Misc

MEASUREMENT OF EARTH RESISTANCES*

A.B. OSLON

Zlatoust

(Received 28 August 1955)

A three-electrode circuit is used to measure the resistances of an earthing system, these being: the earth electrode (earthing circuit), the current electrode and the potential electrode. All quantities referring to the earth electrode are denoted by the K, those referring to the current electrode by subscript T and those referring to the potential electrode by P.

Current is passed through the earth and current electrodes. The potential of the circuit is measured via the potential electrode. The earth resistance equals the measured potential divided by the current passing.

In Fig. 1 the voltmeter and ammeter are instruments specially designed for measuring the resistances of earthing systems.

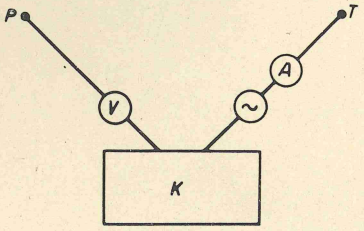

Fig. 1.

It is usually assumed that the current and earth electrodes must be sufficiently far apart not to distort the field and that a sufficiently large zero potential zone remains between them. The potential electrode must be placed in the zero potential zone [1,2].

Let us assume that we already know the earth resistance of the circuit R_K. Is it then possible, having placed the current electrode at an arbitrary point, to so locate the potential electrode that the measured resistance is equal to R_K? If this is possible, how can we determine the 'locus of precise measurements'?

To answer this question we will use the analogy between an electrostatic field and the field due to a current in a conducting medium.

* *Elektrichestvo* No. 2, 56–58 (1957). [Reprint Order No. EL. 10]

Maxwell's equations with potential coefficients for the three electrodes are

$$\phi_K = \alpha_{KK} I_K + \alpha_{KT} I_T + \alpha_{KP} I_P$$

$$\phi_T = \alpha_{TK} I_K + \alpha_{TT} I_T + \alpha_{TP} I_P$$

$$\phi_P = \alpha_{PK} I_K + \alpha_{PT} I_T + \alpha_{PP} I_P$$

Current flow from the electrodes into the ground is taken as positive:

Neglecting the current drawn by the voltmeters we get:

$$I_P = 0, \quad I_T = -I_K$$

The measured resistance is

$$R_{\text{meas}} = \left| \frac{\phi_K - \phi_P}{I_T} \right|$$

Assuming $\alpha_{12} = \alpha_{21}$, we have

$$R_{\text{meas}} = \alpha_{KK} + \alpha_{TP} - \alpha_{KT} - \alpha_{KP} \tag{1}$$

The actual earth resistance

$$R_K = \alpha_{KK}$$

If $R_{\text{meas}} = R_K$, the following condition must be satisfied:

$$\alpha_{TP} = \alpha_{KT} + \alpha_{KP} \tag{2}$$

Equation (2) is the answer to our question. From this we can draw the following conclusions:

(a) It is theoretically possible to measure earth resistances accurately when the measuring and earth electrodes are placed arbitrarily close together

(b) When the measuring electrodes have been placed in a certain way, the result of the measurement is independent of which is the current electrode and which the potential electrode.

From (a) it follows that the measurement may be accurate even when the current electrode distorts the field of the earth electrode, and from (b) that the second electrode need not necessarily be placed in a zone of zero potential.

We will demonstrate the usefulness of (b) for any measurement performed by the 'three-point' method used for obtaining potential distributions in the field, measuring the footing-resistances of steel towers connected through earth wires, when the earthing circuit is disconnected from the base of the tower, etc. For this purpose we will represent the measuring circuit as a passive four-terminal network, all elements being linear over the entire current range. In Fig.2, 1′ and 2′ represent the earth electrode, 1 the current electrode and 2 the potential electrode.

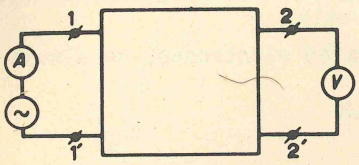

Fig.2

The following relationships apply to such a four-terminal network:

$$U_1 = AU_2 + BI_2, \quad I_1 = CU_2 + DI_2$$

Assuming $I_2 = 0$, we get

$$R_{meas} = \frac{U_2}{I_1} = \frac{I}{C}$$

Let us reverse the current and potential electrodes, (Fig.3). We then get

$$U_2 = DU_1 + BI_1, \quad I_2 = CU_1 + AI_1$$

then $I_1 = 0$ and

$$R'_{meas} = \frac{U_1}{I_2} = \frac{I}{C}$$

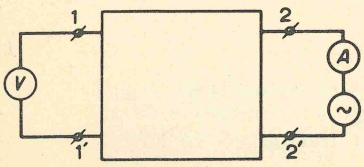

Fig.3

The identity $R_{meas} = R'_{meas}$ is the most general demonstration of (b).

We give below examples of electrode sitings satisfying equation (2). In the examples the soil is assumed to be homogeneous and of resistivity ρ.

A concentrated earth electrode

An earth electrode will be termed concentrated if its field is radial and spherical, at a short distance away (~ a few metres). At this distance (2)

$$\alpha_{KM} = \frac{\rho}{2\pi r_{KM}}$$

where r_{KM} is the distance (subscript M denoting any measuring electrode).

Since the measuring electrodes are concentrated electrodes, we always have

$$\alpha_{KP} = \frac{\rho}{2\pi r_{KP}}$$

These expressions and equation (2) show that for the earth resistance measurement to be accurate we must have

$$\frac{1}{r_{TP}} = \frac{1}{r_{KT}} + \frac{1}{r_{KP}} \qquad (3)$$

or

$$r_{TP} = \frac{r_{KT}\, r_{KP}}{r_{KT} + r_{KP}}$$

In practice it is desirable that the total lead length to the measuring instrument ($r_{KT} + r_{KP}$) should be a minimum, this being the case when $r_{KT} = r_{KP}$.

If r_{KT} must not be less than a certain value for some reason, the same condition must be imposed on r_{KP}, since the conditions applying to both electrodes are similar. In this case

$$r_{TP} = \frac{r_{KM}}{2} \qquad (4)$$

The relative positions of the electrodes are indicated in Fig.4.

A radial earth electrode

The equipotential lines of a radial earth electrode on the surface of the ground are ellipses, so

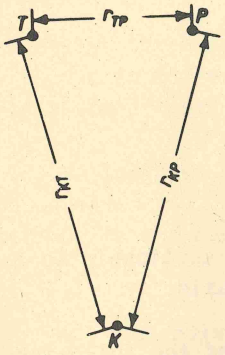

Fig. 4. Recommended positions for the measuring of electrodes when testing a small earth electrode $r_{TP} = r_{KP}/2 = r_{KT}/2$.

$$\phi = \frac{I\rho}{4\pi c} \ln \frac{a + c}{a - c}$$

where a is the semi-major axis, and "c" the focal distance, equal to the length of the earth electrode l; instead of 8π we took 4π, because the ground represents a half-space.

Hence,

$$\alpha_{KM} = \frac{\rho}{2\pi l} \ln \frac{2a + l}{2a - l}$$

where $2a$ is the sum of the distances from the measuring electrode to the ends of the radial earth electrode.

We will measure r_{KM} from the mid-point of the earth electrode.

When $r_{KT} = r_{KP}$ (Fig.5)

$$\alpha_{KM} = \frac{\alpha_{TP}}{2} = \frac{\rho}{4\pi r_{TP}} = \frac{\rho}{8\pi x} = \frac{\rho}{2\pi l} \ln \frac{2a + l}{2a - l}$$

where x and y are the co-ordinates of the measuring electrode in the first quadrant.

Hence,

$$x = \frac{i}{4 \ln \frac{a2a + l}{2a - l}}$$

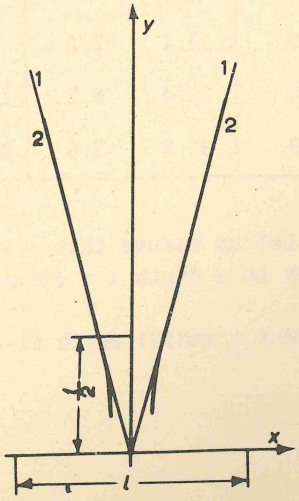

Fig. 5. Resistance measurement for a radial earth electrode. 1. Lines along which equation (4) is satisfied for symmetrically disposed electrodes. For these, $x' = y'\sqrt{15}$; 2. Lines of accurate measurement (columns 3 and 4 of table).

We will find the relation between x and y which assures accurate measurements. From the equation of an ellipse

$$\frac{x^2}{a^2} + \frac{y^2}{b^2} = 1$$

we have

$$y = \sqrt{\frac{b^2(a^2 - x^2)}{a^2}}$$

We have, therefore, obtained a single-valued solution applicable to measuring electrodes disposed symmetrically about the y-axis.

The measured data are given in the first six columns of the following table. As fundamental datum we took the semi-minor axis b of the ellipse.

All distances are in metres.

α/ρ emphasises that the result is independent of the character of the soil (ρ is measured in ohm-metres).

TABLE 1

b	a	x	y	$\frac{\alpha_{PT}}{\rho}$	$\frac{\alpha_{KM}}{\rho}$	x'	$\frac{\alpha'_{PT}}{\rho}$	$\Delta R_K'\%$
2.5	10.6	1.41	2.47	0.00564	0.0282	0.63	0.126	77.4
5	11.2	1.73	4.94	0.0460	0.0230	1.27	0.0625	18.3
10	14.1	2.8	9.8	0.0284	0.0142	2.53	0.0315	3.44
20	22.4	5.2	19.4	0.0154	0.0077	5.0	0.0158	0.45
30	31.6	7.6	29	0.0104	0.0052	7.47	0.0106	0.22

Let us assume that $l = 20$ m, the earth electrode diameter to be $d = 1$ cm, sunk to a depth $t = 50$ cm.

For a radial earth electrode (1)

$$R_K = \frac{\rho}{2\pi l} \ln \frac{l^2}{dt}$$

In our case $R_K = 0.09\rho$.

The table shows that when x has the values given in column 3, we get, with the values of y in column 4, $\alpha_{BT} = 2\alpha_{KM}$ and $\Delta R_K = 0$.

The last three columns show the error of measurements when the electrodes are placed to correspond with equation (4), i.e. on the lines 1 (Fig.5). y' is assumed equal to y, in which case we get practically $\alpha'_{KM} = \alpha_{KM}$.

The table shows that when the electrodes are arranged to correspond with equation (4), distances of $l/2$ from the mid-point of the radial earth electrode to the measuring electrodes are sufficient to assure an accuracy of 5 per cent.

Circuit consisting of linear horizontal segments (polygon, star, etc.)

Each linear segment i sets up a potential

$$\phi_i = \frac{I_i \rho}{2\pi l_i} \ln \frac{2a_i + l_i}{2a_i - l_i}$$

the measuring electrode where $2a_i$ is the sum of the distances from the measuring electrode to the ends of segment i;

l_i being the length of segment i;
I_i the current flowing from it into the ground.

The potential set up at the measuring electrode by the whole circuit becomes

$$\phi_{KM} = \sum \phi_i = \frac{\rho}{2\pi} \sum \frac{I_i}{l_i} \ln \frac{2a_i + l_i}{2a_i - l_i}$$

Let us assume $I_i/l_i = I_K/L$, where $L = \Sigma l_i$. Then,

$$\alpha_{KM} = \frac{\phi_{KM}}{I_K} = \frac{\rho}{2\pi L} \ln \prod_i \frac{2a_i + l_i}{2a_i - l_i}$$

Where Π is the product sign.

We use a rectangular circuit to show that a correct choice of distance from the circuit will give a satisfactory accuracy when the electrodes are placed in accordance with equation (4). Distances are measured from the centre of the circuit.

Fig. 6 shows a rectangular earthing system and also two possible locations for the measuring electrodes. We know [3] that for such a system

$$R_K = \frac{\rho}{2\pi L} \ln \frac{8L^2}{\pi b t}$$

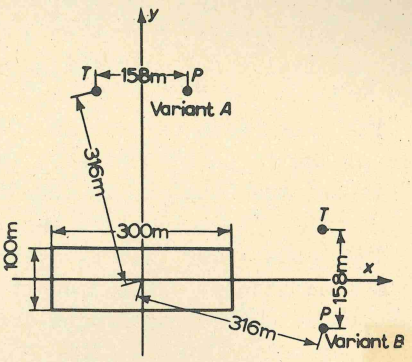

Fig. 6. Earth resistance measurement on a rectangular earthing system.

where L is the perimeter of the circuit; b the width of the earthing strip; t the depth to which it is sunk in the earth.

In our case L = 800 m, b = 50 mm, t = 50 cm. With these parameters, $R_K = 3.58 \times 10^{-3}\rho$.

The above formulae give

	α_{KM}/ρ	α_{TP}/ρ	ΔR_K,
Variant A	0.050×10^{-3}	1.06×10^{-3}	1.7
Variant B	0.574×10^{-3}	1.06×10^{-3}	2.5

By using additional internal strips, vertical earth electrodes, etc. the earth resistances may be reduced, but it cannot be less than the resistance of a hemisphere of diameter equal to the circuit diagonal D = 316 m, for which

$$R_K = \frac{\rho}{\pi D} = 10^{-3}\rho$$

In this extreme case the error reaches 8.8 per cent for B. In general an error of 10 per cent is regarded as acceptable [1,3,4].

In the literature [2–4] recommended for use, when measuring the istance of the earthing of large objects

$$r_{KP} \geqslant 5D; \quad r_{TP} = 40 \text{ m}; \quad r_{KT} \geqslant (5D + 40) \text{ m}$$

These cause exceptionally large errors. Indeed, we would get in our

$= 1580$ m, $\alpha_{KP} = \dfrac{\rho}{2\pi r_{KP}} = 0.1 \times 10^{-3}\rho$; $r_{TP} = 40$ m, $\alpha_{TP} =$

$$= \frac{\rho}{2\pi r_{TP}} = 4 \times 10^{-3}\rho$$

$= 1620$ m, $\alpha_{KT} = \dfrac{\rho}{2\pi r_{KT}} \approx 0.1 \times 10^{-3}\rho$; $\Delta R_K = \alpha_{TP} - \alpha_{KP} - 3_{KT} =$

$$= 3.8 \times 10^{-3}\rho$$

$$\Delta R_{K'} = \frac{\Delta R_K}{R_K} 100 = 3.8 \times 10^{-3}\rho / 3.58 \times 10^{-3}\rho \times 100 = 106\%$$

n the extreme case for $R_K = 1 \times 10^{-3}\rho$

$$\Delta 3_K = 380 \text{ per cent}$$

in measuring the earth resistances of large objects the distance en the measuring electrodes and the centre of the system must not be er than the diagonal of the earth contact, and the interelectrode ice not less than half this.

REFERENCES

. Lur'e; *Testing the Earth Connections of Electrical Plant.* energoizdat (1950).

. Krug; *Fundamentals of Electrical Engineering.* Gosenergoizdat 46).

. Baptiddnov and V.I. Tarasov; *The Electrical Equipment of Power tions and Sub-stations* Vol. II, Gosenergoizdat, (1948).

tection of Industrial Plants and Buildings against Lightning (Edited I.S. Stekol'nikov) Akad. Nauk SSSR (1951).

AUTOMATION OF ELECTRIC DRIVES FOR BUCKET-CHAIN DREDGERS*

L.F. SHKLIARSKII

Bauman Higher Technical College, Moscow.

Automatic load drive and manoeuvring winch control is a current problem in ensuring maximum dredger productivity.

Attempts† had earlier been made to render the drive control automatic, e.g. in 1937 in the "Primorzoloto" trust [1]. They were based on the use of fluid flywheels with servomotors actuated by current relays in the stator circuit of the bucket chain drive motor. Such a stepwise control could not be widely used in practice††.

Therefore the output control required by the soil variations is performed manually in most induction-motor dredgers, viz. by altering the lateral feed rate. Rheostats are used in the manoeuvring winch rotor circuit, the bucket drive motor speed being constant.

The automatic control system described below is based on the manual one, viz. that the lateral feed rate must change with the soil properties, the bucket drive speed being kept practically constant to ensure maximum productivity.

---

* *Elektrichestvo* No.1, pp.22-25, (1957).

† Only a.c. driven dredgers are considered.

†† A design for 0.23 m^3 bucket (1949: "Sibelektromontazh" trust) for both d.c. (generator + motor) and a.c. systems. Provided for automatic rheostat control of the maneouvring winches. But the IZTM works adopted the d.c. drive system for industrial production.

[Reprint Order No. EL.11]

WIND PRESSURE ON OVERHEAD TRANSMISSION LINE CONDUCTORS*

V.V. BURGSDORF

(Received 9 January 1957)

The correct assessment of wind pressure on conductors is of great importance in the design of transmission lines. This applies particularly to double-circuit lines and lines equipped with release clamps and safety (swivelling or collapsible) cross-arms, since in these cases there is an upper limit imposed for the maximum permissible wind loading. In designing large installations, it is necessary to know accurately the aerodynamic characteristics of conductors and the distribution of wind pressure.

As is well known, strong winds are always of turbulent nature and consist of fast-and slow-moving air masses. In other words, the wind velocity is never uniform along the front of a gust. The total load on a long object is therefore determined not by the maximum, but by some mean value, of the wind velocity. For spans longer than 200 m this lack of uniformity may be of considerable importance.

The first experimental investigations to ascertain the extent of the non-uniformity in the distribution of the wind velocities affecting the total load on conductors date back over 25 years [1] and [2]. These tests showed that for wind speeds up to 20 m/sec. this non-uniformity can be neglected for spans up to 100 m. long, but that it becomes sufficiently noticeable on spans about 200 m. long.

Later investigations carried out in Sweden in 1939 revealed a possibility of reducing the design value of wind load because of the finding that the wind pressure becomes less uniform with velocity [3]. Similar experiments were also carried out in other countries: France in 1951 [4] and [5], Australia in 1949 [6]; Belgium in 1952 [7]. Recently investigations were made in West Germany [8] and in the U.S.S.R. where eight experimental stations were erected with span lengths from 220 to 350 m.

The reduction co-efficient considering the non-uniform distribution of the pressure along the span was introduced in the Soviet Regulations for Trans-

* *Elektrichestvo* No.5, 47-52, 1957 [Reprint Order No. EL 23].

mission Lines in 1947 [9]. These regulations recommend the following formula

$$P = aC_x \frac{v^2}{16} \tag{1}$$

where P is wind pressure in kg/m² of projected area;
a is the reduction co-efficient;
C_x is the head resistance of conductor;
v is the wind speed in m/sec.

In the above formula the wind speed is taken usually as the maximum velocity registered by a meteorological station, for a period of 5 to 10 years. The head resistance of the conductor which can be referred to conductor diameter and wind speed, is normally taken as 1.2 [10]. The coefficient a is 0.85.

The coefficient a depends not only on the conditions existing in a given locality, but also on the method of measurement of the wind velocity.

It should be pointed out that the anemometers used in the U.S.S.R. were of the pressure-plate type whereas those used abroad were generally of the pressure – tube type (i.e. working on the Pitot-tube principle). The latter anemometers can register the velocity of a wind gust lasting 10 to 15 sec. whereas the pressure-plate instrument, according to the instruction book, should register a mean position of the plate for 2 min. It is obvious that the maximum velocities as recorded by low-inertia anemometers should be higher than those recorded with the pressure-plate anemometers. This, in fact, explains the various statements on low wind speed prevailing in the U.S.S.R.

The wind load on conductors is usually computed from the measurement of the angle of swing of the insulator string or the coupling link from which the conductor is suspended. This gives directly the horizontal force on the tower and the reduction of the clearance to the tower. To determine the maximum wind loading for a given period of time, continously recording instruments were used in Sweden, Germany, and U.S.S.R. and maximum-swing indicators were used in France and Belgium. The deflection angles thus obtained were checked against records of the maximum wind velocities measured in the immediate vicinity of the experimental span or at a near-by meteorological station.

A visual method of measuring the angle of deflection of the conductor at midspan was used in Australia. Readings were taken "only when the conductor was fairly steady" obviously because such a method is not particularly suitable for measuring maximum deflections. Moreover, the readings were checked against wind velocities measured by a cup-type anemometer and consequently, in this investigation, one can speak only of some average conductor deviation and wind speed. A simultaneous underestimation of conductor deflection and wind speed leads to the cancellation of the error. Thus, such results cannot be accepted as being characteristic of maximum wind loadings and will not be utilized in the following considerations.

In the U.S.S.R. the wind velocity was invariably recorded by means of

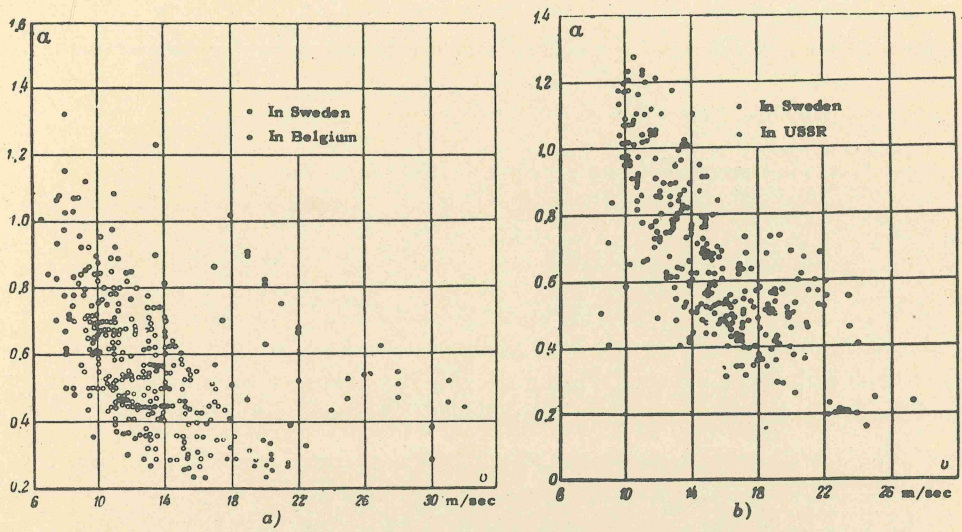

FIG. 1. Relationship between the coefficient α and wind velocity
a — measurements in Sweden (inland regions): d = 25 to 27.7 mm, l = 155 to 300 m; measurements in Belgium: d = 9.5 mm, l = 120 and 190 m;
b — measurements in Sweden: d = 15.8 mm, l = 200 m; measurements in U.S.S.R. (coastal area): d = 19.1 mm, l = 250 m.

pressure plate anemoters, except in one case in which a pressure-tube instrument was used.

The results of various investigations are presented in different ways. For example, Swedish publications give the measured wind pressure on conductors as a fraction of the wind pressure on a large plane ($C_x = 2$), i.e. the measured pressure is characterized by a quantity which is less than the coefficient α; in French investigations the results are expressed in terms of the ratio of the measured to calculated angle of conductor deflection (the calculations being performed in accordance with the method accepted in France). In order to compare the results from various countries the data were recalculated on a common basis. The quantities calculated were the coefficient α from (1) and the effective load per square metre of the projected area normal to the direction of wind*. For each particular case the head resistance was taken as depending on the type of conductor and wind speed in accordance with the results of tests in wind tunnels carried out in the U.S.S.R. [10]. In this way it was possible to arrive at more accurate values of the coefficient α.

The results of this re-calculation are shown in dotted lines on the accompanying figures. Figs. 1,2 and 3 show the values of the coefficient α for the various countries, and Fig. 4 the envelopes drawn through the points of maximum value. Two points differing from the others are shown in Fig. 4 separately.

* It is regretted that the results of German investigations could not be recalculated because of the insufficiency of published data.

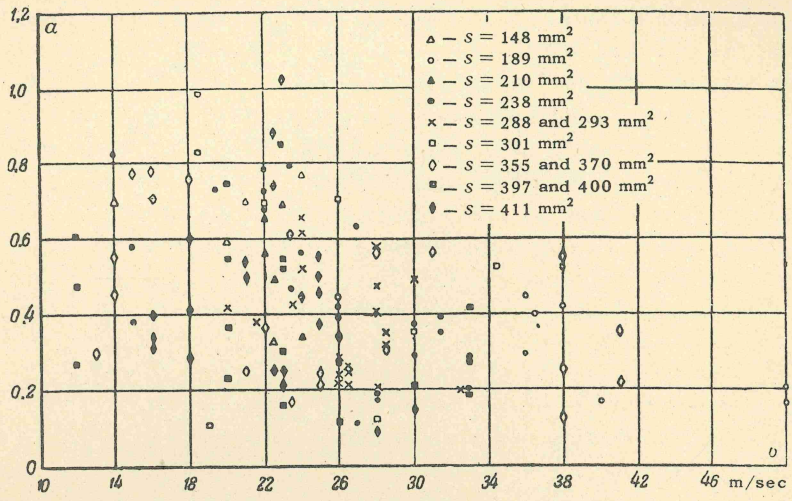

FIG. 2. Relation between the coefficient α and wind speed according to the results obtained in France.

When analysing results of measurements, apart from the non-uniform distribution of the wind speed along the span, one should also consider the case when the wind speed at the span is higher than that at the point of location of the anemometer. In this case the coefficient α becomes greater than unity. It is characteristic that for high wind speeds (20 m/sec and more) no such case has been observed in practice.

The manner in which the experimental points are distributed allows us to establish beyond any doubt the fact that the wind pressure becomes less uniform along the span as the wind becomes stronger. Also, the influence of the different physical and geographical factors pertaining to different geographical areas is clearly brought out. Moreover, this is true not only for coastal and inland regions within one country such as, for example, Sweden. The first measurements carried out in the Leningrad area with low-inertia instruments yielded values * for the coefficient α greater than those obtained for a coastal region in Sweden. Even greater values of the coefficient were obtained in Belgium and yet greater values in France.

In France values between 0.5 and 0.55 were obtained for the coefficient α for wind velocities up to 38 m/sec. It is regrettable that no information is available on the experimental span lengths but it can be taken that in France the span length for conductors of 300 mm² or more† cross-sectional area, is, as a rule, more than 400 m and only rarely 350 m.

* Here and later on the values of the coefficient α are taken for the same, and not for the maximum wind speeds, recorded in the given localities.

† It can be shown that for a wind speed of 34.5 m/sec, $\alpha = 0.52$ (Fig. 2) was recorded on a span 462 m long.

The coefficients a obtained from measurements in the U.S.S.R. by using pressure-plate anemometers with loaded plate (Fig.3) correspond mainly to wind speeds of up to 20 – 25 m/sec. However, there is enough experimental data to establish the fact that the coefficients obtained in this way are greater than those resulting from measurements with low-inertia instruments. One fact stands out, viz. the large number of points whose values are considerably greater than unity for wind speeds up to 18 m/sec and also the number of points having values of the order of 0.8 for wind speeds of about 25 m/sec for long spans.

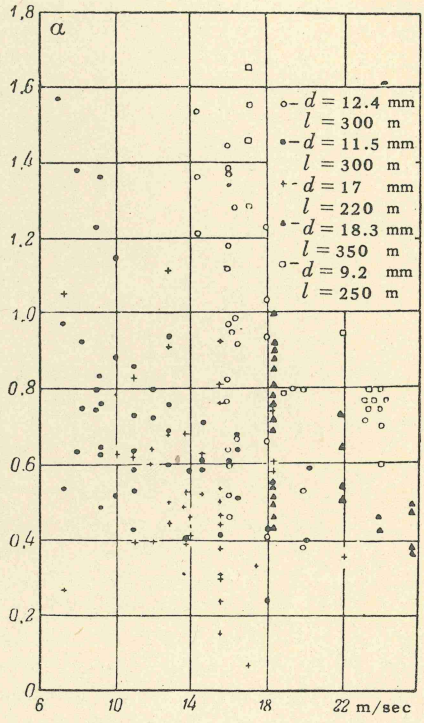

FIG. 3. Relation between coefficient a and wind speed according to results obtained in the U.S.S.R.

A comparison of the curves shown in Fig. 4 indicates that the coefficient a depends on the degree to which a given district is exposed to high winds. In this respect the comparison of the Swedish data for coastal and inland regions and of the Belgian and French data are characteristic. From Fig. 4 it is seen that the curves of the reduction coefficient obtained for different regions are shifted with respect to each other, and the coefficients a for districts subjected to stronger winds are higher than those for districts with less intense winds for a given wind speed. Therefore, if a coefficient a is obtained for a region with strong winds, it cannot be extended to maximum wind speeds of regions with moderate winds. For example, the value of a at 25 m/sec for the region with the design wind speed of 30 or 35 m/sec cannot be applied to a line erected in a region where the design wind speeds is 25 m/sec, since in this latter case the value of a is smaller.

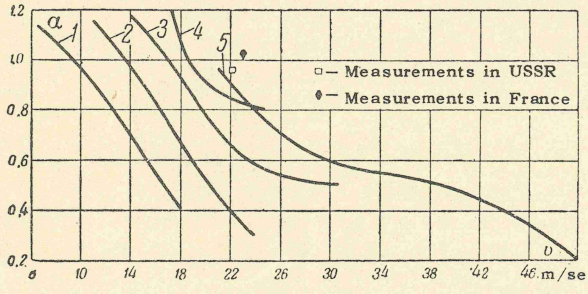

FIG. 4. Relation between greatest values of coefficient a and wind speed as measured in different countries:
1 – in Sweden (inland regions);
2 – in Sweden (coastal regions);
3 – in Belgium;
4 – in U.S.S.R; 5 – in France.

To facilitate further analysis, mean values of wind pressure on a conductor for one span recorded at various wind speeds are plotted in Figs. 5 – 7. The distribution of these points is typical. The curves shown in these figures are drawn from (1) for $C_x = 1.2$ and

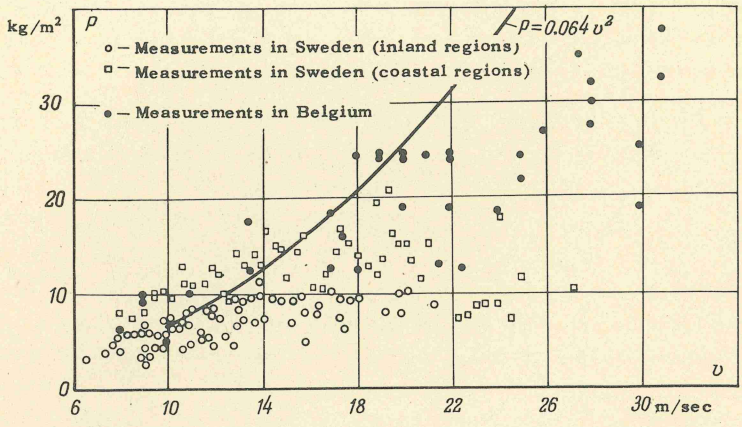

FIG. 5. Relation between wind pressure on conductor projection area normal to wind direction and wind speed according to measurements in Sweden and Belgium.

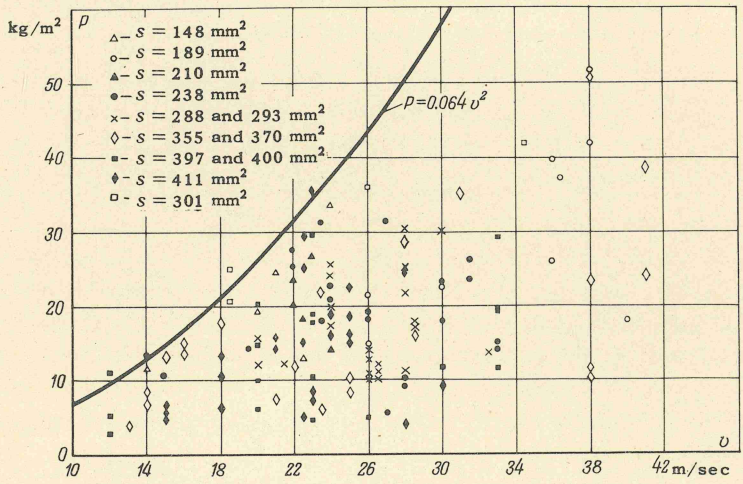

FIG. 6. Relation between wind pressure on conductor projection area normal to wind direction and wind speed according to measurements in France.

α = 0.85 in accordance with the recommendations given in the Regulations for the Erection of Electrical Installations [9].

The practical conductor loading in Sweden (especially in inland regions) is noticeably lower than it is in Belgium and this, in turn, is lower than in France. For wind speeds up to 15 m/sec the experimental points lie not infrequently above the design curve and for velocities of 15 to 20 m/sec they are, in general,

the same as the higher values observed in Belgium and France. At still higher wind velocities the measured wind load is smaller than the calculated one which is obviously due to the lowering of the coefficient a.

Of a similar character is the distribution of experimental points obtained from short-period tests in the U.S.S.R., though the quantitative relations are here different *: wind pressures greater than those given by (1) occur often at speeds of up to 18 or 19 m/sec, and at 25 m/sec they are almost as high as the highest values recorded.

The material presented demonstrates convincingly the importance of the correction factor for wind pressure at high wind speeds. This coefficient should be different for speeds measured with the low-inertia and the pressure-plate anemometers.

The West European investigators working with low-inertia anemometers suggest a value of 0.5 for the reduction coefficient; they are also referring to a considerable local wind speed of 35 m/sec. The investigators in Sweden, where the wind speed has also been measured with low-inertia anemometers, recommend the coefficient $a = 0.4$ on the basis of a wind speed of 28 m/sec. Such a lowering of the coefficient appears to be justifiable on the ground that undoubtedly the winds in Sweden are not so strong as those in Belgium and France.

The value of the coefficient a should be greater if this is worked out from the data on wind velocities obtained with the method which is accepted in the U.S.S.R. The relation between the coefficient obtained with the two types of anemometer is given by

$$\left(\frac{v_{li}}{v_{pp}}\right)^2,$$

where v_{li} is the speed measured with the low-inertia, and v_{pp} with the pressure-plate anemometers. At the present time work is being done to determine this ratio, but it can be said even now that no great reduction can be expected in the present value (0.85) of the coefficient a. Indeed, taking the West European coefficient $a = 0.5$, the ratio

$$\frac{v_{li}}{v_{pp}} = \sqrt{\frac{0.85}{0.5}} = 1.3$$

which may be regarded as a sufficiently realistic figure for the ratio of short duration (10 to 20 sec) to one minute maximum wind velocity.

The above statement is verified by the damages to transmission lines occur-

* This is obviously connected with the different method of measurements (pressure-plate anemometers) used in the U.S.S.R.

ring at strong winds when the effective wind pressure on conductors is nearly 60 kg/m² and the wind speed (measured by pressure-plate anemometer) 32 to 35 m/sec.

A more substantial reduction of the coefficient a can be expected for regions where the design wind speed is 35 m/sec or more, and also where the repetition rate of the assumed design speed comes near the highest observed.

To give a fuller picture of practices in various countries the tables 1 and 2 of design wind loadings on conductors and metal supports were compiled.*

It is seen from Table 1 that the conductor loading used in the U.S.S.R. is about the same, or even sometimes lower, than in other countries.† The lowest wind loading is applied in Finland where, as in the Leningrad district and Karelian A.S.S.R., the wind speeds are not very high due to favourable geographical conditions.

Recent research on the effects of non-uniform wind pressures is now being accepted as a basis for the reduction of the design wind loadings in Belgium and France, where until recently these loadings have been excessively high.

The design wind loadings on supports are invariably higher abroad than in the U.S.S.R., sometimes by as much as 50 or even 100 per cent.

It appears from the foregoing that the design values used in the U.S.S.R. for wind loading are in every respect more modern than in most other countries where only recently the regulations were slightly eased-up, which brings the foreign design values nearer to the Soviet values. It should be made clear, however, that this does not preclude the possibility of a future reduction in the design wind loading for transmission lines.

This further reduction should be well substantiated by more extensive investigations to determine realistic loadings for various regions and to obtain more accurate aerodynamic characteristics of conductors and supports and the possible values of the coefficient a.

From experiments which have been carried out up to now it is possible to reduce the design head resistance to 1.1 for the values of the product $vd \geq$ 400 m/sec. mm. It is also possible to take the coefficient $a = 0.75$ if the supports are checked for the highest wind loads ††. This relaxation of the design conditions can be extended also to localities with the design wind velocity of

* In the U.S.S.R. the loads are taken for the average wind speed of 25 m/sec.

† The accepted thickness of ice for Sweden varies between 1.3 and 3.2 cm. Therefore the resulting wind load on tower becomes considerably greater than in the U.S.S.R.

†† The speeds considered are the maximum values for a given region, occurring once in 5 years, and not the design speeds.

TABLE 1. Design wind loadings on conductor projection area without ice used in various countries.

	Country	USSR	Great Britain	Belgium	Germany	Italy	Canada	USA	Sweden	Switzerland	Finland	France
Design load	kg/m²	40	39	72*** / 45	44-53	72	39	44	25*	50	25	72** / 48
	%	100	97.5	180*** / 112.5	110-130	180	97.5	110	–	125	62.5	180** / 120

* With and without ice load.
** Numerator – present standards; denominator – standards recommended at the present time, publications referred to
*** Numerator – present standards; denominator – proposed new standards with $C_x = 1.2$.

TABLE 2. Design wind loadings on flat tower sections used in various countries.

	Country	USSR	Great Britain	Germany	Italy	Canada	USA	Sweden	Switzerland	Finland	France
Design load	kg/m²	54.9	120	77	120	63	70.5	100	100	100	120
	%	100	220	140	220	115	128	182	182	182	220
Pressure on leeward face %		100	–	81	60-80*	100	100	80/100**	60-80	100	60-80*

* Depending on projected tower area.
** Depending on distance between tower sides.

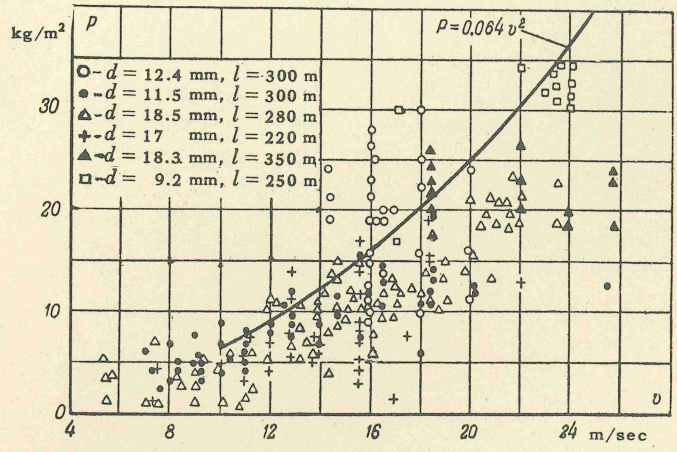

FIG. 7. Relation between wind pressure on conductor projection area normal to wind direction and wind speed according to measurements in the U.S.S.R.

35 to 40 m/sec, except for the regions adjacent to large water areas. The question of specifying more precise value for the coefficient a will be decided from the results of experiments now being carried out in the U.S.S.R.

It is also necessary to consider more closely the actual conditions under which a line is expected to operate. In particular the present practice of extending the design wind speed of 25 m/sec. to regions with light wind should be abandoned. In all cases the design wind speeds should be chosen in accordance with observations. For lines passing through woodlands the design speed should be taken at least 5 m/sec. less than the speed for the main region.

REFERENCES

1. W.D. Tuck, *Variation in Distribution of Wind Pressure on Overhead Lines. Brit. Electr. a. All. Indust. Research Assoc. Tech., rep.* X (1934).
2. R.H. Sherlock and M. Stont, *Storm Loading a. Strength of Wood Pole Lines a. Study of Wind Gusts. Edis. El. Inst.* (1936), *University of Michigan, Anu Arbor.*
3. O.P. Zetterholm and S. Sandin, *Wind Pressure on Overhead Transmission Line Conductors.* CIGRE Rep., 202 (1954).
4. R. Poyart, *Effect of High-Velocity Winds on Overhead Line Conductors. Bull. Soc. France des electriciens,* XI (1953).
5. P. Schuepp *et al, Investigation of Mechanical Overload in Insulators of Transmission Lines Under Normal Service Conditions. Rev. Gen. Electr.,* No. 2 and 3 (1955).
6. H.C. Harrison, *Factors Affecting the Mechanical Design of Transmission Lines.* Pt. 1, CIGRE. Rep. 218 (1956).
7. L.H. Marchal *et al, The Action of Wind on Overhead Line Conductors.* CIGRE. Rep. 206 (1956).
8. H. Mors *et al, Wind Pressure on Overhead Transmission Line Conductors.* CIGRE., Rep. 220 (1956).

REFERENCES (*continued*)

9. *Recommendations for Erection of Electrical Installations. Gosenergoizdat* (1947).
10. V.V. Burgsdorf, *Fundamental Problems in Erection of Overhead Transmission Lines. Trudy Central Scientific Research Electrochemical Laboratory.* 5th Edition.

Note:

(CIGRE *stands for Conference Internationale des Grands Reseaux Electriques.)*

CORONA LOSSES ON LIVE TRANSMISSION LINES*

V.D. KRAVCHENKO, V.I. LEVITOV and V.I. POPKOV

(Received 7 February 1957)

The corona loss on an energized transmission line constitutes only a small fraction of the transmitted energy and is commensurable with or sometimes even smaller than the heat loss. Therefore, it is practically impossible to determine this loss by separating the current component which corresponds to the corona loss from the total line current as measured by conventional methods.

The corona loss is due to the cross currents, that is, the currents that flow between the conductors and between the conductors and earth. If it were possible to measure quantities which are proportional to these currents, or to their corresponding charges this would be the best solution of the problem of measuring the corona losses on energized lines.

Fig. 1 shows an arrangement consisting of a single phase-conductor, 1, and an aerial, 2, which is earthed through a measuring element Z connected to the middle of the aerial.

The e.m.f. induced electromagnetically in an aerial isolated from earth is so distributed that it is zero at the middle of the aerial [1]. Therefore, if this point is earthed through a measuring element Z, no current can flow in the element owing to the magnetic field of the line. The current which flows in the element is determined only by the electrostatic coupling between the line and the aerial.

The minimum height at which conductors are suspended on conventional lines is 7–8 m. At this height the space charge in the region G (Fig. 1) is distributed practically symmetrically with respect to the conductor axis, i.e. the space charge density depends only on the distance from the axis of the conductor of the element of charge considered. Consequently, the integrated electrostatic effect of the space charge on the aerial is the same as that of a linear charge of equal magnitude placed at the axis of the conductor.

For sufficiently small values of the impedance Z the relation between the charge on the aerial and the total charge of the conductor is given by:

$$\alpha_{12}q_1 + \alpha_{22}q_2 = 0 \qquad (1)$$

* *Elektrichestvo* No. 7, 31 – 34, 1957 [Reprint Order No. EL 35].

or

$$q_2 = -\frac{\alpha_{12}}{\alpha_{22}} q_1, \tag{2}$$

where $\alpha_{12} = \frac{1}{2\pi\varepsilon_0} \ln \frac{r'}{r}$ - mutual potential coefficient of the aerial and conductor; $\alpha_{22} = \frac{1}{2\pi\varepsilon_0} \ln \frac{2h}{a_0}$ - self potential coefficient of the aerial (a_0 is the radius of the aerial wire); $q_1 = q_c + q_s$ - total charge of conductor per unit length (q_c is the charge on conductor surface and q_S is the integrated space charge); q_2 - charge per unit length of aerial.

Thus, the charge on the aerial which is earthed at its middle point is proportional to the total charge enclosed in the region G, i.e. is determined by both the charge on the conductor surface and the space charge due to corona.

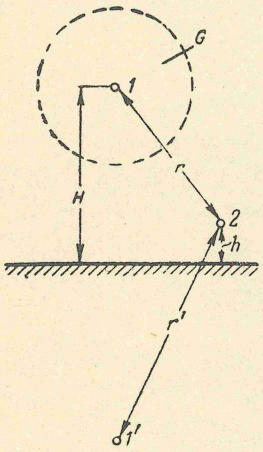

FIG. 1.

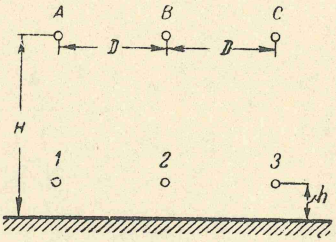

FIG. 2.

Also, the coefficient of proportionality α_{12}/α_{22} is a constant quality depending only on geometrical dimensions of the conductor-aerial arrangement. These circumstances make it possible to use aerials for corona loss measurements.

Three aerials are necessary for measurement on three-phase lines. Fig. 2 shows a possible arrangement of aerials placed directly under the three phase conductors. In this case the relation between the total charges on phase conductors q_A, q_B and q_C and the charges on earthed aerials q_1, q_2 and q_3 is given by the following system of equations:

$$\left.\begin{aligned} -(\alpha_1 q_1 + \alpha_2 q_2 + \alpha_3 q_3) &= \alpha_I q_A + \alpha_{II} q_B + \alpha_{III} q_C; \\ -(\alpha_2 q_1 + \alpha_1 q_2 + \alpha_2 q_3) &= \alpha_{II} q_A + \alpha_I q_B + \alpha_{II} q_C; \\ -(\alpha_3 q_1 + \alpha_2 q_2 + \alpha_1 q_3) &= \alpha_{III} q_A + \alpha_{II} q_B + \alpha_I q_C, \end{aligned}\right\} \tag{3}$$

where $a_1 = a_{11} = a_{22} = a_{33}$; $a_2 = a_{12} = a_{21} = a_{23} = a_{32}$; $a_3 = a_{13} = a_{31}$; $a_1 = a_{1A} = a_{2B} = a_{3C}$; $a_{11} = a_{1B} = a_{2C} = a_{3B} = a_{2A}$; $a_{111} = a_{1C} = a_{3A}$ are self and mutual potential coefficients determined from the geometrical dimensions.

By solving the system of equations (3) with respect to conductor charges q_A, q_B and q_C, we get

$$\left.\begin{aligned} q_A &= A_1' q_1 + A_2' q_2 + A_3' q_3; \\ q_B &= B_1' q_1 + B_2' q_2 + B_3' q_3; \\ q_C &= C_1' q_1 + C_2' q_2 + C_3' q_3. \end{aligned}\right\} \qquad (4)$$

The coefficients A'_i, B'_i and C'_i are composed of potential coefficients a_i which appear in (3). For example,

$$A_1' = \frac{A_1}{\Delta}; \quad A_2' = \frac{A_2}{\Delta}; \quad A_3' = \frac{A_3}{\Delta},$$

where $\Delta = a_1(a_I^2 - a_{III}^2) - 2a_{II}^2(a_I - a_{III})$ - the determinant of the system of equations (3);

$$A_1 = -a_1(a_I^2 - a_{II}^2) + a_2(a_I a_{II} - a_{II} a_{III}) - a_3(a_{II}^2 - a_I a_{III});$$

$$A_2 = -a_2(a_I^2 - a_{II}^2) + a_1(a_I a_{II} - a_{II} a_{III}) - a_2(a_{II}^2 - a_I a_{III});$$

$$A_3 = -a_3(a_I^2 - a_{II}^2) + a_2(a_I a_{II} - a_{II} a_{III}) - a_1(a_{II}^2 - a_I a_{III}).$$

It follows from (4) that the sum of the products of charges on the three aerials, q_1, q_2 and q_3, into their corresponding coefficients A'_i, B'_i and C'_i give the total charges on the phase conductors, q_A, q_B and q_C.

Either capacitors or resistors can be used as the measuring elements. In the first case, the voltages across the elements are proportional to the total charges of phase conductors and in the second case, to their time derivatives, that is to the cross-currents of the line. However, it is preferable to choose capacitors since in this case the measurement will be practically unaffected by the possible h.f. pick-ups of the aerial.

The voltages on the measuring capacitors are given by:

$$U_i = \frac{q_i l}{C} \qquad (5)$$

where U_i - voltages on the aerials; q_i - charges per unit length of the aerials; l - lengths of aerials; C - measuring capacitances.

If follows from (5) that the input voltage to the measuring circuit depends not

only on the coefficients a_i (which are determined by the geometry of the conductor-aerial arrangement) but also on the lengths of aerials and on the values of the me measuring capacitors. The choice of the ratio l/c is governed by the magnitude of the voltage required at the input to the measuring circuit, i.e. it depends on the sensitivity of the measuring device.

The length of the aerial should be such that the part of the conductor catenary which is above the aerial can be taken as being parallel to the ground.* For example, for 220 and 400 kV lines with spans of 450 m this condition is satisfied by an aerial 50 m long placed at mid-span. With this aerial suspended at a height of 0.5 m and with measuring capacitances of the order of 0.1 μF the voltage on the aerial is about 8 to 15 volts.

From the above, a block circuit diagram may be drawn for a device for measuring the corona loss on energized lines. Such a diagram is shown in Fig. 3; A, B and C are line conductors; 1, 2 and 3 aerials; C_u measuring capacitances; $1A$, $1B$ and $1C$ voltage transformers or voltage dividers;

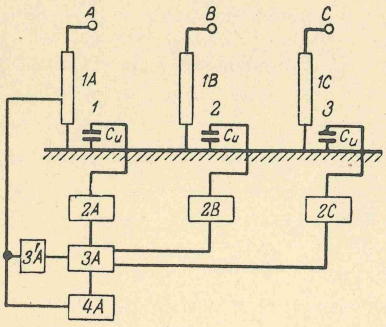

FIG. 3.

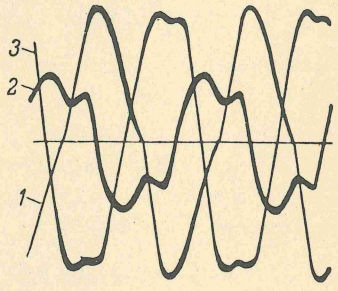

FIG. 4.

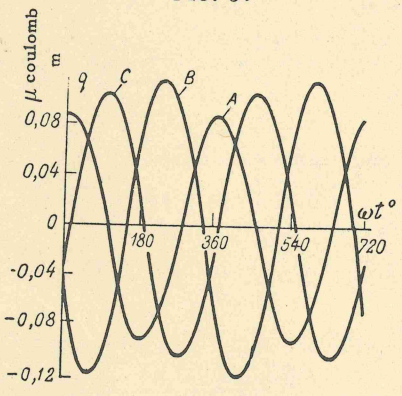

FIG. 5.

$2A$, $2B$ and $2C$ are elements multiplying the voltages corresponding to aerial charges q_1, q_2 and q_3 by their corresponding coefficients A'_i, B'_i and C'_i; $3A$ is an element carrying out the summation of the above products. As a result of this summation we get a voltage (or current) out put proportional to the total charge of phase conductor A; $4A$ is a wattmeter of some sort.

To increase the accuracy of corona loss measurements, particularly at small values of loss, it may be necessary to compensate for the reactive component of the charge q_A.

* In general this condition is not essential, since the effect of the caternary can be taken into account, when calculating potential coefficients. However, it simplifies calculation, if this condition is fulfilled.

Such a compensating voltage may be applied to the integrating element $3A$ by a suitable device indicated by $3'A$.

For simplicity the measuring circuit is drawn for one phase only, the circuits for the remaining two phases are identical.

The assumption made above about the symmetrical distribution of the space charge due to corona with respect to the conductor axis was varified experimentally in the laboratory. A three-phase transmission line model having the following dimensions was set-up: viz. line length - 14.5 m; height of conductor suspension 2 m; interphase clearances - 1.3 m; diameter of polished steel conductors - 1 mm. As aerials copper conductors of 0.83 mm dia, having the same length as the model line were used. One aerial was placed under each phase conductor at a height of 0.27 m above the ground and was earthed through a capacitor. The voltages on the capacitors which are proportional to the charges on the respective aerials were applied in turn (using a special synchronizing device) to the deflecting plates of the CRO and photographed on the same plate. Each oscillogram contains therefore three voltage records. A sample oscillogram obtained with a phase-to-earth voltage of $U = 64\ \mathrm{kV}_{max}$ is shown in Fig. 4.

It is seen from this oscillogram that the curves of the charges on the aerials are irregular and differ from each other. The amplitudes of the charges on the external aerials are approximately the same, but the amplitude of the charge on the middle aerial is about one-half of that of each of the outer aerials. By multiplying the ordinates of the curves by their respective coefficients A'_i, B'_i and C'_i, and adding, we get curves corresponding to equations (4) which are shown on Fig. 5.

It follows from the above that the curves of Fig. 5 should be identical with the curves of the total charges of the experimental conductors in corona conditions. To compare these two sets of curves, an oscillographic record of the volt-coulomb characteristic was obtained for each of the three line conductors. The recording circuit for one phase only is shown in Fig. 6. In this figure the voltage across the capacitor C_q, which is proportional to the total conductor charge, was applied to one pair of deflecting plates of the CRO and the voltage across one arm (C_1) of the capacitance potential divider which is proportional to the voltage of the h.v. transformer T, was applied to the other pair of deflecting plates of the CRO.

With such a circuit the trace on the CRO screen has the form of a closed loop which is known as the volt-coulomb characteristic. The area enclosed by the loop is proportional to the energy loss due to corona for one cycle of the alternating voltage [2].

The volt-coulomb characteristics obtained for the conductors of the experimental line by direct measurement at a phase-to-earth voltage of $U_{ph} = \mathrm{kV}_{max}$ are shown in Fig. 7 (curves drawn in continuous lines). The curves drawn in broken lines represent volt-coulomb characteristics constructed from the data obtained from the aerial measurements (the curves of Fig. 5 and oscillograms of phase-to-earth voltages on the conductors recorded simultaneously with the records of the charges on the aerials), using the same voltage applied to the line.

A good measure of agreement is shown between the volt-coulomb characteristics obtained by the two methods considering the amount of error introduced by the intermediate calculations and constructions in deriving the final curve from the experimental data. The two sets of characteristics agree well as regards the amplitude of the

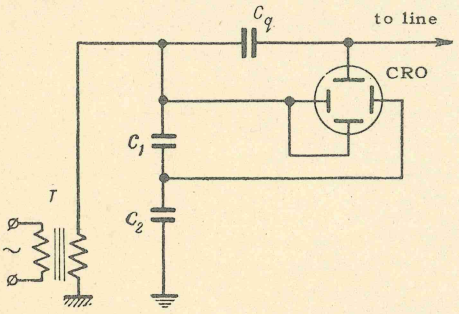

FIG. 6.

charge, the shape of the curve, and the area enclosed by the curve (the last factor being of importance from the point of view of corona loss measurement by means of aerials).

The construction of total charge and volt-coulomb curves was performed for different phase voltages up to a value exceeding three times the critical corona inception voltage. In this way values of corona loss were obtained for the experimental line for a wide range of voltages. These losses are indicated by crosses on Fig. 8 on which are also plotted corona losses derived from the volt-coulomb characteristics obtained by direct measurement. It is seen from this figure that the losses obtained by both methods are practically identical.

Thus, experimental investigations confirm the possibility of measurement of corona loss on live lines by means of aerials and also of verifying the correctness of the assumptions made.

In conclusion it should be mentioned that apart from its application to corona loss measurement the method presented can also be used for investigating other problems; for

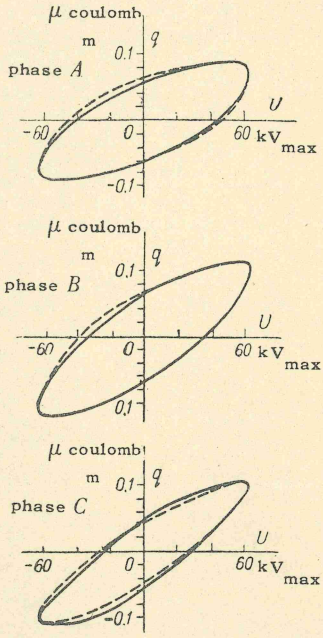

FIG. 7.

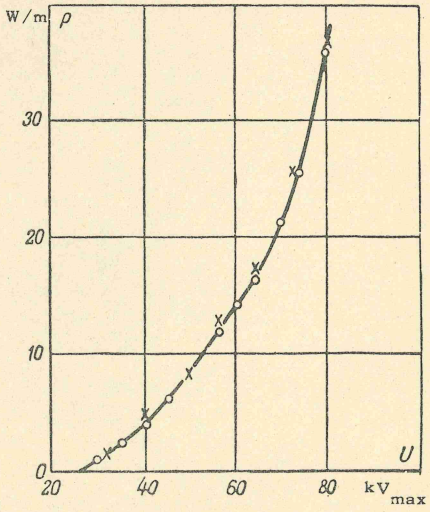

FIG. 8.

example, the distribution of losses along the conductor span, the measurement of charges, etc.

REFERENCES

1. M.I. Mikhailov; *The protection of communication lines. Svyaz'izdat* (1939).
2. H.I. Ryan and H.H. Henline; *The hysteresis character of corona formation. Trans. Amer. Inst. Elect. Engrs.* **43** (1924).

VOLTAGE GRADIENTS IN A LONG-SPARK LEADER CHANNEL*

V.P. LARIONOV

The Lenin All-Union Electrotechnical Institute

(Received 11 June 1956)

Komelkov [1] was the first to show that the leader structure is rather complex in a long-gap spark in air. An extensive ionized region occurs at the tip of the narrow leader channel. This region is composed of separate streamers, i.e. thin, long channels so numerous in the case of a positive discharge that the whole ionized region resembles a cascade of luminous filaments issuing from the tip of the leader. The electrons released at the fronts of the streamers rush along the streamer ducts into the leader channel, leaving positive ions in the ionized region. As the leader penetrates more deeply into the interelectrode space, new streamers appear as the old ones are extinguished, giving an immobile space charge envelope around the narrow leader channel.

The narrow leader channel (the "core") in direct contact with the electrode provides a path along which electrons flow to the electrode in a positive discharge. The voltage gradient along the leader channel determines the ionization conditions at its tip and is therefore the most important parameter. However, this parameter has not yet been fully investigated.

The mean longitudinal gradients were studied at the All-Union Institute of Electrical Engineering by producing an artificial step in the leader channel [2]. The current in the step was first assumed to produce a state of arc-conduction in the channel, the second assumption being that the leader tip potential is unaffected by this, i.e. that the abrupt drop in spark-gap voltage at the instant of producing the step determines the voltage across the channel. Thus, the mean gradients were determined as follows:

$$E_{1m} \approx \frac{U'}{l_1} + E_a \qquad (1)$$

where U' is the abrupt drop in spark-gap voltage.

l_1 is the leader length at the moment of producing the step

E_a is the voltage gradient in the arc channel.

* *Elektrichestvo* No. 4, 80–81 (1957). [Reprint Order No. EL.9]

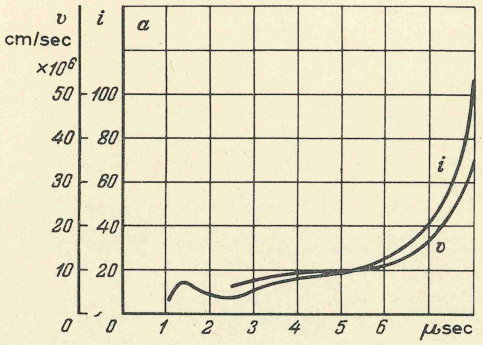

Fig. 1 Leader current and leader tip velocity. Spark gap "rod-plane", 100 cm long. Discharge circuit resistance 2.5 kΩ.

While the first assumption is certainly correct, the second is obviously without foundation. Experience shows that where the step has been formed the current and tip velocity increase considerably; this can only be attributed to an increase in field strength at the tip and therefore to an increased potential on the tip itself. The sudden voltage drop at the instant of step formation does not by any means give the full voltage across the leader channel, so the mean longitudinal voltage gradients calculated from this voltage drop are too low. Using a 200 cm rod-plane gap, the lower values obtained by this method for the mean voltage gradient along the positive leader channel when this was 120 – 140 cm long were found to be between 1200 and 1600 V/cm with discharge circuit resistances of between 140 and 400 kΩ respectively [2]. These figures show that the picture if the developing leader as a highly conducting almost equipotential channel (longitudinal gradients ~ 10 V/cm is not consistent with physical facts.

The longitudinal gradients may be expected to decrease in time owing to the increased current heating the leader channel. It is here of interest to consider the final stages of leader development.

The abrupt drop in spark-gap voltage when the main discharge strikes can be regarded as the sum of the voltage across the leader channel and the potential of its tip immediately before reaching the plane. Thus, assuming that the tip potential is zero near earth, it is possible to obtain a value, which we know to be exaggerated, for the mean longitudinal channel gradient at the instant immediately preceding the main discharge. The gradients obtained under the above test conditions were between 1000 and 1600 V/cm, regardless of the discharge resistance (in 42 tests the drop was between 230 and 370 kV).

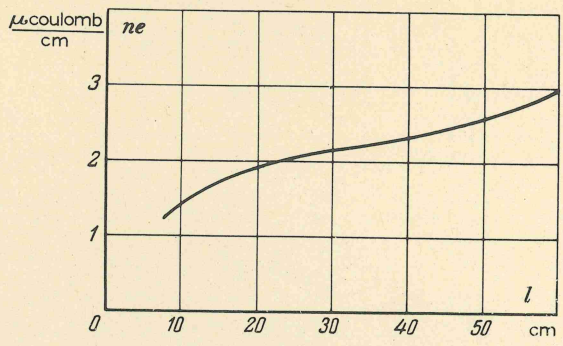

Fig. 2 Distribution of the excess positive charge along the leader (for the discharge of Fig. 1).

Thus, the *lower* limit for the mean channel gradient determined when the leader bridges 60 – 70 per cent of the spark gap is between 1200 and 1600 V/cm, and the *upper* limit, determined immediately before the leader reaches the plane, is between 1000 and 1600 V/cm. This shows that the mean longitudinal gradient decreases considerably during development.

The channel current, i, is given by $i = nev$, where v is the tip velocity, e the electronic charge and n the number of electrons leaving the channel per unit increase in length (ne is numerically equal to the linear excess positive space charge density in the leader envelope). On the other hand, i may be expressed as the number of electrons released during ionization per unit length of the leader, n', and by the electron drift velocity, v' produced by the longitudinal gradients in the channel, viz.

$$i = nev = n'ev', \quad \text{i.e.} \quad nv = n'v' \tag{2}$$

As the tip of the leader approaches the plane, the leader current and the tip velocity increase considerably. Of the two, the current grows more rapidly, which means that the linear density of excess charge increases in the lower part of the leader. The variation in leader current and tip velocity in the rod-plane gap is shown in Fig. 1. In 5 μsec (from 3 μsec to 8 μsec) the current increases ten times, the tip velocity five times, and their ratio $ne = i/v$ two times. The distribution of linear excess charge density along the whole channel for the same discharge is shown in Fig. 2.

v' is less than v [3]. An increase in ne along the leader channel therefore means, in accordance with (2), an increase in n' in the channel plasma.

Let us consider the discharge records for the rod-plane gap shown in Fig.3. The records were obtained with a high-speed rotating camera with a 'Jupiter-3' lens, by the well-known method [1] of photographing simultaneously through a number of slits at different distances from the plane. The records show that at any particular instant (the times are determined by reference to the instant when the main discharge strikes) the channel diameter ("core") is almost constant throughout the length.

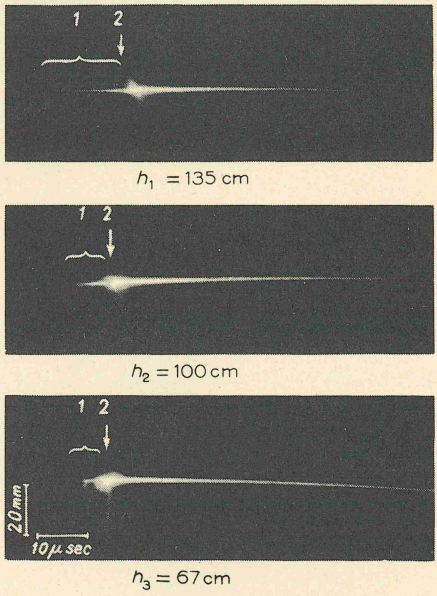

Fig.3 Time-base records for the leader channel. Rod-plane gap, 150 cm long. Discharge circuit resistances 28 kΩ; h = distance, between the leader tip and the plane; 1 - leader stage of the discharge; 2 - main discharge. Side branches round the main channel are visible in the bottom record.

The higher linear electron density in the lower part of the channel (of constant diameter), indicates a higher conductance and a lower longitudinal voltage gradient. The initial voltage gradients therefore vary along the leader channel, being higher at the top, and lower at the bottom. The gradients should fall with time, particularly in the older parts of the channel, owing to thermal ionization.

Since the linear excess positive ion density is constant ($ne = i/v \approx$ const.) Loeb [3] assumes the leader channel homogeneous throughout its length and the voltage gradients constant along the channel.

REFERENCES

1. V.S. Komelkov; The structure and parameters of the leader discharge. *Izv. Akad. Nauk SSSR* (Technical Sciences Section) No.8(1947).
2. V.P. Larionov; The impulse discharge mechanism in a long air gap. *Elektrichestvo* No.7 (1952).
3. L.B. Loeb; Some aspects of breakdown streamers. *Phys. Rev.* **94**, No.2 (1954).

A METHOD OF DERIVING EQUATIONS FOR THE ELECTROMECHANICAL TRANSIENT IN ELECTRIC CIRCUITS*

S.V. STRAKHOV

(Received 5 October 1956)

There are basically two methods of investigating the transient electromechanical processes in electric circuits, viz:

1. Physical modelling.
2. Mathematical modelling, this comprising two sections, viz:
   (a) the section using physical analogs;
   (b) the section using digital computers (integrators) with continuous and discrete action.

The method of physical modelling, comprehensively treated in papers of V.A. Venikov [1-3], M.P. Kostenko [4-6] and of other authors, consists in the replacement of large rotating electric machines and hydraulic turbines by similar units of small ratings with due consideration to the laws of similitude. Transmission lines, tranformers, saturable reactors and static loads are replaced by assemblies of capacitances and inductances, networks with repeated members being used for transmission lines. In other words, in this case the physical character of the model and of the original are the same.

Among the advantages of the method of physical modelling, where rotating machines are concerned, we should mention the possibility of considering eddy currents, saturation, hysteresis, the actual distribution of stator and rotor windings in space, and of other factors. A drawback of this method is the difficulty of varying the parameters of individual machines, usually necessitating the availability of a number of inter-changeable rotors for them. It is, therefore, more convenient to use the method of mathematical modelling in cases where the parameters of the machines must be variable; because this method can deal in a much more simple way with such variations. However, physical modelling will still be preferable in all cases in which the system of differential equations describing the process is very complicated.

* *Elektrichestvo* No. 7, 5-10, 1957 [Reprint Order No. EL 32].

Referring to the first section of the method of mathematical modelling [1, 7 and 8], we note that rotating machines are replaced by equivalent devices (electronic circuits, electrodynamical apparatus), i.e. physical analogs according to the similar structure of their differential equations. In this case the model has a different physical character from the original. If the system contains static elements, for example, transmission lines, they are represented in the same way as in the preceding method, i.e. to these physical modelling is applied. An advantage of this method is the greater convenience of varying the individual parameters of the rotating machines, because it amounts only to a variation of comparatively easily adjustable parameters of the electronic circuits or the physical analogs. On the other hand, since the static elements of circuits consist of assemblies of coils and capacitors, no differential equations have to be set up for them. This is a great advantage of the first section of the method of mathematical modelling over the second section.

The second section of the method of mathematical modelling, consisting of the use of computing mechanisms (integrators) for the investigation of the transient electromechanical processes in the electric circuits, is nowadays widely used. Its importance is still increasing with the growing production of relatively inexpensive computor types suitable for the integration of systems of non-linear differential equations of an over-all order up to 20 – 30.

This method makes it particularly easy to vary the system of parameters within a wide range by an easy regulation of the blocks collecting the coefficients of the individual equations.

This method is suitable not only for the solution of electrical engineering problems, but also for the solution of systems of non-linear differential equations met in physics, mechanics, hydrodynamics, heat engineering, etc. In this sense it is a universal method.

A disadvantage of this method is the necessity of using a whole number of blocks of the integrator for considering the differential equations of the static circuit elements and, in particular, of long lines, since often the greater half of the overall order of the system of differential equations of the circuit is accounted for by the static circuit elements.

However, the integrators may be designed in such a way as to enable the differential equations of only one part of the whole circuit to be represented, whereas the remaining part is actually present in life-size or represented by physical models. The latter condition considerably extends the range of possible users of integrators of this type for investigations of the transient processes in interconnected systems.

Method of setting-up system of differential equations

In order to use the integrator, the system of differential equations of the circuit has to be set up, first of all, in the simplest and the most rational form.

We will then consider the differential equations of the synchronised generator, referred to all coordinate systems rigidly connected with its rotor, the equations of an induction motor and of all the static circuit elements (loads, transformers, transverse capacitances, compensating coils and lines with longitudinal compensating capacitances) referred to coordinated system rotating at an arbitrary speed, as given.

All the equations given below refer to the positive directions of the currents shown in figures.

When setting up the differential equations for any actual system it is, above all, important to choose the most rational system of rotating coordinates to which then the equations of all static circuit elements have to be referred. For symmetrical circuits the equations of the static elements may be referred to axes rigidly connected to the rotor of any of the generators [9], which follows from the symmetry of the circuit.

We will illustrate the method of setting up the system of equations on the example of the circuit of Fig. 1, being practically symmetrical.

We will refer to equations of all elements of the circuit of Fig. 1 (except *SG*2) and the equations resulting from Kirchhoff's first law, to coordinate axes rigidly connected to the rotor of the synchronous generator *SG*1.

The equations for *SG*1 are [10 and 11]:

$$\left.\begin{aligned}
u_{1d} &= -r_{C1}i_{1d} + \frac{d}{dt}(-L_{d1}i_{1d} + M_{f1}i_{1f} + M_{g1}i_{1g}) - \\
&\quad -(-L_{q1}i_{1q} + M_{h1}i_{1h})\frac{d\theta_1}{dt}; \\
u_{1q} &= -r_{C1}i_{1q} + \frac{d}{dt}(-L_{q1}i_{1q} + M_{h1}i_{1h}) + \\
&\quad +(-L_{d1}i_{1d} + M_{f1}i_{1f} + M_{g1}i_{1g})\frac{d\theta_1}{dt}; \\
u_{10} &= -r_{C1}i_{10} - L_{01}\frac{di_{10}}{dt}; \\
u_{1f} &= r_{f1}i_{1f} + \\
&\quad + \frac{d}{dt}\left(-\frac{3}{2}M_{f1}i_{1d} + L_{f1}i_{1f} + M_{fg1}i_{1g}\right); \\
0 &= r_{g1}i_{1g} + \\
&\quad + \frac{d}{dt}\left(-\frac{3}{2}M_{f1}i_{1d} + L_{g1}i_{1g} + M_{fg1}i_{1f}\right); \\
0 &= r_{h1}i_{1h} + \frac{d}{dt}\left(-\frac{3}{2}M_{h1}i_{1q} + L_{h1}i_{1h}\right);
\end{aligned}\right\} \quad (1)$$

$$T_{\partial 1} - \frac{3}{2}\left[(L_{d1} - L_{q1})\, i_{1d}\, i_{1q} - M_{f1}\, i_{1f}\, i_{1g} - \right.$$

$$\left. - M_{g1}\, i_{1g}\, i_{1q} + M_{h1}\, i_{1h}\, i_{1d}\right] = J_1 \frac{d^2\theta_1}{dt^2}\,.$$

In an analogous way, by altering subscript 1 to subscript 2, we write the equations for *SG2*, since we refer to its equations to axes rigidly connected to its rotor.

The equations for *IM1* [10 and 12] are:

$$U_{1d} = r_{\partial 1}\, i_{\partial 1d} + L_{C11}\frac{di_{\partial 1d}}{dt} + L_{ad1}\frac{di_{1pd}}{dt} -$$

$$-(L_{C11}\, i_{\partial 1q} + L_{ad1}\, i_{1pq})\frac{d\theta_1}{dt}\,;$$

$$U_{1q} = r_{\partial 1}\, i_{\partial 1q} + L_{C11}\frac{di_{\partial 1q}}{dt} + L_{ad1}\frac{di_{1pq}}{dt} +$$

$$+(L_{C11}\, i_{\partial 1d} + L_{ad1}\, i_{1pd})\frac{d\theta_1}{dt}\,;$$

$$U_{10} = r_{\partial 1}\, i_{\partial 10} + L_{C01}\frac{di_{\partial 10}}{dt}\,; \qquad (2)$$

$$0 = r_{p1}\, i_{1pd} + L_{p11}\frac{di_{1pd}}{dt} + L_{ad1}\frac{di_{\partial 1d}}{dt} -$$

$$-(L_{ad1}\, i_{\partial 1q} + L_{p11}\, i_{1pq})\left(\frac{d\theta_1}{dt} - \omega_{\partial 1}\right);$$

$$0 = r_{q1}\, i_{1pq} + L_{p11}\frac{di_{1pq}}{dt} + L_{ad1}\frac{di_{\partial 1q}}{dt} +$$

$$+(L_{ad1}\, i_{\partial 1d} + L_{p11}\, i_{1pd})\left(\frac{d\theta_1}{dt} - \omega_{\partial 1}\right);$$

$$0 = r_{p1}\, i_{1p0} + L_{p01}\frac{di_{1p0}}{dt}\,;$$

$$\frac{3}{2}L_{ad1}\,(i_{1pd}\, i_{\partial 1q} - i_{1pq}\, i_{\partial 1d}) - T_{C1} = J_{\partial 1}\frac{d\omega_{\partial 1}}{dt}\,.$$

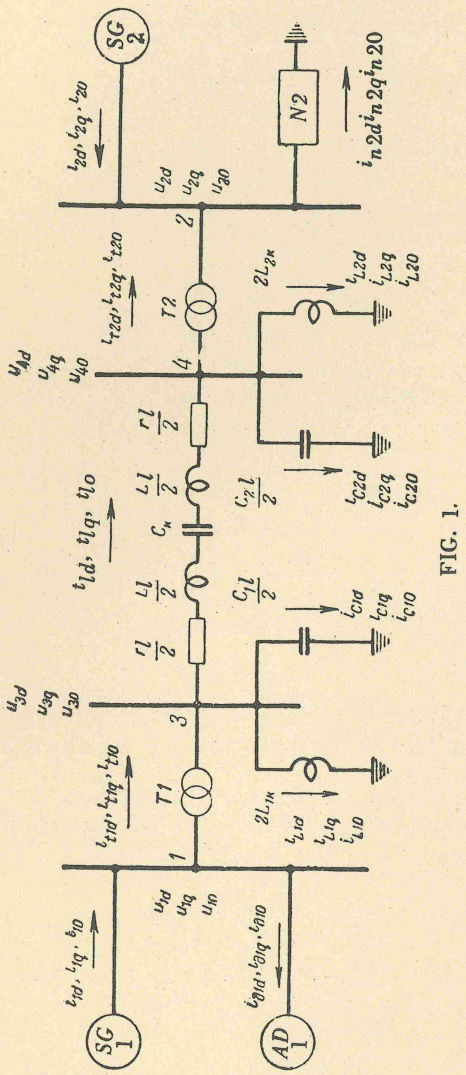

FIG. 1.

The equations following from Kirchhoff's first law [*cf.* (1)] are as follows:

$$\begin{aligned} i_{1d} - i_{\partial 1d} - i_{t1d} &= 0 ; \\ i_{1q} - i_{\partial 1q} - i_{t1q} &= 0 ; \\ i_{10} - i_{\partial 10} - i_{t10} &= 0 . \end{aligned} \tag{3}$$

The equations for static load [9 and 10] are :

$$\begin{aligned} & U_{2d} \cos(\theta_2 - \theta_1) - U_{2q} \sin(\theta_2 - \theta_1) - \\ & - r_{n2}\, i_{n2d} - L_{n2} \frac{di_{n2d}}{dt} + L_{n21}\, i_{n2q} \frac{d\theta_1}{dt} = 0 ; \\ & U_{2d} \sin(\theta_2 - \theta_1) + U_{2q} \cos(\theta_2 - \theta_1) - \\ & - r_{n2}\, i_{n2q} - L_{n21} \frac{di_{n2q}}{dt} - L_{n21}\, i_{n2d} \frac{d\theta_1}{dt} = 0 ; \\ & U_{20} - r_{n2}\, i_{n20} - L_{n20} \frac{di_{n20}}{dt} = 0. \end{aligned} \tag{4}$$

The occurrence of the factor $\cos(\theta_2 - \theta_1)$ and $\sin(\theta_2 - \theta_1)$ is due to the fact that the terminal voltage of *SG*2 is referred to axes rigidly connected to its rotor.

The equations expressing Kirchhoff's first law [9], considering the positive directions of the currents as assumed in Fig. 1 will be:

$$\begin{aligned} & i_{t2d} + i_{2d} \cos(\theta_2 - \theta_1) - i_{2q} \sin(\theta_2 - \theta_1) - \\ & - i_{n2d} = 0 ; \\ & i_{t2q} + i_{2d} \sin(\theta_2 - \theta_1) + i_{2q} \cos(\theta_2 - \theta_1) - \\ & - i_{n2q} = 0 ; \\ & t_{t20} + i_{20} - i_{n20} = 0 . \end{aligned} \tag{5}$$

It should be noted that if the equations of the static load N2 are referred to axes rigidly connected to the rotor of $SG2$, equations (5) will become complicated to the extent equations (4) will be simplified.

Indeed, if we refer the equations of the static load N2 to axes rigidly connected to the axes of the rotor $SG2$ we get [9 and 10] :

$$U_{2d} - r_{n2}\, i_{n2d} - L_{n21}\frac{di_{n2d}}{dt} + L_{n21}\, i_{n2q}\frac{d\theta_2}{dt} = 0;$$

$$U_{2q} - r_{n2}\, i_{n2q} - L_{n21}\frac{di_{n2q}}{dt} - L_{n21}\, i_{n2d}\frac{d\theta_2}{dt} = 0; \tag{4a}$$

$$U_{20} - r_{n2}\, i_{n20} - L_{n20}\frac{di_{n20}}{dt} = 0.$$

Under the same conditions the equations of Kirchhoff's first law [*cf.* (2)] are written as follows :

$$i_{t2d} + i_{2d}\cos(\theta_2 - \theta_1) - i_{2q}\sin(\theta_2 - \theta_1) - i_{n2d}\cos(\theta_2 - \theta_1) + i_{n2q}\sin(\theta_2 - \theta_1) = 0;$$

$$i_{t2q} + i_{2d}\sin(\theta_2 - \theta_1) + i_{2q}\cos(\theta_2 - \theta_1) - i_{n2d}\sin(\theta_2 - \theta_1) - i_{n2q}\cos(\theta_2 - \theta_1) = 0; \tag{5a}$$

$$i_{t20} + i_{20} - i_{n20} = 0.$$

We will further consider in the equivalent circuit of the transformer $T1$ the branch of the no-load current (Fig. 2). For the branches 1 – 7 of the primary winding we get [9 and 10] :

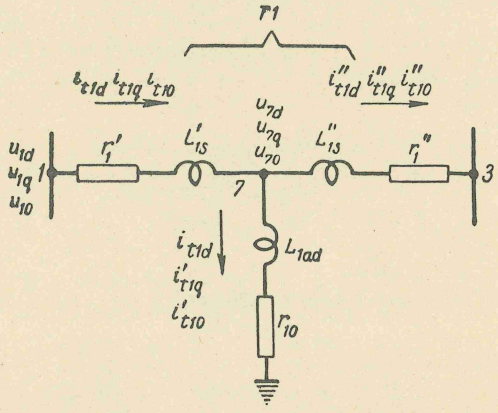

FIG. 2.

$$U_{7d} = U_{1d} - r'_1 i_{t1d} - L'_{1s1} \frac{di_{t1d}}{dt} +$$

$$+ L'_{1s1} i_{t1q} \frac{d\theta_1}{dt};$$

$$U_{7q} = U_{1q} - r'_1 i_{t1q} - L'_{1s1} \frac{di_{t1q}}{dt} - \tag{6}$$

$$- L'_{1s1} i_{t1d} \frac{d\theta_1}{dt};$$

$$U_{70} = U_{10} - r'_1 i_{t10} - L'_{1s0} \frac{di_{t10}}{dt}.$$

Similarly, we get for the branches 7 – 3 of the secondary winding:

$$U_{3d} = U_{7d} - r''_1 i''_{t1d} - L''_{1s1} \frac{di''_{t1d}}{dt} +$$

$$+ L''_{1s1} i''_{t1q} \frac{d\theta_1}{dt}; \tag{7}$$

$$U_{3q} = U_{7q} - r''_1 i''_{t1q} - L''_{1s1} \frac{di''_{t1q}}{dt} -$$

$$- L''_{1s1} i''_{t1d} \frac{d\theta_1}{dt} ; \qquad (7)$$

$$U_{30} = U_{70} - r''_1 i''_{t10} - L''_{1s0} \frac{di''_{t10}}{dt} .$$

For the no-load branch we get :

$$0 = U_{7d} - r_{10} i'_{t1d} - L_{1ad1} \frac{di'_{t1d}}{dt} +$$

$$+ L_{1ad1} i'_{t1q} \frac{d\theta_1}{dt} ;$$

$$0 = U_{7q} - r_{10} i'_{t1q} - L_{1ad1} \frac{di'_{t1q}}{dt} - \qquad (8)$$

$$- L_{1ad1} i'_{t1d} \frac{d\theta_1}{dt} ;$$

$$0 = U_{70} - r_{10} i'_{t10} - L_{1ad0} \frac{di'_{t10}}{dt} .$$

Equations of Kirchhoff's first law [*cf*(7)] are :

$$i_{t1d} - i'_{t1d} - i''_{t1d} = 0 ;$$

$$i_{tq} - i'_{tq} - i''_{tq} = 0 ; \qquad (9)$$

$$i_{t10} - i'_{t10} - i''_{t10} = 0 ;$$

The equations for the compensating coil $2L_{1k}$:

$$0 = U_{3d} - 2r_{1k} i_{L1d} - 2L_{1k1} \frac{di_{L1d}}{dt}$$

$$+ 2L_{1k1} i_{L1q} \frac{d\theta_1}{dt} ; \qquad (10)$$

$$O = U_{2q} - 2r_{1k} i_{L1q} - 2L_{1k1} \frac{di_{L1q}}{dt} -$$

$$- 2L_{1k1} i_{L1d} \frac{d\theta_1}{dt} ; \qquad (10)$$

$$O = U_{30} - 2r_{1k} i_{L10} - 2L_{1k0} \frac{di_{L10}}{dt} .$$

We consider above the branches of the primary and the secondary windings of transformer $T1$, its no-load branch and the branch of the compensating coil as rL-circuits. If the mutual inductance between the phases of these branches may be neglected, the expressions of the parameters after simplying [10] for example, for the compensating coil $2L_{1k}$ we get :

$$L_{1k} = L_{1k1} = L_{1k0}. \qquad (11)$$

The equations for the capacitance $C_{1l}/2$ may be obtained from the identities (3, 5) . . . . (3, 7), given in [10] if we substitute in them

$$C_3 = C1l/2,\ i_{C3d} = i_{C1d},\ i_{C3q} = i_{C1q}, i_{C30} = i_{C10}$$

and $\theta_3 = \theta_1$ since at 3 (Fig. 1) the synchronous generator is not connected, and the voltage u_3 is directly referred to axes rigidly connected with the rotor of $SG1$, viz :

$$U_{3d} = \frac{2}{C_{1l}} \int i_{C1d}\, dt + \int U_{3q} \frac{d\theta_1}{dt}\, dt ;$$

$$U_{3q} = \frac{2}{C_{1l}} \int i_{C1q}\, dt - \int U_{3d} \frac{d\theta_1}{dt}\, dt ; \qquad (12)$$

$$U_{30} = \frac{2}{C_{1l}} \int i_{C10}\, dt.$$

The equations of Kirchhoff's first law [*cf* (3)] are as

$$i''_{t1d} - i_{L1d} - i_{C1d} - i_{ld} = O ;$$

$$i''_{t1q} - i_{L1q} - i_{C1q} - i_{ld} = O ; \qquad (13)$$

$$i''_{t10} - i_{l10} - i_{C10} - i_{lo} = 0. \tag{13}$$

We may get the equations for the line (r_l, L_l) with the compensating capacitance C_{com} connected to it, for example, from the identities (7) and (12), viz:

$$\begin{aligned} U_{4d} &= U_{3d} - r_l i_{ld} - L_{ld} \frac{di_{ld}}{dt} + \\ &+ L_{l1} i_{lq} \frac{d\theta_1}{dt} - \frac{1}{C_k} \int i_{ld}\, dt + \\ &+ \int (U_{4q} - U_{3q} + r_l i_{lq} + L_{l1} \frac{di_{lq}}{dt} + \\ &+ L_{l1} i_{ld} \frac{d\theta_1}{dt}) \frac{d\theta_1}{dt}\, dt; \end{aligned} \tag{14}$$

$$\begin{aligned} U_{4q} &= U_{3q} - r_l i_{lq} - L_{l1} \frac{di_{lq}}{dt} - \\ &- L_{l1} i_{ld} \frac{d\theta_1}{dt} - \frac{1}{C_k} i_{lq}\, dt - \\ &- \int (U_{4d} - U_{3d} + r_l i_{ld} + L_{l1} \frac{di_{ld}}{dt} - \\ &- L_{l1} i_{lq} \frac{d\theta_1}{dt}) \frac{d\theta_1}{dt}\, dt; \end{aligned} \tag{15}$$

$$U_{40} = U_{30} - r_l i_{l0} - L_{l0} \frac{di_{l0}}{dt} - \frac{1}{C_k} \int i_{l0}\, dt. \tag{16}$$

The equations for the capacitance $C_{2l}/2$ of the line will be analogous to (12), viz :

$$U_{4d} = \frac{2}{C_{2l}} \int i_{C2d}\, dt + \int U_{4q} \frac{d\theta_1}{dt}\, dt; \tag{17}$$

$$U_{4q} = \frac{2}{C_{2l}} \int i_{C2q}\, dt - \int U_{4d} \frac{d\theta_1}{dt}\, dt$$

$$U_{40} = \frac{2}{C_{2l}} \int i_{C20}\, dt. \tag{17}$$

The equations for the compensating coil $2L_{2\,com}$ will be analogous to (10) viz :

$$0 = U_{4d} - 2r_{2k}\, i_{L2d} - 2L_{2k1} \frac{di_{L2d}}{dt} + 2L_{2k1}\, i_{L2q} \frac{d\theta_1}{dt};$$

$$0 = U_{4q} - 2r_{2k}\, i_{L2q} - 2L_{2k1} \frac{di_{L2q}}{dt} - 2L_{2k1}\, i_{L2d} \frac{d\theta_1}{dt}; \tag{18}$$

$$0 = U_{40} - 2r_{2k}\, i_{L20} - 2L_{2k0} \frac{di_{L20}}{dt}.$$

The equations of Kirchhoff's first law [*cf* (4)] are

$$i_{ld} - i_{C2d} - i_{L2d} - i_{t2d} = 0;$$

$$i_{1lq} - i_{C2q} - i_{L2q} - i_{lq} = 0; \tag{19}$$

$$i_{l0} - i_{C20} - i_{l20} - i_{t20} = 0.$$

Since the way of considering the no-load current in the equivalent circuit is shown for transformer $T1$, we will write down the equations for transformer $T2$ without considering this factor. These equations may be obtained from the identities (1, 17) . . . . (1, 19) adduced in [10], if we consider that the voltage [*cf* (4)] is referred directly to coordinate axes rigidly connected with the rotor of $SG1$; we have therefore to assume $\theta_3 = \theta_1$. Also having brought the symbols in Fig. 1, 1 of [10] and Fig. 1 of the present paper into agreement, we get

$$U_{3d} = U_{4d};\ U_{3q} = U_{4q};\ U_{30} = U_{40}; \tag{20}$$

$$r_{l2} = r_{t2}\ ;\ L_{l2p} = L_{t21}\ ;\ L_{l20} = L_{t20}\ ;$$
$$i_{l2d} = i_{t2d}\ ;\ i_{l2q} = i_{t2q}\ ;\ i_{l20} = i_{t20}\ . \tag{20}$$

We then get the branch of transformer $T2$

$$U_{2d}\cos(\theta_1 - \theta_2) + U_{2q}\sin(\theta_1 - \theta_2) =$$
$$= U_{4d} - r_{t2}\, i_{t2d} - L_{t21}\frac{di_{t2d}}{dt} + L_{t21}\, i_{t2q}\frac{d\theta_1}{dt}\ ;$$
$$-U_{2d}\sin(\theta_1 - \theta_2) + U_{2q}\cos(\theta_1 - \theta_2) = \tag{21}$$
$$= U_{4q} - r_{t2}\, i_{t2q} - L_{t21}\frac{di_{t2q}}{dt} - L_{t21}\, i_{t2d}\frac{d\theta_1}{dt}\ ;$$
$$U_{20} = U_{40} - r_{t2}\, i_{t20} - L_{t20}\frac{di_{t20}}{dt}\ .$$

Since the equations of the individual circuit elements may be assumed to be known, the whole system of equations can be put together from the individual equations referring to its blocks, which we can immediately write down for each of the circuit elements.

Should it be necessary to consider in any of the synchronous generators or compensating coils the dependence of the inductance on the state of saturation of the steel, this circuit element should be separated and its differential equations be re-written in the proper form, based on the character of the magnetisation curve.

It should be noted that the equations for all the zero-sequence components form a separate system, to be solved independently of the other equations. Their number is 18 in the case of the circuit of Fig. 1.

Determination of the total order of system of non-linear differential equations from structure of circuit

On the above considerations it is possible to determine from the structure of the scheme, without writing down the actual differential equations, the total order to the latter. In doing this we have to bear in mind the following circumstances:

1. For a synchronous machine (generator, synchronous condenser or motor) with in-phase or quadrature damper windings the total order of the equations is

7*, if the circuit contains apart from this at least one more synchronous machine, i.e. a machine of magnetic or electric asymmetry (equations of system (1), except the third).

The order of the equation of motion of the rotor of each of the synchronous machines is 2.

If the circuit contains only one synchronous machine, the total order of the equations for it will be six, because in this case the differential equation of the motion of the rotor will be of the first order and the angle θ will not occur in one of them (by change of the variables $d^2\theta/dt^2 = d\omega/dt$ and $d\theta/dt = \omega$ the order is reduced by one).

2. Neglecting each of the damper windings of the synchronous machine reduces the total order of its defferential equations by one.

3. The total order of the differential equations of an induction machine is 5. This means that each induction machine connected to the system increases the total order of the system of differential equations by 5.

4. The equations of Kirchhoff's first law for the branching points are not differential equations and therefore, do not increase the total order of the equations of the system.

5. The stator circuits of the machines (stationary circuits) must be divided into the simplest independent circuits and their differential equations have to be set up for the in-phase as well as for the quadrature components. This doubles the order of the differential equations for each individual circuit.

6. If a line, system or static load are represented by a coil with resistance and inductance, its series-connexion with the stator of any of the machines does not increase the total order of the differential equations of the system.

7. If the circuit comprises a transformer whose no-load current is not considered, it is represented by a coil. If, however, the no-load current is considered, the equivalent circuit contains a no-load branch (additional circuit), which, together with the necessity of considering the equations of the in-phase and quadrature components, increases the total order of the differential equations of the circuit by 2.

8. If there are no synchronous machines in the circuit (e.g. if one or several induction motors for static loads, etc., are supplied from busbars of infinite power), it is not necessary to set up the equations separately for in-phase and quadrature components. If the complex instantaneous values of currents and voltages are introduced, a static load or transmission line (each of them separately) will be represented by first-order differential equations, and an induction

* This does not take into account the differential equations for the zero-sequence components.

motor by a third-order differential equation. In this case, the connexion of any further induction machine to the circuit increases the total order of the system of differential equations by 3.

Let us determine the total order of the system of differential equations for the circuit of Fig. 3.

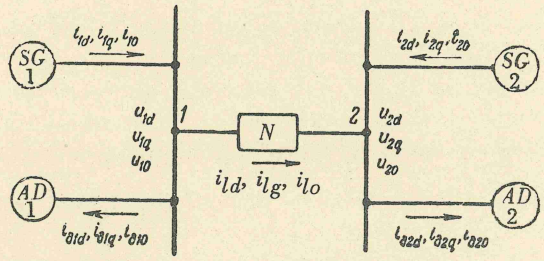

FIG. 3.

In Fig. 3. the stationary part of the circuit is resolved into three circuits, viz:

(a) The stator $SG1$ – stator $IM1$;

(b) Stator $IM1$ – line – stator $IM2$;

(c) Stator $SG2$ – stator $IM2$; for each of which, if the in-phase and quadrature components have to be considered, the differential equation is of the second order, this resulting in the total order of six. Each of the synchronous machines makes a total order of the order of the remaining equations 5, and each of the induction machines involves a total order 3. The total order of the differential equations for the whole circuit will therefore be 22.

In Fig. 1, if the no-load currents of the transformers $T1$ and $T2$ have to be considered, the stationary part of the circuit is resolved into 9 simpler circuits, for example, as follows.

(a) Stator $SG1$ – stator $IM1$ (if it is necessary to consider in-phase and quadrature components, the order of the equations will be 2);

(b) Stator $IM1$ - no - load branch of the equivalent circuit of transformer $T1$ (Fig. 2) (order of the equations-2);

(c) No-load branch of equivalent circuit of transformer $T1$-compensating coil $2L_{1\ com}$ (order of the equations-2);

(d) Compensating coil $2L_{1\ com}$-capacitance of the line $C_{1l}/2$;

(e) Capacitance of the line $C_{1l}/2$ - line - capacitance of the line $C_{2l}/2$ (order of the equations-4).

(f) Capacitance of the line $C_{2l}/2$-compensating coil $2L_{2\ com}$ (order of the equations-4);

(g) Compensating coil $2L_{2\ com}$-no-load branch of equivalent circuit of transformer $T2$ (order of equations-2);

(h) No-load branch of equivalent circuit of transformer $T2$-static load $SL2$ (order of equations-2);

(i) Stator $SG2$-static load $SL2$ (order of equations-2); this adding up to a total order 24. From this figure the fraction concerning transformers $T1$ and $T2$, lines and loads $SL2$, i.e. the static circuit elements amounts to a total order 18. For the two synchronous generators the total order of the determining equations is 10; for the induction motor, 3.

We see, therefore, that the total order of the differential equations for the whole system will be 37.

If the line is not represented by one member but by several T – or π-type members, the fraction of the line elements (series, connected inductances and shunt-capacitances) in the total order of the system of the differential equations of the circuit will increase still further. This fact is very important in the choice of the method for solving the resulting system of differential equations.

If the in-phase and quadrature damper windings of both synchronous generators are not considered, the total order of the equations will be reduced by 4, i.e. to 33. If, furthermore, we neglect the no-load branches in the equivalent circuits of the 2 transformers, the total order of the equations is again reduced by 4, i.e. to 29. If the two compensating coils $2L_{1\ com}$ and $2L_{2\ com}$ are also neglected, the total order of the equation is again reduced by 4, i.e. to 25.

It is worth noting that in the last case again both synchronous and one induction machine together result in a decrease of the total order of differential equations by 13; the remainder, 12, refers as before to the transmission line.

REFERENCES

1. V.A. Venikov; *The adoption of the theory of similarity and physical modelling in electric technology* Gosenergoizdat (1949).
2. V.A. Venikov and A.V. Ivanov-Smolenskii; A synchronous generator for the dynamic modelling of electrical systems. *Elektrichestvo*, No. 8 (1951).
3. V.A. Venikov *et al.; A brief description of dynamic models for electrical systems*, Moscow Power Institute (1955).
4. M.P. Kostenko and E.D. Treivish; Modelling of electrical machinery and transformers in experimental research on the stability of parallel work in power stations. *Transactions of the Leningrad Power Institute* No. 1 (1946).
5. M.P. Kostenko; Electrodynamic model for the study of stability. *Elektrichestvo* No.9 (1951).
6. M.P. Kostenko; The modelling of electrical machinery equipment in the study of stability of parallel work on power systems, linked with long-distance transmission lines *Isz. Akad. Nauk SSSR, Otd. tekh. nauk* No. 12 (1953).

7. V.L. Lossievskii; *The use of the similarity theory and dynamic analogies in problems connected with the modelling of objectives and regulation processes*, Gosenergoizdat (1951).
8. V.A. Trapeznikov; Mathematical modelling of dynamic systems *Elektrichestvo* No. 8 (1955).
9. S.V. Strakhov ; Selection of the co-ordinating systems for calculation of transition processes in chains with synchronous machine *Elektrichestvo* No.6 (1954).
10. S.V. Strakhov; The equating of transition processes in static and rotating elements in electrical chains. *Report on scientific research work. Moscow Power Institute* (1956).
11. R.E. Vowels; Transient Analysis of Synchronous Machines. *Proc. Inst. El. Eng.*, vol. 99 part IV, No. 3 (1952).
12. A.A. Yanko-Trinitskii; The equating of transition electromagnetic processes of an asynchronous motor and their solution. *Elektrichestvo* No. 3 (1951).

THE INDUCTION LAW FOR AN ELECTROSTATIC MACHINE*

A.A. BAL'CHITIS

(Received 19 December 1956)

Introduction

The fundamental equations of the classical theory of electrodynamics, the first and second equations of Maxwell point to two possible methods of conversion of mechanical into electrical energy. For example, by the first equation of Maxwell†

$$\operatorname{curl} \bar{H} = \gamma \bar{E} + \frac{\partial \bar{D}}{\partial t} \tag{1}$$

such a conversion is possible when an electric field changes with time, i.e. by mechanical action on the electric field it is possible to obtain the magnetic field connected with it in space.

According to the second equation

$$\operatorname{curl} \bar{E} = -\frac{\partial \bar{B}}{\partial t} \tag{2}$$

it is possible to obtain an electric field by changing the magnetic field associated with it.

The second equation of Maxwell was the generalized form of Faraday's experimental law of electromagnetic induction, viz.

$$E = B\, l\, v, \tag{3}$$

which was discovered in 1831 and forms the basis of the design of a large variety of electric machines, covered by the general term "electromagnetic machines".

Machines working on the principle of a mechanical change of an electric field (Maxwell's first equation) are not nearly so widely used; they are known as *electrostatic* machines. These machines are used for obtaining high and very high voltages for research purposes.

For a long time electrostatic machines did not find practical uses. The suc-

* *Elektrichestvo* No.7, 11 – 14, 1957 [Reprint Order No.EL33].

† All equations are given in terms of the absolute practical rationalized system of units.

THE NOMOGRAM FOR DETERMINING PROTECTIVE ZONES OF LIGHTNING CONDUCTORS*

L.M. LOPSHITS

(Received 24 April 1956)

This nomogram supersedes an earlier one (*Elektrichestvo*, No. 10, 1947) and is deemed necessary because of the distinction made in the latest instruction book on overvoltage protection of electrical installations for 3 - 220 kV (Gosenergoizdat, 1954) between the formulae for lightning conductors up to and above 30 m.

The nomogram is constructed for single and double lightning conductors up to 150 m using an emphirical formula based on laboratory test results and on the assumption that orientation of the lightning stroke onto the lightning conductor takes place at the height of H = 600 m (for an open country).

The use of the nomogram is explained with three examples.

That part of the latest Code of Practice on protection against overvoltages [1] which deals with protection against direct lightning strokes is based on laboratory investigations carried out at the V.I. Lenin All Union Electro-technical Institute, and differs from the earlier edition of the Code [3] in that in it a distinction has been introduced between the formulae for rod lightning conductors up to 30 m high and above 30 m high. Thus, the earlier nomogram for determining protective zones, constructed for lightning conductors up to 60 m has become obsolete and now may be used only for lightning conductors up to 30 m.

Figs. 1 and 2 give curves constructed from the data included in [2] which describe protective zones of single and double lightning conductors respectively. The geometrical sense of the parameters of the protective zone a, h, ha, h_x, b_x, and r_x is clear from Fig. 4; by H is denoted the height at which orientation of the lightning channel onto the lightning conductor takes place for open country.

For taller lightning conductors, $h > 30$ m, H was taken as 600 m, and for shorter lightning conductors, $h < 30$ m, the constant ratio of $H/h = 600/30 = 20$ was taken. It should be mentioned here that the Code of Practice does not set definite limits within which its recommendations are valid but merely states that the value of $H = 600$ m can be used for "very tall lightning conductors".

The curves given in Figs. 1 and 2 can be applied in these cases when the height of the lightning conductor does not exceed 150 m ($H/h = 4$), which corres-

* *Elektrichestvo* No. 7, 76 – 78, 1957 [Reprint Order No. EL 39].

ponds to the greatest height of chimneys built in power stations.

With the above value assumed for the height at which orientation of the lightning channel takes place, the following empirical expressions can be written for the relations represented on Figs. 1 and 2.

$$\frac{r_x}{h_a} = \frac{1.6}{1+\frac{h_x}{h}} \cdot p_1(h); \tag{1}$$

$$\frac{a}{h_a} = 7\sqrt[1.3]{1-\left(\frac{b_x}{r_x}\right)^{1.4}} \cdot p_2(h), \tag{2}$$

where $p_1(h)$ and $p_2(h)$ are coefficients depending on the height of the lightning conductor (Fig. 3).

It should be noted that in order to simplify calculations the following assumption is made in the Code of Practice*; $p_1(h) = p_2(h) = p(h)$,

where $$p(h) = \sqrt{\frac{30}{h}} \quad (\text{for } h \geqslant 30 \text{ m}).$$

The relation $p(h)$ is shown in Fig. 3 by the curve drawn in a broken line.

Eliminating r_x from (1) and (2) one gets the following formula for the double lightning conductor:

$$\left(\frac{b_x}{1.6h_a \cdot p_1(h)}\right)^{1.4} \times \left(1+\frac{h_x}{h}\right)^{1.4} + \left(\frac{a}{7h_a \cdot p_2(h)}\right)^{1.3} - 1 = 0$$

which if $a = 0$, becomes also valid for the single lightning conductor.

The calculation of the lightning conductor height using this formula is lengthy and tedious; the present nomogram (Fig. 4) removes this disadvantage. The following examples explain the use of the nomogram and illustrate its scope.

Example 1. The given object has the shape of a parallelepiped with the base 48×48 m^2 ($b_x = 24$ m) and the height 15 m. It is located between two lightning rods 49 m high in such a way that a line drawn through the centres of the lightning rods coincides with the axis of symmetry of the object. It is required to verify that the object is protected if the distance between the lightning rods is 60 m.

Place one point of a pair of dividers at the point $a = 60$ m on the abscissa (the scale of centres). Bring the other point to $b_x = 24$ m on the ordinate. Keeping the first point unmoved and without altering the distance between the two points place the second point on the curve $h_x = 15$ m.

Through this point of the nomogram the curve $h_a = 32$ m also passes. Thus, the necessary height of the lightning conductor is $h = h_x + h_a = 15 + 32 = 47$ m. Therefore, with $h = 49$ m the object lies within the protective zone of the lightning conductor.

* There are errors in Figs. 4 and 5 of the Code. Instead of $h_x = 0.7h$ and $h_x = 0.9h$ it should be $h_x \approx 0.6h$ and $h_x \approx 0.7h$ respectively.

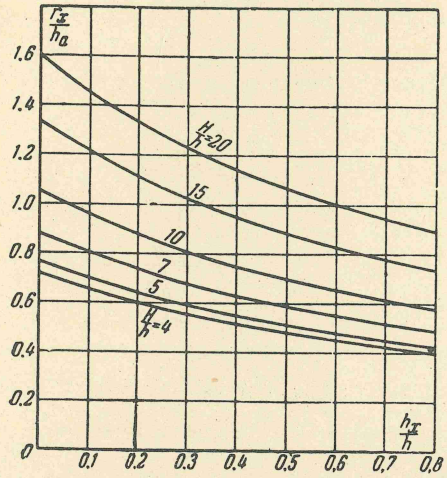

FIG. 1.

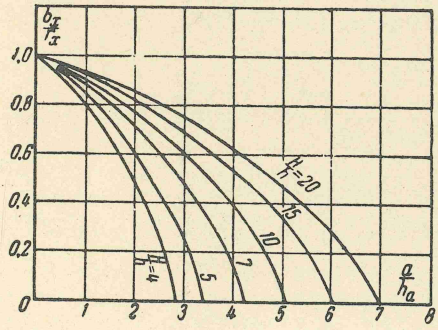

FIG. 2.

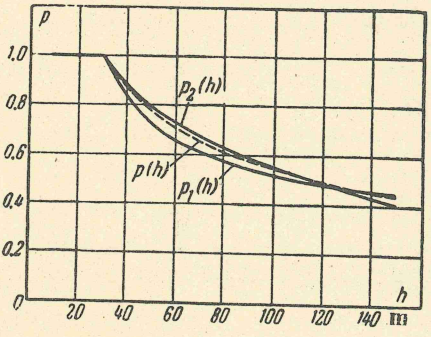

FIG. 3.

The nomogram can also be used in a different way. Set the dividers to the distance between the point $a = 60$ m and the point of intersection of the curves $h_x = 15$ m and $h_a = 49 - 15 = 34$ m. With this distance as radius and with point $a = 60$ m as the centre determine the point at which the ordinate is intersected; this is seen to be at $b_x = 25$ m. It follows then that the given lightning conductor would protect an object for which $b_x = 25$ m.

Example 2. Determine the necessary active height of a single lightning conductor placed in the centre of a structure having a cylindrical form with the diameter 40 m and the height 6 m.

With radius equal to the distance from the origin ($a = 0$) to the point $r_x = b_x = 20$m, determine the point of intersection with the curve $h_x = 6$ m. The curve $h_a = 16$ m which also passes through this point gives the desired value for the active height of the conductor.

Example 3. Find the radius of the protective zone at the level of $h_x = 26$ m for a single lightning conductor 120 m high placed on the chimney of a power station.

With origin as centre and radius equal to the distance from the origin to the point $h_x = 26$ m on the curve for $h = 120$ m, determine the point of intersection with the ordinate; this is found to be $b_x = r_x = 59.5$ m, which is the required value for the radius of protection.

The nomogram has been constructed on the assumption that the distance a between two lightning rods is given, which is normally the case in practice. In these exceptional cases when the distance is to be determined, it may be quickly found using a simple geometrical construction.

From the middle of the line joining the given points b_x (on the ordinate) and h_a

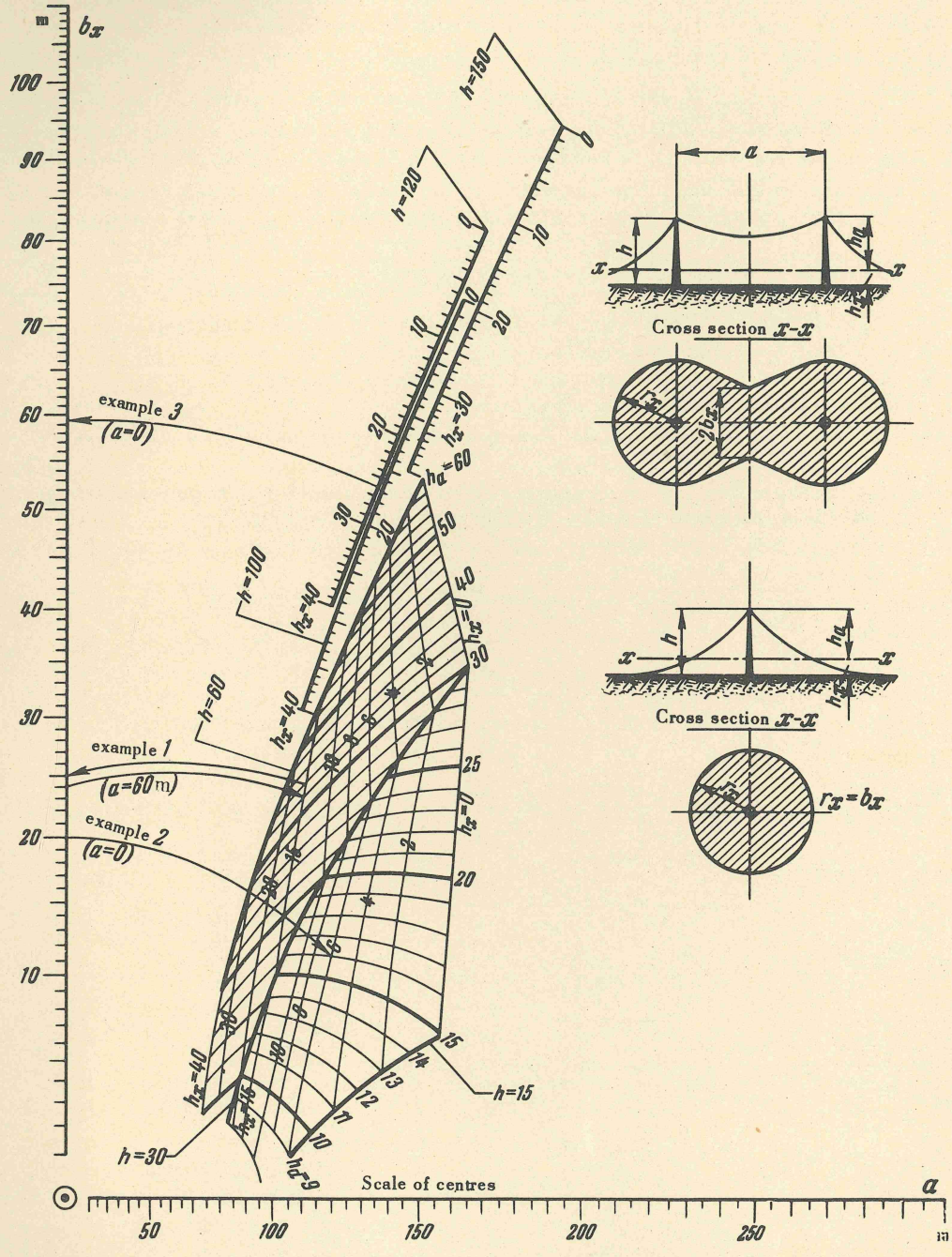

FIG. 4. The nomogram for determining protective zones of rod lightning conductors.

and h_x (the intersection of the corresponding curves) drop the perpendicular on the scale of centres. The point of intersection with this scale gives the required distance between the two lightning rods.

In conclusion it should be mentioned that the Code of Practice considers but in a small degree the critical observations regarding simplification of the contour of the protective zone [5]. In the present edition of the Code it would be desirable to approximate the curvilinear generatrix of the "cone" of the protective zone by a number of straight lines. This should considerably simplify graphical constructions.

REFERENCES

1. *The Code of practice on protection from overvoltages of a.c. electrical installations for* 3 - 220 *kV*. *Gosenergoizdat* (1954).
2. A.A. Akopyan; *Proceedings All-Union Electrotechnical Institute* VOL. 36, *Gosenergoizdat* (1940).
3. *The code of practice on protection from overvoltages of a.c. electrical installations for* 3 - 220 *kV*. *Gosenergoizdat* (1946).
4. L.M. Lopshits; *A Nomogram for determining protective zones of lightning conductors up to* 60 *m high. Elektrichestvo,* No. 10 (1947).
5. I.S. Stekol'nikov *et al; Lightning protection of industrial structures and buildings. Izd. Akad. Nauk SSSR* (1951).

ARCING SHORT-CIRCUITS ON 400 kV TRANSMISSION LINES AND METHODS OF DEALING WITH THEM*

A.S. MAIKOPAR and N.N. BELIAKOV

Central Scientific and Research Electrotechnical Laboratory,
Moscow Electric Station

(Received 19 September 1957)

On 400 kV transmission lines with a solidly earthed neutral, we have to expect mainly single-phase short-circuits to earth. As opposed to the lines with lower voltages, the restoring of the electric strength of the path of the arc after switching off the phase becomes more difficult on 400 kV lines because of appreciable influence of the current at the point of damage caused by capacitive and electromagnetic connections between the disconnected phase and the working phases. The supply current which will flow at the point of the fault, after automatically switching off the faulty section of the line, will sustain the electric arc for a certain time. The next reclosing can be done only after the extinction of the arc and restoration of the electric strength. This circumstance not only defines the placing of protective relays but also exerts an influence on the total lay-out of switchgear on the 400 kV lines. In particular, the problem of connecting shunting reactors directly to the line or through the circuit-breakers is strictly connected with the extinguishing of the sustained current arc. Several works are known dealing with research on the sustained current arcs [1-5]. Nevertheless, they do not give a clear idea of the range of sustained currents, for which it is possible to use single-phase automatic reclosing. As a result of these works, it is assumed that the extinguishing of the sustained current arc is possible for the currents of the order of 12-15 A.

Research into powerful open arcs, carried out by the C.S.R.E.L., has shown that an electric arc is capable of self-extinction even for currents of a few hundred ampres, if the conditions exist for a substantial increase of its length [6]. On this basis the investigations of the sustained current conditions were undertaken. Experiments on a 6 kV model have shown that the extinction of the sustained current arc for gradients of 5-15 kV/m occurs for currents up to 75-100 A, and experiments on a 220 kV grid 750 km long have shown the possibility of

* *Electrichestvo* No.1, 19-25, 1958 [Reprint Order No. EL 43].

extinction of the sustained current arc in the real conditions for currents of 30 A, [7]. Further experiments have been carried out on the 400 kV line from Kuibyshev Hydroelectric Power Station Moscow. The results are given in this article.

The values of the sustained currents and the restoring voltages at the place of flash-over determine to a considerable degree the time of burning of the arc.

In considering various separate cases, used for calculations, it is necessary to bear in mind that in the case of a single-phase automatic reclosing, the phenomenon of the sustained current is conditioned by the presence on the sound phases of the voltage of industrial frequency and of the working current, and, in the case of three-phase reclosing, by the presence of voltages varying in time on the sound phases during their capacitive discharge into the earth.

If a voltage transformer is connected to the 400 kV line, then the discharge of the line into it will have an aperiodic character. For a section of the line 200-500 km long the time constant of the aperiodic discharge is about 0.01 sec. The process of the discharge will be practically finished in 0.05 sec and will not produce any appreciable sustained current phenomenon. Therefore, in future, there is no need to consider this case. If the voltage transformer and the reactor are connected to the line, then the discharge process will be determined by the ratio of the capacitance of the line and the parameters of the reactor, in so far as the resistance of the reactor is smaller than the resistance of the voltage transformer by a few orders of magnitude. In this case, there will be an oscillatory discharge, and the constants of the discharge process will vary according to the length of the disconnected section. These constants are calculated by known formulae. The data, necessary for calculations of the amplitude values of the discharge current, proper frequency and time constant of discharge as a function of the length of the 400 kV line, are given in Table 1.

TABLE 1

Element of the electro-transmission	Values for one phase				
	Resistance of the positive sequence R (Ω)	Inductance of the positive sequence L (H)	Mutual inter-phase inductance M (H)	Phase capacitance with respect to earth C_0 (μF)	Interphase capacitance C_1 (μF)
Line (for 1 km)	0.2	0.93×10^{-3}	0.86×10^{-3}	8.6×10^{-3}	1.28×10^{-3}
Shunting reactor	5.3	3.4	–	–	–

As can be seen from the graphs on Fig.1, the values of the parameters characterizing the discharge of the line in relation to the length of the section vary rather

considerably. Nevertheless, the current of discharge and its proper frequency are of the same order as the working current of the 400 kV line and its working frequency.

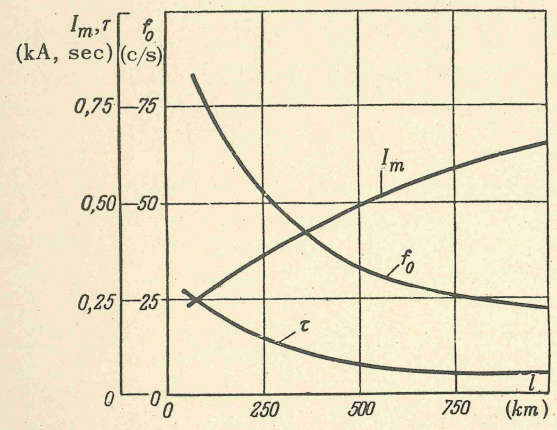

FIG.1. The values of the amplitudes of the discharge current I_m, time constant of the discharge τ and the proper frequency f_0 at the discharge of the line through the shunting reactor as a function of the length of the disconnected section.

The time constant of the discharge τ is equal to a fraction of a second; therefore we have to reckon with the fact that the voltage on the sound phases of the line and the discharge current will maintain sustained current conditions at the faulty place through the disconnected phase for 1 sec or more.

Thus, calculation of the sustained currents and of the recovery voltages should be done for two cases: switching off one phase and switching off all three phases in the presence of a reactor. The general formulae for these quantities are deducted on the basis of the simplified circuit of the line element with distributed constants, as shown in Fig.2. In this diagram, two sound phases are replaced by an equivalent single phase, the voltage along it being assumed constant. This assumption enables us to exclude consideration of the inductance and the resistance of the equivalent phase. The mutual inductance between the sound phases and the disconnected phase of the section is accounted for by the introduction into the faulty phase of the c.m.f. of the mutual inductance.

The differential equation of the line element has the following form:

$$\left.\begin{aligned} -\frac{\partial \dot{U}}{\partial l} &= j\omega L\dot{I} + j\omega M\dot{I}_A; \\ -\frac{\partial \dot{I}}{\partial l} &= j\omega C_0\dot{U} + (\dot{U} - \dot{U}_A)j\omega C, \end{aligned}\right\} \qquad (1)$$

where $\dot{U}_A = 0.5\ \dot{U}_f$; $\dot{I}_A = I_f$; $C = 2C_1$;

$\dot{U}_A$ and $\dot{I}_A$ are the voltage and current in the phase equivalent to the two sound phases;

$\dot{U}_f$ and $\dot{I}_f$ are the voltages and currents in the sound phases; and

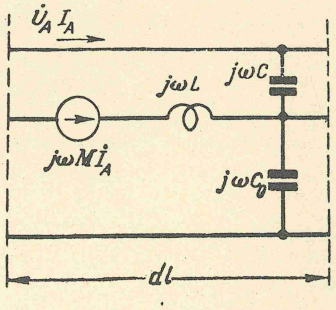

FIG.2. The diagram of the element of the line with distributed parameters for the calculated example.

$\dot{U}$ and $\dot{I}$ are the voltage and current in the disconnected phase.

Solving simultaneously the equations (1) for the section of the line of length l, we have:

$$\dot{U}_2 = \dot{U}_1 \operatorname{ch}\gamma l - \dot{I}_1 Z_c \operatorname{sh}\gamma l + \dot{U}_A \frac{a}{\gamma^2}(1 - \operatorname{ch}\gamma l) - \dot{I}_A \frac{j\omega M}{\gamma}\operatorname{sh}\gamma l;$$
$$\dot{I}_2 = -\frac{\dot{U}_1}{Z_c}\operatorname{sh}\gamma l + \dot{I}_1 \operatorname{ch}\gamma l + \dot{U}_A \frac{a}{Z_c\gamma^2}\operatorname{sh} l - \dot{I}_A \frac{j\omega M}{Z_c\gamma}(1 - \operatorname{ch}\gamma l), \qquad (2)$$

where $a = -\omega^2 LC$; $\gamma = j\omega\sqrt{L(C_0 + C)}$; $Z_c = \frac{j\omega L}{\gamma}$;

$\dot{U}_1$ and $\dot{I}_1$ refer to the beginning of the section; and $\dot{U}_2$ and $\dot{I}_2$ refer to the end of the section.

Let us divide the section of the line in question into two parts: X and l-X. Let us establish for each of them the boundary conditions:

For the beginning of the part X: $\dot{U} = \dot{U}_1$; $\dot{I} = 0$; for the end of the part X: $\dot{U} = \dot{U}_X$; $\dot{I} = \dot{I}_X$; for the beginning of the part $l - X$: $\dot{U} = \dot{U}_X'$; $\dot{I} = \dot{I}_X'$; for the end of the part $l - X$: $\dot{U} = \dot{U}_2$; $\dot{I} = 0$; At the junction of two parts: $\dot{U}_X = \dot{U}_X'$; $\dot{I}_X = -\dot{I}_X'$.

Using equations (2) and the boundary conditions we get the following expressions: for the recovery voltage on the disconnected phase

$$\dot{U}_x = \dot{U}_A \frac{C}{C_0 + C} + j\dot{I}_A \frac{M}{\sqrt{L(C_0+C)}} \times \frac{\frac{1 - \cos\gamma x}{\cos\gamma x} - \frac{1 - \cos\gamma(l - x)}{\cos\gamma(l - x)}}{\tan\gamma x - \tan\gamma(l - x)}; \qquad (3)$$

for the magnetization current

$$\dot{I}_x = -j\dot{U}_A \frac{C}{\sqrt{L(C_0 + C)}}[\tan\gamma x + \tan\gamma(l - x)] + \dot{I}_A \frac{M}{L} \cdot \frac{\cos\gamma(l - x) - \cos\gamma x}{\cos\gamma(l - x)\cos\gamma x}.$$

As can be seen from formulae (3), voltage $\dot{U}_X$ and current $\dot{I}_X$ have two components: the first of them depends on the voltage on the sound phases and is due to the capacitive connexion between sound and faulty phases, and the second depends on currents in the sound phases and is due to the mutual inductance.

On the basis of data given in Table 1, we obtain the distribution of the components of the recovery voltage and of the sustained current for different lengths of the disconnected section of the line in the case of an automatic single-phase reclosing after break. The value of the current I_A is assumed equal to 700 A.

The plotting of graphs of distribution in Figs 3 and 4 is done in such a way that the ordinate axis corresponds to the middle of the disconnected section, and the variable coordinate to the faulty place.

From graphs in Fig. 3 and 4, it is seen that the capacitive component of the recovery voltage does not vary along the section; we can also assume that the capacitive component of the sustained current remains constant along the section.

Inductive components of the sustained current and of the recovery voltage are equal to zero when the short-circuit occurs at the central point of the section, and for short-circuits at the ends of the section they have maximum values. The inductive component of the voltage has a positive value when the short-circuit occurs at one end of the section, and a negative one when it occurs at the other end of the section. The value of the resultant of the inductive and capacitive components depends upon the angle between the current, which produces them, and the voltage on the sound phases; the maximum value of the resultant also occurs at the end of the section.

The above method may also be used for calculations of the sustained current and of the recovery voltage in the case then a shunting reactor is connected at the end of the section of the line. Since, however, the maximum values of these quantities are of primary importance, we give below the formulae for calculations in the case when a short-circuit occurs at the end of the section opposite to that where the shunting reactor is connected. The boundary condition for this case will be: at the end of the section in which the fault occurred $U = U_d$; $I = 0$; at the end of the section with a reactor $U = I_{2j} X_p$; $I = I_2$ where $X_p = \omega L_p$ – inductive reactance of the reactor.

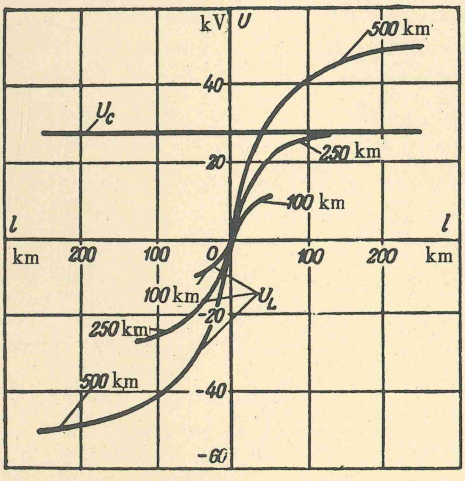

FIG.3. Capacitive U_c and inductive U_l component of the voltage on the disconnected phase (in the absence of the reactor).

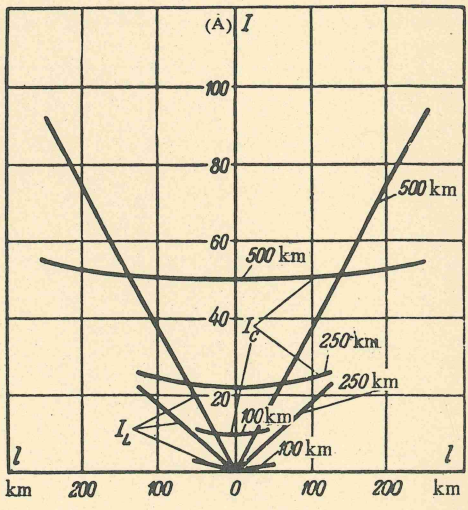

FIG.4. Capacitive I_c and inductive I_l components of the sustained fault current when one phase is disconnected (in the absence of the reactor).

Using equations (2) and the boundary conditions we get:

$$\left.\begin{aligned}
\dot{U}_\partial &= \dot{U}_A \frac{C}{C_0+C} \frac{\sin\gamma l - \frac{Z_c}{x_p}(1-\cos\gamma l)}{\sin\gamma l - \frac{Z_c}{x_p}\cos\gamma l} + \\
&+ jI_A \frac{M}{\sqrt{L(C_0+C)}} \frac{1-\cos\gamma l - \frac{Z_c}{x_p}\sin\gamma l}{\sin\gamma l - \frac{Z_c}{x_p}\cos\gamma l}; \\
\dot{I}_n &= -j\dot{U}_A \frac{C}{\sqrt{L(C_0+C)}} \frac{\sin\gamma l - \frac{Z_c}{x_p}(1-\cos\gamma l)}{\cos\gamma l - \frac{Z_c}{x_p}\sin\gamma l} + \\
&+ I_A \frac{M}{L} \frac{1-\cos\gamma l + \frac{Z_c}{x_p}\sin\gamma l}{\cos\gamma l + \frac{Z_c}{x_p}\sin\gamma l}
\end{aligned}\right\} \quad (4)$$

Here, the recovery voltage and the sustained current also have two components each, one of the components being capacitive and the other inductive.

For calculation of the resultant values of the current and voltage, despite the previously assumed values of different parameters, $\cos\phi$ of the transmission was taken equal to unity, which approximately corresponds to the conditions of normal power. Fig.5 shows the results of calculations for the cases when the reactors are present and when they are absent.

I In the case of a single-phase automatic reclosing after the break and in the absence of a reactor, the recovery voltage varies within the limits 30-60 kV according to the length of the section. In the case when a reactor is present, its inductance and interphase capacitance appear as if connected in series; because of this, voltage resonance is possible, and, hence, a considerable increase of voltage on the faulty phase. Equating to zero the denominator of one of the terms for the voltage (4), we find that the resonance occurs for the length of the section

$$l_{res} = \frac{1}{\omega\sqrt{L(C_0+C)}} \tan^{-1}\frac{Z_c}{\omega L_p}.$$

Calculations show that l_{res} = 290 km. Although, in fact, resonance over-voltage is limited by the saturation of the reactor and the discharge, nevertheless it is necessary to reckon with a considerable increase of voltage. In the presence of a reactor, the sustained current also reaches a considerably higher value than in its absence.

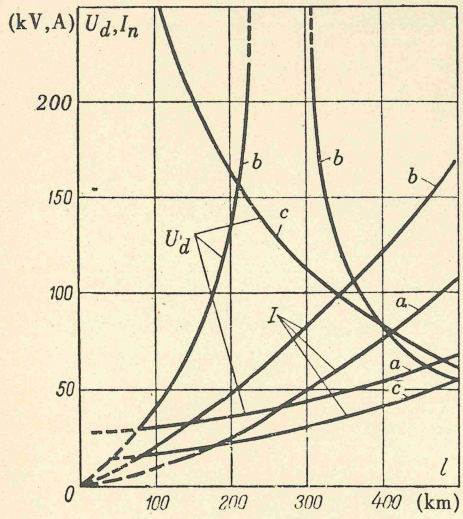

FIG.5. The sustained current and the recovery voltage on the disconnected phase for a point of the end at the section: (a) one phase disconnected, reactor absent; (b) one phase disconnected, reactor present; (c) three phases disconnected, reactor present.

In calculating the sustained current and the recovery voltage for conditions at the three-phase automatic reclosing after break, the values of the discharge current and of the proper frequency of the discharge for each length of the section were taken in accordance with graphs in Fig.1. Voltage on the sound phases was assumed to be equal to the nominal, the damping of the discharge current was disregarded, angles between vectors of the discharge currents and voltages of the sound phases were taken equal to 90 el. deg. The results of calculations are given on Fig.5. The sustained current was a little smaller, and the recovery voltage bigger than for conditions in the case of a single-phase automatic reclosing in the absence of a reactor. The sustained current in the case of a single-phase automatic reclosing in the presence of a reactor was approcimately equal to 0.3 A/km, and in the same case, in the absence of a reactor, to 0.2 A/km. In the case of the three-phase automatic reclosing in the presence of a reactor, the current equalled 0.1 A/km.

The diagram of the 400 kV line Kuibyshev - Moscow, during the experiments carried out by the C.S.R.E.L., is shown on Fig.6. Wind during these experiments was weak.

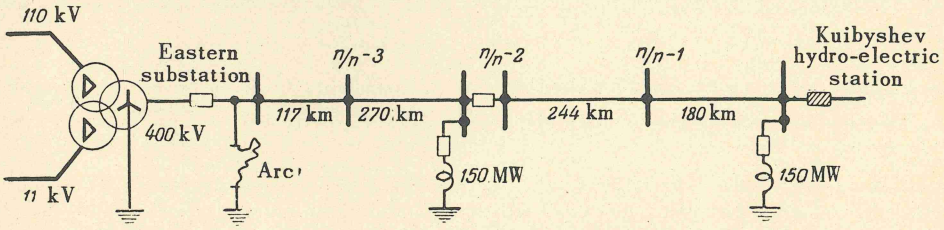

FIG.6. The diagram of the 400 kV Kuibyshev-Moscow line during the experiments with extinction of the sustained faulty current arc.

Arcing short-circuit on the group of insulators of the suspension type was produced by means of a copper wire of 1 mm² cross-section. After fixing the wire, all three phases were switched on and the arc was struck.

The damaged phase was disconnected by a breaker after 0.14 sec, and after this, the sustained current arc remained. The voltages of all three phases, the current of one sound phase, the short-circuit current and the sustained current were recorded by a magneto-electric ossillograph. The photographs of the arc were taken by a cine-camera at the rate of 32 frames/sec. Cine - frames of the experiment on the section of the line 815 km long, in the absence of reactors, are given in Fig.7, and the oscillograms of this experiment in Fig.8.

During the short-circuit stage, the arc on the film appears as a luminous cloud; later the luminous gases, surrounding the arc disperse and the patch of the sustained current arc can be clearly seen; this path gradually becomes longer, bending sideways and upwards, at the expense of thermal forces of the previous short-circuit and due to its own thermal effect; after this comes extinction.

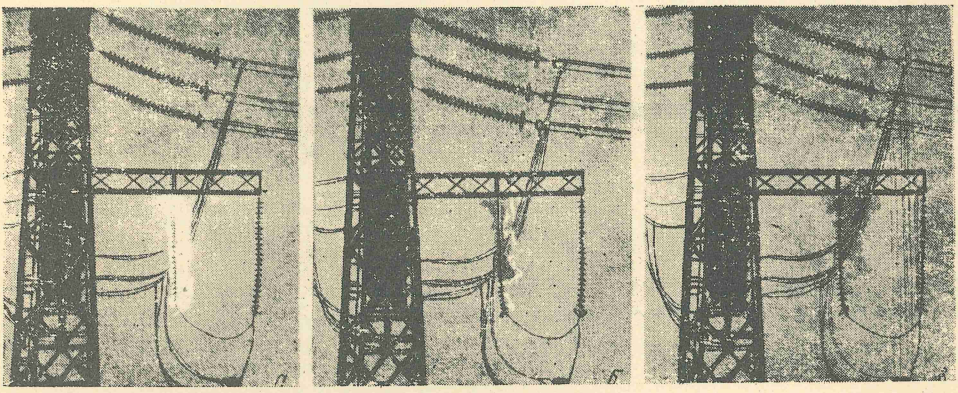

FIG.7. Separate cine-frames of the single-phase short-circuit with the following sustained current arc: (a) short-circuit arc; (b) the sustained current arc before the beginning of extinction; (c) cooling of gases after extinction of the sustained current arc.

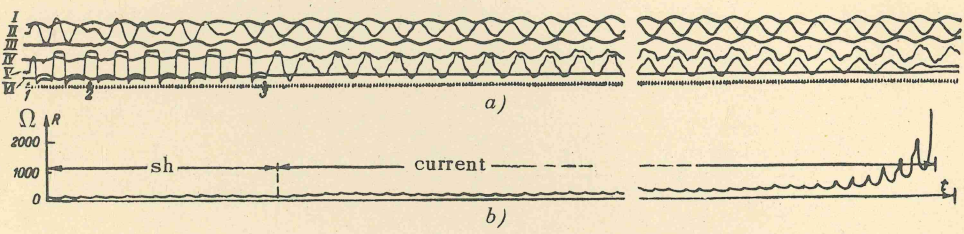

FIG.8. Oscillogram of the experiment (a) and the graph of the resistance of the path of the arc (b) on the single-phase short-circuit and switching off one phase. I – voltage of the "yellow" phase U_y. II – current of the "yellow" phase I_y. III – voltage of the "green" phase U_g. IV – voltage on the arc (of the "red" phase) U_r. V – current I_{su}. VI – short-circuit current I_{sh} (1) the beginning of the short-circuit; (2) connecting of the sound phase with a delay; (3) switching off the "red" phase (the end of the short-circuit).

As can be seen from the oscillogram in Fig.8, after switching off, the sustained current flows through the discharge channel; the current gradually decreases with the lengthening of the channel and the voltage increases on the arc gap. The resistance of the path of the sustained current arc, whose graph of variation is plotted using the oscillogram data, shows a steady increase during the whole process. This arc dies away due to the steady decrease of current caused by the increasing resistance of the path. This process of extinction occurred in all experiments and is typical for the sustained current arc. The extinction of open powerful arcs occurred in a similar way in all the experiments performed by Burgsdorf [6]. In a few cases in these experiments, single restrikes may be observed, these being peculiar to arcs in capacitive networks.

The oscillogram of the experiment on switching-off all three phases on a section of the line 117 km long, without a reactor, is shown in Fig.9a. In this case, the discharge of the sound phases of the line and the sustained current correspond-

ing- to it have an aperiodic character. The discharge lasts only 1.5-2 periods of industrial frequency; therefore, reclosing with a delay of 0.3 sec proves successful.

The oscillograms of the experiment on switching off all three phases on a section of the line 635 km long with the reactor are shown in Fig.9b. In this case, the discharge of sound phases through the reactor, after they have been switched off, proceeds at a frequency of 31 c/s per sec and with small damping, and this agrees with calculations. The curve of the sustained current has an irregular shape, and the extinction of the arc occurs during 0.2 sec. The reclosing after 0.3 sec also proves succesful.

Table 2 shows the results of the experiments carried out on the line from Kuibyshev to Moscow. The experimental values of the sustained current are taken after the first half period after switching off the short-circuit, and the voltage on the disconnected phase is taken at its established value.

In all experiments, the short-circuit current was equal to 2.000 A, and the time of short-circuit 0.14 sec.

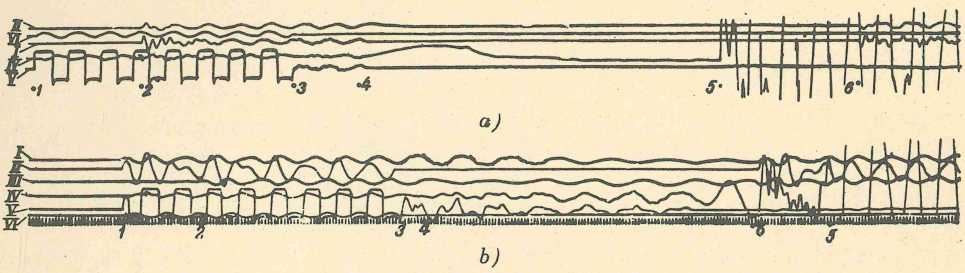

FIG.9. Oscillograms of the experiments with the three-phase switching off and reclosing. (a) section of the line with a voltage transformer; (b) section of the line with a voltage transformer and reactor. I – voltage of the "yellow" phase U_y; II – current of the "yellow" phase T_y; III – voltage of the "green" phase U_g; IV – voltage of the arc (of the "red" phase) U_r; V – current I_{su}; VI – short-circuit current I_{sh}. (1) the beginning of the short-circuit; (2) reclosing of the sound phase with a delay; (3) switching off the "red" phase (the end of the short-circuit); (4) switching off the "yellow" and "green" phases; (5) reclosing of the "red" phase; (6) reclosing of the "yellow" and "green" phases.

The data of the table show a satisfactory coincidence of calculated and measured values of the sustained currents and recovery voltages on the disconnected phase.

Experimentally obtained values of the times of arc extinction in relation to the sustained current for a single-phase automatic reclosing are plotted in Fig.10 as dots. As can be seen from this graph, these points show a considerable dispersion, due to the characteristic instability of the arc.

It is necessary to point out that the experiments were carried out on the line without load, and without the sustained current component, due to the inter-phase

TABLE 2

Kind of experiment	Length of the line (km)	Reactors on phases	Capacitive component of the: Voltage on the disconnected phase (kV) Calculated	Voltage on the disconnected phase (kV) Measured	Sustained current (A) Calculated	Sustained current (A) Measured	Time of burning of sustained current arc (sec)
Single phase A.R.	117	—	28	28	15	17	0.05
" "	391	—	28	28	40	38	0.26
" "	391	—	28	28	40	38	0.34
" "	391	—	28	28	40	38	0.38
" "	391	—	28	28	40	38	0.59
" "	635	Y,G	28	28	67	62	0.25
" "	635	Y,G	28	28	67	62	0.33
" "	635	Y,G	28	28	67	62	0.40
" "	815	Y,G	28	28	82	80	0.35
" "	815	Y,G	28	28	82	80	0.76
" "	815	Y,G	28	28	82	80	1.80
" "	391	Y,G,R	100	92	25	25	0.22
" "	391	Y,G,R	100	92	25	25	0.24
" "	391	Y,G,R	100	92	25	25	0.26
" "	635	Y,G,R	45	50	47	45	0.84
" "	635	Y,G,R	45	50	47	45	1.50
" "	635	Y,G,R	45	50	47	45	1.88
Three phase A.R.	117	—	—	—	—	—	0.02*
" "	635	—	—	—	—	35	0.1
" "	635	—	—	—	65	25	0.15
" "	635	Y,G,R	—	—	65	75	0.20
" "	635	Y,G,R	—	—	65	35	0.08**
" "	635	Y,G,R	—	—	65	70	0.16***

* Reclosing succesfully done after 0.3 sec.
** " " " " " 0.27 sec.
*** " " " " " 0.26 sec.

mutual inductance. If the experiments were carried out on the line with a normal load, the sustained current would have been greater.

Taking into account the maximum durations of time for arc extinction and considering an additional interval of time of the order 0.05 sec, necessary for the recovery of the electric strength of the path after the arc extinction, we can assume, as an approximation, that the sustained current and the duration of the currentless interval for the single-phase automatic reclosing of the line without a reactor, are linearly dependent (straight line on Fig.10). Therefrom we can derive the relationship between the currentless interval and the length of the disconnected section, if the relationship between the length of the section and the sustained current has been determined earlier (see Fig.7). The corresponding approximate formula is

$$t_{Sfar} = 0.003\, l$$

where t_{Sfar} is the necessary currentless interval for the single-phase automatic reclosing (sec) and l is the length of the section (km)

With the reactor, which causes an increase in the recovery voltage, the necessary currentless interval will be appreciably longer than that obtained by formula (6).

In conditions approaching resonance the sustained current arc may remain unextinguished.

So far as the 400 kV line from Kuibyshev to Moscow is concerned, such conditions may occur on the section between the switching points 3 and 2, of length

274 km, and on the section between switching points 2 and 1, of length 244 km, if resonance occurs, as was found earlier, on the length of the disconnected 290 km section.

The resonant increase of the voltage on the disconnected phase can be dangerous for the insulation of the connected transformers and for the shunting reactor. The real value of the over-voltage may be found only experimentally.

For the successful use of the single-phase automatic reclosing on the sections considered of the line from Kuibyshev to Moscow, it is possible, for the single-phase short-circuit, to switch off the shunting reactor simultaneously with switching off the faulty phase. In designing 400 kV lines it is necessary to choose such distances between the switchgears that the conditions for the resonant increase of voltage should not arise when switching off one phase.

If the shunting reactors are sufficiently reliable and damage to them is less probable than serious damage to the line itself, excluding the possibility of its reclosing after break, then we can omit the breaker in the network of the reactor.

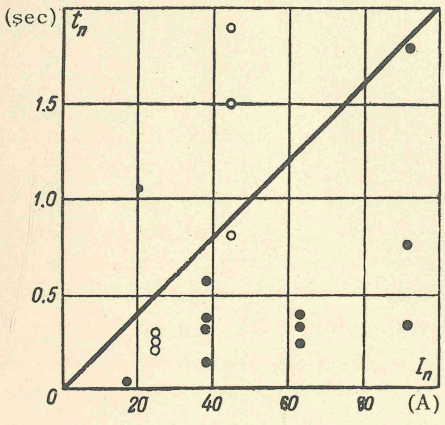

FIG.10. Experimentally found durations of the arc extinction in relation to the current:
● – on the section of the line without a reactor, ○ – on the section of the line with a reactor.

For the three-phase automatic reclosing with a reactor, the durations of arc extinction show a considerable dispersion, but the maximum duration does not exceed 0.2 sec. Therefore, in this case, we may successfully use the so-called quick-acting automatic reclosing, for which the interval is determined by the time of the separation of the arc breaking contacts of the air breaker and their consequent reclosing, this time being equal to 0.27-0.3 sec, as it was during the performed experiments.

In the conditions of dynamic stability of the electro-transmission it is desirable that the currentless interval for the three-phase automatic reclosing should be very small. Nevertheless, the further decrease of the interval of the quick-acting automatic switch-on is inadmissible with shunting reactors, since the relation between the maximum time of the burning of the sustained current arc (0.2 sec), and the maximum interval (0.3 sec) had a limiting value in the experiments. For deionization and the recovery of the electric strength of the path of the arc only 0.1 sec is left.

If, simultaneously with the disconnection of the three-phases of the line, we disconnect the three phases of the shunting reactor as well, then the interval of

the quick-acting automatic reclosing will not be limited by the sustained current arc. In this case, the duration of the pause will be determined by the time of deionization and of the recovery of the electric strength of the path of the short-circuit arc. According to the published data, this time does not exceed 0.2 - 0.25 sec for a large range of short-circuit currents. Taking into consideration that for the 400 kV Kuibyshev - Moscow transmission line, the three-phase short-circuit current varies within the limits 1 - 10 kA, the reduction of the interval of the quick-acting automatic reclosing, the reactor being disconnected, may be brought down to the value of 0.25 sec. The possibility of the further reduction of the interval should be confirmed by additional experiments.

It is necessary to point out that on the section of the line between Moscow and switching point 3, where the reactor is absent, and the extinction of the sustained current arc takes only 0.05 sec, we may successfully use the single-phase quick-acting reclosing.

In conclusion it is necessary to point out that the effectiveness of the automatic reclosing on the 400 kV lines, judging from the experience gained from the exploitation of the 154 kV and 220 kV lines, having analogous electrical and mechanical characteristics, should be high. According to CSREL data, for the period from 1945 to 1954, on the lines with steel cables and the protective angle of 20° or less, there occurred about seventy cases of break - down. Damage due to lightning did not occur. 45 per cent of break-downs were of short duration (dirt, damp insulation in marshy regions, various deposits), and in 55 per cent of cases the break-downs were due to serious and lasting damage, followed by the conductors falling to the ground. It follows that approximately half of the short-circuit cases may be handled without prolonged disconnection of the line.

The authors wish to thank V.V. Burgsdorf for his valuable advice and help given during their work and colleagues who participated in the experiments.

Translated by S. Szymanski

REFERENCES

1. E. Mory; *Bull S.E.F.*, 8 (1945).
2. A. Amstat; *B.B.M.* 7/8 (1948).
3. E. Harrington and E. Starr; *Trans. Amer. Inst. Elect. Engrs. 2* (1949).
4. A. Matthey-Doret and A. Leuthold; *B.B.M.*, 9 (1954).
5. L. Norlin; *Tech. Tijdschro*, 40 (1953).
6. V.V. Burgsdorf; *Elektrichestvo*, No.10 (1948).
7. A.S. Maikopar; *Trud. TsNIEL (CSREL)*, No.2 (1953).

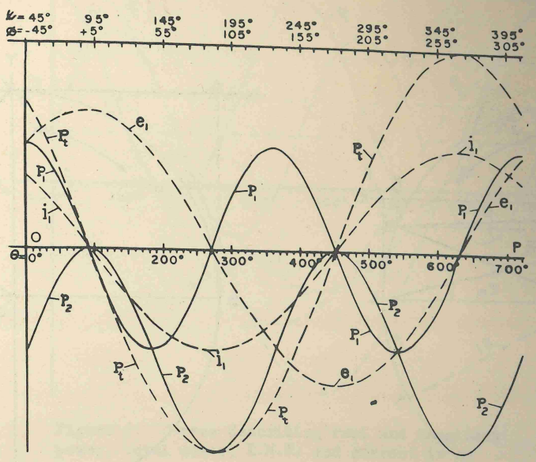

Figure 12. Power curves together with E.M.F. and current in a capacitive circuit with resistance negligible.

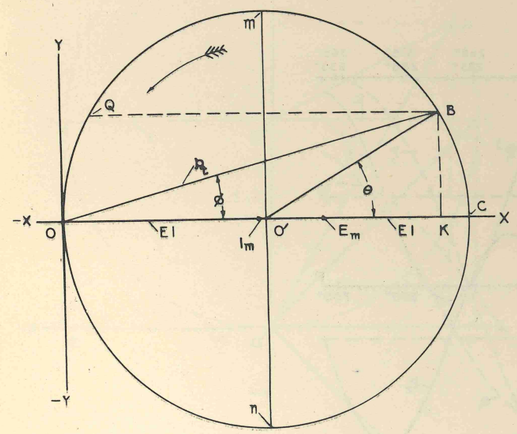

Figure 13. Diagram describing power in a resistive circuit.

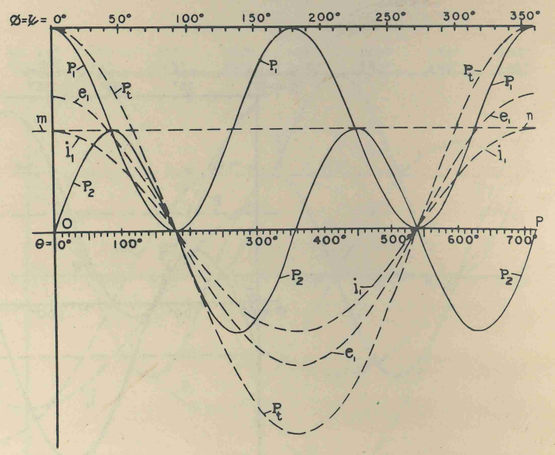

Figure 14. Power curves together with E.M.F. and current in a resistive circuit.

AIEE
Technical Paper
53-81

December 1952
Litho in USA

Discussion for publication
must be postmarked on or before
February 4, 1953.

RECEIVED
DEC 26 1952
ENG. DEPT.

REAL POWER AND IMAGINARY POWER IN ALTERNATING CURRENT CIRCUITS

C. F. Estwick
Member AIEE
43 Cambridge Place
Brooklyn, N. Y.

Advance Copy
Not Released for Publication

All Rights Reserved by the
American Institute of Electrical Engineers
33 West 39th Street, New York 18, N.Y.

A paper recommended by the AIEE Committee on Transmission and Distribution and approved by the AIEE Committee on Technical Operations for presentation at the AIEE Winter General Meeting, New York, N. Y., January 19-23, 1953. Manuscript submitted April 30, 1952; made available for printing December 3, 1952.

PRICE: 30¢ To Members (5¢ per copy additional if
60¢ To Nonmembers first class mailing desired)

REAL POWER AND IMAGINARY POWER

IN ALTERNATING CURRENT CIRCUITS

C. F. ESTWICK
Member AIEE

In examining the theory of power as presented by different writers on the subject there appear to be certain differences in their theories which make the subject difficult to understand. Instead of attempting to reconcile these differences it was decided to make an independent investigation of the subject which has resulted in the development of the theory of real power and imaginary power as described herein.

Instead of attempting to make an intensive study of the literature on the subject it was deemed sufficient to refer to three leading contemporary authorities.

(1) One authority states:
"If we multiply the r.m.s. current by the impressed e.m.f. at standard phase, we obtain the vector power diagram." [1]

(2) The second writer states:
"The symbolic expression of the power vector is obtained by multiplying the E.M.F. vector by the conjugate of the current vector." [2]

(3) A third writer states that the algebraic product of the E.M.F. and the current does not give the power.
He then further states,
"the double frequency vector product denotes more than the mere power, by giving with its two components the true power volt-amperes, or 'effective power', and the wattless volt-amperes, or 'reactive power'." [3]

Although each of the three writers have a different method of solving the problem, they appear to be in agreement in regard to power in the steady state condition, which is the most important case to consider; but they are not in agreement as to what imaginary power really is and only one of the three describes imaginary power, or reactive power as it is sometimes called, under instantaneous conditions.

(1) In regard to imaginary power the first writer states:
"The imaginary component is the reactive power, or the maximum cyclic rate of transferring energy from the mains into the magnetic flux of the coil, and back again."
"The energy of active power is spent outside the circuit; but the energy of reactive power is loaned to the circuit during one half of the energy cycle and returned from the circuit to the source during the other half." [1]

(2) The second writer does not mention "Reactive Power" but, in summing up his discussion, states: [2]
"Hence the effective power $W(=EI\cos\phi)$
is $W = E_1I_1 + E_2I_2$
and the so-called imaginary power $(EI\sin\phi)$
is $W_j = E_1I_2 - E_2I_1$

(3) The third writer has stated as quoted above that
$$P^j = [\dot{E}\dot{I}]^j$$
is "the wattless volt-amperes or reactive power."
Later on he states as follows:
"In an induction motor, for instance, the torque is -------- the product of the secondary current into the component of generated e.m.f. in quadrature therewith in time and space.
Thus, if
$E' = e' + je'' =$ generated e.m.f. in one direction in space,
$I_2 = i' + ji'' =$ secondary current in the quadrature direction in space,
the torque is $D = [\dot{E}\dot{I}]^j = e''i' - e'i''$
By this equation the torque is given in watts, the meaning being that $D = [\dot{E}\dot{I}]^j$ is the power which would be exerted by the torque at synchronous speed, or the torque in synchronous watts.
It is interesting to note that the expression of torque, $D = [e_1i_1]^j$ and the expression of power $P = [\dot{E}\dot{I}]'$, are the same in character, but the former is imaginary, the latter the real component. Mathematically, torque, in synchronous watts, can be considered as imaginary power, and inversely." [3]

The theory of imaginary power described in the latter case is not the same as that proposed by the first author in which imaginary power is referred to as reactive power. The average of the instantaneous values of reactive power taken over one or more complete cycles is zero. This is not the same kind of power as that in the latter case in which imaginary power is described as being the kind of power that could operate an induction motor.

From a summary of the results of this investigation the conclusion reached is that imaginary power is derived from a mathematical theory but it is entirely fictitious and has no physical existence. This does not mean that it is unimportant. The importance and usefulness of the theory of imaginary power has been demonstrated in the solution of power problems under steady conditions.

E.M.F. AND CURRENT IN AN INDUCTIVE CIRCUIT

The E.M.F. and the current flowing in the circuit are assumed to vary sinusoidally and in the steady state condition are represented by E and I which are effective or r.m.s. values taken over one or more complete cycles. In the vector diagram shown in Fig. 1, E_m and I_m represent the maximum values of E.M.F. and current; $E_m = \sqrt{2}E$ and $I_m = \sqrt{2}I$. The vectors OE_m and OI_m rotate continuously about the origin O in the counter-clockwise direction, as indicated by the arrow, at a speed $\omega = 2\pi f$ radians per second where f represents the frequency of the EM.F. and the current. When the vectors are in any momentary position, which may be that shown in the diagram, they can be resolved into rectangular components which represent their real and imaginary values. The real values are laid out on an axis of real values which, throughout this discussion, will be understood to be a fixed axis taken to coincide with the abscissa -XOX and imaginary values are the corresponding ordinates. The position of a vector at any instant is described by the angle it makes with that part of the horizontal axis

OX on the right of the origin. The angle expressed in radians and divided by $2\pi f$ indicates the actual length of time it has taken the corresponding vector to rotate over the angle from the horizontal axis. As the vectors rotate the angles $\varnothing$ and ψ vary in size but their relative phase displacement $\gamma=\varnothing-\psi$ is a constant angle, which is positive in an inductive circuit as shown in the diagram, and negative in a capacitive circuit. The actual values of the E.M.F. and current flowing in the circuit at any instant will be represented by e_1 and i_1 respectively which are equal to the length of the lines oa and ob, then

$$e_1 = E_m \cos\varnothing \qquad \text{---------- (1)}$$

and $$i_1 = I_m \cos\psi \qquad \text{---------- (2)}$$

The imaginary values, e_2 and i_2, are

$$e_2 = E_m \sin\varnothing \qquad \text{---------- (3)}$$

and $$i_2 = I_m \sin\psi \qquad \text{---------- (4)}$$

POWER UNDER INSTANTANEOUS CONDITIONS

In describing power under instantaneous conditions the following symbols will be employed:

P_1 = real power

P_2 = imaginary power

$P_t = \sqrt{P_1^2+P_2^2}$ = total apparent power.

The real power, expressed in watts, is the actual power flowing in the circuit. It consists of two components, one is a steady flow of power from the source of energy into the circuit and is the rate at which energy is dissipated in overcoming resistance, hysterisis and eddy currents, in radiation and in the case of a motor in supplying mechanical energy. This is the power that is measured with a wattmeter in the steady condition. The other component is a flow of energy that surges back and forth between the source of energy and the circuit. In one part of its cycle energy is built up in the magnetic fields of the inductance coils in the circuit and in the other part of the cycle energy is released from the magnetic fields and flows back to the source. In a capacitive circuit the energy flowing back and forth is due to the charging and discharging of the condensers. Imaginary power, usually expressed in vars, is sometimes called wattless power or reactive power and will be described as the imaginary component of the total apparent power. Total power is the geometric sum of the other two; in the steady state condition it is referred to as volt-amperes.

The theory of power, as described herein, has been developed from two equations, one representing real power and the other imaginary power; both equations have been derived from the action of the E.M.F. on the real component of the current. The real component of the E.M.F. acting on the current gives real power which is described by the equation,

$$P_1 = e_1 i_1 = E_m \cos\varnothing \cdot I_m \cos\psi \qquad \text{---------- (5)}$$

(This equation and the curves shown in Fig. 3 and also the vector diagram in Fig. 2 are well known). The action of the imaginary component of the E.M.F. operating on the current gives the following equation for imaginary power which is in quadrature with real power,

$$P_2 = e_2 i_1 = E_m \sin\varnothing \cdot I_m \cos\psi \qquad \text{----------(6)}$$

Equations (5) and (6) may be written in the form,

$$P_1 = \tfrac{1}{2} E_m I_m \cos(\varnothing-\psi) + \tfrac{1}{2} E_m I_m \cos(\varnothing+\psi)$$
$$= EI\cos\gamma + EI\cos\theta \qquad \text{----------(7)}$$

$$P_2 = \tfrac{1}{2} E_m I_m \sin(\varnothing-\psi) + \tfrac{1}{2} E_m I_m \sin(\varnothing+\psi)$$
$$= EI\sin\gamma + EI\sin\theta \qquad \text{----------(8)}$$

in which $\gamma=\varnothing-\psi$ and $\theta=\varnothing+\psi$

STANDARD PHASE

In the solution of problems involving the E.M.F. and the current it is usual to take either the E.M.F. or the current as standard phase at the moment when it is at zero or when it is at a maximum value but in the present case, where it is necessary to consider not only the E.M.F. and the current, but also real power, imaginary power, and total power in their proper phase relations, it has been decided to select as the standard phase, or phase of reference, the instant when real power is a maximum, flowing in a positive direction, and at the same time both the voltage and the current are in the positive direction. At this time vector $O'B$ is in the horizontal position $O'C$ and the voltage and the current are in the positions indicated on the drawings. The curves in the diagrams have been drawn to standard phase assuming that the phase displacement $\gamma=30^\circ$. The magnitudes of the current and voltage have been left arbitrary.

Should it be more convenient, in any particular problem, to change the standard phase this may be accomplished, after the curves have been plotted as described herein, by simply selecting any ordinate on the curves as standard phase and rearranging the horizontal scales of phase angles accordingly. This will not change the curves; they will still show the same magnitudesand relative phase relations although it may be necessary to extend the curves to show at least a full cycle of the current and voltage.

The frequency, angular velocity and time have been eliminated from the equations as far as possible for simplicity. Functions of time may be substituted for the phase angles where it is necessary to compute intervals of time or where intergration or differentiation is required. In making such changes it is usually convenient to select the standard phase as the instant to represent zero-time.

REAL POWER

The vector diagram shown in Fig. 2 has been drawn from Equation (7). The length of the line OO' has been drawn to represent the term $EI\cos\gamma$ and the vector $O'B = EI$ represents any position the vector might assume during its rotation about the point O'. The vector rotates at twice the speed of the E.M.F. and the current in the counter-clockwise direction as indicated. Angle θ describes the instantaneous position of the vector and is measured from OC on the horizontal axis. The projection $O'K$ represents the term $EI\cos\theta$ in the equation. The length of the line OK representing the algebraic sum of the constant term $EI\cos\gamma$ and the variable quantity $EI\cos\theta$,

describes p_1, the instantaneous value of real power. A curve of real power has been drawn from Equation (7) and is shown in the diagram in Fig. 3 together with the E.M.F. and the current. The power curve oscillates about the axis aa′ making two complete cycles during the time the E.M.F. and the current make one cycle. The curves have been extended, in dotted lines, on the left of the zero ordinate to show more clearly that the power curve reaches a maximum value midway in time between the maximum values of the current and voltage. At this particular instant the power lags with reference to the voltage and is leading with reference to the current. It should be understood that the phase displacement between the power vector and either the E.M.F. or the current is changing continuously throughout their cycles of operation because they are rotating at different angular velocities. For this reason it is unusual to attempt to show the voltage and current in the same vector diagram with the power vectors, however, the vectors OE_m and OI_m have been drawn to show their positions when the power vector O′B is in the horizontal position OC.

IMAGINARY POWER

An examination of Equations (7) and (8) will show that they are similar in that the second members of both contain a constant term and a variable, in fact, the second members are identical except that the functions of the phase angles γ and θ are cosine functions in Equation (7) and sine functions in Equation (8). The diagram in Fig. 4, describing imaginary power, has been drawn in a similar manner to that in Fig. 2. Imaginary power is in quadrature with real power and is laid out on the ordinate axis -YY. The length of the line from O to O′ represents the constant term $EI\sin\gamma$ and the projections of the rotating vector O′B on the vertical axis represent the variable term $EI\sin\theta$. The length of the line OQ is, therefore, the algebraic sum of the constant term and the variable term as expressed in Equation (8) and describes instantaneous values of imaginary power.

A curve of imaginary power together with curves of voltage and current may be drawn in a diagram similar to that in Fig. 3, which describes real power, voltage and current, but this is not necessary because these curves are all shown in the diagram in Fig. 6.

VECTOR DIAGRAMS AND CURVES DESCRIBING
POWER IN AN INDUCTIVE CIRCUIT.

In the diagram in Fig. 2, the center of rotation O′ of vector O′B has been located on the horizontal axis but it might have been located at any point on the line ab and the projection of O′B on the horizontal axis would still be the same, that is, the length of the line O′K. The requirement in locating the center of rotation is that it must be displaced horizontally from the origin O, or from the ordinate axis, by a distance equal to OO′ representing $EI\cos\gamma$. In the same manner it becomes evident that the center of rotation O′ in the diagram in Fig. 4 may be located at any point on the line de; the requirement being that it must be located vertically at a distance from the horizontal axis equal to OO′ representing $EI\sin\gamma$. The size and slope of vector O′B in the diagrams in Figs. 2 and 4 are the same, that is, O′B is the same vector shown in both diagrams.

The information regarding vector O′B and the center of rotation makes it possible to combine the diagrams in Figs. 2 and 4 into one diagram as shown in Fig. 5 in which -XX is the abscissa and -YY is the ordinate axis; O is the origin and O′ is the center of rotation of the power vector O′B. The point O′ is displaced horizontally from the ordinate axis by $RO' = OL = EI\cos\gamma$ and is displaced vertically from the horizontal axis by $O'L = EI\sin\gamma$. The length of line $OO' = EI$ is the hypotheneus of the triangle OLO′. This triangle is important because it describes conditions during the steady state, and will be referred to again later. The length of the line LK is the projection of the vector O′B on the horizontal axis and represents the variable term in Equation (7). The line OK is the algebraic sum of OL and LK and expresses the instantaneous value of real power. In a similar manner RQ is the projection of O′B on the vertical axis and represents the variable term in Equation (8). The line OQ, which is the algebraic sum of the constant quantity OR and the variable RQ, expresses the instantaneous value of imaginary power.

When O′B is in the horizontal position O′C real power is represented by OF and imaginary power by $OR = EI\sin\gamma$ In this position of the vector, real power is at its maximum value in the positive direction. When O′B has rotated to the position Om real power is represented by $OL = EI\cos\gamma$ and imaginary power by OT. In this position imaginary power is a maximum value in a positive direction. When O′B reaches the position O′S, the real power is represented by OG which is a negative quantity that describes the condition where energy flows from the circuit back toward the generator. The imaginary power is described by $OR = EI\sin\gamma$ As O′B reaches the origin and coincides with O′O both real power and imaginary power become zero. When O′B reaches the position On real power is equivalent to $OL = EI\cos\gamma$ and imaginary power to OU which is negative and describes the condition where imaginary power is a maximum value in the negative direction.

Referring further to Fig. 5, when O′B is in the position shown on the diagram, the vector OB describes the total apparent power p_t which is the vector sum of the real power OK and the imaginary power KB. At the instant referred to as standard phase the vector OB is in the position OC and is in phase with the voltage OE_m, the phase angle being $\gamma/2 = 15°$. As the vectors rotate the point B moves over the arc of the circle CB. The angles BO′C and BOC both subtend the arc BC; one is at the center of the circle and the other on the circumference. OB, therefore, rotates at half the angular velocity of O′B, that is, the total power vector p_t rotates at the same angular velocity and at the same frequency as the E.M.F. and the current. It can be shown, from the geometry in the diagram, that the angle $AOB = \psi$, which is the phase angle of the current. From the triangle AOB, the size of $P_t = OB = 2EI\cos\psi = E_m I_m \cos\psi$. When OB rotates to OA it reaches its maximum value in a positive direction and as it continues to rotate it varies in size simusoidally until it becomes zero at the origin. The vector OE_m then continues to rotate from the position Oe through 180° to Of. During this time the vector p_t operates around the circle in phase opposition to the voltage. Although this statement is correct it would also be correct to reverse the slope of p_t to bring it in phase with the voltage and at the same time change its size to make it negative instead of positive. This would be difficult to explain from the present diagram but it can easily be proven algebraically in the form of complex quantities as follows:

$$P_t = P_1 + jP_2 \qquad \text{---------- (9)}$$

Substituting from Equations (5) and (6)

$$P_t = E_m I_m \cos\psi \cos\phi + jE_m I_m \cos\psi \sin\phi$$

$$P_t = E_m I_m \cos\psi (\cos\phi + j\sin\phi)$$

$$P_t = E_m I_m \cos\varphi \, \epsilon^{j\varnothing} = |E_m I_m \cos\varphi| \angle\varnothing \qquad \text{---------- (10)}$$

(ϵ is the base of the natural logarithms)

Equation (10) states that the slope of p_t is $\angle\varnothing$, in phase with the voltage, and the size is $E_m I_m \cos\varphi$. The size is negative as the current OI_m, in Fig. 1, operates over the 2nd and 3rd quadrants during which time the voltage and p_t operate from the position Oe to Of in Fig. 5.

Curves have been plotted in Fig. 6, from data already obtained, to describe real power, p_1, imaginary power, p_2, and total power, p_t, and also the E.M.F., e_1, and the current, i_1. These curves have been drawn from the standard phase represented by $\theta = 0°$. Curves p_1 and p_2 have been drawn from the vector diagram in Fig. 5 and p_t from Equation (10), p_1, e_1 and i_1 are the same curves that are shown in Fig. 3. The curves p_1 and p_2 oscillate at twice the frequency of the E.M.F. and the current making two complete cycles to one cycle of e_1, i_1 and p_t. Curve p_1 oscillates about ab as an axis and p_2 oscillates about cd. Portions of the curves above OP represent positive values and those below OP are negative. Curves p_1 and p_2 can be compared with the discussion previously given in describing the vector diagram in Fig. 5. Curve p_t is similar to the curve of the current i_1; it reaches its maximum values and zero points at the same time as the corresponding points on the current curve.

INDUCTIVE CIRCUIT WITH
RESISTANCE NEGLIGIBLE

Conditions in the inductive circuit where the resistance is negligible are determined from Equations (7), (8) and (10). In this case the phase displacement between the E.M.F. and the current $\gamma = 90°$. As shown in the vector diagram in Fig. 7, the center of rotation of O′B is on the ordinate axis -YOY and is displaced from the origin O in a positive direction by the length OO′, which is equivalent to EI. At the time designated as the standard phase the vector O′B coincides with O′C; the current OI_m lags with reference to the horizontal axis -XOX by 45° and the voltage OE_m leads the axis by the same amount. The total power p_t is in phase with the voltage. The real power OF is a maximum in a positive direction and as O′B rotates the power, represented by OK, oscillates back and forth indicating that there is a flow of energy into the circuit from the generator during one half cycle and the same amount of energy flows from the circuit back toward the generator during the other half of the cycle; there is no energy dissipated from the circuit. The imaginary power, represented by OQ, is always positive and oscillates about the axis SC as it varies from a minimum zero to a maximum value $2EI = E_m I_m$.

A better understanding of the conditions in the circuit may be obtained from the curves shown in Fig. 8. Curves p_1 and p_2 were drawn from the diagram in Fig. 7. The values plotted in the curve p_t were computed from Equation (10).

VECTOR DIAGRAMS AND CURVES DESCRIBING
POWER IN A CAPACITIVE CIRCUIT

Power in an electric circuit is determined from the E.M.F., and the current and their relative phase displacement. The principal difference between the capacitive circuit and the inductive circuit is that the phase displacement $\gamma = \varnothing - \varphi$ is negative in the former circuit and positive in the latter. The diagram in Fig. 1 describes the current and voltage in the inductive circuit but it may be redrawn to show the current leading with respect to the voltage. This will show that the Equations (1), (2), (3) and (4), describing the real and imaginary component of the current and voltage, apply to both circuits

and by employing the same method of reasoning as heretofore it then follows that all of the equations that have been given thus far may be employed in the same manner in either case.

The diagram in Fig. 9 describes conditions in the capacitive circuit. The abscissa axis is -XOX and the ordinate axis -YOY; the origin is at the point O. The double frequency power vector O′B rotates about the point O′ in the counter-clockwise direction as indicated on the diagram. The center of rotation is displaced from the ordinate axis by the length RO′=OL which has been drawn to represent $EI\cos\gamma$ and from the horizontal axis -XOX by LO′ which represents $EI\sin\gamma$. The line LO′ in this case is negative and is drawn below the horizontal axis. The line OO′=EI is the hypotheneus of the triangle OLO′. This triangle describes conditions in the steady state in a capacitive circuit. In laying out the diagram in Fig. 9 and the corresponding curves in Fig. 10, it has been assumed that the phase displacement $\gamma = -30°$. The dimensions of the current and the voltage have been drawn to the same dimensions as the corresponding quantities in the previous vector diagrams. Equations (7) and (8) describing real and imaginary power have been employed in the same manner as in the inductive circuit. The constant term in Equation (7) is represented by $OL = EI\cos\gamma$ and the variable term by the projection LK of the vector O′B on the horizontal axis -XOX. The real power, when O′B is in the position shown on the drawing, is represented by OK which is the algebraic sum of OL and LK. As O′B rotates the projections are considered to be either positive or negative depending upon whether they are on the right or the left of point L. In Equation (8) the constant term $EI\sin\gamma$ is represented by LO′=OR which is negative and is drawn on the ordinate axis -YOY below the origin O. The variable term is represented by RQ which is the projection of the vector O′B on the vertical axis. The imaginary power at this moment is OQ, which is the algebraic sum of OR and RQ.

The rotating vector O′B assumes the position O′C at the time described as the standard phase. The real power OF is then at its maximum value in a positive direction and the imaginary power is negative and equal to $OR = EI\sin\gamma$. At this time the phase angle of the E.M.F., OE_m is $\gamma/2 = -15°$ and that of the current OI_m is equal to $+15°$ as indicated on the drawing. When O′B reaches the position O′m the real power is $OL = EI\cos\gamma$ and the imaginary power is OT which is a maximum in a positive direction. As O′B reaches the position O′O both the real power and the imaginary power become zero. When O′B is in the position O′S the real power is OG which is a maximum in a negative direction and represents the flow of energy back toward the generator. The imaginary power is $OR = EI\sin\gamma$. As O′B assumes the position O′n the real power is $OL = EI\cos\gamma$ and the imaginary power is Ou which is a maximum value in the negative direction. Total power p_t is described by the vector OB which is in phase with the voltage. The size of the vector varies as it rotates and it reaches a maximum value in the position OA. By referring to Equation (10) it can be seen that the size of p_t is positive as the vector operates from the position Of to Oe and negative as it operates from Oe to Of.

The diagram in Fig. 10 shows the curves of power in the capacitive circuit together with the current and voltage. Curves p_1 and p_2 were drawn from the diagram in Fig. 9 and the curve p_t from Equation (10).

CAPACITIVE CIRCUIT WITH
RESISTANCE NEGLIGIBLE

In this case the current leads the E.M.F. and the angle of phase displacement $\gamma = -90°$ which make it possible, in the same manner as described heretofore, to draw the vector diagram in Fig. 11. The center of rotation O′ is located on the ordinate axis below the

horizontal axis by the length OO' equivalent to -El. When the vector $O'B$ is in the standard phase position $O'C$ the real power, represented by OF, is a maximum value in the positive direction and the current and voltage are in the positions shown on the drawing; the vector p_t coincides with OC and is in phase with the voltage. There is no real power in the steady condition and no dissipation of energy, but there is a surging of energy back and forth between the generator and the circuit due to the charging and discharging of the condensers. The imaginary power is negative and varies between zero and a maximum value $-2EI = -E_m I_m$ These relations are shown in the form of curves in the diagram in Fig. 12.

VECTOR DIAGRAMS AND CURVES DESCRIBING
POWER IN A RESISTIVE CIRCUIT

In the resistive circuit the phase displacement between the E.M.F. and the current $\gamma = 0°$ so that the constant term in Equation (7) equals EI and the corresponding term in Equation (8) becomes zero. With this information the vector diagram in Fig. 13 was drawn with O' the center of rotation of the vector $O'B$ located on the horizontal axis -XOX at a distance OO', equivalent to EI, from the origin O. When the vector is in the standard phase position it coincides with $O'C$ and the real power p_1 is represented by OC equivalent to $2EI = E_m I_m$ which is at its maximum value in a positive direction. At this time the vectors E_m, I_m and p_t, representing the E.M.F., the current and total power, are in the zero phase position and as they rotate they remain in phase throughout their full cycle. This is the only case in which the flow of energy is always in one direction flowing from the generator into the circuit; there is no storage of energy during the cycle and all of the energy from the source is dissipated from the circuit. This can be seen more clearly in the corresponding curves shown in the diagram in Fig. 14.

Although there is no inductance nor capacitance in the resistive circuit there is imaginary power under instanceous conditions which varies from zero to a maximum, equivalent to EI, in both the positive and negative directions. In this case it can be seen from the vector diagram and from curve p_2 that the mean value is zero. From this it may be stated that under steady state conditions the imaginary power in the resistive circuit is zero.

TRANSITION FROM INSTANTANEOUS
CONDITIONS TO THE STEADY STATE

Real power in the steady state condition is the mean of the momentary values of the real power taken over a complete cycle. Selecting Equation (7) as describing instantaneous conditions and taking the mean value of the second member of the equation this becomes,

$$P_1 = EI\cos\gamma \qquad \text{----------(11)}$$

where P_1 expresses real power in the steady state.

By adopting the same method of reasoning in regard to imaginary power and employing Equation (8) as representing instantaneous conditions, the imaginary power in the steady state, P_2, may be expressed in the following equation:

$$P_2 = EI\sin\gamma \qquad \text{----------(12)}$$

Total power P_t, or volt-amperes, in the steady state, is the geometric sum of P_1 and P_2

$$P_t = \sqrt{P_1^2 + P_2^2} = EI \qquad \text{----------(13)}$$

By combining Equations (7) and (8) into one equation,

$$P_t = EI\cos\gamma + jEI\sin\gamma + EI\cos\theta + jEI\sin\theta$$

$$P_t = EIe^{j\gamma} + EIe^{j(\varnothing+\chi)} = EI\angle\gamma + E\angle\varnothing \cdot I\angle\chi \qquad \text{----------(14)}$$

The first term in the second member describes power in the steady state and the second term represents a transient that reduces to zero under steady conditions. It can be seen that the latter term is the complex algebraic product of the E.M.F. and the current. These relations are shown in the vector diagrams; for instance, the diagram of the inductive circuit in Fig. 5, in which $OO' = EI\angle\gamma$ and $O'B = E\angle\varnothing \cdot I\angle\chi$ OB represents $p = OO' + O'B$ In passing to the steady state the vector $O'B$ reduces to zero and, at the same time, the projections of $O'B$ on both the horizontal and vertical axes become zero leaving only the well known triangle OLO' to describe power under steady state conditions.

CONCLUSIONS

The theory of power has been developed from two independent Equations (5) and (6), the former describing real power and the latter imaginary power.

A question may be asked as to why it was necessary, in developing the equations, to assume that the E.M.F. operates on the current instead of considering the current to act on the E.M.F. In order to obtain a better understanding of the physical action involved, it might be helpful to consider a similar mechanical system. Suppose that, for any particular circuit arrangement, there is an analagous mechanical system in which the application of a mechanical force is similar to the action of the E.M.F. in the electric circuit and that velocity or speed likewise represents the current. From this it may be said that length in the mechanical system is analagous to a quantity of electricity. Speed is a function of distance or length. If a force, in overcoming a resistance, acts over a certain length, in the same direction as the force, there is an expenditure of energy which is equal to the force times the length. The action that takes place is clearly due to the operation of the force and is not due to the length operating on the force. To state that length operates on a force would be expressing an impossibility and would have no physical meaning whatever.

When a force is applied at right angles to a length the product, force times length, gives torque not energy.[3] The subject of torque and energy has previously been discussed by C.P. Steinmetz. Here again, the force operates on the length and not the length on the force. Both real and imaginary power are also due to the action of a force. The force is the operator in each case and the result of the operation is power expended in the direction in which the force is applied.

If there is such a mechanical system which is truly representative of conditions in the electric circuit it may reasonably be assumed that an E.M.F. operates on the current but, from this analogy, it would appear to be incorrect to state that the current operates on the E.M.F.

Vector power, as stated in describing Equation (14), is the sum of the vector describing power in the steady state condition and the complex algebraic product of the E.M.F. and the current. An interesting discussion of the complex algebraic product [2] of the current and voltage under momentary condition has been given by LaCour and Bragstad.

The real component of the E.M.F. operating on the real component of the current gives real power and the imaginary component operating on the real component of the current gives imaginary power. The imaginary component of the current does not appear in the equations; in fact, it is a fictitious quantity that has no physical existence. The same thing may be said about the imaginary component of the E.M.F. The entire theory of imaginary power has been developed from e_2 operating on i_1, as expressed in Equation (6), and, as stated above, must be considered as a methematical expression that has no direct physical meaning. Total power under momentary conditions and volt-amperes in the steady state are also fictitious.

As previously stated, in either an inductive or a capacitive circuit in which effective resistance is negligible there is no real power in the steady condition but under momentary conditions there is real power surging back and forth in the circuit. Similarly, in a resistive circuit in which there is neither inductance nor capacitance, there is no imaginary power in the steady condition but there is imaginary power during the cycle under momentary conditions.

REFERENCES

1. Electric Lines and Nets, A.E. Kennelly, McGraw-Hill Book Co., New York, 1928, pages 121-125, pages 120, 121 and 123, page 186.

2. Electric Currents, J.L. La Cour and O.S. Bragstad, Longmans, Green and Co., London, 1913, page 37, pages 36-37.

3. Alternating Current Phenomena, C.P. Steinmetz, McGraw-Hill Book Co., New York, 1916, page 181, pages 185-186.

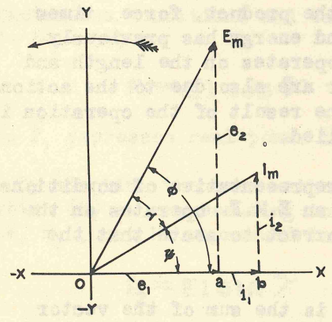

Figure 1. Vector diagram of the E.M.F. and current in an inductive circuit.

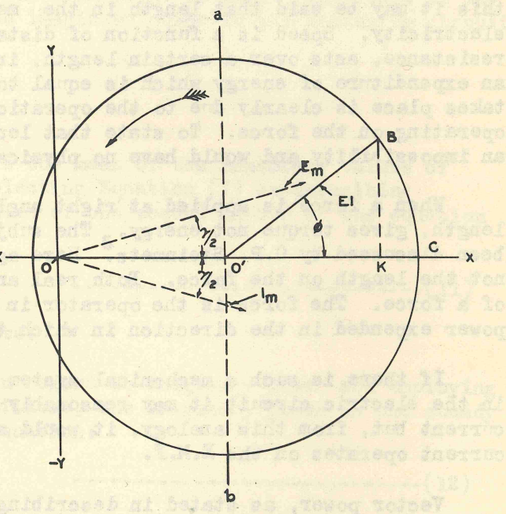

Figure 2. Vector diagram of real power in an inductive circuit.

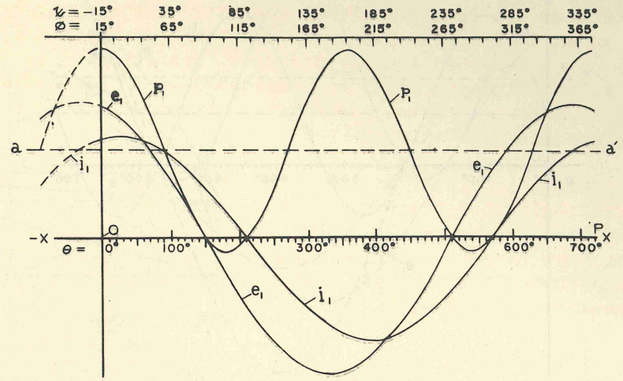

Figure 3. Curves describing real power, E.M.F. and current in an inductive circuit.

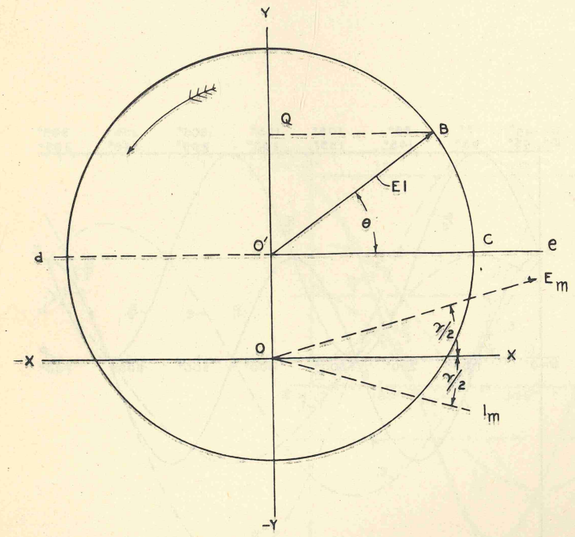

Figure 4. Vector diagram of imaginary power in an inductive circuit.

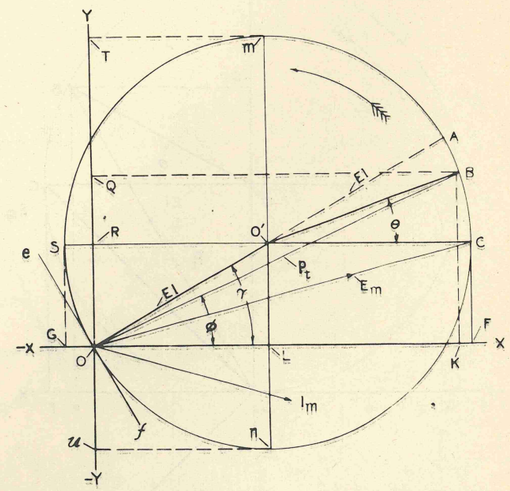

Figure 5. Vector diagram describing real and imaginary power, total power, E.M.F. and current in an inductive circuit.

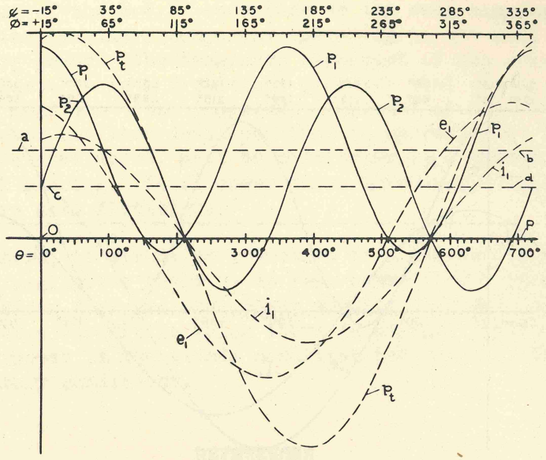

Figure 6. Curves describing real and imaginary power, total power, E.M.F. and current in an inductive circuit.

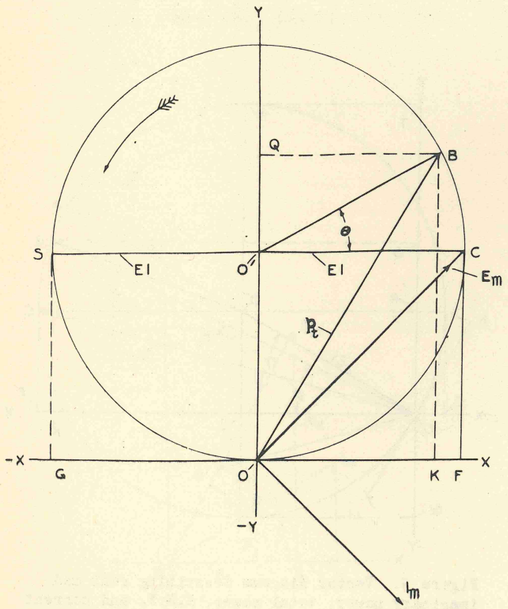

Figure 7. Vector diagram of real and imaginary power and total power in an inductive circuit with resistance negligible.

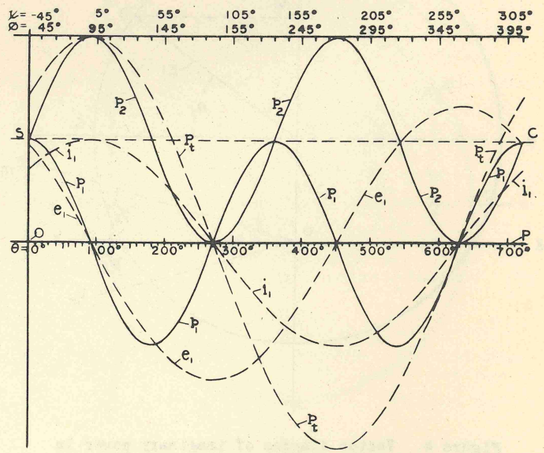

Figure 8. Curves of real and imaginary power, total power, E.M.F. and current in an inductive circuit with resistance negligible.

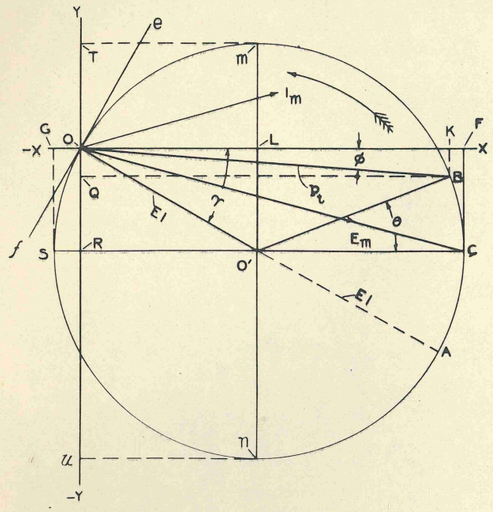

Figure 9. Vector diagram describing power in a capacitive circuit.

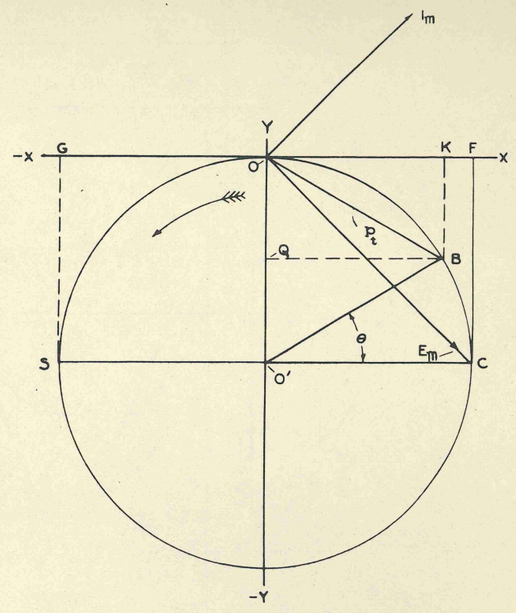

Figure 11. Diagram describing power in a capacitive circuit with resistance negligible.

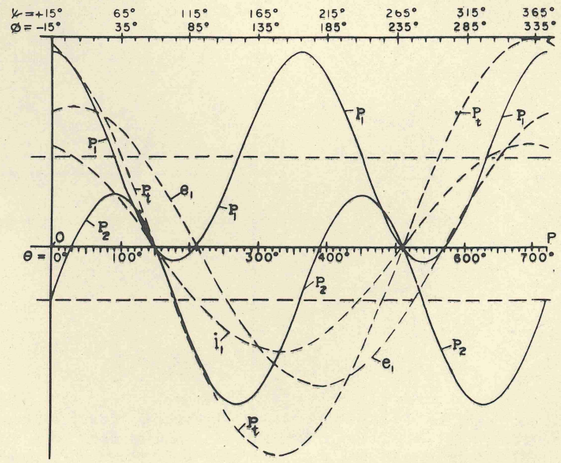

Figure 10. Power curves in a capacitive circuit together with the E.M.F. and current.

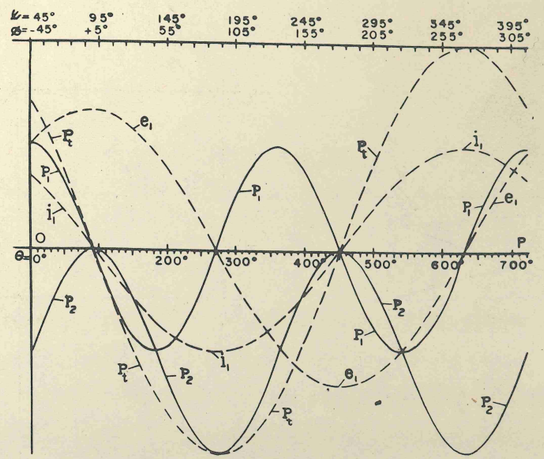

Figure 12. Power curves together with E.M.F. and current in a capacitive circuit with resistance negligible.

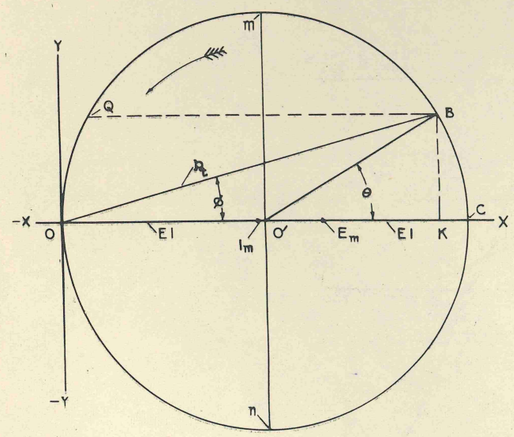

Figure 13. Diagram describing power in a resistive circuit.

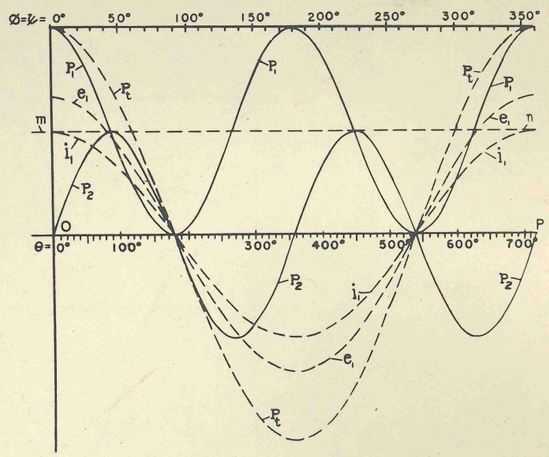

Figure 14. Power curves together with E.M.F. and current in a resistive circuit.

AIEE
Technical Paper
53-81

December 1952
Litho in USA

Discussion for publication
must be postmarked on or before
February 4, 1953.

RECEIVED
DEC 26 1952
ENG. DEPT.

REAL POWER AND IMAGINARY POWER IN ALTERNATING CURRENT CIRCUITS

C. F. Estwick
Member AIEE
43 Cambridge Place
Brooklyn, N. Y.

Advance Copy
Not Released for Publication

All Rights Reserved by the
American Institute of Electrical Engineers
33 West 39th Street, New York 18, N.Y.

A paper recommended by the AIEE Committee on Transmission and Distribution and approved by the AIEE Committee on Technical Operations for presentation at the AIEE Winter General Meeting, New York, N. Y., January 19-23, 1953. Manuscript submitted April 30, 1952; made available for printing December 3, 1952.

PRICE: 30¢ To Members (5¢ per copy additional if
60¢ To Nonmembers first class mailing desired)

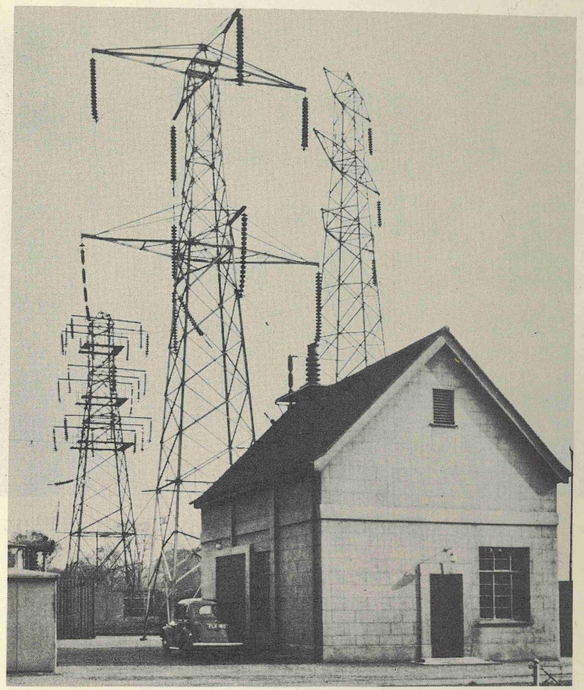

Fig. 5. Croydon Insulator Testing Station.

Conference Paper

RESEARCH BY THE CENTRAL ELECTRICITY AUTHORITY

J. S. Forrest
Nonmember AIEE
Central Electricity Research Laboratories
Leatherhead, Surrey, England

Submitted in abstract or outline form only to the AIEE Committee on Research for the AIEE Winter General Meeting, New York, N. Y., January 30-February 3, 1956. Manuscript submitted November 29, 1955; made available for printing December 9, 1955.

Price: 40¢ To Members
80¢ To Nonmembers
(5¢ per copy additional if first class mailing desired)

All Rights Reserved by the
American Institute of Electrical Engineers
33 West 39th Street, New York 18, N. Y.
Litho in USA

Paper No. CP
56-267

RESEARCH BY THE CENTRAL ELECTRICITY AUTHORITY

By J.S. Forrest *

SUMMARY

The paper describes the organisation of research in the Central Electricity Authority, who, with the Area Boards, are responsible for electricity supply in England. It shows how the Authority's research activities can be broadly classified into
(a) research carried out by the Authority themselves;
(b) co-operative research under the aegis of a Research Association or in collaboration with manufacturers or other users; and
(c) external research carried out for the Authority by a University or other organisation.

Typical research investigations in the fields of generation, transmission, distribution and utilization are described.

---

1. INTRODUCTION.

In the early years of electricity supply in Britain, the Authorised Undertakers, as the supply authorities were called, did little research, and depended largely on the resources of the manufacturing industry for technical developments and improvements in efficiency. The competition between manufacturers for contracts also provided an incentive to give the user something better.

However, with the Electricity (Supply) Act of 1926, and the advent of the Grid transmission system, the opportunity occurred of embarking on research on a national basis, and the Central Electricity Board, the body then responsible for the operation of the Grid system, initiated work on the high-voltage transmission problems which were being encountered for the first

---

* Director of Central Electricity Research Laboratories, Leatherhead, Surrey, England.

time in Britain. This work continued throughout the 20-year period for which the Central Electricity Board functioned, but the building of adequate research laboratories and other facilities, which would have been provided if it had been possible for the work to develop naturally, was prevented by the 1939-1945 war.

As a result of the 1947 Electricity Act, the British Electricity Authority and Area Boards were set up and became responsible for generation, transmission and distribution of electricity throughout Britain (except for the North of Scotland which came under the North of Scotland Hydro-Electric Board). The B.E.A. operated the generating stations and main transmission systems, while distribution was carried out by the fourteen Area Boards.

More recently, a further change in organisation has occurred as a result of the Electricity Re-organisation (Scotland) Act 1954. Under that Act the South of Scotland Electricity Board was established and became responsible for generation and distribution in the former South-East and South-West Scotland areas. The Authority's title was changed to Central Electricity Authority (C.E.A.). Accordingly, the C.E.A. and the twelve Electricity Boards are now responsible for generation, transmission and distribution in England and Wales, i.e. for about 90 per cent of the public electricity supply in Britain. For administrative purposes the Authority have established eleven Generating Divisions who operate the power stations and main transmission systems in their respective areas. The C.E.A. interconnected system comprises 275 stations with a plant capacity of 20,000 MW, 600 circuit miles of 275-kV transmission line and 6,000 circuit miles of 132-kV line.

The energy generated is about 70 x 10^9 kWh per year and the energy sold has increased at an average rate of 8.5 per cent per year during the period 1949-1955. At present practically all the energy is generated in coal-fired steam stations but oil firing is now being used to an increasing extent and plans have been made to build twelve nuclear power stations.

An important feature of the 1947 Electricity Act is that it lays considerable emphasis on research and states (Section 2(i)) that "It shall be the duty of the Central Authority and of any Area Board, in so far as they may be requested by the Central Authority to do so, to conduct research into matters affecting the supply of electricity, and the Central Authority and, in so far as they may be so requested, any Area Board may assist other persons conducting such research". Thus it is a statutory duty of the Authority to carry out research - as well as a necessity for efficient operation.

It is the object of this paper to describe the research organisation of the Central Electricity Authority and to illustrate the working of this organisation by giving examples of typical research investigations.

2. THE RESEARCH ORGANISATION OF THE C.E.A.

Although producers of electricity, the C.E.A. are users of electrical plant, and much of the research work can accordingly be termed "user research". The scope of user research will become clearer in subsequent sections of the paper where typical examples of research are given. Broadly speaking, however, the user lays emphasis on the performance of equipment in service. He is therefore particularly interested in "life tests" and "weathering tests", in which equipment is studied for comparatively long periods under actual operating conditions. Furthermore, the collection and analysis of operating statistics is clearly the province of the user. From such data, improved designs and better methods of maintenance often result. Finally, research of a more fundamental nature may arise from operational problems and the results of the fundamental research may in turn be applied to practical operation.

It should be emphasised that research, from its very nature, cannot be planned in detail, and no attempt should be made to restrict research unnaturally by rigid organisation. Facilities for research must be planned, however, and research programmes can be planned broadly. Nevertheless, the organisation must be very flexible in order to accommodate rapidly the changes in the scope of the work which occur from time to time.

The Authority's research activities can be divided into three groups: Research carried out by the Authority in their central laboratories or in the Divisions, or by the Area Boards, at the request of the Authority; Co-operative Research carried out by a Research Association, or in conjunction with manufacturers or other users; and External Research carried out for the Authority by some other organisation such as a University, Government Establishment, or Research Institute.

It is not possible to state precisely how the work is or should be divided between these three main categories, but broadly, the policy of the Authority is to arrange for the work to be done by the body which is best qualified to do it from the point of view of staff and facilities, and to avoid undesirable duplication. It should be noted also that the above sub-division of research is not in practice as clear-cut as might at first appear. For example, research by the Authority always involves some co-operation with other workers in the same or related fields.

Similarly, external research is more likely to be fruitful if the sponsor is able to make a useful technical or scientific contribution to the work.

In 1949, the Authority appointed an Electricity Supply Research Council composed of external scientists and engineering representatives of the Authority and Area Boards. The external members of the Council are the Chairman and five scientists, mainly drawn from Universities and covering a wide range of interests in the fields of engineering, physics and chemistry. The Authority and the Boards are represented by the Chief Engineer, members of the Research Branches of the Authority, and by the Chief Engineers of two of the Area Boards. It is the function of the Council to advise the Authority on the planning and conduct of research and to make recommendations on research which the Council considers it desirable to initiate.

Under the 1947 Electricity Act the Authority have to carry out research "in accordance with a general programme settled from time to time in consultation with the Minister of Fuel and Power". Accordingly the Authority prepare an annual programme of research covering all aspects of research and including also certain development projects, such as the installation of gas turbines and experimental plant. This programme is discussed and approved by the Research Council before submission to the Minister.

Expenditure on Research. The expenditure on research is often used as a convenient measure of a research effort but it is not a good measure and may be misleading. Good research often costs very little; a competent investigator will make only the essential observations. On the other hand, too much money is sometimes spent on elaborate apparatus or on unnecessarily intricate pilot plant, with the result that an enormous amount of data are accumulated and never properly analysed. Another difficulty lies in deciding what constitutes research and in drawing the line between research and development work. Installing a new experimental machine may legitimately be classified as research but such work soon becomes development and then ordinary commercial operation.

With these reservations, however, it may be of interest to consider the Authority's present annual research budget which is summarised below.

(a) Research by the Authority:

Central Research Laboratories	£175,000
Investigations in power stations in Divisions	65,000
Utilization research	15,000

(b) Co-operative Research:

Research Associations Boiler Availability Committee International Flame Research Committee	170,000

(c) External Research:

Universities Research Institutes	35,000
	£460,000

In addition, about £1 million per year may be spent on development projects such as gas turbines, flue gas-washing, and high temperature steam plant.

The total expenditure is therefore between £½ million and £1½ million depending on the extent to which development and large experimental projects are classed as research. These sums are not large when considered in relation to the Authority's annual income of £350 million, but it has been the policy of the Authority to let the research organisation grow naturally on the operational problems which arise from time to time. In this way it has been possible to build up a more stable organisation than if an attempt had been made to force a large expansion in too short a time. Moreover in research, perhaps even more than in other activities, it is the individual who is of paramount importance, and the time taken to build up a first-rate research laboratory is fundamentally the time required to build up a team of the right men.

2.1 Research by the Authority

It is very desirable for the Authority to conduct a considerable amount of research themselves. In the study of operational problems, and in making investigations in the field, it is clearly more efficient to arrange for the work to be done by the Authority's staff who already have the necessary background knowledge and experience. Furthermore, it is essential for the Authority's staff to have first-hand research experience if they are to take part effectively in co-operative research, and to be in a position to assess the quality of extra-mural work.

The Authority have Headquarters laboratories at Leatherhead, Croydon and Grove Road, London, and Divisional laboratories associated with the power stations throughout the country. The routine work is practically all done in the power station laboratories so that it is possible to devote the resources of the Headquarters laboratories almost entirely to research.

The Leatherhead laboratories (Fig. 1), which were opened in 1950, are the central laboratories of the Authority; their function is to contribute to the solution of any of the problems which may arise in the supply industry and in particular, to serve the Chief-Engineer's Department at Headquarters, the Divisions and the Area Boards. In order to deal with the wide scope of this work the laboratories are divided into six subject sections: Transmission and Distribution, Electronics and Instruments, Generation (Special Problems), Mechanical Engineering, Physics, Chemistry and Metallurgy.

The work of the laboratories is described in Laboratory Reports which are circulated to Headquarters staff and to the Divisional Controllers and Electricity Board Chief Engineers. In this way the results of research are made available throughout the electricity supply industry, and undesirable duplication of work is avoided.

Croydon Testing Station was established by the Central Electricity Board in 1934 in order to study the performance of high-voltage insulators operating outdoors in humid and polluted atmospheres. This work has been continued by the Authority and, in addition, the scope of the Station has been extended to include research on the performance of water-cooling towers and electrostatic precipitators.

Grove Road laboratory was established in 1952 to provide experimental facilities for a group working on internal corrosion in boilers.

Much of the development work on generating plant must be done at the power stations, and furthermore, conclusions reached in the laboratory or with the help of pilot plant must be confirmed by full-scale trials. One of the advantages of a national power system is that power plant investigations can be carried out at the most suitable stations and the results immediately made available for the benefit of other stations. This work is organised by a Generation Research Liaison Committee of Headquarters and Divisional Engineers. Sub-Committees are appointed by the Committee from time to time to work on specific problems, such as Combustion; Flame Radiation; Boiler Corrosion; Electrostatic Precipitators; Atmospheric Pollution; Effluents Testing; District Heating; and Heat Pumps.

Similarly, a Co-ordinating Committee of representatives of the Transmission and Research Departments meets regularly to discuss the progress of research on transmission problems. Furthermore, meetings of Generation and Transmission Divisional and Headquarters engineers are often held at the Research Laboratories in order to ensure full co-operation and to assist in the dissemination of the work of the Laboratories. Progress in research is also reported directly to the Area Board Chief Engineers at their regular Conferences.

2.2 Co-operative Research

The Authority participate in many co-operative research programmes in order to avoid unnecessary duplication of work and also to enable the pooled resources of several organisations to be applied to a problem of mutual interest. Co-operative research is for the most part carried out under the aegis of the appropriate Research Association. The Research Associations are organisations for co-operative industrial research supported by subscriptions from manufacturers and users and by a Government grant related to the amount contributed by industry. The Research Associations conduct research in their own laboratories and also place research contracts with Universities and other research organisations. Their research programmes are organised by a Council and Committees of subscribing members representing the various interests involved, and confidential reports are circulated to the members.

The Authority are members of the Electrical Research Association, the Coal Utilisation Research Association, the Hydromechanics Research Association, the Iron and Steel Research Association and the Non-Ferrous Metals Research Association, and members of the Authority's staff serve on the Councils and Research Committees of these bodies. In addition, the Authority often co-operate directly with Government laboratories such as the National Physical Laboratory, with the research organisations of manufacturers, and with other supply authorities and national bodies at home and abroad. Participation in the work of professional institutions and scientific societies has also been found to be of great value to the research staff. A particularly useful function of such organisations is that they provide a forum for free discussion and publication of research.

2.3 External Research

The work carried out by the Authority and most of the co-operative research would broadly be classed as applied research. The distinction between fundamental and applied research is a rather artificial one, however, and a research project in the Authority's laboratories would not be discontinued merely because it showed signs of becoming too fundamental. This would not be fair to the investigator, and moreover the fundamental research of

today is the applied research of tomorrow. Nevertheless, it is possible to describe certain work as "pure", "long-term" or "fundamental". Work of this type can often be carried out best at a University. Here, operational background knowledge and experience is not required, and may even be a disadvantage as it leads the investigator to think along conventional lines.

The Authority feel that it is important for them to support, and to be associated with, fundamental research on electricity supply. Accordingly, they arrange from time to time for work on specific long-term problems to be carried out at Universities. These external research contracts are placed on the recommendations of the Electricity Supply Research Council. Members of the Council visit the University Departments where the work is being done, discuss the reports received, and in general guide the direction of the researches. In order to co-ordinate the work of the various investigators on a given project and to ensure that each investigator is aware of similar work in progress elsewhere, discussions are arranged when necessary between all interested persons - these discussions are usually held at the Authority's Research Laboratories.

3. RESEARCH AND DEVELOPMENT WORK.

The nature and organisation of the research and development work can best be illustrated by describing briefly some typical investigations in the fields of generation, transmission and distribution which have been undertaken or are now in progress.

3.1 Generation Research

The basic thermal efficiency of generating plant is fixed by thermodynamic considerations, but the operating efficiency from day to day and to a greater extent the availability are determined, not only by the plant design, but also by the skill and knowledge of the operating engineer.

Combustion

The characteristics of the coal available have a very important influence on the operation of boiler plant, and work is continually in progress to ensure that the operating methods used are the most efficient for the coal and boiler plant in question.

An important part of the research on combustion is the study of the formation of deposits which build up on the fire-side of the heating surfaces of boilers. The rate at which these deposits form depends on the temperature of the furnace and on the amount of certain elements, such as sodium, potassium, sulphur, phosphorus and possibly calcium, present in the coal. By analysing the deposits and the coals, and by making trials on

power station boilers, the parts played by various constituents in the coal have been elucidated. This work has led to great improvements in boiler availability and has also shown how unsuitable coal can be used by blending with coal from another source. Experiments are also being made at power stations to determine the effects of increasing the moisture content of the combustion air and of recirculating flue gas to the combustion chamber. New methods of firing, such as spreader-stokers, cyclone and slag-tap furnaces, are investigated extensively. In the laboratory improved rapid methods of analysis based on physical techniques, have been developed which reduce the time required for a complete analysis of a boiler deposit from a week to a day.

Research is also in progress on boiler tube corrosion caused by certain types of deposit, and air-heater corrosion due to sulphur trioxide and moisture condensing on the metal surfaces.

Some of the work on improving boiler availability is done in collaboration with the Boiler Availability Committee; this is a committee for co-operative research on which are represented the manufacturers of boiler plant, the Authority, the Fuel Research Station of the D.S.I.R. and the British Coal Utilisation Research Association. Reports are made to the Committee and circulated to all those interested. Completed investigations are also described in papers to technical journals.

Work is also being carried out on flame radiation in boilers under the aegis of the Flame Radiation Sub-Committee and in collaboration with the International Flame Research Committee, and the University of Sheffield.

Corrosion in boilers

Internal corrosion is another problem in boiler plant operation. Certain broad principles, such as the importance of feed-water treatment, low oxygen concentration and good circulation, are generally recognised as being effective in combating internal corrosion. The detailed picture is much more complicated, however, and there is much conflicting evidence as to the rôle of various factors in the corrosion mechanism. Accordingly, statistical investigations are being made of the incidence of corrosion in power station boilers. In addition, apparatus is being built to study the corrosion of boiler tubes at high temperatures and pressures in the laboratory. In connexion with this work, highly-sensitive methods of estimating dissolved oxygen and copper in feed-water have been devised.

Steam temperature measurement

The accurate measurement of steam temperature is becoming of increasing importance and research has been completed on the

causes of errors in steam-temperature measurements such as poor design of thermometer pocket, incomplete mixing of steam from different sources and the variation in temperature over the cross-section of a steam pipe.

Condenser tubes

Corrosion problems also arise in the low-temperature portion of the steam cycle, and there is need for more information on the corrosion and erosion-resisting qualities of alloys used for condenser tubes. Service trials are therefore continually being made to obtain data on the life and efficiency for different alloys operating under various conditions, such as with sea water, fresh water, sewage effluent, and water with solids in suspension.

In the laboratory measurements are being made of heat transfer through new and used condenser tubes to study the effect of surface conditions and oxide films. It is well-known that the heat transfer coefficient can be increased if the steam condenses on the tubes in the form of drops and not as a film. Various substances have been developed to promote drop-wise condensation, and in collaboration with Queen Mary College (University of London) these materials are being applied to condenser tubes in service to determine their life.

Boiler feed-pump gland seals

Work has recently been started in the laboratory on the performance of various kinds of sealing gland for high-pressure boiler feed pumps. Data are being obtained for plain annular, labyrinth, and helical screw seals with 0.006 in. clearance to the rotating shaft.

Water cooling towers

Cooling towers must be used at stations where there is not an adequate supply of cooling water, and difficulties have often been experienced due to the drizzle produced in the vicinity of the towers. This is particularly objectionable when the temperature is below freezing, as the precipitated moisture will then form a coating of ice on nearby roads. The precipitation is caused by the entrainment of small droplets of water in the air rising through the tower. A small-scale experimental tower in which the rates of flow of air and water can be conveniently controlled was installed at Croydon Testing Station in order to study this problem (Fig. 2). As a result of this work a spray eliminator was designed with a very low resistance to air-flow. The new device, which is relatively inexpensive, has resulted in a very substantial reduction in precipitation without any serious sacrifice in tower performance. Methods of calculating the performance of natural draught water cooling towers have been

developed, and useful design data have been obtained on the heat transfer from water droplets to air and on the pressure drop in various types of cooling tower packing.

Fly ash

The greatly increased use of pulverised fuel firing has led to production of very large quantities of fly ash - about 4×10^6 tons are produced annually in England at present - and problems arise in preventing the emission of ash from chimneys and in disposing of or utilizing the collected ash. The physical and chemical characteristics of fly ash have been studied in order to provide basic data for work on electrostatic precipitation, the dispersal of ash particles from chimneys and various methods of utilization. One of the most important factors in determining the behaviour of the ash is the free-falling speed of the particles in air and apparatus has been developed for grading fly ash in terms of this parameter. An electrostatic precipitator pilot plant has been installed at the laboratory to study the fundamental mechanism of electrostatic precipitation and the effect of different types of electrode and dust characteristics (Fig. 3). A second pilot plant has been erected at Croydon power station for work on flue gas under actual operating conditions.

Concerning the utilization of fly ash, research has been carried out in co-operation with the Building Research Station and other organisations on the use of fly ash for making bricks and building blocks, as a partial replacement for cement in concrete, and as a light-weight aggregate. Work on the mineralogical structure of fly ash and on plant growth in fly ash is being done at several Universities for the Authority.

Turbo-alternators

The vibration of turbine blading is one of the causes of breakdown of turbo-alternator sets and work has been started recently both in the Authority's laboratories and at a University in order to study the natural frequencies of vibration of various types of blade. Operational data on a large number of sets of various designs and vibration measurements in stations will provide a background for this work.

In order to pave the way for higher steam temperatures, research is in progress under the aegis of the Electrical Research Association on the extension of the steam tables and on steels and welded joints for high temperatures.

On the electrical side of the machine, work is being done on stator insulation with a view to developing a site test which will detect faulty insulation before a complete breakdown occurs in service. Research is also in progress on stability problems and on methods of automatic frequency control.

Future energy requirements

The demand for electricity doubles approximately every decade but coal becomes progressively more difficult to mine and the output is remaining fairly constant. It is necessary therefore to use the existing coal more efficiently, and secondly, to find alternative sources of energy.

Progress is being made in the more efficient utilization of coal by using higher steam temperatures and pressures and larger machines. For example, construction has been started on the High Marnham station in Nottinghamshire, which will have five 200 MW sets operating at 1050°F and 2350 lb/in.^{2} with reheating to 1000°F. This station will have a thermal efficiency almost 50 per cent above the present average for all steam stations.

Alternatively, coal could be used more efficiently if the chemical energy in the coal or coal gas were converted into electrical energy in a "fuel cell" without the intermediary of the steam cycle with its inherent thermodynamic limitations. Although fuel cells have been made to work in the laboratory the development of large-scale electricity generation on this principle presents a formidable problem and the prospect becomes relatively less favourable as other energy-converting methods improve in efficiency. Nevertheless the potentialities are so great that the Authority have sponsored work on high-temperature and Redox cells at two Universities and (jointly with the Ministry of Fuel and Power) at a Research Institute.

Considering alternative fuels, oil is being used to an increasing extent in power stations but it is clear that nuclear fuels must take an increasing share in the supply of Britain's energy requirements. The Authority have been co-operating with the U.K. Atomic Energy Authority for some time on the design of nuclear power stations and plans have now been adopted to build twelve stations in the next ten years and thereafter to increase the nuclear power output until it supplies the increase in national load.

3.2 Transmission, Distribution and Utilization Research

Many problems arise in connexion with the design and operation of the 275-kV and 132-kV transmission system and the distribution networks of the Area Boards, and there is scope for research with the objects of improving reliability and decreasing costs.

High-voltage transmission

When it became clear some time ago that higher transmission voltages would be necessary, an experimental high-voltage transmission line was erected at Leatherhead so that data could be

obtained on corona losses and radio noise under various weather conditions at voltages of 275 and 380 kV. The line is 2400 ft long and takes the form of three steel gantries 1200 ft apart from which various arrangements of line conductors can be suspended (Fig. 4). Single and twin conductors have been used and the corona power loss measured in dry weather, rain and snow. Radio noise has also been measured over a frequency range of 0.1 to 150 Mc/s, and figures obtained for the field strength with different conductors and at various distances from the line. Interference with television reception has proved to be a more serious problem than was anticipated, because although the noise field from the line is very much reduced at television frequencies, the level of interference which can be tolerated on the vision channel is much lower than that for a sound channel on the same frequency owing to the wide band-width and other factors. Accordingly the causes of television interference, such as high-resistance contacts between metal fittings in suspension insulator strings are being investigated in some detail. The experimental transmission line is also used for conductor vibration studies, and in particular records are being made of the vibration of single and twin conductors.

Insulators

The flashover of high-voltage insulators in fog or polluted atmospheres is a frequent cause of trouble in heavily industrialised areas. In coastal areas, salt deposited on the insulators is also a source of trouble when gale-force winds blow from the sea. Research on the surface flashover of insulators under such conditions is carried out at Croydon Testing Station where facilities are provided for testing various types of insulator outdoors in a typical polluted atmosphere at voltages of 132 kV, 275 kV and 380 kV (Fig. 5). This work has led to a better understanding of insulator flashover and, in collaboration with the manufacturers, to the development of improved fog-type insulators. In addition, more efficient methods of testing and of cleaning insulators have been devised.

Long-term weathering tests are also made at Croydon on prototype high-voltage plant under conditions simulating the service conditions as closely as possible. In this way weaknesses in lightning arresters, for example, have been discovered before putting the equipment into service.

Conductors

Steel-cored aluminium conductors are mainly used for the transmission lines, and samples of conductor from various parts of the country are examined in the laboratory to ascertain the loss in mechanical strength and determine if replacement is necessary. It has been found that progressive deterioration is occurring in

some industrial and coastal districts. Broadly speaking, two types of corrosion have been encountered: internal corrosion, usually in coastal areas, due to electrolytic action between the aluminium and the steel; and external corrosion, usually in industrial districts, which takes the form of severe pitting on the exposed surface of the aluminium. Methods have been developed of reducing corrosion on new lines by impregnating and coating the conductors with a suitable grease.

Work on new types of overhead-line joints and clamps and on failures in service is continually in progress at the laboratories.

Lightning

Lightning is the greatest single cause of failure of many overhead-line systems, and is responsible for about 40 per cent of the breakdowns on the Grid system. It is natural therefore that supply authorities in all countries should have fostered research on methods of improving the performance of power systems when subjected to surge voltages. In Britain most of the work has been done in co-operation with the Electrical Research Association and the National Physical Laboratory, and some of the more fundamental aspects of electrical discharges are being investigated at Universities. The Authority play an active part in this work and the following lines of investigation are being pursued at present. In the first place, the impulse characteristics of insulating materials, power system plant and protective devices are being studied with the help of the 1400-kV impulse generator at the Leatherhead laboratories. Secondly, radio methods are being used to record atmospherics from lightning flashes. The information obtained is used to give the control engineers objective information on the outbreak of thunderstorms in the areas under their control; the records of atmospherics can also be used as a measure of the severity and frequency of occurrence of thunderstorms. Thirdly, the Authority keep a detailed record of all system breakdowns due to lightning, and a statistical survey of 14 years operating experience has been made to provide a reliable picture of the magnitude of the problem, of the seasonal and diurnal variations in thunderstorm severity and of the fluctuations from year to year. Finally, surge recording instruments, some of a new design, are installed at various points on the system in order to obtain data on the number and magnitude of surges, due to any cause, to which apparatus is subjected in service.

Underground cables

Field trials are made from time to time, in co-operation with the manufacturers, of new designs of high-voltage cable and new types of cable sealing-end. For example, facilities have been provided to test various designs of 275-kV cable by connecting

sample lengths in series with the Staythorpe-West Melton 275-kV line.

Samples of cable from service are frequently examined in the laboratories to find if any deterioration of the paper insulation has occurred.

Attention is also being devoted to the prevention of corrosion of underground cable sheaths, and service experience is being obtained on the efficacy of methods for protecting lead and aluminium cable sheaths. On new cable routes soil samples are examined to determine if the soil is likely to be harmful, and when necessary, special protection is specified for the cable sheath. Examples of sheath corrosion on existing cables are studied in the laboratories, and measurements of stray currents are made in the field with a view to finding the cause and preventing further trouble.

Switchgear and transformer insulation

Every effort is made to forestall major failures of insulation in service by detecting deterioration at an early stage. Various types of testing equipment have been designed for testing insulation in the field by measuring the power factor, the insulation resistance, or some other characteristic of the insulation. In particular, a sensitive and compact electronic megohmmeter was developed, and is widely used for checking the condition of switchgear bushings and other insulating components in the field.

Research on insulating materials forms an important part of the programme of the Leatherhead laboratories; this work is associated partly with service failures and partly with the application of new materials in the supply industry. A D.C. conductivity test has been devised for controlling the condition of insulating oils used in transformers and switchgear. In this connexion the mechanism of conductivity in insulating oil containing very small quantities of free water has been elucidated, and work is in progress on the effect of other impurities, such as metal-organic compounds, on the electrical conductivity. The use of anti-oxidants or inhibitors in transformer oil is being studied; a continuously-recording oxygen absorption apparatus has been constructed in the laboratory to measure the performance of inhibitors, and field trials are being made to obtain practical experience under controlled conditions. Synthetic liquid dielectrics of the chlorinated diphenyl type are also being examined. Some of the work on insulating oils is being done as part of co-operative research programmes organised by the Electrical Research Association or by C.I.G.R.E.

Transformer noise

With the development of the electricity system and the extension of built-up areas, it is inevitable that transformers are more likely to be situated in close proximity to dwelling-houses. The problem of transformer noise is therefore becoming more serious. Complaints of noise are particularly difficult to deal with partly because of the sensitivity of the human ear (it is seldom possible to measure the noise at the position where the complaint is made), and partly because psychological factors are often of importance. There is scope for research on fundamental methods of reducing transformer noise, but it was considered that, from the Authority's point of view, the first step should be to make measurements of the noise emission from transformers of various sizes, and also to obtain data on the attenuation of noise with distance and the effect of screening walls or complete enclosure of the transformer. This work has now been completed and information is available to enable the sound level at a dwelling-house to be estimated in a particular case.

Utilization

As examples of research on utilization, mention may be made of the investigations in progress on district heating, heat pumps, methods of electrical space heating, and the characteristics of industrial, commercial, and domestic loads.

ACKNOWLEDGMENTS

This paper is published by permission of the Central Electricity Authority. The author is indebted to the Authority for making it possible for him to present it in New York and to the American Institute of Electrical Engineers for inviting him to submit it.

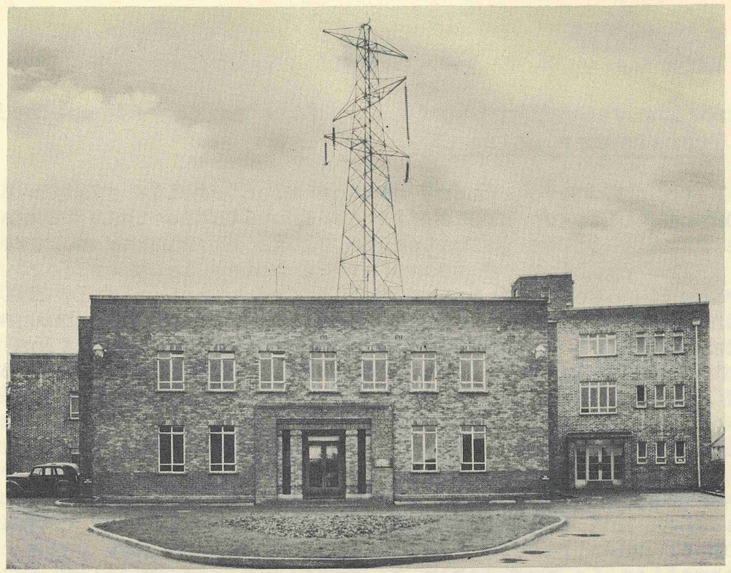

Fig. 1. Central Electricity Authority Research Laboratories at Leatherhead.

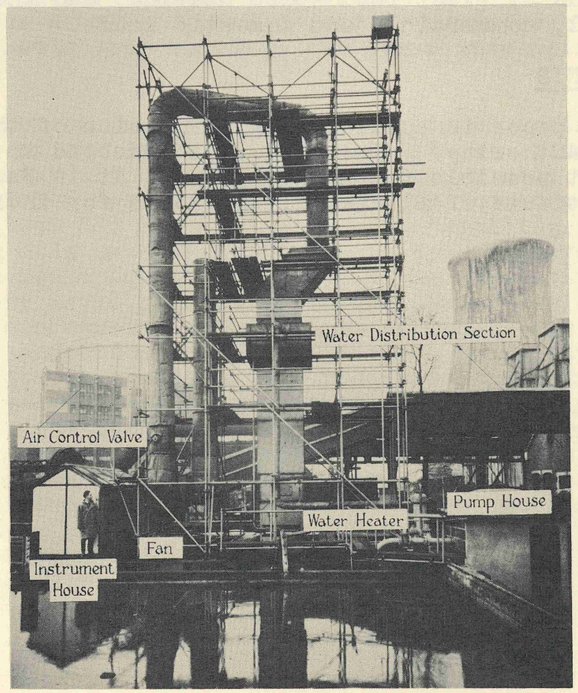

Fig. 2. Experimental water-cooling tower.

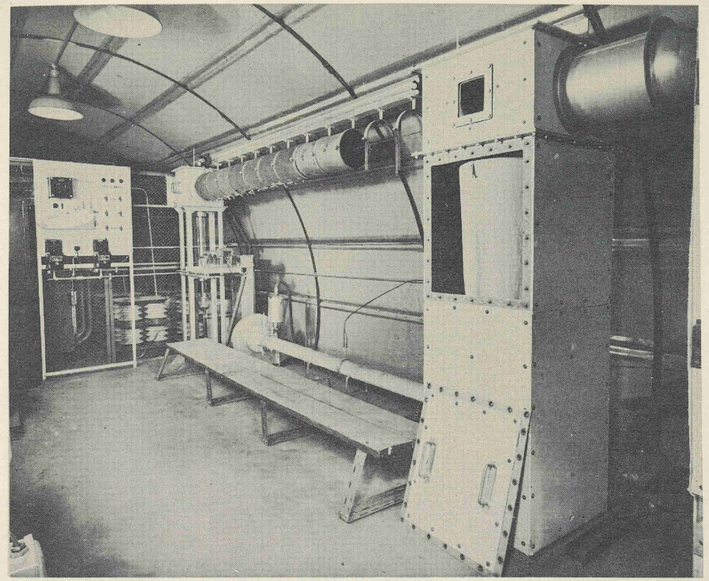

Fig. 3. Electrostatic precipitator pilot plant.

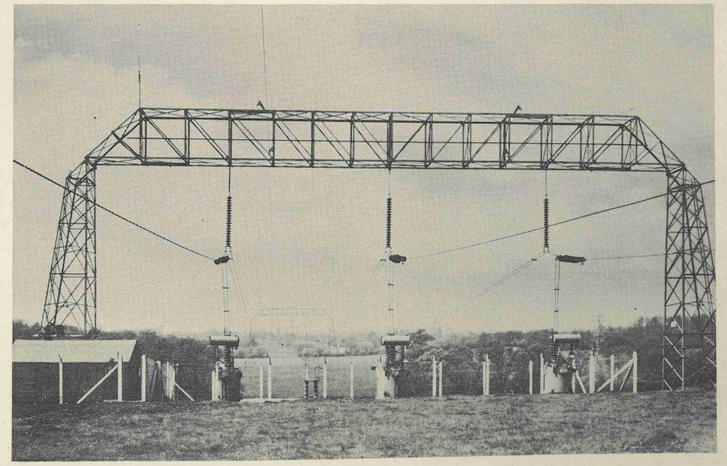

Fig. 4. High-voltage experimental transmission line.

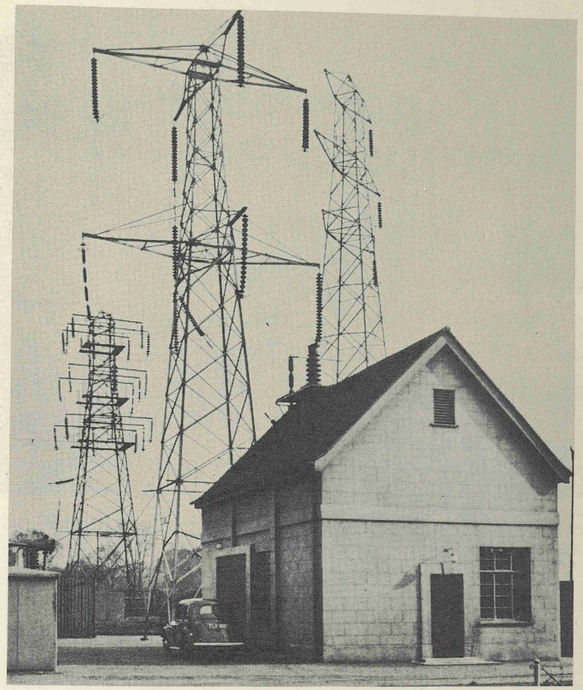

Fig. 5. Croydon Insulator Testing Station.

Conference Paper

RESEARCH BY THE CENTRAL ELECTRICITY AUTHORITY

J. S. Forrest
Nonmember AIEE
Central Electricity Research Laboratories
Leatherhead, Surrey, England

Submitted in abstract or outline form only to the AIEE Committee on Research for the AIEE Winter General Meeting, New York, N. Y., January 30-February 3, 1956. Manuscript submitted November 29, 1955; made available for printing December 9, 1955.

Price: 40¢ To Members
80¢ To Nonmembers

(5¢ per copy additional if first class mailing desired)

All Rights Reserved by the
American Institute of Electrical Engineers
33 West 39th Street, New York 18, N. Y.
Litho in USA

Paper No. CP
56-267

TELEVISION IN THE WORLD TODAY

by

Charles J. Hirsch
Hazeltine Corporation
Little Neck, L.I., N.Y.

A conference paper for presentation at Winter General Meeting of American Institute of Electrical Engineers, New York City, Thursday, February 2, 1956, at 9:30 A.M.

CP 56-354

TELEVISION IN THE WORLD TODAY

INTRODUCTION

The purpose of this report is to discuss the technical standards used for television throughout the world. Eight different sets of standards are in use requiring channel bandwidths of 5, 6, 7, 8, and 14 Mc. Within Europe alone six of these eight standards are currently practiced.

No attempt is made in this report to discuss in detail the reasons for the existence of the multitude of standards. The several systems are described, differences are pointed out, and some comparisons of performance are made, along with some notes on the difficulties which can arise due to the use of many systems.

DESCRIPTION OF STANDARDS

Table I lists the characteristics of the several standards in use at the present time and Table II lists the countries using these standards. The names given to the systems in Table I are those by which the systems are generally known. These, for the most part, are indicative of the country of origin except for system IV. This is usually known as the Gerber system and takes its name from the chairman of a CCIR Study Group XI Committee which recommended the system.

The relative location of sound and picture carriers within the various-width channels is illustrated in Fig. 1.

CHARACTERISTICS COMMON TO ALL STANDARDS

While there are many differences among systems, certain features are common to all. For example all standards now in use:

1. Scan left to right and top to bottom of the picture.

2. Interlace two-to-one.

TABLE I

Characteristics of Television Systems

System	I	II	III	IV	V	VI	VII	VIII
Name of System	British	United States		Gerber	U.S.S.R.	French	Belgian 625	Belgian 819
Number of Lines	405	525	625	625	625	819	625	819
Video Bandwidth Mc	3	4	4	5	6	10.4	5	5
Channel Width Mc	5	6	6	7	8	14	7	7
Sound Carrier Relative to Picture Carrier Mc	-3.5	+4.5	+4.5	+5.5	+6.5	±11.15	+5.5	+5.5
Line Frequency cps	10,125	15,750	15,625	15,625	15,625	20,475	15,625	20,475
Field Frequency cps	50	60	50	50	50	50	50	50
Picture Frequency cps	25	30	25	25	25	25	25	25
Picture Modulation	AM	AM	AM	AM	AM	AM	AM	AM
Sense of Picture Modulation	+	-	-	-	-	+	+	+
Sound Modulation	AM	FM ±25 kc	FM ±25kc	FM ±50 kc	FM ±50 kc	AM	AM	AM
Sync Waveform	Fig. 2	Fig. 3	Fig. 3	Fig. 4	Fig. 4	Fig. 5	Fig. 6,8	Fig. 7,8

TABLE II

Countries Using or Planning to Use the Television Systems of Table I

I	II	III	IV	V	VI	VII	VIII
Great Britain[1]	U.S.A.	Argentina	Norway	U.S.S.R.	France[2]	Belgium	Belgium
Ireland	Canada	Brazil[3]	Sweden	Poland	N. Africa		
New Zealand	Mexico	Venezuela	Denmark	Czechoslovakia	Saar		
	Cuba		Netherlands	E. Germany	Monaco		
	Dominican Republic		Australia	Hungary			
	Guatemala		Austria				
	Uruguay		W. Germany				
	Columbia		Italy				
	Brazil		Luxembourg				
	Philippines		Spain				
	Japan		Switzerland				
	Thailand		Turkey				
	El Salvador						

[1]The London and Northern Ireland transmitters use a 7 Mc channel for double sideband transmission.

[2]Paris has one transmitter operating with 441 lines, AM sound, and 7.6 Mc channel. It is planned to discontinue this channel.

[3]One station in Rio de Janeiro has used this system, but has changed or is about to change to system II.

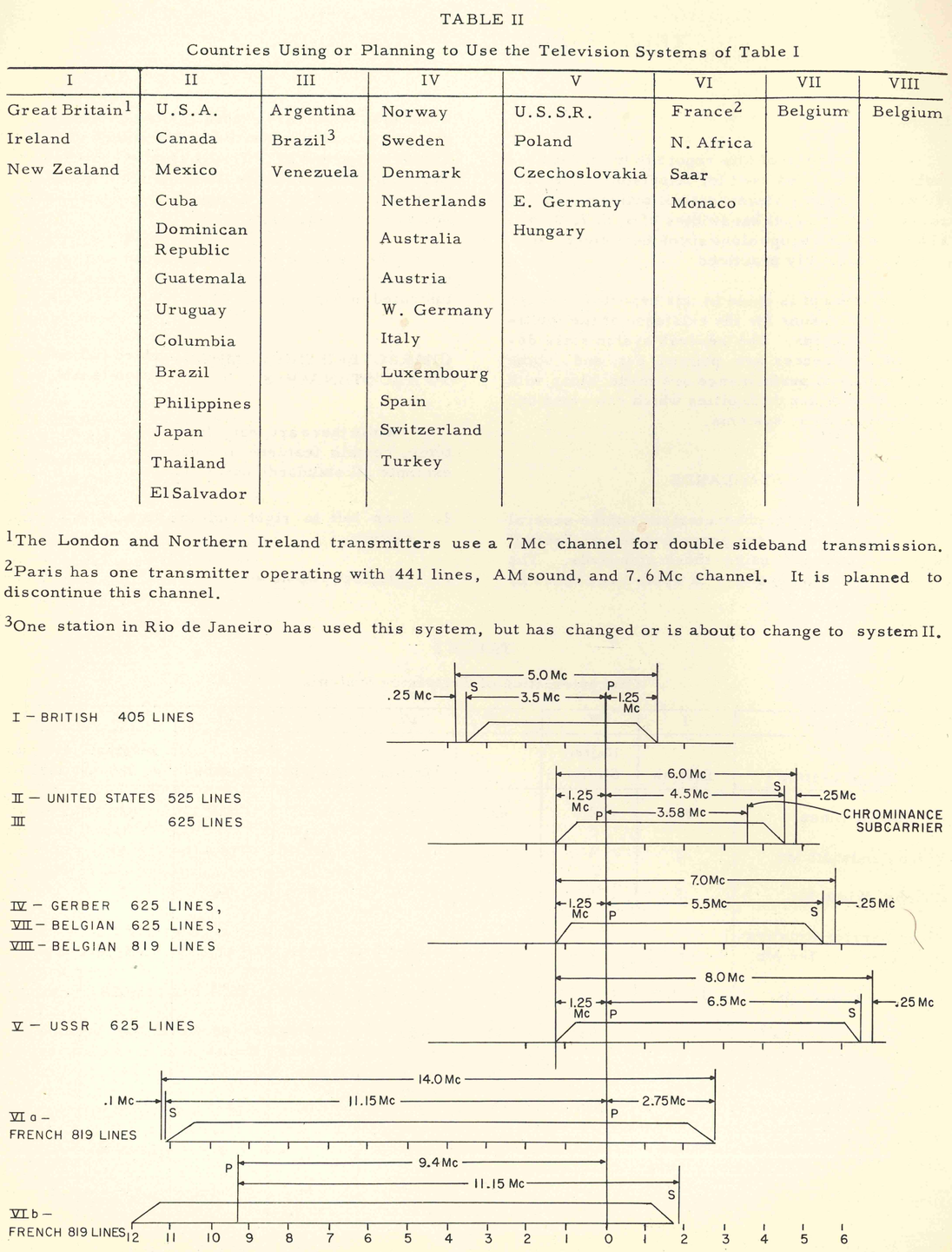

Fig. 1 - Channel Arrangement for Various Systems

3. Use an aspect ratio of four-to-three.

4. Use amplitude modulation for the picture carrier.

5. Use vestigial sideband transmission.

6. Make the black level independent of the picture content (transmit the DC component).

7. Are capable of operating while not synchronized to the electric power systems.

CHARACTERISTICS WHEREIN THE STANDARDS DIFFER

All the systems listed in Table I operate with 50 fields interlaced two-to-one to give 25 pictures per second except the 525 line (United States) system which operates with 60 fields and 30 pictures per second. This difference is primarily due to the use of 50 cycle electric power in Europe and 60 cycle in the United States.

The British 405 line system (system I) is the oldest in operation. Its synchronizing waveform is shown in Fig. 2. It makes no use of equalizing pulses. Positive modulation is used with blanking at 30% and sync at 0-3% of peak white amplitude. The channels are 5 Mc wide with a picture-to-sound carrier spacing of 3.5 Mc. Amplitude modulated sound is used.

The United States 525 line system (system II) uses the synchronizing waveform of Fig. 3. Negative modulation is employed. Blanking occurs at 75% and peak white at 10-15% of peak carrier output. The channels are 6 Mc wide with carrier spacing of 4.5 Mc. Sound is transmitted by FM.

System III has been used to some extent in Latin American countries. Its channel width, carrier spacing, sound and picture modulation, and synchronizing waveform are as used in system II but with 625 lines per picture and 25 pictures per second instead of 525 and 30. This represents only a minor change in horizontal scanning frequency since $525 \times 30 = 15,750$ and $625 \times 25 = 15,625$ lines per second.

The Gerber Standard (system IV) is similar in many respects to the United States system. The channel width and the carrier spacing have been increased to 7 Mc and 5.5 Mc respectively. Negative modulation and FM sound are used. Five equalizing pulses instead of six precede and follow the vertical sync interval which is 2.5 lines in duration instead of three. The synchronizing waveform is shown in Fig. 4.

System V used by the U.S.S.R. and satellite countries differs from system IV only in channel width and carrier spacing which are 8 Mc and 6.5 Mc instead of 7 and 5.5.

The French system (system VI) differs in more respects. Channels are 14 Mc wide with a carrier spacing of 11.15 Mc. Positive modulation is used for the picture information and amplitude modulation for the sound. The number of lines per picture is 819 with 25 pictures per second. No equalizing pulses are used; the vertical sync consists of a single 20 μsec pulse within a 41 line blanking period. The synchronizing waveform is shown in Fig. 5.

The Belgian 625 line system (system VII) uses a 7 Mc channel with 5.5 Mc carrier spacing. Its synchronizing waveform shown in Figs. 6 and 8 is similar to that of the Gerber standard but positive modulation is used. Sound modulation is AM.

The Belgian 819 line system (system VIII) also uses a 7 Mc channel with 5.5 Mc carrier spacing. Here also positive modulation of the picture carrier is employed along with AM sound. The synchronizing waveform shown in Figs. 7 and 8 differs from that of the French 819 line system since here equalizing pulses and normal vertical sync pulses are used. The number of equalizing pulses has been increased to 7 as compared with 6 or 5 for other systems and a proportionate increase has been made in the vertical sync interval.

TECHNICAL CONSIDERATIONS

Picture Repetition Rate

The United States with a 60 cycle electric power system uses 60 fields per second for its television pictures. Europe, with 50 cycle power, uses 50 fields. There are systems operating satisfactorily with 60 fields on 50 cycle power systems in Japan, Thailand, and parts of Latin America. The following paragraphs discuss the factors affecting this choice.

Pictures produced at the rate of 25 per second can be only 16% as bright as those produced under identical conditions at the rate of 30 per second, before the threshold of flicker sets in. However, they can have 20% (30/25 = 1.20) more detail per picture for the same video bandwidth because the information capacity can be used for detail instead of repeating detail already displayed. It appears wrong to many engineers to pay a permanent 20% loss in picture detail just to satisfy the flicker sensitivity of the eye which may be satisfied at a much lower cost. Thus, for example, slow-decaying phosphors, such as those now used in the United States in color television, can produce bright pictures with little flicker although with some blurring on fast motion.

Signal at end of even fields

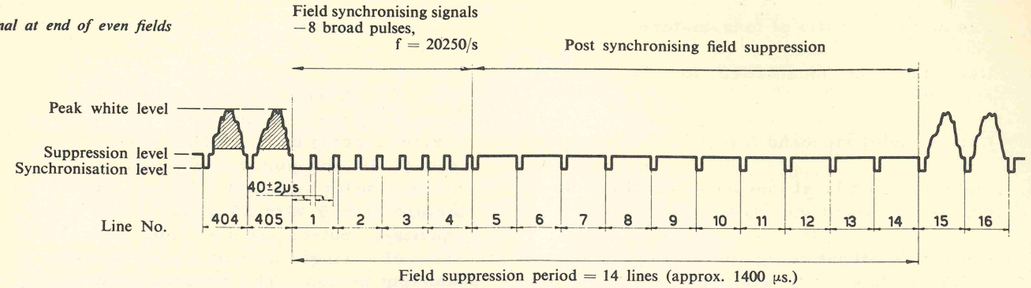

Signal at end of odd fields

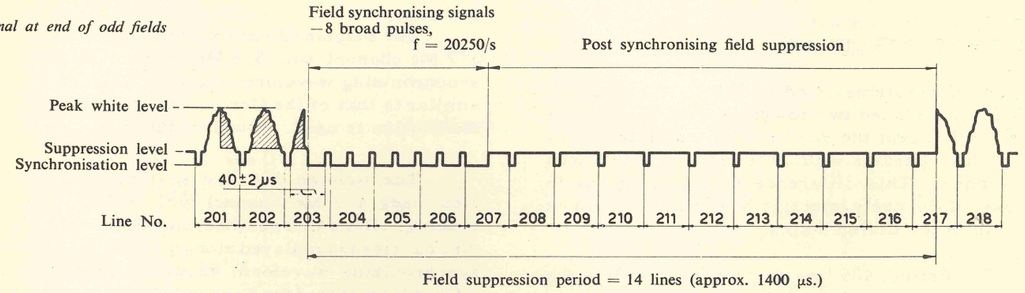

The hatched part of the signal shown can either be occupied by a suppression pulse up to 2 lines in length or by picture signal as shown.
A small pre-synchronising suppression pulse is shown at the opening of the frame suppression. This may be between 0 and 10 µs in length.

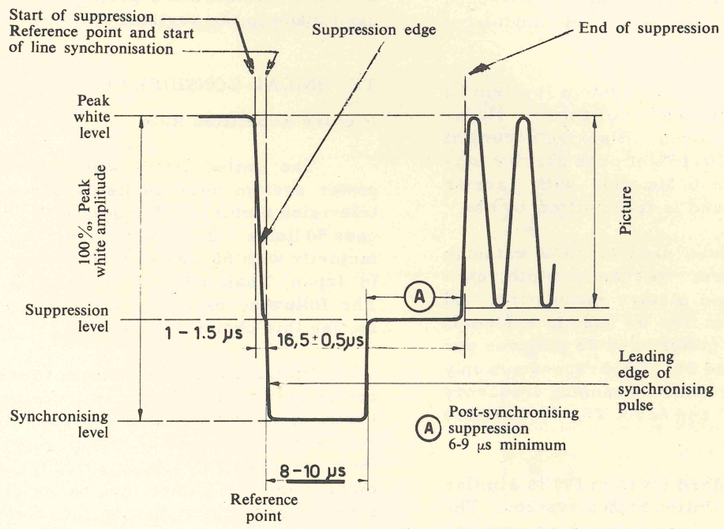

The signal is shown in its video form, but synchronising level corresponds to 0-3%.
Suppression level 30%±3%, and peak white 100% of carrier amplitude.
Time of rise of synchronising pulse (10% to 90%) 0.25 µs.
Time of rise of suppression edge (10% to 90%) should not exceed 1 µs.
Minimum post-synchronising suppression period 6 µs.
Field suppression period 14 lines and variation must be such as not to cause visible jitter on picture
Field frequency is tied to frequency of mains.

Fig. 2 - Synchronizing Waveform, System I

(1) *Even fields*

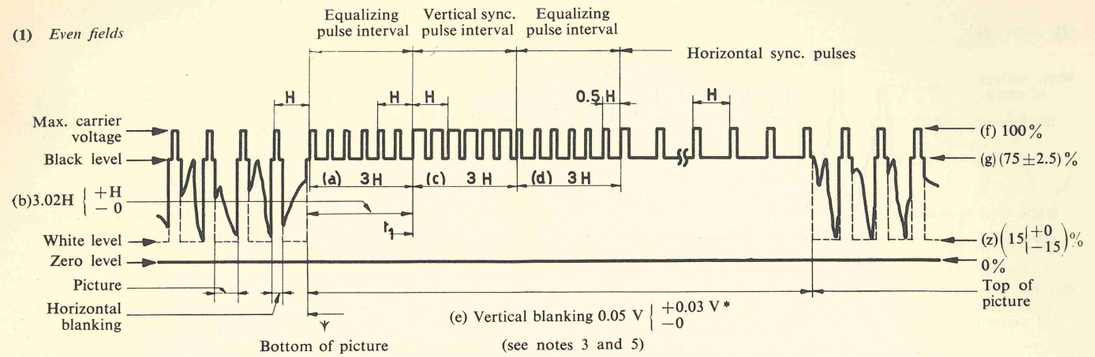

(2) *Odd fields*

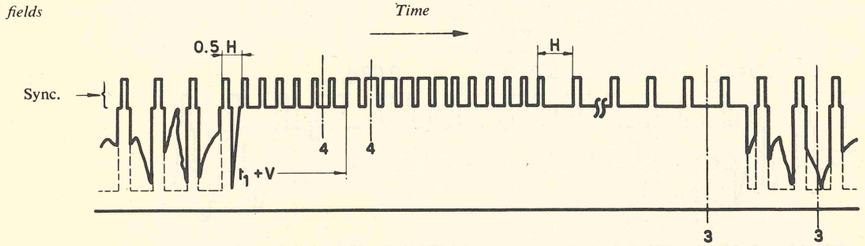

Horizontal dimensions not to scale

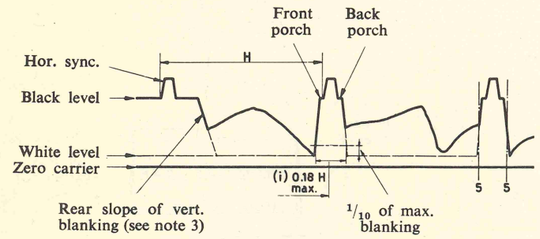

(3) Details between 3-3 in (2)

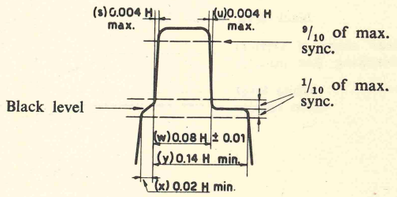

(5) Details between 5-5 in (3)

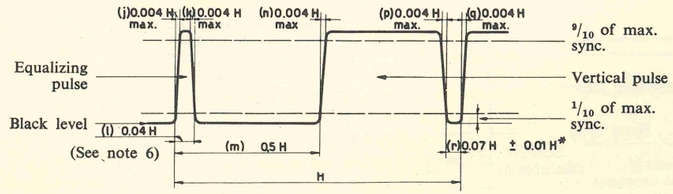

(4) Details between 4-4

Horizontal dimensions not to scale

Fig. 3 - Synchronizing Waveform, Systems II and III

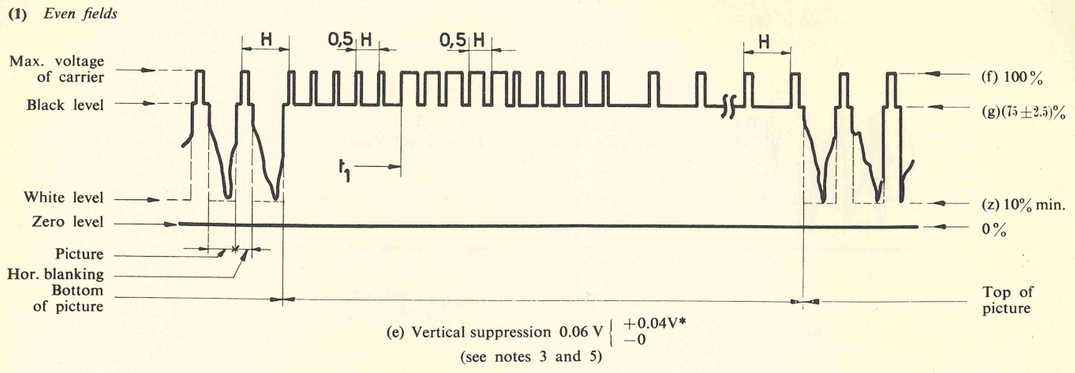

Fig. 4 - Synchronizing Waveform, Systems IV and V

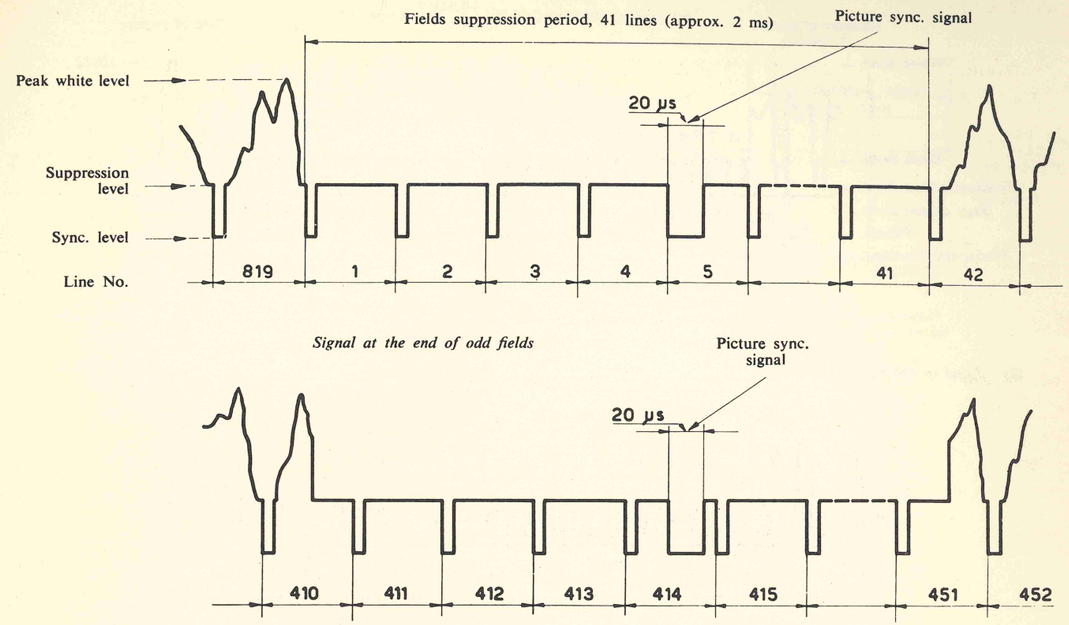

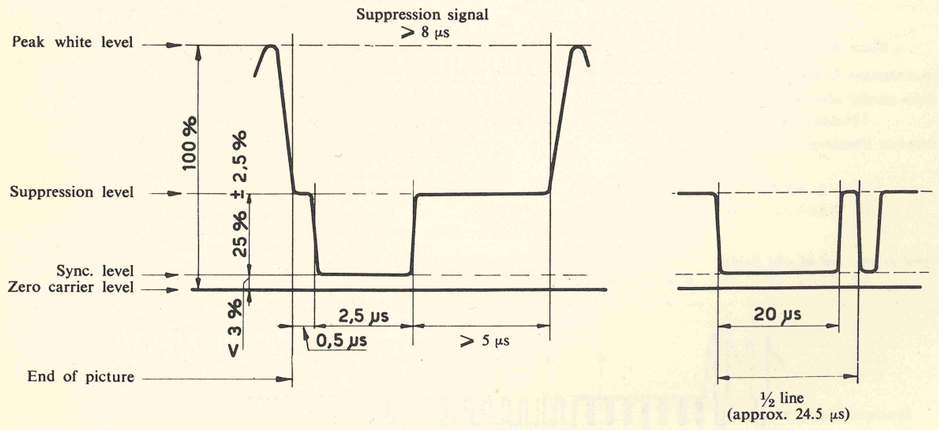

Details of *line* sync. waveform
(High frequency signal)

Details of *picture* sync. signal
(Odd field)

Fig. 5 - Synchronizing Waveform, System VI

(1) *Signal at the end of even fields*

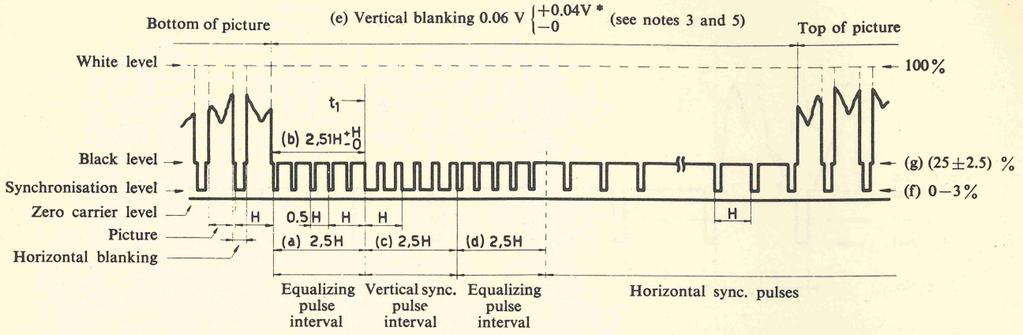

(2) *Signal at the end of odd fields*

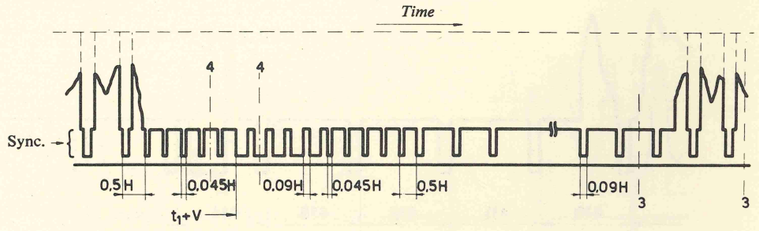

Fig. 6 - Synchronizing Waveform, System VII

(1) *Signal at the end of even fields*

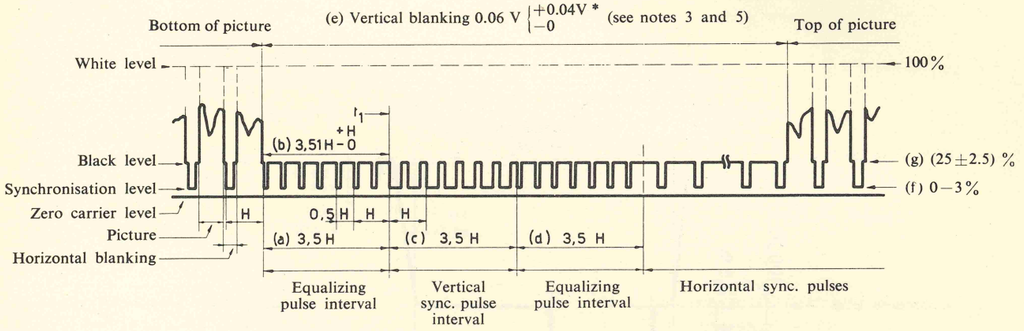

(2) *Signal at the end of odd fields*

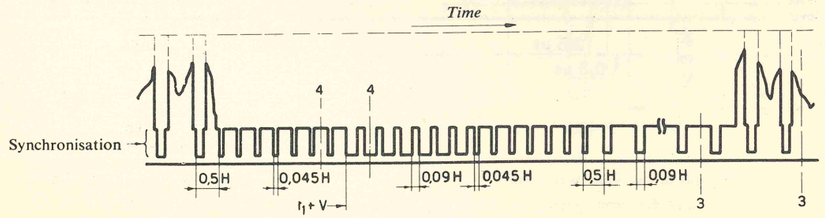

Fig. 7 - Synchronizing Waveform, System VIII

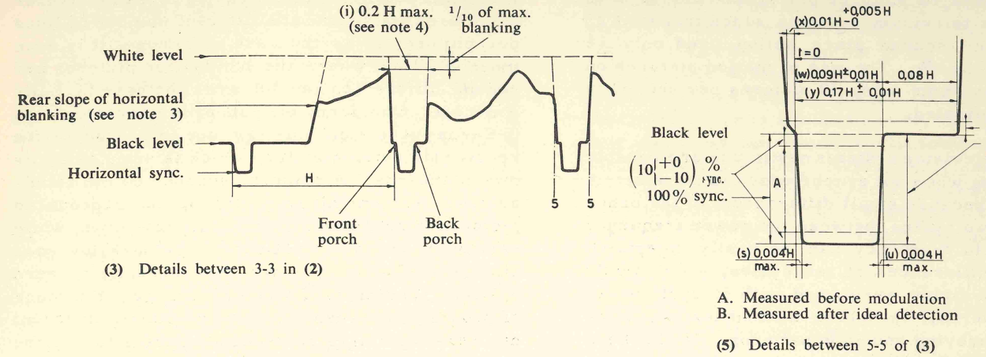

(3) Details betveen 3-3 in (2)

(5) Details between 5-5 of (3)

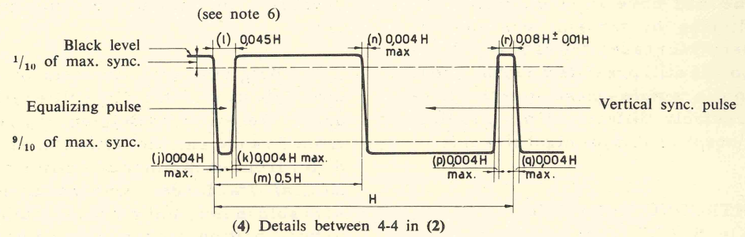

(4) Details between 4-4 in (2)

Fig. 8 - Details of Synchronizing Waveform, Systems VII and VIII

Notes Applying to Figs. 3, 4, 6, 7, and 8

1. H = Time from start of one line to start of next line.
2. V = Time from start of one field to start of next field.
3. Leading and trailing edges of vertical blanking should be complete in less than 0.1 H.
4. Leading and trailing slopes of horizontal blanking must be steep enough to preserve minimum and maximum values of (x + y) and (i) under all conditions of picture content.
5. Dimensions marked with an asterisk indicate that tolerances given are permitted only for long time variations, and not for successive cycles.
6. Equalizing pulse area shall be between 0.45 and 0.5 of the area of a horizontal sync pulse.

Standard motion picture projectors which normally show 24 pictures per second can be used directly on television systems which transmit 25 pictures per second since action need only be speeded up by 4%. The use of motion pictures on television systems using 30 pictures per second is more complicated.

All television systems now in use are capable of operating when not synchronized to the electric power line because small differences, of the order of one or two cycles, between the power frequency and the field frequency can be easily tolerated. However, differences of ten cycles, which would occur if 60 fields were used with 50 cycle power (or vice versa), introduce difficulties such as flicker and moving spurious patterns. While these difficulties can be and have been minimized by adequate hum filtering of transmitters and receivers this remedy increases the cost of all receivers. Some trouble still persists when the scene is illuminated from a single-phase source whose frequency is appreciably different from the field rate such as might occur in outdoor night pickups.

DIFFICULTIES INTRODUCED BY THE MULTIPLICITY OF STANDARDS

The multiplicity of standards results in difficulties with frequency allocation, with the exchange of programs, and complicates those receivers which must receive pictures on multiple standards.

When systems require different channel bandwidths, it is difficult to work out an allocation plan without overlapping some channels. This can produce interference in the overlapping region. Thus, a French 14 Mc channel requires as much spectrum space as two of its neighbors' channels which use only 7 Mc. The interference that can arise from this situation is demonstrated in Fig. 9. This shows the frequency relationships between a station in Koblenz, Germany, and a station in Guebwiller, Alsace, France, approximately 165 miles apart, The German sound carrier can produce a 1.2 Mc beatnote in French pictures. To a lesser degree, the French picture carrier can produce a 4.3 Mc beatnote in the German pictures. The addition of a color subcarrier to the German station (shown as C_K in Fig. 9), can introduce an annoying 200 kc beatnote in receivers tuned to the French station. Likewise, the French picture carrier can interfere with the reception of colored pictures near Koblenz. Since Koblenz uses 625 lines, and Guebwiller uses 819 lines, offset carrier operation cannot be used to reduce the visibility of the interference.

Differences of standards complicate the international exchange of programs. Special techniques are used in Europe where such exchanges are quite frequent. Awkward as it is to exchange programs between systems having the same number of pictures per second and different number of lines per picture, as is the case in Europe, it is even more difficult where the number of pictures per second differs (25 and 30) as is the case in Latin America. One form of standards converter used in Europe uses a cathode ray tube to reproduce the received television picture which is scanned by its own standards. A camera, scanned on the standards to be transmitted, picks up the reproduced picture for retransmission. This technique, while relatively complex, results in remarkably good pictures. Exchanges now occur frequently between almost all countries of Western Europe. Exchange of programs between countries employing different numbers of pictures per second appears to require devices using information storage such as film or tape.

Belgium, with two sets of standards of its own, illustrates the difficulties of multiple standards. Receivers in Belgium can receive programs from France and the Netherlands whose standards differ from each other and differ also from the two Belgian standards. One result is that television sets sold in Belgium must be equipped with at least a two-position switch to receive the two Belgian standards but preferably with a four-position switch to receive all available programs. The same situation exists to a lesser extent in Luxembourg, and along the borders of France. The functions performed by the "standards switch" can be seen by comparing columns IV, VI, VII, and VIII in Table I which lists the characteristics of the different systems. Briefly referring to the table, it is seen that

1. Synchronizing circuits adapted to each system must be switched.

2. The video polarities must be reversed in going from system IV to systems VI, VII, and VIII (or vice versa).

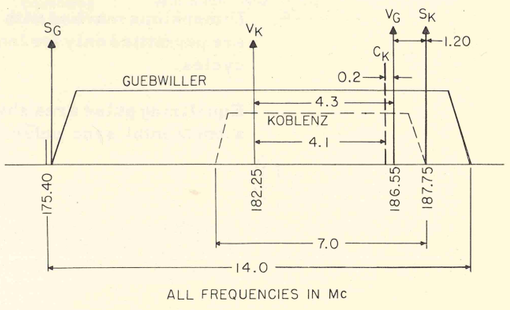

Fig. 9 - Potential Interference Between Systems

3. The scanning frequency must be lowered in going from systems VI and VIII to systems IV and VII.

4. The video bandwidth must be reduced in going from system VI to systems IV, VII, and VIII.

5. The sound system must be changed from FM to AM in going from system IV to systems VI, VII, and VIII.

The 14 Mc bandwidth, required by French standards, seriously reduces the number of channels available wherever this system is used. To provide an adequate number of transmitters, the French have resorted to the so-called "tete-beche" scheme. In this scheme, shown in the lower part of Fig. 1, one section of the radio spectrum is shared by two channels whose transmitters are separated geographically. The relative position, within the passband, of the picture and sound carriers of station 1 are the inverse of the relation for station 2. Only the low energy (high frequency) picture components of station 2 can interfere with the low frequency high energy picture components of station 1. The low frequency components of station 2 which interfere with the fine detail of station 1 can be filtered out at the cost of the fine detail. This scheme can produce high resolution pictures in the vicinity of each transmitter where the interference is low and results in reduced picture detail as the receiving location approaches the interfering station. Recent tests seem to show that the interference is appreciably greater than had been calculated with the result that interference-free coverage is more limited than had been expected.

FREQUENCY BANDS ASSIGNED TO TELEVISION

The Atlantic City Convention in 1947 and subsequent regional authorities allocated the frequency bands shown in Table III for television broadcasting.

TABLE III

Frequency Allocations for Television Broadcasting

Region 1	Band I	Band III	Bands IV & V
Europe, U.S.S. R. inside and outside Europe, Mongolia, Asia Minor, Africa, and additional out-of-band frequencies for:	41-68 Mc	174-216 Mc	470-585 Mc
France		162-174 Mc	
Italy	81-88 Mc		
Belgian, Germany, Switzerland		216-223 Mc	
Region 2			
Western Hemisphere including Hawaii	54-72 Mc 76-88 Mc	174-216 Mc	470-890 Mc
Region 3			
Oceania, Asia (less parts in Region 1)	54-68 Mc 76-88 Mc	174-216 Mc	470-585 Mc 610-940 Mc
Australia	49-56 Mc 63-70 Mc 85-92 Mc 132-146 Mc	174-202 Mc 209-216 Mc	500-855 Mc

RELATIVE PERFORMANCE OF THE DIFFERENT SYSTEMS

The performance of the different systems is compared to that of the United States 525 line system in Table IV and discussed below.

The wider the bandwidth of each channel the fewer the number of channels which can be accommodated. Also, other things being equal, receivers with wide bandwidths cost more. Only the 405 line system is more economical of bandwidth than the 525 line system. (See Item 1 of Table IV).

The brightness at which flicker just appears can be determined from the Ferry-Porter law (see Hazeltine report No. 7142, p. 5). Under equal viewing conditions pictures viewed at 50 fields can only be 0.16 as bright as those viewed at 60 fields. (See Item 2.)

The total number of picture elements per picture is proportional to the video bandwidth divided by the number of pictures per second. Table IV shows that all systems have more detail than the 525 line system except the 405 line system which is quite close. (See Item 4.)

The vertical resolution is proportional to the number of lines if blanking is neglected. Again we see that all systems except the 405 line system are superior in this respect to the 525 line system. (See Item 5.)

The horizontal resolution is proportional to the video bandwidth multiplied by the duration of one line. All systems are at least equal in this respect to the 525 line system except the Belgian 819 line system which is quite close. (See Item 6.)

It should be pointed out that, while there are rather large apparent differences among systems with regard to detail and resolution, these differences are actually of less importance than indicated due to subjective effects in viewing pictures. [1]

ADDITION OF COLOR

All systems can support the addition of a color subcarrier except the French system when it uses the tete-beche scheme. There is a possibility of interference when a non-French transmitter emits color in the vicinity of the French frontier as is discussed above (see Fig. 9). Since all systems have greater horizontal resolution than the 525 line system, the color subcarrier can be placed at a relatively higher frequency than in the United States. This will result in lower visibility of the interfering dot-pattern, or conversely greater luminance resolution.

The 7 Mc (and 8 Mc) systems, except the Belgian 819 line system, might well use their large video bandwidth to achieve better compatibility and simpler color circuits than in the United States. This could be done by choosing a color subcarrier frequency which is about half a megacycle higher (one megacycle for the 8 Mc system) than the United States standard of 3.58 Mc. This will result in better compatibility and luminance resolution by reducing the overlap between the luminance and chrominance signals, and simpler color receiver circuits by allowing essentially symmetrical sidebands for both components of chrominance.

[1] M. W. Baldwin, Jr., The Subjective Sharpness of Television Images, Proc. I.R.E., Vol. 28, pp. 458-468, Oct. 1940.

TABLE IV

Comparison of Performance of Different Television Systems

System	I	II	III	IV	V	VI	VII	VIII
Name of System	British	United States		Gerber	U.S.S.R.	French	Belgian 625	Belgian 819
Number of Lines	405	525	625	625	625	819	625	819
1 - Relative Channel Bandwidth	0.84	1	1	1.17	1.33	2.33	1.17	1.17
2 - Relative Brightness for Threshold of Flicker	0.16	1	0.16	0.16	0.16	0.16	0.16	0.16
3 - Maximum Available Video Bandwidth Mc (Picture Carrier to Sound Carrier Spacing)	3.5	4.5	4.5	5.5	6.5	11.15	5.5	5.5
4 - Relative Number of Picture Elements per Picture	0.93	1	1.2	1.5	1.7	3.0	1.5	1.5
5 - Relative Vertical Resolution	0.8	1	1.2	1.2	1.2	1.6	1.2	1.6
6 - Relative Horizontal Resolution	1.2	1	1	1.2	1.45	1.9	1.2	0.93

TELEVISION IN THE WORLD TODAY

by

Charles J. Hirsch
Hazeltine Corporation
Little Neck, L.I., N.Y.

A conference paper for presentation at Winter General Meeting of American Institute of Electrical Engineers, New York City, Thursday, February 2, 1956, at 9:30 A.M.

CP 56-354

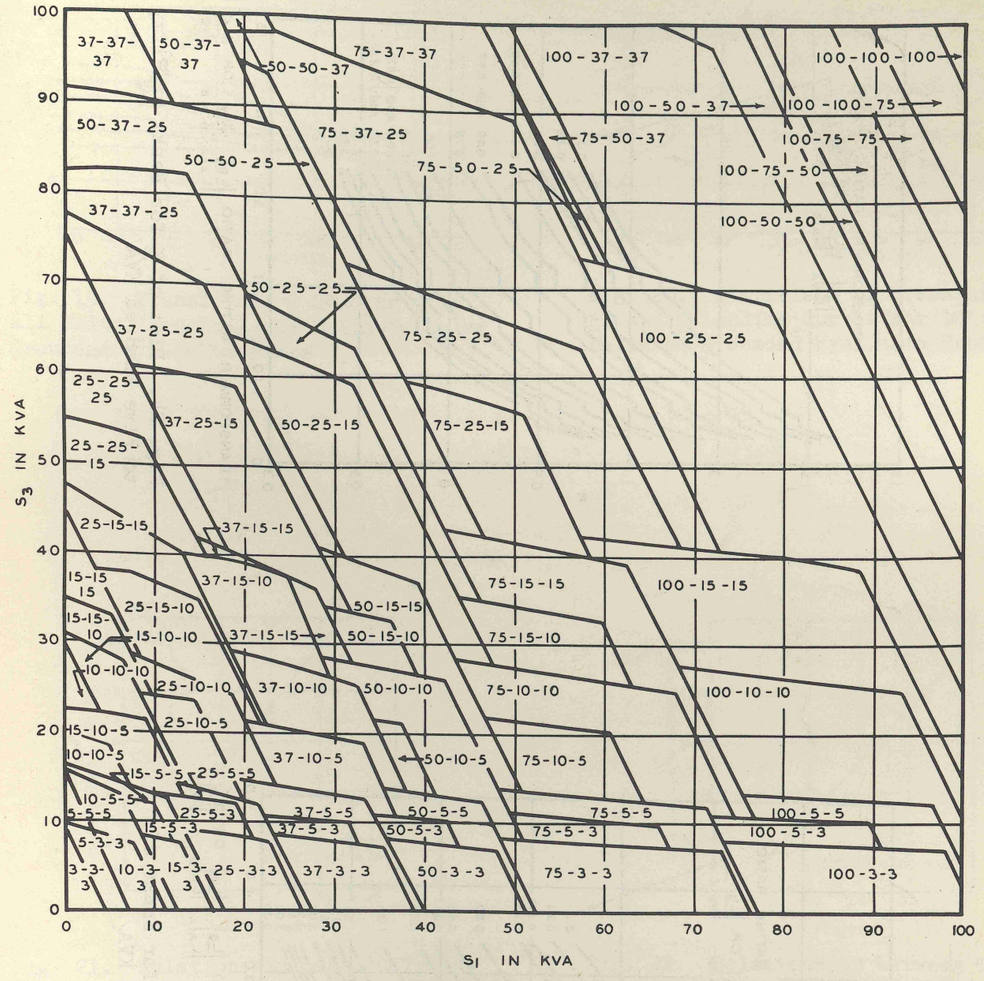

Fig. 25. Preferred Loading Curves with r = 20° for Delta-Delta or Grounded Wye-Delta Banks

RECEIVED
APR -1 1957
ENG. DEPT.

District Conference Paper

UNBALANCED LOADING OF THREE-PHASE TRANSFORMER BANKS

S. W. Anderson
Associate Member AIEE
Middle West Service Company
Chicago, Ill.

RECEIVED
MAR 29 1957
H. A. FREY

A paper recommended by the AIEE Committee on Transmission and Distribution for the AIEE Great Lakes District Meeting, Des Moines, Iowa, April 15-17, 1957. Manuscript submitted January 14, 1957; made available for printing March 14, 1957.

Price: 40¢ To Members
80¢ To Nonmembers
(5¢ per copy additional if first class mailing desired)

All Rights Reserved by the
American Institute of Electrical Engineers
33 West 39th Street, New York 18, N. Y.
Litho in USA

Paper No. DP
57-608

UNBALANCED LOADING OF THREE-PHASE TRANSFORMER BANKS

S. W. Anderson

INTRODUCTION

There appears to be very little published information available on the subject of unbalanced loading of transformers. Yet it is a subject that is becoming of increasing greater importance to both electric utilities and industrial establishments. A certain few authors[1,2,3,4,5] have partially covered the field. However, up to now no thorough analysis appears to be available. Certain "rules of thumb" are available and are quite generally used for selecting transformer sizes. However, in most cases these "rules of thumb" are inadequate, and frequently give incorrect and costly results.

The methods set forth in this study are rigorous and accurate. Yet they are about as simple to use as any approximate method now in use.

ASSUMPTIONS

In this study a number of approximations and assumptions have been made. All transformer banks discussed are made up of single-phase transformers. The exciting branch of each transformer has been ignored on the basis that its effect on the quantities considered will be small. Balanced voltages have been assumed to exist on the primary of any transformer bank.

Grounded wye-delta banks have the characteristic of maintaining three-phase voltage on all three phases beyond a break or open in one phase in the event the grounded wye-delta bank is beyond the break in the phase. Any single-phase load connected to the open phase beyond the break is back fed through the grounded wye-delta bank. Sometimes such load is beyond the capacity of the bank, and the bank is destroyed or damaged. Some companies do not use grounded wye-delta banks for this reason. No account has been taken of this characteristic in this study.

Unbalanced loading is usually confined to distribution transformers. Thus distribution transformer characteristics have been used. Occasionally the problem arises with substation transformers. For such cases, the equations developed in this study are exact. The data pertaining to the particular case under consideration should then be substituted in these equations. It does not appear that it is worth while to develop curves and charts that would apply to substation transformers.

The transformer connections considered are delta-delta, ungrounded wye-delta, grounded wye-delta, and open-delta. The equations for an open-wye open-delta bank are identical with those of an open-delta open-delta bank. In general reference will be made to both cases as open-delta banks in this study. The phase relations of these various cases and a circuit diagram are to be found in Figures 1, 2, 3, 4, 5, and 6.

TRANSFORMER LOADING

The detailed determination of the current and KVA equations is carried out in the Appendix. These equations will now be studied.[6]

Ungrounded Wye-Delta Banks

Equations (37), (38) and (39) of the Appendix may be rearranged as follows:

$$\left|\frac{S_A}{S_3}\right| = \left|\frac{1}{3}\, e^{j0^\circ} + \frac{2}{3}\left|\frac{S_1}{S_3}\right| e^{-jr}\right| \quad - - - - - - - - - - - - - \quad (1)$$

$$\left|\frac{S_B}{S_3}\right| = \left|\frac{1}{3}\, e^{-j60^\circ} + \frac{1}{3}\left|\frac{S_1}{S_3}\right| e^{-jr}\right| \quad - - - - - - - - - - - - - \quad (2)$$

$$\left|\frac{S_C}{S_3}\right| = \left|\frac{1}{3}\, e^{j60^\circ} + \frac{1}{3}\left|\frac{S_1}{S_3}\right| e^{-jr}\right| \quad - - - - - - - - - - - - - \quad (3)$$

Here the vertical lines indicate the absolute value of the quantity enclosed, and the right side of the equation is equal to the ratio of the absolute value of the transformer KVA loading to the absolute value of the three-phase load KVA. Thus if the right side in equations (1), (2), and (3) can be determined, the actual loading on each transformer can easily be determined. It is to be noticed that the expression within the absolute value signs on the right of each equation is the equation of a set of displaced circles and is of the form

$$H\, e^{j\delta} + R\left|\frac{S_1}{S_3}\right| e^{-jr} \quad - - - - - - - - - - - - - \quad (4)$$

This equation can be plotted as in Figures 7, 8, and 9. In these figures O represents the origin, and C the center of the displaced circles. The straight line distance from the point O to any point on one of the circles represents the loading ratio of the left side of Equations (1), (2), and (3) for the particular values of $|S_1|/|S_3|$ and r. Thus a simple convenient method of obtaining the loading on any transformer of an ungrounded wye-delta transformer bank has been obtained. It will be noted that Figures 7, 8, and 9 have been laid out so that an engineers scale can be used to determine loading ratio.

Load limit curves are easily derived from the equations so far presented. Let an expression for $|S_3|$ be derived from each equation in (1), (2), and (3). Let $S_A = L_A$, the maximum allowable load on transformer A, i.e. the load limit of transformer A. Similarly let $S_B = L_B$ and let $S_C = L_C$. Then the following expressions can be obtained:

$$|S_3| = \frac{|L_A|}{\left|\frac{1}{3} + \frac{2}{3}\left|\frac{S_1}{S_3}\right| e^{-jr}\right|} = \frac{|L_A|}{M_A} \quad - - - - - - - - - \quad (5)$$

$$|S_3| = \frac{|L_B|}{\left|\frac{1}{3}\, e^{-j60^\circ} + \frac{1}{3}\left|\frac{S_1}{S_3}\right| e^{-jr}\right|} = \frac{|L_B|}{M_B} \quad - - - - - - - - - \quad (6)$$

$$|S_3| = \frac{|L_C|}{\left|\frac{1}{3}\, e^{j60^\circ} + \frac{1}{3}\left|\frac{S_1}{S_3}\right| e^{-jr}\right|} = \frac{|L_C|}{M_C} \quad - - - - - - - - - \quad (7)$$

Now if each equation is taken in order and the $|L|$ of that equation is let equal 1.00 per unit, for a particular value of r and for various values of the ratio, $|S_1|/|S_3|$, values of M can be determined from Figures 7, 8, and 9. If these values of M are substituted into equations (5), (6), and (7), S_3 and from it S_1 can be determined in per unit of $|L|$. These values can be plotted to give the load limit at that value of r. These curves are shown in Figures 10, 11, and 12. Since the curves are plotted in per unit of allowable transformer load, they are good for any size transformer. Thus only one set of curves need be plotted for the entire range of ungrounded wye-delta transformers from the smallest distribution transformer to the largest power transformer.

It is to be noted that all expressions are independent of all transformer characteristics. Thus the loading of a bank is unchanged by changing any one transformer in the bank, and thus there is one optimum bank combination.

For the case where three-phase power factor is about eighty percent and single-phase power factor is about ninety-five percent, i.e. $r = 20^{o}$, the optimum bank sizes to give no more than 100 percent load on any transformer are as shown in Figure 13 for single-phase and three-phase loads up to 100 KVA.

Open-Delta Banks with Lagging Connection

Lagging connection is defined as that connection that has the single-phase load connected across the transformer through which flows a current that lags that of the other transformer in the bank. The current directions are defined as in Figure 4. The KVA loading equations for the open-delta case in lagging connection are shown in equations (43), (44) and (45) of the Appendix. The loading equation for transformer A is the only one that needs to be considered since the others are simple. It may be rearranged as follows:

$$\left|\frac{S_A}{S_3}\right| = \left|\frac{e^{j30^{o}}}{\sqrt{3}} + \left|\frac{S_1}{S_3}\right| e^{-jr}\right| \quad - - - - - - - - - - - - - - \quad (8)$$

Again it is to be noticed that the expression within the absolute value signs on the right of equation (8) is similar to equation (4) and thus is the equation of a set of displaced circles. It can be plotted as in Figure 14 where O_{Lag} is the origin. The distance from point O_{Lag} to some point on the general circles in this figure can be used, as in Figures 7, 8, and 9, to determine the loading on the lagging transformer when the bank is connected so that the single-phase load is across the lagging transformer.

Load limit curves may be derived for the lagging transformer of the open-delta bank in the same manner as for the ungrounded wye-delta bank. The following expression is the equation from which they may be derived:

$$|S_3| = \frac{|L_A|}{\left|\frac{1}{\sqrt{3}} e^{j30^{o}} + \left|\frac{S_1}{S_3}\right| e^{-jr}\right|} \quad - - - - - - - - - - - - - - \quad (9)$$

The curves derived from this equation are plotted in Figure 15.

For the case where three-phase power factor is about eighty percent and single-phase power factor is about ninety-five percent, i.e. $r = 20^{o}$, the optimum open-delta bank sizes to give no more than 100 percent load on any transformer are as shown in Figure 16 for single-phase and three-phase loads up to 100 KVA.

Open-Delta Banks with Leading Connection

Leading connection is defined as that connection where the single-phase load is connected across the leading transformer of the bank. Here the current directions are defined as in Figure 5. The KVA loading equations for the open-delta case in leading connection are shown in equations (49), (50), and (51) of the Appendix. The loading equation for Transformer A is the only one that needs to be considered since the others are simple. It may be rearranged as follows:

$$\left|\frac{S_A}{S_3}\right| = \left|\frac{1}{\sqrt{3}} e^{-j30^{o}} + \left|\frac{S_1}{S_3}\right| e^{-jr}\right| \quad - - - - - - - - - - - - - - \quad (10)$$

Again this can be plotted as a set of circle diagrams and this has been done on Figure 14 with O_{Lead} considered as the origin. Load limit curves have been plotted on Figure 15. It can be noticed from Figure 15, that for certain values of r, the load on the transformer connected across the single-phase load is less for the one connection than for the other. Thus for a particular load one connection may require smaller transformers than the other connection, and thus there is a saving that may be realized by picking the connection that requires the smallest bank.

Open-Delta Banks with Open Connection

Open connection is defined as that connection where the single-phase load is connected across the open leg of the bank. The KVA loading equations are shown by equations (55), (56), and (57) of the Appendix. The loading equation for Transformer B is trivial. However, the equations for Transformers A and C may be rearranged as follows:

$$\left|\frac{S_A}{S_3}\right| = \left|\frac{1}{\sqrt{3}} e^{j30^{o}} + \left|\frac{S_1}{S_3}\right| e^{-jr}\right| \quad - - - - - - - - - - - - - - \quad (11)$$

$$\left|\frac{S_C}{S_3}\right| = \left|\frac{1}{\sqrt{3}} e^{-j30^{o}} + \left|\frac{S_1}{S_3}\right| e^{-jr}\right| \quad - - - - - - - - - - - - - - \quad (12)$$

It will be noticed that equation (11) is identical with equation (8) and equation (12) is identical with equation (10). Therefore both of these equations are represented by the circle diagrams of Figure 14 and the load limit curves of Figure 15.

Delta-Delta and Grounded Wye-Delta Banks

As is shown in the Appendix, the loading equations of these two connections are identical. Thus the following discussion applies to both cases. The loading equations derived in the Appendix are as follows:

$$S_A = \left[\frac{Z_b}{Z_a+Z_b+Z_c}\right]^{*} \left[\left(\frac{Z_c}{Z_b} a^2-a\right)^{*} \frac{|S_3|}{\sqrt{3}} + \left(\frac{Z_c}{Z_b}+1\right)^{*} |S_1| e^{-j(r-90^{o})}\right] e^{j(\theta-90^{o})} \quad (13)$$

$$S_B = \left[\frac{Z_a}{Z_a+Z_b+Z_c}\right]^{*} \left[\left(\frac{Z_c}{Z_a} -a\right)^{*} \frac{|S_3|}{\sqrt{3}} + |S_1| e^{-j(r-90^{o})}\right] e^{j(\theta+150^{o})} \quad - - - \quad (14)$$

$$S_C = \left[\frac{Z_a}{Z_a+Z_b+Z_c}\right]^{*} \left[\left(\frac{Z_b}{Z_a} -a^2\right)^{*} \frac{|S_3|}{\sqrt{3}} + |S_1| e^{-j(r+90^{o})}\right] e^{j(\theta+30^{o})} \quad - - \quad (15)$$

It is to be noted here that if all transformers in a bank, and thus presumably all impedances, are exactly alike, that equations (13), (14), and (15) degenerate to the equations (37), (38), and (39) of the Appendix, and thus act as if the bank were an ungrounded wye-delta bank. Loading circles and load limit curves for this case only are as shown in Figures 7, 8, 9, 10, 11, and 12. It is of some interest to see how the transformer loading varies with power factor angle for the case where all transformer impedances are identical. Transformer loading ratio is plotted versus r for all transformers in the bank in Figures 17, 18, and 19. A comparison of the three for one value of $|S_1|/|S_3|$ is plotted in Figure 20.

Equations (13), (14), and (15) have six unknowns to deal with, too many to be handled readily. However, they can be put into the following form:

$$\left|\frac{S_A}{S_3}\right| = \left| \frac{(\frac{Z_c}{Z_b} a^2 - a)^*}{\sqrt{3}(1 + 2\frac{Z_c}{Z_b})^*} + \frac{(1 + \frac{Z_c}{Z_b})^*}{(1 + 2\frac{Z_c}{Z_b})^*} \left|\frac{S_1}{S_3}\right| e^{-j(r-90)} \right| \times \left| \frac{(1 + 2\frac{Z_c}{Z_b})^*}{(1 + \frac{Z_c}{Z_b} + \frac{Z_a}{Z_b})^*} \right| \qquad (16)$$

$$\left|\frac{S_B}{S_3}\right| = \left| \frac{(\frac{Z_c}{Z_a} - a)^*}{\sqrt{3}(1 + 2\frac{Z_c}{Z_a})^*} + \frac{1}{(1 + 2\frac{Z_c}{Z_a})^*} \left|\frac{S_1}{S_3}\right| e^{-j(r-90)} \right| \times \left| \frac{(1 + 2\frac{Z_c}{Z_a})^*}{(1 + \frac{Z_c}{Z_a} + \frac{Z_b}{Z_a})^*} \right| \qquad (17)$$

$$\left|\frac{S_C}{S_3}\right| = \left| \frac{(\frac{Z_b}{Z_a} - a^2)^*}{\sqrt{3}(1 + 2\frac{Z_b}{Z_a})^*} + \frac{1}{(1 + 2\frac{Z_b}{Z_a})^*} \left|\frac{S_1}{S_3}\right| e^{-j(r+90)} \right| \times \left| \frac{(1 + 2\frac{Z_b}{Z_a})^*}{(1 + \frac{Z_c}{Z_a} + \frac{Z_b}{Z_a})^*} \right| \qquad (18)$$

These expressions, while they look complicated, are much simpler to handle than those of equations (13), (14), and (15), for it may readily be seen that the following expressions are true:

$$\left|\frac{S_A}{S_3}\right| = M_A\left(\frac{Z_c}{Z_b}, \left|\frac{S_1}{S_3}\right|, r\right) \times K_A\left(\frac{Z_c}{Z_b}, \frac{Z_a}{Z_b}\right) \quad - - - - - - - - - \qquad (19)$$

$$\left|\frac{S_B}{S_3}\right| = M_B\left(\frac{Z_c}{Z_a}, \left|\frac{S_1}{S_3}\right|, r\right) \times K_B\left(\frac{Z_c}{Z_a}, \frac{Z_b}{Z_a}\right) \quad - - - - - - - - - \qquad (20)$$

$$\left|\frac{S_C}{S_3}\right| = M_C\left(\frac{Z_b}{Z_a}, \left|\frac{S_1}{S_3}\right|, r\right) \times K_C\left(\frac{Z_c}{Z_a}, \frac{Z_b}{Z_a}\right) \quad - - - - - - - - - \qquad (21)$$

Here the M's are made up of three unknowns and the K's are made up of two unknowns. The value of M may be calculated separately, the value of K may be calculated separately, and their product is the desired expression.

For large banks, the impedance ratios are approximately real numbers. However, for distribution banks this is not quite true and the impedance ratios are actually complex numbers.

It appears that a discussion of the impedance ratios is in order, particularly with respect to the constant K since it is desirable to plot K versus transformer KVA ratio. If transformer KVA is plotted against the reciprocal of the percent impedance with all percent impedances converted to the same base, a straight line is obtained as is shown in Figures 21 and 22. Note that for transformer sizes of one hundred KVA and below the straight line goes through the origin, while from fifty to five hundred KVA the straight line does not go through the origin. Above five hundred KVA too many other factors such as type of cooling influence the percent impedance so that it appears a straight line relationship may no longer be used.

Circle Diagrams to determine M can be drawn for all possible combinations of transformers. However, this seems impractical. If the angles of the impedance ratios were

all alike, circle diagrams would need only be drawn for the various transformer KVA ratios, and not for every possible transformer combination, thus greatly reducing the volume of work. The phase angle of the impedance ratios for distribution size transformers varies from minus thirteen degrees to plus twenty-five degrees. However, the angles of various transformer combinations that have the same ratio are surprisingly similar. If the mean ratio angle is used, the relationships shown in Table I are valid for transformers from three to one hundred KVA and would introduce a small error only, if used. Thus in this study, data for circle diagrams and the values of K have been determined only for the general transformer KVA ratios and not for every possible bank in the three to one hundred KVA sizes.

In the fifty to five hundred KVA sizes a further complication is introduced by the fact that the KVA ratios are not inversely proportional to impedance ratio. Instead the following transformation may be used:

$$\frac{|L_1| + 50}{|L_2| + 50} = \frac{Z_2}{Z_1} \quad - - - - - - - - - - - - - - - - \qquad (22)$$

This can be derived from Figure 22. This transformation was used in this study to determine data for the circle diagrams and for the values of K.

In general equations (16), (17), and (18) are of the form

$$\left|\frac{S}{S_3}\right| = K \times \left| He^{j\delta} + R\left|\frac{S_1}{S_3}\right| e^{-jr} \right| = KM, \quad - - - - - - - - - \qquad (23)$$

where

$$M = He^{j\delta} + R\left|\frac{S_1}{S_3}\right| e^{-jr} \quad - - - - - - - - - - - - - - \qquad (24)$$

By making use of the impedance relationships of Table 1 the values of H, R, and δ have been determined for the most probable transformer ratios and have been listed in Tables II, III, and IV for transformers of three to one hundred KVA. They have also been determined for transformers of fifty to five hundred KVA and have been listed in Tables V, VI, and VII. From these values of H, R, and δ, circle diagrams to determine M can be easily set up. Values of K have also been determined and have been plotted in Figure 23 for transformers from three to one hundred KVA and in Figure 24 for transformers from fifty to five hundred KVA. Then with K determined from the curves of Figure 23 and 24 and with M determined from the circle diagrams, their product is easily determined. Thus a fairly simple method has been derived for determining the loading of the transformers in a delta-delta or grounded wye-delta transformer bank.

Load limit curves could also be set up for delta-delta or grounded wye-delta banks. The same procedure would be followed as previously. However, a large number of such curves would need be set up and it is felt that it is not desirable to include them in this paper; however, each individual may set up his own as needed.

A plot of the preferred transformer bank sizes for three-phase loads of 80 percent power factor and single-phase loads of 95 percent power factor has been included in Figure 25 and has been set up so that no transformer in any bank carries more than its rated load. If some other limit is desired, the abscissa and ordinate of Figure 25 and incidentally also Figures 13 and 16 should be multiplied by the ratio of the desired limit to rated limit.

CONCLUSIONS

A number of conclusions may be drawn from the preceding investigation. They are as follows:

1. Transformer loading in an ungrounded wye-delta transformer bank is independent of the transformer characteristics and depends only upon the load. Thus there is one optimum size transformer bank that will most nearly match the loading due to a particular unbalanced load.

2. Transformer loading may be very simply determined by a set of circle diagrams. Three sets of circle diagrams are sufficient for any size bank of ungrounded wye-delta transformers.

3. Load limit curves may be set up to handle any combination of unbalanced loads on an ungrounded wye-delta transformer bank. Three sets of curves are sufficient to handle all transformers.

4. Transformer loading in an open-delta transformer bank is independent of the transformer characteristics and depends only upon the load. Thus there is one optimum size transformer bank that will most nearly match the loading due to a particular unbalanced load.

5. In general for an open-delta bank the leading connection with currents defined as in Figure 5 and in the text, the lagging connection with currents defined as in Figure 4 and in the text, and the open connection all load differently. Each should be investigated for a particular load in order that the smallest bank size be used. At power factors normally encountered, the lagging connection usually requires the smallest bank size.

6. Transformer loading in an open-delta bank may be very easily determined from a set of circle diagrams.

7. Load limit curves may be set up to handle any combination of unbalanced loads on an open-delta transformer bank.

8. Transformer loading in a delta-delta or grounded wye-delta bank of transformers is dependent upon the transformer impedances in addition to the power factors and the magnitudes of the single-phase and three-phase loads. For the standard distribution transformers in use, there is one optimum size of transformer bank that will most nearly match the loading due to a particular unbalanced load.

9. Transformer loading in a delta-delta or ungrounded wye-delta bank may be very easily determined by means of circle diagrams. However, in general, in order to cover the range of possible combinations, a large number of circle diagrams will be required. Data for these circles and charts giving the K multiplier are presented here.

10. Load limit curves may be set up following the procedure set forth previously. In general a large number would be required.

APPENDIX

DETERMINATION OF THE LOADING EQUATIONS

Ungrounded Wye-Delta Transformer Banks

From Figure 2 the following current equations are derivable:

$$I_a = I_1 = I_L\, e^{-j\theta} \quad - - - - - - - - - - - - - \quad (25)$$

$$I_b = I_2 + I'' = I_L\, e^{-j(120+\theta)} + I'\, e^{-j(90+\phi)} \quad - - - - - - - - \quad (26)$$

$$I_c = I_3 - I'' = I_L\, e^{-j(240+\theta)} - I'\, e^{-j(90+\phi)} \quad - - - - - - - - \quad (27)$$

The following equations follow from Kirchhoff's laws:

$$I_a = I_{ba} - I_{ac} \quad - - - - - - - - - - - - - - - \quad (28)$$

$$I_b = I_{cb} - I_{ba} \quad - - - - - - - - - - - - - - - \quad (29)$$

$$n(I_{ba} + I_{cb} + I_{ac}) = 0 \quad - - - - - - - - - - - - - - \quad (30)$$

If equations (28), (29), and (30) are solved simultaneously for I_{ba}, I_{ac}, and I_{cb}, the following equations result:

$$I_{cb} = \frac{1}{3} I_a + \frac{2}{3} I_b \quad - - - - - - - - - - - - - - \quad (31)$$

$$I_{ac} = \frac{-2}{3} I_a - \frac{1}{3} I_b \quad - - - - - - - - - - - - - - \quad (32)$$

$$I_{ba} = \frac{1}{3} I_a - \frac{1}{3} I_b \quad - - - - - - - - - - - - - - \quad (33)$$

If equations (25), (26), and (27) are substituted into equations (31), (32), and (33) the following equations result:

$$I_{cb} = \frac{\sqrt{3}}{3} I_L\, e^{-j(\theta+90)} + \frac{2}{3} I'\, e^{-j(\phi+90)} \quad - - - - - - - - \quad (34)$$

$$I_{ac} = \frac{\sqrt{3}}{3} I_L\, e^{-j(\theta-150)} + \frac{1}{3} I'\, e^{-j(\phi-90)} \quad - - - - - - - - \quad (35)$$

$$I_{ba} = \frac{\sqrt{3}}{3} I_L\, e^{-j(\theta-30)} + \frac{1}{3} I'\, e^{-j(\phi-90)} \quad - - - - - - - - \quad (36)$$

Now

$$S_A = E_{cb}\, I_{cb}^* = E_L\, e^{-j90^\circ} \left[\frac{\sqrt{3}}{3} I_L\, e^{j(\theta+90)} + \frac{2}{3} I'\, e^{j(\phi+90)} \right]$$

$$S_A = \sqrt{3}\, \frac{E_L\, I_L}{3}\, e^{j\theta} + \frac{2}{3} E_L\, I'\, e^{j\phi}$$

$$S_A = \frac{|S_3|\, e^{j\theta}}{3} + \frac{2}{3} |S_1|\, e^{j\phi} \quad - - - - - - - - - - - - \quad (37)$$

$$S_B = \frac{|S_3|\, e^{j\theta}}{3} + \frac{|S_1|}{3}\, e^{j(\phi+60)} \quad - - - - - - - - - - - - \quad (38)$$

$$S_C = \frac{|S_3|\, e^{j\theta}}{3} + \frac{|S_1|}{3}\, e^{j(\phi-60)} \quad - - - - - - - - - - - - \quad (39)$$

Open-Delta Banks with Lagging Connection

From Figure 4 the following current equations may be derived:

$$I_{ca} = I_a = I_1 = I_L\, e^{-j\Theta} \quad - - - - - - - - - - - - - - - \quad (40)$$

$$I_{cb} = I_b = I'' + I_2 = I_L\, e^{-j(\Theta+120)} + I'\, e^{-j(\phi+90)} \quad - - - - - - \quad (41)$$

$$I_{ab} = 0 \quad - - - - - - - - - - - - - - - - - \quad (42)$$

The expressions for $\underline{S}$ may be derived as follows:

$$S_A = E_{cb}\, I_{cb}{}^* = E_L\, e^{-j90^\circ} \left[I_L\, e^{+j(\Theta+120)} + I'\, e^{+j(\phi+90)}\right]$$

$$S_A = \frac{|S_3|}{\sqrt{3}}\, e^{j(\Theta+30^\circ)} + |S_1|\, e^{j\phi} \quad - - - - - - - - - - - \quad (43)$$

$$S_B = \frac{|S_3|}{\sqrt{3}}\, e^{-j(\Theta+30^\circ)} \quad - - - - - - - - - - - - \quad (44)$$

$$S_C = 0 \quad - - - - - - - - - - - - - - - - \quad (45)$$

Open-Delta Banks with Leading Connection

From Figure 5 the following current equations may be derived:

$$I_{ba} = I_a = I_1 = I_L\, e^{-j\Theta} \quad - - - - - - - - - - - - - - \quad (46)$$

$$I_{bc} = I_c = I_3 - I'' = I_L\, e^{-j(\Theta+240^\circ)} - I'\, e^{-j(\phi+90^\circ)} \quad - - - - - \quad (47)$$

$$I_{ac} = 0 \quad - - - - - - - - - - - - - - - - \quad (48)$$

The expression for $\underline{S}$ may be derived as follows:

$$S_A = E_{bc}\, I_{bc}{}^* = E_L\, e^{j90^\circ} \left[I_L\, e^{j(\Theta-120^\circ)} + I'\, e^{j(\phi-90^\circ)}\right]$$

From this S_A is as shown below with S_B and S_C similarly derived:

$$S_A = \frac{|S_3|}{\sqrt{3}}\, e^{j(\Theta-30^\circ)} + |S_1|\, e^{j\phi} \quad - - - - - - - - - - - \quad (49)$$

$$S_B = 0 \quad - - - - - - - - - - - - - - - - \quad (50)$$

$$S_C = \frac{|S_3|}{\sqrt{3}}\, e^{j(\Theta+30^\circ)} \quad - - - - - - - - - - - - \quad (51)$$

Open-Delta Banks with Open Connection

From Figure 6 the following current equations may be derived:

$$I_{bc} = I_c = I_3 + I'' = I_L\, e^{-j(\Theta+240^\circ)} + I'\, e^{-j(\phi-150^\circ)} \quad - - - - - \quad (52)$$

$$I_{ba} = I_a = I_1 - I'' = I_L\, e^{-j\Theta} - I'\, e^{-j(\phi-150^\circ)} \quad - - - - - - - \quad (53)$$

$$I_{ac} = 0 \quad - - - - - - - - - - - - - - - - \quad (54)$$

The expressions for $\underline{S}$ may be derived as follows:

$$S_A = E_{bc}\, I_{bc}{}^* = E_L\, e^{j90^\circ} \left[I_L\, e^{j(\Theta+240^\circ)} + I'\, e^{j(\phi-150^\circ)}\right].$$

From this S_A is as shown below with S_B and S_C similarly derived:

$$S_A = \frac{|S_3|}{\sqrt{3}}\, e^{j(\Theta-30^\circ)} + |S_1|\, e^{j(\phi-60^\circ)} \quad - - - - - - - - \quad (55)$$

$$S_B = 0 \quad - - - - - - - - - - - - - - - - \quad (56)$$

$$S_C = \frac{|S_3|}{\sqrt{3}}\, e^{j(\Theta+30^\circ)} + |S_1|\, e^{j(\phi+60^\circ)} \quad - - - - - - - - \quad (57)$$

Delta-Delta Banks

From Figure 1 the following current equations may be derived:

$$I_a = I_1 = I_L\, e^{-j\Theta} \quad - - - - - - - - - - - - - - \quad (58)$$

$$I_b = I_2 + I'' = I_L\, e^{-j(\Theta+120^\circ)} + I'\, e^{-j(\phi+90^\circ)} \quad - - - - - - - \quad (59)$$

$$I_c = I_3 - I'' = I_L\, e^{-j(\Theta+240^\circ)} - I'\, e^{-j(\phi+90^\circ)} \quad - - - - - - - \quad (60)$$

The following equations follow from Kirchhoff's laws:

$$I_a = I_{ba} - I_{ac} \quad - - - - - - - - - - - - - - \quad (61)$$

$$I_b = I_{cb} - I_{ba} \quad - - - - - - - - - - - - - - \quad (62)$$

$$I_{ba}Z_c + I_{ac}Z_b + I_{cb}Z_a = 0. \quad - - - - - - - - - - - - \quad (63)$$

If equations (61), (62), and (63) are solved simultaneously for I_{ba}, I_{ac}, and I_{cb}, the following equations result:

$$I_{ba} = \frac{I_a\, Z_b}{Z_a+Z_b+Z_c} - \frac{I_b\, Z_a}{Z_a+Z_b+Z_c} \quad - - - - - - - - - - - \quad (64)$$

$$I_{ac} = \frac{-I_a(Z_a+Z_c)}{Z_a+Z_b+Z_c} - \frac{I_b\, Z_a}{Z_a+Z_b+Z_c} \quad - - - - - - - - - - - \quad (65)$$

$$I_{cb} = \frac{I_a\, Z_b}{Z_a+Z_b+Z_c} + \frac{I_b(Z_b+Z_c)}{Z_a+Z_b+Z_c} \quad - - - - - - - - - - - \quad (66)$$

If equations (58), (59), and (60) are substituted into equations (64), (65), and (66) and if the operators $\underline{a}$ and $\underline{a^2}$ are employed, where

$$a = e^{j120^\circ} \qquad a^2 = e^{j240^\circ},$$

the following current equations result:

$$I_{ba} = \frac{Z_a}{Z_a+Z_b+Z_c}\left[\left(\frac{Z_b}{Z_a} - a^2\right) I_L\, e^{-j\Theta} - I'\, e^{-j(\phi+90^\circ)}\right] \quad - - - - - \quad (67)$$

$$I_{ac} = \frac{-Z_a}{Z_a+Z_b+Z_c}\left[\left(\frac{Z_c}{Z_a} - a\right) I_L e^{-j\theta} + I' e^{-j(\phi+90^\circ)}\right] \quad - - - - - \quad (68)$$

$$I_{cb} = \frac{Z_b}{Z_a+Z_b+Z_c}\left[\left(\frac{Z_c}{Z_b} a^2 - a\right) I_L e^{-j\theta} + \left(1 + \frac{Z_c}{Z_b}\right) I' e^{-j(\phi+90^\circ)}\right] - - - \quad (69)$$

The expressions for S may be easily derived from equations (67), (68), and (69) by the procedures used for the other connections. They are as follows:

$$S_A = \left[\frac{Z_b}{Z_a+Z_b+Z_c}\right]^* \left[\left(\frac{Z_c}{Z_b} a^2 - a\right)^* \frac{|S_3|}{\sqrt{3}} + \left(1 + \frac{Z_c}{Z_b}\right)^* |S_1| e^{-j(r-90^\circ)}\right] e^{j(\theta-90^\circ)} \quad (70)$$

$$S_B = \left[\frac{-Z_a}{Z_a+Z_b+Z_c}\right]^* \left[\left(\frac{Z_c}{Z_a} - a\right)^* \frac{|S_3|}{\sqrt{3}} + |S_1| e^{-j(r-90^\circ)}\right] e^{j(\theta+150^\circ)} \quad - - \quad (71)$$

$$S_C = \left[\frac{Z_a}{Z_a+Z_b+Z_c}\right]^* \left[\left(\frac{Z_b}{Z_a} - a^2\right)^* \frac{|S_3|}{\sqrt{3}} + |S_1| e^{-j(r+90^\circ)}\right] e^{j(\theta+30^\circ)} \quad - - \quad (72)$$

Grounded Wye-Delta Banks

From Figure 3 the following current equations may be derived:

$$I_a = I_1 = I_L e^{-j\theta} \quad - - - - - - - - - - - - - - - \quad (73)$$

$$I_b = I_2 + I'' = I_L e^{-j(\theta+120^\circ)} + I' e^{-j(\phi+90^\circ)} \quad - - - - - - - \quad (74)$$

$$I_c = I_3 - I'' = I_L e^{-j(\theta+240^\circ)} - I' e^{-j(\phi+90^\circ)} \quad - - - - - - - \quad (75)$$

The following equations come from an application of Kirchhoff's laws to the circuit diagram of Figure 3:

$$I_a = I_{ba} - I_{ac} \quad - - - - - - - - - - - - - - - \quad (76)$$

$$I_b = I_{cb} - I_{ba} \quad - - - - - - - - - - - - - - - \quad (77)$$

$$I_{ba} Z_c + I_{ac} Z_b + I_{cb} Z_a = 0 \quad - - - - - - - - - - \quad (78)$$

But equations (73), (74), (75), (76), (77), and (78) are identical with equations (58), (59), (60), (61), (62), and (63) of the delta-delta bank derivation. Therefore the same derivation applies here, and the results of the delta-delta bank derivation are also the results here.

NOMENCLATURE

a, b, c	Phase designations.
A, B, C	Transformer designations where A represents the transformer connected between phases b and c, B represents the transformer connected between a and c, and C represents the transformer connected between phases a and b.
a, a^2	The operators, e^{j120° and e^{j240° respectively.

$E_a = E_p e^{j0}$	Phase-to-neutral voltage of phase a.
$E_{ba} = \sqrt{3} E_p e^{j30^\circ}$	Phase-to-phase voltage from phase b to a.
E_L	Absolute value of the line voltage in any phase.
H_A, H_B, H_C	Displacement of the center of a circle from the origin.
I_a, I_b, I_c	Current in phase a, b, and c respectively.
I_{ba}, I_{cb}, I_{ac}	Current inside a delta bank from phase b to a, phase c to b, and phase a to c respectively.
$I'' = I' e^{-j(\phi + 90)}$	Current in a single phase load.
I_1, I_2, I_3	Current into a balanced three-phase load in phases a, b, and c respectively.
I_L	Absolute value of the line current in any phase.
K_A	$\frac{Z_b + 2Z_c}{Z_a + Z_b + Z_c}$.
K_B	$\frac{Z_a + 2Z_c}{Z_a + Z_b + Z_c}$.
K_C	$\frac{Z_a + 2Z_b}{Z_a + Z_b + Z_c}$.
$\|L_A\|$, $\|L_B\|$, $\|L_C\|$	Absolute value of the load limits in KVA or pu of transformers A, B, and C respectively.
$\left\|\frac{L_A}{L_B}\right\|_c$	Ratio of transformer A rating to that of B in the determination of K_C.
M_A	$H_A e^{j\delta_A} + R_A \|S_1\| e^{-jr} / \|S_3\|$.
M_B	$H_B e^{j\delta_B} + R_B \|S_1\| e^{-jr} / \|S_3\|$.
M_C	$H_C e^{j\delta_C} + R_B \|S_1\| e^{-jr} / \|S_3\|$.
n	Transformer turns ratio, primary to secondary.
R_A, R_B, R_C	Coefficient of $\|S_1\|/\|S_3\|$ in the radius of the circle to determine M for A, B, and C respectively.
S_1	Single-phase load KVA.
S_3	Three-phase load KVA.
S_A, S_B, S_C	Load on transformers A, B, and C respectively.
Z_a, Z_b, Z_c	Impedance of transformers A, B, and C respectively.

r	$\theta - \phi$.
δ_A, δ_B, δ_C	Angle of H_A, H_B, and H_C .
θ	Three-phase load powerfactor angle.
ϕ	Single-phase load powerfactor angle.
$(a + jb)^*$	$(a - jb)$.
$\lvert\ \rvert$	Absolute value signs.

BIBLIOGRAPHY

1. Two Transformers Serve Better than Three, A. S. Anderson. Electrical World, 143:43 June 13, 1955.

2. Voltage Unbalance in Delta Secondaries Serving Single-Phase and Three-Phase Loads, A. S. Anderson and R. C. Ruete. AIEE Transactions, Vol. 73, 1954, pp. 928-932.

3. Unbalanced Loading and Voltage Unbalance on Three-Phase Distribution Transformer Banks, H. M. Bankus and J. E. Gerngross. AIEE Transactions, Vol. 73, 1954, pp. 367-375.

4. Transformer Engineering, L. F. Blume and A. Boyajian, 2nd Ed., New York: John Wiley & Sons Inc., 1951.

5. Wye-Delta Distribution Transformer Banks: Grounded or Floating Wye Point, P. A. Oakes, The Line. Milwaukee: Line Material Co., July-August 1953.

6. Unbalanced Loading of Three Phase Transformer Banks, S. W. Anderson, Unpublished Doctor of Philosophy Thesis in Engineering, Illinois Institute of Technology, 1957.

Table I. Relationship between KVA Ratio, Impedance Ratio, and Mean Impedance Ratio Angle for Three to One Hundred KVA Transformers

KVA Ratio	Impedance Ratio	Mean Impedance Ratio Angle
0.3	3.33	$-7\frac{1}{2}^\circ$
0.33	3.00	-5°
0.375	2.667	$-2\frac{1}{2}^\circ$
0.4	2.50	$-10\frac{1}{2}^\circ$
0.5	2.00	$-6\frac{1}{2}^\circ$
0.6	1.667	$-\frac{1}{2}^\circ$
0.667	1.50	-5°
0.75	1.33	-2°
1.00	1.0	0°

Table II. Data to Determine Circle Diagram, M_A, for Transformer A, 2400 Volt, Three to One Hundred KVA, Delta-Delta or Grounded Wye-Delta Banks

L_C/L_B	H_A	R_A	δ_A
0.30	0.289	0.576	17.7°
0.33	0.294	0.574	16.2
0.375	0.295	0.578	15.2
0.40	0.288	0.582	14.6
0.50	0.297	0.596	11.2
0.60	0.309	0.616	8.6
0.67	0.303	0.625	6.5
0.75	0.320	0.636	4.5
1.00	0.333	0.667	0
1.33	0.358	0.698	- 4.4
1.50	0.366	0.710	- 6.4
1.67	0.368	0.728	- 8.4
2.00	0.390	0.752	-11.0
2.50	0.419	0.780	-13.5
2.67	0.406	0.783	-13.5
3.00	0.426	0.800	-16.0
3.33	0.437	0.811	-16.5

Table III. Data to Determine Circle Diagram, M_B, for Transformer B, 2400 Volt, Three to One Hundred KVA, Delta-Delta or Grounded Wye-Delta Banks

L_C/L_A	H_B	R_B	δ_B
0.30	0.304	0.131	-71.0°
0.33	0.304	0.143	-72.1
0.375	0.302	0.158	-72.9
0.40	0.315	0.167	-65.9
0.50	0.318	0.200	-66.0
0.60	0.314	0.231	-67.5
0.67	0.322	0.250	-63.6
0.75	0.324	0.273	-63.5
1.00	0.333	0.333	-60.0
1.33	0.346	0.399	-56.0
1.50	0.347	0.428	-55.0
1.67	0.367	0.454	-52.0
2.00	0.376	0.501	-51.3
2.50	0.387	0.558	-48.5
2.67	0.396	0.572	-45.2
3.00	0.413	0.600	-45.0
3.33	0.412	0.625	-44.4

Table IV. Data to Determine Circle Diagram, M_C, for Transformer C, 2400 Volt, Three to One Hundred KVA, Delta-Delta or Grounded Wye-Delta Banks

L_B/L_A	H_C	R_C	δ_C
0.30	0.289	0.131	83.5°
0.33	0.293	0.143	80.3
0.375	0.295	0.158	76.9
0.40	0.286	0.166	81.8
0.50	0.295	0.200	75.5
0.60	0.310	0.230	68.8
0.67	0.306	0.250	69.8
0.75	0.321	0.273	66.0
1.00	0.333	0.333	60.0
1.33	0.358	0.399	54.5
1.50	0.371	0.428	51.8
1.67	0.368	0.456	51.8
2.00	0.396	0.500	47.4
2.50	0.420	0.558	43.5
2.67	0.406	0.570	44.5
3.00	0.420	0.601	42.7
3.33	0.433	0.624	41.5

Table V. Data to Determine Circle Diagram, M_A, for Transformer A, 2400 Volt, Fifty to Five Hundred KVA, Delta-Delta or Grounded Wye-Delta Banks

L_C/L_B	H_A	R_A	δ_A
0.30	0.288	0.579	15.5°
0.33	0.297	0.591	14.0
0.40	0.298	0.598	13.0
0.45	0.298	0.614	9.4
0.50	0.308	0.616	8.5
0.60	0.311	0.634	5.5
0.67	0.312	0.634	5.3
0.75	0.321	0.638	4.4
1.00	0.333	0.666	0.0
1.33	0.347	0.686	- 3.7
1.50	0.358	0.708	- 5.1
1.67	0.364	0.706	- 5.2
2.00	0.376	0.730	- 8.0
2.23	0.373	0.728	- 7.5
2.50	0.387	0.744	-10.4
3.00	0.402	0.763	-12.8
3.33	0.416	0.774	-14.0

Table VI. Data to Determine Circle Diagram, M_B, for Transformer B, 2400 Volt, Fifty to Five Hundred KVA, Delta-Delta or Grounded Wye-Delta Banks

L_C/L_A	H_B	R_B	δ_B
0.30	0.311	0.163	-67.0°
0.33	0.306	0.178	-69.0
0.40	0.315	0.200	-65.4
0.45	0.325	0.226	-63.0
0.50	0.316	0.228	-66.6
0.60	0.323	0.262	-63.0
0.67	0.318	0.262	-64.0
0.75	0.325	0.281	-64.0
1.00	0.333	0.333	-60.0
1.33	0.348	0.390	-56.3
1.50	0.352	0.414	-55.1
1.67	0.348	0.415	-56.0
2.00	0.366	0.458	-52.8
2.23	0.355	0.462	-54.6
2.50	0.367	0.499	-51.0
3.00	0.386	0.534	-48.0
3.33	0.383	0.561	-48.0

Table VII. Data to Determine Circle Diagram, M_C, for Transformer C, 2400 Volt, Fifty to Five Hundred KVA, Delta-Delta or Grounded Wye-Delta Banks

L_B/L_A	H_C	R_C	δ_C
0.30	0.288	0.163	82.5°
0.33	0.297	0.178	76.0
0.40	0.298	0.200	76.0
0.45	0.298	0.226	75.0
0.50	0.307	0.227	70.0
0.60	0.311	0.262	68.0
0.67	0.312	0.262	66.5
0.75	0.321	0.281	64.7
1.00	0.333	0.333	60.0
1.33	0.347	0.390	56.0
1.50	0.358	0.414	54.0
1.67	0.364	0.415	53.0
2.00	0.368	0.455	51.0
2.23	0.373	0.461	49.5
2.50	0.387	0.498	47.2
3.00	0.401	0.533	46.0
3.33	0.416	0.561	43.0

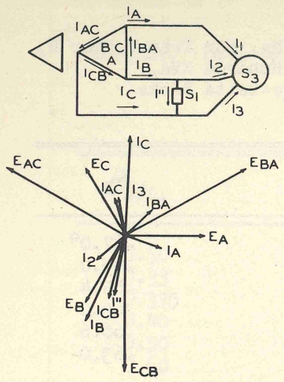

Fig. 1. Circuit Diagram and Phase Relations of a Delta-Delta Transformer Bank

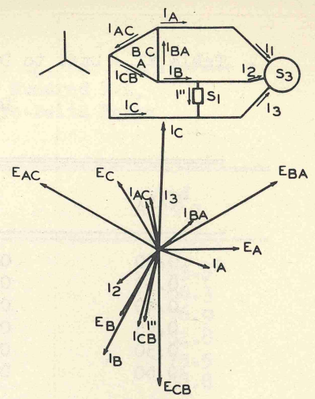

Fig. 2. Circuit Diagram and Phase Relations of an Ungrounded Wye-Delta Transformer Bank

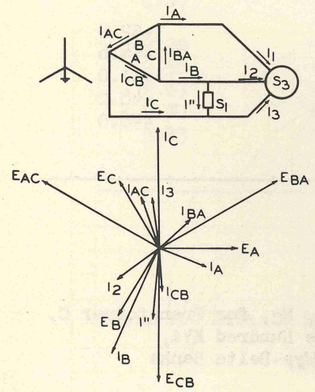

Fig. 3. Circuit Diagram and Phase Relations of a Grounded Wye-Delta Transformer Bank

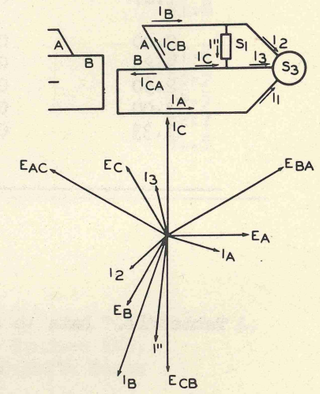

Fig. 4. Circuit Diagram and Phase Relations of an Open-Delta Transformer Bank with a Lagging Connection

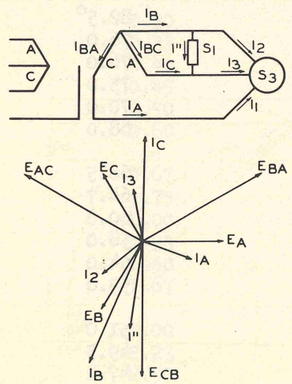
IB
A
C
IBA
IBC
C A
IC
I"
S1
I2
I3
S3
I1
IA
EAC
EC
EBA
EA
EB
EB
EB

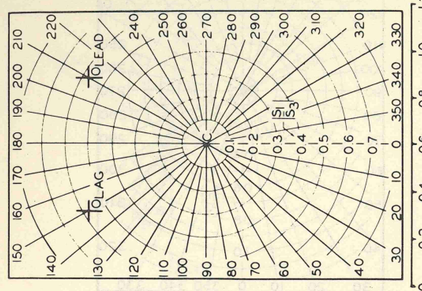

Fig. 14. Transformer Circle Diagram for Open-Delta Banks

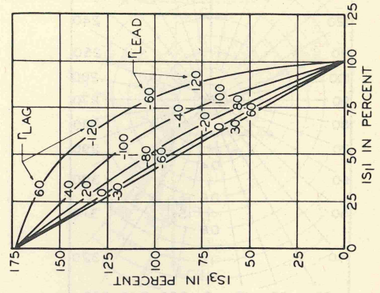

Fig. 15. Load Limit Curves for Open-Delta Banks in Percent of Allowable Load

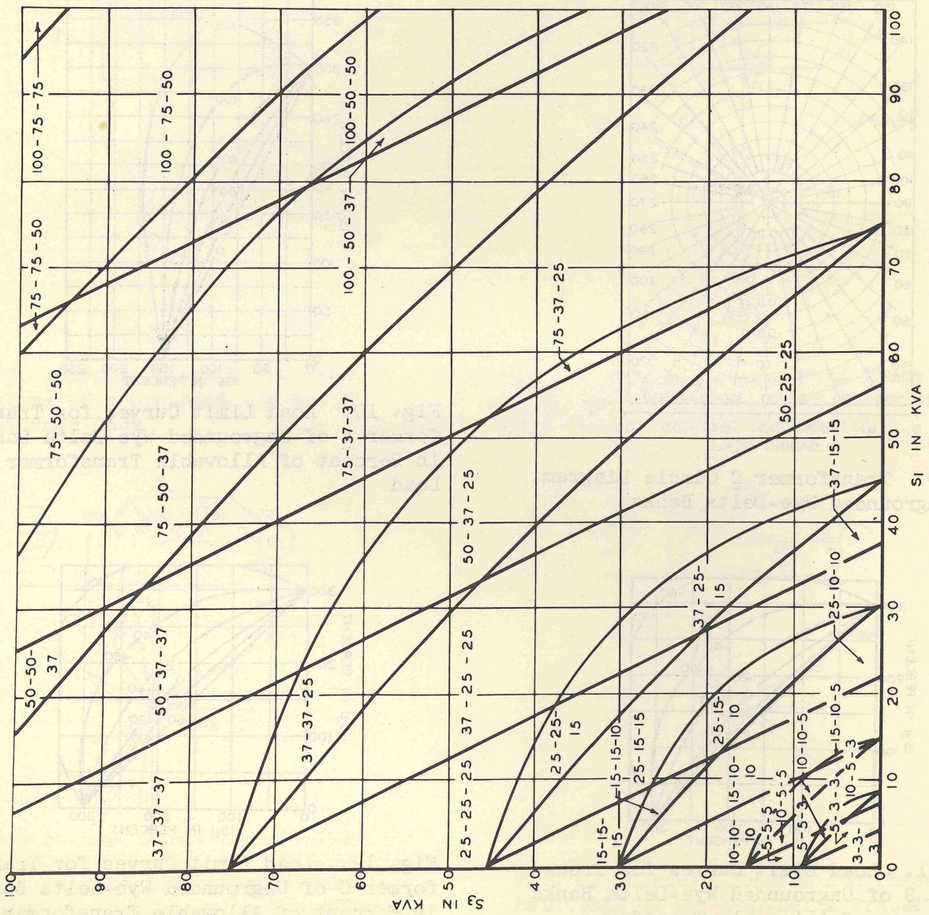

Fig. 13. Preferred Loading Curves with $r = 20^{\circ}$ for Ungrounded Wye-Delta Banks

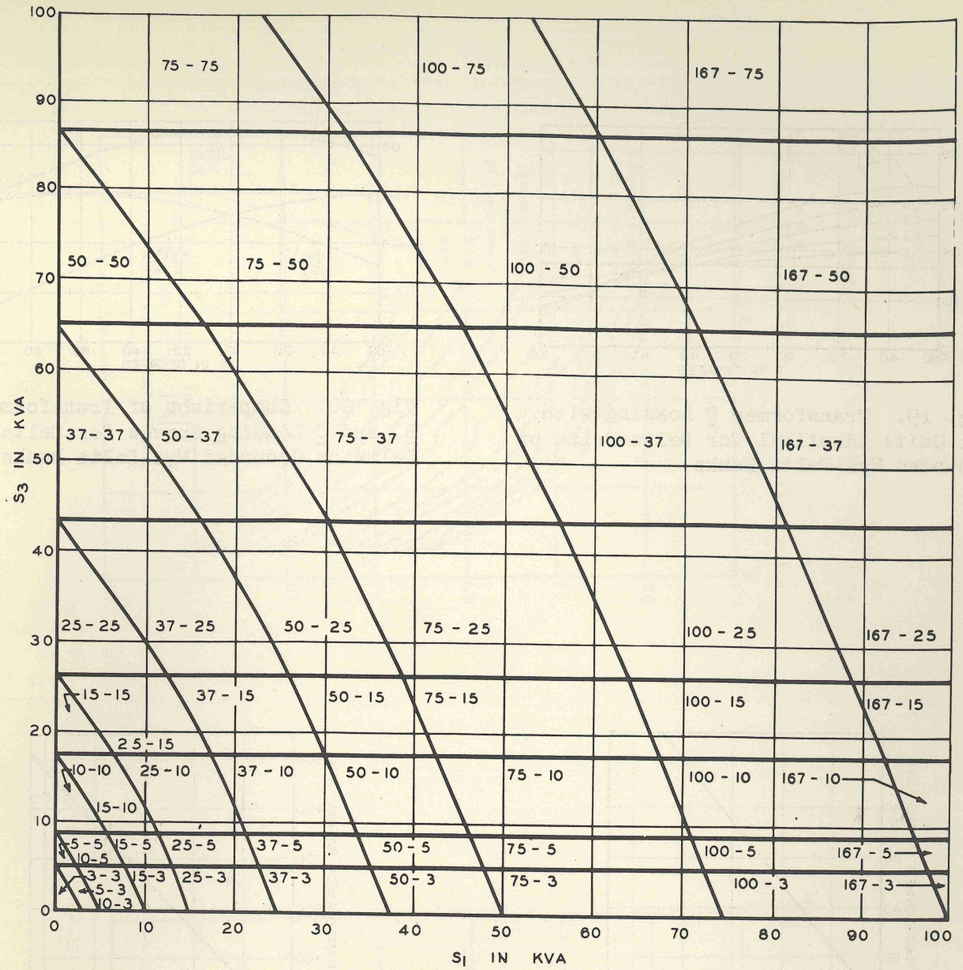

Fig. 16. Preferred Loading Curves with $r = 20^{\circ}$ for Open-Delta Banks

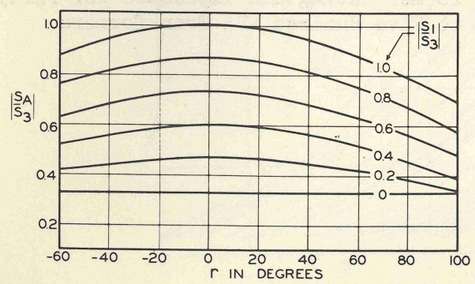

Fig. 17. Transformer A Loading with all Units Identical for Delta-Delta or Grounded Wye-Delta Banks

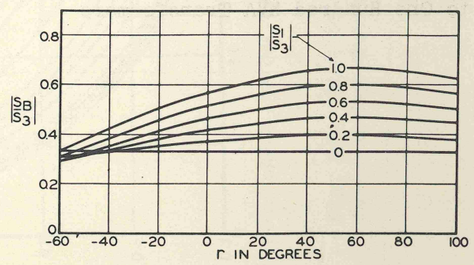

Fig. 18. Transformer B Loading with all Units Identical for Delta-Delta or Grounded Wye-Delta Banks

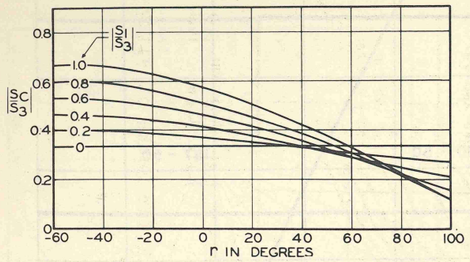

Fig. 19. Transformer C Loading with all Units Identical for Delta-Delta or Grounded Wye-Delta Banks

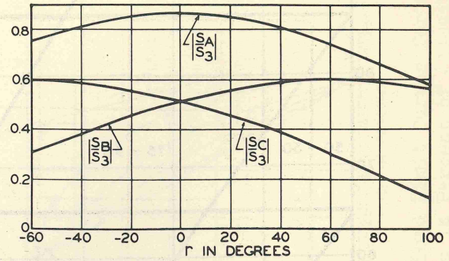

Fig. 20. Comparison of Transformer A, B, and C Loading Curves for Delta-Delta or Grounded Wye-Delta Banks

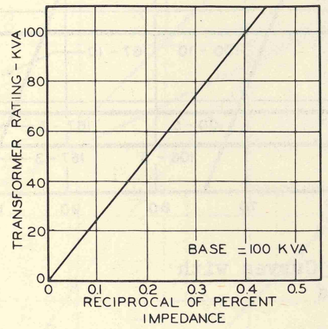

Fig. 21. Relationship between Transformer Rating and Impedance for Three to One Hundred KVA Transformers

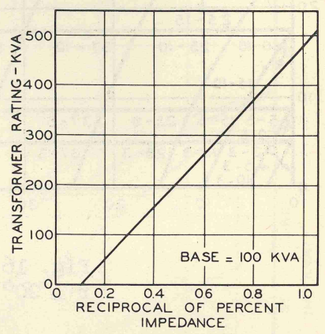

Fig. 22. Relationship between Transformer Rating and Impedance for Fifty to Five Hundred KVA Transformers

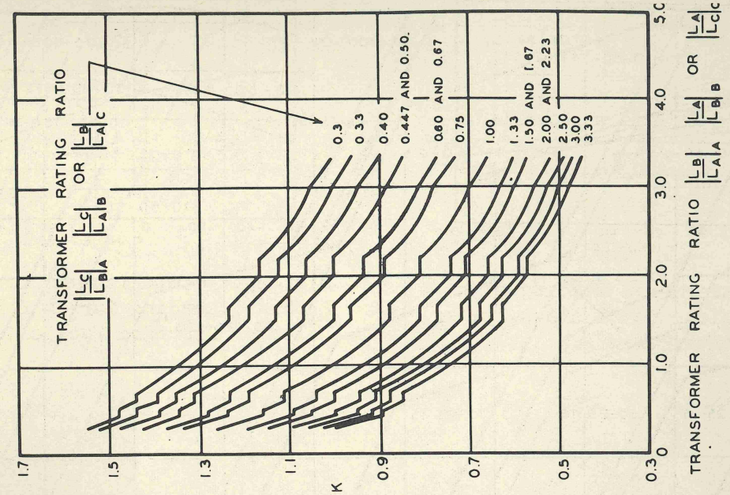

Fig. 24. Plot of K for Banks of Fifty to Five Hundred KVA

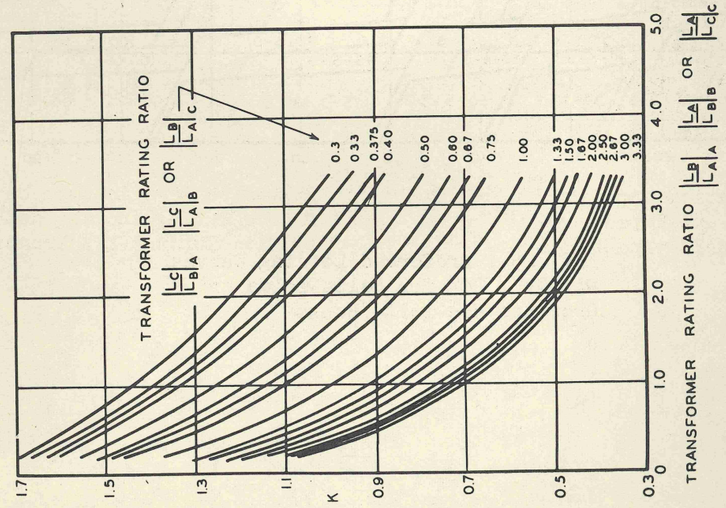

Fig. 23. Plot of K for Banks of Three to One Hundred KVA

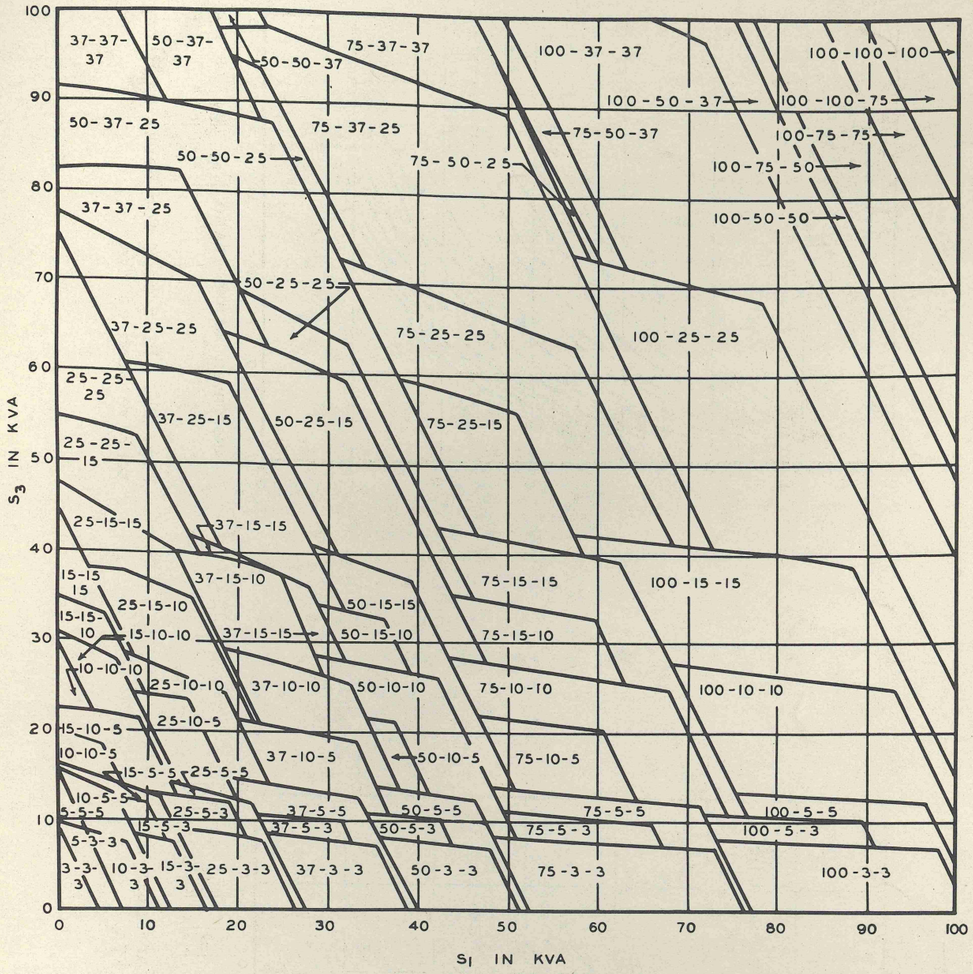

Fig. 25. Preferred Loading Curves with r = 20° for Delta-Delta or Grounded Wye-Delta Banks

RECEIVED
APR -1 1957
ENG. DEPT.

District Conference Paper

UNBALANCED LOADING OF THREE-PHASE TRANSFORMER BANKS

S. W. Anderson
Associate Member AIEE
Middle West Service Company
Chicago, Ill.

RECEIVED
MAR 29 1957
H. A. FREY

A paper recommended by the AIEE Committee on Transmission and Distribution for the AIEE Great Lakes District Meeting, Des Moines, Iowa, April 15-17, 1957. Manuscript submitted January 14, 1957; made available for printing March 14, 1957.

Price: 40¢ To Members
80¢ To Nonmembers

(5¢ per copy additional if first class mailing desired)

All Rights Reserved by the American Institute of Electrical Engineers
33 West 39th Street, New York 18, N. Y.
Litho in USA

Paper No. DP
57-608

INSULATOR DEPARTMENT

GENERAL ELECTRIC COMPANY

Baltimore, Maryland

Technical Report No. LK-647
May 28, 1958

SUBJECT

Knox 6 Inch, 10,000 lb. Suspension Insulator

This report contains:

3 Typewritten Pages

Signed Joseph Kaminski Jr Approved Fred C. Kane

Technical Report No. LK-647
May 28, 1958

Subject:

Knox 6 inch, 10,000 lb. Suspension Insulator

Introduction:

A total of 38 Knox six inch No. 86102 suspension insulators were examined and tested to determine the quality of these insulators.

The units were assembled using Brewer-Titchener hardware. The results are as follows:

I - Physical Measurements

Sample Number	Arcing Distance Inches	Leakage Distance Inches	Weight lbs.-oz.	Unit Spacing Inches
1	4 3/8	7 3/8	5 - 1	5 1/2
2	4 1/4	7 3/16	4 - 13	5 1/2
3	4 1/2	7 5/16	5 - 1	5 1/2

Standard A.S.A. spacing 5 1/2 inches ± 1/8 inches.

II - 60 Cycle Dry Flashover - KV

Single Unit		Two Unit		Three Unit	
Sample No. 1	Sample No. 2	Sample Nos. 1 & 2	Sample Nos. 3 & 4	Sample Nos. 1, 2, 3	Sample Nos. 4, 5, 6
63	60	116	116	157	160
62	62	116	113	160	159
62	60	108	112	157	152
59	60	117	116	159	148
60	58	117	112	156	163
Av. Uncorr. 61.2	60	114.8	113.8	157.8	156.2
Av. Corr. 64.5	63.2(60)	124.8	123.8(115)	171.5	170 (165)

( ) Locke Catalog Values.

III - 60 Cycle Wet Flashover - KV

Single Unit		Two Unit		Three Unit	
Sample No. 1	Sample No. 2	Sample Nos. 1 & 2	Sample Nos. 3 & 4	Sample Nos. 1, 2, 3	Sample Nos. 1, 2, 3
32	29	66	61	80	87
32	30	55	55	79	89
30	30	55	58	78	91
33	29	54	53	80	88
33	29	53	58	75	84
Av. 32	29.4(30)	56.6	57(55)	78.4	87.2(80)

(No Correction)

IV - Impulse Flashover - KV

Single Unit

Pos.	Neg.	Pos. Corr.	Neg. Corr.
94	102	99.3	107
106	100	113(100)	104.5(100)

String of 2 Units

Pos.	Neg.	Pos. Corr.	Neg. Corr.
187	187	202	200
190	180	206(200)	193(180)

String of 3 Units

Pos.	Neg.	Pos. Corr.	Neg. Corr.
267	248	289	265
260	248	282(290)	265(260)

V - Mechanical and Electrical and Ultimate Strength Test (10,000 lb. rating)

Sample Number	M & E Pounds	Ultimate Pounds	Nature of Fracture	Pinhole Depth (Inches)
21	11,600	14,250	Low break	1 11/32
22	9,900	13,400	Low break	1 7/32
23	16,150	16,150	Low break	1 11/32
24	15,800	16,900	Low break	1 12/32
25	16,600	16,600	Low break	1 11/32
26	10,600	11,350	Low break	1 10/32
27	8,100	11,100	Low break	1 7/32
28	10,900	14,000	Low break	1 11/32
29	13,600	14,900	Low break	1 11/32
30	10,050	14,400	Low break	1 12/32
Av.	12,330	14,305		

VI - Mechanical Impact Strength Test (45 in lb. rating)

Sample Number	Ultimate Strength (in lbs.)	Nature of Fracture	Skirt Thickness Inches
11	60	Doughnutted	13/32
12	60	Doughnutted	13/32
13	50	3/4 off	12/32
14	60	Doughnutted	13/32
15	50	Doughnutted	13/32
16	60	Doughnutted	14/32
17	40	2 inch piece out	14/32
18	50	Doughnutted	15/32
19	50	Doughnutted	14/32
20	50	Doughnutted	14/32
Av.	53		

VII - Puncture Under Oil (80 kv rating)

Sample Number	Puncture Value KV	Location of Puncture
1	128	In the head
2	125	Base of cap
3	106	In the head
4	128	In the head
5	106	In the head
6	130	Base of cap
7	125	Base of cap
8	110	In the head
9	110	Base of cap
10	130	Base of cap
Av.	119.8	Percent avg. variation 7.8%

VIII - Porosity Test

Taken from Previous Test	Sample Number	Head	Throat	Skirt
M & E	22	ok	ok	ok
M & E	27	ok	ok	ok
Punct.	3	ok	ok	ok
Punct.	5	ok	ok	ok
Impact	17	ok	ok	ok

IX - Specific Gravity Test

Sample Number	Head	Throat	Skirt
3	2.390	2.363	
5	2.401	2.368	
17	2.408		
22	2.404	2.369	
27		2.380	2.402

Summary:

The combined mechanical and electrical strength tests show that 20% of the units fail to meet rating with a minimum test value of 8,100 lbs. The average mechanical impact strength of 53 in lbs. is only slightly better than the rating of 45 in lbs. Under test section VI headed "Nature of Fracture", it is to be noted that 80% of the units "doughnutted." This type of fracture will result in complete loss of insulation and accompanying damage under the top of the insulator.

F. C. Vose ~~Fcbe~~

GENERAL ELECTRIC COMPANY
INSULATOR DEPARTMENT
Baltimore, Maryland

Technical Report No. LK-646-DR

May 28, 1958

SUBJECT

Knox 10 Inch 15,000 Lb. Insulator

J. Kaminski, Jr.

This report contains:

7 typewritten pages

Signed Joseph Kaminski Jr

Approved Fred C Vose

Knox 10 Inch 15,000 Lb. Insulator

J. Kaminski, Jr.

INTRODUCTION

A total of 46 Knox 10 inch suspension insulators No. 81022 (Locke equivalent 1840-ZG-1) were tested and examined. The units were assembled with Brewer Titchener forged steel caps and ball bolts. The insulators were packed in hexagonal wire bound crates with easily identified markings. The test results are as follows:

I. Physical Measurements

Sample Number	Spacing (Inches)	Arcing Distance (Inches)	Leakage Distance (Inches)	Weight
1	5-9/16	7-9/16	11-9/16	10 lb. 12 oz.
2	5-5/8	7-5/8	11-1/2	11 lb. 1 oz.
3	5-5/8	7-7/16	11-1/8	10 lb. 11 oz.
4	5-5/8			
5	5-11/16			
6	5-5/8			

String Spacing 6 Units

String Number	Spacing (Inches)	ASA Standard (Inches)	Exceed Tolerance
1	33-5/8	34-1/2 ± 1/2	-3/8"
2	33-11/16		-5/16"
3	33-5/16		-11/16"

II. 60 Cycle Dry Flashover - KV

	Single Unit	3 Unit String	6 Unit String	9 Unit String	18 Unit String
	76	201	351	508	960
	73	202	351	508	937
	73	204	351	502	951
	74	198		502	976
	74	202		502	972
Av. Uncorr.	74	201.4	351	504.4	959.2
Av. Corr.	76.8 (80)	212 (215)	383 (380)	550 (540)	1049 (965)

( ) Locke Catalog Values

III. 60 Cycle Wet Flashover - KV

	Single Unit	3 Unit String	6 Unit String	8 Unit String	18 Unit String
	48	128	304	423	796
	46	135	318	427	823
	47	133	284	420	775
	49	137	292	430	692
	49	141	284	412	772
Av. Uncorr.	47.8	134.8	296.4	422.4	719
Av. Corr.	47.6 (50)	134.2 (130)	294.4 (255)	419 (375)	743
					712
					716
					700
				Av. Uncorr.	744.8
	( ) Locke Catalog Values			Av. Corr.	739 (690)

IV. Impulse Flashover - KV

Single Unit

Sample No.	Pos.	Neg.	Poss. Corr.	Neg. Corr.
1	115	130	120 (125)	136 (130)
2	124	150	134 (125)	159 (130)
3	121	128	128 (125)	135 (130)
		String of 3 Units		
	313	328	335 (355)	348 (340)
	303	335	335 (355)	366 (340)
		String of 6 Units		
	552	558	597 (610)	596 (585)
		String of 9 Units		
	791	807	856 (860)	862 (845)
		String of 18 Units		
	1460	1508	1617 (1585)	1647 (1615)

V. Radio Influence Voltage Tests

Single Unit

Test Voltage KV	0	10	15	17	(10)
Noise Level Microvolts	8	8	12	50	(50)

4 Unit String

Test Voltage - KV	0	40	45	50	54	(40)
Noise Level Microvolts	0	9	35	90	200	(200)

8 Unit String

Test Voltage - KV	0	50	60	70	90	100	110	120	135	(85)
Noise Level Microvolts	2	5	20	32	50	100	175	350	500	(500)

10 Unit String

Test Voltage KV	0	75	85	95	105	115	125	135	150	(95)
Noise Level Microvolts	2	2	10	25	45	80	150	250	400	(500)

VI. Mechanical and Electrical and Ultimate Strength Tests

Sample No.	M&E (Pounds)	Ultimate (Pounds)	Nature of Fracture	Pinhole Depth
1	22,400	24,150	low break	1-19/32
2	17,250	26,300	low break	1-16/32
3	23,600	23,600	low break	1-18/32
4	19,000	19,000	low break	1-18/32
5	20,600	20,750	low break	1-17/32
6	16,500	18,600	low break	1-16/32
7	21,400	25,350	pin broke thru shank	-
Av.	20,107	22,535		
Max.	23,600	26,300		
Min.	16,500	18,600		
Range	7,100	7,700		

VII. Time Load Test

Seven samples were placed in the outdoor time load frame and an initial load of 6,000 lbs. applied. The load increased at the rate of 1,000 lbs. per hour until 10,000 lbs. reached. The total load of 10,000 lbs. was held for a period of 10 days. The units were flashed over periodically and after 10 days the units were subjected to M&E and Ultimate tests.

Sample No.	M&E Pounds	Ultimate Pounds	Nature of Fracture	Pinhole Depth
36	20,300	25,200	low break	1-19/32
37	19,500	28,800	low break	1-21/32
38	18,800	29,100	ball sheared off pin	
39	16,900	28,700	pin broke at base of ball	
40	22,400	25,800	one side of ball sheared	
41	18,000	18,450	low break	1-19/32
42	15,400	18,200	low break	1-16/32
Av.	18,757	24,893		

VIII. Thermal Test

Temperature Hot Bath 208°F to 210°F
Temperature Cold Bath 34°F to 36°F

All units passed ten cycles without failure and units given M&E and Ultimate test.

Sample No.	M&E Pounds	Ultimate Pounds	Nature of Fracture	Pinhole Depth
1	20,600	21,100	low break	1-21/32
2	17,900	19,650	low break	1-25/32
3	16,850	21,000	low break	1-18/32
4	15,400	21,300	low break	1-17/32
5	21,300	22,750	low break	1-21/32
6	25,700	25,700	one side of pin sheared	-
7	19,000	24,500	low break	1-20/32
Av.	19,535	22,285		

IX. Mechanical Impact Test

Sample No.	Ultimate Strength - In. Lbs.	Nature of Fracture	Skirt Thickness
15	80	3/4 off	14/32"
16	50	1/4 off	13/32"
17	30	3 inch piece out	15/32"
18	50	6 inch piece out	14/32"
19	40	1/2 off	16/32"
20	70	1/2 off	15/32"
21	40	4 inch piece out	14/32"
Av.	51		

X. Puncture Under Oil Test

Sample No.	Puncture Value	Location of Puncture
8	140 KV	base of cap
9	150	in the head
10	140	in the head
11	142	in the head
12	144	in the head
13	90	in the head
14	135	in the head
Av.	134.4	Percent Average Variation 9.4%

XI. Steep Wave Front Impulse and Puncture Under Oil

Sample No.	No. of Impulse	Puncture Under Oil - KV	Ultimate Strength Pounds	Head Thickness
29	5	96	23,700	20/32"
30	3	-	17,800	18/32"
31	3	-	19,250	18/32"
32	5	162	21,000	20/32"
33	3	-	20,850	21/32"
34	2	-	21,100	18/32"
35	3	-	21,000	17/32"

XII. Porosity Test

Taken from previous test.

	Sample No.	Head	Throat	Skirt
M & E	2	OK	OK	OK
M & E	6	OK	OK	OK
Puncture	13	OK	OK	OK
Puncture	14	OK	OK	OK
Impact	17	OK	OK	OK

Pressure 4,000 lb. per square inch for 15 hours.

XIII. Specific Gravity Test

Sample No.	Head	Throat
2	2.377	2.379
6	2.379	2.354
13	2.395	2.380
14	2.404	2.374
17	2.396	2.395

SUMMARY

All three string lengths checked showed that the units exceeded the permissable tolerances by a considerable margin. The results of the M&E test indicate that 70% of the units failed electrically prior to mechanical failure. This pattern of prior electrical failure continued to evidence itself on the M&E tests that followed both the time load test and thermal test. Experience with our insulators has shown that this type of failure is usually associated with unequal load distribution.

The Knox insulator is particularly poor under impact with 70% failing to meet the standard 55 in. lb. rating. Although only one failure was evidenced by the puncture under oil test the head thickness measurements made on units, following the steep wave front impulse test shows that these units are from 1/16 to 5/32 inches below the minimum allowable head thickness of the 1840 shell. It is expected that with this small head section 14% of the units will continue to fail below 120 KV. The variation in diaphram thickness between individual units of 1/8 of inch indicates a serious lack of control in the shell making operation.

The cotter key and cotter key hole opening were very poorly matched, permitting the key to rotate within the socket even though the ball bolt was in place. With the key turning to an upright position it becomes lodged between ball bolt and cap making it extremely difficult to remove the key.

The hexagonal type crates when piled in stacks show an increased tendency to roll.

GENERAL ELECTRIC

VR-289-58

REV NO.

TITLE

KNOX SUSPENSION INSULATOR

FIRST MADE FOR 15,000 LBS.

CONT ON SHEET

SH NO.

ENSIONS

ANGLES

CONT ON SHEET

SH NO.

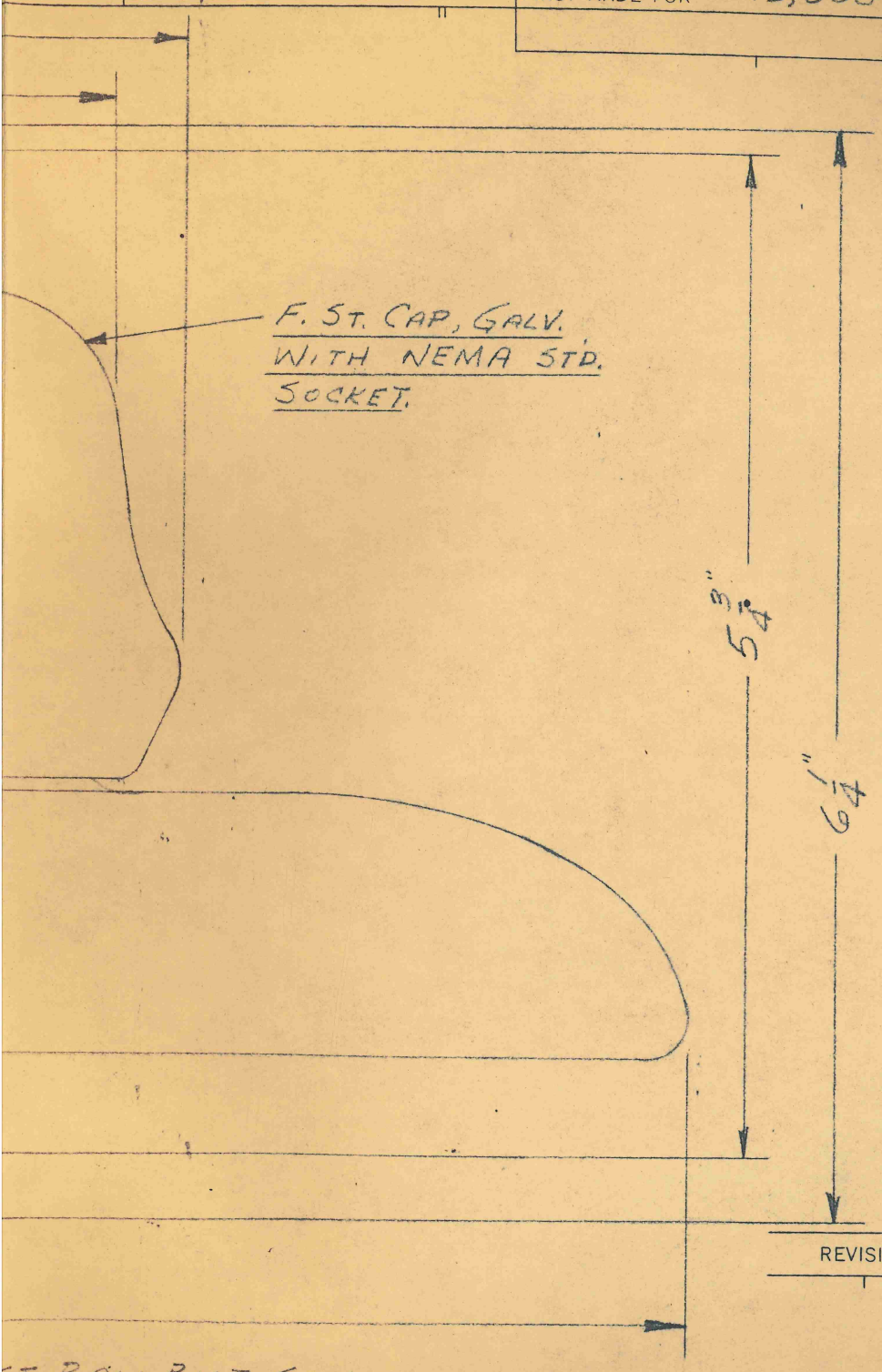

ST. BALL BOLT, GALV.
TH NEMA STD. BALL

REVISIONS

PRINTS TO

MADE BY BL

ISSUED

APPROVALS

INSULATOR DIVISION

DEPT

BALTIMORE, MD. LOCATION

VR-289-58

CONT ON SHEET

SH NO.

DRAWING NO.	CONT ON SHEET
R-289 4-4-58	SH NO
APRIL 15, 1958	

UNLESS OTHERWISE SPECIFIED USE THE FOLLOWING:—			
APPLIED PRACTICES	SURFACES	TOLERANCES ON MACHINED DIMENS	
		FRACTIONS ±	DECIMALS ±
	✓		

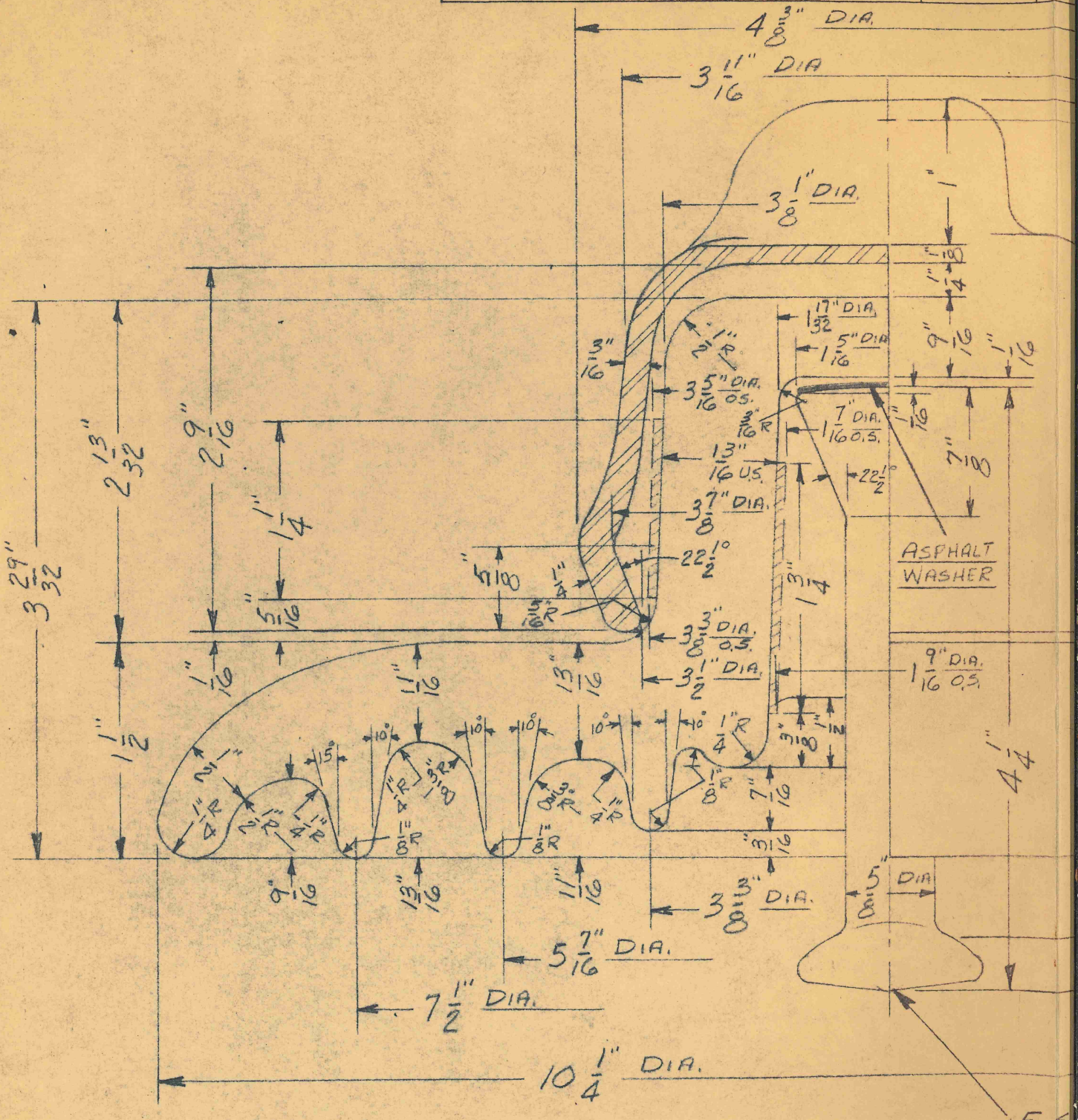

CONT ON SHEET | SH NO.

DRAWING NO.

R-289 4-4-58
APRIL 15, 1958

UNLESS OTHERWISE SPECIFIED USE THE FOLLOWING:—

APPLIED PRACTICES	SURFACES	TOLERANCES ON MACHINED DIMENSIONS		
		FRACTIONS	DECIMALS	ANGLES
	✓	±	±	±

REV NO. | CONT ON SHEET | SH NO.

GENERAL ELECTRIC

VR-289-58
CONT ON SHEET | SH NO.

TITLE
KNOX SUSPENSION INSULATOR
FIRST MADE FOR 15,000 LBS.

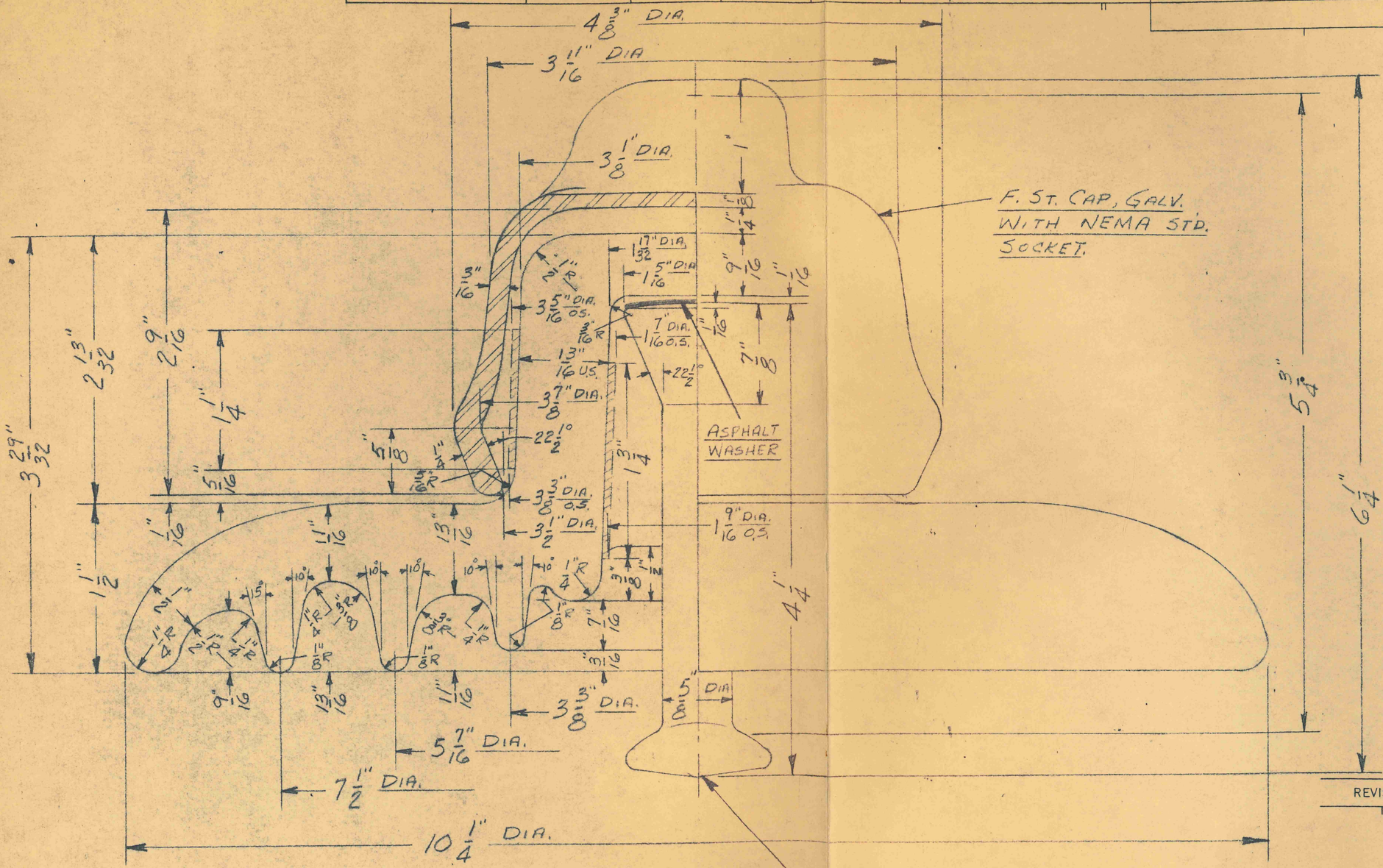

REVISIONS

PRINTS TO

MADE BY BL
ISSUED

APPROVALS

INSULATOR DEPT
BALTIMORE, MD. LOCATION

VR-289-58
CONT ON SHEET | SH NO.

FF-806-PL 7M (1-57) PRINTED IN U.S.A.

Misc.

Conference Paper

RECEIVED
MAY 5 1958
H. A. FREY

R ~~Heller~~
J ~~Kaminski~~
~~J M Jasatko~~
~~J C Rose~~
~~N J Hatter~~
~~L J Stevens~~
~~R N Anderson~~
B E Kingsbury

Circulate

POWER SYSTEM PLANNING ECONOMICS

A. J. Wood
Member AIEE
General Electric Company
Schenectady, N. Y.

A paper recommended by the AIEE System Engineering and Transmission and Distribution Committees for presentation at the AIEE Summer General Meeting and Air Transportation Conference, Buffalo, N. Y., June 22-27, 1958. Manuscript submitted January 31, 1958; made available for printing April 15, 1958.

Price: 40¢ To Members
80¢ To Nonmembers
(5¢ per copy additional if first class mailing desired)

All Rights Reserved by the
American Institute of Electrical Engineers
33 West 39th Street, New York 18, N. Y.
Litho in USA

Paper No. CP
58-870

POWER SYSTEM PLANNING ECONOMICS

A. J. Wood*
Member, AIEE

INTRODUCTION AND SCOPE

In his day-to-day operations, the power system engineer is faced with problems and decisions which must ultimately stand the tests of an economic analysis. This is particularly true of electric utility engineers who perform the system planning function. The elements of the system planning function may be briefly stated as follows:[1]

1. Forecast future system requirements.

2. Devise and test the technical feasibility of various alternative schemes to meet these future requirements.

3. Compare the economic and operating merits of the various alternatives after estimating the investment requirements, charges, and other costs of each scheme.

4. Apply experience and judgment to select a course of action.

5. Proceed with the selected alternative; but continually or periodically when required, review and revise the long range plans.

It is the objective of this paper to discuss briefly a general method of performing the economic comparison of various alternative purposes. The aim of this paper is not to discuss in detail the more involved and complex relationships which may arise. Other authors have, in fact, discussed some of these important, but rather involved points.[2,3,4,5] It is hoped that by the use of a simple example, the general technique and elementary arithmetic operations may be explained.

The purpose of scrutinizing all technical engineering plans in terms of dollars is to estimate the difference in the revenue requirements between the alternatives in order to assist management in making decisions. As such, the engineering economic study is not an end in itself, but is only a useful tool for the planning engineer; similar to other tools such as the A-C Network Analyzer. The importance of utility engineering economic studies should be obvious because of the very nature of the electric utility business. Fig. 1 shows the historical, annual capital expenditures of American electric light and power companies. A small percentage saved annually by the prudent use of economic analyses will result in a very large reduction in the revenue dollars required in an industry which invests 4 to 5 billion dollars yearly for capital equipments. By 1970, it has been predicted that the industry's capital expenditures will reach an annual level of over 10 billion. These monies have been allocated in the past approximately 33 to 40%, each, for generation and distribution additions, and 15 to 16% for new transmission facilities. In the future, technological and economic developments may shift this balance so that larger portions will be allocated for transmission with a corresponding reduction in generation outlay.

In short, because the electric utility business requires tremendous capital investments, because it is a growing industry, and because the utility company managements must serve their shareowners and bondholders wisely, the electric utility engineer must ultimately examine all future plans in terms of the revenue requirements for each plan.

* General Electric Company, Schenectady, New York

ENGINEERING ECONOMIC STUDIES

General Procedure

There are many procedures suggested in the literature for conducting engineering economic studies.[5,6] Those techniques which involve no short cuts of dubious rigor should all yield the same result when properly applied since they are all based on the same mathematical foundations. However, the most straightforward and generally applicable technique to use in power system investment problems is that of making economic comparisons on the basis of the present worth of all future revenue requirements. That is, the criteria used in deciding which is the economic choice is that the most economically attractive is the one which has the minimum future revenue requirements. With this as a criteria, the procedure for making an economic comparison between alternatives is a simple, two-step operation. That is:

1. Estimate for each alternative the annual revenue requirements for each year.*

2. If these annual revenue requirements are not uniform, calculate the present worth of all required annual expenditures.

This procedure will always lead to the economic choice, is easy to apply to many situations, and requires only a knowledge of simple financial arithmetic.

Of course, for rare situations in which the future annual revenue requirements are estimated to be uniform for each alternative, there is no point in computing present worths since the economic choice may be based on the annual data.

Financial Arithmetic

Since the second step in the economic comparison procedure requires the calculation of present worth values, at this point it might be well to review some fundamentals of financial arithmetic.[7] The appendix contains a simple derivation of some of these relationships so that only the resultant relationships are listed below. A present sum, P, invested at an interest rate, i, will be worth,

$$S = P\,(1 + i)^n \tag{1}$$

at the end of n interest periods. Conversely, the present worth of a future lump sum payment, S, is,

$$P = S\left[\frac{1}{(1 + i)^n}\right] \tag{2}$$

That is, the amount, P, must be invested now at interest, i, to be worth the sum, S, at the end of n interest periods. The bracketed factor in equation (2) is known as the "single payment present worth factor".

Other simple relationships may be derived which involve a uniform series of payments. If a uniform investment, R, is made at the end of each of n interest periods, the accumulated lump sum, S, at the end of these n periods will be,

$$S = R\left[\frac{(1 + i)^n - 1}{i}\right] \tag{3}$$

* Although not strictly correct, the terms "annual revenue requirements" and "annual costs" have through usage come to mean the same thing.

Equation (3) may be solved for R in order to determine what equal series of annual investments is required to accumulate a total sum, S, at the end of n periods. That is,

$$R = S \left[\frac{i}{(1+i)^n - 1} \right] \qquad (4)$$

The bracketed term is known as the "sinking fund factor". It is a useful relationship in engineering economics because this factor gives the annual depreciation rate at which funds must be accumulated in order to recover the original capital investment.

With the aid of equation (1), the uniform series of payments, R, required to pay back a present debt, P, in n periods may be calculated. That is,

$$R = P \left[\frac{i}{(1+i)^n - 1} + i \right] \qquad (5)$$

This factor is designated as the "capital recovery factor" in the literature. The above relationship will also assist in answering the question, "What is the present worth (P) of uniform series of payments (R)?" The answer is, of course,

$$P = R \left[\frac{(1+i)^n - 1}{i\,(1+i)^n} \right] \qquad (6)$$

The bracketed term in this expression is also a present worth factor and is sometimes referred to as the "uniform annual series present worth factor". This present worth factor plus that of equation (2) are the relationships which are most useful in engineering economic studies. Fortunately, the numerical values of these factors are widely available in texts on economics or mathematics handbooks so that the equations need not be used directly.[7]

Annual Revenue Requirements

The two-step operation for comparing on an economic basis various alternative proposals may be restated briefly as:

1. Estimate future annual revenue requirements (i.e., annual costs).

2. Calculate the present worths of these revenue requirements for nonumiform annual expenditures.

The tools necessary for the computations required in the second step have been outlined above. A convenient and widely used technique for estimating the annual costs is that of using an annual carrying charge. If the expected capital expenditures in a given year are designated as E, and the annual carrying charge is I, (a decimal number) then the annual revenue requirement for these capital expenditures (C) is,

$$C = E \times I \qquad (7)$$

In the usual situations encountered, there will be other annual revenue requirements in addition to those for capital expenditures. Such things as estimated operating and maintenance and charges for energy losses where applicable must be added to C in order to determine the total annual cost.

The annual carrying charge is made up of a sum of four categories of required rates of return. This number must include:

1. A rate of return for depreciation.

2. A rate of return for the cost of capital funds.

3. A rate of return for income taxes.

4. A rate of return for other expenses, such as local and other taxes and insurance costs.*

The use of a uniform annual carrying charge greatly facilitates the estimation of annual costs. In some areas, different rates are used for different portions of a power system (e.g., generation, transmission, and distribution) but for many preliminary studies a common charge for the entire system may be found to be adequate.

For a "typical" present day, investor-owned American utility, these rates of return are about as follows:

Item	Required Annual Rate of Return
Other Expenses }	7.7%
Income Taxes }	
Depreciation	1.3%
Capital Costs	6.0%
Total	15.0%

There are, of course, many variations of these rates throughout the industry, but they will usually vary between limits of 10 to 17%, depending upon the nature and location of the particular company. Expenses and taxes probably depend the most on locality. Fortunately, it is usually a relatively easy matter to obtain an estimate of the annual return rate required for these items from the accounting and other historical data of a particular utility.

The rate required for depreciation is a matter of some dispute in the industry. This rate depends upon the estimated life of the equipments, its estimated scrap value, whether or not dispersion must be considered, and in some instances, the type of depreciation funding actually used. Where depreciation rates are of some concern, they are probably handled best by separating the depreciation revenue requirements from the annual carrying charge. In that case, a year-by-year estimate may be made, the present worth of these depreciation requirements calculated, and if so desired, an equivalent uniform annual rate may be calculated using the capital recovery factor given in equation (5). This equivalent uniform annual rate then plays the same role as that assumed here. The 1.3% figure above was calculated from the sinking fund factor of equation (4). That is, the annual depreciation rate is,

$$d = R/S \qquad (8)$$

* In some situations, it also may be appropriate to include maintenance charges (as a percentage of capital costs) in the other expense category.

and the 1.3% figure was arrived at by assuming a 6% cost of money (i) and zero scrap value at the end of a 30 year life (n).

The capital costs (i.e., interest rate or "cost of money") for a utility depend upon the method of borrowing used. For the most part, long term capital funds are obtained by the selling of stocks and bonds. Historically, the capitalization of an electric light and power company is usually split equally between stocks and bonded indebtedness. For example, the weighted cost of capital may be estimated as shown in the following:

	Approximate % of Capitalization	Approximate Rate of Return	Weighted Capital Cost
Bonds	50%	4%	2.0%
Common Stock	35	10	3.5%
Preferred Stock	15	4	0.6
Totals	100%		6.1%

The 10% rate of return for common stock includes earnings and surplus which is plowed back into the company as well as the paid-out dividends to the shareowners. This weighted cost of capital for long term investments will usually run between 5 and 7%, varying for local conditions and, of course, with the over-all economic situation. Where short term capitalization enters the economic picture, the rate at which bank loans are made may have to be used in estimating the over-all cost of capital.

In making these engineering economic studies, a question which may arise is, "How long should the study period be?" There are many answers to this question for specific situations. In general, however, the purpose of the engineering economic analysis is to determine the most economic choice between alternatives. Since this is the case, it is sufficient to use a study period which is long enough so that the present worths of the differentials in annual revenue requirements between the various alternatives are negligible. If this criteria is adhered to, then the economic choice will not be influenced by neglecting future annual cost differences. Usually a study period of from 30 to 50 years will be found to suffice.

For illustrative purposes in the example which follows, the "typical values" (viz, i = 6%, I = 15%, n = 50 years) will be utilized. It may seem that the procedure has been too greatly over-simplified. However, the controversial items in the theory of engineering economic analyses (primarily concerned with depreciation) will not influence the over-all procedure and general technique discussed here. Both the simplest and the most difficult engineering economic analyses are identical in the conceptual problems they present. It is usually only in the details of calculating the annual carrying charge rate that these controversial difficulties enter in.

TRANSMISSION ECONOMICS EXAMPLE

The example to be used has been chosen because it illustrates the basic concepts and required arithmetic computations, and further, it illustrates how generalized data on annual revenue requirements (i.e., costs) may be utilized to provide rapid estimates of an economic situation. The problem briefly stated is as follows. A new station, located 100 miles from a 115 KV load area is to be built with an ultimate capacity of 600 MW.

300 MW will be installed initially and it has been estimated that the remaining 300 MW unit will be in service five years later. The system is shown on Fig. 2. Two plans have been suggested and tested for technical feasibility. Both have been shown to be equally attractive from a technical and operating viewpoint. The first plan calls for installing two 230 KV circuits initially to deliver the 300 MW load, and then in five years, when the capacity is 600 MW, installing two additional 230 KV circuits. The alternative is to install two 345 KV circuits. Initially, at the 300 MW level, they will be moderately loaded. However, when the system load is 600 MW, the two 345 KV circuits will be economically loaded. The question to be answered is which is the most economic voltage, while the over-all problem is to select the proper voltage level.

Since only the transmission system is involved in the choice, only the annual revenue requirements chargeable to this portion of the system need to be estimated. The annual cost of transmission, C_T, has been calculated from general system studies and presented in the literature.[8,9] This annual cost may be calculated as a function of the peak received power, P_r, in kilowatts on a per circuit basis. The general method of calculating these annual transmission costs is presented in reference 9 and is repeated briefly below. Referring to Fig. 2, it may be seen that the revenue requirements assignable to each transmission circuit must include returns for capital expenditures for:

1. The installed cost of 100 miles of line.
2. The installed cost of four HV breakers and associated equipments.
3. The installed cost of both sending and receiving end transformers.
4. The installed cost of the required KVAR support at the receiving end.
5. The cost of the additional generating capacity to accommodate the peak losses.

In addition, there is an annual revenue requirement to pay for the energy losses (KWH) of the transmission system.

In symbolic form, the annual transmission cost in dollars per KW received per circuit, C_T, is,

$$C_T = \frac{I}{P_R}\left[C_{LINE} + 4C_{CB} + C_{TRF} + C_{KVAR} + C_{LOSS}\right] + \frac{AC_{EL}}{P_R} \qquad (9)$$

where:

C_{LINE}, C_{CB}, . . . etc. = investment costs in dollars for the equipment, associated gear, buildings and installation

AC_{EL} = annual cost of KWH losses, dollars

P_R = peak received KW per circuit

With an annual carrying charge (I) of 15% and with system cost assumptions similar to

those of reference 9, the annual transmission cost for the 230 and 345 KV systems are as shown on Fig. 3. These data are very similar to the data of the reference except for a change in units and for the 15% carrying charge.* In fact, since the annual cost is almost directly proportional to the carrying charge rate, the data of Fig. 3 could be estimated quite accurately by direct ratioing from the data of the reference.

From the curves of Fig. 3, the annual revenue requirements of both schemes may be obtained for both phases of the planned expansion. These annual costs are shown in Table I below.

Table I
Annual Transmission Cost Data

Phase	System Load MW	Annual Costs					
		230 KV			345 KV		
		Circuits	$/KW	Total*	Circuits	$/KW	Total*
1	300	2	7.05	2.12	2	9.36	2.81
2	600	4	7.05	4.23	2	6.50	3.90

*Total annual costs are expressed in millions of dollars

From this tabulation it may be seen that the annual revenue requirements are nonuniform for the 345 KV system. At the 300 MW level during phase 1, using the two 230 KV circuits will save almost $700,000 yearly. On the other hand, when the 345 KV circuits are more fully utilized during the second phase, the higher voltage scheme will require $330,000 less in revenue annually. Obviously, the most economic choice will depend upon the time delay before the station reaches full capacity.

Assuming now that the second phase will start in five years, the present worths of both schemes may be calculated as follows for phase 1,

$$P_1 = \left(\begin{array}{l}\text{Uniform Series PWF for}\\ \text{a series five years long}\end{array}\right) \times \left(\begin{array}{l}\text{Annual Costs}\\ \text{during phase 1}\end{array}\right)$$

while for the second phase, the present worth is,

$$P_2 = \left\{\left(\begin{array}{l}\text{Uniform Series PWF for}\\ \text{a series 45 years long}\end{array}\right) \times \left(\begin{array}{l}\text{Annual Costs}\\ \text{during phase 2}\end{array}\right)\right\} \times \left\{\begin{array}{l}\text{Lump Sum PWF for}\\ \text{a payment 5 years}\\ \text{in the future}\end{array}\right\}$$

The total present worth of the revenue requirements of each plan is, of course, the sum of the present worth values of the annual requirements during each phase. For example, for the 230 KV alternative and in millions of dollars;

$P_1 = 4.21 \times 2.12 = \$\ 8.9$

$P_2 = (15.46 \times 4.23) \times 0.75 = \underline{48.8}$

$P = P_1 + P_2 = \$57.7$

* For a load factor of 65% and a loss factor of 54.5%, the dollars per KW figures may be converted to mills per KWH by dividing by a factor of 5.694.

That is, the future annual revenue requirements for the 230 KV system are 57.7 million dollars. By a similar simple calculation, the revenue requirements of the 345 KV alternative may be shown to be 56.8 million dollars. Therefore, the economic evaluation has indicated that the two alternatives are very close with the higher voltage scheme having a slight economic margin.

Because there is no overwhelming economic choice, it may be of interest to repeat the calculation to show the influence of the time to full capacity on the economic choice. Fig. 4 shows the present worths of future revenue requirements for both alternatives as a function of the number of years required to reach the 600 MW level. From this Fig. it may be noted that if the time to full capacity is six years of longer, then the lower voltage, lower investment cost alternative is most attractive. On the other hand, if the 600 MW level is reached in less than six years, the 345 KV alternative offers an economic advantage.

These simple calculations permit an answer to the question of which is the most economic voltage for the proposed system. The answer to the economic problem depends upon the time delay involved in utilizing the full station capacity and the answer to the over-all planning problem of which is the proper voltage choice may depend not only upon the economic answer, but also on many other factors. For example, the remainder of the particular transmission system may consist of heavily loaded 115 KV circuits which require reinforcing at the 345 KV level, while on the other hand, there may already be new 230 KV class lines being built in the particular system and its neighbors so that an eventual interconnection could easily be made at 230 KV. These remarks are intended to emphasize that the economic evaluation of the various alternatives in planning for future conditions is only part of the over-all evaluation that must be made.

CONCLUSIONS

In discussing the role of economics in power system planning, many topics and related subjects enter in. These include such important areas as the effect of inflation and the evaluation of the cost of system losses. These and other interesting topics have been covered by other authors.[10,11,12] This paper has been confined to a simple discussion of the place of economic evaluation in power system planning. It has been illustrated by a transmission economics problem that the economic choice between several alternatives is that plan which has the lowest present worth of all future revenue requirements. Further, it has been shown that the engineering economic evaluation consists basically of two relatively simple steps; estimating the annual costs and calculating the present worth of these annual revenue requirements.

APPENDIX

Simple Financial Mathematics

The relationships, nomenclature, and derivations presented here are essentially the same as those given by Grant in "Principles of Engineering Economy."[7] All of these relationships are concerned with and based on the concept of interest. Interest is the cost of money or, to be more verbose, interest is the return obtainable by the productive investment of capital.

For a nomenclature let,

i = the interest rate expressed as a decimal

n = the number of interest periods

P = a present sum

S = a sum equal to P at the end of n interest periods with interest rate i, and

R = annual payment in a uniform series continuing for n periods.

At the end of a single period, a single investment, P, is worth

$$S = P(1 + i)$$

Now, a simple computation will show the value of a present investment left at compound interest for n periods.

Time	Value of Investment		
	Principle	Interest	Total
0 (now)	P	0	P
1 period	P	i P	P(1 + i)
2 periods	P(1 + i)	i P(1 + i)	$P(1 + i)^2$
3 periods	$P(1 + i)^2$	$i P(1 + i)^2$	$P(1 + i)^3$
⋮	⋮	⋮	⋮
n periods	$P(1 + i)^{n-1}$	$i P(1 + i)^{n-1}$	$P(1 + i)^n$

That is,

$$S = P(1 + i)^n$$

gives the value of P at the end of n periods.

Now, for a uniform series of investments at the end of each interest period, a similar tabulation will show the total value of the investment at the end of n periods.

Time End of Period Number	Investment	Value of Investment at the end of n Periods
1	R	$R(1 + i)^{n-1}$
2	R	$R(1 + i)^{n-2}$
3	R	$R(1 + i)^{n-3}$
⋮	⋮	⋮
n	R	R

The total value is obviously the sum of the values of each individual payment. That is,

$$S = R + R(1 + i) + R(1 + i)^2 + \ldots + R(1 + i)^{n-1}$$

or,

$$S = R\left(1 + (1 + i) + (1 + i)^2 + \ldots + (1 + i)^{n-1}\right)$$

Therefore,

$$S(1 + i) = R\left((1 + i) + (1 + i)^2 + (1 + i)^3 + \ldots + (1 + i)^n\right)$$

and subtracting this from the previous equation gives,

$$iS = R\left((1 + i)^n - 1\right).$$

This may be seen to be equation (3) of the paper.

REFERENCES

1. "Long Range Planning Essential," H. L. Melvin and P. E. Gourdon, Electrical World, Oct. 3, 1955, pp. 98-99.
2. "Annual Carrying Charges in Economic Comparisons of Alternate Facilities," P. H. Jeynes, A.I.E.E. Transactions, Vol. 70, 1951, pp. 1942-1953.
3. "Operating and Maintenance Costs for Use in the Economic Comparison of Alternative Facilities," W. E. Slemmer, A.I.E.E. Transactions, Vol. 70, 1951, pp. 1954-1955.
4. "Some New Mathematical Aspects of Fixed Charges," C. W. Bary and W. T. Brown, A.I.E.E. Technical Paper 57-152.
5. "The Criterion of Economic Choice," P. H. Jeynes and L. Van Nimwegen, A.I.E.E. Technical Paper 58-113.
6. "Present Worth, or the Time Cost of Money, as a Factor in the Economic Comparison of Alternative Facilities," P. H. Jeynes, A.I.E.E. Transactions, Vol. 70, 1951, pp. 1956-1962.
7. "Principles of Engineering Economy," (Book), E. L. Grant, The Ronald Press Co., New York, Third Edition, 1950.
8. "Economics of Long-Distance A-C Power Transmission," S. B. Crary and I. B. Johnson, A.I.E.E. Transactions, Vol. 66, 1947, pp. 1092-1099.
9. "An Economic Study of High Voltage Transmission," J. M. Henderson and A. J. Wood, A.I.E.E. Transactions, Vol. 75, Part III, 1956, pp. 695-700.
10. "Evaluation of Energy Differences in the Economic Comparison of Alternative Facilities," A. P. Fugill, A.I.E.E. Transactions, Vol. 70, 1951, pp. 1854-1860.
11. "Economic Studies Applied to Industrial Power Systems," H. B. Backenstoss, A.I.E.E. Transactions, Vol. 75, Part II, 1956, pp. 61-70.
12. "Economic Evaluation of Industrial Power System Reliability," W. H. Dickinson, A.I.E.E. Transactions, Vol. 76, Part II, 1957, pp. 264-272.

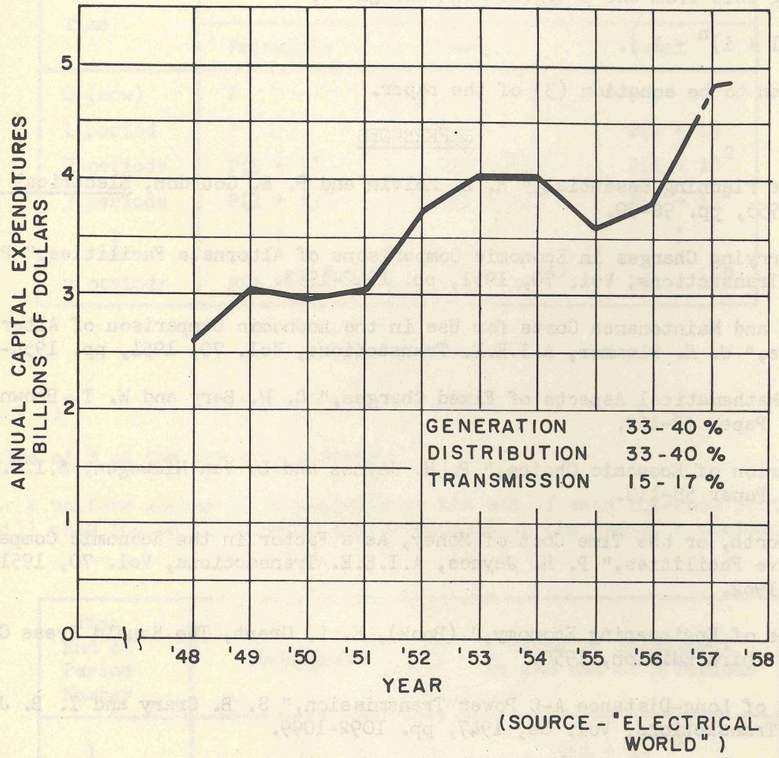

Fig. 1. Annual level of capital expenditures by American Electric Utilities

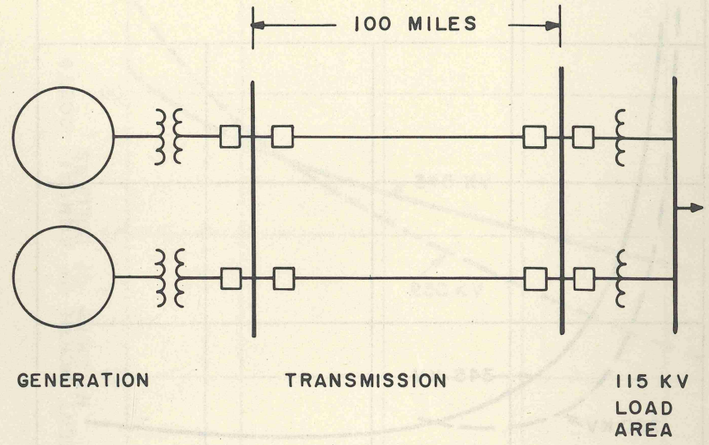

Fig. 2. 100 mile transmission system for economic example

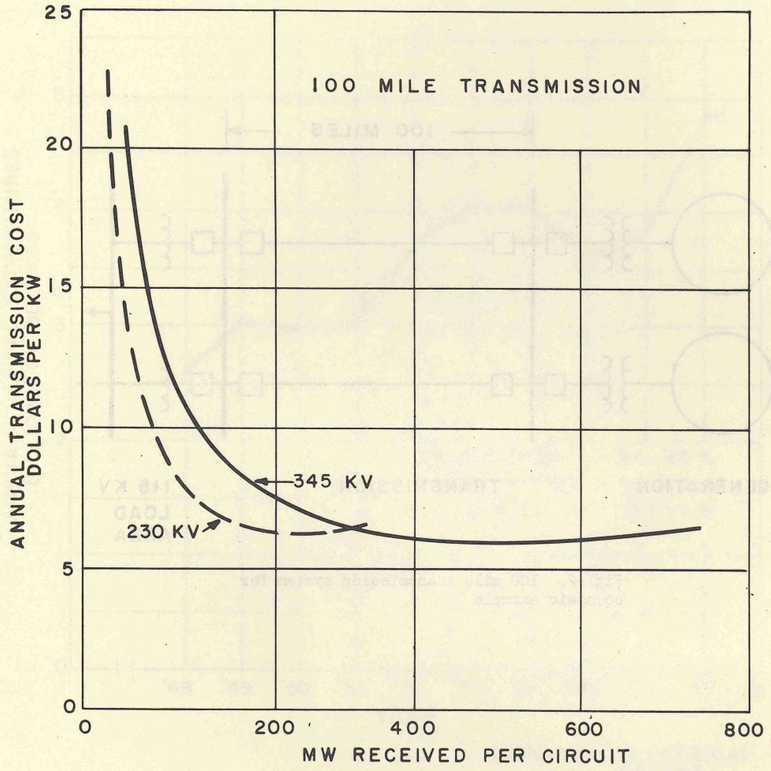

Fig. 3. Annual revenue requirements for 100 mile transmission system at a 15 percent annual carrying charge rate

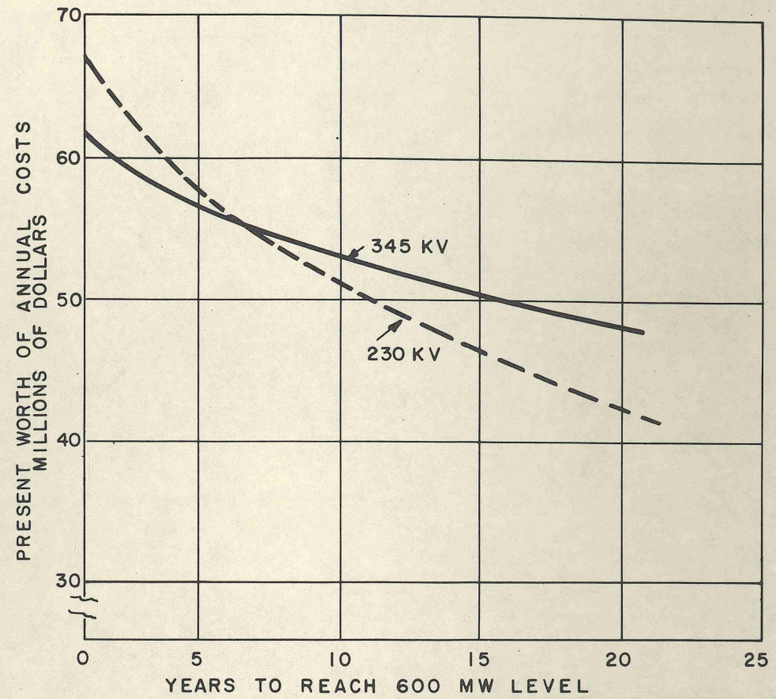

Fig. 4. Revenue requirements for 100 mile transmission as a function of the time to full utilization of the station capacity

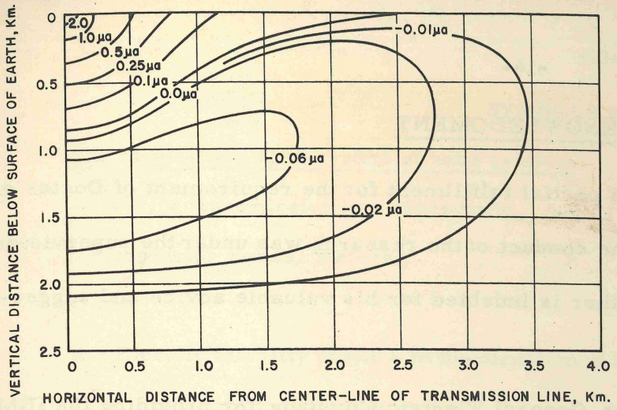

Figure 3. Constant current density plot of the imaginary component of zero-sequence current density in microamps per square meter per amp of zero-sequence current per phase. Conductor height 20 meters, spacing 10 meters and earth conductivity 10 micromhos/meter.

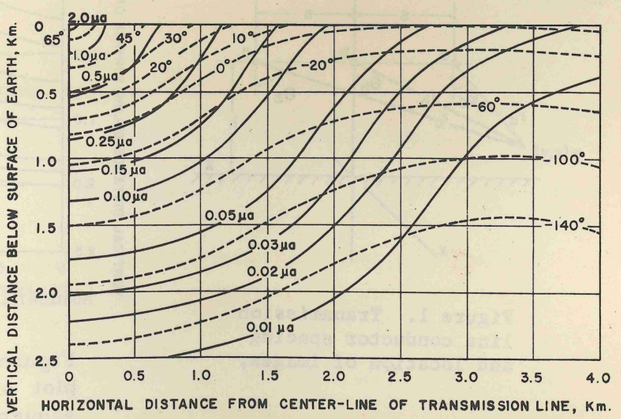

Figure 4. Constant current density plot of the magnitude and phase angle of the zero-sequence current density in microamps per square meter per amp of zero-sequence current per phase. Conductor height 20 meters, spacing 10 meters and earth conductivity 10 micromhos/meter.

RECEIVED
NOV 20 1958
H. A. FREY

Paper No.
59-893

Milton
" Kamichi
" Kingsbury

Miss.

Transactions Paper

(Reviewed and Accepted for Publication)

ZERO-SEQUENCE CURRENT DENSITY IN THE EARTH

Marion E. Forsman
Member AIEE
University of Florida
Gainesville, Fla.

A paper recommended by the AIEE Transmission and Distribution Committee and approved by the AIEE Technical Operations Department for presentation at the AIEE Summer and Pacific General Meeting and Air Transportation Conference, Seattle, Wash., June 21-26, 1959. Manuscript submitted July 29, 1955; made available for printing May 1, 1959.

Price: 40¢ To Members
80¢ To Nonmembers

(5¢ per copy additional if first class mailing desired)

All Rights Reserved by the
American Institute of Electrical Engineers
33 West 39th Street, New York 18, N. Y.
Litho in USA

RECEIVED
MAY 6 1959
RECEIVED
MAY 26 1959
ENG. DEPT.
ENG. DEPT.

Discussion in Duplicate Due July 10, 1959.

ZERO-SEQUENCE CURRENT DENSITY IN THE EARTH

Marion E. Forsman

Many authors have published articles concerning the zero-sequence impedance of transmission lines with ground return, but few, if any, have been concerned with the distribution of current in the earth under the transmission line. Since this distribution of current is a major factor in the variations in impedance, a more thorough knowledge of its behavior should contribute to the general understanding of transmission line theory. It is therefore the objective of this paper to develop an equation for this current density and to determine the zero sequence current density in the earth under a three-phase transmission line twenty meters high with ten meters between conductors. The earth is assumed to be homogeneous with a conductivity of 0.01 mhos/meter.

Carson[1] developed the equations for determining the impedance of transmission lines with ground return as well as the electric intensity in the ground. This derivation for the three-phase transmission line follows the method introduced by Carson.

While it is recognized that the ideal case assumed does not yield results which are representative of installed transmission lines, it is shown that current flow at some distance from the transmission line cannot be neglected. Additional investigations assuming a nonhomogeneous earth should be made in order to determine the effect of low conductivity layers beneath the surface.

The current density in the earth under a transmission line is dependent on the characteristics of both the earth and the transmission line. A better understanding of transmission line characteristics should develop if the physical phenomena associated with short circuit current flow in the earth is better known. This paper is intended to develop the equations of the current density in the earth and, by example, show the distribution of zero sequence current in the earth under a three-phase transmission line with ground return assuming ideal conditions. The derivation used here follows the method developed by J. R. Carson.

The determination of the zero-sequence current density under a transmission line is dependent on the configuration of the line. A general configuration would assume each conductor at a different height above the earth and no two equal spacings between conductors. Since the general configuration is not often used, the derivation of equations will be made for a less general case. Figure 1 is the cross-section of the transmission line which will be used for derivation.

The following assumptions were made:

1. The earth is a homogeneous conductor of conductivity σ

2. The permeability, μ, of the earth is equal to that of free space and the capacivity is not greater than 30 times that of free space
3. In the earth all current flow is parallel to the axis of the transmission line
4. All voltages and currents are sinusoidal and contain the exponential $e^{(j\omega t-\gamma z)}$
5. The transmission line is perfectly transposed
6. The free charge density in the earth is zero.

The wave equation for the electric intensity is:

$$\nabla^2 E = -j\omega\mu(-\sigma + j\omega\epsilon)E. \tag{1}$$

The symbols are defined in the Symbols and Units.

From assumption 3, $E_x = E_y = 0$ and from assumption 4, $E_z = |E_z|e^{(j\omega t - \gamma z)}$.

Thus:

$$\nabla^2 E = \frac{\partial^2 E_z}{\partial x^2} + \frac{\partial^2 E_z}{\partial y^2} + \frac{\partial^2 E_z}{\partial z^2}. \tag{2}$$

Since z is constant,

$$\nabla^2 E = \frac{\partial^2 E_z}{\partial x^2} + \frac{\partial^2 E_z}{\partial y^2}. \tag{3}$$

Substitution of equation (3) into equation (1) yields

$$\frac{\partial^2 E_z}{\partial x^2} + \frac{\partial^2 E_z}{\partial y^2} = -j\omega\mu(-\sigma + j\omega\epsilon)E_z. \tag{4}$$

If $\frac{\omega\epsilon}{\sigma}$ is less than 0.01, the term $j\omega\epsilon$ may be neglected. Assuming the minimum conductivity of the earth to be 10 μmhos/meter and the frequency to be 60 cps,

$$\frac{\omega\epsilon}{\sigma} = \frac{120\pi(10^5)(30)}{36\pi(10^9)} = 0.01 \tag{5}$$

Therefore the wave equation may be written

$$\frac{\partial^2 E_z}{\partial x^2} + \frac{\partial^2 E_z}{\partial y^2} = j\omega\mu\sigma E_z \tag{6}$$

for the assumed conditions.

A general solution of equation (6) with the electric field symmetrical about the x-axis may be obtained from the infinite integral[1]

$$E_z = -\int_o^\infty F(u)\cos(xu)\, e^{y\psi(u)}\, du \qquad (7)$$

$F(u)$ is finite

$\psi(u)$ is finite and positive

$y \leqq 0$.

After evaluating the functions $F(u)$ and $\psi(u)$ by applying the proper boundary conditions, equation (7) may be written[2]

$$E_z = \frac{-I}{6\pi}\int_o^\infty \frac{j\omega\mu\, e^{y\sqrt{u^2 + j\omega\mu\sigma}}\cos(xu)\, e^{-hu}}{\sqrt{u^2 + j\omega\mu\sigma} + u}\left\{\frac{1}{\cos(xu)}\left[\cos(x+s)u + \cos(xu) + \cos(x-s)u\right] + \frac{1}{\sin(xu)}\left[\sin(x+s)u + \sin(xu) + \sin(x-s)u\right]\right\} du. \qquad (8)$$

Applying the proper trigonometric identities yields

$$E_z = -\frac{j\omega\mu I}{3\pi}\int_o^\infty \frac{e^{-(hu - y\sqrt{u^2 + j\omega\mu\sigma})}\cos(xu)\,[2\cos(su) + 1]}{-\sqrt{u^2 + j\omega\mu\sigma} + u} du$$

$$= -\frac{\omega\mu I}{3\pi\omega\mu\sigma}\int_o^\infty (\sqrt{u^2 + j\omega\mu\sigma} - u)\, e^{-(hu - y\sqrt{u^2 + j\omega\mu\sigma})}\cos(xu)\,[2\cos(su) + 1]du. \qquad (9)$$

Let

$$\begin{aligned} \sqrt{\omega\mu\sigma} &= \alpha \\ S &= \alpha s \\ D &= \alpha h \\ X &= \alpha x \\ Y &= \alpha y \\ u &= \alpha v \end{aligned} \qquad (10)$$

and substitute into equation (9). This substitution will not change the limits and therefore

$$E = -\frac{\omega\mu I}{3\pi}\int_o^\infty (\sqrt{v^2 + j} - v)\, e^{-(Dv - Y\sqrt{v^2 + j})}\cos(Xv)\,[2\cos(Sv) + 1]dv. \qquad (11)$$

Equation (11) gives the electric field intensity in the earth in integral form. A solution to this equation, when multiplied by $-\sigma$, will give the current density as a function of x, y, h, and s. A general solution for this equation was not available and attempts to solve it by series expansion were not successful. It was decided that a numerical solution for particular values of s and h would be made. Since the IBM facilities available could solve only problems involving real quantities, the integral was put into a form which

contained a real term and an imaginary term.

The term $\sqrt{v^2 + j}$ is the only term in the equation which is complex and the angle associated with the term is always less than 90°. Assume that

$$\sqrt{v^2 + j} = \delta + j\beta \qquad (12)$$

where δ and β are real numbers and positive.

The solution to equation (12) gives

$$\delta = \sqrt{\frac{v^2 + \sqrt{v^4 + 1}}{2}} = \frac{m}{\sqrt{2}} \qquad (13)$$

$$\beta = \frac{1}{\sqrt{2(v^2 + \sqrt{v^4 + 1})}} = \frac{1}{m\sqrt{2}} \qquad (14)$$

Substituting equations (13) and (14) into equation (11) gives

$$E_z = -\frac{\omega\mu I}{3\pi}\int_o^\infty \left[\frac{1}{\sqrt{2}}\left(m + \frac{j}{m}\right) - v\right]e^{-\left[Dv - \frac{Y}{\sqrt{2}}\left(m + \frac{j}{m}\right)\right]}\cos(Xv)\,[2\cos(Sv) + 1]dv. \qquad (15)$$

Since $i_z = -\sigma E_z$ and since this solution is restricted to $y \leqq 0$,

$$i_z(R) = \frac{\omega\mu\sigma I}{3\pi}\int_o^\infty [2\cos(Sv) + 1]\cos(Xv)e^{-(Dv + |Y|\frac{m}{\sqrt{2}})}\left[\left(\frac{m}{\sqrt{2}} - v\right)\cos\frac{|Y|}{m\sqrt{2}} + \frac{1}{m\sqrt{2}}\sin\frac{|Y|}{m\sqrt{2}}\right] dv \qquad (16)$$

$$i_z(\mathfrak{J}) = \frac{\omega\mu\sigma I}{3\pi}\int_o^\infty [2\cos(Sv) + 1]\cos(Xv)e^{-(Dv + |Y|\frac{m}{\sqrt{2}})}\left[\frac{m}{\sqrt{2}}\cos\frac{|Y|}{m\sqrt{2}} - \left(\frac{m}{\sqrt{2}} - v\right)\sin\frac{|Y|}{m\sqrt{2}}\right] dv. \qquad (17)$$

Where

$|Y|$ = absolute value of Y

$i_z(R)$ = real component of current density

$i_z(\mathfrak{J})$ = imaginary component of current density.

Simpson's Rule[3] was used to obtain numerical solutions for a conductor height of 20 meters and a conductor spacing of 10 meters. The error[3] involved in using Simpson's Rule was calculated in order to determine the proper intervals between ordinates for a given accuracy.

The IBM general purpose CPC system used for the calculations was known as the SEMAC (Series Evaluated functions, Mixed decimal, Arithmetic Computor). The machine was capable of processing about 80 to 100 cards per minute and required between 15 to 120 minutes to evaluate equations (16) and (17) for a single point P (x, y). The SEMAC had sufficient storage capacity to obtain the solutions to both of the equations at the same time. The length of time for the evaluation depends on the rate of convergence of the integrand as well as the rate of curvature. The details of programming the problem on the IBM punch cards and the method of operating the machine will not be discussed. The data obtained with the IBM facilities are plotted on Figures 2, 3, and 4 for $\sigma = 0.01$ mhos/meter.

The true accuracy of the calculations is not known, however, the error due to Simpson's Rule was less than 3 per cent. The error caused by the substitution of a finite upper limit for the infinite limit in equations (16) and (17) is also not known. Calculations were carried on until the value of the ordinate calculated was less than 5 per cent of the sum of the ordinates for small values of Y and less than 1 per cent for large values of Y. Errors in obtaining the value of the integrals near zero were probably quite large because of the finite value used for the upper limits.

It should be noted that the solutions may be used for other values of s, h, ω, and σ provided the values of S and D are not changed and the ratio s/h is held constant.

The curves shown in Figures 2, 3, and 4 represent the zero-sequence current distribution in the earth under the three-phase transmission line assumed for this study. The real component of current density shown in Figure 2 is the determining factor in the value of the zero-sequence reactance. A method for calculating this reactance is indicated in Appendix II.

Figure 4 shows the magnitude and phase angle of the current density and was obtained from Figures 2 and 3. The magnitude of the current density may be used to determine the resistive component of the zero-sequence impedance. A method for this determination is shown in Appendix II. The zero-sequence impedance value obtained using these data is compared with the value obtained using Carson's method in Appendix II also.

Figure 3 shows the reactive component of current density. At the surface of the earth directly under the transmission line this component leads the real component. This is in contradiction to Rudenberg's derivation[4] although this difference in phase angle

alone would not change the magnitude of impedance obtained using his method. The fact that the impedance for each tube of current in the earth varies in accordance with its location has a much greater effect on the total impedance than the phase angle difference at the surface.

The data presented indicate that the earth must be homogeneous for a vertical distance in excess of 2 to 2.5 km and a horizontal distance in excess of 3 to 4 km to obtain accurate calculations of the current density.

Since the assumptions made in deriving the equations do not represent the true condition existing in the earth, it might appear that the results of this study are not valid. However, the conditions assumed are not different from those assumed when solving for the transmission line impedance using the accepted methods. Certainly the current density will vary with conductivity and the nonhomogeneous earth will not allow the current to flow in straight smooth lines. A layer of high conductivity soil over a mass of low conductivity rock could distort the current distribution considerably. Without investigating the particular case, it is impossible to predict the results.

A continuing investigation of this problem should include the two layer earth. Before a complete understanding of the current density is obtained, considerable additional research is necessary.

APPENDIX I

The derivation of the axial electric intensity in the ground: The wave equation for this paper has been written

$$\frac{\partial^2 E_z}{\partial x^2} + \frac{\partial^2 E_z}{\partial y^2} = j\omega\mu\sigma E_z \qquad \text{(see Eq. 6)}$$

A general solution of this equation with the electric field symmetrical about the x-axis may be obtained from the infinite integral.[1]

$$E_z = -\int_0^\infty F(u)\cos(xu)\, e^{y\psi(u)}\, du \qquad (18)$$

$F(u)$ is finite

$\psi(u)$ is finite and positive

$y \leq 0$.

Substituting (18) into (6),

$$\int_0^\infty u^2 F(u)\cos(xu)\, e^{y\psi(u)}\, du$$

$$-\int_0^\infty F(u)\cos(xu)\,[\psi(u)]^2\, e^{y\psi(u)}\, du$$

$$+ j\omega\mu\sigma\int_0^\infty F(u)\cos(xu)\, e^{y\psi(u)}\, du = 0 \qquad (19)$$

or

$$\int_0^\infty F(u)\cos(xu)\, e^{y\psi(u)}\,[u^2 - \psi(u)^2 + j\omega\mu\sigma]\, du = 0\,. \qquad (20)$$

Since equation (20) is identically zero for all values of x, and y,

$$\psi(u) = \sqrt{u^2 + j\omega\mu\sigma}\,. \qquad (21)$$

Therefore

$$E_z = -\int_0^\infty F(u)\cos(xu)\, e^{y\sqrt{u^2 + j\omega\mu\sigma}}\, du. \qquad (22)$$

Since

$$\nabla \times E = i\frac{\partial E_z}{\partial u} - j\frac{\partial E_z}{\partial x} = -\mu\left(i\frac{\partial H_x}{\partial t} + j\frac{\partial H_y}{\partial t}\right)\,. \qquad (23)$$

$$\left.\begin{aligned}\frac{\partial E_z}{\partial y} &= -j\omega\mu H_x \\ \frac{\partial E_z}{\partial x} &= -j\omega\mu H_y\,.\end{aligned}\right\} \qquad (24)$$

Substituting equation (22) into equation (24) gives

$$H_x = \frac{1}{j\omega\mu}\int_0^\infty F(u)\sqrt{u^2 + j\omega\mu\sigma}\,\cos(xu)\, e^{y\sqrt{u^2 + j\omega\mu\sigma}}\, du \qquad (25)$$

and

$$H_y = \frac{1}{j\omega\mu}\int_0^\infty uF(u)\sin(xu)\, e^{y\sqrt{u^2 + j\omega\mu\sigma}}\, du\,. \qquad (26)$$

In the dielectric above the surface of the earth, the magnetic intensities may be written

$$H_x = H_{xa} + H_{xb} + H_{xc} + H_{xg} \qquad (27)$$

$$H_y = H_{ya} + H_{yb} + H_{yc} + H_{yg}\,. \qquad (28)$$

where the subscripts a, b, and c indicate the magnetic intensities due to the conductors a, b, and c as shown in Figure 1 and the subscript g indicates the intensity due to the current in the earth.

Assuming that the current flow in the conductors has a radial symmetry, that the total current, I, divides equally between conductors, i.e., applying assumption 6, and recognizing that $\sigma = 0$ in the dielectric, the magnetic intensities due to current flowing in the wires may be written

$$\left.\begin{aligned}H_{xn} &= \frac{I}{6\pi}\,\frac{\cos\theta_n}{r_n} \\ H_{yn} &= \frac{I}{6\pi}\,\frac{\sin\theta_n}{r_n}\end{aligned}\right\} \qquad n = a,\ b,\ c \qquad (29)$$

where (see Figure 1)

$$\left.\begin{aligned} r_a &= \sqrt{(x+s)^2 + (y-h_a)^2} \\ r_b &= \sqrt{x^2 + (y-h_b)^2} \\ r_c &= \sqrt{(x-s)^2 + (y-h_a)^2} \end{aligned}\right\} \qquad (30)$$

and

$$\left.\begin{aligned} \cos\theta_n &= \frac{h_n - y}{r_n} \\ \sin\theta_a &= \frac{x + s_a}{r_a} \\ \sin\theta_b &= \frac{x}{r_b} \\ \sin\theta_c &= \frac{x - s_c}{r_c} \quad . \end{aligned}\right\} \qquad (31)$$

The magnetic field intensity in the dielectric due to the current in the earth may be obtained from the infinite integral [1]

$$H_{xg} = + \int_0^\infty G(u)\cos(xu)\, e^{-yu}\, du \qquad y \geq 0 \qquad (32)$$

$$H_{yg} = - \int_0^\infty G(u)\sin(xu)\, e^{-yu}\, du \qquad y \geq 0 \quad . \qquad (33)$$

At the surface of the earth where y = 0, the magnetic intensities may be written [5]

$$\left.\begin{aligned} H_{xa} &= \frac{I}{6\pi} \int_0^\infty e^{-h_a u} \cos(x+s)u\, du \\ H_{xb} &= \frac{I}{6\pi} \int_0^\infty e^{-h_b u} \cos(xu)\, du \\ H_{xc} &= \frac{I}{6\pi} \int_0^\infty e^{-h_a u} \cos(x-s)u\, du \end{aligned}\right\} \qquad (34)$$

and

$$\left.\begin{aligned} H_{ya} &= \frac{I}{6\pi} \int_0^\infty e^{-h_a u} \sin(x+s)u\, du \\ H_{yb} &= \frac{I}{6\pi} \int_0^\infty e^{-h_b u} \sin(xu)\, du \\ H_{yc} &= \frac{I}{6\pi} \int_0^\infty e^{-h_a u} \sin(x-s)u\, du \quad . \end{aligned}\right\} \qquad (35)$$

Combining equations (32) and (33) for y = 0 with equations (34) and (35) respectively, yields

$$H_x = \int_0^\infty \left\{ G(u)\cos(xu) + \frac{I}{6\pi}\left[e^{-h_a u}\cos(x+s)u + e^{-h_b u}\cos(xu) + e^{-h_a u}\cos(x-s)u\right]\right\} du \qquad (36)$$

$$H_y = \int_0^\infty \left\{ -G(u)\sin(xu) + \frac{I}{6\pi}\left[e^{-h_a u}\sin(x+s)u + e^{-h_b u}\sin(xu) + e^{-h_a u}\sin(x-s)u\right]\right\} du \qquad (37)$$

From assumption 2, the normal and tangential components of magnetic intensity are continuous across the boundary at the surface of the earth. Therefore, the values of H_x and H_y of equations (25) and (26), with y = 0, are equal to H_x and H_y of equations (36) and (37) respectively. Thus

$$\frac{1}{j\omega\mu}\sqrt{u^2 + j\omega\mu\sigma}\, F(u)\cos(xu) - G(u)\cos(xu) - \frac{I}{6\pi}\left[e^{-h_a u}\cos(x+s)u + e^{-h_b u}\cos(xu) + e^{-h_a u}\cos(x-s)u\right] = 0 \qquad (38)$$

and

$$\frac{u}{j\omega\mu} F(u)\sin(xu) + G(u)\sin(xu) - \frac{I}{6\pi}\left[e^{-h_a u}\sin(x+s)u + e^{-h_b u}\sin(xu) + e^{-h_a u}\sin(x-s)u\right] = 0 \quad . \qquad (39)$$

Simultaneous solution of equations (38) and (39) gives

$$F(u) = \frac{I}{6\pi} \frac{j\omega\mu}{\sqrt{u^2 + j\omega\mu\sigma} + u} \left\{ \frac{1}{\cos(xu)} \left[e^{-h_a u} \cos(x + s)u + e^{-h_b u} \cos(xu) + e^{-h_a u} \cos(x - s)u \right] + \frac{1}{\sin(xu)} \left[e^{-h_a u} \sin(x + s)u + e^{-h_b u} \sin(xu) + e^{-h_a u} \sin(x - s)u \right] \right\} \quad (40)$$

and

$$G(u) = \frac{I}{6\pi} \left(1 - \frac{u}{\sqrt{u^2 + j\omega\mu\sigma} + u}\right) \frac{1}{\sin(xu)} \left[e^{-h_a u} \sin(x + s)u + e^{-h_b u} \sin(xu) + e^{-h_a u} \sin(x - s)u \right] - \frac{I}{6\pi} \left(\frac{u}{\sqrt{u^2 + j\omega\mu\sigma} + u}\right) \frac{1}{\cos(xu)} \left[e^{-h_a u} \cos(x + s)u + e^{-h_b u} \cos(xu) + e^{-h_a u} \cos(x - s)u \right] . \quad (41)$$

Substituting the value of F (u) into equation (22) gives the value of E_z in the earth.

$$E_z = \frac{-I}{6\pi} \int_o^\infty \frac{j\omega\mu \, e^{y\sqrt{u^2 + j\omega\mu\sigma}} \cos(xu)}{\sqrt{u^2 + j\omega\mu\sigma} + u} \left\{ \frac{1}{\cos(xu)} \left[e^{-h_a u} \cos(x + s)u + e^{-h_b u} \cos(xu) + e^{-h_a u} \cos(x - s)u \right] + \frac{1}{\sin(xu)} \left[e^{-h_a u} \sin(x + s)u + e^{-h_b u} \sin(xu) + e^{-h_a u} \sin(x - s)u \right] \right\} du. \quad (42)$$

There are two general configurations which are in common use in three-phase transmission line construction. For one configuration $h_a < h_b$ while for the other $h_a = h_b$. For the remainder of this derivation assume that $h_a = h_b = h$. Substituting this value into equation (42) and applying the proper trigonometric identities yields

$$E_z = -\frac{j\omega\mu I}{3\pi} \int_o^\infty \frac{e^{-(hu - y\sqrt{u^2 + j\omega\mu\sigma})} \cos(xu)}{\sqrt{u^2 + j\omega\mu\sigma} + u} \left[2\cos(su) + 1\right] du \quad (43)$$

This is equation (9) in the article.

APPENDIX II

Reactance and Resistance Calculations from Figures 2 and 4

In order to check the validity of the calculated current density, the impedance of the transmission line was determined, using conventional methods, and compared with the results of this investigation.

The reactance calculation may be made assuming that the earth may be divided into a finite number of conductors of circular cross section with each conductor carrying a particular portion of the current. For this calculation, only the real component of current density was considered because the imaginary flux linkages are zero. Figure 2 was used to determine the currents and distances to be used in the equation for the reactance and was divided into the assumed conductors by drawing circles between current density lines tangent to the curves and the adjacent circles. The current carried by each assumed conductor was determined by drawing a line from one current density line to the next through the points of tangency of the adjacent circles, measuring this area with a planimeter, and calculating the current using an average value of current density. The average value used was not an arithmetic average but a value obtained by assuming the curves to be conic in shape and therefore dependent on the square root of the sum of the squares of the radii of the bounding curves.

Summing the reactance of the assumed conductors in the normal manner gives the total reactance. This calculation yields a total reactance of 2.00 ohms/mile/phase which compares well with the 2.04 ohms/mile/phase obtained using the method of Carson and others.

Calculation of the resistive component may be made using either Figure 4 or Figures 2 and 3. This calculation consists of a graphical integration of the I^2R losses and then dividing the total power loss by the square of total current. The incremental areas used were those included between the constant current density lines, and the average value of the current density was computed in a manner similar to that used for the reactance calculations. A resistance value of 0.270 ohm/mile/phase obtained by this method compares with 0.272 ohm/mile/phase calculated using the method of Carson.

REFERENCES

1. Wave Propagation of Overhead Wires with Ground Return, John R. Carson. Bell System Technical Journal, volume 5, 1926, pages 539-54.
2. Zero-Sequence Impedance of a Three-Phase Transmission Line with Ground Return (thesis), Marion E. Forsman. Iowa State College, 1954.
3. Numerical Mathematical Analysis (book), James B. Scarborough. The Johns Hopkins Press, 1950, second edition, page 132.
4. Transient Performance of Electric Power Systems (book), R. Rudenberg. McGraw-Hill Book Co., Inc., 1950, pages 392-402.
5. Nouvelles tables d'intégrales definies. D. Bierans De Haan. G. E. Stechert & Co. 1929, page 383.

SYMBOLS AND UNITS

The rationalized MKS system of units is used.

a, b, c, = transmission line conductors

d = conductor radius, meters

D = αh

E = Electric intensity positive in the direction of increasing potential, volts/meter

F(u), ψ(u) = arbitrary functions of u

h = transmission line conductor height, meters

I = zero-sequence current, amperes

i = current density, microamperes/meter^2

$\mathfrak{I}$ = imaginary component

j = operator $\sqrt{-1}$

L = inductance, henries

m = defined function of v

R = real component

S = αs

s = transmission line conductor spacing, meters

t = time, seconds

u, v = variables of integration

X = αx

x, y, z = rectangular coordinates, meters

Y = αy

$\alpha^2 = \omega\mu\sigma$

γ = attenuation constant, per meter

δ, β = real positive constants

ϵ = dielectric constant of free space

σ = conductivity of the earth, mhos/meter

ω = angular frequency, radians/second

μ = permeability of free space

ρ = radial distance from transmission line, meters

ACKNOWLEDGMENT

This research was performed in partial fulfillment for the requirement of Doctor of Philosophy at Iowa State College. The conduct of the research was under the supervision of Dr. W. B. Boast to whom the author is indebted for his valuable advice and suggestions during the investigation.

Appreciation is expressed to the General Electric Company for providing the IBM facilities and to Messrs. P. M. Thompson, D. O. Banks, D. D. McCracken and other members of the Computing Unit at the Hanford Atomic Products Operation for their assistance in programming the numerical solution and in operating the IBM equipment.

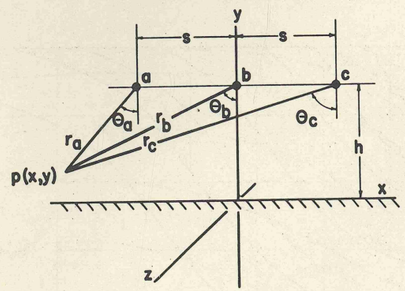

Figure 1. Transmission line conductor spacing and location of images.

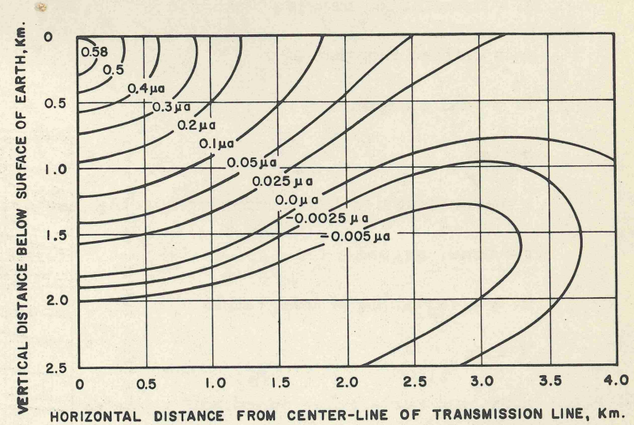

Figure 2. Constant current density plot of the real component of zero-sequence current density in microamps per square meter per amp of zero-sequence current per phase. Conductor height 20 meters, spacing 10 meters and earth conductivity 10 micromhos/meter.

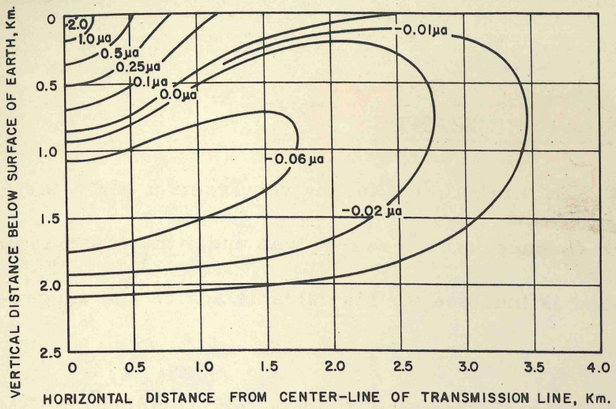

Figure 3. Constant current density plot of the imaginary component of zero-sequence current density in microamps per square meter per amp of zero-sequence current per phase. Conductor height 20 meters, spacing 10 meters and earth conductivity 10 micromhos/meter.

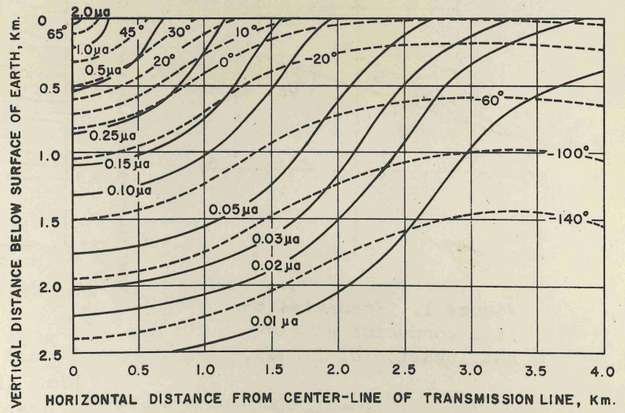

Figure 4. Constant current density plot of the magnitude and phase angle of the zero-sequence current density in microamps per square meter per amp of zero-sequence current per phase. Conductor height 20 meters, spacing 10 meters and earth conductivity 10 micromhos/meter.

RECEIVED
NOV 30 1959
M. A. FREY

Paper No.
59-893

Transactions Paper

(Reviewed and Accepted for Publication)

ZERO-SEQUENCE CURRENT DENSITY IN THE EARTH

Marion E. Forsman
Member AIEE
University of Florida
Gainesville, Fla.

A paper recommended by the AIEE Transmission and Distribution Committee and approved by the AIEE Technical Operations Department for presentation at the AIEE Summer and Pacific General Meeting and Air Transportation Conference, Seattle, Wash., June 21-26, 1959. Manuscript submitted July 29, 1955; made available for printing May 1, 1959.

Price: 40¢ To Members
80¢ To Nonmembers

(5¢ per copy additional if first class mailing desired)

All Rights Reserved by the
American Institute of Electrical Engineers
33 West 39th Street, New York 18, N. Y.
Litho in USA

RECEIVED
MAY 6 1959
RECEIVED
MAY 26 1959
ENG. DEPT.
ENG. DEPT.

Discussion in Duplicate Due July 10, 1959.

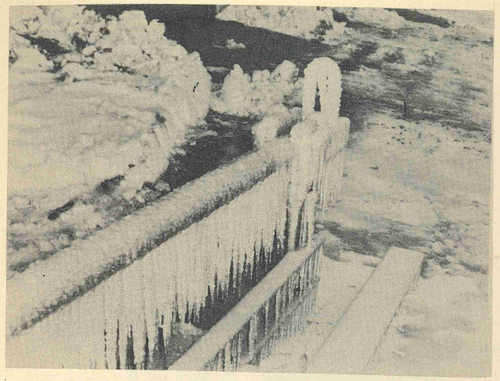

Fig. 14. Ice Test 1600 Amp. 161 KV Switch. From Closed to Open - Switch Shown Frozen in Closed Position.

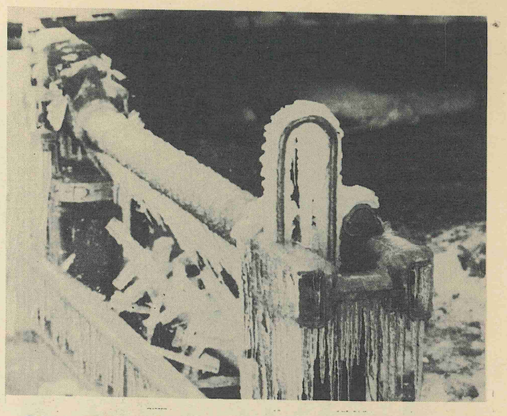

Fig. 15. Ice Test 1600 Amp. 161 KV Switch. Next Stage - Beginning of Opening Phase.

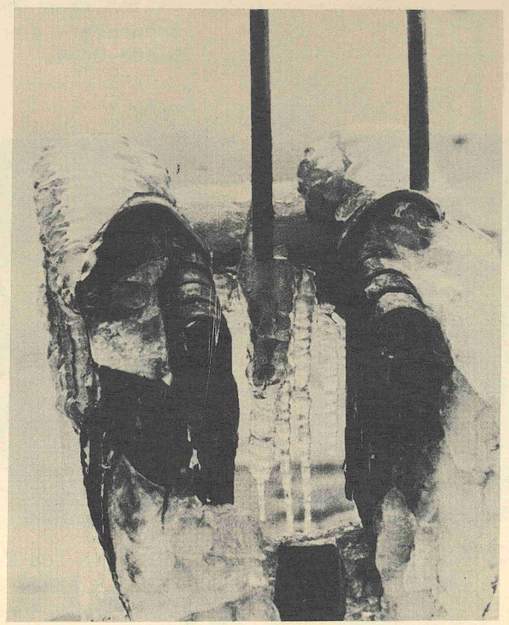

Fig. 16. Ice Test 1600 Amp. 161 KV Switch. Jaw Assembly When Blade Reached Fully Open Position.

District Conference Paper

MAGNETIC LOOP CONTACTS FOR OUTDOOR GROUP-OPERATED SWITCHES

Eugene Gorin
Member AIEE
Memco Engineering & Mfg. Co., Inc.
Commack, L. I., N. Y.

A paper recommended by the AIEE Switchgear Committee for presentation at the AIEE Middle Eastern District Meeting, Baltimore, Md., May 19-21, 1959. Manuscript submitted March 12, 1959; made available for printing March 20, 1959.

Price: 40¢ To Members
80¢ To Nonmembers

(5¢ per copy additional if first class mailing desired)

All Rights Reserved by the American Institute of Electrical Engineers
33 West 39th Street, New York 18, N. Y.
Litho in USA

Paper No. DP
59-653

MAGNETIC LOOP CONTACTS FOR OUTDOOR GROUP-OPERATED SWITCHES

Eugene Gorin

INTRODUCTION

Higher generating capacities and the use of larger single generating units result in an enormous concentration of power and danger of highly destructive short-circuit currents on switches, buses, and allied equipment.

Present NEMA Standards[1] for air switches specify momentary current ratings up to 50 times the continuous current ratings. The growth of power systems has already made the NEMA momentary ratings inadequate in some cases, and continued growth will certainly necessitate higher momentary ratings in the near future.

The jaw contacts of air switches are most vulnerable to the destructive effects of high short-circuit currents. When these contacts are subjected to a current beyond their limit, failure usually occurs for one or both of two reasons:

1. The metal of the contacts is literally melted by the I^2R loss
   or
2. The contacts are blown open by electromagnetic forces.

An obvious method of increasing the ability of switches to withstand momentary current is to reduce the heating at the jaw contacts and to eliminate or greatly reduce the magnetic forces tending to move the blade with respect to the stationary contact members.

Fig. 1 shows a single pole of a group-operated switch with magnetic loop jaw contacts. The loops utilized the magnetic field created by short-circuit currents to increase the contact pressure and maintain the blade in its normal position. Loop contacts have large heat radiating capacity.

DESCRIPTION OF MAGNETIC LOOP CONTACTS

Practical application of magnetic loop contacts for 600, 1200, 1600, and 2000 amp vertical-break switches are illustrated in Fig. 2, 1, 3, and 4, respectively. Fig. 5 shows a typical application for 161 kv, 1200 amp horizontal double-break switch. The continuous current ratings and corresponding numbers of loops are given in Table I.

Each loop, Fig. 2, is formed from a relatively flexible beryllium-copper strip into which is brazed a solid copper block faced with a rolled silver contact strip. The beryllium-copper loop applies conventional high pressure contact and radiates heat during normal operation. The copper block absorbs heat during short-circuit conditions, and the silver contact provides low contact resistance.

During short-circuit conditions, magnetic forces tend to expand the loop against the restraint of the blade, with a resulting increase in contact pressure. With loop contacts, the magnetic field around the blade tip is symmetrical with respect to the centerline of the loops and locks the blade in the central position.

THEORY

The magnetic loop contact is shown schematically in Fig. 6. The oval in the center represents the switch blade; the two loops on each side are the magnetic loop contacts; S_1 and S_2 are the fixed jaw supports of the switch.

The paths of current are indicated by the heavy arrows. Note that each loop provides two current paths (one up and one down) from the blade to the fixed jaw supports and that the currents in the two sides of the same loop flow in opposite directions. This produces a magnetic field around each loop, as indicated by the symbols (+) and (•).[5]

The magnetic lines will be uniformly spaced on the straight portions of the loops. There will be twice as many inside as outside (the sum of the magnetic lines produced by each leg). Inside the curves there will be a considerable concentration of magnetic lines. Consequently, the denser magnetic field inside the loop will push the free side of the loop toward the center of the jaw where the field is less concentrated. Naturally, the loop will also be affected by the proximity of the other currents, such as the opposite loop and loop supports.

The total effect of the momentary current on the loops is determined by the vectorial sum of all forces produced simultaneously by the action between the loop and all other paths.

Contact pressure, which is the horizontal component of this above vector, will increase with the square of the current as indicated by equation (1):

$$F = 80 + 1.56\ (I_1^1)^2 \times 10^{-6}\ \text{Lbs} \qquad (1)$$

Fig. 7 gives the relationship between contact pressure and momentary current per pair of loops in the case of a 1200 amp assembly, as calculated in Appendix A.

Magnetic Blade Restraint

Conventional "offset" jaw contacts transfer current from the blade to the jaw (or vice versa) in such a way that the current must "turn a 90 degree corner" as indicated in Fig. 8. This action sets up an electromagnetic field which is more dense around the inside of the "corner" and less dense around the outside of the "corner." The blade tends to move towards the field of minimum density. It has been demonstrated that during high short-circuit this motor action may be of sufficient magnitude to blow the blade out of the jaw contacts. Even when the blade movement is less drastic, an undesirable "commutation" effect usually

damages the contact surfaces to some degree. Attempts have been made to avoid this blade movement by the use of mechanical latches, but these have proved ineffective or, at best, undesirable.

Magnetic loop contacts eliminate or greatly reduce the above-described blow-out effect by splitting the current at the "corner" into two paths, 180 degrees apart, as indicated in Fig. 9. This configuration produces a symmetrically balanced electromagnetic field which tends to magnetically lock the blade in the center of the jaw during short-circuit conditions.

To better understand the locking effect of the magnetic field produced by loop contacts, it is necessary to return to Fig. 6 and assume that the blade is located above the horizontal centerline of the loops. The impedance of paths $A_1B_1C_1$ and $A_2B_2C_2$ (upper portion of loops) will decrease, while the impedance of paths $A_1D_1C_1$ and $A_2D_2C_2$ (lower half of the loops) will increase; thus currents going up (I_1' and I_2') will become greater than the currents going down (I_1'' and I_2'') and create a denser magnetic field above the blade. The resultant magnetic force will be directed down. The opposite will happen if the blade is placed below the centerline of the loop.

The above theoretical condition can be closely associated with "in line" loop contacts (practical application Fig. 3, 4, 5). In case of "offset" loop contacts, the symmetrical pattern of current paths is partially disturbed by jaw supports, and no general theory applies. However, the practical effects of the secondary field produced by currents in the jaw supports appear to be insignificant. This was demonstrated in a test (Table II, Test No. 12) to destruction in which the blade remained in the center of the contacts even after it had burned free of the loops as indicated in Fig. 10.

Contact Temperature

The contact temperature rise of any switch, during normal conditions, is a function of the I^2R loss per unit of area of heat radiating surface. The maximum current per loop circuit for magnetic loop contacts, Table I, is 100 amperes for switches rated up to and including 2000 amperes. This maximum normal current of 100 amperes is transferred from the blade to each loop circuit through wiping silver-to-copper contacts having a nominal pressure of 80 pounds. Each loop has a heat radiating surface of 33 square inches, exclusive of supporting structure. The resulting maximum temperature rise of the loops measured on a continuous heat run test was approximately 20 C.

During short-circuit conditions (defined as 10 cycles for momentary current rating), the elapsed time is too short for the heat radiating surfaces of the loop to have any significant effect on the temperature rise, but three other factors combine to limit the temperature to an extremely low value:

1. The multiple loop circuits subdivide the current and effectively reduce the I^2R loss; e.g., a 1200 ampere contact passes a 96000 ampere short-circuit with only 8000 amperes in each of its 12 loop circuits.

2. The mass of the copper contact blocks act as a "heat sink."

3. Contact pressure is greatly increased by magnetic forces.

The calculated maximum temperature rise at the end of 10 cycles with a 90000 amp momentary for a 1200 amp assembly is only 26.5 C.

TESTS

Temperature rise tests conducted on 1200, 1600, and 2000 amp switches demonstrated that magnetic loop contacts have a maximum temperature rise of between 18.4 and 20 C when carrying rated current (above ambient of 24 C).

The results of a series of short-time current tests are given in Tables II, III, and IV. These tests were conducted on completely assembled single-pole switches, including insulators, connected to the source of power with a split return to simulate adjacent phases under service conditions. The spacing of the return conductors was calculated by the equation (2):

$$A = \frac{B \times C}{C - B} \qquad (2)$$

where A - normal phase spacing
B - near return spacing
C - far return spacing

For the 161 kv switch assembly, for A = 108", B = 18", and C = 21.6". The return conductor was 2" I.P.S. copper tubing located approximately in the same horizontal plane with switch blade in closed position.

Observation during the short-circuit tests and examination of contacts and final results fully confirm the theory of the behavior of magnetic loop contacts:

1. Contact pressure increased considerably with current--as evidenced by slight pressure marks on the contact surfaces of the silver inlays (Fig. 2 and 3).

2. Short-circuit capacity of the loop contacts is much higher than that of conventional contacts. Results indicate the possibility of loop contacts being used for higher momentary currents than presently specified by NEMA.

3. Fig. 10 illustrates a 600 amp assembly tested to destruction. Note that burned portion is limited to the original position of blade. This indicates the effectiveness of magnetic locking:even after blade burned free of the loops and was no longer held by friction, it remained on neutral centerline.

Ice Test

The flexibility of contact loops best explains why heavy ice incrustations shatter when the switch is operated. The following photographs taken during the ice test of 161 kv, 1600 amp switch illustrate this point:

Fig. 11 - jaw assembly frozen with switch open.

Fig. 12 - shows the action of the blade coming down. Note how ice shattered by the blade springs away due to loop deflection.

Fig. 13 - illustrates the same jaw after blade was brought down to fully closed position. Note that contact surfaces are now completely free of ice.

Fig. 14 - same switch is again shown solidly frozen in closed position.

Fig. 15 - illustrates the opening of the blade and the crumbling of the ice.

Fig. 16 - a close-up photograph of jaw assembly when blade reached fully open position. Note that contact portion of the loops are free from ice.

CONCLUSIONS

1. Magnetic loop contacts operate at a lower temperature than conventional contacts:

   (a) During normal conditions because of multiple current paths and large heat radiating surfaces.

   (b) During short-circuit conditions because of multiple current paths and greatly increased contact pressure.

2. Loop contacts, because of their elastic nature, shed ice promptly. Therefore, they are particularly suitable where heavy ice formations are prevalent.

3. The electromagnetic field around loop contacts effectively locks the switch blade in the closed position and prevents it from being blown open during short-circuits.

4. Switches equipped with magnetic loop contacts have greater ability to withstand higher momentary current than switches utilizing conventional contacts.

5. The jaw contacts of switches in service may be replaced with magnetic loop contacts and thereby extend the useful life of old switches installed in growing power systems.

APPENDIX A

To illustrate the relationship between contact pressure and current, a specific example of 1200 amp switch jaw assembly is analyzed below:

Contact pressure F, Fig. 6, on blade is a combination of mechanical and magnetic forces applied to the loop. The mechanical force, same as in a conventional design, results from deflection of contacts. In this specific case it is 80 lbs (F_o) per loop. This is the initial pressure which insures safe and effecient operation with silver-to-copper contacts at rated currents.

The electromagnetic force exerted between two current-carrying conductors is a function of current, its decrement rate, shape and arrangement of conductors. In the case of two parallel conductors, the electromagnetic force is expressed by equation (3):

$$F_1 = M \times K \times L \times \frac{0.45 \times I_1 \times I_2}{D \times 10^7} \qquad (3)$$

where F force in lbs.

M multiplying factor depending on shape of current wave which, for a completely offset wave, is the square of the ratio between crest and rms value, or M = 8.

K "shape" factor in case under consideration using methods and curves suggested by H. B. Dwight varies between 0.96 and 0.98 and for practical purposes is assumed to be unity.7

I_1 & I_2 short-circuit currents in amps in two conductors under consideration.

D spacing between centerlines of conductors in inches.

L length of parallel conductor in inches.

The total electromagnetic force acting on a loop is the resultant of individual electromagnetic forces produced by each individual current path under consideration. Referring to Fig. 6, the following components are involved:

Force F_1 on $A_1 B_1$. Between $A_1 B_1$ and $B_1 C_1$

Distance between center of conductors D_1 = 1.26".

Current I_1^1 flows in opposite directions in two opposite sides of the loop. Therefore, conductors will be forced apart.

Force F_1 on leg $A_1 B_1$ is directed from left to right, or positive.

Substituting in equation (3): $I_1 = I_2 = I_1^1$, L_1 = 3.5" length of half loop; F_1 will become:

$$F_1 = 3.5 \times \frac{8 \times 0.45\ (I_1^1)^2}{1.26 \times 10^7} = 1.0 \times 10^{-6}(I_1^1)^2 \qquad (4)$$

Force F_2 on A_1 B_1. Between A_1 B_1 and A_2 B_2.

Current I_1^1 and I_2^1 are in the same direction. Magnetic force is attraction between two paths and the direction of Force F_2 is from left to right, or positive.

$I_1^1 = I_2^1$ because of symmetry of loop contacts.

$D_2 = 3.24"$ $L_2 = 3.5"$

Substituting in equation (3)

$$F_2 = 3.5 \times \frac{8 \times 0.45\ (I_1^1)^2}{3.24 \times 10^7} = 0.388 \times 10^{-6}\ (I_1^1)^2 \qquad (5)$$

Force F_3 on A_1 B_1. Between A_1 B_1 and B_2 C_2

$I_1^{11} = I_2^{11}$ $D_3 = 4.5"$ $L_3 = 3.5"$

In this case currents are in opposite directions. Force will be repulsion and direction will be negative.

$$F_3 = -3.5 \times \frac{8 \times 0.45\ (I_1^1)^2}{4.5 \times 10^7} = -0.28 \times 10^{-6}\ (I_1^1)^2 \qquad (6)$$

Force F_4 on A_1 D_1. Between A_1 D_1 and S_1 (left jaw support)

Since I_1 and I_1^{11} are in the same direction, F_4 will be directed from right to left, or negative.

$I_1 = I_1^1 + I_1^{11} = 2I_1^1$ $I_1^{11} = I_1^1$

$D_4 = 2.26"$ $L_4 = 3.5"$

$$F_4 = -3.5 \times \frac{8 \times 0.45\ (2\ I_1^1 \times I_1^1)}{2.26 \times 10^7} = -1.11 \times 10^{-6}(I_1^1)^2 \qquad (7)$$

Force F_5 on A_1 D_1. Between A_1 D_1 and S_2 (right jaw support)

I_1^{11} and I_2 are in the same direction, F_5 is from left to right, or positive.

$I_2 = 2 \times I_1^1$ $I_1^{11} = I_1^1$

$D_5 = 5.5"$ $L_5 = 3.5"$

$$F_5 = 3.5 \times \frac{8 \times 0.45\ (2 \times I_1^1 \times I_1^1)}{5.5 \times 10^7} = 0.46 \times 10^{-6}\ (I_1^1)^2 \qquad (8)$$

Total horizontal force acting on free side of loop BAD will become:

$$F = F_0 + 2\ (F_1 + F_2 - F_3) - F_4 + F_5 \quad \text{or} \qquad (9)$$

$$F = 80 + (I_1^1)^2 \left[2\ (1.0 + 0.388 - 0.28) - 1.11 + 0.46\right] \times 10^{-6} = \qquad (1)$$

$$= 80 + 1.56 \times 10^{-6}\ (I_1^1)^2$$

For 1200 amp assembly $I_1^1 = \frac{I_o}{12}$

Blade Current (amp) I_o	Loop Circuit (amp) I_1^1	Contact Pressure (lbs) F
12,000	1,000	81.56
24,000	2,000	86.24
48,000	4,000	104.96
60,000	5,000	119.00
72,000	6,000	135.16
84,000	7,000	156.44
96,000	8,000	179.84

APPENDIX B

The temperature rise at the end of 10 cycles, assuming no heat dissipation, may be determined by the following equation:

$$I_1^1 = \sqrt{\frac{G \times 4.74 \times A^2 \times 10^5 \times 103{,}500 \log_{10} \frac{T_2 + 234}{T_1 + 234}}{t}} \qquad (10)$$

where T_1 initial temperature assumed 40 C.

T_2 temperature at the end of 10 cycles.

A cross section of loop = 0.102 sq. in.

t 10 cycle = 0.167 seconds.

G per cent conductivity I.A.C.S. = 46%

for I_o = 90,000 amp, I_1^1 = 7500 amp.

substituting in equation (10)

$$T_2 = 26.5 \text{ C}$$

ACKNOWLEDGMENT

The author expresses his gratitude to those members of the staff of Memco Engineering & Manufacturing Co., Inc., who cooperated in the preparation of this paper. He wishes to thank particularly Mr. E. A. Williams, who sponsored this work and who offered much helpful assistance and guidance.

TABLE I

CURRENT DISTRIBUTION IN JAW WITH LOOP CONTACTS

Amps/Assembly	Number of Loops	Amps/Loop	Amps/Loop Circuit
600	4	150	75
1200	6	200	100
1600	8	200	100
2000	10	200	100

TABLE II

SHORT-CIRCUIT TEST - TYPE R-15 SWITCH
69 KV, 600 AMP 4-LOOP ASSEMBLY
NEMA MOMENTARY RATING 40,000 AMP

Test No.	Current Amperes rms at Half Cycle	Duration Cycles	Observations
1	15,800	10	No effect
2	29,000	10	No effect
3	30,100 *	240	No effect
4	36,500 *	240	No effect
5	39,000	10	No effect
6	45,000	10	No effect
7	48,500	10	No effect
8	53,500	10	No effect
9	60,000	10	Slight mark on contact
10	60,000	10	Slight mark on contact
11	68,000	10	Definite mark on contact
12	75,200	10	Destroyed

* rms current effective for duration of test.

TABLE III

SHORT-CIRCUIT TEST - TYPE R-15 SWITCH
161 KV, 1200 AMP 6-LOOP ASSEMBLY
NEMA MOMENTARY RATING 61,000 AMP

Test No.	Current Amperes rms at Half Cycle	Duration Cycles	Observations
1	47,000	10	No effect
2	47,000 *	248	No effect
3	60,200	10	No effect
4	68,500	10	No effect
5	78,500	10	Slight mark on contact
6	83,500	10	Definite mark on contact

* rms current effective for duration of test.

TABLE IV

SHORT-CIRCUIT TEST - TYPE R-15 SWITCH
161 KV, 1600 AMP 8-LOOP ASSEMBLY
NEMA MOMENTARY RATING 70,000 AMP

Test No.	Current Amperes rms at Half Cycle	Duration Cycles	Observations
1	47,000	10	No effect
2	48,400	10	No effect
3	60,500	10	No effect
4	70,200	10	No effect
5	72,000 *	144	No effect
6	77,000	10	No effect
7	77,000	10	No effect
8	83,500	10	No effect
9	89,000	10	No effect
10	95,000	10	Slight mark on contact
11	97,000	10	Slight mark on contact

* rms current effective for duration of test.

REFERENCES

1. NEMA Power Switching Equipment Publication #SG6-1954.

2. Results of High Current Tests on 161 kv Disconnecting Switches, A. M. McNerney. AIEE Transactions preprint Paper #55-9, Feb. 16, 1955.

3. Switches for 300 to 500 kv - Some New Concepts, Arem Foti and E. A. Williams. AIEE Transactions preprint Paper #54-229, July 9, 1954.

4. Calculation of Magnetic Forces on Disconnecting Switches, Herbert Bristol Dwight. AIEE Transactions, vol. 39, 1920, pp. 1337-1350.

5. Modern College Physics (book), Harvey E. White, Ph.D., D Van Nostrand Co., Inc., New York, N. Y., 1957, p. 528.

6. Dielectric and Other Problems in the Design of a New 330 kv Outdoor Switch, A. H. Powell, AIEE Technical preprint Paper #54-33.

7. H. B. Dwight, Electrical World, Vol. 70, 1917, p. 523.

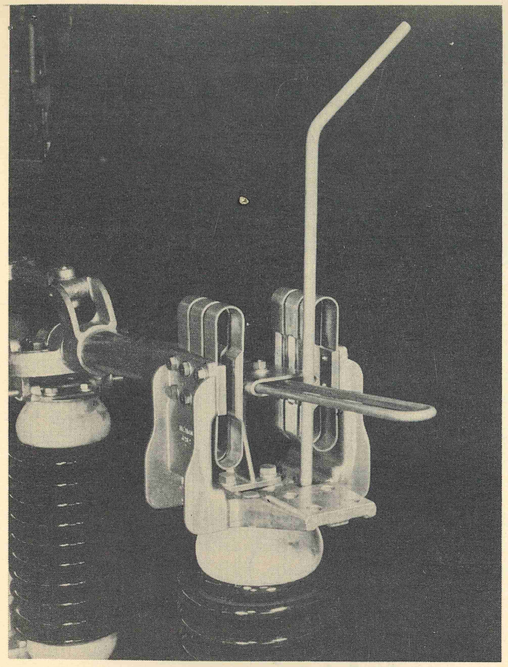

Fig. 1. 34.5 KV 1200 Amp. Switch with Loop Contacts.

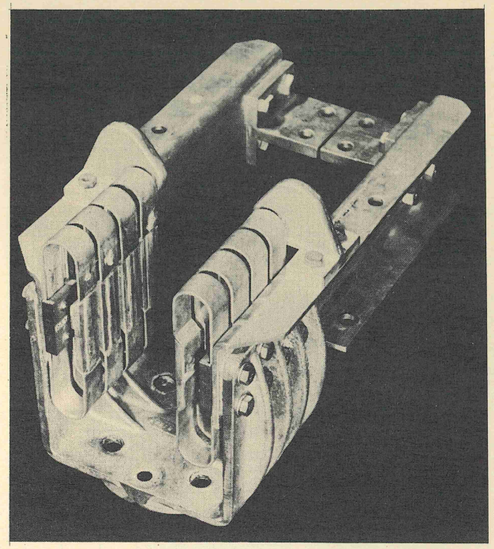

Fig. 3. Jaw Assembly after Momentary Tests Table IV.

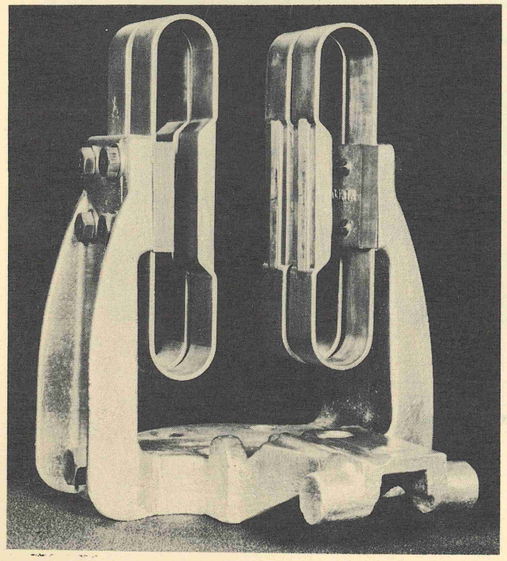

Fig. 2. Jaw Assembly with Loop Contacts for 600 Amp. Switch, ~~15 1200 Amp. Switch~~.

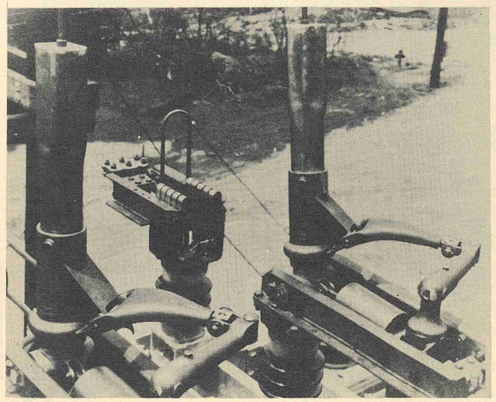

Fig. 4. Installation of 15 KV, 2000 Amp. Switch.

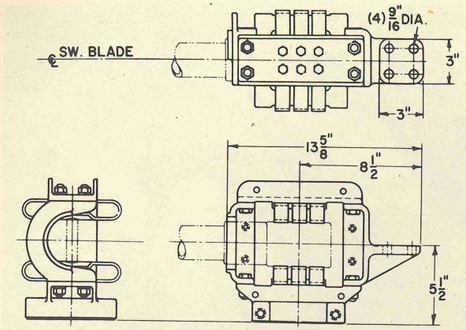

Fig. 5. Jaw Assembly 1200 Amp. 161 KV Horizontal Double Break Switch.

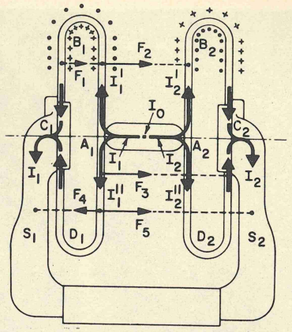

Fig. 6. Distribution of Currents and Magnetic Fields in Loop Contact Assembly.

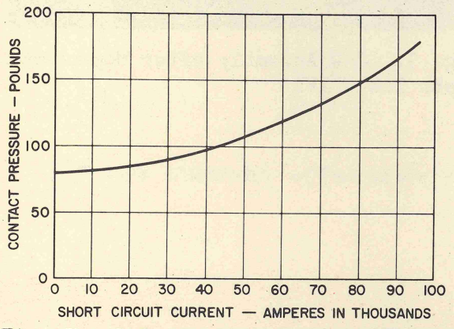

Fig. 7. Relationship between Short-Circuit Current and Contact Pressure in 1200 Amp. Loop Contact Assembly.

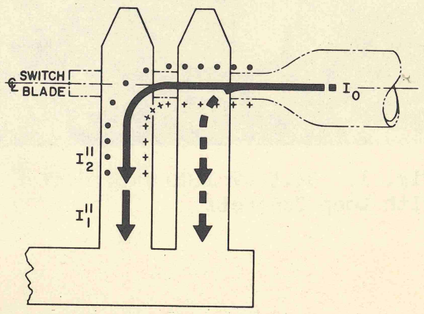

Fig. 8. Current and Field Distribution in "Offset" Jaw with Conventional Contacts.

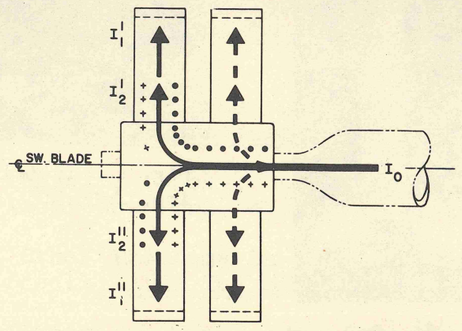

Fig. 9. Current and Field Distribution in "Offset" Jaw with Loop Contacts.

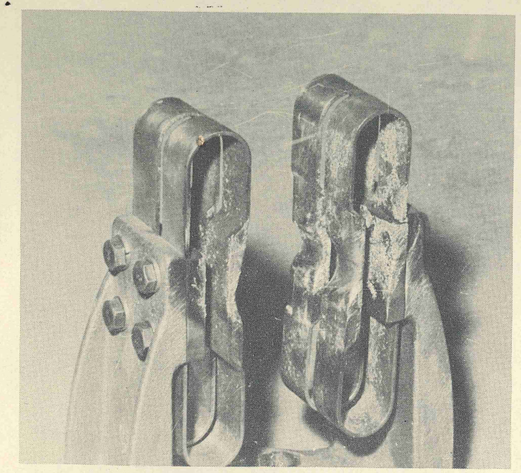

Fig. 10. Loop Contact Assembly Tested to Destruction; Table II Test No. 12; with Current for above NEMA Momentary Rating.

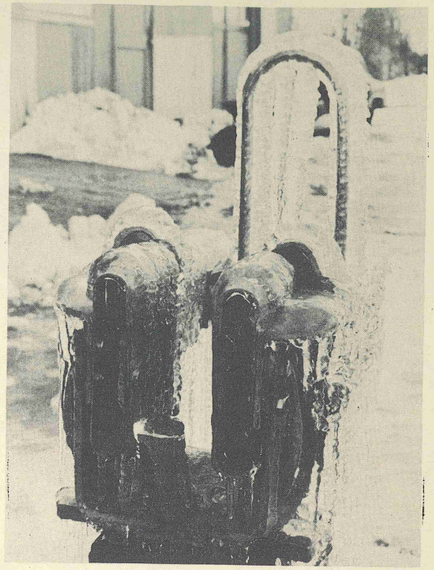

Fig. 11. Ice Test 1600 Amp. 161 KV Switch From Open to Close. First Sequence - Jaw Assembly Frozen with Blade Open.

Fig. 12. Ice Test 1600 Amp. 161 KV Switch. Second Stage - Blade Coming Down in Jaw.

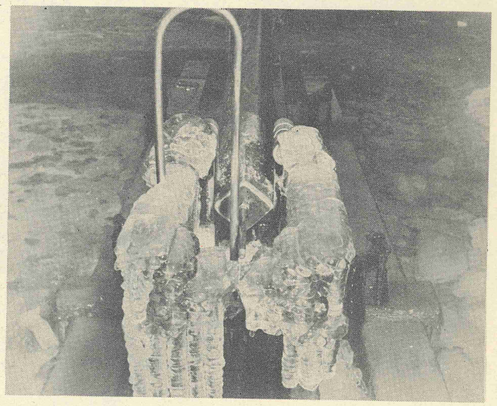

Fig. 13. Ice Test 1600 Amp. 161 KV Switch. Final Stage - Jaw Assembly After Blade Reached Fully Closed Position.

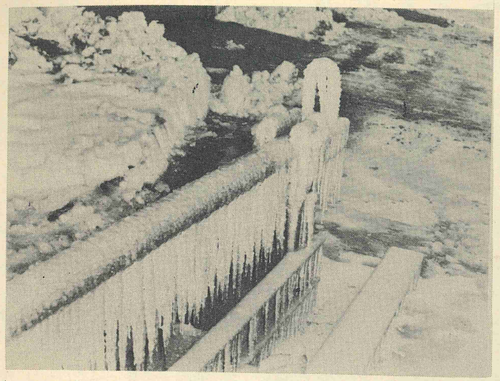

Fig. 14. Ice Test 1600 Amp. 161 KV Switch. From Closed to Open - Switch Shown Frozen in Closed Position.

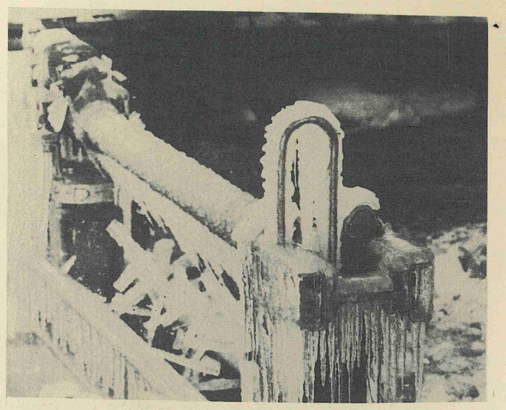

Fig. 15. Ice Test 1600 Amp. 161 KV Switch. Next Stage - Beginning of Opening Phase.

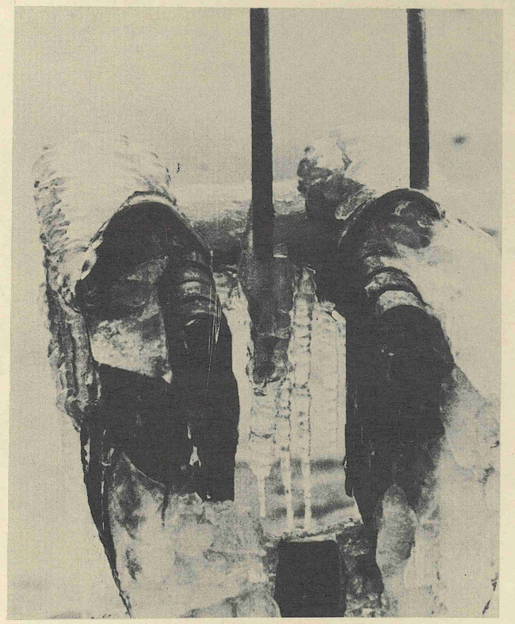

Fig. 16. Ice Test 1600 Amp. 161 KV Switch. Jaw Assembly When Blade Reached Fully Open Position.

District Conference Paper

MAGNETIC LOOP CONTACTS FOR OUTDOOR GROUP-OPERATED SWITCHES

Eugene Gorin
Member AIEE
Memco Engineering & Mfg. Co., Inc.
Commack, L. I., N. Y.

A paper recommended by the AIEE Switchgear Committee for presentation at the AIEE Middle Eastern District Meeting, Baltimore, Md., May 19-21, 1959. Manuscript submitted March 12, 1959; made available for printing March 20, 1959.

Price: 40¢ To Members
80¢ To Nonmembers

(5¢ per copy additional if first class mailing desired)

All Rights Reserved by the
American Institute of Electrical Engineers
33 West 39th Street, New York 18, N. Y.
Litho in USA

Paper No. DP
59-653

CRITICAL-PATH PLANNING AND SCHEDULING

A SUMMARY

by

J. E. Kelley, Jr.

and

Morgan R. Walker

Mauchly Associates, Inc.

Ambler, Pa.

May 1960

SUMMARY

CRITICAL-PATH PLANNING AND SCHEDULING

>>>>> <<<<<

During the past three years a new technique for project planning, scheduling, and cost control has been developed, tested and applied. It is called the Critical-Path Method.

Significant results have been obtained by applying the method to the design, procurement and fabrication functions of a variety of project types. The following list of applications is merely suggestive:

1) All types of construction and maintenance
2) Retooling programs for high-volume production
3) Low-volume production scheduling
4) Missile countdown procedures
5) Budget planning
6) Mobilization planning
7) Strategic and tactical planning
8) New product launching, marketing
9) Assembly and testing of electronic systems
10) Utility billing procedures

The Plan

The first major departure of the Critical-Path Method from traditional techniques is the separation of the planning and scheduling functions. As is easily perceived, the building blocks of any project are functions, activities and jobs. For example, in projects concerned with construction we have jobs like building forms, pouring concrete, erecting steel, etc., as well as the activities of procuring the materials and equipment required. These activities have one underlying characteristic - they must be performed in a well-defined order. Planning consists in stating the project activities and the order in which they are to be performed, while scheduling is the act of putting the plan on a calendar timetable. Traditional methods attempt to do both simultaneously.

The plan of a project is formed by listing all the jobs in the project and determining the order in which they must be performed. This process is done graphically by representing each job by an arrow which depicts its existence and the direction of time-flow (time flows from tail to head). The arrows are then interconnected to show the sequence in which the jobs must be performed.

This graphical form of the project provides planners with several benefits:

1) It provides a disciplined basis for planning a project.

2) It provides a clear picture of the scope of a project that can be easily read and understood.

3) It provides a vehicle for evaluating alternative strategies and objectives.

4) It tends to prevent the omission of jobs that naturally belong to the project.

5) In showing the interconnections among the jobs it pinpoints the responsibilities of the various operating departments involved.

6) It is an aid to refining the design of a project.

7) It is an excellent vehicle for training project personnel.

Time and Cost

Based on operating knowledge and experience, upper and lower bounds on elapsed time for each activity are determined. A point of diminishing returns fixes the upper bound. The lower bound is set by the minimum time in which the activity can feasibly be performed.

The cost of an activity, which varies with its duration, is estimated for each of the two bounds. The cost at the upper bound represents normal operating procedure; cost at the lower bound reflects overtime, changes in method, and possibly premium rates for obtaining materials and is certainly greater than for normal operation. These costs are direct costs and include everything except overhead and distributives.

The technology of the method enables a selection of solutions of different durations for each job. By means of a specially developed mathematical procedure, the durations of certain jobs in the project are changed. Starting with a schedule in which each job is done in the normal fashion, the project time is decreased by expediting certain jobs so that the project cost goes up by the least amount. The result is a breakdown which gives minimum cost schedules for each of the various project durations.

What You Learn

Management thus comes into possession of a spectrum of possible schedules, each with an engineered sequence, a known elapsed time span, and a known cost. At this point, the indirect costs for each computed schedule are prepared and added to direct costs. The result is the total investment required for each possible project completion date.

Management is now in a position to select one schedule from many alternatives - a luxury unavailable from traditional methods. Which schedule is selected depends on many factors. For example, if the project objective is to launch a product in a rising or falling market, maximizing return on investment is the criteria.

Once a schedule is selected on an objective basis, it becomes necessary to furnish the entire organization with a detailed working schedule that conforms to the management decision. Knowing the project completion date and the elapsed time for each job, the Critical-Path Method indexes all critical jobs - those for which any slippage will delay the entire project.

In an identical way all delivery information, including limiting deliveries, is computed.

Just as some jobs are critical, others have more time available to do them than they require. Timing information about these jobs is also provided.

In effect, the method determines who needs what detail when. It is so designed that it is a simple matter to reflect progress, delays and changes at any level of operation or organization.

Cost Control

Each job in a project is assigned a cost account number. With this data a structure is set up for accruing costs against proper accounts as the project proceeds.

Since each job has costs associated with it, estimated individual job costs are computed for each computed schedule. This gives management and supervision the basis for project cost control. As actual costs are incurred, they can be compared with estimated costs and analyzed for exceptions.

With the Critical-Path Method costs are always accrued so that they are easily identified and apportioned to the proper facility. This expedites closing the project to capital investment accounts. Similarly, the method

makes it easy to estimate in advance capital expenditures for labor, equipment and materials. This can mean many dollars in savings by efficient capital usage.

Computer Usage

The Critical-Path Method has been programmed for several data processing systems, both medium and large-scale. However, significant portions of the technique can be used without the aid of computers. The size of the application and the extent to which the technique is applied dictate the requirements for various-sized computing facilities for economical processing.

What You Can Expect

Significant accomplishments have been demonstrated by the practical applications of the Critical-Path Method: Personnel can readily be trained to collect pertinent data and develop consistent and detailed project schedules faster than it normally takes. Entire projects consisting of hundreds of activities can successfully be depicted in their proper technological sequence by means of arrow diagrams. This diagramming technique has been extremely helpful, not only by giving a visual representation of a project, but also for indicating important revisions in project design, defining goals and fixing responsibilities. The mass of detailed information required for large projects can be processed with dispatch by a computer, and by such means, schedules can readily be updated. The output from the Critical-Path Method is far more accurate and useful than that obtained from traditional methods. There is a high correlation between the forecasted direct cost of a schedule and that actually experienced. Current experience indicates that the savings which accrue from the use of the method far outweigh any investment required.

James E. Kelley, Jr.
Morgan R. Walker
Mauchly Associates, Inc.
50 E. Butler Ave.
Ambler, Pa.

May 1960

This table shows the present standard practice with respect to system nominal, transformer secondary and motor voltage. It should be noted that without use of taps excessive voltage to 265/460-volt secondaries could be expected when using the overhead type on overhead systems. Also as the same rating utilization equipment is served from both overhead and network systems a lower network primary voltage would be required to provide the same utilization voltage, which is obviously undesirable. Although not shown in the table, it is interesting to note that on 7200/12470 network systems both the primary and secondary ratings are 5 per cent higher than system nominals. In other words, the transformers are rated 7500/13000 to 125/216 volts, which is the same transformer ratio.

CONCLUSION

It is recommended that if and when the 240/416 volt three-phase and the 240/480-volt single-phase systems are made standard that the following voltage ratings be adopted:

SINGLE-PHASE NOMINAL 240/480-VOLT SYSTEM

Item	Nominal or Nameplate Voltage
Transformer Secondary	240/480 volts
Utilization Equipment	240 volts, 2-wire*

*Design Voltage may remain 230 volts

THREE-PHASE NOMINAL 240/416-VOLT SYSTEM

Transformer Secondary	240/416 volts
Utilization Equipment	240/416 volts 3 or 4 wire

TABLE I

TRANSFORMER AND MOTOR VOLTAGE RATINGS
7620/13200Y NOMINAL PRIMARY SYSTEMS

System Nominal	Transformer Type	Transformer Primary Voltage	Transformer Secondary Rating	Transformer Size Kva	Motor Voltage
120/240 1-phase	OH Single Phase	7620	120/240	5 to 500	115, 230 1-phase 230 3-phase
120/240 3-phase	OH Single Phase	7620/ 13200	120/240	5 to 500	115 and 230 1-phase
120/208 3-phase	OH Three Phase	7620/ 13200	120/208	112,150 225,500	208 and 220 3-phase
265/460 3-phase	OH Three Phase	7620/ 13200	277/480	225,500	440 3-phase
120/208 3-phase	Network Three Phase	7620/ 13200	125/216	300 to 1000	208 and 220 3-phase
265/460 3-phase	Network Three Phase	7620/ 13200	277/480	500 to 2500	440 3-phase

misc.

Conference Paper

VOLTAGE NOMENCLATURE - SECONDARY AND UTILIZATION SYSTEMS

A. S. Anderson
Fellow AIEE
Ebasco Services Inc.
New York, N. Y.

A paper recommended by the AIEE Transmission and Distribution Committee for presentation at the AIEE Summer General Meeting, Atlantic City, N. J., June 19-24, 1960. Manuscript submitted March 22, 1960; made available for printing May 4, 1960.

Price: $ .50 To Members
$1.00 To Nonmembers

(5¢ per copy additional if first class mailing desired)

All Rights Reserved by the
American Institute of Electrical Engineers
33 West 39th Street, New York 18, N. Y.
Litho in USA

Paper No. CP
60-842

VOLTAGE NOMENCLATURE - SECONDARY AND UTILIZATION SYSTEMS

A S Anderson, Fellow AIEE Ebasco Services Incorporated

INTRODUCTION

The greatest obstacle to standardization of utilization equipment and distribution equipment particularly transformers is in the voltage designation. The evolutionary change from 110 volts to 115 volts to 120 volts in secondary systems is the basic reason for the present variations in not only utilization voltage nomenclature but in the voltage nomenclature of both secondaries and primaries of transformers. The situation as it now exists is the result in many instances of choosing on the basis of immediate expediency.

In the evolution of utilization system voltage change it was necessary and economical to manufacture and use incandescent lamps rated for each voltage. In most other equipment it was neither necessary or economical to do so. For some equipment design voltages were changed. For others it was not. The three-phase motor rating of 220 and 440 volts is an example of the latter.

In the process of evolution there finally developed an example of voltage nomenclature which is the ultimate result of a process of expedient solutions without a long range plan. The example is the present situation with respect to the 265/460-volt system. The motor rating for this system is 440 volts and the secondary transformer rating is 277/480 volts.

PURPOSE

A large part of the utility industry favors the nominal 240/416-volt system for service to consumers. This system is not standard and neither are the motors or three-phase transformers to serve them. However, because of its great advantages and the seriousness with which it is being advocated, it seems timely to consider the rating of transformer secondary and the motors for use with the 240/416-volt system.

The present pattern of voltage ratings for motor, transformer and system for the non-standard 265/460-volt level is an evolutionary development and not the result of planning ahead. The purpose of this presentation is to recommend voltage ratings that seem more logical and will cause less confusion than now exists.

DISCUSSION

System Nominal Voltage and Voltage Range

The nominal voltage of a secondary supply system is a value used for the purpose of convenient designation. It is generally recognized that the actual value of voltage at any time or at any location may not always be of this value. Most utility supply and consumers' wiring systems are designed and operated so that the voltage at the point of utilization is not less than 90 per cent of nominal or more than 105 per cent of nominal. These limits are within the favorable zone as listed in EEI-NEMA "Preferred Voltage Ratings for A-C Systems and Equipment" ASA C84.1-1954.

Transformer Secondary Rating

As indicated above the maximum utilization voltage to be expected is 105 per cent of nominal. There hardly seems need to use a transformer secondary voltage rating of 105 per cent of nominal because:

1. According to ASA C57.12-00.411 "transformers shall be capable of delivering rated output kva at 5 per cent above rated secondary voltage without exceeding the guaranteed temperature rise. This requirement applies to load power factors of 80 per cent or higher."

2. According to ASA C57.12-00.412 "transformers shall be capable of operating at 10 per cent above rated output voltage at no load without exceeding the guaranteed temperature rise."

3. According to ASA C57.12-00.414 "The foregoing requirements apply to rated voltage and rated kva for any tap."

Two reasons have been given by others to support their feeling that a secondary rating of 5 per cent above nominal is required.

(a) To avoid excessive core loss.

(b) To keep the noise level lower.

This approach does not recognize that the ASA requirements would have the effect of limiting core losses to practical values that are encountered for the varying loads and voltages on a primary feeder. In the case of network transformers it may be desirable to operate at lower core losses and noise level in some situations. Rather than change primary and secondary voltage ratings of all network transformers to accomplish this, it would seem more desirable to design another line of transformers for these special applications.

Nameplate Voltages - Utilization Equipment

Utilization equipment is marked with either the design voltage or the nominal voltage of the system on which it is to be used. In the case of the 208-220 volt three-phase motor, the first value indicates that it is usually satisfactory to operate the motor on a 208-volt system. The second value is the design value of the motor which may be operated on 240-volt nominal systems.

It would be preferable that as a general principle utilization equipment should be marked with the system nominal voltage for which it is designed. Motor nameplates should also carry the design voltage and be so identified.

Motors have a satisfactory operating range of plus and minus 10 per cent. Since utilization voltages have a lesser range than this, it seems appropriate that the motor voltage as shown on the nameplate be the same as system nominal. It is claimed by many that the system nominal should be 5 per cent higher than a motor rating to assure adequate starting torque. Another claim is that motors should generally be operated on undervoltage because of better economy. While these are conflicting reasons, neither would seem to be a good reason for having a nameplate designation other than system nominal. Proper design and correct motor application will avoid the need for having other than system nominal voltage on the nameplate.

The Existing Situation

It is not necessarily intended in this presentation to indicate that anything should be done in the present situation. However, an example of conditions now existing is shown in Table I in the interest of encouraging the use of a simpler system when the 240-volt-to-neutral systems are adopted.

This table shows the present standard practice with respect to system nominal, transformer secondary and motor voltage. It should be noted that without use of taps excessive voltage to 265/460-volt secondaries could be expected when using the overhead type on overhead systems. Also as the same rating utilization equipment is served from both overhead and network systems a lower network primary voltage would be required to provide the same utilization voltage, which is obviously undesirable. Although not shown in the table, it is interesting to note that on 7200/12470 network systems both the primary and secondary ratings are 5 per cent higher than system nominals. In other words, the transformers are rated 7500/13000 to 125/216 volts, which is the same transformer ratio.

CONCLUSION

It is recommended that if and when the 240/416 volt three-phase and the 240/480-volt single-phase systems are made standard that the following voltage ratings be adopted:

SINGLE-PHASE NOMINAL 240/480-VOLT SYSTEM

Item	Nominal or Nameplate Voltage
Transformer Secondary	240/480 volts
Utilization Equipment	240 volts, 2-wire*

*Design Voltage may remain 230 volts

THREE-PHASE NOMINAL 240/416-VOLT SYSTEM

Transformer Secondary	240/416 volts
Utilization Equipment	240/416 volts 3 or 4 wire

TABLE I

TRANSFORMER AND MOTOR VOLTAGE RATINGS
7620/13200Y NOMINAL PRIMARY SYSTEMS

System Nominal	Transformer Type	Transformer Primary Voltage	Transformer Secondary Rating	Transformer Size Kva	Motor Voltage
120/240 1-phase	OH Single Phase	7620	120/240	5 to 500	115, 230 1-phase 230 3-phase
120/240 3-phase	OH Single Phase	7620/ 13200	120/240	5 to 500	115 and 230 1-phase
120/208 3-phase	OH Three Phase	7620/ 13200	120/208	112,150 225,500	208 and 220 3-phase
265/460 3-phase	OH Three Phase	7620/ 13200	277/480	225,500	440 3-phase
120/208 3-phase	Network Three Phase	7620/ 13200	125/216	300 to 1000	208 and 220 3-phase
265/460 3-phase	Network Three Phase	7620/ 13200	277/480	500 to 2500	440 3-phase

misc.

Conference Paper

VOLTAGE NOMENCLATURE - SECONDARY AND UTILIZATION SYSTEMS

A. S. Anderson
Fellow AIEE
Ebasco Services Inc.
New York, N. Y.

A paper recommended by the AIEE Transmission and Distribution Committee for presentation at the AIEE Summer General Meeting, Atlantic City, N. J., June 19-24, 1960. Manuscript submitted March 22, 1960; made available for printing May 4, 1960.

Price: $ .50 To Members
$1.00 To Nonmembers

(5¢ per copy additional if first class mailing desired)

All Rights Reserved by the
American Institute of Electrical Engineers
33 West 39th Street, New York 18, N. Y.
Litho in USA

Paper No. CP
60-842

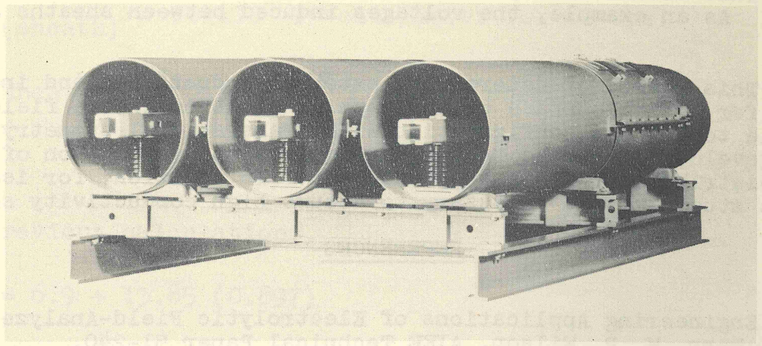

Fig. 1. Typical isolated-phase bus

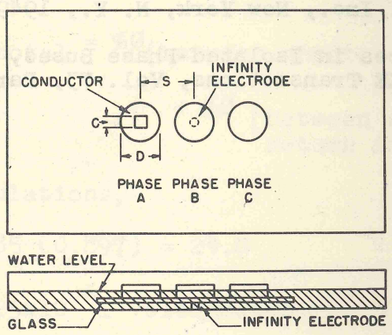

Fig. 2. Field analyzer set-up of isolated-phase bus

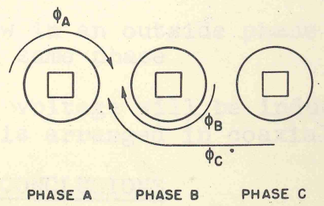

Fig. 3. Flux pattern between sheaths of isolated-phase bus

Mr Weller
Misc.

Conference Paper

THE USE OF THE ELECTROLYTIC TANK FOR DETERMINING EXTERNAL INDUCTANCES OF ENCLOSED CONDUCTORS

L. L. Mankoff
Associate Member AIEE

R. H. Brealey, Jr.
Nonmember AIEE

Both of:
General Electric Co.
Philadelphia, Pa.

Submitted in abstract or outline form only to the AIEE Special Instruments and Auxiliary Apparatus Committee for presentation at the AIEE Winter General Meeting, New York, N. Y., January 31-February 5, 1960. Manuscript submitted November 25, 1959; made available for printing December 14, 1959.

Price: $ .50 To Members
$1.00 To Nonmembers

(5¢ per copy additional if first class mailing desired)

All Rights Reserved by the
American Institute of Electrical Engineers
33 West 39th Street, New York 18, N. Y.
Litho in USA

Paper No. CP
60-176

THE USE OF THE ELECTROLYTIC TANK FOR DETERMINING EXTERNAL INDUCTANCES OF ENCLOSED CONDUCTORS

L. L. Mankoff R. H. Brealey, Jr.

INTRODUCTION

A knowledge of the impedance of the bus is of value in applying enclosed conductors of the isolated-phase bus type. Lengthy equations for calculating inductances may be found in the literature for some conductors such as square-tubular and double-channel conductors. However, the methods of calculation found in the literature did not include the effects on inductance of non-magnetic, conducting sheaths surrounding conductors of these shapes.

A new, rapid technique, using the electrolytic field analyzer (1), has been developed and applied to determine the external inductances of isolated-phase bus for all types of current flow, balanced three-phase current, and all possible fault current conditions. The new method was also applied to determine the voltages induced by the electromagnetic field between sheaths of isolated-phase bus. This method may be used to determine the voltage induced in a loop external to isolated-phase bus. For the case of a closed, conducting loop, this technique of determining the flux through the loop, plus a knowledge of the impedance of the loop to current flow, would make it possible to approximate eddy current flow in the loop.

The manner in which this new technique was applied assumes uniform current distribution within each of the bus conductors. For the case of isolated-phase bus, (Fig. 1) where conductor separation is large compared to conductor size, and where the individual sheaths tend to shield each conductor from the field effects of the other conductors, this assumption is reasonable. In addition, the analysis assumes that the sheaths of the isolated-phase bus are of high conductivity aluminum and of a thickness consistent with current practice.

GENERAL DESCRIPTION OF THE TEST TECHNIQUES

For years we have employed the electrolytic field analyzer (flux plotter) to determine the inductance of a single-phase configuration with translational symmetry (1). To do this it is only necessary to make a scale model and measure the resistance between electrodes. The inductance per-unit length is:

$$L = uu_o \frac{R_e}{R_s} \qquad (1)$$

where u = relative permeability of the medium

$u_o = 4\pi \times 10^{-7}$ - henries/meter

R_e = resistance between electrodes - ohms

R_s = resistance per square of the electrolyte - ohms

By definition, $L = \frac{\phi}{I}$ for a single-turn circuit. Therefore, ϕ, the total flux per-unit length, is merely:

$$\phi = I\, uu_o \frac{R_e}{R_s} \text{ or } \frac{\phi}{I} = uu_o \frac{R_e}{R_s} \text{ flux per-unit current} \qquad (2)$$

The quantity ϕ, the total flux, is necessary to determine the flux distribution for purposes of finding induced voltages in the flux field.

The same analogy which relates water resistance to inductance provides a potential distribution in the water equal to the relative flux distribution in the device under consideration. Hence, for the single-phase case, inductance may be obtained directly and flux distribution may be obtained easily by combining the total flux with the relative flux distribution obtained from the potential distribution in the water.

The extension of this technique to three-phase conditions presents additional complications. Three-phase power at 1000 cps, (the field analyzer frequency) is not readily available. Three-phase measurements in the field analyzer often require the measurement of phase angle in the analyzer, a more difficult problem in instrumentation. The concept of total flux is not easily applied for three-phase conditions where non-symmetrical arrangement of conductors produce a total flux linking a conductor which is not exactly in phase with the current in the conductor.

The approach used in this new method makes use of simple, single-phase measurements combined vectorially to provide results produced by balanced three-phase currents. The total flux and the relative flux distribution for each phase is studied in turn in the field analyzer between the conductor and an electrode in the analyzer which represents infinity. Infinity is accurately represented by means of a small cylindrical electrode in the lower half of the double-tank setup (2). The flux distribution is determined from potential measurements and the total flux by a resistance measurement from the conductor to "infinity" and by using equation (2). By properly combining the quantities obtained for each conductor, remembering that they are 120° apart, the desired results are achieved, inductance or induced voltage. In essence, we represent three balanced three-phase currents at infinity. Each is a return current for a single-phase current in one of our three conductors. These currents at infinity must cancel and consequently produce no net effect on the flux in question (3).

EXAMPLES OF APPLICATION OF THE METHOD

External Inductances

A. External Inductance Per Phase of Three-Phase-Isolated Phase Bus.

The inductance of a conductor is defined as the total flux linking the conductor per-unit current flowing in the conductor. To find external inductance it is necessary to add all the flux linkages starting at the conductor boundary and extending to infinity.

The electrolytic field analyzer was set up as shown in Fig. 2. The geometric parameters set to scale in the analyzer were:

D = 32 3/8"
S = 44"
C = 12" square conductor

A 6" diameter sheath was used in the analyzer. The water resistivity was 2170 ohms per square for each level. The potential of the conductor was 100% and the "infinity" electrode was at 0% potential.

The data obtained are shown in Table I, below:

Table I. Electrolytic Field Analyzer Data for Determining the External Inductances of a Three-Phase, Isolated-Phase Bus.

Conductor Position	Percent Potential at Sheath			Average Value of Resistance Between Conductor and "Infinity", R_e
	A	B	C	
A	88.1	74.4	67.5	
B	76.2	87.8	76.2	2357 Ohms
C	67.5	74.4	88.4	

The inductance per phase with balanced three-phase currents is calculated in the following manner.

1. Percent total flux linking conductors A or C.

By symmetry, the magnitude of the total flux linking conductors A or C must be the same. To reduce errors resulting from slight imperfections in the tank such as minor variations in level or the wax bottom, the data for conductors A and C are averaged.

The percent of the total flux from conductor to "infinity" linking a conductor, for example conductor A, is called %Ø linking A. Also, for purposes of calculation I_A is assumed to be at 0°, I_B at 120° and I_C at 240°. Then:

	Average Value	%Ø Linking A	%Ø Linking C
%Ø Linking A due to $I_A = 100$	100%	$100/0^\circ$	$100/240^\circ$
%Ø Linking C due to $I_C = 100$			

To determine the %Ø linking A or C due to I_B we must look at the data of Table I. With the conductor in position B, 76.2% of the total flux of conductor B is between the sheath of A and "infinity." It is assumed with good approximation that no flux from conductor B penetrates sheath A (4). In other words, the sheath is a perfect conductor. Consequently, 76.2% of the total flux of conductor B links conductor A. Then:

	Average Value	%Ø Linking A	%Ø Linking C
%Ø Linking A due to $I_B = 76.2$	76.2%	$76.2/120^\circ$	$76.2/120^\circ$
%Ø Linking C due to $I_B = 76.2$			

The remaining component of flux is the %Ø from conductor A linking conductor C and vice versa. By the same method described above:

%Ø Linking A due to $I_C = 67.5/240^\circ$,
%Ø Linking C due to $I_A = 67.5/0^\circ$.

The total external flux linkages for conductor A or C will be:

%Ø Linking A (total) = $100/0^\circ + 76.2/120^\circ + 67.5/240^\circ$,
%Ø Linking C (total) = $100/240^\circ + 76.2/120^\circ + 67.5/0^\circ$.

Combining vectors we obtain:

%Ø Linking A (total) = $29.2/15.0^\circ$,
%Ø Linking C (total) = $29.2/225.0^\circ$.

2. Percent total flux linking conductor B

Using the same approach as was used for conductors A and C, the fluxes linking conductor B are:

%Ø Linking B due to $I_A = 74.4/0^\circ$,
%Ø Linking B due to $I_B = 100/120^\circ$,
%Ø Linking B due to $I_C = 74.4/240^\circ$.

Combining vectors we obtain:

%Ø Linking B (total) = $25.6/120^\circ$.

3. External Inductance

The total flux $Ø_T$ is determined by means of equation 2 and the resistance data from Table I, using an average value for R_e.

$$Ø_T = u_o I \frac{R_e}{R_s} = 4\pi \times 10^{-7} \frac{2357}{2170} I, \text{ or}$$

$$Ø_T = 1.38 \times 10^{-6} I \text{ weber/meter.}$$

Combining $Ø_T$ with the various %Ø (total) we obtain:

ϕ Linking A = 0.403×10^{-6} I_A weber/meter $\angle 15^\circ$,

ϕ Linking B = 0.352×10^{-6} I_B weber/meter $\angle 120^\circ$,

ϕ Linking C = 0.403×10^{-6} I_C weber/meter $\angle 225^\circ$.

Since inductance is defined as total flux linking the conductor divided by the current in the conductor,

$L_A = 0.403 \times 10^{-6}$ henry/meter,

$L_B = 0.352 \times 10^{-6}$ henry/meter,

$L_C = 0.403 \times 10^{-6}$ henry/meter.

B. External Inductances for Phase-to-Phase and Phase-to-Ground Faults

During phase-to-phase or phase-to-ground faults, single-phase current flows. For this condition inductances may be obtained in the field analyzer either by means of direct resistance measurements (1) or by the use of the return at "infinity" technique. The latter method was used since data obtained for three-phase calculations was applicable to the single-phase cases.

1. Phase-to-Phase Faults

a. Fault current flowing in the center phase and an outside phase

From the data in Table I, the percentage of flux due to I_A between conductors A and B is, 100 - 74.4 = 25.6.

The percentage of flux between conductors A and B due to I_B is, 100 - 76.2 = 23.8. Therefore,

$\%\phi_{\text{total (A-B)}} = 25.6 + 23.8 = 49.4$, and

$L_{AB} = 1.38 \times 10^{-6} \times 0.494 = 0.681 \times 10^{-6}$ henry/meter, or

$L = 0.341 \times 10^{-6}$ henry/meter per conductor.

b. Fault current flowing in outside phases

From the data in Table I, $\%\phi_{A-C}$ due to $I_A = 32.5$ and $\%\phi_{A-C}$ due to $I_C = 32.5$.

Then L_{AC} (loop) $= 0.895 \times 10^{-6}$ henry/meter, or

$L = 0.448 \times 10^{-6}$ henry/meter per conductor.

2. Phase-to-ground faults

The latest design of the authors' company of isolated-phase bus utilizes the sheath of one of the outside phases for a continuous ground.

Therefore, any phase-to-ground fault will consist of current in any of the three conductors returning in one of the outside phase sheaths. Table I contains all the data required to find the relative flux distributions. The total flux for current in a sheath returning at "infinity" is slightly different than that for the conductor. The resistance between sheath and "infinity" was measured and found to be 2108 ohms. This is a reduction by $\frac{2108}{2357}$ or 0.897 total flux from the grounded sheath compared to the total flux from a conductor.

a. Fault current flowing in an outside phase conductor and returning in the other outside phase sheath

From Table I, the average percent flux between an outside phase conductor and the other outside phase sheath is 32.5%. The percent flux between outside sheaths due to current in a sheath of an outside phase is the average of (88.4-67.5) and (88.1-67.5), or 20.75.

Then $\%\phi_{\text{total}} = 32.5 + (20.75)\ (0.897) = 51.05$

And as before $\phi = 1.38 \times 10^{-6} I \times 0.5105 = 0.705 \times 10^{-6} I$ weber/meter,

or $L = 0.705 \times 10^{-6}$ henry/meter

b. Fault current flowing in the center phase conductor returning in an outside phase sheath

From Table I, the percent flux from conductor B to sheath C (or sheath A) is 23.8%. The percent flux between sheath A or C and sheath B is 13.7 or 14.0, an average value of 13.85%. Then

$\%\phi_{\text{total}} = 23.8 + (13.85)\ (0.897) = 36.2$, and

$\phi = 1.38 \times 10^{-6} I \times 0.362 = 0.499 \times 10^{-6}$ I weber/meter, or

$L = 0.499 \times 10^{-6}$ henry/meter.

c. Fault current flowing in an outside phase conductor returning in the sheath of the same phase

For this case, coaxial current flow, all the flux between conductors is that produced by conductor C or A to the internal boundary of its sheath. From Table I,

$\%\phi$ = 11.9 or 11.6 = 11.75 (average). Then

$\phi = 0.162 \times 10^{-6}$ I weber/meter, or

$L = 0.162 \times 10^{-6}$ henry/meter.

VOLTAGES INDUCED BETWEEN SHEATHS

As an example of the application of the electrolytic field analyzer to determine induced voltages, consider the open loop formed by two

sheaths of isolated-phase bus and the single ground connection for the three sheaths per sheath section. Isolated-phase bus design provides insulation at intervals between sheaths of different phases.

A. Induced voltage for balanced three-phase currents

It is apparent from symmetry considerations for sheaths of high conductivity that the voltage between sheaths A and B and between sheaths B and C must have the same magnitude. As before, average values will be used to minimize the effects of any tank inaccuracies. From the data of Table I,

	Average Value	$\%\phi_{AB}$	$\%\phi_{BC}$
$\%\phi$ between sheaths A and B due to I_A=13.7 $\%\phi$ between sheaths B and C due to I_C=14.0	13.85	$13.85\angle 0$	$13.85\angle 240$
$\%\phi$ between sheaths A and B due to I_B=11.6 $\%\phi$ between sheaths B and C due to I_B= 11.6	11.6	$11.6\angle 120$	$11.6\angle 120$
$\%\phi$ between sheaths A and B due to I_C= 6.9 $\%\phi$ between sheaths B and C due to I_A= 6.9	6.9	$6.9\angle 240$	$6.9\angle 0$

From Figure 3, it is apparent that,

$\%\phi_{AB}$(between sheaths) $=\%\phi_{AB}$ (due to I_A) $-\%\phi_{AB}$(due to I_B) $-\%\phi_{AB}$(due to I_C),

and

$\%\phi_{BC}$(between sheaths) $=\%\phi_{BC}$(due to I_C) $-\%\phi_{BC}$(due to I_B) $-\%\phi_{BC}$(due to I_A).

Combining vectors we obtain,

$\%\phi_{AB}$ (between sheaths) $= 23.5\angle -10.2^\circ$

$\%\phi_{BC}$ (between sheaths) $= 23.5\angle 249.9^\circ$

As before $\phi = \%\phi \times \phi_T$, where $\phi_T = 1.38\text{x}10^{-6}$I weber/meter, and

$\phi_{AB} = 0.324\angle -10.2^\circ \times 10^{-6}$I weber/meter, and

$\phi_{BC} = 0.324\angle 249.9^\circ \times 10^{-6}$I weber/meter.

By Faraday's Law, $V = -\frac{\partial\phi}{\partial t}$ or,

$V = jw\phi = j377\phi$ (for 60 cps).

Then $V_{AB\ (sheaths)} = 122\text{x}10^{-6}$ I volts/meter at 79.8°, and

$V_{BC\ (sheaths)} = 122\text{x}10^{-6}$ I volts/meter at 339.7°.

B. Induced voltages for phase-to-phase and phase-to-ground faults.

1. Phase-to-phase faults

a. Fault current flow between the center phase and an outside phase

From above, $\%\phi$ between A and B or B and C due to I_A or I_C is 13.85%. Similarly the flux due to I_B is 11.6%.

Then $\%\phi_{\ total} = 25.45$ and, for 60 cps,

$V_{AB\text{ or }BC\ (sheaths)} = 132\text{x}10^{-6}$I volts/meter.

The other voltage induced for a phase-to-phase fault is small compared to that induced between the sheaths whose conductors are involved in the fault. In other words for a fault between phase A and phase B, the induced voltage between sheath C and B would be found by using 11.6% - 6.9% or 4.7%, or $24.5\text{x}10^{-6}$I volts/meter.

b. Fault current flow between outside phases

From above, the contribution to flux between sheaths A and B or B and C are,

$\%\phi_{\ total} = 13.85 + 6.9 = 20.75$.

Then $V_{AB\text{ or }BC\ (sheaths)} = 108\text{x}10^{-6}$ I volts/meter (for 60 cps).

2. Phase-to-ground faults

a. Fault current flow in an outside phase conductor returning in the other outside phase sheath

For $V_{AB\ (sheath)}$, $\%\phi_{\ total} = \%\phi$ (between sheaths due to I_A)

$+\%\phi$(between sheaths due to ground return in sheath C).

From previous calculations,

$\%\phi_{total} = 13.85 + 6.9\ (0.897)$, or

$\%\phi_{total} = 20.04$.

Then $V_{AB\ (sheath)} = 104 \times 10^{-6} I$ volts/meter for 60 cps.

For $V_{BC\ (sheath)}$, $\%\phi_{\ total}$ = $\%\phi$ (between sheaths due to I_A)

+$\%\phi$ (between sheaths due to ground return in sheaths).

From previous calculations,

$\%\phi_{\ total} = 6.9 + 13.85\ (0.897)$

$\%\phi_{\ total} = 19.3$

Then $V_{BC(sheath)} = 100 \times 10^{-6} I$ volts/meter for 60 cps.

b. Fault current flow in the center phase conductor returning in the outside phase sheath

For $V_{BC\ (sheath)}$, $\%\phi_{\ total}$ = $\%\phi$ (between sheaths due to I_B)

+ $\%\phi$ (between sheaths due to ground return in sheath C).

From previous calculations,

$\%\phi_{\ total} = 11.6 + 13.85\ (0.897) = 24.0$

Then $V_{BC\ (sheath)} = 125 \times 10^{-6} I$ volts/meter.

Similarly for $V_{AB(sheath)}$

$\%\phi_{\ total} = 11.6 - 6.9\ (0.897) = 5.4$, and

$V_{AB\ (sheath)} = 28.2 \times 10^{-6} I$ volts/meter.

c. Fault current flow in an outside phase conductor returning in the sheath of the same phase

It is obvious that no voltage will be induced between sheaths since the total current is arranged in coaxial flow.

CONCLUSIONS

1. A new technique utilizing the electrolytic field analyzer has been devised and applied to determine the external inductances of isolated-phase bus for all types of current flow.

2. This method also provides a simple means for determining induced voltages. As an example, the voltages induced between sheaths are determined.

3. This method of determining external inductances and induced voltages for a single-phase or three-phase electromagnetic field is applicable to any bus configuration with translational symmetry. The present development of the technique requires the assumption of uniform current distribution within the conductor. In addition, for isolated-phase bus studies it is necessary to assume high conductivity sheaths.

REFERENCES

1. Some Engineering Applications of Electrolytic Field-Analyzer, H. K. Farr, W. R. Wilson, AIEE Technical Paper 51-240.

2. An Electrolytic Tank for the Measurement of Steady-State Response, Transient Response, and Allied Properties of Networks, A.R. Boothroyd, E.C. Cherry, R. Makar, Proceedings, Institute of Electrical Engineers Volume 96, Part 1, Number 99, May 1949, Pages 163-177.

3. Electrical Transmission of Power and Signals (book) E.W. Kimbark. J. Wiley and Sons, Inc., New York, N. Y., 1949.

4. Short-Circuit Forces in Isolated-Phase Buses, W. R. Wilson, L. L. Mankoff, AIEE Transactions, Vol. 73, Part III-A, 1954, Pages 382-390.

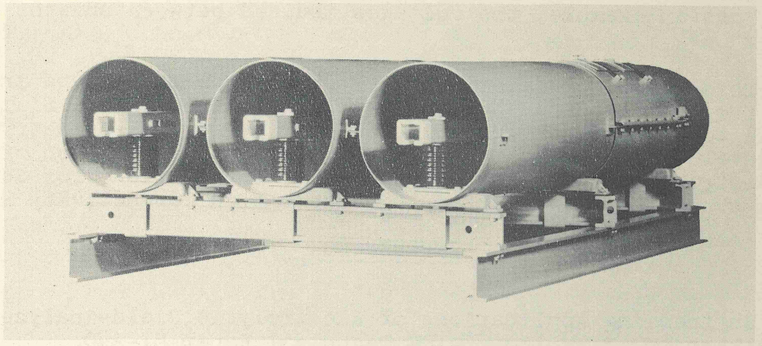

Fig. 1. Typical isolated-phase bus

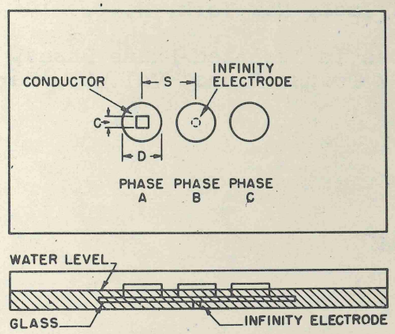

Fig. 2. Field analyzer set-up of isolated-phase bus

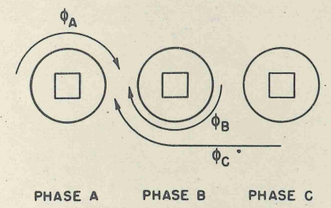

Fig. 3. Flux pattern between sheaths of isolated-phase bus

Mr Weller
Misc.

Conference Paper

THE USE OF THE ELECTROLYTIC TANK FOR DETERMINING EXTERNAL INDUCTANCES OF ENCLOSED CONDUCTORS

L. L. Mankoff
Associate Member AIEE

R. H. Brealey, Jr.
Nonmember AIEE

Both of:
General Electric Co.
Philadelphia, Pa.

Submitted in abstract or outline form only to the AIEE Special Instruments and Auxiliary Apparatus Committee for presentation at the AIEE Winter General Meeting, New York, N. Y., January 31-February 5, 1960. Manuscript submitted November 25, 1959; made available for printing December 14, 1959.

Price: $ .50 To Members
$1.00 To Nonmembers

(5¢ per copy additional if first class mailing desired)

All Rights Reserved by the American Institute of Electrical Engineers
33 West 39th Street, New York 18, N. Y.
Litho in USA

Paper No. CP
60-176

District Conference Paper

Misc

MEASUREMENT OF FLICKER RESULTING FROM LARGE ARC FURNACE OPERATIONS

D. E. Simmons
Associate Member AIEE
Houston Lighting and Power Co.,
Houston, Tex.

Submitted in abstract or outline form only to the AIEE Transmission and Distribution Committee for presentation at the AIEE Southwest District Meeting, Houston, Tex., April 4-6, 1960. Manuscript submitted January 28, 1960; made available for printing February 10, 1960.

Price: $ .50 To Members
$1.00 To Nonmembers

(5¢ per copy additional if first class mailing desired)

All Rights Reserved by the
American Institute of Electrical Engineers
33 West 39th Street, New York 18, N. Y.
Litho in USA

r No. DP
-517

RECEIVED
MAR 17 1960
H. A. FREY

RECEIVED
MAR 18 1960
ENG. DEPT.

MEASUREMENT OF FLICKER RESULTING FROM LARGE ARC FURNACE OPERATIONS

D. E. Simmons

Whenever a large arc furnace is considered for installation on a utility system there is always the question of how much voltage flicker will result and what corrective or limiting devices may be required to keep the voltage flicker within acceptable limits. Although calculations can be made to predict the amount of voltage fluctuations, there is a question of how much to allow for variables such as contribution of motors and resistance of furnace electrodes and steel in the current path. In order to take into consideration these rather indeterminate factors it was decided to conduct tests to establish some correlating factor to apply to the calculated figure in order to obtain a value more closely approximating the actual flicker which would result for different operating conditions. This paper will show how this correlating factor was determined and how it was used to predict the amount of flicker which would result from future additions of large arc furnaces at one particular location.

Electric arc furnace loads are generally considered quite desirable additions to a utility system because of the high load factor which usually prevails. However, the very rapid load variation characteristics of the arc furnace causes deviations in frequency, tie-line interchange, and voltage which must be corrected or limited to values which will not be objectionable to other customers on the system. The frequency and tie-line prolonged deviations can be corrected with modern high speed load-frequency control equipment. Voltage variations usually can be kept within acceptable limits by proper design of equipment and utilization of auxiliary devices such as buffer reactors, synchronous condensers, and capacitors. It is the responsibility of the utility to protect all its customers from objectionable variations in the electric supply furnished to them. To do this there must be some method used to accurately predict the effect of future furnace installations and determine the necessary auxiliary corrective equipment required. This was the purpose of the tests to be described in this paper.

TEST DETAILS

The particular location considered here is a steel mill served by the Houston Lighting & Power Company from two 69 KV lines. The two arc furnaces located at this steel mill are each rated 75 ton 20 MVA, direct arc, three phase, with automatic electrode control. Figure one shows the arrangement of serving these furnaces including the reactor and synchronous condenser. Arrangements were made to vary the reactor setting, take the condenser out of service when required, and to vary generation on Houston Lighting & Power Company system. Tests were then made under the following conditions:

Study Number	Reactor Setting	Synchronous Condenser	System
1	15%	On	Normal
2	Out	On	Normal
3	Out	Off	Normal
4	Out	On	Reduced Generation
5	Out	Off	Reduced Generation

Various parameters were recorded at the Deepwater, Greens Bayou, and Steel Mill 69 KV busses, but the only one to be considered herein will be the oscillographic voltage records taken at these three locations. The oscillograms were made with a voltage biasing circuit shown in figure two. This arrangement permits greater sensitivity and resolution by recording only the tops of one half of the voltage waves. Figures three, four, and five show portions of the oscillographic voltage records obtained during these tests. Both furnaces were in operation on the highest voltage tap of 430 volts when the oscillographic records were made.

Since only one oscillograph was available for this test it was not possible to get simultaneous oscillograms at different locations. Consequently this is one of the limitations of this test and comparisons of the oscillograms between locations cannot be made directly. Examination of the oscillograms shows varying amounts of voltage flicker under different conditions.

CORRELATION FACTOR DEVELOPMENT

Calculations were made of predicted voltage flicker at the three locations under consideration. These calculations were based on known impedances of transmission lines, equipment, and the system. By obtaining the division of load between the two supplying stations on a DC network analyzer the current flow from each station was determined. The voltage drop from each of the busses back to the system then was computed to arrive at the calculated voltage flicker. These calculations were all based on single furnace operation. To obtain the flicker for two furnace operation a factor of 1.20 was applied to the single furnace voltage flicker value. This is in accordance with Ramsaur and Treweek who advocate that a factor of the fourth root of the number of furnaces in operation should be applied to single furnace flicker to obtain the value for multiple furnace operation [1]. A tabulation of both calculated and test values is shown in table one.

In order to develop a correlation factor, the ratio of test to calculated flicker values was determined and is shown as follows:

Study Number	Steel Mill	Greens Bayou	Deepwater
1	.63	.68	.83
2	.30	.38	.54
3	.37	.39	.52
4	-	-	.68
5	-	-	.78

Examination of these values shows that studies 2 and 3 resulted in ratios much less than the other studies. This indicates that the test values were not obtained at times of worst flicker. On this basis these values were disregarded. The average of the remaining ratios is .72 with a maximum of .83. Taking this into consideration it was decided to use a correlation factor of .80 for predicting future voltage flicker conditions due to arc furnace operation at this location. This factor was utilized in predicting voltage flicker for additional furnace installations at this steel mill served with different arrangements from the Houston Lighting & Power Company system.

CYCLIC FLICKER

Examination of the oscillograms obtained during these tests confirmed the contention that these furnaces were producing "cyclic flicker". This is defined in the AIEE sub-

committee report as voltage variations at a rate greater than one per second.[2] The experience of other companies indicates that the tolerable level of voltage flicker in this cyclic range may be as low as one half to one fourth that which may be permitted at slower rates.[2, 4] Restrictions have been placed on these furnaces so that operation over a prolonged period of time will not permit more than one per cent voltage flicker at the utility substation bus. This is considered a border line value particularly for "cyclic flicker". It is believed that voltage flicker greater than one per cent will produce some voltage flicker complaints.

CONCLUSIONS

Analysis of oscillograms taken during these tests showed that "cyclic flicker" was present. This will require continued caution to protect other customers from objectionable voltage flicker.

By comparing the measured flicker as determined on the oscillograms with calculated flicker values for the same operating conditions a correlation factor was developed for application to calculations for additional furnace operations under different system conditions. It is felt that the use of this correlation factor has permitted a more realistic evaluation of auxiliary corrective equipment required to serve future furnaces while also assuring other customers of adequate protection from objectionable voltage flicker.

REFERENCES

1. System Capacity Required for 3 - Phase Arc Furnaces, Oliver Ramsaur, J. E. Treweek. AIEE Transactions, Vol. 73, 1954, Part III-B, pp 1373-1374.

2. Survey of Arc-Furnace Installations on Power Systems and Resulting Lamp Flicker, AIEE subcommittee report. AIEE Transactions, Vol. 76, 1957, Part II, pp 170-183.

3. Transmission Line and System Problems in Supplying Large Electric Arc Furnaces During Wartime, B. M. Jones. AIEE Transactions, Vol. 62, 1943, pp 197-202.

4. Two Large Electric Arc Furnaces - Electrical Characteristics and Corrective Equipment, S. W. Luther, J. D. Ghesquiere, C. E. Quick. AIEE Transactions, Vol. 74, 1956, Part III, pp. 1401-1407.

STUDY NO.	SYSTEM CONDITIONS	SYN. COND.	REACT.	STEEL MILL 13.8KV BUS VOLT.	NO. OF FURNACES	PERCENT FLICKER VOLTAGES 69KV BUS STEEL MILL	69KV BUS G.B. 3 & 4	69KV N. BUS D/W
1.	NORMAL TRANSMISSION LINE ARRANGEMENT - G.B. 3 & 4 WITH BOTH UNITS ON - D/W N. BUS WITH NO. 4 GEN. ONLY ON.	ON	15%	79.3%	1	1.73	0.53	0.61
					2	2.06	0.63	0.73
			TEST VALUES→		2	1.30	0.43	0.61
2.	SAME AS STUDY NO. 1 EXCEPT NO GENERATION ON D/W N. BUS.	ON	0%	86.2%	1	2.71	0.77	1.01
					2	3.22	0.92	1.20
			TEST VALUES→		2	0.96	0.35	0.65
3.	SAME AS STUDY NO. 2.	OFF	0%	81.0%	1	4.02	1.33	1.68
					2	4.78	1.58	2.00
			TEST VALUES→		2	1.75	0.61	1.04
4.	NORMAL TRANSMISSION LINE ARRANGEMENT - G.B. 3 & 4 WITH ONE UNIT ON - D/W N. BUS WITH NO GENERATION.	ON	0%	86.2%	1	2.82	1.15	1.30
					2	3.35	1.37	1.54
			TEST VALUES→		2	—	—	1.04
5.	SAME AS STUDY NO. 4.	OFF	0%	80.4%	1	4.27	1.68	1.88
					2	5.07	2.00	2.24
			TEST VALUES→		2	—	—	1.74

Table I. Tabulation of calculated and test voltage flicker values.

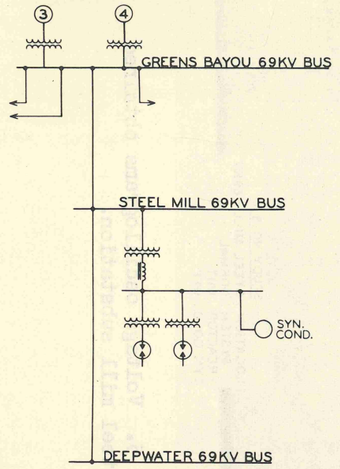

Fig. 1. Method of serving arc furnaces

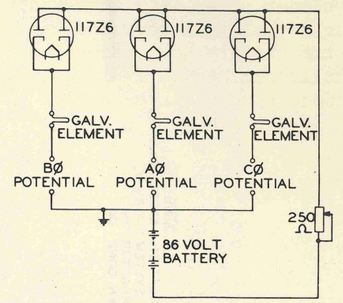

Fig. 2. Oscillograph voltage biasing circuit.

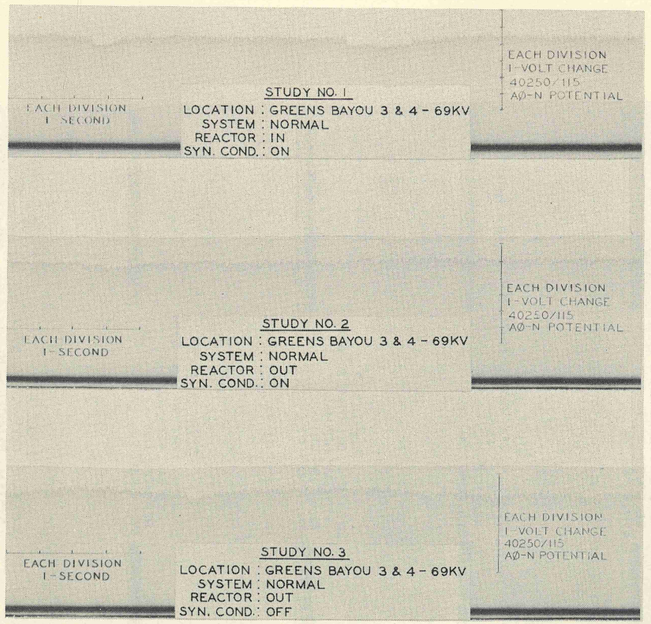

Fig. 3. Voltage oscillograms obtained at Greens Bayou Substation.

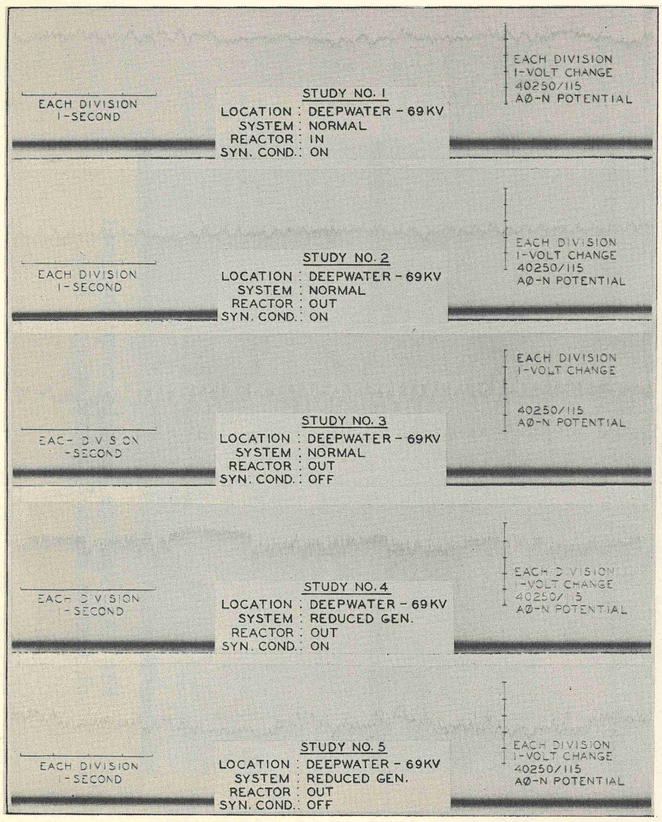

Fig. 4. Voltage oscillograms obtained at Deepwater Substation.

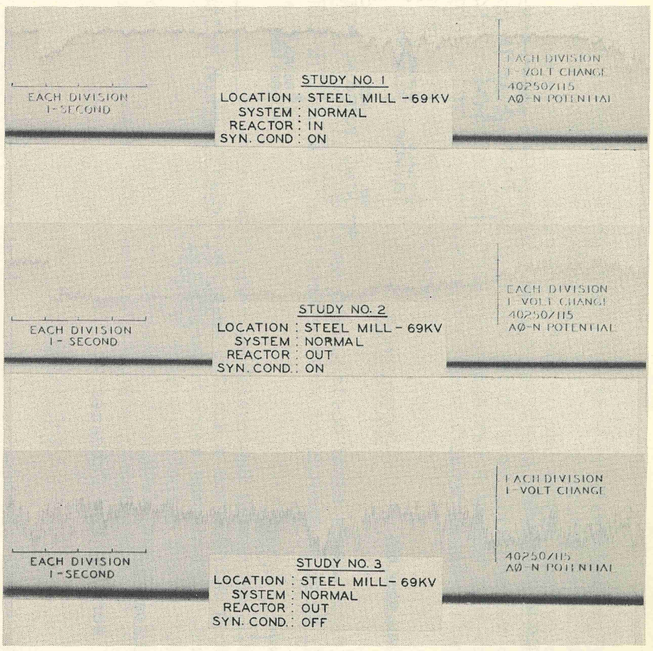

Fig. 5. Voltage oscillograms obtained at steel mill substation.

B. Kingsbury.
Ins - Dielectrics

GENERAL ELECTRIC COMPANY

INSULATOR DEPARTMENT

Technical Report No. LK-183-CR

July 22, 1960

SUBJECT

THEORETICAL MODEL FOR VOLTAGE STRESS AND PUNCTURE STRENGTH OF PORCELAIN DIELECTRIC PLATES

Ronald H. Lester

INFORMATION CONTAINED IN
THIS REPORT IS RESTRICTED
TO GENERAL ELECTRIC COMPANY

This report contains:

8 typewritten pages

Baltimore, Maryland

Signed Ronald H Lester

Approved R. B. Horton

THEORETICAL MODEL FOR VOLTAGE STRESS AND PUNCTURE STRENGTH OF PORCELAIN DIELECTRIC PLATES

Ronald H. Lester

ABSTRACT

Recently a new porcelain composition, #25B, was developed. One unique characteristic of this composition is an exceptionally high dielectric strength. In an effort to explain this phenomena, a model for internal voltage stress has been devised. This report presents the theory and gives data which supports a dielectric constant stress distribution as the main cause for dielectric failure of the matrix material in electrical porcelain.

INTRODUCTION

Standard electrical porcelain (740-1 body) consists of quartz bonded in a matrix of glass and mullite. The percent of quartz added to the composition is 20% by weight, some of which is dissolved in the matrix during firing. The matrix is made from 30% feldspar and the balance clay. The dielectric strength of this body at a thickness of .22" = 230 v/mil. The high strength composition (304 body) consists of alumina bonded in a matrix of glass and mullite. The alumina content is 40% by weight and is substantially inert in the firing operation. The matrix is made from 25% feldspar and the balance is clay. The dielectric strength of this body at a thickness of .22" = 220 v/mil.

The 25B composition consists of fractionated quartz bonded in a matrix of glass and mullite. The percent quartz added is 30% and because of its intermediate particle size, little loss occurs in firing. The matrix is similar to the 304 body and is made with 25% feldspar. The dielectric strength of this composition at a thickness of .22" = 311 v/mil.

The matrix of the 304 body and the 25B body is very similar and the volume fraction of filler (quartz or alumina) is approximately the same. Why then is the 25B composition so much stronger electrically? In considering the improvement of the 25B composition over the 740-1 body, an additional factor is the slight difference in matrix. The matrix in the 740-1 body has fissures caused by the cracks surrounding the quartz grains and also differs in that 5% more glass forming feldspar enters the composition. With the former in mind, the following theoretical model was established:

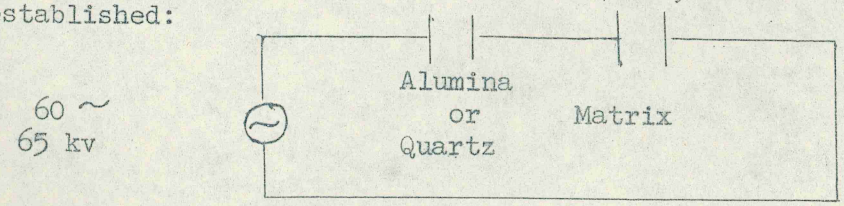

The dielectric is considered to be made of two capacitors in series. One capacitor represents the alumina or quartz filler and the other capacitor the matrix or glass and mullite.

The voltage stress is considered to divide itself according to the capacitance of the alumina, quartz and matrix. The thickness of the capacitors is based upon the volume percent of the phase present.

PROCEDURE:

In order to make the required calculations the following information was needed:

740-1 Body:
- Density of quartz
- Density of matrix
- Dielectric constant for quartz
- Dielectric constant for matrix
- Dielectric strength of matrix
- Dielectric strength of 740-1 body

304 Body:
- Density of alumina
- Density of matrix
- Dielectric constant for alumina
- Dielectric constant for matrix
- Dielectric strength of matrix
- Dielectric strength of 304 body

25B Body:
- Density of quartz
- Density of matrix
- Dielectric constant for quartz
- Dielectric constant for matrix
- Dielectric strength of matrix
- Dielectric strength of 25B body

The information desired was obtained as follows:

DENSITY

Quartz	= 2.65	Reference: Handbook of Physical Constants
Alumina	= 3.80	Reference: Geological Society of America Special Papers No. 36
Matrix 740-1 Body	= 2.42	Measured in Ceramic Laboratory Procedure #12
Matrix 304 Body	= 2.42	Measured in Ceramic Laboratory Procedure #12
Matrix 25B Body	= 2.42	Measured in Ceramic Laboratory Procedure #12

DIELECTRIC CONSTANT

Quartz	= 4.8 Reference: Handbook of Physical Constants
Alumina	= 9.5 Reference: G. E. Insulation Handbook
Matrix 740-1 Body	= Assumed equal to 25B because K of 740-1 body $\cong$ K of 25B
Matrix 304 Body	= Assumed equal to 25B because matrix similar
Matrix 25B Body	= 5.8 Measured in High Voltage Laboratory

DIELECTRIC STRENGTH

Matrix 740-1 Body	= 245 v/mil. at .22" Measured in High Voltage Lab.
Matrix 304 Body	= Assumed equal to 25B body because matrix similar
Matrix 25B Body	= 269 v/mil. at .22" Measured in High Voltage Lab.
740-1 Body	= 230 v/mil. at .22" Measured in High Voltage Lab.
304 Body	= 220 v/mil. at .22" Measured in High Voltage Lab.
25B Body	= 310 v/mil. at .22" Measured in High Voltage Lab.

CALCULATIONS:

740-1 Body

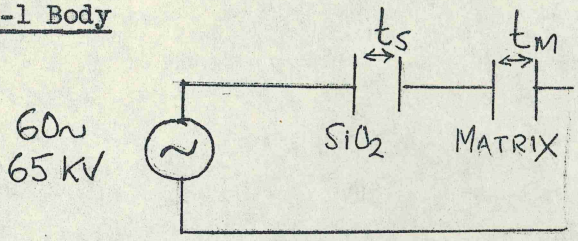

$t_s + t_M = .22''$

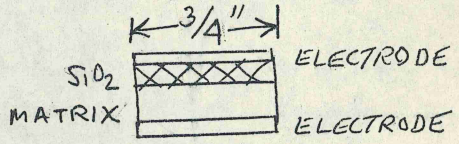

1) 20% flint at density = 2.65 gm/cc = 18.6% by Vol
   80% Matrix at density = 2.42 gm/cc = 81.4% by Vol

2) Volume of a cylinder - 3/4" in diameter and .22" thick

$V = \pi r^2 h = \frac{22}{7} \frac{3}{8} \times \frac{3}{8} \times .22 = .0975$ cu. inches and Area = $.442\ \square''$

3) $.186 \times .0975 = .0181$ and $\frac{.0181}{.442} = .041$ inches = ts

4) $.814 \times .0975 = .0792$ and $\frac{.0792}{.442} = \frac{.179 \text{ inches}}{\Sigma .22 \text{ inches}}$ = tm

5) $C_{Flint} = .2249 \left(\frac{4.8 \times .442}{.041}\right) = 11.65$ mmfd

$C_{Matrix} = .2249 \left(\frac{5.8 \times .442}{.179}\right) = 3.22$ mmfd

6) $\frac{1}{C_t} = \frac{1}{11.65} + \frac{1}{3.22} = \frac{14.87}{3.22 \times 11.65}$

$C_t = 2.52$ mmfd

7) $Z_t = \frac{7 \times 10^{12}}{2640 \times 2.52} = 10.5 \times 10^8 \Omega$

8) $I_t = \frac{65000}{10.5 \times 10^8} = .618 \times 10^{-4}$ a

9) X_c Flint $= \frac{7 \times 10^{12}}{2640 \times 11.65} = 2.28 \times 10^8 \Omega$

10) E Flint $= .618 \times 10^{-4} \times 2.28 \times 10^8 = 14{,}100$ volts

E Matrix = 65,000 - 14,100 = 50,900 volts

11) The dielectric strength of the 740-1 Matrix = 245 v/mil. at .22" or 54 kv

$\frac{54}{.22} = \frac{x}{.179}$ x = 44 kv breakdown voltage of matrix

$\frac{50.9}{65} = \frac{.44}{y}$ y = 56.2 kv = Breakdown voltage of porcelain
= 256 volts/mil

304 Body

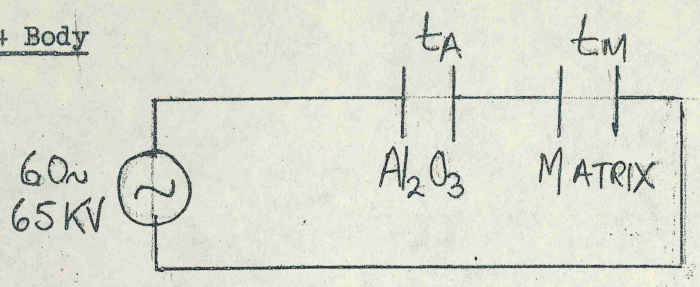

$t_s + t_m = .22''$

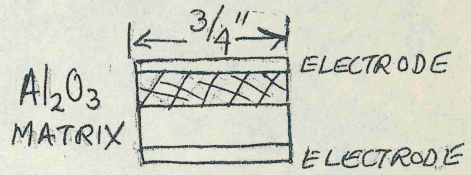

1) 40% Al_2O_3 at density = 3.8 gm/cc = 29.6% by Vol

   60% Matrix at density = 2.42 gm/cc = 70.4% by Vol

2) Volume of cylinder - 3/4" in diameter and .22" thick = .0975 cu.inch
   Area of 3/4" electrode = .442 sq. inch

3) .296 x .0975 = .0289 and $\frac{.029}{.442}$ = .065 inches = ta

4) .704 x .0975 = .0686 and $\frac{.0686}{.442}$ = .155 inches = tm

   Σ .22

5) $C_{Al_2O_3} = .2249 \left(\frac{9.5 \times .442}{.065}\right) = 14.5$ mmfd

   $C_{Matrix} = .2249 \left(\frac{5.8 \times .442}{.155}\right) = 3.72$ mmfd

6) $\frac{1}{C_t} = \frac{1}{14.5} + \frac{1}{3.72} = \frac{18.22}{14.5 \times 3.72}$

   $C_t = 2.96$ mmfd

7) $Z_t = \frac{7 \times 10^{12}}{2640 \times 2.96} = 8.95 \times 10^8 \Omega$

8) $I_t = \frac{65000}{8.95 \times 10^8} = .726 \times 10^{-4}$ a

9) $X_c\ Al_2O_3 = \frac{7 \times 10^{12}}{2640 \times 14.5} = 1.83 \times 10^8 \Omega$

10) $E_{Al_2O_3} = 1.83 \times 10^8 \times .726 \times 10^{-4} = 13{,}300$ Volts

    E Matrix = 65,000 - 13,300 = 51,700 Volts

11) The dielectric strength of the 304 Matrix = 269 v/mil. at .22" or 59.2 kv

    $\frac{59.2}{.22} = \frac{x}{.155''}$ x = 41.7 kv Breakdown voltage of Matrix

    $\frac{51.7 \text{ kv}}{65 \text{ kv}} = \frac{41.7}{y}$ y = 52.5 kv Breakdown voltage of porcelain
    = 238 volts/mil.

25B Body

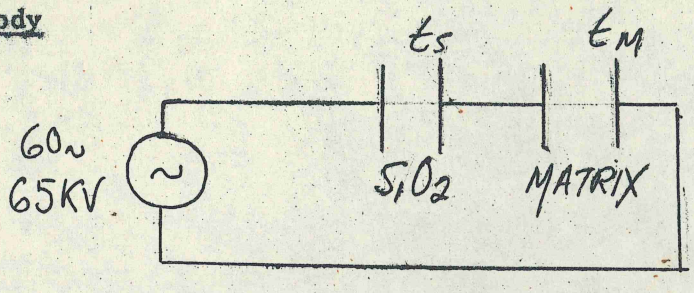

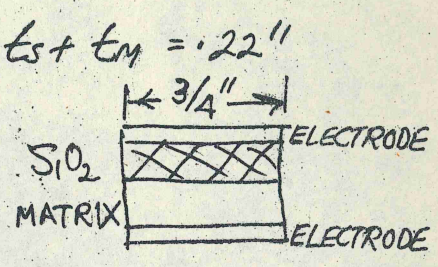

1) 30% Flint at density = 2.65 gm/cc = 27.9% by Vol

   70% Matrix at density = 2.42 gm/cc = 72.1% by Vol

2) Volume of capacitor = .0975 cu. inch and area of electrode = .442 sq. in.

3) $.279 \times .0975 = .0272$ and $\frac{.0272}{.442} = .061$ inches = ts

4) $.721 \times .0975 = .0703$ and $\frac{.0703}{.442} = \frac{.159}{.22}$ inches = tm

5) $SiO_2 = .2249 \left(\frac{4.8 \times .442}{.061}\right) = 7.82$ mmfd

   Matrix $= .2249 \left(\frac{5.8 \times .442}{.159}\right) = 3.63$ mmfd

6) $\frac{1}{Ct} = \frac{1}{7.82} + \frac{1}{3.63} = \frac{11.45}{7.82 \times 3.63}$

   $Ct = 2.48$ mmfd

7) $Zt = \frac{7 \times 10^{12}}{2640 \times 2.48} = 10.7 \times 10^{8} \Omega$

8) $I_t = \frac{65000}{10.7 \times 10^{8}} = .606 \times 10^{-4}$ a

9) $X_{SiO_2} = \frac{7 \times 10^{12}}{2640 \times 7.82} = 3.40 \times 10^{8} \Omega$

10) $E_{SiO_2} = 3.40 \times 10^{8} \times .606 \times 10^{-4} = 20{,}600$ Volts

    $E_{Matrix} = 65{,}000 - 20{,}600 = 44{,}400$ Volts

11) The dielectric strength of the 25B Matrix = 269 v/mil. at .22" or 59.2 kv

    $\frac{59.2}{.22} = \frac{x}{.159}$ x = 42.8 kv Breakdown of Matrix

    $\frac{44.4}{65} = \frac{42.8}{y}$ y = 62.7 kv Breakdown of Porcelain
    = 285 volts/mil.

SUMMARY:

740-1 Body

	Voltage Distribution	Mils.	Voltage	Breakdown Voltage
Quartz	298 v/Mil.	41	12,200	56.0 kv
Matrix	245 v/Mil.	179	43,800	254 v/Mil.
304 Body				
Alumina	167 v/Mil.	65	10,800	52.5 kv
Matrix	269 v/Mil.	155	41,700	238 v/Mil.
25B Body				
Quartz	326 v/Mil.	61	19,900	62.7 kv
Matrix	269 v/Mil.	159	42,800	285 v/Mil.

DISCUSSION:

The dielectric strength of #304 body is inferior because of the decreased quantity of matrix material and resulting higher voltage stress on the matrix. This is the result of the high capacitance of the (Al_2O_3) alumina oxide phase. The capacitance is high because of the high dielectric constant of Al_2O_3.

The dielectric strength of 25B body is high because of the lower capacitance of the quartz phase (caused by increased quantity of flint) and because of the higher dielectric strength of the matrix composition.

The results of this study indicate that the weak link in the electrical strength of porcelain is the matrix and that this is so because the greater quantity of material present is matrix. This is seen by considering that the voltage is divided according to capacitive reactance; i.e., directly as the thickness of the chemical phase present and inversely as the dielectric constant. It is apparent that since K deviates from 5 to 6 only in the case of Alumina (9.5), that the voltage distribution in an alumina free body is according to the volume fraction of the chemical phase present.

Note that in the summary table that the quartz can withstand only 298 volts/Mil. in the 740-1 body but 326 volts/Mil. in the 25B body. It is apparent that the limiting factor is not the quartz but the matrix. Only limited data is available on matrix dielectric strengths and for a better understanding of the dielectric strength of porcelain compositions, the dielectric strength of the matrix composition should be measured. In this study the dielectric strength of the matrix was measured at a thickness of .22 inches. For a more accurate analysis, the dielectric strength should be measured on a plate of matrix having the same thickness as the matrix in the dielectric plate of porcelain. For example, a plate of 740-1 body .220' inches in thickness has a matrix thickness of .159 inches. It is to be noted that the term matrix is defined as the mixture of glass, mullite, and voids with their gas or partial vacuum. It is impossible to make an exact replica of the 740-1 body matrix because of the reduced number of thermal cracks which are generated by the large quartz grains which are bonded in the matrix. These cracks caused by differential expansion will lower the dielectric strength of the actual matrix from the value obtained on the synthetic matrix. This will be in part the reason the

740-1 composition made with fractionated flint will have a higher dielectric strength than that made with standard flint.

A further correction which should be made in the calculations is that for the loss in weight of the matrix batch. For example, in the 740-1 body the following is true:

Batch		After Firing	New Wt. %
Clay	49% by Wt.	43%	} 78.7
Spar	31%	31%	
Quartz	20%	20%	21.3

It may be argued that the capacitance model is not correct and that the materials do not behave as two capacitors in series; however, I offer the following as further proof of a series capacitor arrangement:

740-1 Body

1) $C_{Flint} = 11.65$ $\mu\mu fd$
$C_{Matrix} = 3.22$
$C_{Total} = 2.52$

2) $C_{Air} = .2249 \left(\frac{1 \times .442}{.22}\right) = .452$ $\mu\mu fd$

3) $K = \frac{C_t}{C_{Air}} = \frac{2.52}{.452} = 5.6$

This value agrees with the value of K reported on Engineering Characteristic Sheet No. 1520; i.e., 5.6.

304 Body

1) $C_{Al_2O_3} = 14.5$ $\mu\mu fd$

$C_{Matrix} = 3.72$

$C_t = 2.96$

2) $C_{Air} = .452$ $\mu\mu fd$

3) $K = \frac{2.96}{.452} = 6.5$

Again this value agrees with the value of K reported on Engineering Characteristic Sheet No. 1521; i.e., 6.4.

It is possible to refine the model used to include the loss factor and additional phases. The following model is offered:

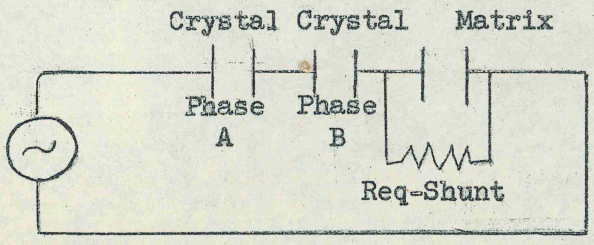

Since the crystals are almost true capacitors and the matrix is the lossy material, the above is believed to represent the actual conditions. The imperfect matrix capacitor is resolved into a perfect capacitor and an equivalent shunt resistance equal electrically to the internal resistance of the capacitor.

In closing the writer wishes to express his appreciation for the testing performed by B. Kingsbury and his staff and of the help of R. Gregory in fabrication of the test specimens used in the investigation.

McCoy

GENERAL ELECTRIC COMPANY

INSULATOR DEPARTMENT

Technical Report LK-694-DR

October 10, 1961

Subject:

NINE INCH SUSPENSION INSULATOR E1763

J. Kaminski, Jr.

This report contains:

6 typewritten pages

Baltimore, Maryland

Signed Joseph Kaminski Jr. Approved Fred C. Vose

NINE INCH SUSPENSION INSULATOR E1763

J. Kaminski, Jr.

PURPOSE:

Design and develop a nine inch suspension insulator utilizing electrical characteristics equivalent to the standard ten inch (1840) suspension insulator.

Prior to the time this initial prototype tests were completed, it was established by tests on Lapp Insulator Company units of equivalent design that the mechanical strength of such insulators were substantially in excess of the advertised 14,000 lb. M & E rating assigned to their insulator. Consequently, a competitive insulator must meet the performance of the Lapp units.

CONCLUSIONS:

The investigations covered 740, 304 and 21R (fractionated flint) type bodies and all shells were made by the jiggering process. The 21R (fractionated flint body) provides the best opportunity to meet the performance of Lapp equivalent units. The 740 body strength is insufficient from a mechanical strength standpoint. The 304 body is inadequate from a dielectric strength standpoint and is estimated to be at least twenty cents per shell more expensive than the 740 body.

Maximum mechanical strength was exhibited by insulators utilizing a single step pin, thereby necessitating a ball bolt design having a reduced shank under the cement line. Further improvement in mechanical strength is expected by increasing the pinhole diameter permitting the use of a ball bolt with an increased shear plane.

PROCEDURE:

All shells were made as per drawing E1763A by the jiggering process. The basic shell revisions when compared with the head of a standard six inch shell provided an increased external and internal radii at the top of the head section as well as a reduced sidewall thickness.

All tests were standard except steep wave front and M & E and ultimate. On M & E test, all insulators were loaded rapidly to 9500 lbs. then at 4000 lbs. per minute to failure.

All insulators were assembled with 16583KF forged steel caps nominally used on six inch suspension insulators. The ball bolts were machined from standard 5/8 inch 92674 ball bolts.

Puncture Under Oil, KV

740 Body	304 Body	21-R Body
120 Head	112 Head	120
126 "	104 "	126
130 "	120 B.C.	134
120 "	117 Head	140
124 "	127 "	122
123 "	———	———
Average 123.8	115.4	128.4

Must meet 110 KV minimum. The 304 body puncture values are too low to provide acceptable values.

Impact, Inch-Lbs.

740 Body	304 Body	21-R Body
90	170 No Break	130
70	170 No Break	140
80	170 No Break	100
90	170 No Break	80
55	170 No Break	120
Average 77		114

Standard rating = 55 inch-lbs. The 740 body exhibits marginal impact performance.

M & E and Ultimate, Lbs.

740 Body				304 Body				21-R Body			
(A)		(B)		(C)		(D)		(E)		(F)	
1 Step Pin		2 Step Pin		1 Step Pin		2 Step Pin		1 Step Pin		2 Step Pin	
M & E	Ult.	M & E	Ult.	M & E	Ult.	M & E	Ult.	M & E	Ult.	M & E	Ult.
12500	12500	13250	13250	17650	17650	16100	16100	18150	18150	17350	17350
13900	14400	14150	14150	17650	17650	15850	15850	18600	18600	17150	17150
13900	13900	15300	15300	16300	16300	16000	16000	18200	18200	17500	17500
14500	14500	14350	14350	18000	18000	13800	13800	17000	17000	17050	17050
13000	13000	14700	14700	15600	15600	15100	15100	18850	18850	17950	17950
14450	14450	12650	12650								
Average:											
13708	13791	14066	14066	17040	17040	15370	15370	18160	18160	17400	17400

(G)	
M & E	Ult.
12900	12900
12900	12900
13750	13750
AU 13183	13183

Groups A, B, C, and D assembled with standard six inch insulator cement. Groups E, F, and G assembled with 10 inch insulator cement. Four out of five insulators in Group A failed electrically simultaneously with mechanical failure. All of group D and F breakdowns resulted from pin pull-outs.

Steep Wave Front Impulse

All insulators were subjected to five impulses with energy input of 7000 watt seconds at approximately 500 kv and an estimated surge current of 7000 amps. A tensile load of 2000 lbs. was applied continuously during impulse test. All units remaining intact were then subjected to puncture under oil test.

740 Body	304 Body	21-R Body
Punct. 2nd Impulse	Punct. 4th Imp.	100 KV - Head
120 KV - Head	Punct. 3rd Imp.	132 KV - B.C.
Punct. 3rd Impulse	Punct. 3rd Imp.	146 KV - B.C.
130 KV - B.C.	Punct. 3rd Imp.	140 KV - B.C.
142 KV - B.C.	Punct. 4th Imp.	Punct. 5th Imp.

The performance of the 21-R body appears to be equivalent to the normal expectancy of the 1840 insulator using the 740 body in this same test.

Sixty Cycle Dry Flashover, KV

Sample 6 made from 304 body, all other samples 740 body.

Sample No.	1	2	3	4	5	6	
	80	78	81	80	82	80	Bar. 29.97
	78	78	82	80	80	80	D.B. 75°F
	78	76	77	78	78	78	W.B. 69°F
	75	75	79	79	78	79	Vap. 0.647
	77	77	77	78	81	82	Hum. 0.987
							Rad. 1.002
Av. Uncorr.	77.6	76.8	79.2	79	79.8	79.8	
Av. Corr.	76	75.8	78.2	78	78.7	78.7	

1840 Rating = 80 KV

Sixty Cycle Wet Flashover, KV

All samples used were 740 body shells.

Sample No.	1	2	3	4	5
	47	45	50	47	46
	45	48	50	48	48
	48	47	49	46	45
	46	44	48	48	48
	46	46	50	45	45
Av. Corr.	46.4	46	49	46.8	46.4

Bar. 29.86
D.B. 75.5°F
Rain Fall 0.19"/min.
Resistivity 7590 ohms per cubic inch
Pressure 37#/sq. in.
R.A.D. 1.000

1840 Rating = 50 KV

Impulse Test, KV

Samples 1, 2, 3, 4, 5, 304 Body. Sample 6, 740 Body.

Sample No.	1		2		3	
	Pos.	Neg.	Pos.	Neg.	Pos.	Neg.
Uncorrected	111	124	114	130	116	140
Corrected	113	126	116	132	118	142.5

Bar. 30.02"
W.B. 68°F
D.B. 81°F
V.P. 0.54
Pos. Hum. 1.013
Neg. Hum. 1.011
R.A.D. 0.995

1840 Rating = 125 KV Pos., 130 KV Neg.
Insulators cleaned with Trichlorethylene.

Sample No.	1		2		3		4		5		6	
	Pos.	Neg.	Pos.	Neg.	Pos.	Neg.	Pos.	Neg.	Pos.	Neg.	Pos.	Neg.
Uncorr.	119	132	119	132	116	134	113	136	118	140	118	140
Corr.	123.5	137.5	123.5	137.5	120.5	139.5	117.5	141.5	122.5	146	122.5	146

Bar. 29.99"
W.B. 64°F
D.B. 80°F
V.P. 0.422

Pos. Hum. 1.043
Neg. Hum. 1.037
R.A.D. 0.996

It is apparent that the single unit does not meet the rated flashover of the 1840 insulator.

Physical Characteristics

Arcing Distance - 7-3/8", 7-5/8"

Leakage Distance - 11-1/8"

Insulator Weight: 740 Body - 7 lbs.-8 oz., 7 lbs.-2 oz., 7 lbs.-7 oz.

304 Body - 8 lbs.-8 oz., 8 lbs.-3 oz., 8 lbs.-3 oz.

Estimated Costs of New Insulator
Per 100 Based on Use of Malleable Iron Caps

	740		21-R		304	
	Material	Labor	Material	Labor	Material	Labor
Shell	13.61	7.940	15.21	7.940	29.86	7.940
Ball Bolt	16.77	.292	16.77	.292	16.77	.292
Cap	47.25	1.055	47.25	1.055	47.25	1.055
Assembly	2.72	5.300	2.72	5.300	2.72	5.300
Sub Total	80.35	14.59	81.95	14.59	98.60	14.59
Wage Adj. 62%						
Sub Total	80.35	23.64	81.95	23.64	98.60	23.64
TOTAL - Labor and Material	103.99		105.59		122.24	

Miscellaneous

	740	21-R	304
Packing Materials	9.00	9.00	9.00
Outgoing Freight	22.50	22.50	25.50
	31.50	31.50	34.50

Comparative Evaluation of Factors Effecting Costs

	740	21-R	304	1840
Total	135.49	137.09	156.74	166.61
Below 1840 Costs	31.12	29.52	9.87	

The 1840 body shows the most favorable cost reduction when compared to 1840 insulators. Should it be necessary to furnish a forged steel cap, the margin between 1840 and nine inch suspension insulator costs should be reduced by at least four cents.

SUMMARY OF RESULTS:

These tests have shown the cement strength and ball bolt design to be a critical factor in the mechanical strength of the smaller head insulator. Insulators assembled with six inch insulator grade cement produced unfavorable results. The two step ball bolt shows a clear tendency to shear cement with pin pull-outs, a common occurrence. It is doubtful that the top step of the pin contributes anything to the strength of the assembly. Since the pinhole area proved to be the highest stressed area improvement in the insulator strength should result from increasing the cement bearing area of both the pinhole and the pin. The steep wave

front impulse results indicate the inherent dielectric strength weakness of the 304 body. The M & E and impact strength tests demonstrate the incapability of the 740 body to meet minimum requirements. It is expected that a plunged shell will exhibit greater impact strength then the jiggered shell, but there is no evidence to support any significant improvements in the M & E strength since our 16583 strength is substantially the same as that obtained on insulators used in these tests.

HIGH LINE TOOLS

FOR HIGH VOLTAGE LINES

AND HEAVY CONDUCTORS

PAST, PRESENT AND FUTURE

by

CLETUS R. BREWER
Chief Hot Line Tool Demonstrator
James R. Kearney Corporation
St. Louis, Missouri

Presented At:

Pacific Coast Electrical Association
Engineering and Operating Meeting
Overhead Transmission and Distribution Group

March 23, 1962

San Francisco, California

Slide 1-1

Living and working within a few short feet of wires humming with live power has produced a breed that fears nothing, but that has a quiet respect for a high voltage line...the linemen. It is our good fortune that there is a rich photographic literature of linemen at work, dating back to the very beginning of high line maintenance and repair. The slides you are about to see have been prepared from old photos, Polaroid snapshots, sets of color slides, and even from 16-mm movie film. They have been selected as being typical of the eras they represent, so that I might show you, by means of a series of slides, the linemen using their unique tools on high voltage lines and heavy conductors in the past and at present. Then I will offer you some ideas of possible future developments in the high line tool industry.

YESTERDAY

By comparison to many other industries, electrical transmission and distribution is almost a new field. In 1882--only 80 years ago--power was being transmitted at 110 volts, DC. Four years later the first AC system was put into operation, and by 1888 alternators were delivering 1100 volts. One of the first electric plants was built in 1893 in Monticello,

Slide 1-2

Georgia. As the story goes, this plant, which supplied power for street lights at a flat rate, operated on what was called a "moonlight schedule." If there was a bright moon shining down on Monticello, the street lights were turned off and Mother Nature provided the illumination. And, by the way, you might have noticed that even back then the power house gang had their "pin-up girls."

From the very beginning, the electrical industry was on the go, growing almost too fast to follow. By 1902 transmission voltage was up to 80 KV. In a short 20 years it jumped to 220 KV; and 30 years later, in 1952, a 330 KV line was put into service.

In spite of how well the engineers design electrical systems, there has always been a need for line maintenance. Parts failure, the forces of nature--such as lightning and storm damage--and vandalism can cause interruptions of service that

must be restored as soon as possible. To keep the lines in service, there has grown up in the power industry that highly specialized sort of maintenance man, the lineman, with his equally specialized working equipment, high line tools.

Here is one of the early linemen.

Slide 1-3

This gentleman, a Mr. Robert Hamilton, started out in the electrical industry in the days when Ulysses S. Grant was President. Working alone, he patrolled an area that could be covered by walking--and pushing a wheelbarrow. Over his right shoulder he carries what looks like an instrument for ringing out lines. Safety strap and tool belt are over his left shoulder. In the barrow there are rolls of wire and insulators, hammer, saw, ladder, and brace and bit. Yes, back in the days of low voltages, the tools used were about the same as in any other trade. High line tools, made special for the lineman, had not yet come into existence.

Handpowered trouble shooting wagons were popular around the turn of the century.

Slide 1-4

It was lineman leg power that sent this rig and its crew of four there and back on trouble calls in the Chambersburg, Pennsylvania, area many years ago. The roll of wire looks like Weatherproof No. 2 solid copper, and with that solder pot by Junior's foot, you can be sure there are no compression fittings in the cart.

Between 1900 and 1910 there occurred two important developments that were to have a strong influence on the growth of transmission and distribution lines. Wet process porcelain was available by then, and in 1907 the first flexible suspension insulators were put to use. Now that high voltage insulation was practical, lines to handle high voltages were being worked on, and in 1910 ACSR made its appearance.

Along with higher voltages, the length of transmission lines increased beyond the distance that a crew on foot could cover.

Slide 1-5

So the crew of linemen was provided with a horse and spring wagon. Old Dobbin was considered a member of the crew. He

was very well cared for; the crew took as much pride in him as was taken in the fire engine horses in the good old days. Why? Well, they had a saying, "Spare the horse, but not the man." You could hire a man, but you had to buy a horse.

Slide 1-6

By its very nature, electricity is a "natural" for those classes of service that would be most seriously hurt by a power interruption. From the beginning, operators and linemen have realized that power lines had to be worked "hot" so that there would be the fewest possible number of outages. Electrical transmission and distribution wires can be worked on while they are energized provided that the tools that are used put an adequate barrier of insulation between the lineman's hands and the conductors he is working on.

At the start, wood was the only material used for the poles and handles on power line tools. Wood has certain natural qualifications for this duty: It is readily available; it is moderately lightweight and strong; and, so long as it is dry, it is a reasonably good insulator. Not totally dry, for a wood pole robbed of all its moisture is quite brittle. It will fail in cantilever. Tests have shown that a moisture content of 6% to 7% is the most desirable, as this amount provides maximum strength with the least sacrifice of dielectric properties. To preserve these dielectric properties of wood poles, certain routine precautions are necessary: Tools are stored in heated drying enclosures. All scratches, nicks, and scars on the surface are promptly repaired. Poles are cleaned whenever they are dirty, damp, or greasy.

Slide 1-7

Here is a copy of the earliest known picture of a set of insulated tools. They were made of dried and seasoned hardwood, and used for insulator and crossarm changeouts. The "Christmas tree" in the center of the picture is a telescoping tool for lifting all the wires of a three-phase system at the same time. The lower end was lashed to the utility pole, and blocks were used to raise the triple yoke which picked up all three phase wires on its way up. Judging from the spacing, which is about 2½ feet between center and end phase wires, it looks like this tool was used on a 22 KV line. The "push-stick" at the right is a hardwood pole with a porcelain insulator fastened on the

top. These, and the other tools shown in the picture, were stored in the big box in the background. Taking care of tools even so crude as these was important; they had to be kept clean and dry--otherwise brush discharge would cause them to become "fuzzy" and be unsafe for use. In fact, these uncoated wood-pole tools were sometimes called "fuzz sticks" for that very reason. Even though they were homemade, these tools were ingenious, and certainly did the job they were intended to do. The worst that can be said about them is that they were heavy and clumsy, so that rigging them took a lot of muscle power.

In 1918 the first high line tool maker began to manufacture hot sticks, some of which are shown in this picture. Here

Slide 1-8

are hand poles, lift poles, and insulated links that look very much like the ones used today. The rigging--lifting out one phase at a time with poles and blocks--also has a familiar look. So, at the time of this picture--30 years after the first transmission line started into operation--specialized tools for the lineman had been devised and were being put to good use.

Of course, high line tools improved with each passing year, but the main change was in the quality of the tools. You will notice very little difference in their appearance.

Slide 1-9

A picture taken in the 30's shows the same sort of job as in the previous slide--an insulator changeout, again on a 22 KV line. The same style of rigging is used, but with refinements. Notice the lever lifts on the lift poles for the outer phases, and the pole saddles supporting the stick that holds the top phase aloft. Those are modern screw-type clamping heads on both the hand poles and the lift poles. This picture shows very clearly the two basic purposes of hot sticks: to provide an insulating support for conductors, and to isolate the conductors from each other as well as from the lineman.

In another picture taken in the 30's, a typical hotstick crew of those days poses with their working equipment. It is

Slide 1-10

the combined maintenance and line crew that re-insulated the McCammon, Idaho, to Downey, Idaho, line from 11 KV to 44 KV.

The crew consisted of foreman, three linemen, and three groundmen. Their tools were of modern design and fully adequate for the job; only by the age of their line truck is it apparent that this is a hot line crew of a quarter of a century ago.

Replacement of damaged insulators is, by far, the most

Slide 1-11

common job of high line maintenance and repair. This is true of both pintype insulators and suspension strings. Designing tools to do this job has offered a constant challenge to the high line tool industry. Many clever tools have been made and tried out; some few of them are still in use. Here is a set of tools that allows the lineman to take out a faulty insulator "bell" from a suspension string without removing the rest of the string. It is a heavy duty utility deadend tool being used on a 220 KV line. Being suspended from the tower arm, it lifts the conductor, taking all the down strain off the insulators. With the tension removed, it is possible for the lineman, with his insulated tools, to reach the cotter keys, and uncouple the ball and socket joints between bells, so that

Slide 1-12

the faulty unit can be removed. A closer look at this operation shows the lineman's view at the time the faulty insulator is being lifted out. The strain relieving lever system of the deadend tool is seen to be spaced by the reach bar that it pivots on. The rope block in the foreground takes up the slack. To keep the lower section of the insulator string from leaning over, it is held upright by a braced pole having an end that is shaped like a forked scoop. Meanwhile, a lineman is removing the defective insulator with a tool called a Disk Insulator Tong.

A different approach to the same maintenance problem is seen next. Working off a double circuit 3-way tower, the lineman has rigged a platform that makes it easy to get to

Slide 1-13

the insulator string with his hand tool. The insulators are cradled in a heavy duty deadend tool which takes the place of

the insulators in supporting the conductor while the insulator string is being repaired. At the time this picture was taken, there were several spectators in the tower watching the job. The line superintendent stands at the top of the tower. Two of his linemen are right below him watching the job.

Double string insulators presented another problem. What kind of tool would take the strain off one set of insulators while allowing the set next to it to remain in suspension? A tool was devised, and here it is. As you know, double insu-

Slide 1-14

lator strings are massive; the lines are heavy; the tool must be strong enough to bear the conductor load and insulator weight, yet not so massive or clumsy as to hamper its installation or to interfere with working through and around it. This group is inspecting the double string deadend tool fol-

Slide 1-15

lowing the demonstration of an insulator changeout on a 230 KV line. Lightweight aluminum castings combined with insulated poles make up the tool. The yoke on the left can be adjusted along the poles to match the length of the insulator string. Take-up screws going through the yoke on the right are tightened to take the strain off the insulators. Since they are removable, the two yokes can be interchanged to make the tool either left-handed or right-handed. Hookeyes on the two yokes allow the entire cradle assembly to be positioned by clamp-sticks. This style of tool is the forerunner of today's double string insulator and deadend tools.

TODAY

In the early 50's an event occurred that gave a tremendous boost to the quality of hot sticks. A usable pole made of epoxy-bonded glass fibers was developed and made available to the field. This Fiberglas pole is stronger and lighter than an equivalent wood pole, especially in the smaller diameters. Fiberglas, by its nature, will not absorb moisture,

Slide 1-16

and therefore requires less special care to maintain its voltage rating. However, the accumulation of surface moisture still must be avoided because of the leakage paths it can cause. Fiberglas is a better insulator by 1/3 than wood; consequently, the published test ratings of poles jumped from 75,000 to 100,000 volts per foot (based on 5-minute tests). Because of its smooth non-porous finish, the Fiberglas pole is easier to keep clean; and since it is tougher than the surface of a wood pole, it is less likely to be damaged in handling and use. Surface scuffing can be repaired with a suitable epoxy cement, but a pole with damaged glass fibers cannot be satisfactorily repaired. There are a few more steps in fastening tool heads to Fiberglas poles, but once they are attached, they are on for good--the two-component epoxy cement used hardens like porcelain. Live line Fiberglas poles consist

Slide 1-17

of a core of expanded plastic (unicellular polyurethane) on top of which there are formed several layers of glass fibers and epoxy sealer. Layers of glass fibers lying lengthwise on the core are alternated with layers wound around the core, giving great strength to the finished pole. The outer layer is wound spirally on the pole and sealed with the resin binder. The binder has a characteristic color generally selected to make the hotstick clearly visible even under conditions of obscure light. The finished pole is smooth and glossy; it has a very high electrical resistance, approaching that of air; it is not affected by most solvents, creosote, or petroleum products such as gasoline, oil, or grease.

Except for certain applications, wood poles and handles are going out of the picture. Some day they will all be replaced by Fiberglas. Both mechanically and electrically the Fiberglas pole is better than the wood pole, and is competitively priced.

At the present time, ideas for high line tools and work methods often come from a cooperative effort among operators, linemen, and tool demonstrators. In some instances, a lineman's idea for a new and useful device will be taken by a tool demonstrator to his company...and a new tool is born. Working the other way around, the tool demonstrators often take prototypes of a proposed new tool out into the field to find out from the linemen's reaction how well the tool will do the job.

And in yet another direction, a tool company will undertake to manufacture some tool developed by a power company. Everyone benefits from this type of cooperation, and I know I speak for the entire tool industry when I say that we are willing and anxious to work with the power companies in this way.

An interesting project handled cooperatively between the tool company's demonstrators and a power company back in 1955 involved an insulator changeout on a 345 KV line, worked entirely from inside the tower structure. A custom-made tool--good for suspension insulators only, and that could be rigged in place by hotsticks alone--was made for this job. Fortunately, several excellent slides were obtained at the time the tool was demonstrated. The first one shows the string of eighteen

Slide 1-18

insulators selected for the trial run.

The suspension insulator change-out tool is a combination

Slide 1-19

of stock items and parts made special for the job. The Fiberglas reach poles and the jack screws are standard, but the metal assembly was tailor-made to this particular tower arm,

Slide 1-20

and probably will not fit most other towers. An installing tool, having a roller which rides along the far-side upper beam, is used to position the insulator tool. The roller is not visible in this view; it is behind the lineman. The installing tool also is a special item made just for this job, and is not catalogued. (However, let me mention here that the manufacture of "specials" like this can be worked out to fit the needs of any operating company.) The installing

Slide 1-21

tool gives excellent control over the suspension insulator tool which can be easily rolled out alongside the insulators, swung around, then positioned over the string. Observe also, at the ends of the reach poles, the hooks that will pick up the conductor.

The final maneuver to set the tool in place in the tower arm is shown here up close. The roller on the installing tool

Slide 1-22

is just visible. The hand line on the roller block helps to keep the installing tool and its load from running downhill too fast along the tower beam that acts as its track, while the insulator tool is being worked into position.

Tower work can sometimes be exasperating because it is so hard to find a place to hang the insulator tool on the tower arm. And, since for best results the tool should be fastened directly in line with the insulator support on the tower arm, it is almost always necessary to build a custom-

Slide 1-23

made cross head to fit the design of the tower arm. This one has several interesting features. It hangs solidly on the tower arm in the best position for relieving the insulator strain--right above the insulator string. Both reach bars are on pivots so that the conductor will be free to swing or sway. Alongside the top of the crosshead there is a bar

Slide 1-24

that the installing tool grabs. Notice the eye ring located on the square handle of the installing tool. The roller is fastened here when the installing tool is used to retrieve insulators, or in the eye ring farther back on the handle (where it now is) when the tool is used to work reach bars. The purpose of the big hook is now apparent; it hooks onto

Slide 1-25

the tower arm at a V-joint, giving an unusually sturdy hanging support for the insulator tool. At the base of the hook there is a block that sits solidly on the end of the tower arm.

Slide 1-26

The crosshead bracket-and-hook are the heart of this tool. The bracket is made approximately 20 inches long so

that the reach bars hanging down from it will just straddle the insulator string. Bracket and hook together weigh about 35 pounds. They represent the major weight of the tool as the 2" diameter Fiberglas reach poles are very light.

Slide 1-27

When the suspension insulator tool is solidly in place, the installing tool can be uncoupled from it and rigged to hang below the tower arm, then rolled out to engage a bell in the insulator string. Being fork-shaped, it can pick up a single bell, or the entire string, as required.

Slide 1-28

The final slide of this series shows the tool fully rigged. The safe working load rating of this tool is 10,000 pounds, which is more than adequate for suspension insulator change-outs on most lines.

As the size of conductors increases and spans get longer, there is the problem of how to grab the wire to relieve the strain on the insulators, particularly at deadends. A Cuma-long is not always adequate for the heavy weight to be handled, and it is not advisable to grip the deadend shoe. Any gripping tool that scars the conductor encourages corona discharge. It would be ideal if there were permanently placed between the end bell and the deadend shoe a link having a hook, a knob, or

Slide 1-29

a stud that could be engaged by the deadend tool. Tests of several such links have proved them fully satisfactory. Not only do they offer an easy way to grip the conductor, but also support the weight of the deadend shoe and the deadend jumper without the need of any extra rigging. They have the enthusiastic approval of the power companies that have seen them in use.

Slide 1-30

Here are some Polaroid pictures of a conductor grip that has met with considerable success. Called a bullnose clamp, it is placed over the conductor with a clampstick, so that it butts up against the deadend shoe. Its far side is rounded

and provides a knob that can be gripped onto. On the end of

Slide 1-31

the deadend tool there is a slotted bracket or socket (also called a bullnose, because of its shape). It fits around the clamp on the conductor forming a sort of ball-and-socket joint. In this view, the bullnose is being put in place. The conductor grip is being tried out at a deadend on a 230 KV line.

Slide 1-32

After the reach bars are located, a cradle is swung under the insulator string and fastened in place. A chain around the

Slide 1-33

power line pole serves as an anchor for the eyelet of the insulator tool. The lineman can work from a convenient loca-

Slide 1-34

tion on a platform to tighten the jack screws on the reach bars, relieving the strain on the insulators. To complete the story, we must borrow a picture from another installation.

Slide 1-35

At this stage, the insulator bells have been removed, and the conductor load is being carried by the reach bars. This point-blank view clearly shows how the bullnose socket grabs the conductor fitting. Although this particular clamp and socket do afford a workable wire-gripping means, it is easy to see how much better it would be to have a fitting made especially for gripping purposes that would be put between the deadend and the insulators, as part of the original power

Slide 1-36

line installation. The location of the bullnose socket 'way out on the end of the deadend tool can be seen in this picture of its use in yet another application. In this instance, the bullnose was not the conductor grip; instead a pair of hooks on the same casting with it holds the conductor in suspension. The hooks will take rodded conductors up to 2-1/8" diameter.

To illustrate the versatility of the deadend tool, it is shown here being used on a 230 KV tower at a running corner.

Slide 2-1

Unlike the changeout shown earlier as being handled from inside the tower structure, this one is being worked with the help of an insulated ladder. At the stage shown, the cradle

Slide 2-2

for the string of bells has been placed under the reach bars. The lineman at the right of center holds a hand line that is to be tied to the top of the string of insulators. The final slide of this operation shows how the bottom bell is coupled

Slide 2-3

or uncoupled from the conductor clamp by the man on the ladder.

The four examples shown so far have been of individual tools for high voltage work. Much of the experience gained from them has gone into the preparation of a complete tool set designed for one of the major utilities; it is capable

Slide 2-4

of taking care of single and double insulator string work on their 230 KV lines. Being a complete working set, many of the tools are, of course, standard. But the ones of main concern are the semi-custom-made types. Some of these are relatively simple; others are multiple assemblies. A few are quite new and unusual, and it is these which reflect current engineering trends in high line tools for high voltages and heavy conductors.

In those cases where the build of the tower arm interferes with using a top-mounted reach bar, an underslung

Slide 2-5

insulator tool is used. It consists simply of a cast aluminum crosshead that will take either the U-bolt yoke shown on it or the one below.

Quite often, when using a new tool whose appearance is out of the ordinary, linemen will give it a nickname that is both colorful and descriptive. They call this one the "milking stool." It has several unusual features. It puts no bind on

Slide 2-6

the conductor it is supporting during changeout. The cross-head is free to slide back and forth in its supporting tube far enough to accommodate conductor movement, and the conductor pick-up hooks are swivel-mounted to allow for the tilt of the conductor. The length of the reach bars can be adjusted to match up with the number of bells in the insulator string. Taking a closer look at one of them, it is seen that the end

Slide 2-7

of the inner pole has a drilled hole that can be aligned with any of the holes in the row on the outer sleeve. The adjustments are in 2-inch steps and cover a range of 2 feet. At any

Slide 2-8

particular adjustment the inner pole and the outer sleeve are held together with a locking pin that goes through both. It is one of the quick-operating types that is released by pushing on the button in the center of the handle, which allows it to be pulled straight out.

The "milking stool" drops over I-beams or inverted L's,

Slide 2-9

then two bars are bolted to the bottom of it, clamping the tool tightly on the beam at the desired spot. As shown at the lower left, the barrel can also be used with suitably formed yokes for hanging the tool below tower arms. At the lower right, almost out of the picture, is a barrel with U-bolts for attachment at swinging corners. With such an assortment of fittings, the insulator tool can be rigged on almost any type of structure. On the hollow tubular tower now showing on the screen, a heavy conductor is being held

Slide 2-10

in free-floating suspension while one string of insulators

from a V-configuration is being charged out. A U-bolt yoke over the tubular arms clamps the crossbar in place immediately above the conductor. A typical application of the "milking stool" tower arm clamp is shown next.

Slide 2-11

These last two slides were taken from 16-mm film frames.

When the insulator string must be eased down from an angle, such as at deadends and swinging corners, a tool designed to cradle the string is easier to handle; also it

Slide 2-12

reduces changeout time. The carrier that hauls the cradle

Slide 2-13

out into place is held onto the cradle by cushioned hooks. Both carrier and cradle are built up on lightweight Fiberglas

Slide 2-14

poles. The use of aluminum end castings is essential so that

Slide 2-15

the tool can be rigged with hotsticks. Observe the casting at the lower end of the cradle--it has a shoulder that fits around the insulator skirt, holding the string from accidentally falling out. At the top of the tool are two studs that can be grabbed with hotsticks, keeping the cradle under precise control while it is being swung in. The cradle is, as you might imagine, fully adjustable, and is usually set

Slide 2-16

to the length of the insulator string before being lifted into working position. For all its size, the tool weighs only about 75 pounds and can be raised with a hand line. In this view of a deadend string, the insulator cradle lies

Slide 2-17

inside of a deadend tool that is carrying the conductor strain.

A tower boom controls the tool as it is swung with its insulator load back to a tower position or lowered to the ground.

As an example of the way that a technique which proves successful in one application is modified to fit others, the reach bar installing tool previously shown being rolled along a tower beam inspired the tool that is shown in the next

Slide 2-18

sequence. It is called the monorail; it is a tool for grasping and hauling in a string of insulators. The "rail" itself is a 2½" Fiberglas pole. Its outer end is attached to the tower arm in a position above the insulator string. Its inner end is firmly anchored by a tower saddle. A pulley wheel rides the rail; suspended below it is a long-handled scoop.

Slide 2-19

The tool is used here to change out a suspension string on a 230 KV tower. In this view, reach bars are being put in place, and the monorail is coming up the side of the tower.

Slide 2-20

Looking down the tower arm, one can see the rigging for the monorail and how the scoop is cupped under the insulator bell. Notice the reach bars and their supporting yoke hooked into the "V" at the end of the tower arm.

Slide 2-21

At the lower end of the string, reach bars support the conductors. Hotsticks are in position to uncouple the bottom insulator from the conductor clamp.

Slide 2-22

There are 13 fog-type insulators in the string. At this stage the top bell has been loosened from the tower arm and the monorail tool is just about to be set into motion. The scoop can

Slide 2-23

be engaged under either the top insulator or the one below it. In this case, it was more convenient to reach under the second

bell. A curved flange on the scoop surrounds the skirt on the insulator so that when it is tipped at even a greater angle than is shown here, there is no likelihood of the string falling out. The almost negligible bending of the monorail with a heavy string of insulators at the midpoint shows very well the strength of the Fiberglas rail pole. This is the most unusual tool of the set shown earlier, and has been received with great enthusiasm by linemen and operators because of simplicity of rigging, the excellent control of the insulator string, and the speed and ease of changeout.

Quite a few of the tools I have shown you are bigger and bulkier than they need to be only because they must include an apparatus for tower arm attachment. Actually the tools are not complicated, it is just that so many fixtures, adapters, and connectors are needed. The tool does not exactly fit all towers, and rigging it is invariably time-consuming. It has been felt for some time that modern towers themselves should have a built-in means for attachment of conductor and insulator tools. Here are two examples that show how easily that could be done.

Slide 2-24

It is possible to design into a suspension tower arm a bracket, such as the channel section shown here in red. At the ends there are two holes spaced far enough apart so that reach bars run through them will properly clear the string of insulators. With these built-in yokes at each suspension point, a pair of reach bars are all that is needed to relieve the strain on the insulators, and a monorail tool could finish

Slide 2-25

the changeout quickly and efficiently. At deadends, a different sort of approach would be required...some device that could be set to the angle between the deadend string and the tower arm. A two-piece fixture is shown here. The stud would be a permanent part of the tower arm. On it, the tubular fitting would be placed, positioned toward the insulator string, and bolted down tight. Through the tubular portion would be attached the yoke of a deadend tool.

Both of these drawings of tower arm attachments have been made in a style intended simply to illustrate the principle.

To our way of thinking, including the reach bar yoke and the deadend stud on tower arms, and installation of the wire grip link shown earlier, as an integral part of the tower and line installation, would represent a notable advance in high line maintenance procedure.

TOMORROW

Right now, technical advances are so rapid that to estimate or guess what trends high line maintenance will follow must surely fall short of reality. A steady flow of new materials, devices and processes is being made available and is being used by our engineers. Breakthroughs are as prevalent in this industry as in any other. So, to be realistic, it is best to limit our discussion to developments in the near future as indicated by present-day experimental effort.

Every increase in transmission voltage and every increase in conductor diameter has allowed more electric power to be delivered more economically. One wonders if there is any technical or economic limit to transmission voltage and conductor size!

Slide 2-26

At the Extra High Voltage Laboratory set up by the Ontario Hydro-Electric Power Commission, one mile of bundled conductor is under test, operating at voltages from 460 KV to 600 KV. The northern half of the line consists of a bundle

Slide 2-27

of four conductors, each 954 MCM; and the southern half mile is also a 4-conductor bundle of 397.5 MCM conductors. Individual conductors are at the corners of a 16" square. The phase spacing is 32 feet. Each phase has its own transformer and voltage regulator. Suspension insulators of German manufacture are used because they were the only kind available with measured losses.

Slide 2-28

The test line was built on wood poles for cost economy. The lines are 80 feet above the ground. Even at that distance,

Slide 2-29

the static field produced by the conductors at around half a million volts causes hair on a man's arm to stick straight up when he walks under the span. All line trucks in the area must be grounded so that workmen will not get a shock when coming in contact with the body of the truck. A lineman working on an insulated platform acquires a capacitive charge that must be discharged slowly. High voltage experts estimate that if the lineman is discharged quickly--as, for instance, by coming into contact with a tower member--the shock can be fatal when the charge was accumulated from lines having a phase-to-phase voltage of 400 KV or higher.

About a year after the Coldwater project's lines were energized, experimental methods of suspension and deadend insulator maintenance were put to test. It was realized that, for safety, the lineman had to be kept at ground potential while at work. For the insulator changeout at this steel tower,

Slide 2-30

a ladder covered with grounded bronze mesh was rigged for a lineman to work at the conductor end of the insulator string. The linemen working on the top of the tower have a leg bracelet that is attached to a trailing ground. With reach bars in place, the man on the ladder uncoupled the insulator string from the conductor spreader yoke. The string was then swung up to tower position by reach bars. As the lower bell moved away from the conductor yoke, a loud hissing noise, audible on the ground below, was heard. Aside from the grounding safety measure, this changeout was performed in a routine manner.

So that the regular test line would not be disturbed, a separate line was erected for the purpose of a deadend insu-

Slide 2-31

lator changeout. A ground wire was run up the side of the pole for attachment of the trailing wires from the metal bands worn by the linemen. A lead from the ankle bracelet worn by the man on the platform can be seen nearby his feet. In climbing the pole, the linemen reported that when they were not grounded they received a distinct shock at each step upon

coming in contact with the pole ground wire. Again, in this instance, the change was accomplished without incident, using the newer type of insulator tools.

As part of the procedure of keeping the lineman at ground potential, the platform was covered with steel mesh. It was

Slide 2-32

also found that linemen on this platform tended to remain at ground potential when wearing leather soled shoes, while those wearing shoes with rubber soles attained a potential which caused a slight sting each time they came in contact with ground or with a person wearing leather soles.

Another device for keeping the lineman grounded is these

Slide 2-33

coveralls which they called the "monkey suit." It has bronze mesh sewed on front and back. You can see the bonding wire and ground rod near the lineman's left hand.

Slide 2-34

The suit was fitted with tabs for the attachment of an electrostatic voltmeter. A lineman wearing the "monkey suit" was posi-

Slide 2-35

tioned on an insulated platform at a specified distance from the line conductor, while another lineman read a meter which had been placed on a smaller platform nearby. Readings were compared with those taken with the lineman wearing normal clothing. Typical test results showed that the lineman wearing normal clothing acquired a potential of 11½ KV at a distance of 12 feet from the conductor, while the lineman with conducting clothing and shoes remained at zero potential with respect to ground.

Although these tests firmly established the effectiveness of the "monkey suit," it was believed that other grounding methods would stand a better chance, since the linemen found that the conducting suit was uncomfortable and hampered their free movement.

Slide 2-36

Heavier conductors require stronger tools; higher voltages require safer tools. Both the materials and the experience are available for manufacturing products to fit these requirements. There are, on the drafting boards, designs for tools with great strength, and with configurations that lower corona breakdown. There are under test several hydraulic and pneumatic take-up devices for use in those jobs where conductor weight rules out the use of ordinary blocks and jacks. Indeed, the range of materials and designs for tool manufacture is so vast that there is often the question of which to use, especially when there are several equally good ones to choose from. In effect, it all boils down to what kind of tool does the power company require. "Let us work with you to build the tools needed to do the job safer and better," is the present-day attitude of high line tool manufacturers.

It is the goal of the tool manufacturers to turn out the most efficient, useful and safe products possible for hot line maintenance work. Safe methods of insulator, tower, pole, and crossarm changeouts, repair of conductors, armor rodding--in fact, all kinds of maintenance on 230, 345, and 725 KV lines are being devised--using hot line tools. Progress in this sort of tool development is most rapid when there is close cooperation between the power companies and the tool manufacturers.

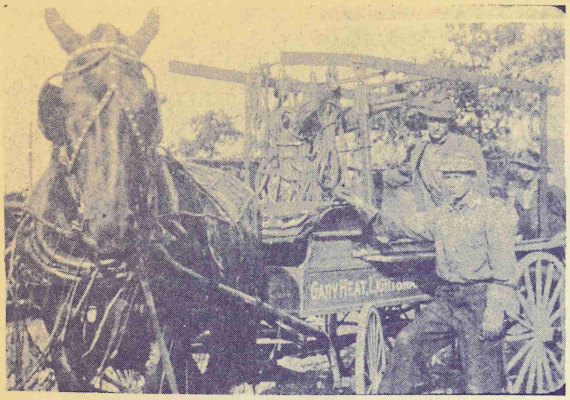

Slide 1-5

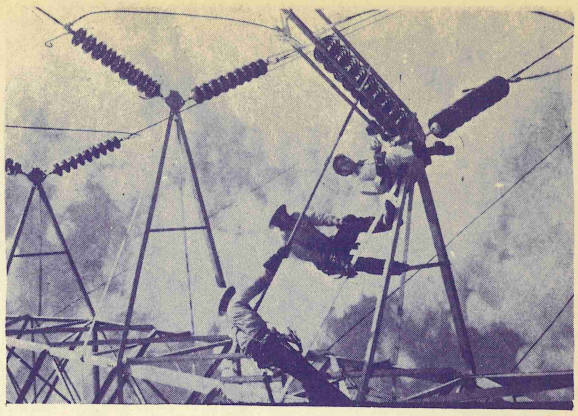

Slide 1-1

Slide 1-6

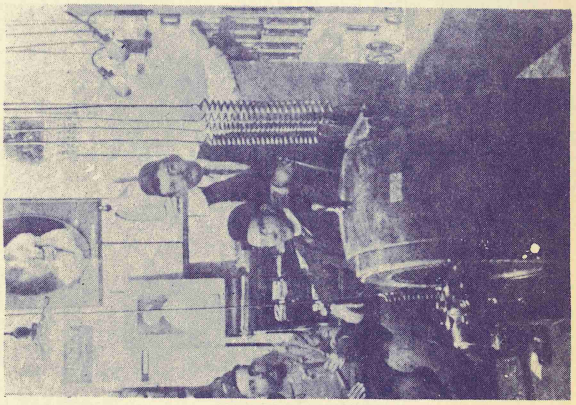

Slide 1-2

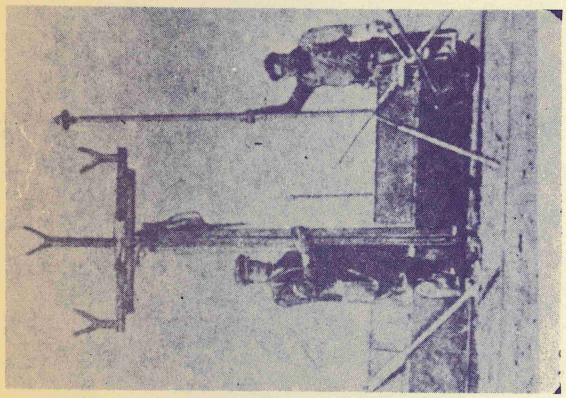

Slide 1-7

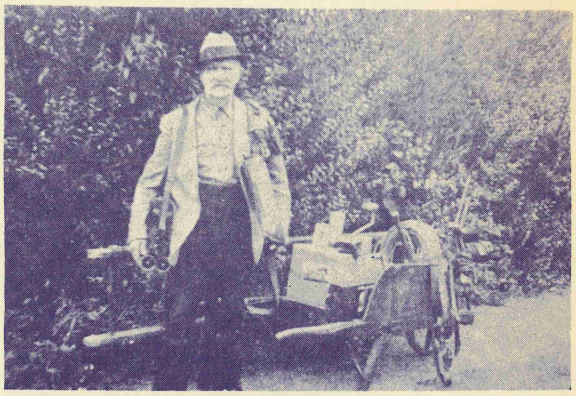

Slide 1-3

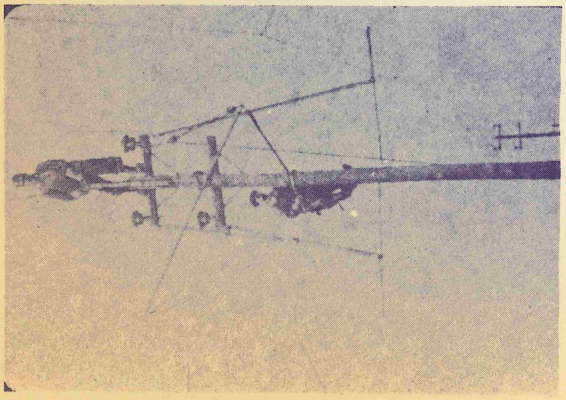

Slide 1-8

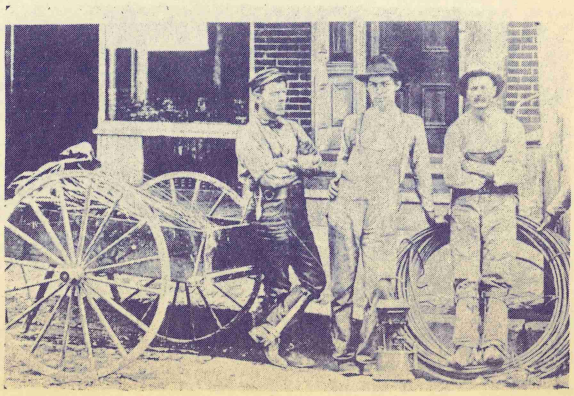

Slide 1-4

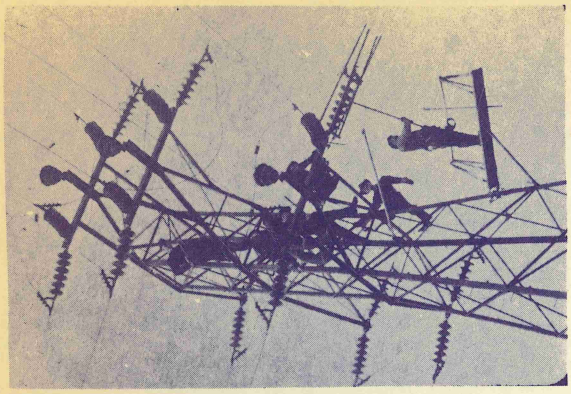

Slide 1-13

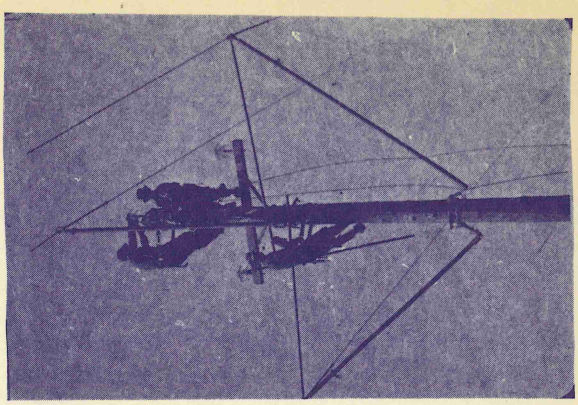

Slide 1-9

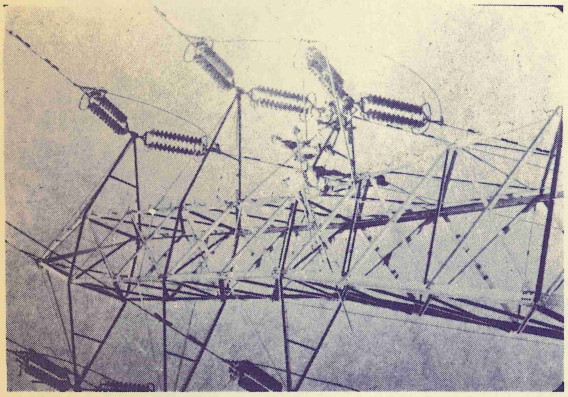

Slide 1-14

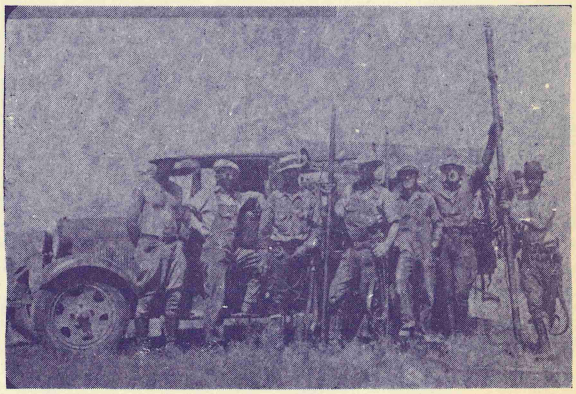

Slide 1-10

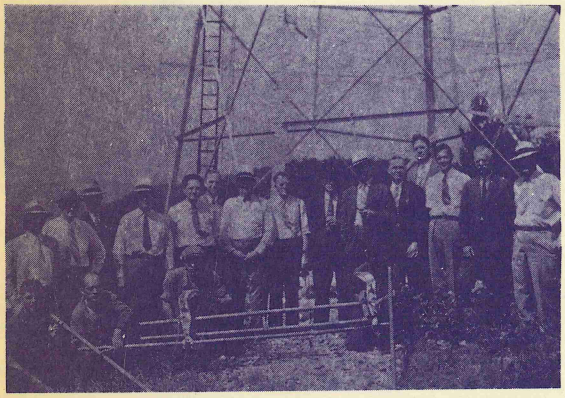

Slide 1-15

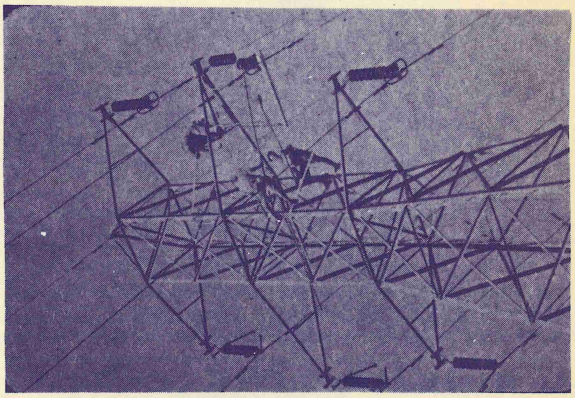

Slide 1-11

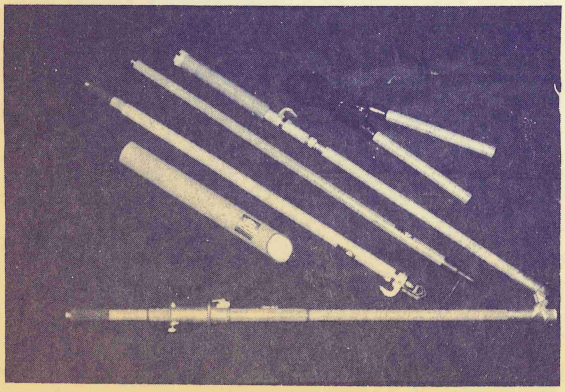

Slide 1-16

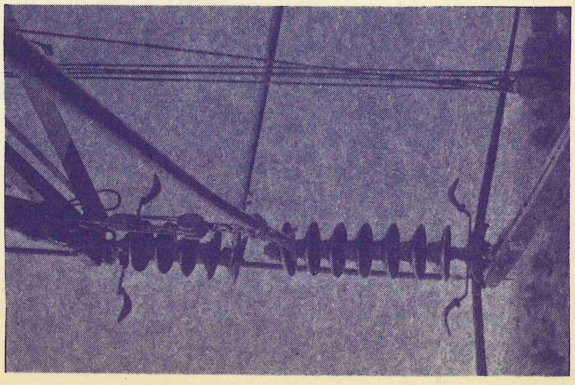

Slide 1-10

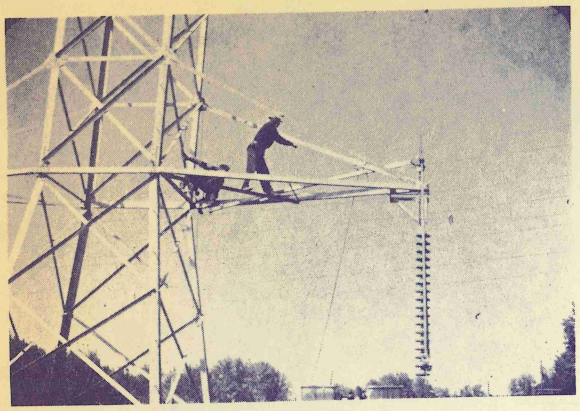

Slide 1-21

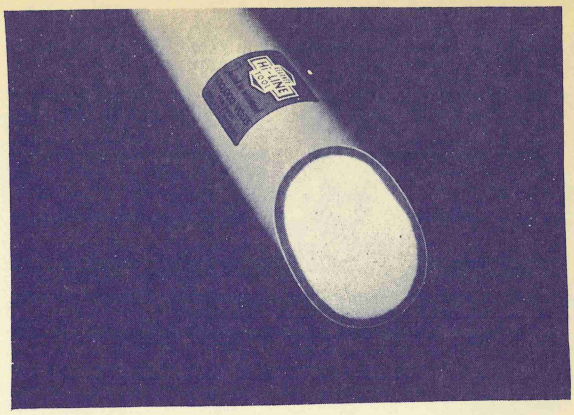

Slide 1-17

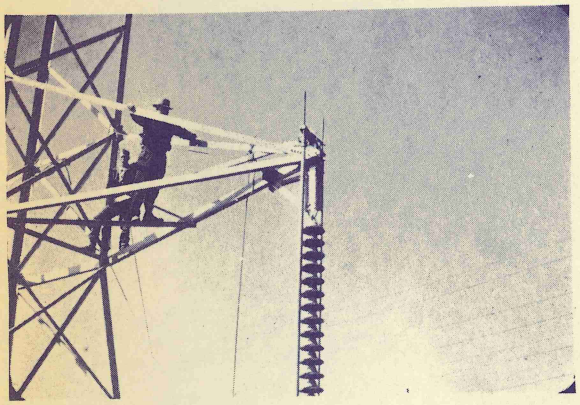

Slide 1-22

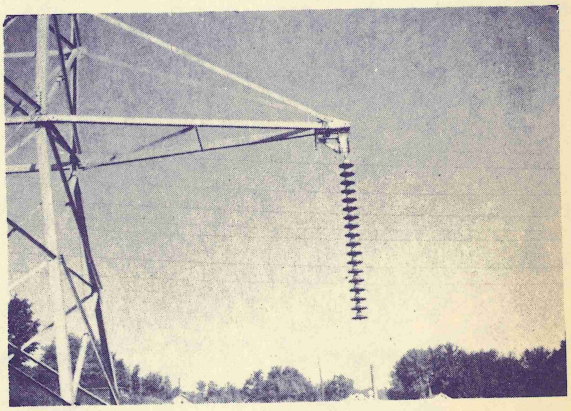

Slide 1-18

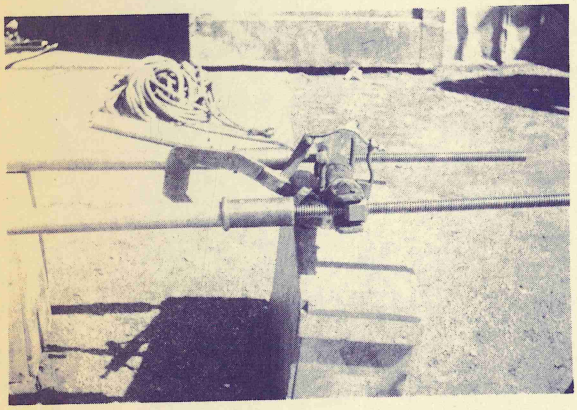

Slide 1-23

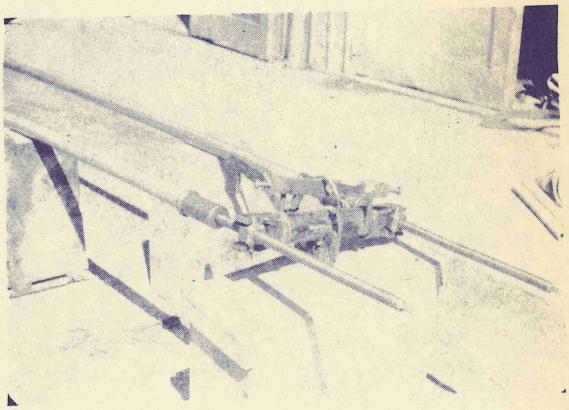

Slide 1-19

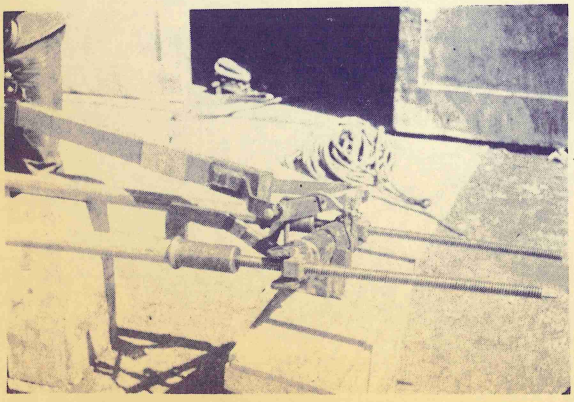

Slide 1-24

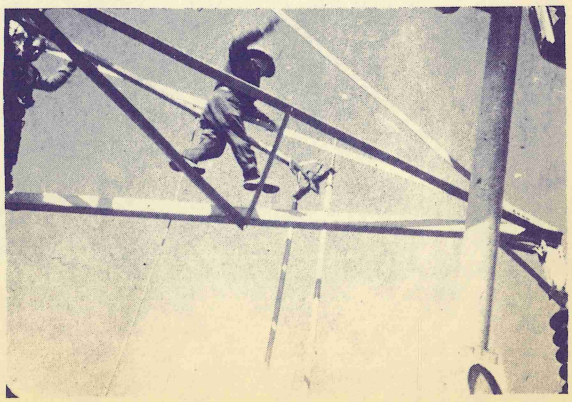

Slide 1-20

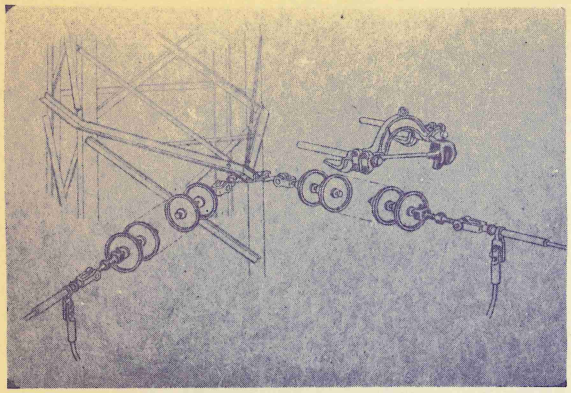

Slide 1-29

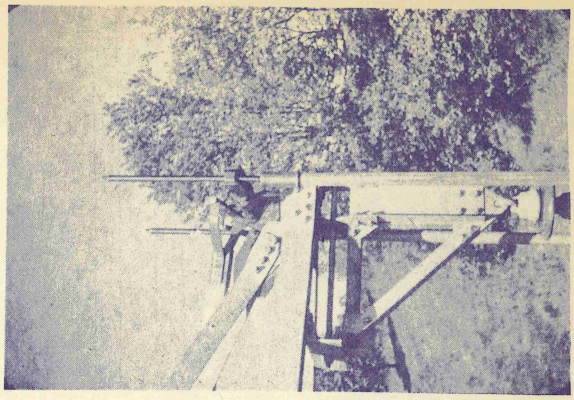

Slide 1-25

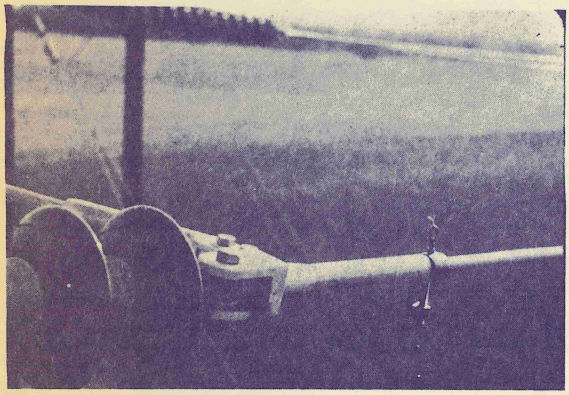

Slide 1-30

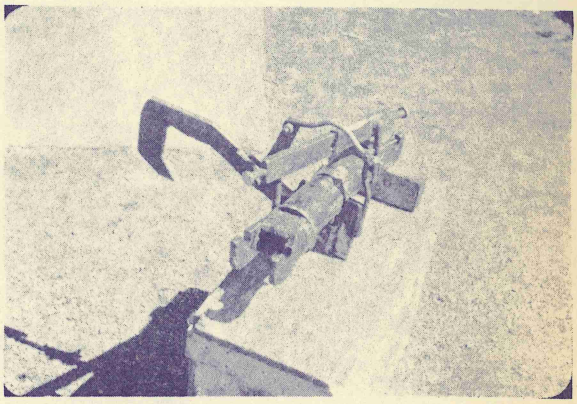

Slide 1-26

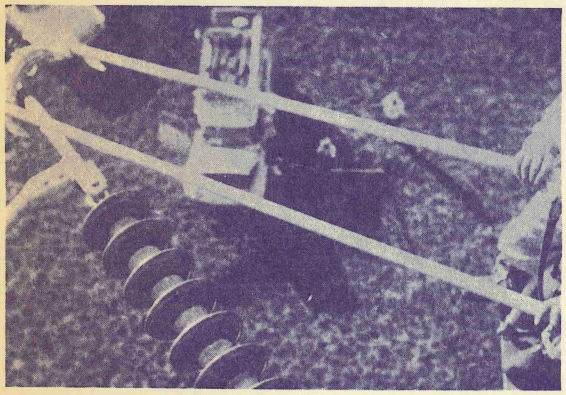

Slide 1-31

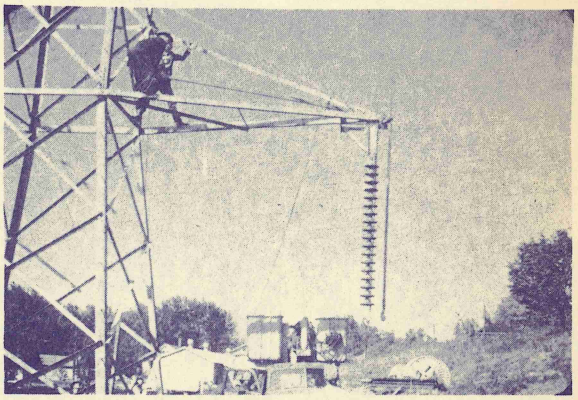

Slide 1-27

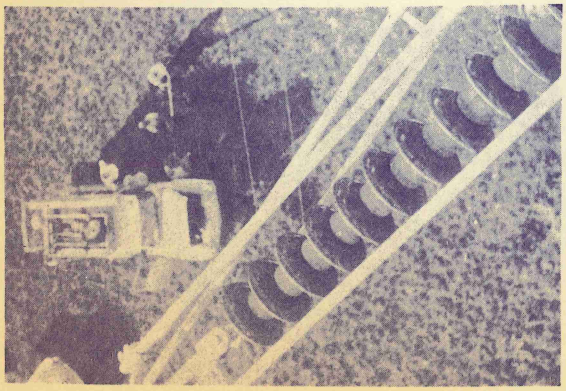

Slide 1-32

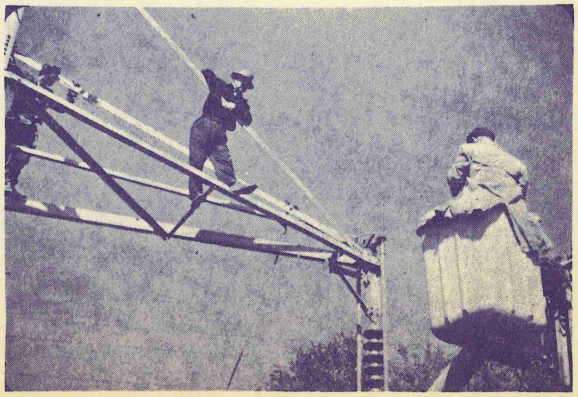

Slide 1-28

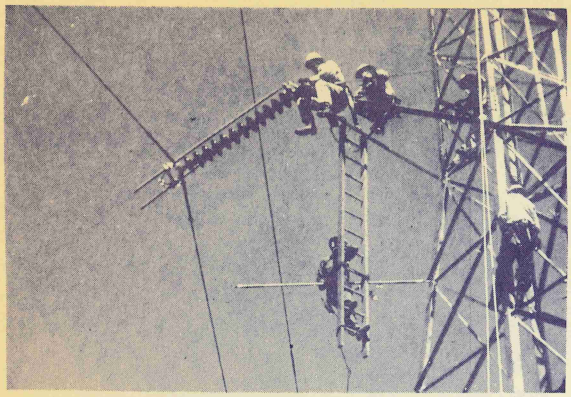

Slide 2-1

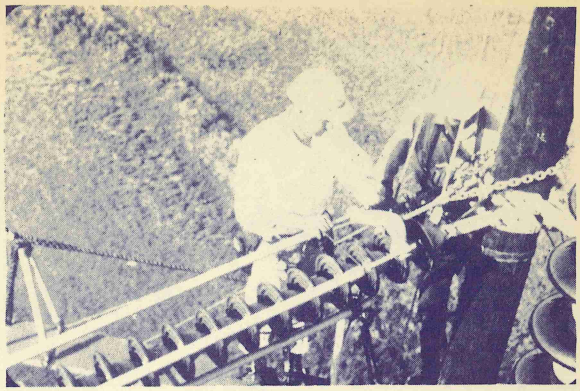

Slide 1-33

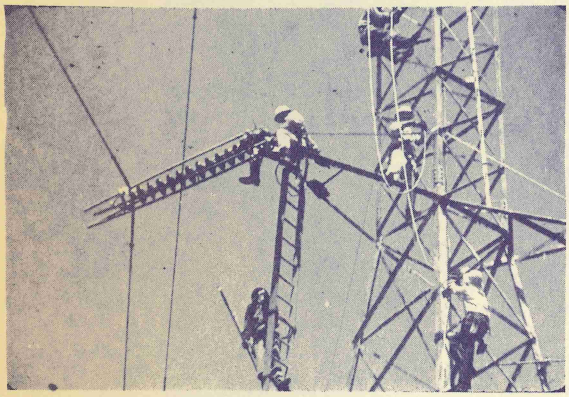

Slide 2-2

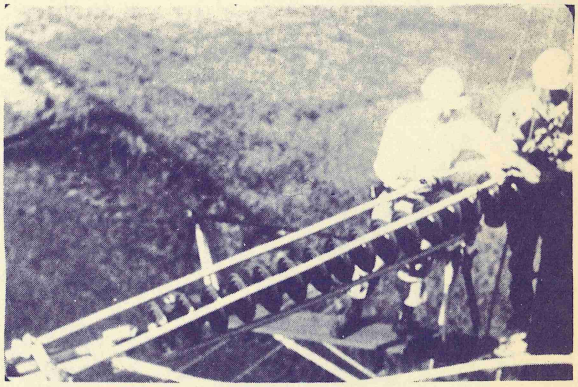

Slide 1-34

Slide 2-3

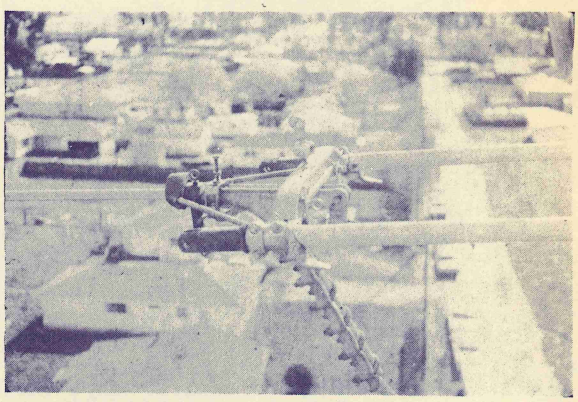

Slide 1-35

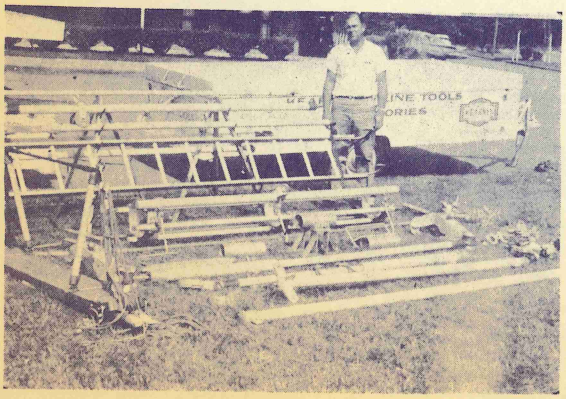

Slide 2-4

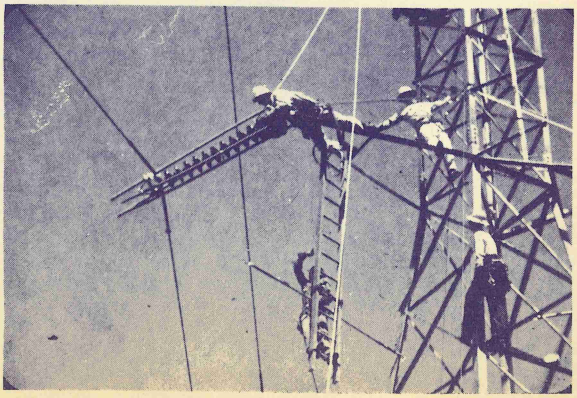

Slide 1-36

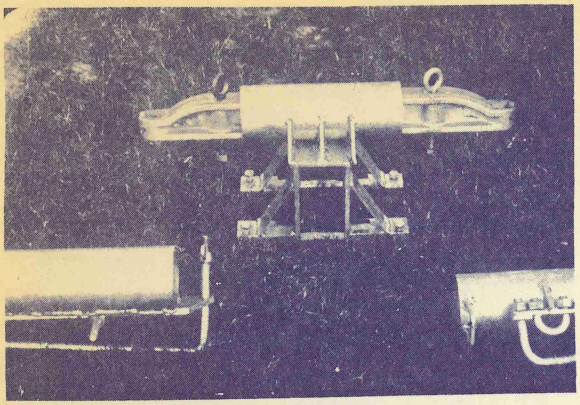

Slide 2-9

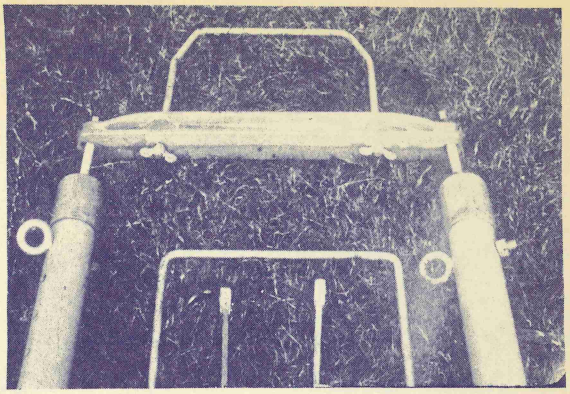

Slide 2-5

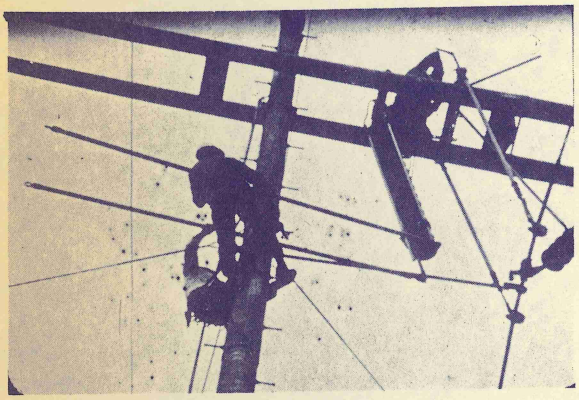

Slide 2-10

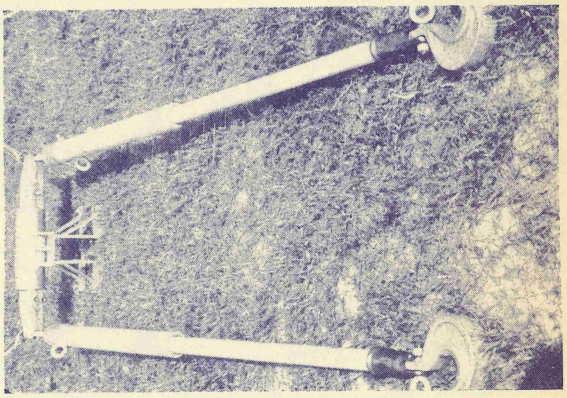

Slide 2-6

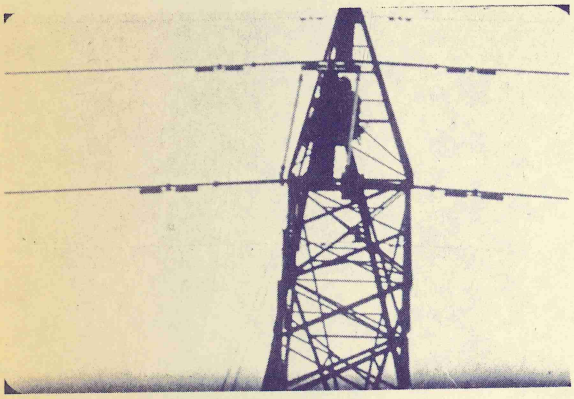

Slide 2-11

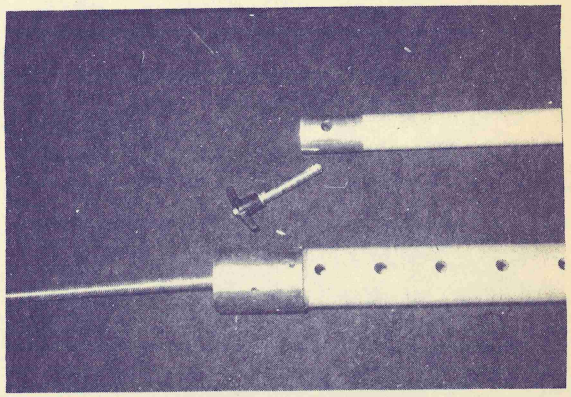

Slide 2-7

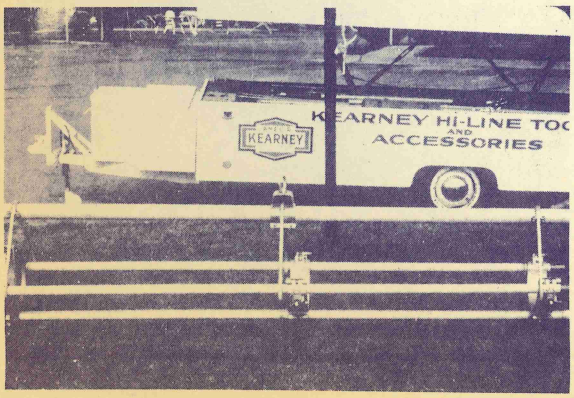

Slide 2-12

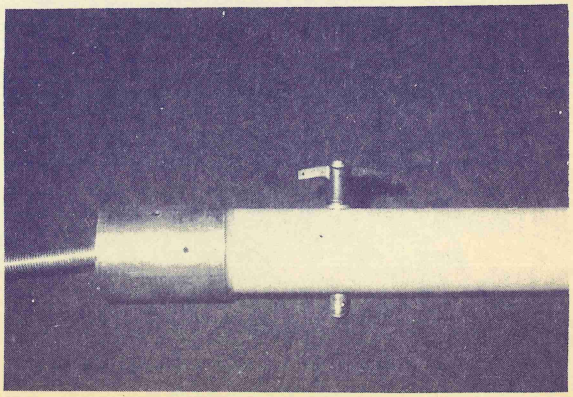

Slide 2-8

Slide 2-17

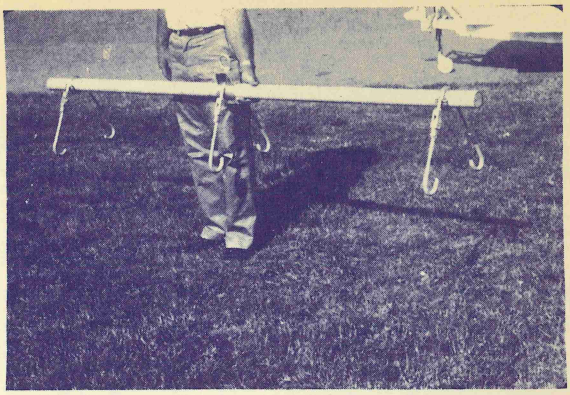

Slide 2-13

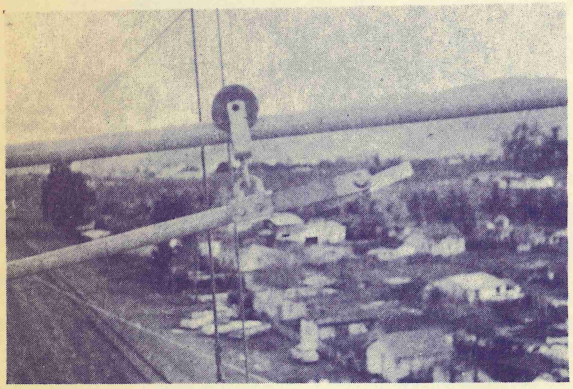

Slide 2-18

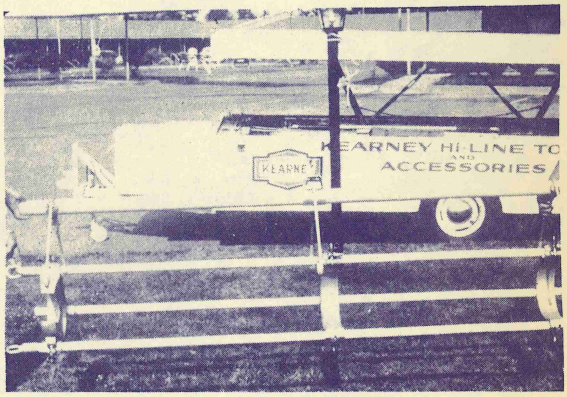

Slide 2-14

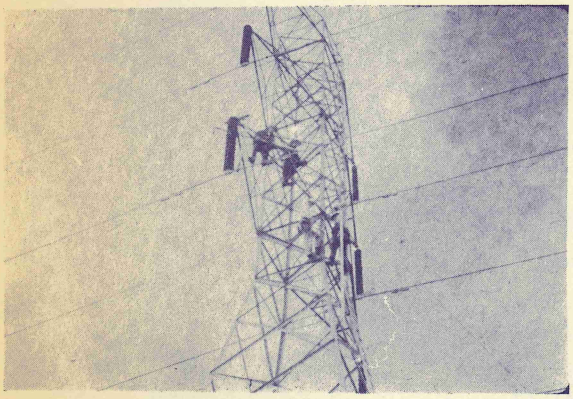

Slide 2-19

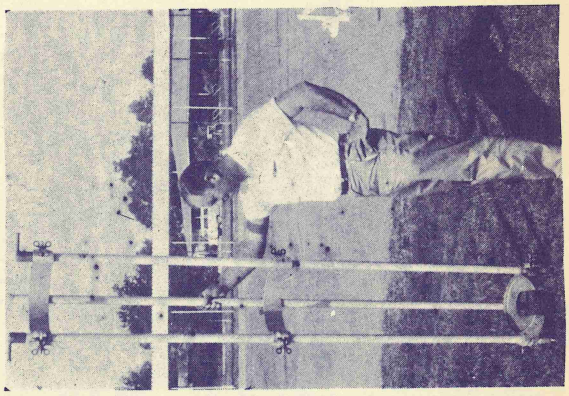

Slide 2-15

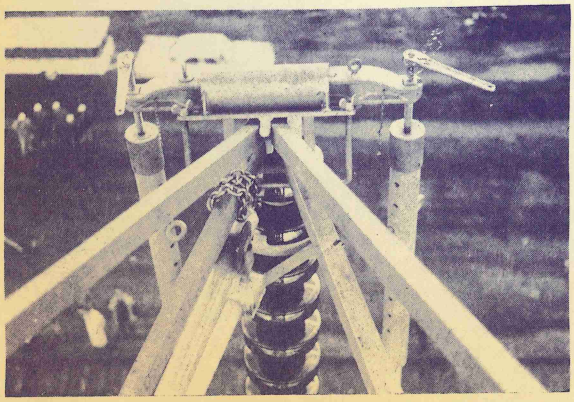

Slide 2-20

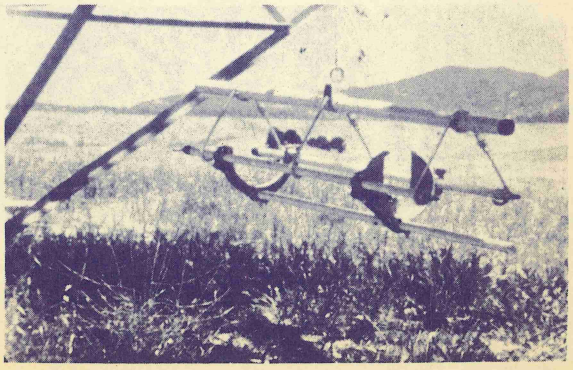

Slide 2-16

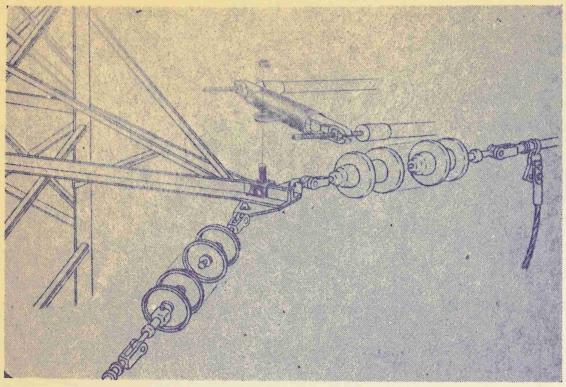

Slide 2-25

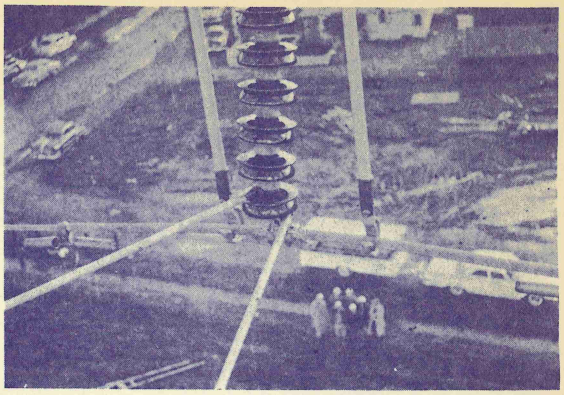

Slide 2-21

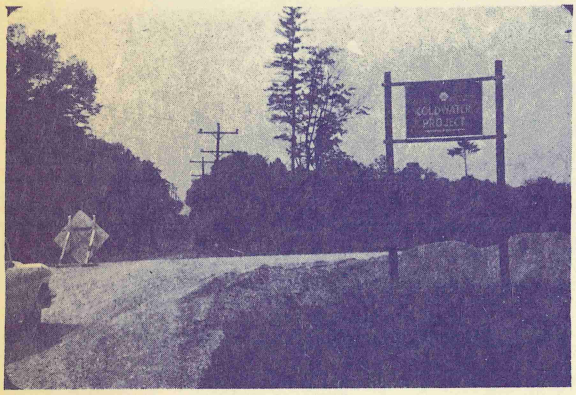

Slide 2-26

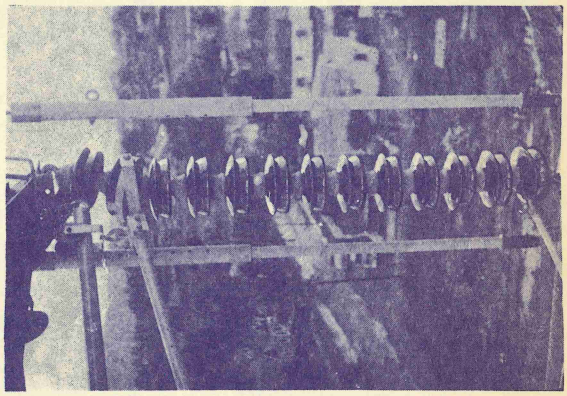

Slide 2-22

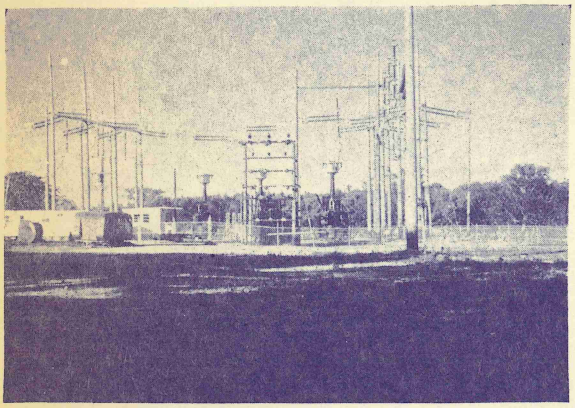

Slide 2-27

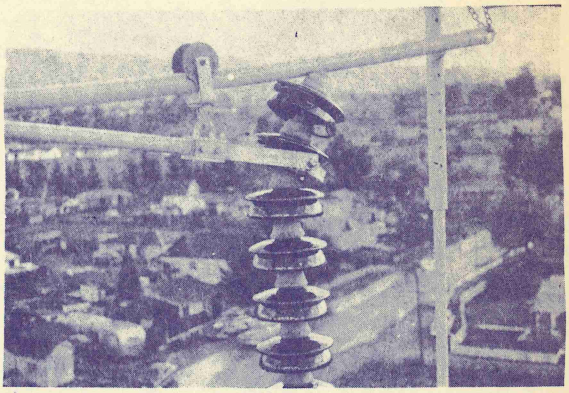

Slide 2-23

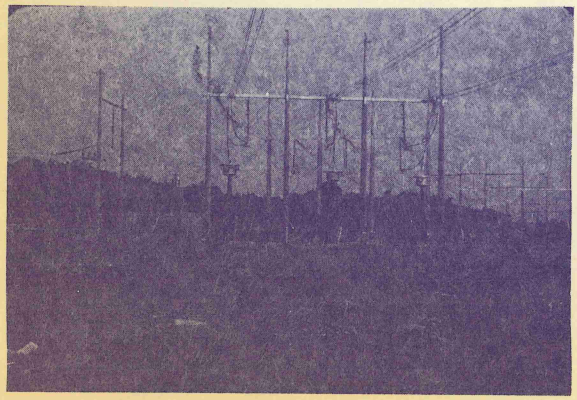

Slide 2-28

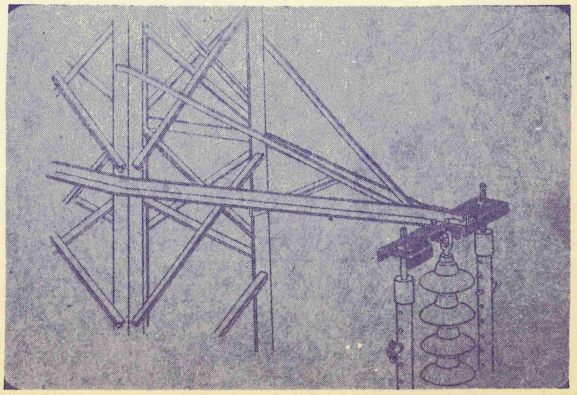

Slide 2-24

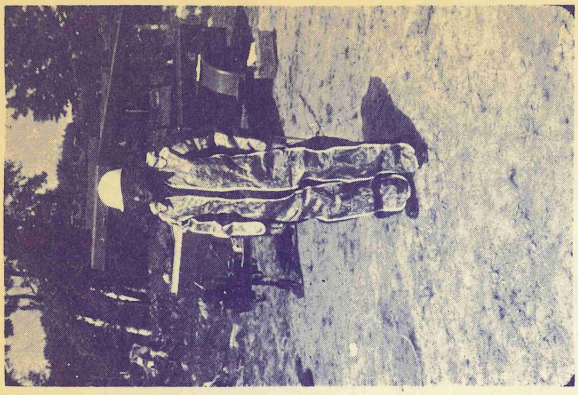

Slide 2-33

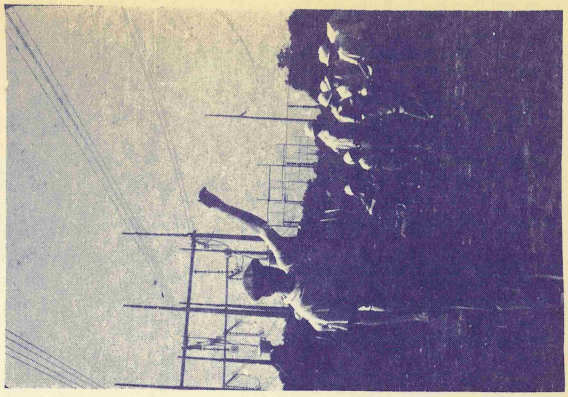

Slide 2-29

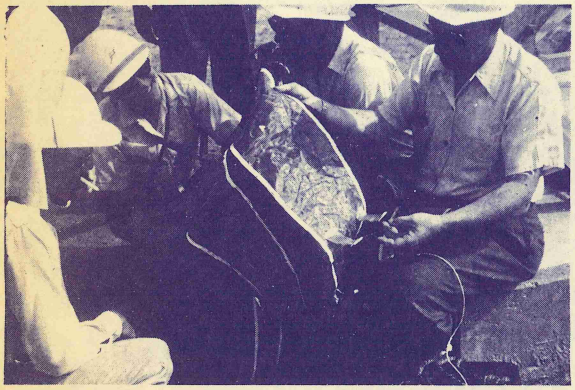

Slide 2-34

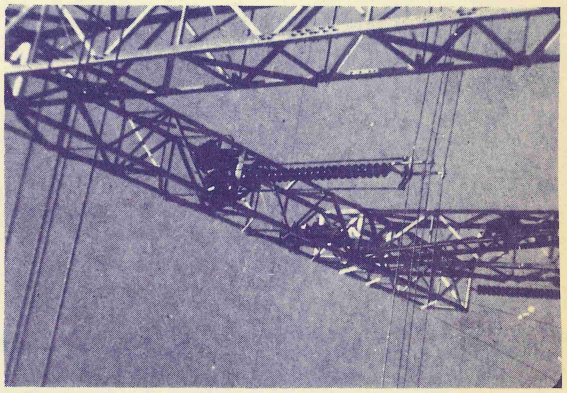

Slide 2-30

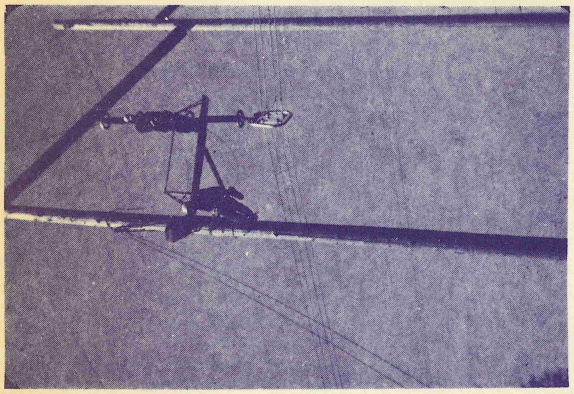

Slide 2-35

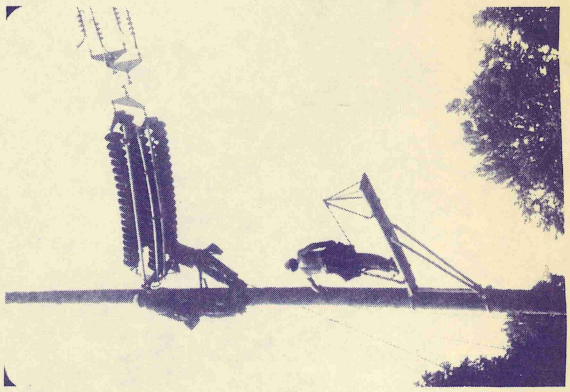

Slide 2-31

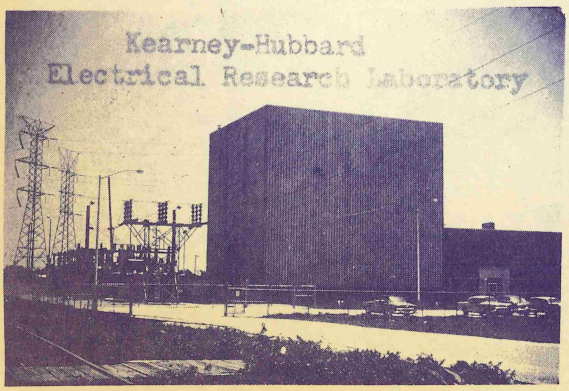

Slide 2-36

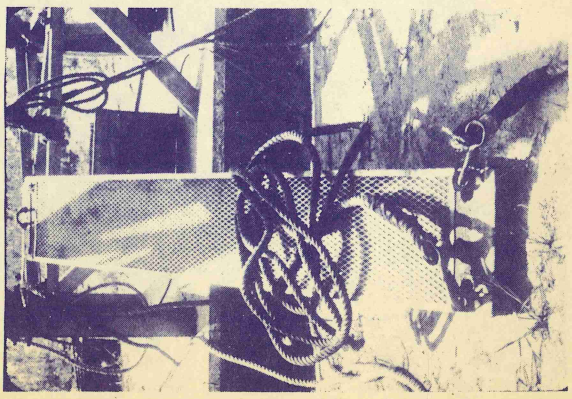

Slide 2-32

Transactions Paper

(Reviewed and Accepted for Publication)

RAINFALL RATE AND RESISTIVITY AT EAST PITTSBURGH, PA.

D. L. Whitehead
Fellow AIEE
Westinghouse Electric Corp.
East Pittsburgh, Pa.

A paper recommended by the AIEE Transmission and Distribution Committee and approved by the AIEE Technical Operations Department for presentation at the AIEE Summer General Meeting, Denver, Colo., June 17-22, 1962. Manuscript submitted November 24, 1961; made available for printing March 29, 1962.

Price: $ .50 To Members
$1.00 To Nonmembers

(5¢ per copy additional if first class mailing desired)

All Rights Reserved by the
American Institute of Electrical Engineers
345 East 47th Street, New York 17, N. Y.
Litho in U.S.A.

Paper No.
62-1025

Discussion in Duplicate Due July 6, 1962.

RAINFALL RATE AND RESISTIVITY AT EAST PITTSBURGH, PA.

D. L. Whitehead

SUMMARY

A new type of rainfall gauge has been built to read instantaneous rates of rainfall and resistivity. Construction details are given. Maximum rate of rainfall recorded during the period May-November, 1961 at East Pittsburgh was 0.07 in./min. The minimum resistivity was 1500 ohms/in. cube and the maximum resistivity 40,000 ohms/in. cube. These values are to be compared with standard wet test values of 0.2 in./min. and 7000 ohms/in. cube.

INTRODUCTION

The wet flashover characteristics of outdoor insulation is influenced to a considerable degree by the rate of rainfall and by the resistivity of the rain water. Tests 1, 2 have shown that the flashover voltage of some types of insulation may be reduced 50% by decreasing the resistivity of the water used in a wet test from 10,000 ohms per inch cube to 2000 ohms per inch cube. Likewise, increasing the precipitation rate from 0.1 in./min. to 0.2 in./min. in a typical case may reduce the flashover voltage 25%. This immediately raises the question of the appropriateness of our wet test standard resistivity of 7000 ohms/ in. cube and 0.2 in./min. rainfall rate. To measure the resistivity and rate of natural rainfall a gauge has been designed and installed on the roof of the new High Power Laboratory in East Pittsburgh, Fig. 1. This gauge is designed to record rainfall resistivity and rate continuously throughout a rainfall period. This offers considerable advantage in the amount of information gained over the conventional cup method of sample collecting, which gives only the average values for the period involved.

RAINFALL GAUGE

The standard laboratory method of measuring rainfall rate using a cup and stop watch gives average rate over the interval of time measured. It was thought that more information would be gained if a gauge were used that would measure instantaneous rates. To achieve this result a gauge was designed to record instantaneous rainfall resistivities and rates.

The gauge consists of two collection trays, one of four square feet and one of one square foot surface area which drain the rain water into an open ended U-tube. The two trays are connected in series with an electrically operated valve for diverting the flow from the larger tray during periods of heavy rainfall. The U-tube has three holes drilled at different heights as shown in Fig. 2. The holes act as metering orifices whose discharge rates are proportional to the height of the water in the tube. The height of the water is measured electrically by probes in the tube wall as shown in Fig. 3. As the water rises in the tube the 96 ohm resistor sections are shunted which changes the current through the meter element of a series connected a-c recording voltmeter. The recording instrument will indicate a step change at the time the probe is shunted, consequently it is not necessary to use a precision recording instrument. The change in water resistivity has no influence on the gauge calibration, since such a change simply changes the height of the recorded steps. To provide sufficient sensitivity for very low rates of rainfall and still have sufficient capacity for the highest rates encountered, it was necessary to use an electrically operated valve, V Fig. 3, that diverts four-fifths of the rainfall, when energized through relay SG_2 which operates when the water reaches the top probe in the U-tube. The scale change valve could be eliminated if sufficient space were available to permit the use of a U-tube of greater length.

To calibrate the gauge, water is admitted to the collecting trays and adjusted to a steady rate at one of the probe positions. The recording meter reading is noted and the discharge from the U-tube is collected and weighed for a measured time

interval. From the known surface area of the trays, the rate in inches per minute can be calculated. The procedure is repeated for different rates until calibration for each probe position is obtained.

The rainfall resistivity is measured by using a glass funnel fitted with platinum electrodes as shown in Fig. 4. It was found necessary to enclose the resistivity gauge in a dust tight box to prevent contamination. A rain sensing detector such as used to raise unattended convertible automobile tops has been included as shown in Fig. 3. The detector requires 6 V. d.c. for operation which is supplied by T_1, through a small full wave rectifier. A single raindrop on the detector will energize R_1, and SG_1, which will open the lid of the box and start the recording instruments. After the rain has stopped, a small heating element under the detector quickly drys the detector, causing the lid to close and the recording instruments to stop. To further insure freedom from contamination, each day the guages are cleaned with distilled water and blown dry.

RESULTS

The results of 34 rains during the period, May to November 1961 are summarized in Table 1. Although a number of the rains appeared to be very heavy, the highest rate recorded was 0.070 in./min., about 1/3 of the rate used in standard tests. The lowest resistivity recorded was 1500 ohms/in. cube and the highest resistivity was 40,000 ohms/in. cube. In all cases the initial rainfall had a low resistivity which increased to a very high value if the rain was prolonged. It was first thought that the gauge was being contaminated between rains, however, a program of daily maintenance insured that this was not the case. It became apparent that the initial rain contained considerable contamination that was gradually removed as the rain progressed.

It is planned to move the rain gauge to the Trafford High Voltage Laboratory in the spring of 1962 in order to obtain data in a second location. It is hoped that other investigators will make similar measurements throughout the country to provide additional data for a realistic evaluation of our present standard rainfall rate and resistivity.

SUMMARY

Initial rainfall resistivity was measured as low as 1500 ohms/in. cube. The highest rainfall rate measured was 0.07 in./min. The resistivity at the beginning of rainfall was in all cases the lowest value observed. The low initial resistivity usually prevailed only a few minutes and then increased gradually to as high as 40,000 ohms/in. cube. The rate of increase in resistivity can be roughly correlated to the rate and duration of rainfall during the period. It is believed that the raindrops are initially formed about conducting dust particles as nuclei and as the rain progresses the dust is gradually washed from the atmosphere. This would explain the initial low value of resistivity with improvement as the rain progresses. Based on the results from this station which is located in a heavy industrial area, it is believed that for such locations wet tests made with 7000 ohm water are highly optimistic, whereas the 0.2 in./min. rate is quite pessimistic. This also emphasizes that insulation designed to meet standard conditions may be quite adequate for most locations but may be deficient when located in areas of heavy air contamination.

REFERENCES

1. The Influence of Water Resistivity and Precipitation Rate Upon Sixty-Cycle Wet Flashover Voltage

AIEE Committee Report

AIEE Vol. 77 pt. I 1958 P. 350-7

2. Rainfall Resistivity and 60 Cycle Wet Flashover Of Suspension Insulators

R. I. Mather and M. G. Poland

AIEE Vol. 79 pt. III 1960 P. 900-904

Table I. Rainfall Rates and Resistivities Measured at East Pittsburgh, Pa. during the period May-November 1961.

Date	Min. Resistivity ohms/in. cube	Max. Resistivity* ohms/in. cube	Max. Rate in./min.
5-5-61	2,100	7,200+	-
5-8-61	3,400	7,200+	-
5-9-61	1,500	7,200+	-
5-15-61	3,400	7,200+	0.046
5-16-61	2,900	7,200+	0.070
5-25-61	3,800	7,200+	0.007
5-26-61	7,200+	7,200+	0.007
5-29-61	3,400	7,200+	0.057
6-6-61	7,200+	7,200+	0.007
6-8-61	6,400	7,200+	0.046
6-9-61	3,800	7,200+	0.008
6-14-61 (11:00)	7,200+	7,200+	0.015
6-14-61 (2:00)	7,200+	7,200+	0.005
6-14-61 (3:00)	7,200+	7,200+	0.012
6-21-61	30,000	30,000	0.052
6-23-61	3,600	20,000	0.029
7-13-61	2,800	15,000	0.029
7-17/61	9,000	13,000	0.002
7-19-61	6,500	9,000	0.029
7-21-61	2,500	7,500	0.015
7-24-61	6,000	17,500	0.015
7-28-61	3,200	7,500	0.009
7-31-61	3,500	3,500	0.011
8-2-61	4,500	13,000	0.050
8-4-61	3,500	4,500	0.015
8-11-61	4,500	11,000	0.002
9-1-61	4,000	14,000	0.052
9-14-61	5,000	22,000	0.030
9-20-61	4,800	22,000	0.014
10-2-61	3,300	40,000	0.002
10-13-61	3,700	40,000	0.004
10-27-61	5,000	6,200	0.004
11-3-61	4,000	13,500	-
11-6-61	2,100	17,500	0.005

*7200 ohms maximum that could be read until meter was changed to read maximum of 50,000 ohms on June 21st.

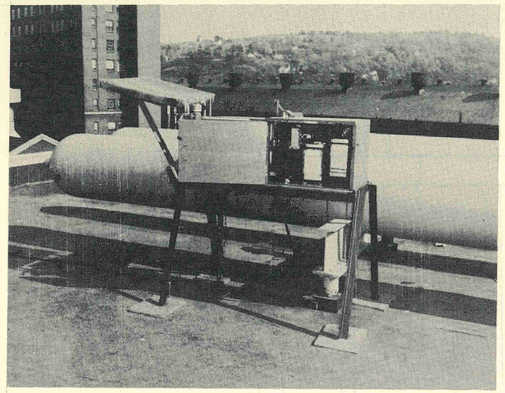

Fig. 1. Rainfall gauge located on roof of the new High Power Laboratory at East Pittsburgh, Pa.

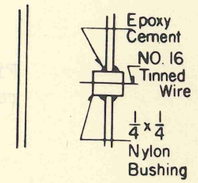

PROBE DETAIL

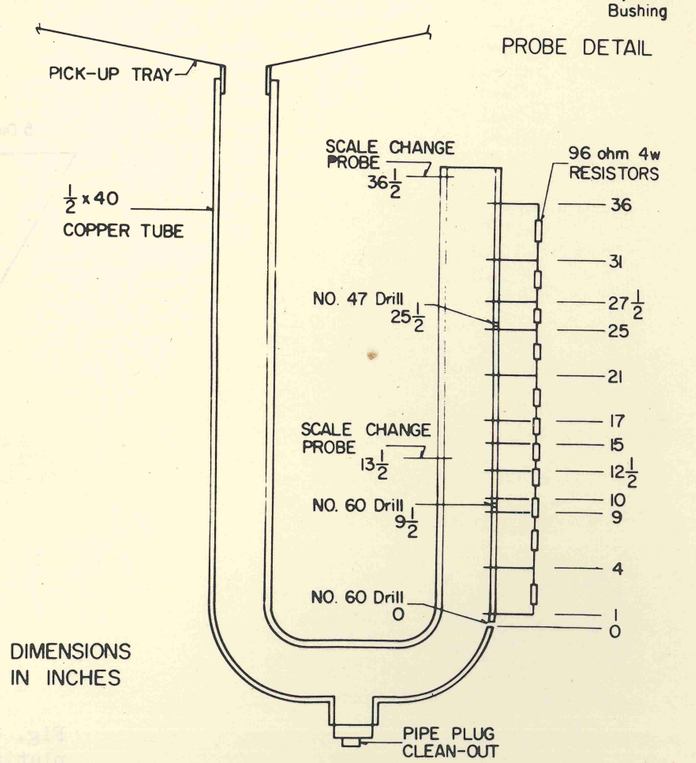

Fig. 2. U-tube rainfall rate gauge

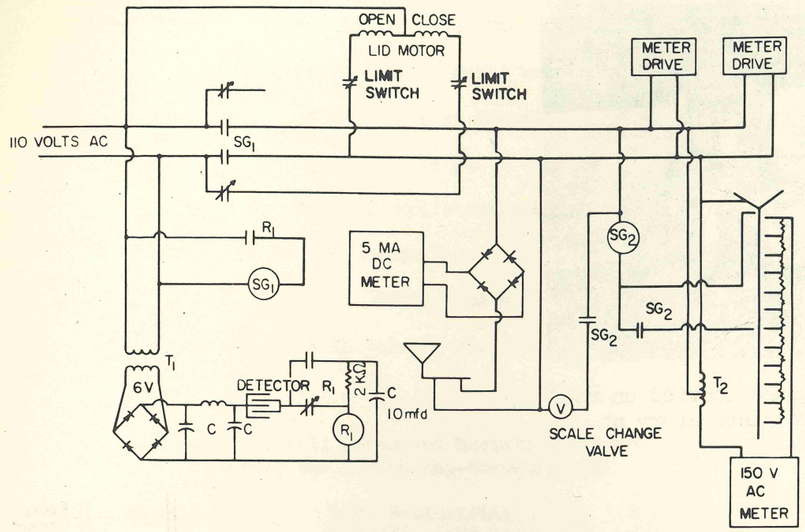

Fig. 3, Schematic wiring diagram for rainfall rate and resistivity gauges

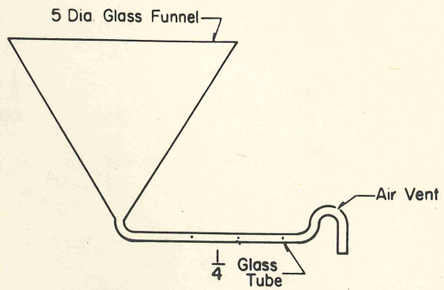

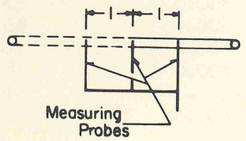

Fig. 4. Resistivity gauge with platinum electrodes

CONTROL CARD:

No. of cond.'s	Earth Resistance ohms/m.^{3}	Frequency c.p.s.	Carson's Correction KLASS	Output Z & P PRINT	Calculate Z or P TYPE	Output Y & S RECIP	Miscell. KODE	Date Yr.	Mo.	Day
2	5	12	19	25	31	37	43	48		

DATA CARDS:

Conductor Resistance ohms/mile	Reactance to 1' spacing ohms/mile	$\log_{10}$ d = O.D. nom. feet	Height at tower feet	Horizontal Coordinate feet	Midspan Height feet	Bundle with #	G.W. Code	
1	9	17	27	35	43	51	55	58

Fig. 6. Sheet for Listing Input Data

Conference Paper

ELECTROMAGNETIC AND ELECTROSTATIC TRANSMISSION LINE PARAMETERS BY DIGITAL COMPUTER

M. H. Hesse
Member AIEE
Electric Utility Analytical Engineering
General Electric Company
Schenectady, N.Y.

A paper recommended by the AIEE Transmission and Distribution Committee for presentation at the AIEE Fall General Meeting, Chicago, Ill., October 7-12, 1962. Manuscript submitted June 7, 1962; made available for printing August 31, 1962.

Price: $ .60 To Members
$1.00 To Nonmembers

(10¢ per copy additional if first class mailing desired)

(Minimum Mail Order $1.00)

All Rights Reserved by the
American Institute of Electrical Engineers
345 East 47th Street,
New York 17, N. Y.

Litho in USA

Paper No. CP
62-1387

ELECTROMAGNETIC AND ELECTROSTATIC TRANSMISSION LINE PARAMETERS BY DIGITAL COMPUTER

M. Harry Hesse

SUMMARY. This paper describes a versatile digital computer program for calculating electromagnetic and electrostatic parameters for an untransposed section of overhead line. Applications to current distribution, electromagnetic and electrostatic unbalance, voltage gradients on conductor surfaces, and other problems are discussed. A technique for establishing upper and lower bounds for Carson's earth-return correction and a modified symmetrical component transformation are introduced as new concepts. The flexibility of the proposed computer program offers a means for solving a large variety of related electromagnetic problems.

INTRODUCTION

Of increasing significance in the design of modern EHV systems using series capacitors and bundle conductors is the question of the possible adverse effects of electromagnetic and electrostatic unbalance of untransposed line sections. The results of previous work[5-10] indicate that a greater accuracy is required in the analysis, particularly for EHV systems where line sections of a hundred or more miles in length are common and where the use of bundle conductors makes it desirable to avoid transpositions except at existing intermediate stations. Furthermore, adjacent rights-of-ways are becoming increasingly loaded with larger numbers of conductors. As a result, the calculation of line parameters becomes a laborious and time-consuming problem. To facilitate the determination of these parameters, a large-scale high speed digital computer program is desirable.

During the initial formulation of the proposed computer program, consideration was given to the many problem areas which are closely related to the determination of transmission line constants. Among these were included such problems as current distribution among conductors, subconductors, and neutral returns; charge distribution among the conductors and ground wires; voltage gradients on the surfaces of conductors and ground wires; reduction of a large multi-circuit configuration to a single- or reduced multi-circuit configuration; neutral current return in lead sheaths and in adjacent conducting surfaces by conductor simulation techniques; zero sequence impedance of aircraft feeder cables adjacent to conducting surfaces.

As a consequence, the proposed digital computer program combines high speed of calculation with considerable versatility. The basic concept of matrix analysis underlies the entire program. The complete impedance and potential coefficient matrices, as well as their inverses (admittance and capacitance coefficient) for an untransposed section containing up to 110 conductors are calculated and printed. The calculations are performed in three stages. In the first stage, every conductor, sub-conductor, and ground wire retain their identities. The corresponding admittance matrix, for example, allows for the determination of current distribution among each conductor. In the second stage, sub-conductors are combined and ground wires are eliminated mathematically to obtain a single equivalent conductor per phase per circuit. By proper coding, for example, several parallel circuits may be reduced to a single equivalent circuit also. In the first two stages, the problem need not be restricted to a three-phase system. In the third stage, the symmetrical component parameter matrices are calculated. Here, for example, the availability of all mutual elements in the output matrix allows the determination of negative and zero sequence currents flowing due to non-transposition of the line section.

The direct matrix inversion technique used in this program is the same as that described in references 11 and 12. Considerable computer time is saved by using this method and by taking advantage of the matrix symmetry which exists in the first two stages of the calculation. Since the conventional symmetrical component parameter matrices are not generally symmetrical, a modified transformation is introduced which attains the

desired matrix symmetry while maintaining the identities of the conventional symmetrical component elements. Consequently, only triangular matrix outputs are necessary.

The corrections applied to the impedances to reflect the influence of earth-return are generally limited to considering the first term in Carson's infinite series.[3] It is often desirable to determine the error involved by neglecting the remaining terms in the series. A convergent alternating series is introduced from which an evaluation of the first term leads to one bound, and evaluation of the first two terms leads to the other bound, and where the answer obtained by evaluating the entire infinite series lies between these two bounds. A code input calling for the first order correction leads to the correction most generally used in calculations. A code input calling for a zero order correction causes no correction to be applied as this may be desirable in other areas as, for example, aircraft power system analyses.

And finally, provision has been made to insert external series impedance into the line representing loads, transformers, generators, series capacitors, etc., after the final stage of the symmetrical component impedance calculation. The program will invert the modified impedance matrix from which a more realistic value of electromagnetic unbalance can be obtained.

The calculations have been programmed and tested for a 32,000 word IBM digital computer (FORTRAN II) with punched card input and tape output. Only a few minutes of computer running time are required to obtain all twelve outputs for an average multi-circuit configuration.

ANALYSIS

Since the process of computing capacitance coefficients is analagous to that for computing impedances, only the latter will be outlined. The voltage equations for a system of conductors is conveneintly expressed in matrix notation $e = Z \cdot i$ whereby Z represents an impedance matrix. The impedance matrix for a physical system is square with a row and column for each conductor and it is symmetrical about the main diagonal. Therefore, only a lower or upper triangle, including the main diagonal need be computed. The conventional symmetrical component impedance matrix is not, however, symmetrical about the main diagonal. A related symmetrical matrix can be formed by means of an artifice as will be shown later.

The physical location of each conductor above ground (and its image below ground) is described by x and y coordinates, the former being the horizontal distance in feet from an arbitrary vertical reference line, the latter being the conductor height above ground in feet. The effective conductor height is computed by the program as the height at the tower minus one-third of the sag. The off-diagonal terms of the Z-matrix are logarithms of the distances between conductors, the main-diagonal terms being the self-impedances of the conductors as obtained from the input cards. This is illustrated in Fig. 1. In the computer memory, the upper triangle of the matrix area is reserved for the Z-matrix, the lower triangle for the P-matrix. Thereby, logarithmic terms which are common to Z and P (including earth-return corrections) can be stored simultaneously and need be computed only once. The main diagonal terms for P and Z are stored in separate columns until needed in the triangular matrix.

According to coded input, three choices for earth-return corrections are possible (see Appendix I). This correction is then applied to the previous Z-matrix and the resultant matrix may be printed out. This may be followed by a matrix inversion (according to Appendix III) which may also be printed out without disturbing the original Z-matrix. In the second stage, bundle-conductors are combined into a single equivalent phase conductor as shown in Appendix II. Also, the rows and columns corresponding to ground and neutral wires are eliminated. This results in a Z-matrix for an equivalent

conductor configuration containing only one conductor per phase for each circuit which may be printed out. This may be followed by a matrix inversion, without disturbing the original matrix. The first two stages are not limited to three-phase systems. Provided that consecutive phase sequence of phase conductor input is observed, any single- or multi-phase system Z-matrix can be computed. Furthermore, there are no system frequency limitations except those imposed by the restrictions on Carson's correction terms and the validity of the assumed voltage equations. Particularly where there is no earth-return, this program will be satisfactory for aircraft power system frequencies, ground power supply frequencies, etc.

In the third stage, the Z-matrix for the physical equivalent configuration is transformed into symmetrical components. In terms of matrix notation explained in Appendix II, $Z_c = S\ Z_e S^{-1}$ represents the conventional spinor transformation and Z_c is no longer symmetrical. This leads to the problem of non-reciprocal mutual impedances in symmetrical component networks representing untransposed and unsymmetrical transmission line systems. This problem can be overcome in two ways:

1. Choose a different set of coordinates, i.e., a different transformation.
2. Force symmetry by means of an artifice.

The first approach, that of defining a new transformation for each configuration, is physically and mathematically the most elegant. For example, a determination of the eigenvalues and eigenvectors for the general Z_e-matrix will establish the characteristic coordinates and the natural modes of operation for the system of conductors. Stated simply, the resultant component Z-matrix has only diagonal terms and no reciprocal mutual impedance problems exist. There is no coupling between the component networks and model network techniques are practical. Except for special studies,[4] this approach would result in new terminology and in serious data correlation problems.

The second approach, as used here and discussed in Appendix III, has the advantage of maintaining the well-known symmetrical component terminology. Although the resultant symmetrical matrix is used to advantage in the present computer program, mutual resistance and negative resistance terms which appear in the matrix do not lend themselves to model techniques except in special cases where these terms may be small enough to be neglected entirely.

In the third stage, therefore, we perform $Z_s = S\ Z_e S/3$ and we may print out the lower triangle of the resultant Z_s-matrix. If the rows and columns of the output are properly labeled, the conventional symmetrical component impedances may be found directly. The conventional form Z_c may also be readily formed by completing the upper triangle of Z_s, cutting out and interchanging <u>columns</u> 2 and 3, 5 and 6, 8 and 9, etc. The inversion of Z_s may also be performed and printed out, whereby <u>rows</u> 2 and 3, etc. of the output must be interchanged to conform to the conventional Y_c format.

Where both EM and ES parameters are required, the potential coefficients are calculated first. Since no resistive elements are involved in the first two stages of the ES calculation, the matrix inversion is performed in the real field thus maintaining the original matrix in the imaginary field. In the third, or symmetrical component stage, both real and imaginary terms exist. After the original ES matrix is printed out, the inversion may take place and will destroy the original matrix.

In the EM calculations, the ES triangular field is no longer required and is available for intermediate storage of the original EM matrix while the inversion is being performed. Therefore, at the end of the calculations of all twelve outputs, the original EM symmetrical component matrix is still available. External impedances may be added

to this matrix and by inverting, the electromagnetic unbalance currents may be determined under more realistic conditions. The requirement of matrix symmetry restricts all external impedances to satisfying $Z_1 = Z_2$. In order to properly include generator impedances where $Z_1 \neq Z_2$, an external program for inverting unsymmetrical matrices must be employed.

<u>Input</u>

The first input card must contain an integer $1 \leq N \leq 999$ punched in columns 1 to 3. The succeeding N cards may contain any desired alpha-numeric headings or comments punched in columns 2-72. The versatility of this feature is evident from the sample output shown in Fig. 3.

The commentary deck is followed by any number of data input decks, one for each case. The first card in each data deck must contain the following information:

<u>Col.</u>	<u>Type</u>	<u>Data</u>
2-4	Integer	Total number of conductors involved
5-11	Floating pt.	Earth resistivity (ohms/m^3)
12-18	Floating pt.	System frequency (cps)
19-24	Integer	Earth return correction (see Appendix I) 0 = No earth 1 = First order correction (conventional) 2 = Second order correction
25-30	Floating pt.	Outputs desired for Z and P 0.= None 1.= Original configuration 2.= Equivalent configuration 3.= Both 1. and 2. 4.= Symmetrical components 5.= Both 1. and 4. 6.= Both 2. and 4. 7.= All 1. and 2. and 4.
31-36	Floating pt.	Type of calculation 1.= Electrostatic (P or P^{-1}) 2.= Impedance (Z or Z^{-1}) 3.= Both 1. and 2.
37-42	Floating pt.	Outputs desired for Z^{-1} and P^{-1} (analogous to Col. 25-30)
43-47	Integer	Provision for supplementary functions which may be desired. 0 = No changes in symmetrical component matrix 2 = Change in symmetrical component matrix
49-54	Integer	Date. This number serves the purpose of a consecutive run numbering device.

After the control card in each deck, there follows a data card for each conductor. These cards must be arranged in a specific sequence since the output reflects this arrangement. The first three cards shall represent a single conductor per phase of the first circuit arranged in phase sequence a, b, and c. The next three cards shall similarly represent the second circuit, etc. Following this there shall be a card for each sub-conductor arranged in any phase sequence (where this sequence will be maintained for the original configuration output). Finally, there shall be a card for each ground wire. Each of the above cards must contain the following information.

Col.	Type	Data
2-8	Floating pt.	Conductor resistance (ohms/mile)
9-16	Floating pt.	Conductor reactance at one foot spacing (ohms/mile)
17-26	Floating pt.	$\log_{10}$d, d = nominal cond. diam. in feet
27-34	Floating pt.	Height above ground at tower, feet.
35-42	Floating pt.	Horiz. dist. from arbitrary reference, feet
43-50	Floating pt.	Height above ground at midspan, feet
51-54	Floating pt.	0. = for main conductors For sub-conductors, enter the main conductor number with which the sub-conductor is to be bundled.
55-57	Floating pt.	0. = for all main and sub-conductors 1. = for ground wires

Fig. 6 shows a sample sheet for listing input data and Fig. 2 illustrates the card arrangement.

In general, the rows and columns of the output matrix will proceed in the sequence dictated by the input. The knowledge of this fact is important when the output reflects every conductor in the original configuration. The insistence upon phase sequencing a, b, and c for the main conductors is required for the symmetrical component transformation.

If the code in columns 43-47 of the first card in a data deck is 2, i.e., if changes are to be made in the symmetrical component matrix, additional data are required. These should be supplied as follows:

Col.	Format	Data
1-8	F8.4	Change in series resistance (ohms/mile)
9-16	F8.4	Change in series reactance (ohms/mile)
17-26	F10.6	New value to replace the code in columns 43-47 of the first card in this data deck 0 = no further changes to be made 2 = data for another change follow that for this change
51-54	F4.0	The number of the circuit in which the change is to be made
55-57	F3.0	Place of change 0. = change in zero sequence 1. = change in positive or negative sequence

Thus one card of data will be required for each of the two possible changes per circuit. (The maximum number of circuits possible is 36.) The end of a set of changes is indicated when the number of the circuit in which the change is to be made is equal to zero. If no further changes in the symmetrical component matrix are to be made for a particular case, a blank card will signify both the end of a set of changes and the end of the case. If, however, additional sets of changes are to be made for the same case, a card with a code of 2 in columns 17-26 should be used in place of the completely blank card at the end of each set of changes, except, of course, the last one.

Following the last data input deck there must appear a blank card which signals the end of the run. This means that if the last deck of data contained any symmetrical component matrix changes, there must be two blank cards at the end of the data decks. If the last case contained no symmetrical component matrix changes, one blank card is sufficient.

Output

The printed output is in the form of a lower triangular matrix where the upper triangular matrix can be found by symmetry about the main diagonal. Because of space limitations, a width of nine columns is printed at one time. For large systems, the triangle can be formed by cutting and properly placing succeeding sections of the output adjacent to the first and largest section. For the output relating to the original configuration, the phase sequence of rows and columns corresponds to the input data sequence. For the output related to the equivalent configuration, row and column phase sequence proceeds from top to bottom and from left to right, respectively, according to a, b, c, and circuits I, II, etc.

The symmetrical component output is also in the form of a triangular matrix obtained by the artifice discussed in Appendix II. For the symmetrical component impedance and capacitive reactance output, the rows proceed from top to bottom in sequence 0, 1, 2, 0, 1, 2, etc., in ascending order of circuit number. The columns proceed in sequence 0, 2, 1, 0, 2, 1, etc. For the symmetrical component admittance and susceptance output, the rows proceed in sequence 0, 2, 1, 0, 2, 1, etc., and the columns proceed according to sequence 0, 1, 2, 0, 1, 2, etc.

APPLICATIONS

This program computes accurately and efficiently the overhead line parameters required in load flow studies, stability analyses, protection coordination, transient analyzer studies, etc. The flexibility of the program becomes apparent when we consider some of the possible applications.

1. Accurate and reliable determination of impedance and capacitive reactance for load flow, short circuit, stability, relaying and other system studies. Maintained outputs for an entire system serve as a uniform reference source and can easily be justified economically.

2. The inductances and capacitances are easily evaluated by removing the factor $2\pi f$ from the reactance computations. Thus, transient analyzer and traveling wave and radio noise propagation studies can be performed with improved input data including earth-return effects.

3. Although voltages and currents are not included in the computation, they may easily be constructed for the implied matrix equations e = Z i and i = Y e. From the latter the current distribution in conductors, sub-conductors, ground wires, etc., may be obtained if Y represents the admittance matrix for the original configuration. If Y represents the symmetrical component admittance matrix, the unbalanced currents flowing due to untransposed lines may be calculated.[5-10]

4. Related to the current distribution problem, because of the 110 conductors which are available, many basic physical studies can be analyzed in an approximate manner. For example, in the determination of zero sequence impedances of three-phase feeder cables adjacent to metal plates or aluminum skins, the metal plates can be simulated by a large number of individual conductors. This can be very useful in zero sequence impedance calculations of aircraft power system feeder cables.

5. In a similar manner, the current distribution between earth-return and lead sheaths in overhead aerial cable can be determined by simulating the sheath with a large number of individual conductors. Neutral current return in messenger cables neutral returns, etc., can also be determined. If the demand for this type of calculation is sufficiently great, the program itself can be modified to expedite shielded cable calculations.

6. From the susceptance matrix and the voltage matrix, we can calculate the capacitive current flow. By factoring out $2\pi f$ we can determine the charge residing on each conductor. Dividing this charge by the diameter of the conductor and multiplying by a constant we have the average field gradient on each conductor and ground wire in KV/cm. The determination of voltage gradients at the surface of phase conductors, ground wires, etc., is of importance in corona and radio noise studies, especially in EHV systems.

7. In many types of studies, it is necessary to take cognizance of adjacent parallel circuits although it is not always necessary to maintain their identities. Because of this program's capability for handling up to 110 conductors, the "bundling" technique can be employed to accurately reduce a large multi-circuit configuration to an equivalent smaller configuration. This may be particularly important where other digital computer programs such as load flow or short circuit programs are restrictive in this sense.

8. Outside the realm of the computer program's initial capabilities, it is sufficiently flexible to allow for modification or extension in several areas. For example, a subroutine has been included by which a series balanced impedance (such as loads, transformers, etc.) may be added to the line impedance. In this manner, a more realistic electromagnetic unbalanced current can be determined. This subroutine can be requested by KODE=2 on the input data sheet. In addition, instead of a symmetrical component transformation, an α, β, 0 or an eigenvalue analysis could be included. The latter leads to principal, normal, or modal components which have already become basic to radio noise and traveling wave propagation problems.

CONCLUSION

A high speed digital computer program for accurately determining overhead transmission line parameters for an untransposed section of line has been developed. Twelve triangular matrix outputs including impedance, potential coefficient, admittance, and capacitive reactance for the original physical configuration, an equivalent configuration, and in terms of symmetrical components can be obtained in less than 30 minutes of computer running time for an average system of 50 varied configurations. The parameter matrices are calculated and printed out completely including every mutual element both in physical and symmetrical component quantities. Applications of this program to the determination of electromagnetic and electrostatic unbalance, current distribution, charge distribution, conductor surface voltage gradient, etc., are described.

The capability of the computer program to handle up to 110 conductors makes it suitable for related electromagnetic calculations such as current distribution in conducting surfaces adjacent to feeders, zero sequence impedance calculation of aircraft feeder cables, neutral current return in lead sheaths, etc. Additional series impedances such as series capacitors, transformer reactances, load impedances, etc. can be included to obtain a more realistic calculation of the electromagnetic unbalance currents which are caused to flow when lines are not transposed. A simple means for determining the upper and lower bounds of the influence of earth return on the zero sequence impedance of a line and a modified symmetrical component transformation which maintains matrix symmetry are also introduced.

NOMENCLATURE

$Z_{ii} = R_{ii} + \Delta r_{ii} + j(X_{ii} + \Delta X_{ii})$

$Z_{ik} = \Delta r_{ik} + j(\Delta X_{ik} - X_{ik})$

$P_{ii} = j\, p_{ii}$

$P_{ik} = j\, p_{ik}$

R_{ii} = resistance of conductor i, ohms per mile

$X_{ii} = 0.27942\ (f/60)\ \log_{10} 1/GMR_i$ = inductive reactance of conductor i at 1 foot spacing, ohms per mile.

GMR_i = geometric mean radius of conductor i, feet.

$X_{ik} = 0.27942\ (f/60)\ \log_{10} D_{ik}$ = inductive reactance between conductors i and k, ohms per mile.

$D_{ik} = \sqrt{(x_i - x_k)^2 + (y_i - y_k)^2}$ = center to center distance between conductors i and k, feet.

x_i, y_i = coordinates of conductor i, feet.

f = system frequency, cycles per second.

$p_{ii} = (4.099)(10^6)(60/f)\ \log_{10} 4(y_i/d_i)$ = capacitive reactance of conductor i to ground, ohm miles.

d_i = nominal diameter of conductor i, feet.

$p_{ik} = (4.099)(10^6)(60/f)\ \log_{10} D'_{ik}/D_{ik}$ = capacitive reactance between conductors i and k, ohm miles.

$D'_{ik} = \sqrt{(x_i - x'_k)^2 + (y_i - y'_k)^2} = \sqrt{(x'_i - x_k)^2 + (y'_i - y_k)^2}$

= center to center distance between conductors i and k' (or i' and k), feet.

x'_i, y'_i = coordinates of the image of conductor i, feet.

$\Delta r_{ii}, \Delta r_{ik}, \Delta X_{ii}, \Delta X_{ik}$ = Carson's earth-return corrections (see Appendix I).

ρ = earth resistivity, ohm-meters (i.e., ohms of a one-meter cube).

APPENDIX I

Carson's Earth Return Corrections

$$\Delta r_{ii} = 0.09530327\ (f/60) \;-\; 0.09798\ (f/60)(y_i/10^3)\sqrt{f/\rho}$$
$$+\ 0.1024284\ (f/60)(y_i/10^3)^2(f/\rho)\ \log_{10}(2291\sqrt{\rho/f}\ /y_i) \;+\; \cdots\cdots\cdots\cdots$$

$$\Delta r_{ik} = 0.09530327\ (f/60) \;-\; 0.09798\ (f/60)\sqrt{f/\rho}\ (y_i+y_k)/2000$$
$$+\ 0.1024284\ (f/60)(f/\rho)(y_i+y_k)^2/2000^2\ \log_{10}(4582\ \cos\theta_{ik})\sqrt{\rho/f}\ /(y_i+y_k) \;-\; \cdots\cdots$$

$$\Delta X_{ii} = 0.27942\ (f/60)\ \log_{10}\ 2162.5361\sqrt{\rho/f} \;+\; 0.09798\ (f/60)(y_i/10^3)\sqrt{f/\rho}$$
$$-\ 0.03495\ (f/60)(y_i/10^3)^2(f/\rho) \;+\; \cdots\cdots\cdots\cdots\cdots\cdots\cdots\cdots\cdots\cdots$$

$$\Delta X_{ik} = 0.27942\ (f/60)\ \log_{10} 2161.5361\sqrt{\rho/f} \;+\; 0.09798\ (f/60)(y_i+y_k)\sqrt{f/\rho}\ /2000$$
$$-\ 0.03495\ (f/60)(f/\rho)(y_i+y_k)^2 \;+\; \cdots\cdots\cdots\cdots\cdots\cdots\cdots\cdots\cdots\cdots$$

$$\cos\theta_{ik} = (y_i+y_k)D'_{ik}$$

Carson's solution for the earth-return problem resulted in an infinite series of Bessel functions.[2] An equivalent, but less formidable, infinite series is given in reference 3 from which the above terms have been extracted. The IBM-704 computer program under discussion allows for three possible alternatives:

1. No correction (for no earth-return).
2. First order correction wherein only the first term of each series is employed.
3. Second order correction wherein the first two terms in each series are employed.

The first order correction neglects the effects of conductor height above ground, is the one most commonly used, and is generally satisfactory for single tower configurations. The second order correction allows for conductor height above ground and distance between adjacent circuits and may be significant where circuits are located on adjacent towers or rights-of-way. Within the limitations expressed in reference 3, the infinite series represented by the above terms is a convergent series. It follows, therefore, that the first order correction is too large for Δr_{ii}, Δr_{ik}, and too small for ΔX_{ii}, ΔX_{ik}. The second order correction overcompensates this condition. The true correction lies between these two bounds thus establishing a means for gauging the error involved.

APPENDIX II

Voltage Equations

$$\begin{bmatrix} e_1 \\ e_2 \\ e_3 \\ e_4 \end{bmatrix} = \begin{bmatrix} Z_{11} & Z_{12} & Z_{13} & Z_{14} \\ Z_{21} & Z_{22} & Z_{23} & Z_{24} \\ Z_{31} & Z_{32} & Z_{33} & Z_{34} \\ Z_{41} & Z_{42} & Z_{43} & Z_{44} \end{bmatrix} \begin{bmatrix} i_1 \\ i_2 \\ i_3 \\ i_4 \end{bmatrix} \quad \text{(II-1)}; \qquad \begin{bmatrix} v_1 \\ v_2 \\ v_3 \\ v_4 \end{bmatrix} = \begin{bmatrix} P_{11} & P_{12} & P_{13} & P_{14} \\ P_{21} & P_{22} & P_{23} & P_{24} \\ P_{31} & P_{32} & P_{33} & P_{34} \\ P_{41} & P_{42} & P_{43} & P_{44} \end{bmatrix} \begin{bmatrix} q_1 \\ q_2 \\ q_3 \\ q_4 \end{bmatrix} \quad \text{(II-2)}$$

Bundling

Assume that conductor #4 is in parallel with conductor #1; i.e., $e_4 = e_1$, $v_4 = v_1$. This might be the case where conductor #4 is a sub-conductor of conductor #1 in a bundle, or conductor #4 may be a conductor of another circuit which is electrically in parallel with #1. We perform the bundling mathematically by subtracting the first rows of the Z and P matrices from the fourth rows of the Z and P matrices, respectively. This results in a Z matrix, for example, as follows:

$$\begin{bmatrix} e_1 \\ e_2 \\ e_3 \\ 0 \end{bmatrix} = \begin{bmatrix} Z_{11} & Z_{12} & Z_{13} & Z_{14} \\ Z_{21} & Z_{22} & Z_{23} & Z_{24} \\ Z_{31} & Z_{32} & Z_{33} & Z_{34} \\ (Z_{41}-Z_{11}) & (Z_{42}-Z_{12}) & (Z_{43}-Z_{13}) & (Z_{44}-Z_{14}) \end{bmatrix} \begin{bmatrix} i_1 \\ i_2 \\ i_3 \\ i_4 \end{bmatrix} \quad \text{(II-3)}$$

and by subtracting e_1 from e_4 the equivalency of the system of simultaneous equations is maintained. In order to restore symmetry to the Z matrix, a related operation is performed on the columns of the Z matrix and on the 'i' matrix resulting in the following form:

$$\begin{bmatrix} e_1 \\ e_2 \\ e_3 \\ 0 \end{bmatrix} = \begin{bmatrix} Z_{11} & Z_{12} & Z_{13} & (Z_{14}-Z_{11}) \\ Z_{21} & Z_{22} & Z_{23} & (Z_{24}-Z_{21}) \\ Z_{31} & Z_{32} & Z_{33} & (Z_{34}-Z_{31}) \\ (Z_{41}-Z_{11}) & (Z_{42}-Z_{12}) & (Z_{43}-Z_{13}) & (Z_{44}-Z_{14}-Z_{41}+Z_{11}) \end{bmatrix} \begin{bmatrix} i_1+i_4 \\ i_2 \\ i_3 \\ i_4 \end{bmatrix} \quad \text{(II-4)}$$

where again the equivalency of the system of simultaneous equations is maintained. It follows from the definitions given in Appendix I that

$$Z_{ik} = Z_{ki}, \quad P_{ik} = P_{ki} \quad \text{(II-5)}$$

so that it will be recognized that the Z-matrix in Equation (II-4) is also symmetrical about the main diagonal. The resultant equation #4 in (II-4) is of the same form as that for a ground wire with no externally applied emf. It may, therefore, be eliminated by the method shown in the next paragraph.

Ground Wire Removal

If, in matrix equation (II-1), the fourth conductor is assumed to be a ground wire solidly grounded at least at both ends and with no source emf, we may write

$$\begin{bmatrix} e_1 \\ e_2 \\ e_3 \\ 0 \end{bmatrix} = \begin{bmatrix} Z_{11} & Z_{12} & Z_{13} & Z_{1gw} \\ Z_{21} & Z_{22} & Z_{23} & Z_{2gw} \\ Z_{31} & Z_{32} & Z_{33} & Z_{3gw} \\ Z_{gw1} & Z_{gw2} & Z_{gw3} & Z_{gw-gw} \end{bmatrix} \begin{bmatrix} i_1 \\ i_2 \\ i_3 \\ i_{gw} \end{bmatrix} \quad \text{(II-6)}$$

From the fourth equation in (II-6) we may solve for i_{gw}:

$$i_{gw} = -\ (Z_{gw-gw})^{-1}\ (Z_{gw1}\ i_1 + Z_{gw2}\ i_2 + Z_{gw3}\ i_3) \quad \text{(II-7)}$$

If this is substituted in the first three equations, a reduced system is obtained as follows:

$$\begin{bmatrix} e_1 \\ e_2 \\ e_3 \end{bmatrix} = \begin{bmatrix} Z'_{11} & Z'_{12} & Z'_{13} \\ Z'_{21} & Z'_{22} & Z'_{23} \\ Z'_{31} & Z'_{32} & Z'_{33} \end{bmatrix} \begin{bmatrix} i_1 \\ i_2 \\ i_3 \end{bmatrix} \qquad \text{(II-8)}$$

where $Z'_{ik} = Z_{ik} - Z_{igw} \; (Z_{gw\text{-}gw})^{-1} \; Z_{gwk}$.

Where more than one ground wire exists, the original Z matrix may be partitioned and the reduction according to (II-8) would proceed in terms of matrix inversion and multiplication. For purposes of the IBM 704 program discussed in this paper, a single row and column elimination method was found more advantageous. Again, the Z-matrix (and similarly the P-matrix) in (II-8) is symmetrical.

Symmetrical Components

In a three-phase system, bundling and ground wire elimination result in Z and P matrices 3C by 3C in size where C is the number of circuits involved. In the simplest case, the equations for a single circuit are

$$\begin{bmatrix} e_a \\ e_b \\ e_c \end{bmatrix} = \begin{bmatrix} Z_{aa} & Z_{ab} & Z_{ac} \\ Z_{ba} & Z_{bb} & Z_{bc} \\ Z_{ca} & Z_{cb} & Z_{cc} \end{bmatrix} \begin{bmatrix} i_a \\ i_b \\ i_c \end{bmatrix} \qquad \text{(II-9)}$$

or, in abbreviated matrix notation,

$$[e_\phi] = [Z_\phi] \; [i_\phi] \qquad \text{(II-10)}$$

We define symmetrical component voltages as

$$\begin{bmatrix} e_0 \\ e_1 \\ e_2 \end{bmatrix} = \frac{1}{3} \begin{bmatrix} 1 & 1 & 1 \\ 1 & a & a^2 \\ 1 & a^2 & a \end{bmatrix} \begin{bmatrix} e_a \\ e_b \\ e_c \end{bmatrix} \qquad \text{(II-11)}$$

where

$$a = -\frac{1}{2} + j \frac{\sqrt{3}}{2} = \varepsilon^{j \frac{2\pi}{3}} \qquad \text{(II-12)}$$

In abbreviated form

$$[e_c] = \frac{1}{3} [S] \; [e_\phi] \qquad \text{(II-13)}$$

Similarly, we define

$$[i_c] = \frac{1}{3} [S] \; [i_\phi] \qquad \text{(II-14)}$$

We transform equation (II-10) conventionally as follows:

$$[e_c] = [S] \; [Z_\phi] \; [S]^{-1} \; \frac{1}{3} \; [S] \; [i_\phi] = [S] \; [Z_\phi] \; [S]^{-1} \; [i_c] = [Z_c] \; [I_c] \qquad \text{(II-15)}$$

where

$$[Z_c] = \begin{bmatrix} Z_{00} & Z_{01} & Z_{02} \\ Z_{10} & Z_{11} & Z_{12} \\ Z_{20} & Z_{21} & Z_{22} \end{bmatrix} \qquad \text{(II-16)}$$

and

$$[S]^{-1} = 1/3 \begin{bmatrix} 1 & 1 & 1 \\ 1 & a^2 & a \\ 1 & a & a^2 \end{bmatrix} \qquad \text{(II-17)}$$

If the expansion of (II-15) is carried out in detail, it will be found that (II-16) is no longer a symmetrical matrix; e.g., $Z_{20} \neq Z_{02}$, etc. This is attributable to the fact that

$$\left\{ [S] \; [Z_\phi] \; [S]^{-1} \right\}' = [S]^{-1} \; [Z_\phi] \; [S] \neq [S] \; [Z_\phi] \; [S]^{-1} \qquad \text{(II-18)}$$

We may overcome this unfortunate relationship by writing instead

$$[Z_c] = 1/3 \; [S] \; [Z_\phi] \; [S] \;\; 1/3 \; [S]^{-1} \; [S]^{-1} = 3 \, [Z_s] \; [S]^{-1} \; [S]^{-1} \qquad \text{(II-19)}$$

where

$$[Z_s] = 1/3 \; [S] \; [Z_\phi] \; [S] \qquad \text{(II-20)}$$

Now

$$\left\{ [S] \; [Z_\phi] \; [S] \right\}' = [S] \; [Z_\phi] \; [S] \qquad \text{(II-21)}$$

so that $[Z_s]$ is a symmetrical matrix. Also,

$$3 \, [S]^{-1} \; [S]^{-1} = \begin{bmatrix} 1 & 0 & 0 \\ 0 & 0 & 1 \\ 0 & 1 & 0 \end{bmatrix} \qquad \text{(II-22)}$$

Expansion of (II-20) will show that

$$\left[Z_s\right] = \begin{bmatrix} Z_{00} & Z_{02} & Z_{01} \\ Z_{10} & Z_{12} & Z_{11} \\ Z_{20} & Z_{22} & Z_{21} \end{bmatrix} \qquad \text{(II-23)}$$

which is symmetrical and postmultiplication of this matrix by (II-22), which is nothing more than an interchange of columns two and three in (II-23), results in the conventional form (II-16) for Z_c. In this paper, the lower triangular matrix of (II-23) is printed out.

If the system under consideration consists of more than one circuit, the transformation in (II-13) must be expanded so that [S] becomes a 3C by 3C matrix whose main diagonal is made up of partitioned matrices [S] as defined in (II-11), and whose off-diagonal partitioned matrices are all zero.

Although the symmetrical component printed output is not in conventional format, it is a simple matter to number the rows 'i' in sequence 0, 1, 2 from top to bottom, and the columns 'k' in sequence 0, 2, 1 from left to right and to use these numbers in determining the desired Z_{ik} or P_{ik} as indicated in (II-23). For systems of more than one circuit, a modified numbering sequence is required to obtain the mutual sequence impedances between sequence networks representing the various circuits. For example, $Z_{i'k}$ might indicate the mutual impedance between 'i' of the second circuit and 'k' of the first circuit.

APPENDIX III

Matrix Inversion

Although there are any number of ways in which a matrix can be inverted, we wish to choose a mechanism whereby:

1. Advantage of matrix symmetry can be utilized;
2. Minimum computer memory storage is required;
3. Computer programming is simple;
4. Computational procedure is reasonably efficient.

The mechanism used in Appendix II for eliminating ground wires is partially a matrix inversion process and can be made to suit the above conditions. We prove this as follows:

Given $[E] = [A][I]$ (III-1)

for which we wish to find $[I] = [A]^{-1}[E]$ (III-2)

Write $[A][I] - [U][E] = [Z]$ and $[U][I] - [Z][E] = [I]$ (III-3)

where $[U]$ is a unit matrix and $[Z]$ is a null matrix.

In complete partitioned matrix format, then:

$$\begin{bmatrix} Z \\ I \end{bmatrix} = \begin{bmatrix} O \\ I \end{bmatrix} = \begin{bmatrix} A & U \\ U & Z \end{bmatrix} \begin{bmatrix} I \\ E \end{bmatrix} \qquad \text{(III-4)}$$

which is of the form (II-6) shown in Appendix II. Therefore, using the same row and column elimination technique as described in Appendix II, we may reduce (III-4) to

$$[I] = [Z] - [U][A]^{-1}[U][E] \quad \text{or} \quad [I] = -[A]^{-1}[E] \qquad \text{(III-5)}$$

whereby the change in sign may be performed after the inversion. Since the coefficient matrix in (III-4) is symmetrical (provided that [A] is symmetrical), then only the lower triangular matrix need be retained. The first column of the triangular matrix which is to be eliminated, is stored temporarily in an adjacent location. The elimination process applies corrections to the remainder of the A-matrix, the first row of the U-matrix, and the first diagonal element of the Z-matrix. As the computation proceeds, the corrected elements are shifted diagonally leftward and upward.

Because of the uniqueness of the U and Z matrices, these are not actually stored in memory, especially since only a single row of the U-matrix and a single element of the Z-matrix are affected at each step.

In this manner, only a single additional temporary storage column for the real and imaginary parts, respectively, are required for the matrix inversion process, and the inverse matrix can be located in the same memory field previously occupied by the supplanted original matrix.

Since the first two stages of the potential coefficient matrix consist of only imaginary values, the remaining matrices being complex in value, a real and a complex number inversion subroutine is programmed. As explained in the paper, by proper scheduling of computation and location of the results of the inversion process, only the memory field of the original matrix is required, thereby maximizing the size of the problem which may be handled by this program. Furthermore, this elimination process is well suited for the inversion of symmetrical matrices since only a triangular portion need be inverted.

REFERENCES

1. Digital Calculation of Overhead Transmission Line Constants, D. Coleman, F. Watts, R. B. Shipley. AIEE Transactions, vol. 78, pt. III, February 1959, pp. 1266-1270.

2. Wave Propagation in Overhead Wires with Ground Return, John R. Carson. Bell System Tech. Journal, vol. 5, 1926, pp. 539-554.

3. Circuit Analysis of A-C Power Systems (book), Edith Clarke. John Wiley & Sons, Inc., New York, N.Y., vol. I, 1948, pp. 372-384.

4. The Present Status of Wire Transmission Theory and Some of Its Outstanding Problems, John R. Carson. Bell System Tech. Journal, vol. 7, 1928, pp. 268-280.

5. Transposition of High-voltage Overhead Lines and Elimination of Electrostatic Unbalance to Ground, Eric T. B. Gross, Andrew H. Weston. AIEE Transactions, vol. 70, pt. II, 1951, pp. 1837-44.

6. Unbalances of Untransposed Overhead Lines, Eric T. B. Gross. Journal, Franklin Institute, Philadelphia, Pa., vol. 254, 1952, pp. 487-97.

7. Electrostatic Unbalance to Ground of Twin Conductor Lines, Eric T. B. Gross, William J. McNutt. AIEE Transactions, vol. 72, pt. III, Dec. 1953, pp. 1288-1297.

8. Electromagnetic Unbalance of Untransposed Transmission Lines, Eric T. B. Gross, M. Harry Hesse. AIEE Transactions, pt. III, vol. 72, Dec. 1953, pp. 1323-1336.

9. Electromagnetic Unbalance of Untransposed Transmission Lines, II. Single Lines with Horizontal Conductor Arrangement, Eric T. B. Gross, S. W. Nelson. AIEE Transactions, pt. III, vol. 74, Oct. 1955, pp. 887-93.

10. Electromagnetic Unbalance of Untransposed Transmission Lines, III. Double Circuit Lines, Eric T. B. Gross, John H. Drinnan, Erich Jochum. AIEE Transactions, pt. III, vol. 78, Dec. 1959, pp. 1362-1371.

11. A New Direct Matrix Inversion Method, R. Bruce Shipley, D. Coleman. AIEE Transactions, pt. I, vol. 78, November 1959, pp. 568-572.

12. Some Improved Methods for Digital Network Analysis, A. Brameller, J. K. Denmead. IEE Proceedings, vol. 108, pt. A, February 1962, pp. 109-116.

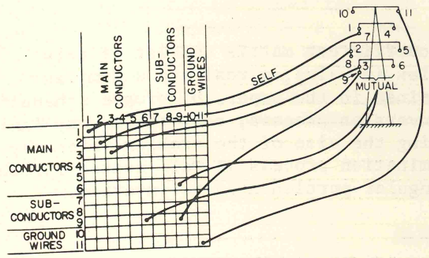

Fig. 1. Relationship Between System Configuration and Parameter Matrix.

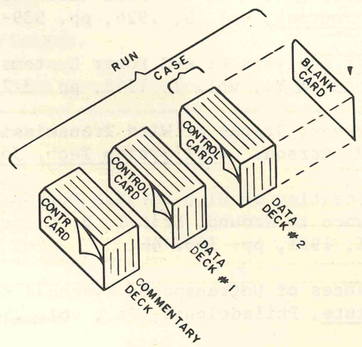

Fig. 2. Arrangement of Data Input Cards

```
                    UNTRANSPOSED TRANSMISSION LINE PARAMETERS

GENERAL ELECTRIC CO.
SCHENECTADY, NEW YORK
APRIL 18, 1962

SAMPLE CALCULATIONS FOR
AIEE ILLUSTRATION PURPOSES

                    (13)          I        (14)
                     X            I         X
                                  I
              (1,7) 00            I     00 (4,12)
                                  I
        (2,8) 00                  I           00 (5,11)
                                  I
              (3,9) 00            I     00 (6,10)
                                  I
                                  I
                                  I
                                  I
                                  I
                                  I
                    ----------------------------
                    ////////////////////////////

PHASE ARRANGEMENT
     (1) A          (8) B
     (2) B          (9) C
     (3) C         (10) G
     (4) A         (11) B
     (5) B         (12) A
     (6) C         (13) GW
     (7) A         (14) GW

    THE FOLLOWING OUTPUT CONTAINS THE RESULTS OF THE CALCULATION OF
OVERHEAD TRANSMISSION LINE PARAMETERS FOR THE SAMPLE CONFIGURATION AND
PHASE ARRANGEMENT SHOWN ABOVE.  THE OUTPUT WHICH YOU ARE NOW READING AS
WELL AS ALL OF THE PREVIOUS TEXT IS A PORTION OF THE AVAILABLE 999
LINES OF COMMENTARY WHICH MAY BE USED TO ADEQUATELY DESCRIBE THE
INFORMATION PERTINENT TO THE PROBLEM.
    NOTE THAT THE OUTPUT FOR THE ORIGINAL CONFIGURATION CONTAINS A ROW
AND A COLUMN FOR EACH INDIVIDUAL CONDUCTOR.  THE ADMITTANCE MATRIX
ALLOWS FOR THE DETERMINATION OF CURRENT DISTRIBUTION AMONG EACH

CONDUCTOR.  THE SUSCEPTANCE MATRIX ALLOWS FOR THE DETERMINATION OF
SURFACE VOLTAGE GRADIENT ON EACH CONDUCTOR AND GROUND WIRE.
    FOR THE EQUIVALENT CONFIGURATION, THE SUBCONDUCTORS ARE BUNDLED
TO FORM AN EQUIVALENT CONDUCTOR, AND THE GROUND WIRES ARE ELIMINATED
MATHEMATICALLY SUCH THAT ONLY AN EQUIVALENT CONDUCTOR PER PHASE PER
CIRCUIT REMAINS.  WHERE A LARGE NUMBER OF PARALLEL CIRCUITS ARE
INVOLVED, THE BUNDLING TECHNIQUE MAY BE APPLIED TO ENTIRE CIRCUITS SO
THAT A REDUCTION TO A DESIRABLE SMALLER NUMBER OF EQUIVALENT CIRCUITS
MAY BE OBTAINED.
    FINALLY, THE SYMMETRICAL COMPONENT ADMITTANCE AND SUSCEPTANCE
MATRICES ALLOW THE CALCULATION OF ELECTROMAGNETIC AND ELECTROSTATIC
UNBALANCED CURRENTS.  PROVISION HAS BEEN MADE FOR THE INSERTION OF
ADDITIONAL BALANCED SERIES IMPEDANCES TO ALLOW THE UNBALANCE
DETERMINATION FOR A SYSTEM INCLUDING TRANSFORMERS, LOADS, ETC.
```

```
                    RECORD OF INPUT DATA                                RUN-CASE-PAGE
                                                                        96125  1  1
    14 100.00  60.00     1     7.     8.     7.    -0  96125
  0.0657  0.2650 -0.912730  140.00    7.00  110.00  -0.-0.
  0.0657  0.2650 -0.912730  105.00    0.     75.00  -0.-0.
  0.0657  0.2650 -0.912730   70.00    7.00   40.00  -0.-0.
  0.0657  0.2650 -0.912730  140.00   60.00  110.00  -0.-0.
  0.0657  0.2650 -0.912730  105.00   67.00   75.00  -0.-0.
  0.0657  0.2650 -0.912730   70.00   60.00   40.00  -0.-0.
  0.0657  0.2650 -0.912730  140.00    0.50  110.00  1.-0.
  0.0657  0.2650 -0.912730  105.00    1.50   75.00  2.-0.
  0.0657  0.2650 -0.912730   70.00    0.50   40.00  3.-0.
  0.0657  0.2650 -0.912730   70.00   50.50   40.00  6.-0.
  0.0657  0.2650 -0.912730  105.00   65.50   75.00  5.-0.
  0.0657  0.2650 -0.912730  140.00   50.50  110.00  4.-0.
  0.5000  0.4040 -1.210000  140.00    2.00  130.00  -0. 1.
  0.5000  0.4040 -1.210000  140.00   65.00  130.00  -0. 1.
```

Fig. 3. Commentary and Record of Input Data

ADMITTANCE MATRIX FOR THE SYSTEM OF PHYSICAL CONDUCTORS (MHO MILES)
ROWS AND COLUMNS PROCEED IN SAME SEQUENCE AS CARD INPUT

RUN-CASE-PAGE
96125 1 12

0.21862E-00
-0.15320E 01

-0.22698E-03
0.76918E-01

0.26996E-02
0.35615E-01

0.59900E-02
0.45362E-01

0.66106E-02
0.30020E-01

0.33313E-02
0.24053E-01

-0.15528E-00
0.82249E 00

-0.29556E-03
0.76485E-01

0.27534E-02
0.34735E-01

0.31671E-02
0.24032E-01

0.32883E-02
0.31564E-01

0.52142E-02
0.49538E-01

-0.78027E-01
0.11086E-00

-0.17629E-01
0.43495E-01

0.28624E-00
-0.15134E 01

-0.35048E-02
0.88883E-01

0.27686E-02
0.34059E-01

-0.79167E-02
0.21164E-01

-0.11711E-01
0.27198E-01

IMPEDANCE MATRIX FOR THE SYSTEM OF PHYSICAL CONDUCTORS (OHMS/MILE)
ROWS AND COLUMNS PROCEED IN SAME SEQUENCE AS CARD INPUT

RUN-CASE-PAGE
96125 1 10

0.16100E-00
0.13277E 01

0.95303E-01 0.16100E-00
0.52093E 00 0.13277E 01

0.95303E-01 0.95303E-01 0.16100E-00
0.44720E-00 0.52093E 00 0.13277E 01

0.95303E-01 0.95303E-01 0.95303E-01 0.16100E-00
0.40096E-00 0.44814E-00 0.41971E-00 0.13277E 01

0.95303E-01 0.95303E-01 0.95303E-01 0.95303E-01 0.16100E-00
0.44814E-00 0.45252E-00 0.44814E-00 0.52093E 00 0.13277E 01

0.95303E-01 0.95303E-01 0.95303E-01 0.95303E-01 0.95303E-01 0.16100E-00
0.41971E-00 0.44814E-00 0.48096E-00 0.44720L-00 0.52093E 00 0.13277E 01

0.95303E-01 0.95303E-01 0.95303E-01 0.95303E-01 0.95303E-01 0.95303E-01 0.16100E-00
0.91352E 00 0.52703E 00 0.44718E-00 0.48445E-00 0.45042E-00 0.42096E-00 0.13277L 01

0.95303E-01 0.95303E-01 0.95303E-01 0.95303E-01 0.95303E-01 0.95303E-01 0.95303E-01 0.16100E-00
0.52983E 00 0.91352E 00 0.52983E 00 0.45042E-00 0.45527E-00 0.45042E-00 0.52093E 00 0.13277E 01

0.95303E-01 0.95303E-01 0.95303E-01 0.95303E-01 0.95303E-01 0.95303E-01 0.95303E-01 0.95303E-01 0.16100E-00
0.44718E-00 0.52703E 00 0.91352E 00 0.42096E-00 0.45042E-00 0.44445E-00 0.44720E-00 0.52893E 00 0.13277E 01

0.95303E-01 0.95303E-01 0.95303E-01 0.95303E-01 0.95303E-01 0.95303E-01 0.95303E-01 0.95303E-01 0.95303E-01 0.95303E-01
0.42096E-00 0.45042E-00 0.48445E-00 0.44718E-00 0.52703E 00 0.91352E 00 0.42219E-00 0.45272E-00 0.44803E-00

0.95303E-01 0.95303E-01 0.95303E-01 0.95303E-01 0.95303E-01 0.95303E-01 0.95303E-01 0.95303E-01 0.95303E-01 0.95303E-01
0.45042E-00 0.45527E-00 0.45042E-00 0.52983E 00 0.91352E 00 0.52983E 00 0.45272E-00 0.45806E-00 0.44272E-00

0.95303E-01 0.95303E-01 0.95303E-01 0.95303E-01 0.95303E-01 0.95303E-01 0.95303E-01 0.95303E-01 0.95303E-01 0.95303E-01
0.44445E-00 0.45042E-00 0.42096E-00 0.91352E 00 0.52703E 00 0.44718E-00 0.44803E-00 0.45272E-00 0.42219E-00

96125 1 11

0.95303E-01 0.95303E-01 0.95303E-01 0.95303E-01 0.95303E-01 0.95303E-01 0.95303E-01 0.95303E-01 0.95303E-01
0.59554E 00 0.47639E-00 0.41652L-00 0.46321E-00 0.42644F-00 0.39563E-00 0.59312E 00 0.47646E-00 0.41639E-00

0.95303E-01 0.95303E-01 0.95303E-01 0.95303E-01 0.95403E-01 0.95303E-01 0.95303E-01 0.95303E-01 0.95303E-01
0.46321E-00 0.42344E-00 0.39563E-00 0.59554E 00 0.47639E-00 0.41652E-00 0.46604E-00 0.42507E-00 0.39455F-00

0.16108E-00
0.13277E 01

0.95303E-01 0.16108E-00
0.52093E 00 0.13277E 01

0.95303E-01 0.95303E-01 0.16108E-00
0.44720E-00 0.52094E 00 0.13277E 01

0.95303E-01 0.95303E-01 0.95303E-01 0.40230E 00
0.39659E-00 0.42567E-00 0.46804E-00 0.14467E 01

0.95303E-01 0.95303E-01 0.95303E-01 0.95303E-01 0.40230E 00
0.41639E-00 0.47646E-00 0.59312E 00 0.45999E-00 0.14467E 01

Fig. 4. Output for Original Configuration

ADMITTANCE MATRIX FOR THE SYSTEM OF EQUIVALENT PHASE CONDUCTORS (MHO MILES)
ROWS AND COLUMNS PROCEED IN SEQUENCE A,B,C,D,E,ETC.

RUN-CASE-PAGE
96125 1 14

0.38018E-00
0.14795E 00

0.41928E-02
-0.57915E-01

0.13527E-01
-0.65149E-01

0.27845E-00
0.71801E 00

0.23149E-01
-0.46167E-01

-0.93146E-02
-0.76837E-01

IMPEDANCE MATRIX FOR THE SYSTEM OF EQUIVALENT PHASE CONDUCTORS (OHMS/MILE)
ROWS AND COLUMNS PROCEED IN SEQUENCE A,B,C,D,E,ETC.

RUN-CASE-PAGE
96125 1 15

0.12627E-00
-0.14284E 01

-0.12721E-01
0.40147E-00

0.11808E-01
0.13612E-00

0.20631E-01
0.19077E-00

0.12824E-01
0.12727E-00

0.12649E-01
0.79858E-01

SYMMETRICAL COMPONENT ADMITTANCE MATRIX (MHO MILES)
ROWS PROCEED IN SEQUENCE 0,1,2,0,1,2, ETC., AND COLUMNS PROCEED IN SEQUENCE 0,1,2,0,1,2, ETC.

RUN-CASE-PAGE
96125 1 13

-0.38726E-01
-0.07658E 00

0.48119E-01
-0.51124E-01

-0.51238E-02
-0.52845E-01

0.24022E-01
0.44064E-00

-0.15259E-01
-0.13659E-01

0.36277E-01
-0.63803E-02

SYMMETRICAL COMPONENT IMPEDANCE MATRIX (OHMS/MILE)
ROWS PROCEED IN SEQUENCE 0,1,2,0,1,2, ETC., AND COLUMNS PROCEED IN SEQUENCE 0,1,2,0,1,2, ETC.

RUN-CASE-PAGE
96125 1 16

0.12627E-00
-0.14284E 01

-0.12721E-01
0.40147E-00

0.11808E-01
0.13612E-00

0.20631E-01
0.19077E-00

0.12824E-01
0.12727E-00

0.12649E-01
0.79858E-01

0.10841E-00 0.14674E-00
0.28984E-00 0.21240E-00

0.44427E-01 0.08644E-01
0.21240E-00 0.23968E-00

0.91177E-01 0.10359E-01 0.48293E-01 0.91359E-01 0.95981E-01 0.11589E-00
0.23978E-00 0.12451E-00 0.12451E-00 0.23978E-00 0.24218E-00 0.79517E 00

Fig. 5. Output for Equivalent Configuration and Symmetrical Components

CONTROL CARD:

No. of cond.'s	Earth Resistance ohms/m.3	Frequency c.p.s.	Calculate Z or P TYPE	Output Y & S RECIP	Miscell. KODE	Date Yr.	Mo.	Day	Carson's Correction KLASS	Output Z & P PRINT
2	5	12	31	37	43	48			19	25

DATA CARDS:

Conductor Resistance ohms/mile	Reactance to 1' spacing ohms/mile	$\log_{10}$ d = O.D. nom. feet	Height at tower feet	Horizontal Coordinate feet	Midspan Height feet	Bundle with #	G.W. Code	
1	9	17	27	35	43	51	55	58

Fig. 6. Sheet for Listing Input Data

Conference Paper

ELECTROMAGNETIC AND ELECTROSTATIC TRANSMISSION LINE PARAMETERS BY DIGITAL COMPUTER

M. H. Hesse
Member AIEE
Electric Utility Analytical Engineering
General Electric Company
Schenectady, N.Y.

A paper recommended by the AIEE Transmission and Distribution Committee for presentation at the AIEE Fall General Meeting, Chicago, Ill., October 7-12, 1962. Manuscript submitted June 7, 1962; made available for printing August 31, 1962.

Price: $ .60 To Members
$1.00 To Nonmembers

(10¢ per copy additional if first class mailing desired)

(Minimum Mail Order $1.00)

All Rights Reserved by the
American Institute of Electrical Engineers
345 East 47th Street,
New York 17, N. Y.

Litho in USA

Paper No. CP
62-1387

Conference Paper

HIGH SPEED THREE POLE RECLOSING

Report of the Arc Deionization Times Working Group

of the AIEE General Systems Subcommittee

For presentation at the AIEE Summer General Meeting, Denver, Colorado, June 17-22, 1962.

Arc Deionization Times Working Group: H. M. Ellis, Chairman; O. A. Demuth, L. O. Barthold, A. E. Kilgour, D. F. Shankle, W. Watson, E. T. B. Gross, R. E. Stade.

Paper No. CP
62-1316

REPORT OF ARC DEIONIZATION TIMES WORKING GROUP ON HIGH SPEED THREE POLE RECLOSING

SUMMARY

A review has been made of the available technical literature on arc deionization times of the fault arc for successful high speed three pole reclosing. Laboratory and field tests as well as operating experience were summarized and estimates made of the minimum deionization times as a function of voltage.

GENERAL

With the high capital investment required today for high voltage transmission systems, high speed reclosing is recognized by transmission engineers in North America as one of the most economical methods of:

1. Increasing the maximum power which can be transmitted over long high voltage transmission lines without loss of synchronism following a fault. The importance of reclose time is shown by the fact that the transient stability of a system can be improved by twenty-five per cent to fifty per cent by reducing the reclose time from thirty-five to twenty-five cycles. 67

2. Reducing system disturbance by reclosing before large swings occur between two parts of a system.

3. Reducing line outage time and improving service to customers.

4. In low lightning areas it is possible to reduce the capital investment in the transmission line by eliminating the overhead groundwires and special tower grounding by employing high speed reclosing.

Unfortunately, because of the number of variables affecting the dead time required to ensure deionization of the power arc, the results of many tests under various conditions, as well as operating experience, must be analysed in order to select dead times which ensure dependable performance of a reclosing system.

Factors affecting deionization time are as follows:

1. Magnitude of the short circuit current. In general, the higher the fault current, the larger the amount of ionized gas generated. This may be offset by the greater turbulence in the air and the magnetic blowout action, both of which increase with higher current.

2. Duration of the short circuit current. The longer the fault current flows, the greater the amount of ionized gases. This is offset also by greater turbulence, longer magnetic blowout action and thermal convection currents in the air.

3. Magnitude and duration of capacitive and magnetic coupling current which may flow due to induced voltage from adjacent conductors which remain energized. This assumes particular

importance for single pole reclosing or for three pole reclosing of one circuit on a double circuit line.

4. Magnitude and duration of resistance follow current which flows through shunting resistors on some types of circuit breakers.

5. Magnitude of re-energization voltage applied.

6. Point of wave at which circuit is re-energized. This determines the magnitude of the surge and will account for much of the randomness of the results obtained.

7. Magnetic forces on the arc due to circuit configuration.

8. Length of insulator string which determines the minimum length of the flashover path.

9. Weather conditions - particularly the wind effect.

10. Shape of grading rings and other parts which determine dielectric stress on reapplication of voltage.

In addition to the above factors which affect the required dead time for a successful reclosing cycle, the following factors will limit the per cent successful reclosing sequences:

1. Permanent faults resulting from mechanical failures and foreign objects (estimates indicate up to twenty-five per cent for wood pole lines and less than five per cent for steel tower lines 12).

2. Multiple component lightning strokes with a duration greater than the total reclose time. Some ten per cent of strokes have durations greater than 0.40 seconds (twenty-four cycles) and thirty per cent greater than 0.20 seconds (twelve cycles). 101. Hence the stroke duration places a real limitation on the minimum reclose interval.

Fortunately, the deionization time required for each stroke component is less than one half cycle, hence, no appreciable increase in dead time is required to allow for the deionization of multiple components. 40

DEFINITION OF HIGH SPEED RECLOSING CYCLE

By definition, reclosing time of a circuit breaker is the time required from energizing the circuit breaker trip coil to the re-contacting of the arcing contacts.

Reclosing times of thirty-five cycles or less are considered as high speed. A reclose is considered successful only if both ends reclose. As a measure of successful reclosing on the basis of deionization time, a percentage successful is tabulated strictly on a reignition basis where possible. The deionization time is the time from final fault current zero to the re-establishment of voltage on the faulted circuit.

Where secondary current flow extends beyond final current zero of the main fault current, this should be noted as a separate parameter.

SUMMARY OF LABORATORY AND FIELD TESTS

Reference No. 18

Ultra High Speed Reclosing of High Voltage Transmission Lines, P. Sporn and D.C. Prince, AIEE Trans. 1937, pp. 81-90.

The authors carried out some 250 laboratory tests simulating the reignition characteristics of a string of insulators at 132 kv, with a restriking voltage of 80 kv under 0-20 m.p.h. wind conditions with fault current of 800 to 6,000 amperes. At 800 amperes and 0-5 m.p.h. wind the minimum dead time was 7 to 8 cycles, whereas with 6,000 amperes it was 10 to 12 cycles. Increasing the wind to 10 to 20 m.p.h. reduced the dead times to 5 to 6 cycles and 9 to 10 cycles, respectively. The study concluded that a minimum dead time of 12 cycles was necessary to provide little probability of a restrike. This might be reduced to 10 cycles with over ninety per cent probability of successful reclosure.

A reclose time of 21 to 22 cycles was obtained during field tests of high speed reclosing on a fifty-nine mile 132 kv line. On all tests the line was successfully re-energized without restriking of the arc for a dead time of 10.7 to 12 cycles for a line to ground fault. For the case of a line-to-line fault, the line was de-energized for 11.5 to 14.1 cycles but only for 14 cycle dead time was re-energization successful. For a double line to ground fault, the re-energization was successful with a dead time of 13.3 cycles.

Reference No. 40

Dielectric Recovery Characteristics of Large Air Gaps, G.D. McCann, J.J. Clark, AIEE Trans. Vol. 62, 1943, pp. 45-52.

For an impulse type gap discharge with varying magnitude and wave shape, the gap recovery to fifty per cent of initial strength, i.e. capable of withstanding normal power frequency voltage, occurs in less than one half cycle. Hence lightning discharges have a negligible effect on reclosing times. However, the time element introduced by multiple strokes of appreciable duration must be considered in determining the reclose time in addition to the rate of recovery of dielectric strength of the power arc.

Reference No. 43

Tests of 230 KV High Speed Reclosing Oil Circuit Breaker, Schwager, AIEE Trans. Vol 63, 1944, pp. 784-788.

Describes tests carried out on a single phase 230 kv, 2500 MVA oil circuit breaker employing a high speed spring operating mechanism. Contact opening speeds of 28 feet per second and reclosing time of 17 cycles (13 cycle dead time) were obtained.

Reference No. 61

Performance Test of the Allegemaine Eleckricitats Gesellschaft Free-Jet Air-Blast 220 KV, 2500 MVA Reclosing Circuit Breaker, Dovjikov, Diemond, AIEE Trans. Vol. 68, 1948, pp. 295-304.

Field tests performed on a 220 kv, 50 cycle, 2500 MVA, AEG Free Stream Air Blast Circuit Breaker on the Bonneville Power Administration System. Three-phase to ground fault currents of 1,350 amperes were interrupted in 6 to 7 cycles and reclosed successfully with a dead time of 12 to 14 cycles, giving a reclose time of the order of 18 to 21 cycles. For a dead time of

Reference No. 61 - Continued

6 to 7 cycles and a reclose time of 12 to 14 cycles, the reclosure was unsuccessful. The fault was applied across a string of sixteen five-inch insulators for a fault length of eighty inches. The paper indicates that minimum possible deionization time of a fault arc across a sixteen-unit insulator string may range between 8 and 12 cycles.

Reference No. 84

Short Circuit Test With Rapid Reclosing on the 220 KV Mettlen-Lavorgo Line, F. Shar and P. Baltensperger, Bulletin Schwiezeirscher Electrotechnisher Verein (Sev) November 17, 1955, Also AIEE Trans. Vol. 75, Part III, 1956, pp. 1137-1146.

High speed reclosing tests were carried out on the 230 kv, sixty-two mile Mettlen-Lavorgo line in Switzerland. For line-to-line faults a dead time of 0.25 seconds (15 cycles) provided successful reclosure.

Reference No. 67

Insulator Flashover Deionization Times as a Factor in Applying High-Speed Reclosing Circuit Breakers, A.C. Boisseau, B.W. Wyman, W.F. Skeats, AIEE Trans. Vol. 68, 1949, pp. 997-1004.

Report investigates minimum deionization times for insulator flashovers on 69 to 230 kv circuits under varying conditions. When capacitive coupling is not present, the de-energization time increases linearly with fault current on 230 kv systems, is practically constant on 132 kv systems and decreases at high currents on 69 kv systems. The duration of the fault current did not show any appreciable effect at 230 kv for an 8,000 ampere fault current with fault durations from 2 to 10 cycles. High speed three-pole reclosing on double circuit transmission lines require 1 or 2 cycles additional dead time to allow for capacitive coupling from the unfaulted circuit for coupled voltages of less than 10 kv. The magnitude of the coupled voltage appears more significant than the arc current as 5 ampere arcs required as long to interrupt as 50 ampere arcs. Calculations indicate that coupled voltages on 230 kv double circuit lines are of the order of 5 kv untransposed and 3 kv transposed.

The dead time for 60 kv circuits varied from 6 to 9 to 6 cycles for fault currents from 1,000 to 8,000 to 22,000 amperes. The dead time at 132 kv was constant over the 8,000 to 22,000 ampere range at 9 cycles. For 230 kv the dead time increased from 8 to 14 cycles for fault current increasing from 1,000 to 22,000 amperes. Tests made on circuit breakers equipped with resistors indicate that the resistor current duration can affect the dead time, particularly for reclosing of long lines.

Tests made for an 8,000 ampere flashover at 230 kv show that the deionization time increased by some 3 cycles (from 7 to 10 cycles) when the reclosing occurred at voltage maximum rather than voltage zero. All data are given for voltage maximum condition.

Reference No. 66

Deionization Time of High-Voltage Fault-Arc Paths, Everett J. Harrington, E.C. Starr, AIEE Trans. Vol. 68, 1949, pp. 997-1004.

Suggests that the limitation on high speed reclosing may be the duration of multiple

lightning strokes. Meager data available to the authors indicates that ten per cent of strokes persist for more than 0.25 seconds or 15 cycles. Tests were performed on the BPA 115 kv system to obtain data on deionization of fault-arc paths produced by SLG faults of 3,000 to 15,000 amperes of varying duration. In preliminary deionization tests at 13.8 kv, recovery was rapid, never exceeding 3 cycles from current interruption to full recovery of rated voltage for fault currents in the range 600 to 1,000 amperes. In the 115 kv tests, it is assumed that recovery is complete when the recovery voltage has reached 150 per cent of normal voltage. This corresponded to a fault path resistance of 0.25 megohms. A large effect of fault current duration was obtained; for example, a 11,000 ampere fault current of 8.6 cycles duration resulted in a recovery time of 8.2 cycles, whereas for a 1.6 cycle duration the recovery time was only 4.2 cycles.

Authors conclude that deionization time is primarily a function of fault duration. It is estimated that 10 cycle dead time is required for a 4 cycle fault, 7 cycles for a 3 cycle fault, and 5 cycles for a 2 cycle fault on a 115 kv system.

Reference No. 71

Dielectric-Recovery Characteristics of Power Arcs in Large Air Gaps, by G.D. McCann, J.E. Conner and H.M. Ellis, AIEE Trans. Vol. 69, Part I, 1950.

Report presents data on effect of arc length, current magnitude and duration on the dielectric recovery characteristics of 6 and 11 inch air gaps. The results indicate minor effect of current magnitude and duration of arc on the recovery characteristics and that the recovery is approximately proportional to the length of the arc. The time required to recovery of fifty per cent of the dielectric strength of the gap was approximately 5 cycles for 300 and 800 ampere fault currents with no wind. This was reduced to 1 and 2 1/2 cycles with a wind velocity of the order of 10 and 5 m.p.h., respectively. This indicates the relative importance of wind in assessing recovery characteristics.

Reference No. 79

Rapid Reclosing Tests on a 30 KV Distribution Network, B. Thoren, ASEA Journal, Vol. 25, 1952, pp. 102-108.

Report describes a number of high speed reclosing tests carried out on a 30 kv distribution system to determine the necessary dead time to deionize arcs caused by line faults and the effect of motor load on the deionization period. The results show a small affect of fault current magnitude on dead time. The dead time required was generally less than 0.10 seconds (6 cycles) with the longest dead time of 0.15 seconds (9 cycles). To allow for motor loading on feeders the dead time increased to 0.20 to 0.25 seconds (12 to 15 cycles) in order to ensure successful high speed reclosing.

Reference No. 102

Arcing Short Circuits on 400 KV Transmission Lines and Methods of Dealing with Them, A.S. Maikopar, N.N. Beliskon, Electrickestro No. 1, 1958, pp. 19-25, Translated in Electric Technology USSR, December 1958, pp. 27-38.

Three-pole reclosing tests were carried out on Russian 400 kv transmission lines having lengths of 117 and 635 Km (72 and 397 miles) and including the effect of shunt reactors. The fault current magnitude was 2,000 amperes and the duration 0.16 seconds (9.6 cycles of 60 cycle fault current).

Successful three-pole reclosing was obtained with total reclosing times of 0.27 to 0.30 seconds (16 to 18 cycles on a 60 cycle system). For shunt reactors connected to the line section disconnected, the time could be reduced to 0.20 to 0.25 seconds (12 to 15 cycles on a 60 cycle system). The longest sustained current arcing time was 0.20 seconds. The sustained current time is lower than for single pole reclosing case (0.1 amps /KM with reactors on). Allow 0.1 second for deionization of the gap in establishing reclosing time.

SUMMARY OF OPERATING EXPERIENCE

Reference No. 18

On four single-line-to-ground faults on the 59-mile Fort Wayne - Deer Creek 132 kv line, the average dead time was 13.0 cycles with a total reclosing time of 22 cycles and there was no arc restriking. The author concluded as early as 1937 that on high voltage overhead lines, outages caused by lightning might be reduced some 75 per cent by ultrarapid reclosing.

Reference Nos. 25 Experience with Ultra-High-Speed Reclosing of High-Voltage Transmission Lines, P. Sporn and C. A. Muller, AIEE Trans. Vol. 58, 1939, pp. 625-636.

34 Five Years' Experience with Ultra-High-Speed Reclosing of High-Voltage Transmission Lines, Sporn and Muller, AIEE Trans. Vol. 60, 1941, pp. 241-246.

45 Nine Years' Experience with Ultra-High-Speed Reclosing of High-Voltage Transmission Lines, Sporn and Muller, AIEE Trans. Vol. 64, 1945, pp. 225-228.

These three papers cover three, five and nine years of operating experience, respectively, of high speed reclosing on 66 and 132 kv lines of American Gas and Electric. Reclosing time was adjusted for 20 cycles with 12 cycle dead time. The first paper deals with the development of equipment for high speed reclosing. Experience from May, 1936, to November, 1944, includes 635 cases of flashover on 66 and 132 kv lines. Of the total, 531 were on single circuit lines and 104 on double circuit lines.

Successful Reclosures	570	(90%)
Unsuccessful Reclosures	65	
Total	635	

Of the 65 unsuccessful reclosures, 8 were permanent faults, which results in a 91% successful reclosure rate. Data is not available as to reignitions on unsuccessful reclosures, however, the authors state that some failures were due to relay operations due to swings on reclosing between two systems. Others were a result of a line dead time of 3 to 4 cycles when trouble occurred on a double circuit line and clearing was not simultaneous at all terminals. From a reignition basis, the percentage of successful reclosures would be even higher than 91%.

Reference No. 58

Experience with Operating Automatic Reclosing of Breakers after Line Faults by G. Jancke, CIGRE 12, 1948, Report 306.

Describes experiences of Swedish State Power Board up to 1948 of high speed reclosing

on large 220, 132 and 44 kv networks.

(1) 11-44 kv Radial Lines

Reclosing first placed in service in 1933 on a 44 kv radial line. 0.10 to 0.15 second dead times resulted in a large percentage of unsuccessful high speed reclosures on temporary faults. Dead time of 0.20 to 0.25 seconds was generally employed.

Experience with 1,084 disturbances:

885 (82%) - successful high speed reclosing
154 (14%) - unsuccessful high speed reclosing but were successfully reclosed in three minutes
45 (4%) - permanent faults necessitating repairs

Since 45 of the faults were permanent, the successful reclosing percentage is increased to 85%.

During the period 1940-1943 faults caused by drifting barrage balloons resulted in unsuccessful reclosure which would account for part of the 154 unsuccessful reclosures.

(2) 77-220 kv Loops and Tie Lines

Tests established a dead time of 0.25 to 0.30 seconds at 220 and 132 kv. Actual dead times will be less than these due to varying fault times. Total fault time including relay time is 0.11 seconds. Experience with 14 high speed reclosures is as follows:

8 - successful (57%)
1 - unsuccessful - permanent fault
2 - unsuccessful - circuit breaker fault or other station fault
1 - breaker failed to open
2 - system instability
14 - Total

On the basis of reignition only, the percentage successful would increase to 100%.

Reference No. 63

Experience with High Speed Reclosing, G.E. Dana, Electrical Engineering October 1948, pp. 942-944.

Operating experience is given from 1945-1948 with high speed reclosing on two 114 kv lines of New York State Electricity and Gas Corporation. Reclosing time was 20 cycles with 12 - 15 cycles of dead time.

Successful Reclosures	31	(78%)
Unsuccessful Reclosures	9	
Total	40	

Unsuccessful Reclosures:
1 - permanent fault; 2 - reignition

One line of 82 miles length without groundwires had 39 operations, second line 20 miles long with groundwire had one operation.

Reference No. 60

Staged Tests and Operating Results on an 8 KV Overhead Line System Using High-Speed Automatic Reclosing, by Naef and J. Wild, CIGRE 12, 1948, Report 331.

This report gives data on high speed reclosing on an 8 kv distribution system. The reclose time is 18 cycles with a dead time of approximately 14 cycles. Statistics are given for a four year period on six 8 kv feeders and on the 8 kv network for one year. In the latter case, the results are tabulated below:

Successful Reclosures	67	(64%)
Unsuccessful Reclosures	37	
Total	104	

In twenty out of the thirty-seven unsuccessful reclosures the breaker could be reclosed manually. If it is assumed that the remaining seventeen were permanent faults, the successful reclosures increase to 78%.

Laboratory tests were carried out by the authors to determine the required dead time at 6 to 10 kv for fault currents in the 3,000 - 8,000 ampere range. The tests indicated that the effect of current, voltage and gap separation were very slight on arc deionization time. There were no reignitions of the arc for a dead time of over 3 cycles, therefore, the authors concluded that in the 10 kv range a dead time of 6 cycles should be sufficient to avoid reignition of the arc.

Reference No. 83

Operating Experience with 230 KV Automatic Reclosing on Bonneville Power Administration System, D.A. Gillies, AIEE Trans. Vol. 73, 1955, pp. 1692-96.

Operating experience on the 230 kv system of BPA, 1950-54. Reclosing times were initially set at 45 to 60 cycles but have been reduced to 20 cycles with a trial installation of 15 cycles. For dead times of 20 cycles or less, the experience is as follows:

Successful Reclosures	87
Unsuccessful Reclosures	15
Total	102

Unsuccessful Reclosures:
12 - permanent faults; 3 - resulted in reignitions

Thus, 96% of the reclosures were successful based on temporary faults. BPA's objective is to establish practical limits of high speed reclosing by reducing the reclose time until failures due to insufficient deionization or repetitive strokes become too high. The author indicated that high speed reclosing provides a means of lightning protection that is now considered preferable to the use of overhead groundwires.

Reference No. 95

Ultra High-Speed Reclosing Experience, Barnes, Hauspurg and Kinghorn, AIEE Trans. Vol. 77, part III, 1958, pp. 137-144.

Two years of high speed reclosing experience on twenty 345 kv lines of American Electric Power. As there was no previous experience with reclosing times at 345 kv, the dead time was determined by extrapolation of existing data to 345 kv. Principal factors influencing the duration of the de-energized time were:

(1) Magnitude of fault current.
(2) Point of voltage wave at which reclosing occurs.
(3) Capacitance coupling of parallel energized circuit.

Calculations indicated a reclose time of 37 cycles, however, based on a reasonable fault magnitude and other factors, a reclose time of 28 cycles was used.

Operating experience is as follows:

Successful Reclosures	90	(59%)
Unsuccessful Reclosures	62	
Total	152	

Of the unsuccessful reclosures:

11 - permanent faults; 28 - reignitions; 23 - successful reclose from one end.

Considering the reignition only as unsuccessful exclusive of permanent faults, the successful reclosure would amount to 80%. Further cataloguing of the data on a purely reignition basis indicates the following:

Lightning

Successful	98	(96%)
Unsuccessful	4	

	Single Circuit	Double Circuit
Successful	40	58
Unsuccessful	0	4

Sleet

Successful	15	(39%)
Unsuccessful	24	
Total	39	

The authors point out that analysis under sleet conditions is difficult but that performance was disappointing. Indication is that success under sleet conditions is a function of mechanical de-

sign factors of the line.

The success in reclosing for single circuit against double circuit lines (100% vs. 94%) suggests that coupling from energized circuit has an effect although the authors state that there is no effect on required dead time for lines under 62 miles in length. Conclusions reached by the authors is that reclosing time is adequately long for lightning flashovers and possibly could be shortened. Further study required as to record under sleet conditions and the effect of coupling voltage on double circuit lines.

In his discussion of this paper, Mr. B. L. Lloyd commented that a study of available laboratory tests and operating experience indicated a consistent trend in required dead time with increasing voltage. He concurred with the reclosing time selected by the authors for 345 kv.

Reference No. 105

The 345 KV Transmission Systems of the American Electric Power Company and the Ohio Valley Electric Corporation, F. M. Porter and H. P. St. Clair, CIGRE #407, 1960.

With 28 cycle reclosing time (equivalent to approximately 24 cycle dead time) the 345 kv lines were re-energized after lightning faults from one or both ends 96% of the time. Field tests conducted in 1957 indicated that the reclosing time could be reduced substantially in areas experiencing moderate short circuit duties without appreciably decreasing the percentage successful reclosures. Accordingly, in 1958 all AEP lines were changed to 22 cycle reclosing (equivalent to a dead time of approximately 18 cycles). Based on lightning faults, the lines were successfully re-energized 22 times out of 23 operations, or 95.6%. Thus reducing the reclosing time to 22 cycles has not changed the overall performance.

Reference No. 104

Field Tests on 345 KV High Capacity Oil Circuit Breaker at Philip Sporn Power Plant, O. Naef, J. D. M. Phelps, W. R. Wilson, A. L. Streater, Power Apparatus and Systems, October 1959, pp. 829-843.

For high speed three pole reclosing, six fault tests were initiated across on 18 unit suspension insulator string. The reclosing time was 15 to 16 cycles. On four tests the reclosure was successful and on two tests the arc restruck across the insulator. The average dead time on these tests was 12 cycles, some 7 cycles less than the minimum now used on the AEP system.

Reference No. 106

Report on the Work of Study Committee No. 9 on Extra High Voltage AC Transmissions, P. H. Sporn, F. Cohen, M. Magnien, CIGRE #416, 1960.

Summarizes the reclosing performance of seven countries. The percentage successful reclosure where the line was restored to service almost immediately is as follows:

Type of Fault	% Successful Reclose
Lightning	83%
Fog	87%
Icing	12%

Type of Fault	% Successful Reclose
Other Faults	54%
Overall Performance	70%

Generally speaking, the auto-reclose of EHV circuits is very successful in clearing non-persistent faults, such as caused by lightning and fog.

Reference No. 107

Minimum Time of Automatic Reclosing, A.S. Maikopar, Electric Technology U.S.S.R., Vol. 2, May 1960.

This paper contains a summary of twenty-nine references on three-pole and single-pole reclosing including the dead time required for reclosing at different voltages. The conclusions are that single and multiple lightning strokes do not affect the dead time required due to the brevity of their duration and rapid recovery of dielectric strength on the lightning channels; wind plays an important part in the recovery of dielectric strength; and the dead time increases with current duration up to a point where the volume of luminous gases ceases to increase due to the upward convection of cold air currents and may even decrease. At higher voltages the insulator string is longer and the effect of the convection currents is less, thus resulting in a longer deionization time.

If the influence of the duration of the short circuit and wind speed are ignored, the basic factors influencing the dead time are the magnitude of current and line voltage. For comparison purposes the range of required dead times obtained in this paper are shown in Table I.

COMMENTS AND CONCLUSIONS

Table I and Figure I summarize the results of all data analysed by the committee on the minimum deionization times of the fault arc for successful three pole high speed reclose.

The summary of laboratory and field tests versus operating experience indicates an increased allowance of some 5 cycles for a minimum dead time under operating conditions as compared with test results for successful three-pole reclosing. Where the variables influencing the required dead time allow, it may be possible to reduce the dead time under operating conditions closer to the minimum as determined under laboratory and field test conditions. Certainly further basic research into ion behavior and arc deionization characteristics should be carried out in order to increase our understanding of the parameters affecting the minimum dead time.

The following factors influence the minimum arc deionization or dead time:

(1) Circuit breaker with resistor

The additional dead time required for resistor current duration following clearing of the main fault current appears to vary with the conditions. Conservatively, the dead time should be increased in accordance with resistor current duration.

(2) Capacitive and inductive coupling from a parallel circuit on a double circuit line.

Only a small amount of information is available at 230 kv on this point which suggests that

a small current flow will continue for several cycles beyond the clearing of the fault. Because of the small amount of ionization and short duration of sustained current, no additional dead time was considered necessary. At higher voltages, this may assume increased importance.

(3) Swing angle between the two parts of the system when reclosure occurs.

The angle of swing will introduce a switching transient proportional to the angular difference between the systems which, according to one reference, increases with line length.

(4) Multiple component lightning strokes having a duration greater than the reclosing time.

Based on statistical data available, 10% of strokes have durations exceeding 0.40 seconds (24 cycles) and 30% greater than 0.20 seconds (12 cycles). This duration will not have much effect on reclose times for system voltage above the 345 kv level as dead times are of this order of magnitude.

(5) Additional factors which affect deionization time include wind, arc current magnitude and duration, rate of rise of recovery voltage and magnitude of recovery voltage, etc.

A considerable amount of operating experience on three pole high speed reclosing is now available; unfortunately, much of this data has not been compiled in sufficient detail to provide a dependable basis for analysis of operating experience. There is much to be gained by up-to-date tabulation of the operating experience of high speed reclosing as operating data is the proving ground for reclosing times and arc deionization times. With the present widespread use of automatic monitoring equipment, the analysis of this operational data should be greatly facilitated. There is at present no standard for classifying reclosing data. Accordingly, the Working Group recommend the recording and classifying of this experience as shown in Table II.

There are a number of arc deionization characteristics which appear to be inconsistent under different conditions. For example, the effects of arc duration and current magnitude vary widely in the different references. Because of the effects of arc configuration, thermal convection currents, magnetic effect of leads, variation in wind, etc., these differences are not surprising. There also appears to be some variation in the required deionization time as a function of the type of fault, i.e. single line-to-ground versus line-to-line.

As more test data and operating experience become available, particularly at system voltages up to 500 kv, the minimum reclosing times for high speed three pole reclosing will become more firmly established and our understanding of the effects of the various parameters on this arc deionization time better understood. The reduction in transmission system investment obtained by possible reduction in the arc deionization time is significant, hence there is a real incentive for carrying out further arc deionization tests particularly at 230 kv and above.

TABLE I
ESTIMATED MINIMUM DEIONIZATION OR DEAD TIME REQUIRED FOR AUTOMATIC THREE-POLE RECLOSING

Rated Voltage	From Ref. No. 107	Minimum Deionization Time (Cycles of 60 Cycle) Based on Laboratory and Field Tests	Based on Operating Experience
23	6 to 7.5	6.5	11
46	-	7	12
69	8.5 to 9.6	7.5	12.5
115	-	9	14
132	10.2	9.5	14.5
230	11.5 to 15	12.5	17
345	-	15.5	20.5
400	15 to 21	17	22
500	-	20	25

TABLE II
SUMMARY OF OPERATING EXPERIENCE ON THREE-POLE RECLOSING

SYSTEM
OPERATING VOLTAGE - KV
LENGTH - Miles
CIRCUIT CONFIGURATION - (Single or Double Circuit)
YEARS EXPERIENCE
RECLOSING TIME - Total
- Dead Time
- Secondary Arc due to Resistor, Coupling, etc.

SUMMARY OF RECLOSING OPERATIONS

	Lightning		Sleet			
	Single Circuit	Double Circuit	Single Circuit	Double Circuit	Other	Total
No. Successful						
No. Unsuccessful						
(a) No. Permanent						
(b) No. Reclosed on one end only						
(c) No. Relayed off due to Swing						
(d) No. Failed due to Reignition or Repetitive Lightning Stroke						
% Successful						
% Successful Based on Reignition Failure or Repetitive Lightning Stroke Only						

SUMMARY AND REMARKS

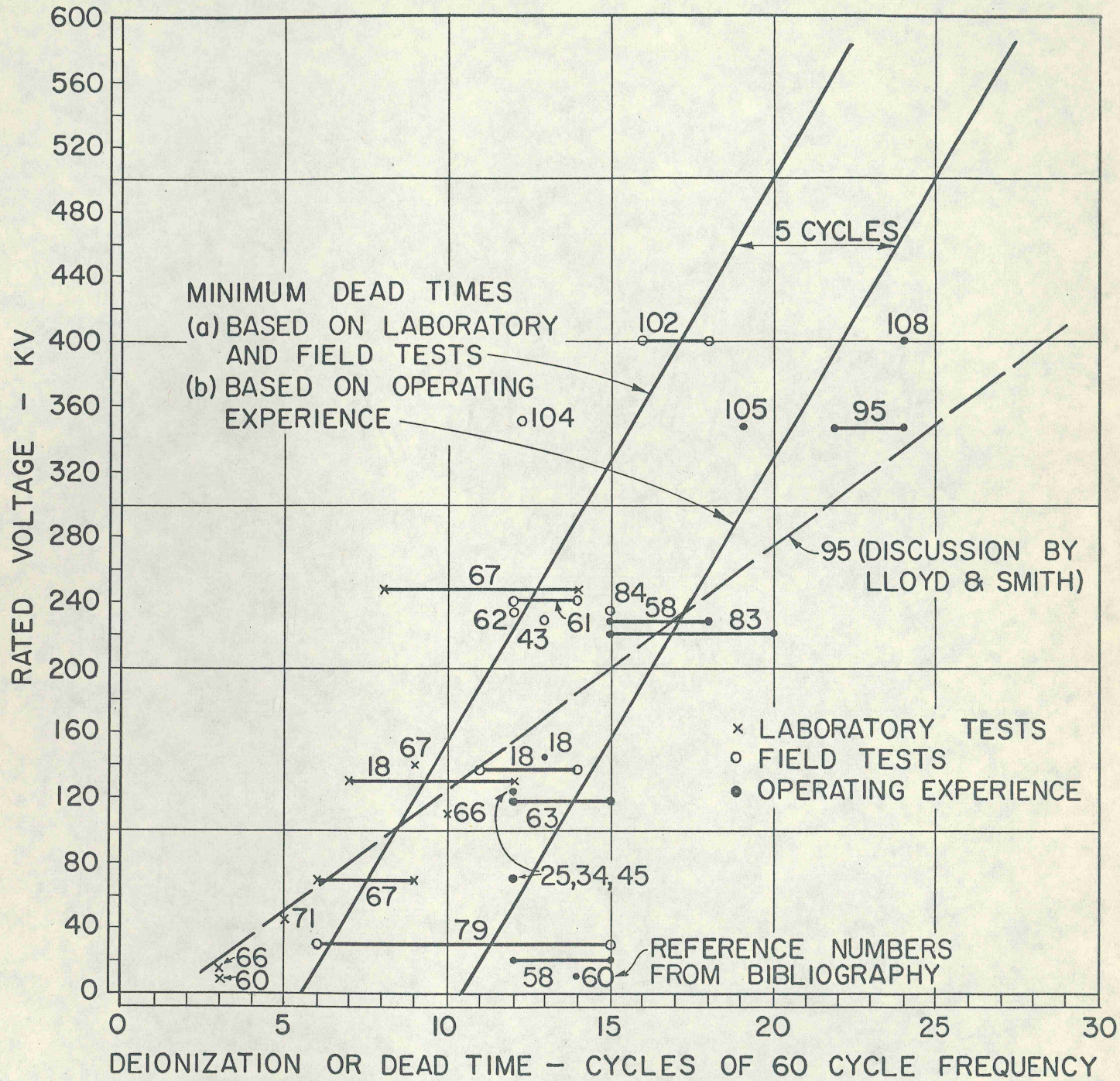

FIG. 1.- HIGH SPEED THREE-POLE RECLOSING DEIONIZATION TIME

BIBLIOGRAPHY

ARC DEIONIZATION TIMES FOR HIGH SPEED THREE POLE RECLOSING

Before 1930

1. Thermal Ionization Theory of Positive Column of Arc, K.T. Compton, Physics Review, 1923, Vol. 21, p. 286.

2. Extinction of an A-C Arc, J. Slepian, AIEE Trans. Oct. 1928, Vol. 47.

1930 - 1934

3. Selecting Breaker Speeds for Stable Operation, R.D. Evans, W.A. Lewis, Electrical World, February 15, 1930, pp. 336-340.

4. Extinction of a Long A-C Arc, J. Slepian, AIEE Trans. April 1930, Vol. 49.

5. Extinction of Short A-C Arcs, T.E. Browne, Jr., F.C. Todd, Physics Review, 1930, Vol. 36, p. 726.

6. Restriking of Short Magnetic Arcs, F.D. Todd, T.E. Browne, Jr., Physics Review, 1930, Vol. 36, p. 732.

7. Reignition of Metallic A-C Arcs in Air, S.S. Attwood, W.C. Dow, and W. Krausnick, AIEE Trans. Sept. 1931, Vol. 50, p. 854.

8. Extinction of Short A-C Arcs, T.E. Browne, Jr., AIEE Trans. Dec. 1931, Vol. 50, p. 1461.

9. Reactance Relays Negligibly Affected by Arc Impedance, A.R. Warrington, Electrical World, New York, N.Y. No. 48, 1931, pp. 502-505.

10. Theory of Oil Blast Circuit Breakers, D.C. Prince, AIEE Trans. March 1932, Vol. 51.

11. Extinction of A-C Arcs in Turbulent Cases, T.E. Browne, Jr., AIEE Trans. March 1932, Vol. 51.

12. Keeping the Line in Service by Rapid Reclosure, S.V. Griscom and J.J. Torok, Electrical Journal, May 1933, p. 201.

13. Dielectric Recovery of Turbulent Arcs, T.E. Browne, Jr., Physics, 1934, Vol. 5, pp. 103-113.

1935 - 1939

14. Das Schaltproblem der Hochspannungstechnik, F. Kesselring and F. Koppelmann, Arch. F. Elektrotechnik, 1935, S. 11.

15. La Frequence Propre et le pouvoir de coupre des disjoncteurs a grande puissance, F. Kesselring, CIGRE 1935, Rapp. 131.

16. Anomalous Secondary Electron Emission, A New Phenomenon, L. Malter, Physics Review, 1936, Vol. 49, p. 478.

17. Carrier Relaying and Rapid Reclosing at 110 KV, R.E. Pierce, R.E. Powers, E.C. Stewart, and G.E. Heberlien, Electrical Engineering, Vol. 55, 1936, pp. 1120-29.

18. Ultra High-Speed Reclosing of High Voltage Transmission Lines, P. Sporn and D.C. Prince, AIEE Trans. 1937, pp. 81-90.

19. Sind Hochleistungs-Pruffelder-uberflussing? F. Kesselring and W. Kaufmann, ETZ 1937, S. 724.

20. Untersuchung einer Bogenentladung mit schnellen Spannung sstossen Wissensch, F. Koppelmann, Verroff, aux dem stemans-Konzern 1937.

21. Kurzschlussfortschaltung, O. Mayr, VDE Fachberichte 10, 1938, pp. 32-35.

22. Effects of Oxides and Impurities on Metallic Arc Reignition, J.D. Cobine , Physics Review, 1938, Vol. 53, p. 911.

23. Recovery Voltage Characteristics of Typical Transmission Systems and Relation to Protector-tube Application, R.D. Evans and A.C. Monteith, AIEE Trans. August 1938, Vol. 57, pp.432-40.

24. Power System Transients Caused by Switching and Faults, R.D. Evans, A.C. Monteith, and R.L. Witzke, AIEE Trans. 1939, Vol. 58, pp. 386-394.

25. Experience with Ultra-High-Speed Reclosing of High-Voltage Transmission Lines, P. Sporn and C.A. Muller, AIEE Trans. Vol. 58, 1939, pp. 625-636.

26. Application of Heat and Transfer Data to Arc Characteristics, C.G. Suits and H. Poritsky, Physics Review 1939, Vol. 55, p. 1184.

27. Convection Currents in Arcs in Air, C.G. Suits, Physics Review, 1939, Vol. 55, p. 198.

28. Investigations on High-Speed Reclosing on the Occurrence of Short Circuits in Overhead Line Systems and the Application of the Air-Blast High-Speed Circuit Breaker for this Purpose, H. Thommen, CIGRE 10, 1939, Rapp. 108.

29. Nouveau genre d'interrupteur pour la coupre d'une mise a la terre out d'un court-circuit, F. Kesselring and W. Kaufmann, CIGRE 1939, Rapp. 104.

30. Impulse Characteristics of Oil Gaps for the standpoint of Insulation Coordination, G.D. McCann, Ph. D. Thesis, California Institute of Technology, 1939.

31. Die Loschung Von Lichtbogenkurzschlussen Durch Kurzzeitiges Abschalten, W. Kaufmann,

ETZ 60, 1939, pp. 241-245.

1940 - 1944

32. Protector Tubes for Power Systems, H.A. Peterson, W.J. Rudge, Jr., A.C. Monteith, and L.R. Ludwig, AIEE Trans. May 1940.

33. Displacement and Diffusion in Fluid Flow Arc Extinction, J. Slepian, AIEE. Trans. 1941, p. 162.

34. Five Years' Experience with Ultra-High-Speed Reclosing of High Voltage Transmission Lines, Sporn and Muller, AIEE Trans., Vol. 60, 1941, pp. 241-246.

35. Gaseous Conductors, J.D. Cobine, McGraw-Hill, 1941, p. 520.

36. Lightning Phenomena, W. Wagner and G. McCann, Electrical Engineering, Vol. 60, No. 10 (1941).

37. High Speed Reclosing, J.E. Hobson, Proceedings of the Midwest Power Conference, Vol. 5, 1942, pp. 156-164.

38. Analysis of the Application of High Speed Reclosing Breakers to Transmission Systems, S.B. Crary, L.F. Kennedy, C.A. Woodrow, Electrical Engineering, AIEE Trans. Vol. 61, 1942, pp. 339-348.

39. Interim Report on Application and Operation of Automatic Reclosing Equipment on Stub Feeders, AIEE Trans. (Committee Report), Vol. 62, 1943, pp. 536-540.

40. Dielectric Recovery Characteristics of Large Air Gaps, G.D. McMann, J.J. Clarke, AIEE Trans. 1943, Vol. 62, pp. 45-52.

41. High-Voltage Oil Circuit Breakers for Rapid Reclosing Duty, Hill, Leeds, AIEE Trans. Vol. 63, 1944, pp. 113-118.

42. Reclosing of Single Tie Lines Between Systems, Parker, Travers, AIEE Trans. Vol. 63, 1944, pp. 119-122.

43. Tests of 230 KV High-Speed Reclosing Oil Circuit Breaker, Schwager, AIEE Trans. Vol. 63, 1944, pp. 784-788.

44. Hi-Voltage Interconnections made Reliable by Single-Pole Switching, J.J. Trainor, H.N. Muller, Jr., Power Plant Engineering (Chicago, Illinios) Vol. 48, June 1944, pp. 77-79.

1945 - 1949

45. Nine Years' Experience with Ultra-High-Speed Reclosing of High-Voltage Transmission Lines, Sporn and Muller, AIEE Trans. Vol. 64, 1945, pp. 225-228.

46. A High-Capacity High Voltage Three-Cycle Oil Circuit Breaker, H.L. Byrd, E.B. Rietz,

AIEE Trans., Vol. 64, 1945, April, pp. 160-163.

47. Three-Cycle, 3500-megavolt-ampere Air Blast Circuit Breaker for 138,000 volt Service, H.L. Byrd, B.S. Beall, III, AIEE Trans., Vol. 64, May 1945, pp. 229-232.

48. Field Test and Performance of Heavy-Duty High-Speed 138 KV Circuit Breakers Oil and Air-Blast, Philip Sporn, H.P. St. Clair, AIEE Trans. May 1945.

49. Reclosing Single-Circuit Tie Lines, H.N. Muller, Jr., W.W. Parker, Westinghouse Engineer (East Pittsburgh, Pa.) Vol. 5, March 1945, pp. 60-63.

50. Systematic Tests with Automatic High-Speed Reclosing in the Goesten and Laufenburg Power Systems, W. Wagner, The Brown Boveri Review (Baden, Switzerland), December, 1945.

51. The Application of Ultra-High-Speed Reclosure to Distribution Networks, by S. Teszner and R. Chambrillon, CIGRE 11, 1946, Report 331.

52. Dielectric Recovery by an A-C Arc in an Air Blast, T.E. Browne, Jr., AIEE Trans., 1946, pp. 169-175.

53. Dielectric Strength of Station and Line Insulation to Switching Surges, Bellaschi and Rademacher, AIEE Trans. 1946, Vol. 65.

54. Resultats d'Essais de Reenclenchement Automatique Effectu es sur un Reseau de Transport di Energie a 150 KV, by C. Dietsch, Soc. Franc. Electr. Bull. 6, 1946, pp. 321-328.

55. Construction et Exploitation des Reseaux de Transport et de Distribution d'Energie Electrique, by Lagoutt, C. Dietsch, F. Cahen, others, Soc. Franc. Electr. Bull. 7, 1947, pp. 209-236.

56. Lightning and 60 Cycle Power Tests on Wood Pole Line Insulation, P.L. Bellaschi and Rademacher, AIEE Trans. 1947, Vol. 66, pp. 838-850.

57. On the Localized after-glow Observed with Long Sparks in Various Gases, J.D. Craggs, W. Hopwood and J.M. Meek, J. Appl. Physics, October 1947, Vol. 18, pp. 919-927.

58. Experience with Operating Automatic Reclosing of Breakers after Line Faults by G. Jancke, CIGRE 12, 1948, Report 306.

59. Power System Stability Requirements Determined by A-C Calculating Board Study and Operating Performance Proved by Staged Fault Tests, by W.A. Morgan and B. Evans, CIGRE 12, 1948, Report 319.

60. Staged Tests and Operating Results on an 8 KV Overhead Line System Using High-Speed Automatic Reclosing, by Naef and J. Wild, CIGRE 12, 1948, Report 331.

61. Performance Test of the Allegemaine Eleckricitats Gesellschaft Free-Jet Air-Blast 220 KV, 2,500 megavolt-ampere Reclosing Circuit Breaker, Dovjikov, Diemond, AIEE Trans. Vol. 68, 1948, pp. 295-304.

62. Field Tests for Development of 10,000,000 KVA 230 KV Oil Circuit Breakers for Grand Coulee Power Plant. C.L. Killgore and W.H. Clagett, AIEE Trans. Vol. 67, Part 1, 1948, pp. 271-287.

63. Experience with High Speed Reclosing, G.E. Dana, Electrical Engineering, October 1948, pp. 942-944.

64. Circuit Breakers and Neutral Point-Earthing, H. Thommen, Brown Boveri Review, 1948, Vol. 35, pp. 227-230.

65. New Investigations on Dielectric Strength of Gas, N. Felici and Y. Marchal, Revue Generale de l'electricite, April 1948, Vol. 57, pp. 155-162.

66. Deionization Time of High-Voltage Fault-Arc Paths, Everett J. Harrington, E.C. Starr, AIEE Trans. Vol. 68, 1949, pp. 997-1004.

67. Insulator Flashover Deionization Times as a Factor in Applying High-Speed Reclosing Circuit Breakers, A.C. Boisseau, B.W. Wyman, W.F. Skeats, AIEE Trans. Vol. 68, 1949, pp. 1058-1067.

68. A-C Tripping and Reclosing of Line Sectionalizing Circuit Breakers, Winegartner, Boneheimer, AIEE Trans. Vol. 68, 1949, pp. 1357-1359.

1950 - 1954

69. Consideration of Requirements and Limitations of Relaying and High-Speed Reclosing on Long and Heavily Loaded Transmission Lines, Parks, Brownlee, AIEE Trans. Vol. 60, 1950, pp. 103-107.

70. The Bonneville Power Administration Relaying and Reclosing Program, Diemond, Wylei, AIEE Trans. Vol. 60, 1950, pp. 1039-46.

71. Dielectric-Recovery Characteristics of Power Arcs in Large Air Gaps, by G.D. McCann, J.E. Conner and H.M. Ellis, AIEE Trans. Vol. 69, Part I, 1950.

72. Modernized Indoor Air-Blast High-Speed Circuit Breakers, by H. Thommen, Brown Boveri Review, Vol. 37, 1950, pp. 143-153.

73. Protection of Transmission Systems Against Lightning (book) by W.W. Lewis, John Wiley & Sons, New York, N.Y., 1950.

74. High-Speed Reclosure of Circuit Breakers, by J.R. Mortlock, BTH Activities 21, 1950, pp. 188-192.

75. Automatic Reclosing As A Means of Lightning Protection During Storms, N.N. Beliakov and A.I. Gershengorn. Trud. nauch-tekh. sessii po perenapriazheniam. Gosenergoizdat (1950).

76. Factors Affecting the Rate of Dielectric Recovery of Power Arcs in Long Air Gaps, Ph. D.

Thesis, California Institute of Technology, 1951, H.M. Ellis.

77. High Speed Multiple Reclosing Oil Circuit Breaker for 161 KV 10,000,000 KVA, Baker Cushing, Vol. 71, AIEE 1952, pp. 22-28.

78. Developing a Super Speed Trip-Free Reclosing Circuit-Breaker Mechanism, Linde, Peak, AIEE Trans. Vol. 71, 1952, pp. 734-742.

79. Rapid Reclosing Tests on a 30 Distribution Network, by B. Thoren, ASEA Journal, Vol. 25, 1952, pp. 102-108.

80. High Speed Motion Picture Photography of Electrical Arcs on a High Voltage Power System, E.J. Harrington and H.C. Ramberg, Journal of the Society of Motion Picture and Television Engineers, June 1953, Vol. 60, pp. 675-679.

81. Protection Test with Rapid Reclosing in an EHV Network, by A. Matthey-Doret and A. Leuthold, Brown Boveri Review, Vol. 41, No. 1, 1954, pp. 351-353.

82. The Supply Arc During the Elimination of Earth Faults in 400 KV Lines. A.S. Maikopar. Trud. TSNIEL (Proceedings of Central Electrical Research Institute), Vol. II (1954).

1955 - 1960

83. Operating Experience with 230 KV Automatic Reclosing on Bonneville Power Administration System, D.A. Gillies, AIEE Trans. Vol. 73, 1955, pp. 1692-96.

84. Short Circuit Test With Rapid Reclosing on the 220 KV Mettlen-Lavorgo Line, F. Shar and P. Baltensperger, Bulletin Schwiezeirscher Electrotechnisher Verein (Sev) November 17, 1955, also AIEE Trans. Vol. 75, Part III, 1956, pp. 1137-1146.

85. Automatic Circuit Reclosers, G.F. Peirson, A.H. Pollard, N. Care, IEE Proceed. Vol. 102, Pt. A. (Power Eng.) No. 6, Dec. 1955, pp. 749-764.

86. Wood versus Steel Transmission Lines - L.M. Robertson, Electrical World, February 7, 1955.

87. Kurzunterbrechung in Verteilungsnetzen (Short Interruption in Distribution Networks). H. Baatz. ETZ-A, No. 18 (1955).

88. Development and Testing of 300 KV Air-Blast Circuit Breaker for Severe Duties, J. Christie, D.F. Amer, A.F.B. Young, AIEE Trans. Vol. 75, Part III, No. 27, December 1956, pp. 1056-1064.

89. New High Power Cathode Circuit Breaker, L.D. McMonnell, J.D. Findley, AIEE Trans., Vol. 75, Part II, No. 23, March 1956, pp. 39-43.

90. Testing of High-Voltage Circuit Breakers, L.R. Bergstrom, ASEA Journal, Vol. 29, No. 6, 1956, pp. 71-81.

91. Air-Blast Circuit Breakers for High Voltage Networks, C.H. Flurscheim, Metropolitan

Vickers Gazette, Vol. 27, No. 445, August 1956, pp. 235-244.

92. High-Voltage Circuit Breakers-Performance and Selection, C.S. Scrrenivasan, Power Eng. (India) Vol. 6, No. 4, October 1956, pp. 236-245.

93. The Transition of High-Power Impulse Flashover Into a Power Arc in Overhead Transmission Lines. A.S. Maikopar, Trud. TSNIEL. Vol. V (1956).

94. Study of High-Power Impulse Discharge in Air at Atmospheric Pressure, V.V. Burgsdorf and A.S. Maikopar, Elekt. No. 12 (1957).

95. Ultra High-Speed Reclosing Experience, Barnes, Hauspurg and Kinghorn, AIEE Transmission, Vol. 77, Part III, 1958, pp. 137-144.

96. Impulse System for Arc Recovery Strength Measurements, J.D. Cobine, E.E. Burger, G.A. Farrall, AIEE Trans. Vol. 77, pp. 1094-1101.

97. Air Blast Circuit Breakers for Very High Voltage, G.K. Simpson, IEE Journal Vol. 4, No. 41, May 1958.

98. The Design of 330 KV Transmission System for Rhodesia, IEE Proc., Pt.A., December 1958 (including discussion by Mortlock).

99. High Temperature Effects on Flashover in Air, IEE Proc., Pt.A., Vol. 105, No. 24, December 1958.

100.

100. Experience with Ultra High-Speed Reclosing of Transmission Lines on 345 KV Systems in the U.S.A., by J.J. Kinghorn, H.C. Barnes, Al Hauspurg, CIGRE 1958, No. 121.

101. A Lightning Stroke Component Counter, H.M. Ellis and H. Link, CIGRE No. 308, 1958.

102. Arcing Short Circuits on 400 KV Transmission Lines and Methods of Dealing with them, A.S. Maikopar, N.N. Beliskon, Electrickestro No. 1, 1958, pp. 19-25, Translated in Electric Technology USSR, December 1958, pp. 27-38.

103. National Advisory Committee for Aeronautics, Technical Note 4150 - "Approximations for the Thermodynamic and Transport Properties of High Temperature Air", by C. Frederick Hansen, NACA, Washington, March 1958.

104. Field Tests on a 345 KV High Capacity Oil Circuit Breaker at Philip Sporn Power Plant by O. Naef, J.D.M. Phelps, W.R. Wilson and A.L. Streater, AIEE Paper No. 59-188.

105. The 345 KV Transmission System of the American Electric Power Company and the Ohio Valley Electric Corporation, F.M. Porter and H.P. St. Clair, CIGRE No. 407, 1960.

106. Report on the Work of Study Committee No. 9 on Extra High Voltage A-C Transmissions, P. Sporn, F. Cohen, M. Magnien, CIGRE No. 416, 1960.

107. Minimum Time of Automatic Reclosing, A.S. Maikopar, Electric Technology USSR, Vol. 2, May 1960.

108. Swedish 380 KV System, book printed in Stockholm, 1960, p. 38.

Fundamental Aspects of Some Switching Overvoltages on Power Systems

J. ZABORSZKY
FELLOW AIEE

J. W. RITTENHOUSE
FELLOW AIEE

Summary: System overvoltages caused by switching are of interest in insulation coordination problems. This paper treats such overvoltages in a graphical fashion, so that a visual concept of overvoltage versus time is provided in both single- and 3-phase cases involving resistive loads, inductive loads, and capacitive loads. As special cases, attention is given to a neutral inversion problem and to a case of coupled circuits.

THE INCREASING complexity of power systems has created difficulty in analyzing specific cases of trouble which seem to stem from system overvoltages. It is believed that some of this difficulty can be minimized if one has a thorough grasp of the causes of overvoltages.

It is the purpose of this paper to demonstrate and review a few of the fundamental conditions that can cause overvoltages. In particular, overvoltages arising from switching operations will be discussed.

It is believed that the graphical approach that is followed provides an easy means of conducting a review in providing a good physical concept of the basic causes of many kinds of overvoltage phenomena.

Restrikes in a Single-Phase Resistive Circuit

A single-phase radially fed pure resistive load is shown in Fig. 1. The line itself is assumed to be purely resistive, and while this is admittedly not a practical combination, it is included here as an introduction to practical but more complicated situations which will be dealt with later.

Current is interrupted at time t_1; prior to that there is a voltage drop, with a peak value of ΔE, on the line. This, for the resistive circuit shown, is exactly in phase with the current, I, which in turn is exactly in phase with the source voltage E_α. Following current interruption at t_1, the voltage E_a remains zero, while the source end of the switch follows the source voltage $E_A = E_\alpha$.

The difference between the E_A and E_a curves, $E_a - E_A$, is the recovery voltage which is being built up across the gap of the switch.

If at some time after t_1 the recovery voltage exceeds the dielectric strength between the switch contacts, a restrike will occur. The potentially most dangerous time for this is t_2 when the peak recovery voltage is reached. Nothing unpleasant happens, however, in this purely resistive circuit. The current is re-established, and it instantaneously assumes the value it would have had at the instant of restrike if there had been no interruption.

The voltages of the terminals a and A instantaneously shift to satisfy the condition $E_A = E_a$ which would have existed with the load connected and if no interruption had occurred.

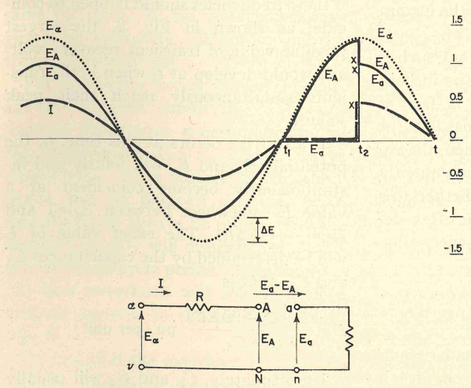

Fig. 1. Circuit, voltages, and current considered in the single-phase resistive restrike and energizing cases (left)

Fig. 2. Circuit and voltages considered in the 3-phase resistive restrike and energizing cases (right)

Restrikes in a 3-Phase Resistive Circuit

Conditions for the 3-phase purely resistive circuits are shown in Fig. 2. The line resistances have been omitted in this illustration to keep it as uncluttered as possible.

Current (not shown) in phase A is interrupted at time t_a. From here on $E_a = E_n$, and since n now is simply the midpoint of a voltage divider between points b and c, also $E_a = (E_b + E_c)/2$.

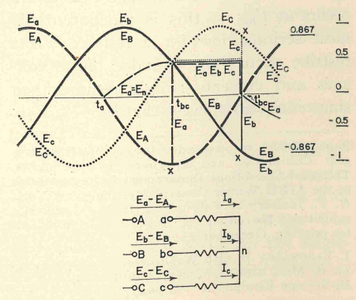

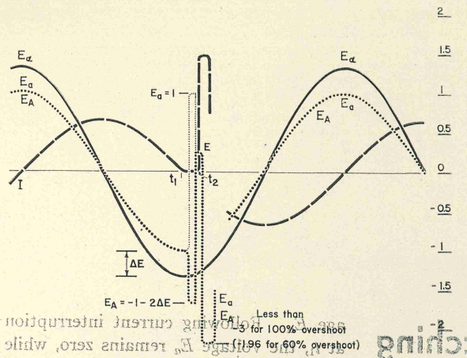

Fig. 3. Circuit, voltages, and current considered in the single-phase inductive restrike case (left)

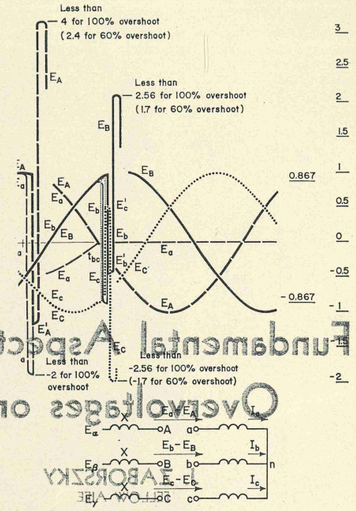

Fig. 4. Circuit and voltages considered in the 3-phase inductive restrike case (right)

$E_a'=E_A$ is the recovery voltage which reaches its peak at t_{bc}. Even in this case a restrike causes no undue disturbance. The current (not shown) instantaneously resumes its steady-state variations, just as in the single-phase case, and the voltage E_a shifts over to coincide with E_A which in this circuit is also the source voltage.

If no restrike occurs at t_{bc}, E_a will, of course, not drop to the E_A' curve as shown. Furthermore, since the single-phase current in phases B and C is passing through zero at t_{bc}', t_{bc}' is a logical time for interruption in these phases.

Accordingly, assuming no restrike at t_{bc} in phase A, and assuming current interruption in phases B and C at t_{bc}', the voltages E_a, E_b, and E_c will undergo a change in behavior after t_{bc}.

If there were truly no capacitance in the system as indicated by Fig. 2, these voltages would simply drop to zero at t_{bc}'. More realistically, though, there actually is stray capacitance between the ground and the load resistors; so actually E_a, E_b, and E_c will tend to remain constant at $E_a'=E_b'=E_c'=0.5$ after the interruption of phases B and C currents.

The maximum value of recovery voltage across the switches in phases B and C occurs at t_{bc}'; so this is the potentially most serious time for a restrike. If a restrike occurs, the B and C phase voltages and currents simply resume their sinusoidal variations so that $E_B'=E_b$, $E_C'=E_c$, and E_a resumes the relationship $E_a'=E_n'=E_b'+E_c'/2$.

Practical circuits will always have at least small amounts of inductance which prevent instantaneous current changes. Consequently, all transitions will cease to be instantaneous, they will become slightly gradual and the corners denoted by x in Figs. 1 and 2 will become rounded. More precisely a transient will occur, and the transition will become an exponential function of time.

Energizing Resistive Circuits

A restrike re-energizes a circuit a short time after it is interrupted. This phenomenon is similar, but not necessarily identical, to the phenomenon of energizing a circuit after it has been de-energized for a long time.

The difference is that in restriking the re-energizing occurs a short time after de-energizing; so there is a possibility that some energy in the form of still persisting charges, or transient currents, will be present in the circuit at the instant of re-energizing.

It is easy to see, however, that such is not the case for resistive circuits in both Figs. 1 and 2. The circuit is free of charges or transients at the times t_{bc}, or t_{bc}' or at any other time when the re-energizing might occur; consequently there will be no difference whether this re-energizing occurs 1/2 cycle after de-energizing or a week after de-energizing.

Restrikes in Single-Phase Inductive Circuits

For this case the conditions under study are represented in Fig. 3. The circuit is a lossless, nominal π equivalent through which an inductive load is fed.

At time t_1 the current is passing through zero; so it can be interrupted. If it is interrupted, the normal current flow through the load ceases, of course, and the voltage E_a will tend toward zero.

Since there will usually be some small distributed capacitances, C_a, in the load no instantaneous shift is possible, but an undamped, high-frequency oscillation will result which will tend to swing the voltage all the way over in the positive direction from its original value of -1, to an overshoot value of $+1$.

At the same time the voltage E_A will try to shift to the no-load value which is nearly equal to E_a. Here too, though, an oscillation with an initial overshoot which is equal to the original difference will result.

The oscillations of E_a and E_A are not likely to be of the same frequency, but if these frequencies should happen to coincide, as shown in Fig. 3, the largest possible value of transient recovery voltage would develop at t_2 when both transients simultaneously reach their peak values.

If a restrike occurs at this time, t_2, the potentials E_A and E_a will jointly and instantaneously become coincident at a value E somewhere between $E_a=1$ and $E_A=-1-2\Delta E$. The exact value of E will be determined by the capacitances C_A and C_a; that is

$$E=\frac{C_a-C_A-2\Delta E C_A}{C_a+C_A}\ \text{pu (per unit)}$$

Unfortunately, C_a and C_A will usually

Paper 62-276, recommended by the AIEE Switchgear Committee and approved by the AIEE Technical Operations Department for presentation at the AIEE Winter General Meeting, New York, N. Y., January 28–February 2, 1962. Manuscript submitted November 8, 1961; made available for printing December 21, 1961.

J. Zaborszky is with Washington University, St. Louis, Mo., and J. W. Rittenhouse is with the Hi-Voltage Equipment Company, Cleveland, Ohio.

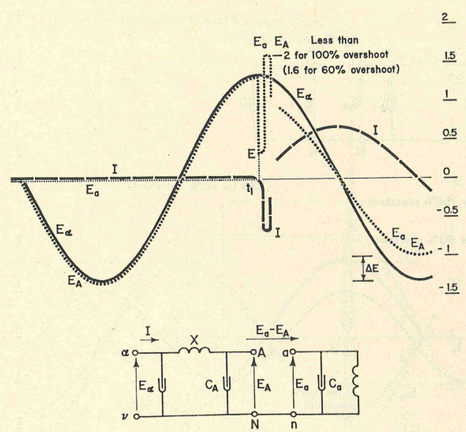

Fig. 5. Circuit, voltages, and current considered in the single-phase inductive energizing case (left)

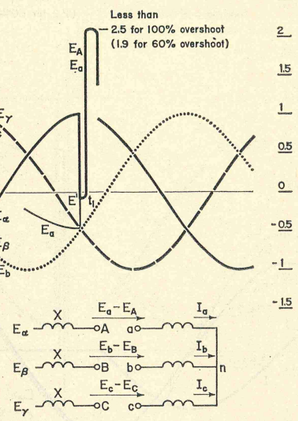

Fig. 6. Circuit and voltages considered in the 3-phase inductive energizing case (right)

be unknown; in fact, the lumped values shown in Fig. 3 are highly oversimplified approximations of much more complicated distributed constant circuits. Accordingly, the exact value of E will rarely be known.

Whatever the value of E is, though, the voltage of points a and A will now tend toward the steady-state sine wave $E_a=E_A$, and since the system shown is lossless this voltage will overshoot by about the original amount of the deviation between E and $E_a=E_A\cong-1$. This overshoot will carry the value of $E_a=E_A$ beyond the normal steady-state peak value; so an overvoltage is present.

As can be seen, the value of this overvoltage will always be less than three times the peak of the steady-state voltage. The value 3 will be reached in the unlikely situation of $C_a>>C_A$ which is about equally as unlikely as having the same transient frequency on either side of the switch. Accordingly, this value should be viewed as an outside limit which can occur only under extreme conditions of coincidence and only on lossless circuits.

A high-frequency current wave of the same frequency as the voltage, but lagging it by 90 degrees, will accompany the transient voltage wave.

For the lossless circuit shown, the voltage and current waves should be undamped sine waves superimposed upon the steady-state $E_a=E_A$ and I waves respectively. In a realistic circuit these waves will be damped sinusoids since resistance will always be present; so the transient usually will disappear in a fraction of the 60-cycle period. Furthermore, the first overshoot will seldom exceed 60% in contrast to the 100% shown in Fig. 3.

In general if the overshoot ratio is $P\%$ in both transients, the maximum overvoltage will reach a value of

$$E_o=1+\frac{P}{100}\left[1+\frac{P}{100}\right]\ \text{pu}$$

Another guide value, but not necessarily an outside limit, is

$$E_o'=1+\frac{P}{100}\left[1-\frac{\Delta E}{2}\left(1+\frac{P}{100}\right)\right]\ \text{pu}$$

This represents the case of $C_A=C_a$ which should not be too widely different from reality.

To keep the illustration clear, Fig. 3, as do many of the other illustrations, shows only stylized forms of the first lobes of the transient waves.

Restrikes in 3-Phase Inductive Circuits

For this case the conditions under study are represented in Fig. 4. The principal differences between this and the single-phase case is that there are more voltages and more combinations in a 3-phase circuit; consequently there can arise more situations which are potentially critical as far as the height of the overvoltage is concerned.

The current of phase A (not shown) can be interrupted at t_a when its value is zero. After this interruption, voltage E_a tends toward $(E_b+E_c)/2$ because points a and n simply become the midpoint of a symmetrical voltage divider, but it overshoots to $E_a=-2$ in this inductive, capacitive (distributed capacitance not shown), lossless, circuit. Voltage E_A tends toward the source voltage, but for clarity in Fig. 4 it is assumed that $E_a\cong E_A$.

A restrike at the peak of the transient recovery voltage, E_a-E_A, will immediately bring E_A and E_a together at E'_A, a value determined by the (unfortunately, usually unknown) stray capacitances at the two contacts of the switch and at adjoining conductors.

From E'_A the voltage seeks to assume the steady E_A variations through a transient which swings it from its original value and polarity to a value of the opposite polarity equal to $E_A+(E_A-E'_A)$. As can be seen, in the unlikely but conceivable case when $E'_A\cong-2$ this overshoot may produce an overvoltage of four times the normal peak. This can be shown to be the absolute maximum possible value of overvoltage for ungrounded 3-phase inductive switching.

With an overshoot ratio of $P\%$, the maximum possible overvoltage is

$$E_o=\frac{1.5P}{100}\left(1+\frac{P}{100}\right)+1\ \text{pu}$$

and if $C_a\cong C_A$

$$E_o'=1+\frac{1.5P}{100}\ \text{pu}$$

The last value is quite realistic, but it is not necessarily on the safe side.

If phase A remains interrupted, phases B and C can be interrupted at $t=t_{bc}$ since this is the instant of current zero in the single-phase current that flows in phases B and C after interruption in phase A. A restrike here, however, only produces overvoltages of less than 2.56 times normal peak, as shown in Fig. 4 for 100% overshoot. For $P\%$ overshoot

$$E_o=\frac{\sqrt{3}}{2}\left[1+\frac{P}{100}\left(1+\frac{P}{100}\right)\right]\ \text{pu}$$

The explanation given for time t_a is believed to be sufficient to enable the reader to follow from Fig. 4 what happens after a restrike in phases B and C at t_{bc}. The remarks on damping given for the single-phase case above apply equally for the 3-phase case.

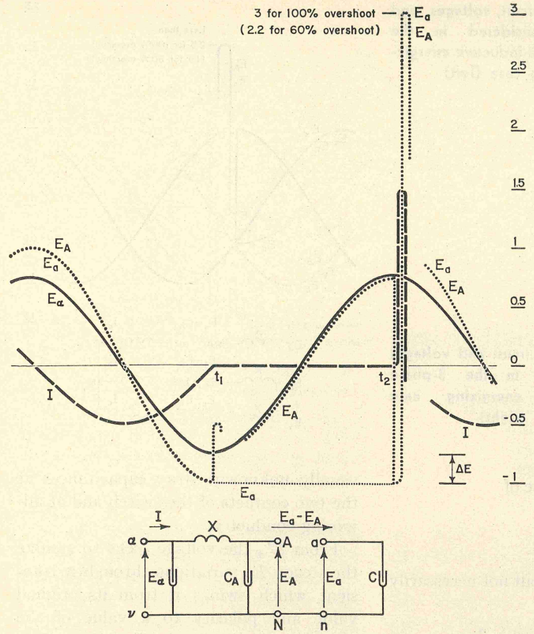

Fig. 7. Circuit, voltages, and current considered in the single-phase capacitive restrike case

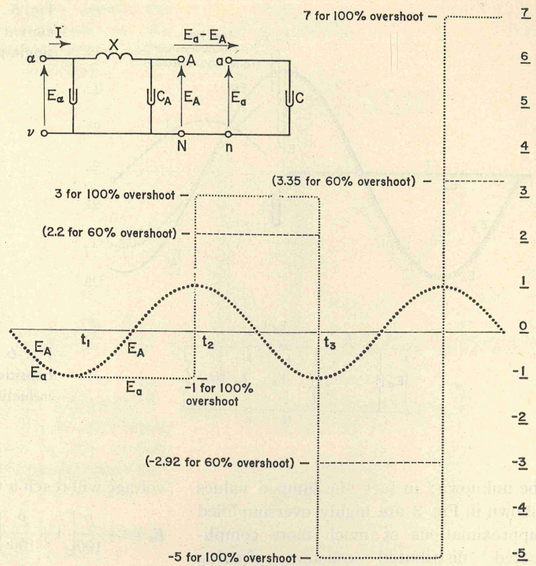

Fig. 8. Voltage build-up attending repetitive restrikes in single-phase capacitive case

Energizing a Single-Phase Inductive Circuit

Some of the results of energizing a lossless single-phase inductive circuit are shown in Fig. 5. The circuit is assumed to have been de-energized for a long time prior to energizing. At time t_1 the switch is closed and voltages E_A and E_a join at a value E which, according to the findings in the preceding sections, is determined by the capacitances C_A and C_a.

For Fig. 5 at time t_1

$$E=\frac{(1+\Delta E)C_A}{C_a+C_A}\ \text{pu}$$

Immediately following the closing of the switch (i.e., following t_1), the joint voltage $E_a=E_A$ seeks, through a transient, coincidence with the steady, loaded, voltage variations of the $E_a=E_A$ curve. In the lossless case the transient carries the voltage above the $E_A \cong E_a$ curve by an amount equal to the oringinal difference, at t_1, between E and the value that E_A would have had if the switch had been closed a long time prior to t_1.

As can be observed from Fig. 5, this overshoot can never produce an overvoltage in excess of twice the normal peak voltage at the switch. This contrasts with an overvoltage of less than 3 (Fig. 3) on de-energizing. For a $P\%$ overshoot ratio the maximum is

$$E_o=1+\frac{P}{100}\ \text{pu}$$

and for $C_a=C_A$

$$E_o'=1+\frac{0.5P}{100}\ \text{pu}$$

The generalized remarks made earlier in connection with the improbability of encountering this maximum limit, and the significance of the $C_a=C_A$ case, also apply to the situation described here. It should be mentioned, however, that if the energizing occurs at a time other than the normal current zero, there will be an additional current transient resulting in a slowly decreasing displacement of the current wave (inrush phenomenon). Discussion of this is beyond the scope of this analysis since this study is concerned with overvoltages.

Energizing a 3-Phase Inductive Circuit

Some of the consequences of energizing a long-dead 3-phase circuit are shown in Fig. 6. The highest possible overvoltage will occur in this case if phase A is closed at a time t_1, following the prior closing of phases B and C.

As before, the voltage E_A will shift to point E' which lies between $E_A=1$ and $E_a=E_b=E_c=-0.5$ at t_1 (prior to t_1, E_a is determined by the voltage divider effect of the phases B and C loads). Again, the value of E' is undefined in terms of quantities which are commonly available for the system.

The maximum possible value of the overvoltage can be found from Fig. 6 to be less than 2.5 times normal peak voltage as compared with four times in the case of restriking (Fig. 4). For a $P\%$ overshoot ratio

$$E_o=1+\frac{1.5P}{100}\ \text{pu}$$

and for $C_a=C_A$

$$E_o'=1+\frac{0.75P}{100}\ \text{pu}$$

It is significant that the overvoltage values which can occur in inductive switching are, in general, not defined in terms of available quantities. Only maximum limits can be found.

Restrikes in Single-Phase Capacitive Circuits

The capacitive circuit considered is shown in Fig. 7 as a purely capacitive load supplied from a lossless line represented for simplicity by a nominal π circuit. The current is assumed to be interrupted at time t_1 leaving the capacitor charged to voltage $E_a=-1$.

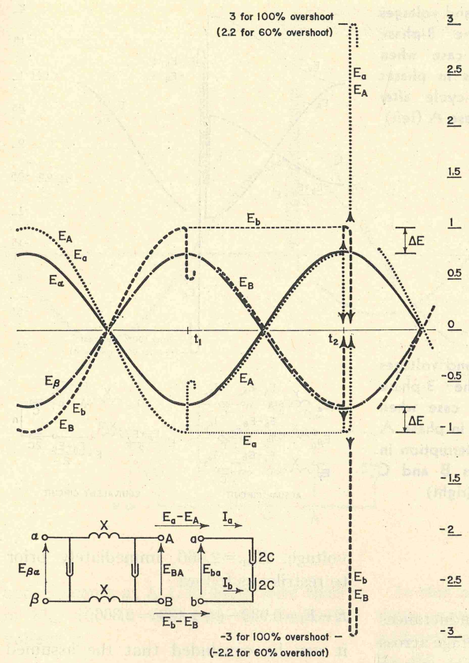

Fig. 9. Circuit, voltages, and current considered in the single-phase capacitive restrike case when both sides of the line contain impedance (left)

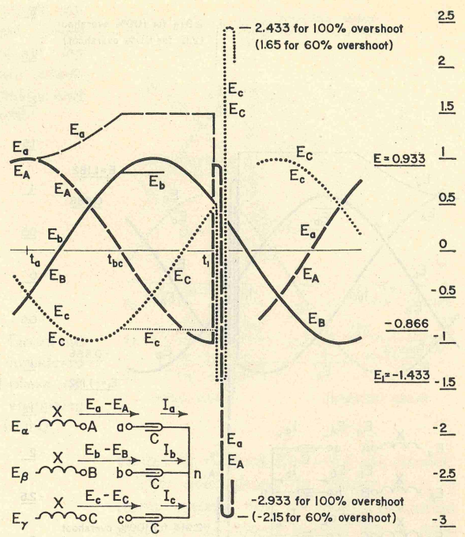

Fig. 10. Circuit and voltages considered in the 3-phase capacitive restrike case when the restrike occurs in phases A and C 1/2 cycle after interruption in phase A (right

The recovery voltage, E_a-E_A, across the switch $A-a$ will then develop in the manner described in a previous paper,[1] and the largest value of the recovery voltage will be reached at t_2. This, then, is the likely critical time for a restrike.

A restrike is assumed at t_2, and since the switched capacitor C is much larger than the equivalent capacitance of the line C_A, voltage E_A at t_2 will shift essentially instantly to join the voltage E_a at $E_a=E_A=-1$.

From this value a transient will try to carry the voltage $E_A=E_a$ to its steady-state condition as indicated by the sine wave after t_2.

In the lossless circuit assumed in this case, the overshoot of the transient will be unrestrained; so the voltage will rise to three times normal peak voltage. The high-frequency transient voltage, after t_2, will be an undamped sinusoid superimposed on the $E_a=E_A$ curve if there is no loss in the circuit.

In the more realistic case which includes losses, the high-frequency transient will be damped out within a fraction of a 60-cycle period, and with a 60% overshoot ratio the overvoltage will be 2.2 times normal peak. In general, for $P\%$ overshoot,

$$E_o=1+\frac{2P}{100}\ \text{pu}$$

In this type of capacitor switching the frequency of the transient is likely to be a small fraction of the frequency encountered in inductive switching because of the large value of the switched capacitor. Bank-to-bank switching, however, results in much higher frequencies (but no significant overvoltages) and high transient currents.[2]

The high-frequency transient voltage in Fig. 7 is accompanied by a transient current of equal frequency leading the voltage by 90 degrees; so in Fig. 7 the current will be zero when the transient voltage is at its peak value.

Should the current be interrupted at the first zero on the transient wave, the capacitor will be left charged at a voltage of three times normal in the lossless case. (2.2 times normal for 60% overshoot). This represents a danger peculiar to capacitor switching in that properly timed, successive interruptions and restrikes can result in a gradual buildup of the overvoltage and recovery voltage. Fig. 8, representing an initial current interruption at t_1, illustrates the consequences of such a sequence of interruptions and restrikes (for simplicity $\Delta E=0$ in this figure).

If at time t_2 a restrike and a successive high-frequency current interruption leaves the capacitor charged to three times normal peak voltage, another restrike occurring at t_3 will cause the voltage in the undamped circuit to swing over to five times normal. If again the arc extinguishes at the first high-frequency current zero, the capacitor will remain charged to five times normal peak voltage, and so on.

Of course, the probability of occurrence of such a uniquely timed series of interruptions and restrike is very small since many conditions in sequence must be met. Specifically all restrikes must occur exactly at the peaks of recovery voltages, and the currents must always be interrupted at the first high-frequency current zeros. Furthermore, the system must be undamped to provide the overshoot ratio of 100%, otherwise the buildup of voltage is much smaller as shown by the 60% overshoot values in Fig. 8.

Even if such a regular sequence does not occur, though, repeated restrikes in a capacitive circuit can cause overvoltages in excess of three times normal.

So far in this section, the examination based on the conditions shown in Fig. 7 has ignored the effects of reactance in the neutral, or return side, of the single-phase source. Fig. 9 takes into account the existence and effects of such a reactance.

An analytical comparison of Fig. 9 with Fig. 7 will reveal that either half of the symmetrical single-phase circuit of Fig. 9 will behave in the manner of the circuit of Fig. 7. The center may be grounded or floating as long as the symmetry is maintained, and the results are the mirror-image-type voltage and current variations in Fig. 9. Each image is individually identical to its equivalent single trace in Fig. 7.

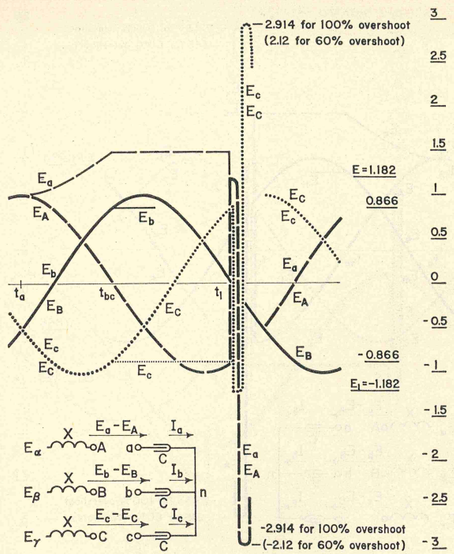

Fig. 11. Circuit and voltages considered in the 3-phase capacitive restrike case when the restrike occurs in phases A and C 7/12-cycle after interruption in phase A (left)

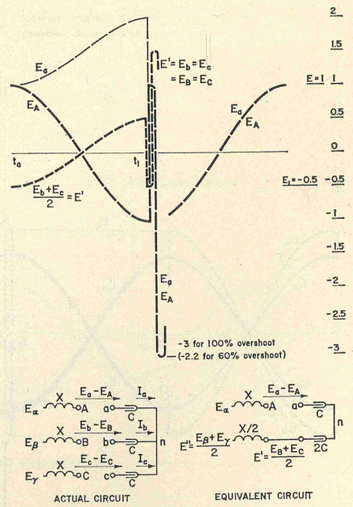

Fig. 12. Circuit and voltages considered in the 3-phase capacitive restrike case when the restrike occurs in phase A 1/2 cycle after interruption in phase A. Phases B and C are closed (right)

The overvoltages above ground are also the same (three or 2.2 times normal). Of course, if the neutral is floating and asymmetrical these overvoltages could be larger by the amount of the asymmetry.

Restrikes in 3-Phase Capacitive Circuits

It is apparent that 3-phase grounded neutral circuits behave like three independent single-phase circuits of the type of Fig. 7, so this situation needs no further analysis. For ungrounded neutral systems, though, additional analysis is warranted.

Fig. 10 depicts a case in which phase A is interrupted at t_a, and phases B and C are interrupted at t_{bc}. Restrikes across switches A-a and C-c are assumed to occur at t_1.

Immediately following the interruptions of the phase currents, the recovery voltages build up across the switches as described in a previous paper.[1] This buildup is such that at t_1 there is a total recovery voltage, E_r, of

$$E_r = E_a - E_A - (E_c - E_C)$$
$$= 1.5 + 1 + 0.866 + 0.5 = 3.866$$

and a trapped voltage, E_{cap}, on the capacitors of

$$E_{cap} = E_a - E_c$$
$$= 1.5 + 0.866 = 2.366$$

At the moment of the restrike, the recovery voltage will disappear across switches A-a and C-c (Fig. 10) and will instantaneously appear across inductances X in phases A and C. The voltage across the capacitors will, of course, remain momentarily unchanged.

Since the line inductances are equal, they will assume equal shares of the recovery voltage, and since the restrike establishes an arc across switch A-a, E_A must immediately become identical to E_a (neglecting the small arc voltage). Let it be assumed that E_A and E_a merge at $E = E_A = E_a = 0.933$ as shown in Fig. 10. Then across the reactance, X, in phase A there is an instantaneous voltage of

$$E_A - E_\alpha = 0.933 + 1 = 1.933$$

Pursuing logic similar to that above, it can be assumed that $E_1 = E_c = E_C = -1.433$ immediately following the restrike; then the instantaneous voltage, $E_\gamma - E_C$, across the reactance, X, in phase C will be

$$E_\gamma - E_C = 0.5 + 1.433 = 1.933$$

The values of $E = E_A = E_a = 0.933$ and $E_1 = E_C = E_c = -1.433$ assumed above have resulted in the required condition that the voltages $E_A - E_\alpha$ and $E_\gamma - E_C$ across the phase A and C reactances, X, are equal immediately following restrike. Furthermore, the sum of these two voltages, $E_A - E_\alpha + E_\gamma - E_C$, is equal to the recovery voltage, $E_r = 3.866$, immediately before restrike as follows:

$$E_A - E_\alpha + E_\gamma - E_C = 0.933 + 1 + 0.5 + 1.433$$
$$= 3.866$$

and since the difference between these assumed values is equal to the capacitor voltage, $E_{cap} = 2.366$, immediately prior to restrike as follows

$$E - E_1 = 0.933 - (-1.433) = 2.366$$

it can be concluded that the assumed instantaneous voltage distribution immediately following restrike is a valid one.

These assumed values could, of course, be determined, and, in fact, they have been, by setting up and solving simultaneous equations.

Once the restrike has occurred, and the terminals A-a have been bridged by an arc, the voltage $E_A = E_a$ will immediately start to change from its immediate post-restrike value of $E = E_A = E_a = 0.933$ back to the steady sinusoidal variations established by the source.

In the first instants of this transient interval it will try to assume the value of $E_A = E_a = -1.0$. However, because of the intertia inherent in the system it will overshoot. If the system is truly lossless, as shown in Fig. 10, the overshoot will be 100%, the maximum system overvoltage will be 2.933 times normal, and the transient oscillation will have an infinite decay time. If, however, the realistic condition of losses exists, the overshoot will be less than 100%, the maximum system overvoltage will be less than 2.933 (for 60% overshoot it will be only 2.15), and the transient will attenuate quite rapidly.

The maximum overshoot voltage for a circuit having an overshoot ratio of P% is

$$E_o = 1 + 1.933 \frac{P}{100} \text{ pu}$$

The conditions depicted in Fig. 11 are similar to those discussed for Fig. 10. They differ in that the restrike in phases A and C occurs at t_1 1/12 cycle later than in Fig. 10. In this case the recovery voltage is

$$E_r = E_a - E_A - (E_c - E_C)$$
$$= 1.5 + 0.866 + 0.866 + 0.866 = 4.096$$

and the trapped voltage on the capacitor is

$$E_{cap} = E_a - E_c$$
$$= 1.5 - (-0.866) = 2.366$$

As was shown in a previous paper,[1] the above value of $E_r = 4.096$ is the largest possible value of recovery voltage for the circuit of Fig. 11.

Pursuing the same logic that was followed in the case of Fig. 10, but assuming in this case that

$$E = E_A = E_a = 1.182$$

$$E_1 = E_C = E_c = -1.182$$

it is apparent that

$$E_A - E_\alpha = 1.182 + 0.866 = 2.048$$

and

$$E_\gamma - E_C = 0.866 + 1.182 = 2.048$$

so the voltages across the A and C phase reactances X are equal. Furthermore, the additional required conditions that

$$E_r = E_A - E_\alpha + E_\gamma - E_C$$
$$= 2.048 + 2.048 = 4.096$$

and

$$E - E_1 = 1.182 - (-1.182) = 2.366$$
$$= E_{cap}$$

are satisfied (except for round-off errors).

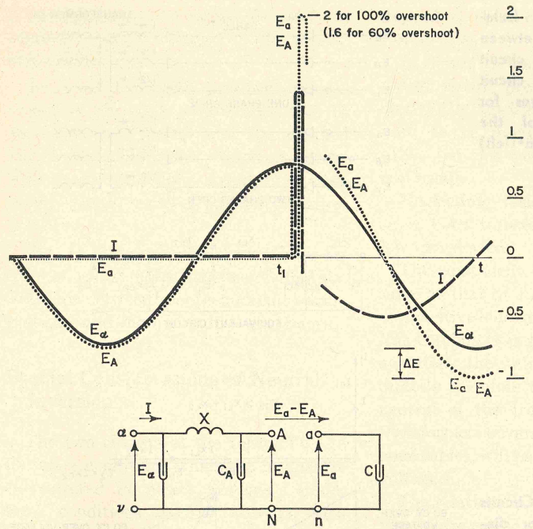

Fig. 13. Circuit, voltages, and current considered in the single-phase capacitive energizing case (left)

Fig. 14. Circuit and voltages considered in the 3-phase capacitive energizing case (right)

In this case the overvoltages are 2.914 times normal for 100% overshoot, and 2.12 times normal for 60% overshoot. Or for P% overshoot

$$E_o = 0.866 + 2.048 \frac{P}{100} \text{ pu}$$

Finally, Fig. 12 represents the case in which a restrike occurs at t_1 in phase A (following an interruption at t_a) before phases B and C have interrupted. The recovery voltage at the time of restrike, t_1, is three times normal, and the total capacitor voltage from point a to point b in the circuit is 1.5 times normal. The principal difference between this and the previous cases is that phases B and C in this case are effectively in parallel as shown in the equivalent circuit of Fig. 12.

The result is that the net reactance of the paralleled phases C and B is half that of phase A; so it will absorb only 1/3 of the recovery voltage.

The voltages E_a and E_A shift to $E = 1$ while $E_b = E_B$ and $E_c = E_C$ go to $E_1 = -0.5$.

The recovery voltage is $E_r = 3$, so,

$$E_A = E_\alpha = 1 + 1 = 2$$

$$E'' - E' = 0.5 + 0.5 = 1$$

The required condition that

$$E_A - E_\alpha + E'' - E' = E_r$$

is satisfied, and the requirement that

$$E_{cap} = E_a - E'$$
$$= 1 + 0.5 = 1.5$$

is met; therefore the previously assumed values $E_A = 1$ and $E' = -0.5$ are correct.

The overvoltage in phase A is 3 times normal for a 100% overshoot ratio, or 2.2 times normal for a 60% overshoot ratio. For P%

$$E_o = 1 + 2 \frac{P}{100} \text{ pu}$$

Phases B and C reach voltages of 1.5 and 1.1 times normal for these respective overshoot ratios.

Energizing Single-Phase Capacitive Circuits

The events accompanying the energizing of a single-phase capacitor bank and the circuit under consideration are shown in Fig. 13.

Since the worst overvoltage condition that can occur attends closing at the peak of supply voltage, as at t_1 in Fig. 13, this is the most interesting case to investigate. This case is even more pertinent to the practical situation if the closing switch is one whose closing contact velocity is slow in comparison to the power frequency period. Such a contact velocity will almost certainly insure that the closure of the circuit will be accomplished by a sparkover of the closing contacts at, or near, a peak of voltage.

Prior to t_1 the voltages at terminals α and A will be about the same: $E_A \cong E_\alpha$. At the instant of closing E_A drops to zero, the voltage of the large uncharged capacitor, compared to which C_A is negligible. Momentarily the total source voltage, E_α, is absorbed by the line reactance X because at the first instant of closure C appears as a short circuit.

Following this momentary dip, E_A starts to swing toward the value $E_A = E_a \cong 1$ which would, in a normal steady-state condition with the switch closed, be its value at t_1. In the absence of damping,

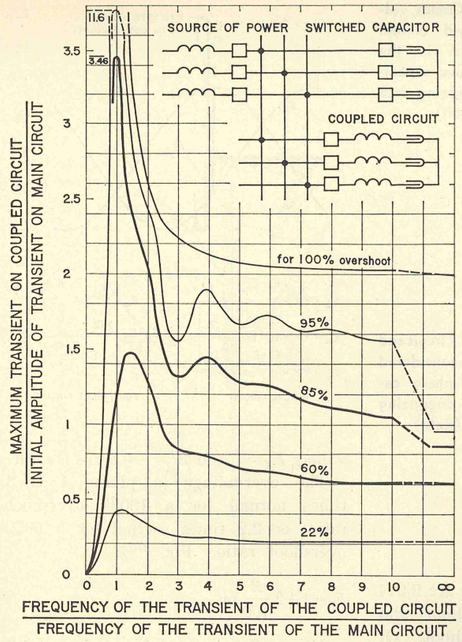

Fig. 15. Relationship between coupled circuit and main circuit overvoltages for circuits of the type shown[3] (left)

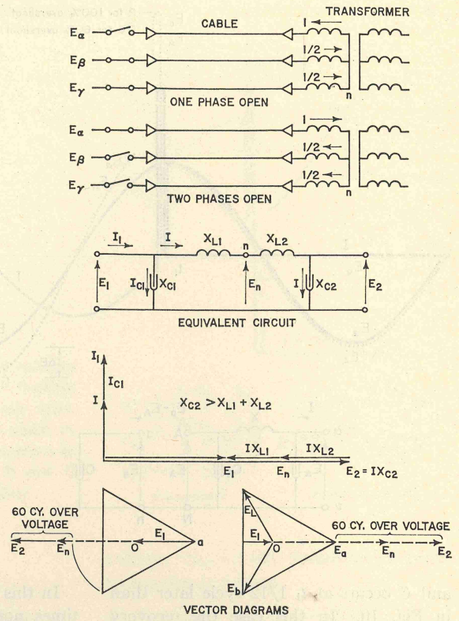

Fig. 16. Circuits and vector diagrams considered in the case of neutral inversion (right)

it overshoots 100% to twice normal peak voltage. With enough damping to cause a 60% overshoot ratio it would go to 1.6 times normal peak voltage. For P% overshoot ratio

$$E_o = 1 + \frac{P}{100} \text{ pu}$$

Energizing 3-Phase Capacitive Circuits

For the 3-phase ungrounded case, Fig 14 shows the pertinent circuit and curves. The maximum overvoltage occurs, as in Fig. 13, when the switch is closed at the peak value of one phase voltage after the other two phases have previously closed. In this example, closure is assumed at t_1, the peak of phase A voltage. At this instant terminals b and c are at the same voltage

$$E'' = \frac{E_\beta + E_\gamma}{2}$$

$$= -0.5$$

This suggests the equivalent circuit of Fig. 14 in which

$$E'' = \frac{E_\beta + E_\gamma}{2}$$

and

$$E' = \frac{E_B + E_C}{2}$$

The total voltage across the equivalent circuit terminals at t_1 equals 1.5; so immediately after closure of the circuit this voltage must be absorbed by the line reactances, X and $X/2$.

The phase A line reactance will assume twice as much voltage

$$E_\alpha - E_A = 1 - 0 = 1$$

as does the net impedance of the paralleled phases B and C

$$E_B - E_\beta = E_C - E_\gamma$$

$$= 0 + 0.5 = 0.5$$

Applying the same logic in this case as before reveals that $E_A = E_B = E_C = 0$ at the instant of closure, t_1, satisfies the requirements to justify this as a valid assumption for the case of Fig. 14.

In swinging back to their steady-state variations, an overvoltage of twice normal appears in phase A without damping, while a 60% overshoot ratio results in an overvoltage of 1.6. For P% overshoot

$$E_o = 1 + \frac{P}{100} \text{ pu}$$

It is interesting that in capacitor switching the maximum overvoltages are the same for single-phase or 3-phase switching, whether the system is grounded or ungrounded, i.e., three times normal on restrikes and twice normal on energizing. This is in contrast to the comparative recovery voltages which differ widely, to the extent of a ratio of more than two.

Overvoltages on Coupled Circuits

Up to this point the investigation of capacitor switching has been directed at the overvoltages produced by restrikes or prestrikes of switches located at the terminals of the capacitor being switched. Frequently, in addition to the source-capacitor circuit, there are other circuits present which are capable of oscillating at frequencies not very different from the frequency of the main circuit considered.

For instance, the bus on which switching occurs may be connected through a transformer to a distribution line at the end of which there are one or more smaller banks. If, by coincidence, in such a situation the frequencies of the main and coupled circuits happen to be not very different, a resonance-like phenomenon may raise the overvoltage on the coupled circuit to values very much higher than those produced on the main circuit.

At exact resonance with very small damping this may be as high as 11.6 times the initial transient amplitude in the main circuit, as shown in Fig. 15.[3] It may be as much as 3.46 times the initial main circuit transient amplitude with practical damping ratios. The frequencies of the main and coupled circuits will be equal if switching the two capacitors produces equal percentage voltages on the respective circuits.

To avoid too many variables, the assumption was made in preparing Fig. 15 that the main circuit and the coupled circuit have the same overshoot ratios. This is a reasonable assumption since damping ratio is rather uniform on power systems.

Fig. 15 represents the quantitative results of an extensive analysis of the relationship between coupled-circuit overvoltages and main-circuit overvoltages.

Special Considerations of Neutral Inversion

The two circuits at the top of Fig. 16 illustrate conditions which are frequently encountered in power systems. Under these conditions neutral inversion with accompanying high overvoltages can occur. This condition would arise if the switch opens one phase long enough ahead of the other two (or if it keeps one phase closed after opening the other two) to permit the intervening transients to die down.

For either case the equivalent circuit is the third figure from the top, but $X_{L1} =$ while $X_{L1} = 2X_{L2}$, and $X_{C1} = 2X_{C2}$ for one line closed, while $X_{L1} = X_{L2}/2$, and $X_{C1} = X_{C2}/2$ for one line open.

It can be seen that the capacitive charging current of the cable flows through the transformer in a manner reminiscent of normal 3-phase magnetizing currents; consequently the reactances X_{L1} and X_{L2} are the large magnetizing reactances rather than the small leakage reactances. In fact, these can be easily of the same order of magnitude as the cable-charging reactances, X_{C1} and X_{C2}, depending upon cable length and transformer size.

It should be mentioned that the equivalent circuit presupposes some type of electrically shielded cable, and it would need to be modified for belt-insulated cable, but this would not affect the general result.

Neglecting resistances is reasonable since both transformers and cables are low-loss devices.

The equivalent circuit obviously is the same as that of an inductive line feeding a capacitive load, and it is well known that this combination results in a rising voltage along the inductive line. It follows directly therefore that the voltage at the neutral of the transformer, and at the transformer terminals connected to the open cables, will be higher than the supply voltage E_1.

The relations of the vector diagrams of Fig. 16 are easily solved to yield

$$E_n = E_1\left(\frac{X_{C_2} - X_{L1}}{X_{C_2} - X_{L1} - X_{L_2}}\right)$$

$$E_2 = E_1\left(\frac{X_{C_2}}{X_{C_2} - X_{L1} - X_{L^2}}\right)$$

Specifically if E_α is the normal phase voltage, X_C is the capacitive reactance of one cable phase, X_L is the magnetizing reactance of one phase of the transformer, and one line is closed,

$$E_n' = E_\alpha\left(\frac{X_C - 2X_L}{X_C - 3X_L}\right)$$

$$E_2' = E_\alpha\left(\frac{X_C}{X_C - 3X_L}\right)$$

For one line open and $X_C > 1.5\ X_L$,

$$E_n'' = \frac{E_\alpha}{2}\left(\frac{X_C - X_L}{X_C - 1.5X_L}\right)$$

$$E_2'' = \frac{E_\alpha}{2}\left(\frac{X_C}{X_C - 1.5X_L}\right)$$

Using these relations, the 60-cycle overvoltages for one line closed and $3X_L < X_C < 6X_L$ are readily available as

$$\text{60-cycle overvoltage} = E_\alpha\left(\frac{6X_L - X_C}{X_C - 3X_L}\right)$$

For one line open, and $1.5\ X_L < X_C < 3X_L$

$$\text{60-cycle overvoltage} = \frac{E_\alpha}{2}\left(\frac{3X_L - X_C}{X_C - 1.5X_L}\right)$$

It can be seen from these equations that one of these overvoltages could become very large if either $X_C \cong 3X_L$ or $X_C \cong 1.5X_L$.

Of course, the infinite value of voltage which is indicated for exact equality will not develop since the rise of the voltage will be checked after a while by saturation and resistance. Nevertheless, substantial overvoltages can occur in cases of unfortunate coincidences.

Conclusions

It is hoped that this paper will be looked upon as an introductory review and that it will serve as a stimulus to conduct a more detailed analysis of the overvoltage situations discussed herein.

References

1. Some Fundamental Aspects of Recovery Voltages, **J. Zaborszky, J. W. Rittenhouse.** See pp. 815–22 of this issue.

2. Selecting Damping Resistors for Vacuum Switches in Bank-to-Bank Switching, **J. Zaborszky, J. W. Rittenhouse, E. L. Luehring.** *AIEE Transactions*, pt. III-A (*Power Apparatus and Systems*), vol. 78, Apr. 1959, pp. 18–22.

3. Capacitor-Switching Phenomena with Resistors, **R. C. Van Sickle, J. Zaborszky.** *Ibid.*, pt. III-B, vol. 73, Aug. 1954, pp. 971–77.

A reprint from **POWER APPARATUS AND SYSTEMS,** published by The Institute of Electrical and Electronics Engineers, Inc.
Copyright 1963, and reprinted by permission of the copyright owner
The Institute assumes no responsibility for statements and opinions made by contributors.
Printed in the United States of America

February 1963 issue

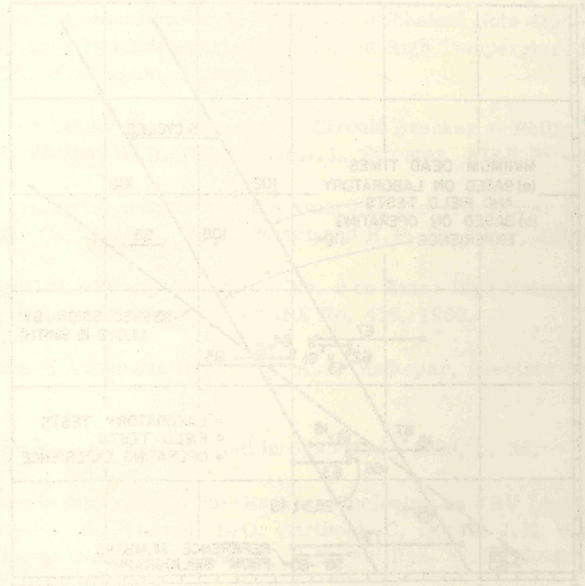

Transactions Paper

(Reviewed and Accepted for Publication)

Discussion in Duplicate Due July 5, 1963.

ARC DEIONIZATION TIMES ON HIGH SPEED THREE POLE RECLOSING

IEEE Working Group on Arc Deionization Times
of the
General Systems Subcommittee
of the
IEEE Transmission and Distribution Committee

A paper recommended by the IEEE Transmission and Distribution Committee and approved by the IEEE Technical Operations Committee for presentation at the IEEE Summer General Meeting and Nuclear Radiation Effects Conference, Toronto, Ont., Canada, June 16-21, 1963. Manuscript submitted April 20, 1962; made available for printing April 18, 1963.

Members of the IEEE Working Group on Arc Deionization Times of the General Systems Subcommittee: H. M. Ellis, Chairman; O. A. Demuth, L. O. Barthold, A. E. Kilgour, D. F. Shankle, E. T. B. Gross, R. E. Stade.

Price: $ .60 To Members
$1.00 To Nonmembers

(10¢ per copy additional if first class mailing desired)

(Minimum Mail Order $1.00)

All Rights Reserved by
The Institute of Electrical and Electronics Engineers, Inc.,
P. O. Box A,
Lenox Hill Station,
New York 21, N. Y.

Litho in USA

Paper No.
63-938

ARC DEIONIZATION TIMES ON HIGH SPEED THREE POLE RECLOSING

by IEEE WORKING GROUP ON ARC DEIONIZATION TIMES
OF THE GENERAL SYSTEMS SUBCOMMITTEE*

SUMMARY

A review has been made of the available technical literature on arc deionization times of the fault arc for successful high speed three pole reclosing. Laboratory and field tests as well as operating experience were summarized and estimates made of the minimum deionization times as a function of voltage.

INTRODUCTION

With the high capital investment required today for high voltage transmission systems, high speed reclosing is recognized by transmission engineers in North America as one of the most economical methods of:

1. Increasing the maximum power which can be transmitted over long high voltage transmission lines without loss of synchronism following a fault. The importance of reclose time is shown by the fact that the transient stability of a system can be improved by twenty-five per cent to fifty per cent by reducing the reclose time from thirty-five to twenty-five cycles.[67]

2. Reducing system disturbance by reclosing before large swings occur between two parts of a system.

3. Reducing line outage time and improving service to customers.

4. In low lightning areas it is possible to reduce the capital investment in the transmission line by eliminating the overhead groundwires and special tower grounding by employing high speed reclosing.

Unfortunately, because of the number of variables affecting the dead time required to ensure deionization of the power arc, the results of many tests under various conditions, as well as operating experience, must be analysed in order to select dead times which ensure dependable performance of a reclosing system.

Factors affecting deionization time are as follows:

1. Magnitude of the short circuit current. In general, the higher the fault current, the larger the amount of ionized gas generated. This may be offset by the greater turbulence in the air and the magnetic blowout action, both of which increase with higher current.

2. Duration of the short circuit current. The longer the fault current flows, the greater

*The members are: H.M. Ellis, Chairman; O.A. Demuth, L.O. Barthold, A.E. Kilgour, D.F. Shankle, W. Watson, E.T.B. Gross, R.E. Stade.

the amount of ionized gases. This is offset also by greater turbulence, longer magnetic blowout action and thermal convection currents in the air.

3. Magnitude and duration of capacitive and magnetic coupling current which may flow due to induced voltage from adjacent conductors which remain energized. This assumes particular importance for single pole reclosing or for three pole reclosing of one circuit on a double circuit line.

4. Magnitude and duration of resistance follow current which flows through shunting resistors on some types of circuit breakers.

5. Magnitude of re-energization voltage applied.

6. Point of wave at which circuit is re-energized. This determines the magnitude of the surge and will account for much of the randomness of the results obtained.

7. Magnetic forces on the arc due to circuit configuration.

8. Length of insulator string which determines the minimum length of the flashover path.

9. Weather conditions - particularly the wind effect.

10. Shape of grading rings and other parts which determine dielectric stress on reapplication of voltage.

In addition to the above factors which affect the required dead time for a successful reclosing cycle, the following factors will limit the percent successful reclosing sequences:

1. Permanent faults resulting from mechanical failures and foreign objects (estimates indicate up to twenty-five per cent for wood pole lines and less than five per cent for steel tower lines[12]).

2. Multiple component lightning strokes with a duration greater than the total reclose time. Some ten per cent of strokes have durations greater than 0.40 seconds (twenty-four cycles) and thirty per cent greater than 0.20 seconds (twelve cycles).[101] Hence the stroke duration places a real limitation on the minimum reclose interval.

Fortunately, the deionization time required for each stroke component is less than one half cycle, hence, no appreciable increase in dead time is required to allow for the deionization of multiple components.[40]

Definition of High Speed Reclosing Cycle

By definition, reclosing time of a circuit breaker is the time required from energizing the circuit breaker trip coil to the re-contacting of the arcing contacts.

Reclosing times of thirty-five cycles or less are considered as high speed. A reclose is considered successful only if both ends reclose. As a measure of successful reclosing on the basis of deionization time, a percentage successful is tabulated strictly on a reignition bases where possible. The deionization time is the time from final fault current zero to the re-establishment of voltage on the faulted circuit. Where secondary current flow extends beyond final current zero of

the main fault current, this should be noted as a separate parameter.

SUMMARY OF LABORATORY AND FIELD TESTS

Sporn and Prince[18] carried out some 250 laboratory tests simulating the reignition characteristics of a string of insulators at 132 kv, with a restriking voltage of 80 kv under 0-20 m.p.h. wind conditions with fault current of 800 to 6,000 amperes. At 800 amperes and 0-5 m.p.h. wind the minimum dead time was 7 to 8 cycles, whereas with 6,000 amperes it was 10 to 12 cycles. Increasing the wind to 10 to 20 m.p.h. reduced the dead times to 5 to 6 cycles and 9 to 10 cycles, respectively. The study concluded that a minimum dead time of 12 cycles was necessary to provide little probability of a restrike. This might be reduced to 10 cycles with over ninety per cent probability of successful reclosure.

A reclose time of 21 to 22 cycles was obtained during field tests of high speed reclosing on a fifty-nine mile 132 kv line. On all tests the line was successfully re-energized without restriking of the arc for a dead time of 10.7 to 12 cycles for a line to ground fault. For the case of a line-to-line fault, the line was de-energized for 11.5 to 14.1 cycles but only for 14 cycles dead time was re-energization successful. For a double line to ground fault, the re-energization was successful with a dead time of 13.3 cycles.

McCann and Clark[40] determined that for an impulse type gap discharge with varying magnitude and wave shape, the gap recovery to fifty per cent of initial strength occurs in less than one half cycle, i.e. capable of withstanding normal power frequency voltage. Hence lightning discharges have a negligible effect on reclosing times. However, the time element introduced by multiple strokes must be considered in determining the reclose time in addition to the rate of recovery of dielectric strength of the power arc.

Schwager[43] describes tests carried out on a single phase 230 kv, 2500 MVA oil circuit breaker employing a high speed spring operating mechanism where contact opening speeds of 28 feet per second and reclosing time of 17 cycles (13 cycle dead time) were obtained.

Dovjikov and Diemond[61] carried out reclosing tests on a 220 kv, 50 cycle, 2500 MVA, AEG Free Stream Air Blast Circuit Breaker on the Bonneville Power Administration System. Three-phase to ground fault currents of 1,350 amperes were interrupted in 6 to 7 cycles and reclosed successfully with a dead time of 12 to 14 cycles, giving a reclose time of the order of 18 to 21 cycles. For a dead time of 6 to 7 cycles and a reclose time of 12 to 14 cycles, the reclosure was unsuccessful. The fault was applied across a string of sixteen five-inch insulators for a fault length of eighty inches. The paper indicates that minimum possible deionization time of a fault arc across a sixteen-unit insulator string may range between 8 and 12 cycles. Similar high speed reclosing tests carried out on the 230 kv, sixty-two mile Mettlen-Lavorgo line in Switzerland by Shar and Baltensperger[84] for line-to-line faults resulted in a dead time of 0.25 seconds (15 cycles) for successful reclosure.

Boisseau, Wyman and Skeats[67] reported minimum deionization times for insulator flashovers on 69 to 230 kv circuits under varying conditions. When capacitive coupling is not present, the de-energization time increases linearly with fault current on 230 kv systems, is practically constant on 132 kv systems and decreases at high currents on 69 kv systems. The duration of the fault current did not show any appreciable effect at 230 kv for an 8,000 ampere fault current with fault durations from 2 to 10 cycles, however, the deionization time increased by some 3 cycles (from 7 to 10 cycles) when the reclosing occurred at voltage maximum rather than voltage zero. All data are given

for voltage maximum condition. High speed three-pole reclosing on double circuit transmission lines requires 1 or 2 cycles additional dead time to allow for capacitive coupling from the unfaulted circuit for coupled voltages of less than 10 kv. The magnitude of the coupled voltage appears more significant than the arc current as 5 ampere arcs required as long to interrupt as 50 ampere arcs. Calculations indicate that coupled voltages on 230 kv double circuit lines are of the order of 5 kv untransposed and 3 kv transposed.

The dead time for 60 kv circuits varied from 6 to 9 to 6 cycles for fault currents from 1,000 to 8,000 to 22,000 amperes. The dead time at 132 kv was constant over the 8,000 to 22,000 ampere range at 9 cycles. For 230 kv the dead time increased from 8 to 14 cycles for fault current increasing from 1,000 to 22,000 amperes. Tests made on circuit breakers equipped with resistors indicate that the resistor current duration can affect the dead time, particularly for reclosing of long lines.

Harrington and Starr[66] suggest that the limitation on high speed reclosing may be the duration of multiple lightning strokes. Meager data available to the authors indicates that ten per cent of strokes persist for more than 0.25 seconds or 15 cycles. Tests were performed on the BPA 115 kv system to obtain data on deionization of fault-arc paths produced by SLG faults of 3,000 to 15,000 amperes of varying duration. In preliminary deionization tests at 13.8 kv, recovery was rapid, never exceeding 3 cycles from current interruption to full recovery of rated voltage for fault currents in the range 600 to 1,000 amperes. In the 115 kv tests, it is assumed that recovery is complete when the recovery voltage has reached 150 per cent of normal voltage. This corresponded to a fault path resistance of 0.25 megohms. The authors conclude that deionization time is primarily a function of fault duration. It is estimated that 10 cycle dead time is required for a 4 cycle fault, 7 cycles for a 3 cycle fault, and 5 cycles for a 2 cycle fault on a 115 kv system at a fault current of 11,000 amperes.

McCann, Conner and Ellis[71] report the effect of arc length, current magnitude and duration on the dielectric recovery characteristics of 6 and 11 inch air gaps. The results indicate minor effect of current magnitude and duration of arc on the recovery characteristics and that the recovery is approximately proportional to the length of the arc. The time required for recovery of fifty per cent of the dielectric strength of the gap was approximately 5 cycles for 300 and 800 ampere fault currents with no wind. This was reduced to 1 and 2 1/2 cycles with a wind velocity of the order of 10 and 5 m.p.h., respectively. This indicates the relative importance of wind in assessing recovery characteristics.

Thoren[79] describes high speed reclosing tests carried out on a 30 kv distribution system to determine the necessary dead time to deionize arcs caused by line faults and the effect of motor load on the deionization period. The results show a small affect of fault current magnitude on dead time. The dead time required was generally less than 0.10 seconds (6 cycles) with the longest dead time of 0.15 seconds (9 cycles). To allow for motor loading on feeders the dead time increased to 0.20 to 0.25 seconds (12 to 15 cycles) in order to ensure successful high speed reclosing.

Three-pole reclosing tests were carried out on Russian 400 kv transmission lines having lengths of 117 and 635 Km (72 and 397 miles) including the effect of shunt reactors by Maikopar and Beliskon[102]. The fault current magnitude was 2,000 amperes and the duration 0.16 seconds (9.6 cycles of 60 cycle fault current). Successful three-pole reclosing was obtained with total reclosing times of 0.27 to 0.30 seconds (16 to 18 cycles on a 60 cycle system). For shunt reactors connected to the line section disconnected, the time could be reduced to 0.20 to 0.25 seconds (12 to 15 cycles on a 60 cycle system).

SUMMARY OF OPERATING EXPERIENCE

On four single-line-to-ground faults on the 59-mile Fort Wayne-Deer Creek 132 kv line[18], the average dead time was 13.0 cycles with a total reclosing time of 22 cycles and there was no arc restriking. Sporn and Prince concluded as early as 1937 that on high voltage overhead lines, outages caused by lightning might be reduced some 75 per cent by ultrarapid reclosing.

Nine years of operating experience of high speed reclosing on 66 and 132 kv lines of American Gas and Electric are described in references 25, 34 and 45 by Sporn and Muller. Reclosing time was adjusted for 20 cycles with 12 cycle dead time. Experience includes 635 cases of flashover on 66 and 132 kv lines. Of the total, 531 were on single circuit lines and 104 on double circuit lines.

Successful Reclosures	570 (90%)
Unsuccessful Reclosures	65

Of the 65 unsuccessful reclosures, 8 were permanent faults. Some unsuccessful reclosures were due to relay operations due to swings between two systems while others were a result of a line dead time of 3 to 4 cycles when trouble occurred on a double circuit line and clearing was not simultaneous at all terminals. On a reignition basis, the percentage of successful reclosures is considerably better than 90%.

Jancke[58] describes experiences of Swedish State Power Board up to 1948 with high speed reclosing on large 220, 132 and 44 kv networks. Reclosing was first placed in service in 1933 on a 44 kv radial line. Dead times of up to 0.15 seconds resulted in a large percentage of unsuccessful high speed reclosures on temporary faults. Operating experience with 1084 disturbances were based on dead times of 0.20 to 0.25 seconds:

885 (82%) - successful high speed reclosing
154 (14%) - unsuccessful high speed reclosing but successful reclosure in three minutes
45 (4%) - permanent faults.

Since 45 of the faults were permanent, the successful reclosing percentage is increased to 85%. Also, during the period 1940-1943, faults caused by drifting barrage balloons resulted in unsuccessful reclosure which would account for part of the 154 unsuccessful reclosures. Tests established a dead time of 0.25 to 0.30 seconds at 220 and 132 kv for a total fault time, including relay time of 0.11 seconds. Experience with 14 high speed reclosures is as follows:

8 - successful (57%)
1 - unsuccessful - permanent fault
3 - unsuccessful - circuit breaker fault or other station fault
2 - system instability.

On the basis of reignition only, the percentage successful would increase to 100%.

Operating experience is given from 1945-1948 with high speed reclosing on two 114 kv lines of New York State Electricity and Gas Corporation by Dana[63]. Reclosing time was 20 cycles with 12-15 cycles of dead time. Experience is as follows:

Successful Reclosures	31 (78%)
Unsuccessful Reclosures	9

Naef and Wild[60] report on high speed reclosing on an 8 kv distribution system. The reclose time is 18 cycles with a dead time of approximately 14 cycles. Statistics for the 8 kv network are tabulated below:

Successful Reclosures	67 (64%)
Unsuccessful Reclosures	37

In twenty out of the thirty-seven unsuccessful reclosures the breaker could be reclosed manually. If it is assumed that the remaining seventeen were permanent faults, the successful reclosures increase to 78%. Laboratory tests were carried out by the authors to determine the required dead time at 6 to 10 kv for fault currents in the 3,000-8,000 ampere range. The tests indicated that the effect of current, voltage and gap separation were very slight on arc deionization time. There were no reignitions of the arc for a dead time of over 3 cycles, therefore, the authors concluded that in the 10 kv range a dead time of 6 cycles should be sufficient to avoid reignition of the arc.

Operating experience on the 230 kv system of BPA, 1950-54 is described by Gillies[83]. Reclosing times were initially set at 45 to 60 cycles but have been reduced to 20 cycles with a trial installation of 15 cycles. For dead times of 20 cycles or less, the experience is as follows:

Successful Reclosures	87 (85%)
Unsuccessful Reclosures	12 - permanent faults
	3 - resulted in reignition.

Thus, 96% of the reclosures were successful based on temporary faults. BPA's objective is to establish practical limits of high speed reclosing by reducing the reclose time until failures due to insufficient deionization or repetitive strokes become too high. The author indicated that high speed reclosing provides a means of lightning protection that is now considered preferable to the use of overhead groundwires.

Two years of high speed reclosing experience on twenty 345 kv lines of American Electric Power is described by Barnes, Hauspurg and Kinghorn[95]. As there was no previous experience with reclosing times at 345 kv, the dead time was determined by extrapolation of existing data to 345 kv. Principal factors influencing the dead time were: magnitude of fault current, point of wave at which reclosing occurs and capacitance coupling of parallel energized circuits. Calculations indicated a reclose time of 37 cycles, however, based on a reasonable fault magnitude and other factors, a reclose time of 28 cycles was used. Operating experience is as follows:

Successful Reclosures	90 (59)
Unsuccessful Reclosures	11 - permanent faults
	28 - reignitions
	23 - successful reclose from one end.

Considering only reignitions as unsuccessful exclusive of permanent faults, the successful reclosure would amount to 80%. Further cataloguing of the data on a purely reignition basis indicates the following:

		Single Circuit	Double Circuit
Lightning	Successful	40 (100%)	58 (94%)
	Unsuccessful	0	4

		Single Circuit	Double Circuit
Sleet	Successful	15 (39%)	
	Unsuccessful	24	

The authors point out that analysis under sleet conditions is difficult but that performance was disappointing. Indication is that success under sleet conditions is a function of mechanical design factors of the line. The success in reclosing for single circuit against double circuit lines (100% vs. 94%) suggests that coupling from energized circuit has an effect although the authors state that there is no effect on required dead time for lines under 62 miles in length. Conclusion reached by the authors is that reclosing time is adequately long for lightning flashovers and possibly could be shortened. Further study is required as to record under sleet conditions and the effect of coupling voltage on double circuit lines. In discussion, Mr. B. L. Lloyd commented that a study of available laboratory tests and operating experience indicated a consistent trend in required dead time with increasing voltage.

With 28 cycle reclosing time (equivalent to approximately 24 cycle dead time) the 345 kv lines of American Electric Power Company and the Ohio Valley Electric Corporation were re-energized after lightning faults from one or both ends 96% of the time. Field tests reported by Porter and St. Clair[105] in 1957 indicated that the reclosing time could be reduced substantially in areas experiencing moderate short circuit duties without appreciably decreasing the percentage successful reclosures. Accordingly, in 1958 all AEP lines were changed to 22 cycle reclosing (equivalent to a dead time of approximately 18 cycles). Based on lightning faults, the lines were successfully re-energized 22 times out of 23 operations (96%). Thus reducing the reclosing time to 22 cycles has not changed the overall performance.

Further field tests were carried out at 345 kv by Naef, Phelps, Wilson and Streater[104] at the Philip Sporn Power Plant. Six fault tests were initiated across an 18 unit suspension insulator string with a reclosing time of 15 to 16 cycles. On four tests the reclosure was successful and on two tests the arc restruck across the insulator. The average dead time on these tests was 12 cycles, some 7 cycles less than the minimum now used on the AEP system.

A Task Force under Mr. I. B. Johnson[109] made extensive system fault tests to obtain precise data on fault arc de-energization times at 345 kv at fault current levels including 20,000 amperes, to explore the effects of coupling from an adjacent twin circuit line and the severity of reclosing transient voltage as a function of fault location and angle of reclosing on the source voltage. The required dead time on the 345 kv system was indicated in the following relationship:

$$T = 9.0 - 0.057\,Ka + 0.0075\,Kv + 0.00053\,KaKv$$

where T = dead time in cycles on a 60 cycle system
Ka = RMS current in first cycle of fault current
Kv = crest value of reclosing voltage.

For example, at 10,000 amperes fault current and a 2.0 p.u. crest reclosing voltage, the dead time would be 16.6 cycles. This compares with the minimum dead time of some 16 cycles at 345 kv shown in Fig. 1 of this report.

A report of the work of CIGRÉ Study Committee No. 9[106] summarizes the reclosing performance of seven countries. The percentage successful reclosure where the line was restored to service almost immediately is as follows:

Type of Fault	% Successful Reclose
Lightning	83%
Fog	87%
Icing	12%
Other Faults	54%
Overall Performance	70%

Generally speaking, the auto-reclose of EHV circuits is very successful in clearing non-persistent faults, such as caused by lightning and fog and very poor for sleet and ice fault conditions.

A Russian report by Maikopar[107] contains a summary of twenty-nine references on three-pole and single-pole reclosing including the dead time required for reclosing at different voltages. The conclusions are that single and multiple lightning strokes do not affect the dead time required due to the brevity of their duration and rapid recovery of dielectric strength on the lightning channels; wind plays an important part in the recovery of dielectric strength; and the dead time increases with current duration up to a point where the volume of luminous gases ceases to increase due to the upward convection of cold air currents and may even decrease. At higher voltages the insulator string is longer and the effect of the convection currents is less, thus resulting in a longer deionization time.

If the influence of the duration of the short circuit and wind speed are ignored, the basic factors influencing the dead time are the magnitude of current and line voltage. For comparison purposes the range of required dead times obtained in this paper are shown in Table I.

COMMENTS AND CONCLUSIONS

Table I and Figure I summarize the results of all data analysed by the committee on the minimum deionization times of the fault arc for successful three pole high speed reclose.

The summary of laboratory and field tests versus operating experience indicates an increased allowance of some 5 cycles for a minimum dead time under operating conditions as compared with test results for successful three-pole reclosing. Where the variables influencing the required dead time allow, it may be possible to reduce the dead time under operating conditions closer to the minimum as determined under laboratory and field test conditions. Certainly further basic research into ion behavior and arc deionization characteristics should be carried out in order to increase our understanding of the parameters affecting the minimum dead time.

The following factors influence the minimum arc deionization or dead time:

1. Circuit breaker with resistor.

   The additional dead time required for resistor current duration following clearing of the main fault current appears to vary with the conditions. Conservatively, the dead time should be increased in accordance with resistor current duration.

2. Capacitive and inductive coupling from a parallel circuit on a double circuit line.

   Only a small amount of information is available at 230 kv on this point which suggests that a small current flow will continue for several cycles beyond the clearing of the fault. Because of the small amount of ionization and short duration of sustained current, no additional dead time was considered necessary. At higher voltages, this may assume increased importance.

3. Swing angle between the two parts of the system when reclosure occurs.

   The angle of swing will introduce a switching transient proportional to the angular difference between the system which, according to one reference, increases with line length.

4. Multiple component lightning strokes having a duration greater than the reclosing time.

   Based on statistical data available, 10% of strokes have durations exceeding 0.40 seconds (24 cycles) and 30% greater than 0.20 seconds (12 cycles). This duration will not have much effect on reclose times for system voltage above the 345 kv level as dead times are of this order of magnitude.

5. Additional factors which affect deionization time include wind, arc current magnitude and duration, rate of rise of recovery voltage and magnitude of recovery voltage, etc.

A considerable amount of operating experience on three pole high speed reclosing is now available; unfortunately, much of this data has not been compiled in sufficient detail to provide a dependable basis for analysis of operating experience. There is much to be gained by up-to-date tabulation of the operating experience of high speed reclosing as operating data is the proving ground for reclosing times and arc deionization times. With the present widespread use of automatic monitoring equipment, the analysis of this operational data should be greatly facilitated. There is at present no standard for classifying reclosing data. Accordingly, the Working Group recommend the recording and classifying of this experience as shown in Table II.

There are a number of arc deionization characteristics which appear to be inconsistent under different conditions. For example, the effects of arc duration and current magnitude vary widely in the different references. Because of the effects of arc configuration, thermal convection currents, magnetic effect of leads, variation in wind, etc., these differences are not surprising. There also appears to be some variation in the required deionization time as a function of the type of fault, i.e. single line-to-ground versus line-to-line.

As more test data and operating experience become available, particularly at system voltages up to 500 kv, the minimum reclosing times for high speed three pole reclosing will become more firmly established and our understanding of the effects of the various parameters on this arc deionization time better understood. The reduction in transmission system investment obtained by possible reduction in the arc deionization time is significant, hence there is a real incentive for carrying out further arc deionization tests particularly at 230 kv and above.

TABLE I

ESTIMATED MINIMUM DEIONIZATION OR DEAD TIME REQUIRED FOR AUTOMATIC THREE-POLE RECLOSING

Rated Voltage	Minimum Deionization Time (Cycles of 60 Cycle) From Ref. No. 107	Based on Laboratory and Field Tests	Based on Operating Experience
23	6 to 7.5	6.5	11
46	-	7	12
69 69	8.5 to 9.6	7.5	12.5
11 115	-	9	14
132	10.2	9.5	14.5
230	11.5 to 15	12.5	17
345	-	15.5	20.5
400	15 to 21	17	22
500	-	20	25

TABLE II - Suggested form of reporting reclosing experience

SUMMARY OF OPERATING EXPERIENCE ON THREE-POLE RECLOSING

SYSTEM
OPERATING VOLTAGE - KV
LENGTH - Miles
CIRCUIT CONFIGURATION - (Single or Double Circuit)
YEARS EXPERIENCE
RECLOSING TIME - Total
- Dead Time
- Secondary Arc due to Resistor, Coupling, etc.

SUMMARY OF RECLOSING OPERATIONS

	Lightning		Sleet			
	Single Circuit	Double Circuit	Single Circuit	Double Circuit	Other	Total
No. Successful						
No. Unsuccessful						
(a) No. Permanent						
(b) No. Reclosed on one end only						
(c) No. Relayed off due to Swing						
(d) No. Failed due to Reignition or Repetitive Lightning Stroke						
% Successful						
% Successful Based on Reignition Failure or Repetitive Lightning Stroke Only						

SUMMARY AND REMARKS

BIBLIOGRAPHY

Prior to 1935

1. Thermal Ionization Theory of Positive Column of Arc, K.T. Compton, Physics Review, 1923, Vol. 21, p. 286.

2. Extinction of an A-C Arc, J. Slepian, AIEE Trans. 1928, Vol. 47.

3. Selecting Breaker Speeds for Stable Operation, R.D. Evans, W.A. Lewis, Electrical World, February 15, 1930, pp. 336-340.

4. Extinction of a Long A-C Arc, J. Slepian, AIEE Trans. 1930, Vol. 49.

5. Extinction of Short A-C Arcs, T.E. Browne, Jr., F.C. Todd, Physics Review, 1930, Vol. 36, p. 726.

6. Restriking of Short Magnetic Arcs, F.D. Todd, T.E. Browne, Jr., Physics Review, 1930, Vol. 36, p. 732.

7. Reignition of Metallic A-C Arcs in Air, S.S. Attwood, W.C. Dow, and W. Krausnick, AIEE Trans. 1931, Vol. 50, p. 854.

8. Extinction of Short A-C Arcs, T.E. Browne, Jr., AIEE Trans. 1931, Vol. 50, p. 1461.

9. Reactance Relays Negligibly Affected by Arc Impedance, A.R. Warrington, Electrical World, No. 48, 1931, pp. 502-505.

10. Theory of Oil Blast Circuit Breakers, D.C. Prince, AIEE Trans. 1932. Vol. 51.

11. Extinction of A-C Arcs in Turbulent Cases, T.E. Browne, Jr., AIEE Trans. 1932, Vol. 51.

12. Keeping the Line in Service by Rapid Reclosure, S.V. Griscom and J.J. Torok, Electrical Journal, May 1933, p. 201.

13. Dielectric Recovery of Turbulent Arcs, T.E. Browne, Jr., Physics, 1934, Vol. 5, pp. 103-113.

1935-1939

14. Das Schaltproblem der Hochspannungstechnik, F. Kesselring and F. Koppelmann, Arch. F. Elektrotechnik, 1935, S. 11.

15. La Frequence Propre et le pouvoir de coupre des disjoncteurs a grande puissance, F. Kesselring, CIGRÉ 1935, No. 131.

16. Anomalous Secondary Electron Emission, A New Phenomenon, L. Malter, Physics Review, 1936, Vol. 49, p. 478.

17. Carrier Relaying and Rapid Reclosing at 110 kv, R.E. Pierce, R.E. Powers, E.C. Stewart, and G.E. Heberlien, Electrical Engineering, Vol. 55, 1936, pp. 1120-29.

18. Ultra High-Speed Reclosing of High Voltage Transmission Lines, P. Sporn and D.C. Prince, AIEE Trans. 1937, pp. 81-90.

19. Sind Hochleistungs-Prüffelder-überflüssig?, F. Kesselring and W. Kaufmann, ETZ 1937, S. 724.

20. Untersuchung einer Bogenentladung mit schnellen Spannungsstössen Wissensch, F. Koppelmann, Verroff, aus dem Siemens-Konzern 1937.

21. Kurzschlussfortschaltung, O. Mayr, VDE Fachberichte 10, 1938, pp. 32-35.

22. Effects of Oxides and Impurities on Metallic Arc Reignition, J.D. Cobine, Physics Review, 1938, Vol. 53, p. 911.

23. Recovery Voltage Characteristics of Typical Transmission Systems and Relation to Protector-tube Application, R.D. Evans and A.C. Monteith, AIEE Trans. August 1938, Vol. 57, pp. 432-40.

24. Power System Transients Caused by Switching and Faults, R.D. Evans, A.C. Monteith, and R.L. Witzke, AIEE Trans. 1939, Vol. 58, pp. 386-394.

25. Experience with Ultra-High-Speed Reclosing of High Voltage Transmission Lines, P. Sporn and C.A. Miller, AIEE Trans. Vol. 58, 1939, pp. 625-636.

26. Application of Heat and Transfer Data to Arc Characteristics, C.G. Suits and H. Poritsky, Physics Review 1939, Vol. 55, p. 1184.

27. Convection Currents in Arcs in Air, C.G. Suits, Physics Review, 1939, Vol. 55, p. 198.

28. Investigations on High Speed Reclosing on the Occurrence of Short Circuits in Overhead Line Systems and the Application of the Air-Blast High-Speed Circuit Breaker for this Purpose, H. Thommen, CIGRÉ 10, 1939, No. 108.

29. Nouveau genre d'interrupteur pour la coupre d'une mise à la terre ou d'un court-circuit, F. Kesselring and W. Kaufmann, CIGRÉ 1939, No. 104.

30. Impulse Characteristics of Oil Gaps for the standpoint of Insulation Coordination, G.D. McCann, Ph. D. Thesis, California Institute of Technology, 1939.

31. Die Löschung von Lichtbogenkurzschlüssen durch Kurzzeitiges Abschalten, W. Kaufmann, ETZ 60, 1939, pp. 241-245.

1940-1944

32. Protector Tubes for Power Systems, H.A. Peterson, W.J. Rudge, Jr., A.C. Monteith, and L.R. Ludwig, AIEE Trans. 1940.

33. Displacement and Diffusion in Fluid Flow Arc Extinction, J. Slepian, AIEE Trans. 1941, p. 162.

34. Five Years' Experience with Ultra-High-Speed Reclosing of High Voltage Transmission Lines, Sporn and Muller, AIEE Trans., Vol. 60, 1941, pp. 241-246.

35. Gaseous Conductors, J.D. Cobine, McGraw-Hill, 1941, p. 520.

36. Lightning Phenomena, W. Wagner and G. McCann, Electrical Engineering, Vol. 60, No. 10 (1941).

37. High Speed Reclosing, J.E. Hobson, Proceedings of the Midwest Power Conference, Vol. 5, 1942, pp. 156-164.

38. Analysis of the Application of High Speed Reclosing Breakers to Transmission Systems, S.B. Crary, L.F. Kennedy, C.A. Woodrow, Electrical Engineering, AIEE Trans. Vol. 61, 1942, pp. 339-348.

39. Interim Report on Application and Operation of Automatic Reclosing Equipment on Stub Feeders, AIEE Trans., Vol. 62, 1943, pp. 536-540.

40. Dielectric Recovery Characteristics of Large Air Gaps, G.D. McMann, J.J. Clarke, AIEE Trans. 1943, Vol. 62, pp. 45-52.

41. High-Voltage Oil Circuit Breakers for Rapid Reclosing Duty, Hill, Leeds, AIEE Trans. Vol. 63, 1944, pp. 113-118.

42. Reclosing of Single Tie Lines Between Systems, Parker, Travers, AIEE Trans. Vol. 63, 1944, pp. 119-122.

43. Tests of 230 kv High-Speed Reclosing Oil Circuit Breaker, Schwager, AIEE Trans. Vol. 63, 1944, pp. 784-788.

44. Hi-Voltage Interconnections made Reliable by Single-Pole Switching, J.J. Trainor, H.N. Muller, Jr., Power Plant Engineering Vol. 48, June 1944, pp. 77-79.

1945-1949

45. Nine Years' Experience with Ultra-High-Speed Reclosing of High-Voltage Transmission Lines, Sporn and Muller, AIEE Trans. Vol. 64, 1945, pp. 225-228.

46. A High-Capacity High Voltage Three-Cycle Oil Circuit Breaker, H.L. Byrd, E.B. Rietz, AIEE Trans., Vol. 64, 1945, pp. 160-163.

47. Three-Cycle, 3500-megavolt-ampere Air Blast Circuit Breaker for 138,000 volt Service, H.L. Byrd, B.S. Beall, III, AIEE Trans., Vol. 64, 1945, pp. 229-232.

48. Field Test and Performance of Heavy-Duty High-Speed 138 kv Circuit Breakers Oil and Air-Blast, Philip Sporn, H.P. St. Clair, AIEE Trans. 1945.

49. Reclosing Single-Circuit Tie Lines, H.N. Muller, Jr., W.W. Parker, Westinghouse Engineer Vol. 5, March 1945, pp. 60-63.

50. Systematic Tests with Automatic High-Speed Reclosing in the Goesten and Laufenburg Power Systems, W. Wagner, The Brown Boveri Review, December, 1945.

51. The Application of Ultra-High-Speed Reclosure to Distribution Networks, by S. Teszner and R. Chambrillon, CIGRÉ 11, 1946, No. 331.

52. Dielectric Recovery by an A-C Arc in an Air Blast, T.E. Browne, Jr., AIEE Trans., 1946, pp. 169-175.

53. Dielectric Strength of Station and Line Insulation to Switching Surges, Bellaschi and Rademacher, AIEE Trans. 1946, Vol. 65.

54. Résultats d'Essais de Réenclenchement Automatique Effectués sur un Réseau de Transport d'Energie a 150 kv, by C. Dietsch, Soc. Franc. Electr. Bull. 6, 1946, pp. 321-328.

55. Construction et Exploitation des Réseaux de Transport et de Distribution d'Energie Electrique, by Lagoutt, C. Dietsch, F. Cahen, others, Soc. Franc. Electr. Bull. 7, 1947, pp. 209-236.

56. Lightning and 60 Cycle Power Tests on Wood Pole Line Insulation, P.L. Bellaschi and Rademacher, AIEE Trans. 1947, Vol. 66, pp. 838-850.

57. On the Localized after-glow Observed with Long Sparks in Various Gases, J.D. Craggs, W. Hopwood and J.M. Meek, J. Appl. Physics, October 1947, Vol. 18, pp. 919-927.

58. Experience with Operating Automatic Reclosing of Breakers after Line Faults by G. Jancke, CIGRÉ 12, 1948, No. 306.

59. Power System Stability Requirements Determined by A-C Calculating Board Study and Operating Performance Proved by Staged Fault Tests, by W.A. Morgan and B. Evans, CIGRÉ 12, 1948, No. 319.

60. Staged Tests and Operating Results on an 8 kv Overhead Line System Using High-Speed Automatic Reclosing, by Naef and J. Wild, CIGRÉ 12, 1948, No. 331.

61. Performance Test of the Allegemeine Eleckricitäts Gesellschaft Free-Jet Air-Blast 220 kv, 2,500 megavolt-ampere Reclosing Circuit Breaker, Dovjikov, Diemond, AIEE Trans. Vol. 68, 1948, pp. 295-304.

62. Field Tests for Development of 10,000,000 KVA 230 kv Oil Circuit Breakers for Grand Coulee Power Plant, C.L. Killgore and W.H. Clagett, AIEE Trans. Vol. 67, Part 1, 1948, pp. 271-287.

63. Experience with High Speed Reclosing, G.E. Dana, Electrical Engineering, October, 1948, pp. 942-944.

64. Circuit Breakers and Neutral Point-Earthing, H. Thommen, Brown Boveri Review, 1948, Vol. 35, pp. 227-230.

65. New Investigations on Dielectric Strength of Gas, N. Felici and Y. Marchal, Revue Generale de l'Electricite, 1948, Vol. 57, pp. 155-162.

66. Deionization Time of High-Voltage Fault-Arc Paths, Everett J. Harrington, E.C. Starr, AIEE Trans. Vol. 68, 1949, pp. 997-1004.

67. Insulator Flashover Deionization Times as a Factor in Applying High-Speed Reclosing Circuit

Breakers, A.C. Boisseau, B.W. Wyman, W.F. Skeats, AIEE Trans. Vol. 68, 1949, pp. 1058-1067.

68. A-C Tripping and Reclosing of Line Sectionalizing Circuit Breakers, Winegartner, Boneheimer, AIEE Trans. Vol. 68, 1949, pp. 1357-1359.

1950-1954

69. Consideration of Requirements and Limitations of Relaying and High-Speed Reclosing on Long and Heavily Loaded Transmission Lines, Parks, Brownlee, AIEE Trans. Vol. 60, 1950, pp. 103-107.

70. The Bonneville Power Administration Relaying and Reclosing Program, Diemond, Wylie, AIEE Trans. Vol. 60, 1950, pp. 1039-46.

71. Dielectric-Recovery Characteristics of Power Arcs in Large Air Gaps, by G.D. McCann, J.E. Conner and H.M. Ellis, AIEE Trans. Vol. 69, Part I, 1950.

72. Modernized Indoor Air-Blast High Speed Circuit Breakers, by H. Thommen, Brown Boveri Review, Vol. 37, 1950, pp. 143-153.

73. Protection of Transmission Systems Against Lightning, W.W. Lewis, John Wiley & Sons, New York, N.Y., 1950.

74. High-Speed Reclosure of Circuit Breakers, by J.R. Mortlock, BTH Activities 21, 1950, pp. 188-192.

75. Automatic Reclosing As A Means of Lightning Protection During Storms, N.N. Beliakov and A.I. Gershengorn. Trud. nauch-tekh. sessii po perenapriazheniam. Gosenergoizdat (1950).

76. Factors affecting the Rate of Dielectric Recovery of Power Arcs in Long Air Gaps, Ph. D. Thesis, California Institute of Technology, 1951, H.M. Ellis.

77. High Speed Multiple Reclosing Oil Circuit Breaker for 161 kv 10,000 KVA, Baker Cushing, Vol. 71, AIEE 1952, pp. 22-28.

78. Developing a Super Speed Trip-Free Reclosing Circuit-Breaker Mechanism, Linde, Peak, AIEE Trans. Vol. 71, 1952, pp. 734-742.

79. Rapid Reclosing Tests on a 30 Distribution Network, by B. Thoren, ASEA Journal, Vol. 25, 1952, pp. 102-108.

80. High Speed Motion Picture Photography of Electrical Arcs on a High Voltage Power System, E.J. Harrington and H.C. Ramberg, Journal of the Society of Motion Picture and Television Engineers, 1953, Vol. 60, pp. 675-679.

81. Protection Test with Rapid Reclosing in an EHV Network, by A. Matthey-Doret and A. Leuthold, Brown Boveri Review, Vol. 41, No. 1, 1954, pp. 351-353.

82. The Supply Arc During the Elimination of Earth Faults in 400 kv Lines, A.S. Maikopar, Trud. TSNIEL (Proceedings of Central Electrical Research Institute), Vol. II (1954).

1955-1960

83. Operating Experience with 230 kv Automatic Reclosing on Bonneville Power Administration System, D.A. Gillies, AIEE Trans. Vol. 73, 1955, pp. 1692-96.

84. Short Circuit Test with Rapid Reclosing on the 220 kv Mettlen-Lavorgo Line, F. Shar and P. Baltensperger, AIEE Trans. Vol. 75, Part III, 1956, pp. 1137-1146.

85. Automatic Circuit Reclosers, G.F. Peirson, A.H. Pollard, N. Care, IEE Proceed. Vol. 102, Pt. A. (Power Eng.) No. 6, 1955, pp. 749-764.

86. Wood versus Steel Transmission Lines, L.M. Robertson, Electrical World, February 7, 1955.

87. Kurzunterbrechung in Verteilungsnetzen (Short Interruption in Distribution Networks), H. Baatz, ETZ-A, No. 18 (1955).

88. Development and Testing of 300 kv Air-Blast Circuit Breaker for Severe Duties, J. Christie, D.F. Amer, A.F.B. Young, AIEE Trans. Vol. 75, Part III, No. 27, 1956, pp. 1056-1064.

89. New High Power Cathode Circuit Breaker, L.D. McMonnell, J.D. Findley, AIEE Trans., Vol. 75, Part II, No. 23, 1956, pp. 39-43.

90. Testing of High-Voltage Circuit Breakers, L.R. Bergstrom, ASEA Journal, Vol. 29, No. 6, 1956, pp. 71-81.

91. Air-Blast Circuit Breakers for High Voltage Networks, C.H. Flurscheim, Metropolitan Vickers Gazette, Vol. 27, No. 445, 1956, pp. 235-244.

92. High-Voltage Circuit Breakers-Performance and Selection, C.S. Scrrenivasan, Power Eng. (India) Vol. 6, No. 4, 1956, pp. 236-245.

93. The Transition of High-Power Impulse Flashover Into a Power Arc in Overhead Transmission Lines, A.S. Maikopar, Trud. TSNIEL, Vol. V (1956).

94. Study of High-Power Impulse Discharge in Air at Atmospheric Pressure, V.V. Burgsdorf and A.S. Maikopar, Elekt. No. 12 (1957).

95. Ultra High-Speed Reclosing Experience, Barnes, Hauspurg and Kinghorn, AIEE Transactions Vol. 77, Part III, 1958, pp. 137-144.

96. Impulse System for Arc Recovery Strength Measurements, J.D. Cobine, E.E. Burger, G.A. Farrall, AIEE Trans. Vol. 77, pp. 1094-1101.

97. Air Blast Circuit Breakers for Very High Voltage, G.K. Simpson, IEE Journal Vol. 4, No. 41, 1958.

98. The Design of 330 kv Transmission System for Rhodesia, IEE Proc., Pt. A., 1958.

99. High Temperature Effects on Flashover in Air, IEE Proc., Pt. A., Vol. 105, No. 24, 1958.

100. Experience with Ultra High-Speed Reclosing of Transmission Lines on 345 kv Systems in the U.S.A., by J.J. Kinghorn, H.C. Barnes, A. Hauspurg, CIGRÉ 1958, No. 121.

101. A Lightning Stroke Component Counter, H.M. Ellis and H. Linck, CIGRÉ No. 308, 1958.

102. Arcing Short Circuits on 400 kv Transmission Lines and Methods of Dealing with them, A.S. Maikopar, N.N. Beliskon, Electric Technology USSR, December 1958, pp. 27-38.

103. National Advisory Committee for Aeronautics, Technical Note 4150 - "Approximations for the Thermodynamic and Transport Properties of High Temperature Air", by C. Frederick Hansen, NACA, Washington, March 1958.

104. Field Tests on a 345 kv High Capacity Oil Circuit Breaker at Philip Sporn Power Plant by O. Naef, J.D.M. Phelps, W.R. Wilson and A.L. Streater, AIEE Paper No. 59-188.

105. The 345 kv Transmission System of the American Electric Power Company and the Ohio Valley Electric Corporation, F.M. Porter and H.P. St. Clair, CIGRÉ No. 407, 1960.

106. Report on the Work of Study Committee No. 9 on Extra High Voltage A-C Transmissions, P. Sporn, F. Cohen, M. Magnien, CIGRÉ No. 416, 1960.

107. Minimum Time of Automatic Reclosing, A.S. Maikopar, Electric Technology USSR, Vol. 2, May 1960.

108. Swedish 380 kv System, book printed in Stockholm, 1960, p. 38.

109. Fault Arc Deionization and Circuit-Breaker Reclosing on EHV Lines, Field, Laboratory and Analytical Results, B. Johnson, L.O. Barthold, C. Dorsa, J.H. Hagenguth, A. Hauspurg, J.H. Kinghorn, O. Naef, J.D. Phelps, V.E. Phillips, W.F. Skeats, C.H. Titus and F.C. Vose, CIGRÉ 1962, No. 307.

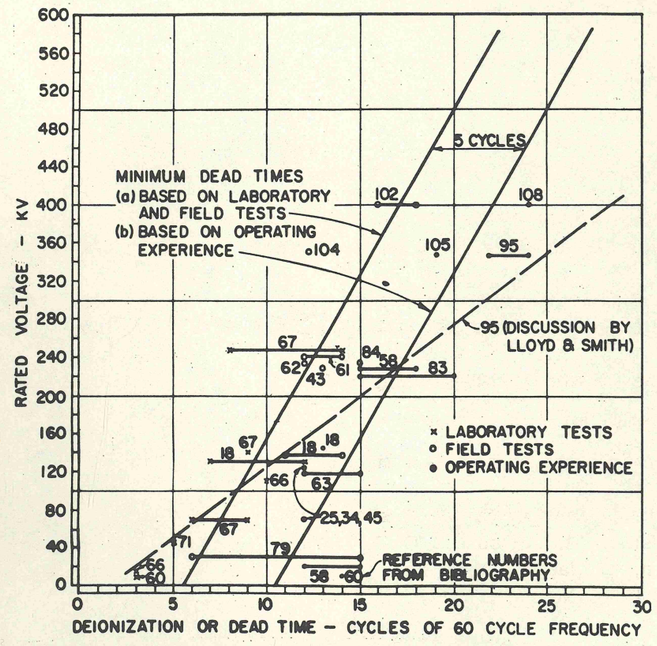

Fig. 1. High Speed Three-Pole Reclosing Deionization Time